# Design, Synthesis and Biological Evaluation of Glycosidase Inhibitors in an Anti-Cancer Setting


Andreas F. G. Glawar

St. John's College, University of Oxford

Trinity Term, 2013

A thesis submitted in partial fulfillment of the requirement for the degree of Doctor of Philosophy (D. Phil.) in Organic Chemistry

# DESIGN, SYNTHESIS AND BIOLOGICAL EVALUATION OF GLYCOSIDASE INHIBITORS IN AN ANTI-CANCER SETTING

Andreas F. G. Glawar, St. John's College, University of Oxford

Doctor of Philosophy in Organic Chemistry

Trinity Term, 2013

The aim of the work described in this thesis was to explore the synthesis of glycosidase inhibitors and to evaluate their potential as anti-cancer agents. Glycosidases catalyze the fission of glycosidic bonds and are involved in vital biological functions. With regard to their potential for anti-cancer therapy, two glycosidases were identified: α-*N*-acetyl-galactosaminidase and β-*N*-acetyl-hexosaminidase. The former has been implicated in causing immunosuppression in advanced cancer patients by negating the effect of the macrophage activating factor (MAF), while the latter is secreted by invading cancer cells and hence associated with metastasis formation.

The synthetic focus was on generating piperidine and azetidine iminosugars, carbohydrate mimetics with their endocylic oxygen replaced by nitrogen. Their structural similarity to carbohydrates make iminosugars excellent inhibitors of glycosidases. Following synthesis of a pipecolic amide, its previously reported potent β-*N*-acetyl-hexosaminidase inhibition was confirmed. This data, along with inhibition profiles of several pyrrolidines, allowed the generation of a molecular model for predicting activity of β-*N*-acetyl-hexosaminidase inhibitors. The model was used to select azetidines in the D/L-*ribo* and D-*lyxo* configuration as suitable candidates to be explored in novel chemical space, leading to the first synthesis of a fully unprotected 3-hydroxy-2-carboxy-azetidine. The potent α-*N*-acetyl-galactosamindase inhibitor 2-acetamido-1,2-dideoxy-D-*galacto*-nojirimycin (DGJNAc) was successfully derivatised *via* *N*-alkylation.

Important structural discoveries with regard to glycosylation of vitamin $D_3$-binding protein, the precursor of MAF, were made using MALDI mass-spectrometry. By comparing the enzymatic and cellular inhibition of *N*-alkylated derivatives of DGJNAc and a pyrrolidine the following generalization on iminosugar biodistribution was found: *N*-butylation promotes uptake into the cell/organelles, while hydrophilic side-chains restrict cellular access. An *in vitro* assay evaluating cancer cell invasion was devised and β-*N*-acetyl-hexoamindase inhibitors were shown to retard cell migration, including with the highly metastatic breast cancer cell line MDA-MB-231. Additive effects where found when the iminosugar was combined with a protease inhibitor, suggesting potential for future combination therapy.

## Acknowledgments

First and foremost I would like to thank my joint supervisors Professor George Fleet and Dr. Terry Butters. It is their guidance, knowledge and support that has made this interdisciplinary project possible. Dr. Butters was always available to patiently answer my questions regarding biochemistry in general and glycobiology in particular, for which I am extremely grateful. Professor Fleet has guided my scientific development for over a decade, beginning with my chemistry undergraduate interview at St. John's College. It has been a privilege and a pleasure to work in the laboratories of two such outstanding scientists, who are so well able to bridge the gap between diverse scientific disciplines.

I would like to thank all of the Butters group for welcoming a chemist to their glycobiology ranks. In particular, I would like to acknowledge Dr. Dom Alonzi for teaching me the FOS HPLC technique, Dom and Mr. Jonny Howe for half-marathon training runs, Dr. Sarah Allman for her positive input at group meetings and especially for appreciating the chemistry, Mr. Adrien Peron for work on isolation of DBP from blood plasma and Dr. Holger Kramer for teaching me to use the MALDI-MS. I would furthermore like to thank Miss Iona Easthope, Miss Laura Pritchard, Dr. Dele Ashiru, Dr. Aime Lopez Aguilar, Dr. Nikolay Kukushkin, Dr. Katy Patzel and Mrs. Gabriele Twigg for being a great crowd of people to work with.

In the Fleet lab, I would like to acknowledge all the help and support from Dr. Sarah Jenkinson, especially with proofreading of any kind, running my crystals in X-ray crystallography and her synthesis of the pyrrolidine iminosugars. I would also like to thank Sarah and Dr. Noelia Araújo for closing my *trans*-azetidine, Dr. R. Fernando Martínez for help with using the supercomputer in Spain, Dr. Gabriel Lenagh-Snow for all the groundwork in azetidine iminosugars and Dr. Ben Ayers for exploring all 16 pyrrolidine amides. Thank you to Fernando and Noelia for making me an honorary member of the Spanish lunchtime mafia. For making life in G3 an enjoyable experience, I would like to thank: Dr. Elizabeth Crabtree, Dr. Scott Newberry, Dr. Loren Parry, Miss. Katy Rutherford, Miss. Dona Dai, Mr. James Mui, Mr. Mike Hollas and Mr. Nigel Ngo.

The contributions of our collaborator Professor Atsushi Kato, the NMR and CRL staff and especially Dr. Amber Thompson in the crystallography department are gratefully acknowledged. I would like to extend my thanks to the Glycobiology Institute and the Organic Chemistry Department with their respective heads of department Professor R. A. Dwek and Professor C. J. Schofield. I would also like to thank Mrs. Lynda Butters for her support of all students in the Glycobiology Institute. I am grateful to St. John's College, which has been a good home for 9 years and of which I will always be a proud member.

Funding from Cancer Research UK (CRUK) in the Medicinal Chemistry for Cancer programme directed by Professor Len Seymour and Dr. Angela Russell, and from the Glycobiology Institute/Biochemistry Department, is gratefully acknowledged.

Mr. Ben Galpin and Dr. Nattapong Paiboonvorachat better known as Foam I would like to thank for our years of friendship going back to undergraduate times. My time at Oxford would have

not been the same without you. Back in my Munich home I would like to thank Mr. Johannes Hunger and Mr. Otto Reinke, for staying in touch with me despite my prolonged absence and for being welcoming and a joy to meet every time I do return.

It is a matter close to my heart to thank Dr. Sarah Remmert for all her support and valuable discussions on molecular modeling.

Zuletzt möchte ich Worte des Dankes an meine ganze Familie richten. Meine Oma trieb mich zwar nicht zur Eile an, fragte aber immer gerne nach, wann meine Doktorarbeit nun ein Ende finden würde. Meinem Patenonkel Volker möchte ich für sein beständiges Interesse an meiner persönlichen Entwicklung und Karriere danken. Meine Schwester möchte ich danken, dass sie mich daran erinnert, was im Leben wirklich wichtig ist. Meine Eltern sind zwei großartige Menschen, die immer alles daran gesetzt haben, ihren Kindern Alles zu ermöglichen. Ohne ihre bedingungslose Unterstützung, ihre Aufopferung und ihren weisen Rat wäre ich nicht, wo ich heute bin und dafür werde ich ihnen immer dankbar sein.

## Table of Contents

## Concerning Nomenclature

The naming and numbering conventions used throughout this thesis are in accordance with the guidelines proposed by IUPAC.[#] Exceptions to this rule are where the sugar denominator has been retained for consistency in NMR data, which will be clearly indicated and the IUPAC name given in parenthesis. Where applicable, the corresponding amino acid name is equally given in the experimental section.[$] Representative examples are shown below.

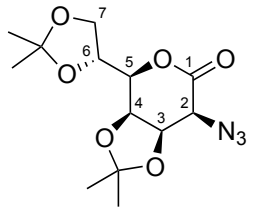

2-*O*-Azido-2-deoxy-3,4:6,7-di-*O*-isopropylidene-D-*glycero*-D-*talo*-heptono-1,5-lactone

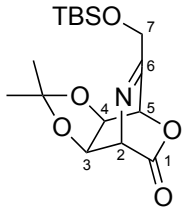

7-*O*-*tert*-Butyldimethylsilyl-2,6-deoxy-2,6-imino-3,4-*O*-isopropylidene-D-*talo*-6-heptulosono-1,5-lactone

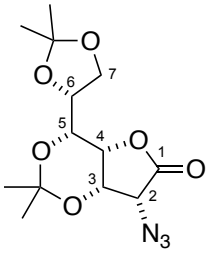

*2*-Azido-2-deoxy-3,5:6,7-di-*O*-isopropylidene-D-*glycero*-D-*gulo*-heptono-1,4-lactone

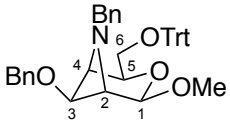

Methyl *N*-benzyl-3-*O*-benzyl-2,4-dideoxy-2,4-imino-6-*O*-trityl-β-D-*talo*-pyranoside

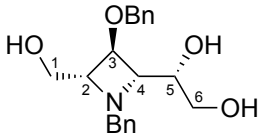

*N*-Benzyl-3-*O*-benzyl-2,4-dideoxy-2,4-imino-D-talitol

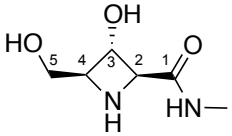

Methyl 2,4-dideoxy-2,4-imino-L-ribonamide

or (2*S*,3*S*,4*S*)-3-hydroxy-4-(hydroxymethyl)-*N*-methylazetidine-2-carboxamide

# McNaught, A. D.; Nomenclature of carbohydrates. Recommendations 1996. *Carbohydr. Res.* **1997**, *297*, 1-92.

$ Nomenclature and symbolism for amino acids and peptides. Recommendations 1983. *Eur. J. Biochem.* **1984**, *138*, 9-37.

## List of abbreviations

| | |
|---|---|
| 2-AA | anthranilic acid |
| ACE | angiotensin-converting enzyme |
| AcOH | acetic acid |
| ATCC | American Type Culture Collection |
| Aze | L-azetidine-2-carboxylic acid |
| b.w. | by weight |
| BCR | breakpoint cluster region |
| br. | broad |
| CAM | chick chorioallantoic membrane |
| cAMP | 3',5'-cylcic adenosine monophophate |
| cat | catalyst |
| CD | circular dichroism |
| CEA | carcinoembryonic antigen |
| CHCA | α-cyano-hydroxycinnamic aicd |
| CML | chronic myelogenous leukemia |
| conc. | concentrated |
| COX-2 | cyclooxygenase-2 |
| CRUK | Cancer Research UK |
| d | doublet |
| DBP | vitamin $D_3$ binding protein |
| DCM | dichloromethane |
| DFT | density functional theory |
| DGJ | deoxy-*galacto*-nojirimycin |
| DGJNAc | 2-acetamido-1,2-dideoxy-D-*galacto*-nojrimycin |
| DHF-DA | dihydrofluoresceine diacetate |
| DMDP | 2,5-dideoxy-2,5-imino-D-mannitol |
| DMP | Dess Martin periodinane |
| DNJ | deoxynojirimycin |
| DTI | direct thrombin inhibitor |
| DTT | dithiothreitol |
| ECM | extra cellular matrix |
| EHS | Engelbreth Holm-Swarm |
| ER | endoplasmic reticulum |
| ERAD | ER-associated degradation |
| ERK | extracellular-signal-regulated kinase |
| ERT | enzyme replacement therapy |
| FDA | Food and Drug Administration |
| FGF-2 | fibroblast growth factor |
| FOS | free oligosaccharide |
| GAG | glycoaminoglycan |
| GC | group specific protein |
| Gly | glycine |
| GSL | glycosphingolipid |
| GUs | glucose units |
| HCC | human hepatocellular carcinoma |
| HEC | human endothelial cells |
| HIF | hypoxia-inducible transcription factor |
| HMBC | heteronuclear multiple-bond correlation spectroscopy |
| HMCV | human cytomegalovirus |
| HMJ | Homomannojirimycin |
| HML | human macrophage C-type lectin |
| HNJ | Homonojirimycin |
| HRMS | high resolultion MS |
| HRP | horseradish peroxidase |
| Hyp | (2*S*,4*R*)-4-hydroxyproline |
| IR | infra red |
| LABNAc | 2-acetamido-1,4-imino-1,2,4-trideoxy-L-arabinitol |

| | |
|---|---|
| LB | Lineweaver Burk plot |
| lit. | literature |
| LPS | lipopolysaccharide |
| LSD | lysosomal storage disorder |
| Lyso-PC | lysophosphatidylcholine |
| m | medium |
| m.p. | melting point |
| MA | mugineic acid |
| MAF | macrophage activating factor |
| MALDI | matrix-assisted laser desorption/ionization |
| MAPK | mitogen-activated protein kinase |
| MCH | melanin-concentrating hormone |
| MCP-1 | monocyte chemotactic protein-1 |
| MDP | meylin basic protein |
| MeCN | acetonitrile |
| MGL | macrophage galactose/N-acetylgalactosamine-specific C-type lectin |
| MMP | matrix metallo proteinase |
| MS | mass spectrometry |
| mTORC1 | mammalian target of rapamycin complex 1 |
| MTS | 3-(4,5-dimethythiazol-2-yl)-5-(3-carboxymethoxyphenyl)-2-(4-sulfophenyl)-2H-tetrazolium |
| NA | nicotianamine |
| ND | Not determined |
| NI | No inhibition |
| NJ | nojirimycin |
| NMR | nuclear magnetic resonance |
| NO | nitric oxide |
| NOE | nuclear Overhauser enhancement |
| P3H | prolyl 3-hydroxylase |
| P4H | prolyl 4-hydroxylase |
| PCC | pyridinium chloro chromate |
| Pd/C | palladium on charcoal |
| PPII | polyproline type II |
| PPTS | pyridinium toluene-*p*-sulfonate |
| Pro | proline |
| PSA | prostate-specific antigen |
| quant | quantitative |
| ROI | reactive oxygen intermediate |
| RT | room temperature |
| s | IR: strong; NMR: singlet |
| SAR | structure activity relationship |
| SCC | squamous cell carcinoma |
| SCID | severe combined immunodeficient |
| $SIP_1$ | sphingosine phosphate receptor-1 |
| SRT | substrate reduction therapy |
| t | triplet |
| TDP-43 | TAR DNA-binding protein of 43-dDa |
| TLC | thin layer chromatography |
| TNF-α | tumor necrosis factor α |
| uPA | urokinase plasminogen activator |
| uPAR | urokinase receptor |
| VEGF | vascular endothelial growth factor |
| VLA-4 | very late activating antigen-4 |
| w | weak |
| WHO | World Health Organization |

# 1 GENERAL INTRODUCTION

## 1.1 Overview

The subject of the work described in this thesis will be to explore the design and synthesis of iminosugars and to develop *in vitro* assays for their biological evaluation against two glycosidases, which represent potential novel anti-cancer targets.

## 1.2 Iminosugars

Iminosugars are carbohydrate mimetics in which the endocyclic ring oxygen is replaced by nitrogen. In 1962 one of the earliest examples of this compound class was synthesized by Paulsen in the form of piperidine **1**, which is the iminosugar analogue of D-*xylo*-pyranose (Figure 1.1).[1] However, the real starting point for the field of iminosugars was his synthesis of deoxynojirimycin (DNJ) **4** from a sorbose derivative in 1966.[2] Having the hemiaminal functionality removed, DNJ **4** is the more stable analogue of nojirimycin (NJ) **3**, which is the nitrogen analogue of the most common monosaccharide D-glucose **2**.[3] NJ **3** has been isolated from fermentation broths of *Streptomyces* bacteria,[4] while DNJ **4** was shown to be produced by *Bacillus* bacteria.[5] In 1979 both NJ **3** and DNJ **4** were shown to be potent inhibitors of carbohydrate processing enzymes and the parent scaffold of DNJ **4** is found in two iminosugars in current clinical use.[5] Therefore, we can see how these discoveries sparked enormous interest in the synthesis, natural isolation and biological evaluation of iminosugars.

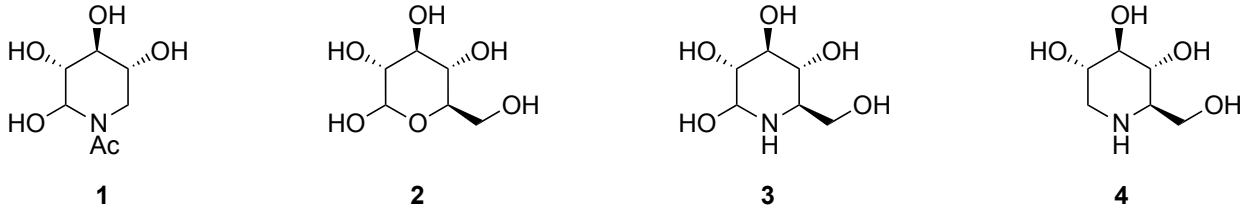


**Figure 1.1** Example of early iminosugar synthesis and relation of nojirimycin and its more stable analogue deoxynojirimyin to D-glucose.

### 1.2.1 Synthesis and natural isolation

The main classes of iminosugars besides the already mentioned piperidines are pyrrolidines, pyrrolizidines, indolizidines and nortropanes.[6] Representatives from of each of these classes are shown in Figure 1.2 and typical synthetic routes to these compounds involve introduction of nitrogen into a suitable carbohydrate starting material. Standard strategies of nitrogen introduction include: a) reductive amination of an azido-ketose, b) intramolecular amine closure onto a leaving group and c) intermolecular closure *via* displacement of a doubly functionalized substrate with primary amine or ammonia. A detailed description of these approaches towards compounds from the classes named above, and additionally including 7-membered and multi-fused nitrogen heterocycles, is presented in the book by El Ashry and El Nemr.[7] Furthermore strategies involving non-carbohydrate starting materials for devising iminosugar libraries based on the decoration of a parent schaffold are becoming more popular.[8] Further synthetic efforts have included the generation of iminosugars, which retain aglycone-specific information but don't suffer the instability of hemiaminal containing derivatives like NJ **3** and these include 1-azasugars and *C*-glycosides.[9]

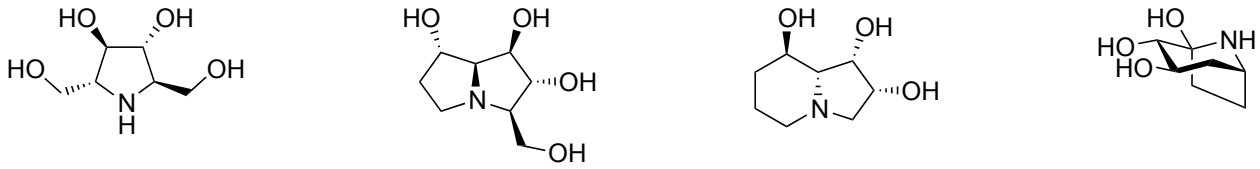


**5** DMDP | **6** (+)-Alexine | **7** (-)-Swainsonine | **8** Calystegin $A_3$

**Figure 1.2** Representative examples of the main classes of iminosugars.

Iminosugars are also found in abundance as natural products from plants and micro-organisms.[10] For example 2,5-dideoxy-2,5-imino-D-mannitol (DMDP) **5** was isolated from the leaves of *Derris elliptica*,[11], (+)-alexine **6** from dried pods of *Alexa leiopetala*,[12] (-)-swainsonine **7** from *Swainsona canescens*[13] and calystegin $A_3$ **8** from roots of *Calystegium sepium* (Figure 1.2).[14]

Therefore a wide variety of iminosugars are readily available both as natural and synthetic products.

### 1.2.2 Biological activity of iminosugars - glycosidase inhibition

One motivation for the large body of iminosugar synthesis and natural isolation publications is the diverse biological effects displayed by these compounds. These can be majorly derived from their inhibition of glycosyltransferases,[15] nucleoside processing enzymes,[16] and especially glycosidases, amongst other carbohydrate processing enzymes.[17] Glycosidases catalyse the fission of glycosidic bonds and can be found in the digestive tract and within cellular organelles including the lysosome, endoplasmic reticulum and the Golgi apparatus. They fulfil many vital functions in the body encompassing the digestive breakdown of oligosaccharides into easily absorbed mono-saccharides, catabolism of glycoconjugates and biosynthesis of glycoproteins, which are responsible for cellular structure, recognition and communication.[10a]

Due to their structural similarity to the natural carbohydrate substrates of glycosidases, iminosugars make excellent inhibitors of this class of enzymes. Additionally the protonation of the endocylic nitrogen under physiological conditions creates a positive charge,[18] which resembles the charge distribution of the oxocarbenium ion-like transition state intermediate found in the glycosidase active site (Figure 1.3).[19]

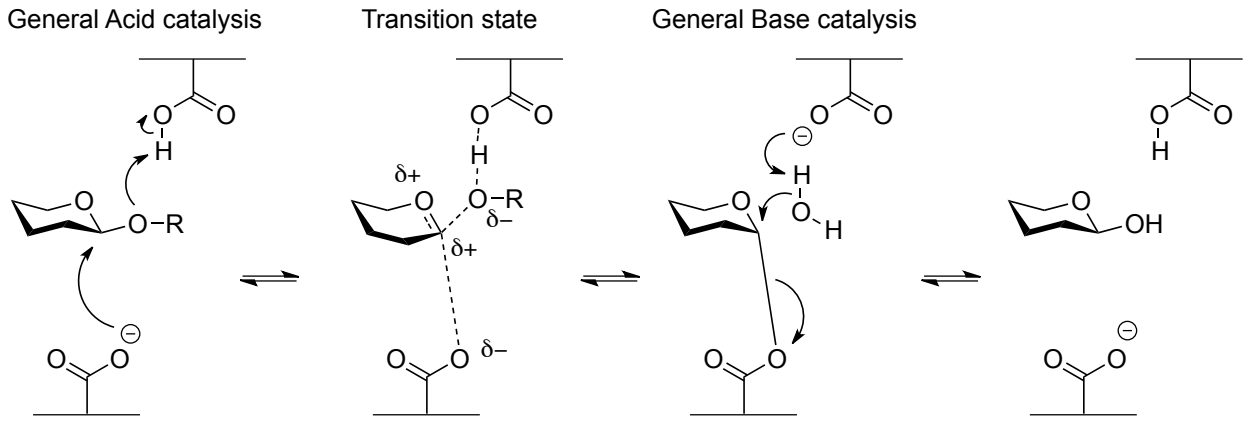


**Figure 1.3** "Classical" hydrolysis mechanism of a generic glycosidase with retention of stereochemistry. Charge distribution for oxocarbenium ion-like transition state is indicated.[19-20]

### 1.2.3 Therapeutic applications of iminosugars

As a result of their diverse bioactivity, iminosugars have found many therapeutic applications for a wide range of ailments including glycolipid lysosomal storage disorders (LSD), diabetes, viral infections and cancer.[6, 17b] LSDs are caused by limited or absent function of lysosomal glycosidases and the standard treatment constitutes enzyme replacement therapy (ERT), which although well established, has several limitations. This includes the inability of the recombinant enzyme to cross the blood brain barrier (lysosomal storage of glycolipids effects neural cells particularly), the high number of required infusions and associated costs (e.g. for Gaucher disease $ 90,000 – 720,000 average cost per patient and year).[21] Although it seems paradoxical to use a glycosidase inhibitor for a disease whose origin is impaired enzyme activity, in terms of the use of iminosugars, two schools of thought have emerged. In most patients residual enzyme activity still remains, so iminosugar-based inhibition of the anabolic glycosphingolipid cascade that generates substrate for an impaired enzyme, reduces substrate build-up and hence lysosomal storage.[22] This approach has been dubbed substrate reduction therapy (SRT).[23] Chaperone therapy on the other hand, uses iminosugar inhibitors specific for the damaged enzyme, but at subinhibitory concentrations.[24] The iminosugar binds to the active site of the enzyme, which as a result folds correctly and is able to escape the ER-associated degradation (ERAD) process. It is trafficked more efficiently through the Golgi apparatus to the lysosome, where the iminosugar becomes displaced due to the high substrate concentration. A phase III trial on Fabry disease using the chaperone approach is currently ongoing with the iminosugar migalastat (DGJ).[25]

Anti-viral properties of iminosugars are the result of inhibition of the host cell's glycoprotein processing glucosidases, the correct function of which are required by viruses, which bud from the ER to acquire their envelope.[26]

Several anti-cancer effects have been ascribed to iminosugar inhibitors.[27] One example is the potent mannosidase and glucosidase inhibitor swainsonine **7**, which was able to restrict tumor

growth and metastatsis formation (Figure 1.2). The underlying molecular mechanism is believed to be the inhibition of α-mannosidase II in the Golgi apparatus, which restricts the expression of complex-type oligosaccharides, a requirement for cancer cell invasion.[28] Animal trials were encouraging and swainsonine **7** progressed to phase II clinical trials before being terminated because of lack of *in vivo* activity against metastatic renal cell carcinoma.[29] Further uses of iminosugars as potential anti-cancer agents, however, are still being explored and this thesis aims to expand our understanding in this area.

### 1.2.4 Clinical use of iminosugars

There is ongoing commercial interest in progressing further iminosugars through clinical trials towards their successful application as therapeutic agents in man.[30] The iminosugars Miglustat (*N*-butyl-DNJ) and Miglitol (*N*-hydroxyethyl-DNJ) are already in current clinical use for the treatment of the LSD Gaucher disease and type II diabetes respectively.[31] Miglustat was marketed by Actelion under the trade name of Zavesca® and relies on the principle of SRT for treating Gaucher disease. This orally available compound inhibits one of the early steps in the synthesis of glycosphingolipids (GSL) and hence prevents the build-up and lysosomal storage of more complex GSLs. Miglitol is marketed as Glyset™ by Pfizer, but was developed by the Bayer company with its mode of action relying on the inhibition of α-1,4-glucosidases in the intestine to prevent postprandial hyperglycemia. The success of these two iminosugars in the clinic displays the potential that this unusual class of compounds might hold for future therapy.

## 1.3 Selective Anti-cancer therapy

According to Cancer Research UK (CRUK) more then 300,000 new cases of cancer and 150,000 cancer caused deaths were recorded in 2010 in the U.K..[32] The World Cancer Report released by the World Health Organization (WHO) reports 12.4 million new cancer cases for 2008 and 7.6 million cancer deaths worldwide.[33] These numbers show the enormous problem this disease

represents for humanity, which is only set to become more fierce with an increasingly aging population (between 2008 and 2030 the proportion of over 65 year old is set to increase from 5.3% to 9.8% in less developed and from 14.6% to 22.6% in more developed countries), as the incidence of cancer is closely correlated with increasing age of the individual. The WHO report forecasts by 2030 numbers of new cancer cases to rise to 20.0 million with 12.9 million of cancer associated deaths and as a result Macmillan Cancer Support predicts that by 2020 47% of the U.K. population could be expected to get cancer during their lifetime.[34] This increasing cancer burden displays the ever increasing need for new and more selective cancer therapies.

### 1.3.1 Traditional chemotherapy vs. selective anti-cancer therapy

The main approaches for cancer treatment currently used in the clinic are surgical removal, chemotherapy and radiotherapy. In some cases this therapy can be extremely effective e.g. 95.1% of melanoma *in situ* operations are curative.[35] However, for common solid tumors like lung cancer, the 5 year survival rate is still limited to 14%.[36] Especially in the cases of metastatic spread of the disease, chemotherapy is the only option and success rates can be very low. Chemotherapy, by definition, is just the use of a chemical in a therapeutic setting, however, in the area of oncology it usually refers to the use of cytotoxic agents in order to treat cancer tissue and is often associated with major side effects.[37] Traditional cytotoxic compounds either target DNA directly, for example *via* crosslinking and alkylating compounds, or processes and proteins associated with the DNA, like the spindle apparatus. However, the interference with these processes will also affect the normal cells in the body, which particularly can be observed in tissues with a faster turnover rate, like hair follicles, bone marrow and gastrointestinal mucosa. The negative effect on these tissues leads to the typical chemotherapy associated side effects of hair loss, immunosuppression and nausea. The beneficial effect of chemotherapy is derived from the fact that the DNA repair mechanism of malignant cells is usually impaired and hence they recover more slowly then normal tissue. Fractionated chemotherapy is therefore designed to

inflict maximal damage on the malignant growth, while giving normal tissue, especially the bone marrow, sufficient time to recover and controlling side effects by co-administration of antiemetics and antibiotics. However, even in this setting the emergence of resistance is common and the therapeutic window is small with patients succumbing to disease relapse or secondary infections due to immunosuppression caused by their impaired bone marrow.

As a result of tireless effort over the last 50 years, biological targets have been discovered, that allow malignant growth to be fully differentiated form normal tissue and hence avoiding the collateral damage on normal tissue caused by the "friendly fire" of the traditional chemotherapy. A toxin selective for such a target would be as close as we can get to Paul Ehrlich's magic bullet for treating cancer. Although our understanding of the molecular basis of cancer has increased enormously, the high levels complexity of cellular signaling has made the identification of suitable targets exceedingly difficult. However, one of the rare examples of such a target is explained in more detail below.

### 1.3.2 Selective therapy showcase – Imatinib

In 1960 a group of scientists in Philadelphia noticed the exceedingly small size of chromosome 22 presented in the cells of chronic myelogenous leukemia (CML).[36] Since then this abnormal Philadelphia chromosome, which is the product of a translocation between chromosome 9 and 22, has been discovered in 95% of CML cases. This translocation places the *ABL* gene (Abelson, named due to its sequence analogy to the virus with murine cells transforming ability) next to the *BCR* (breakpoint cluster region) leading to the expression of a multifunctional fusion protein. One of the discovered functions of the fusion protein was a constitutively active tyrosine kinase, which could be shown to be the origin of the transforming ability of ABL. The cancer was shown to be dependent on the activity of this kinase, as mutations of the kinase active site lead to the loss of all transforming ability. In the 1990s a small molecule inhibitor was developed for

this particular kinase and was found in the form of imatinib **9** (Gleevec or Glivec).[38] The structure of Imatinib is shown in Figure 1.4 and the cross-section through the X-ray crystal structure shows the close fit of the inhibitor in the ATP binding site of the kinase. Imatinib was found to be highly specific, inhibiting only 4 of the 90 kinases found in the human body and due to its highly successful clinical trials gained FDA approval for the treatment of CML.[39] The success of Imatinib stresses the importance of identifying novel biological anti-cancer targets that will allow for future selective anti-cancer therapies.

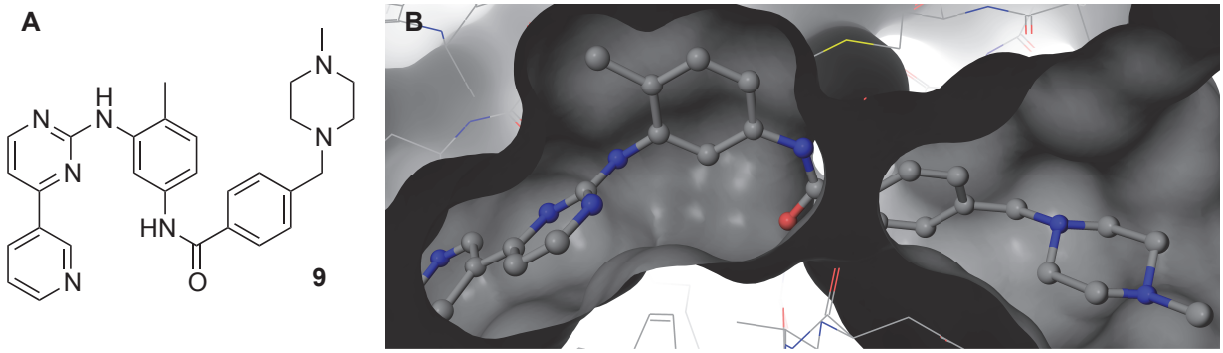


**Figure 1.4** Imatinib (Gleevec or Glivec) A) Structural representation; B) Imatinib bound in active site of the kinase domain of murine c-Abl according to PDB entry 1IEP.[40]

### 1.3.3 Iminosugars as selective anti-cancer agents – glycosidases as novel targets

Two such biological targets could be represented by the glycosidases α-*N*-acetyl-galactosaminidase and β-*N*-acetyl-hexosaminidase, which are implicated in immunosuppression in advanced cancer patients and degradation of the extra cellular matrix respectively. A detailed introduction to these enzymes and their possible role in anti-cancer therapy will be given in Chapter 4, which focuses on the biological evaluation of iminosugars. This work aims to add an exciting new angle on anti-cancer treatment and yet a further therapeutic application to the highly versatile compound class of iminosugars.

## 1.4 Thesis structure summary

This thesis is roughly divided into the two topical areas of iminosugar synthesis and their biological evaluation. Chapter 2 and 3 are both dedicated to the former and overall they sketch

the synthetic journey taken from 6-membered ring piperidine to 4-membered ring azetidine iminosugars. Molecular modeling, which included structures of 5-ring pyrrolidine iminosugars, allowed the bridging of the two different ring sizes resulting in the development of a structure activity model of β-*N*-acetyl-hexosaminidase inhibitors. Chapter 4 on the other hand introduces the two glycosidases, α-*N*-acetyl-galactosaminidase and β-*N*-acetyl-hexoaminidase along with their potential anti-cancer role, in more detail and the biological evaluation can be further subdivided into three segments. Two are dedicated to the development of *in vitro* assays for each of the two glycosidases of interest, while the third more generally explores the effects of *N*-alkylation of iminosugars in a cellular context.

Overall highlights of this thesis include the synthesis of potent β-*N*-acetyl-hexosaminidase inhibitors based on an azetidine framework in novel chemical space, successful activity predictions of iminosugars using molecular modeling, derivatisation of the most powerful α-*N*-acetyl-galactosamindase inhibitor known to date and proof of principle reduction of invasion of a highly aggressive cancer cell line using iminosugars in a combination setting.

## 1.5 References Chapter 1


1. Paulsen, H., Preparation of 5 - Acetamido - 5 - deoxy - D - xylopiperidinose. *Angew. Chem. Int. Ed.* **1962**, *1*, 597.

2. Paulsen, H., Carbohydrates Containing Nitrogen or Sulfur in the "Hemiacetal" Ring. *Angew. Chem. Int. Ed.* **1966**, *5*, 495-510.

3. Inouye, S.; Tsuruoka, T.; Ito, T.; Niida, T., Structure and synthesis of nojirimycin. *Tetrahedron* **1968**, *24*, 2125-2144.

4. (a) Inouye, S.; Tsuruoka, T.; Nida, T., The structure of nojirimycin, a piperidinose sugar antibiotic. *J. Antibiot.* **1966**, *19*, 288-292; (b) Ishida, N.; Kumagai, K.; Niida, T.; Tsuruoka, T.; Yumoto, H., Nojirimycin, a new antibiotic. II. Isolation, characterization and biological activity. *J. Antibiot.* **1967**, *20*, 66-71.

5. Schmidt, D. D.; Frommer, W.; Müller, L.; Truscheit, E., Glucosidase-Inhibitoren aus Bazillen. *Naturwissenschaften* **1979**, *66*, 584-585.

6. Asano, N.; Nash, R.; Molyneux, R.; Fleet, G., Sugar-mimic glycosidase inhibitors: natural occurrence, biological activity and prospects for therapeutic application. *Tetrahedron: Asymmetry* **2000**, *11*, 1645-1680.

7. El Ashry, E. S. H.; El Nemr, A., *Synthesis of naturally occurring Nitrogen Heterocycles from Carbohydrates*. Blackwell Publishing Ltd: Oxford, 2005.

8. La Ferla, B.; Cipolla, L.; Nicotra, F., Chapter 3: General strategies for the synthesis of iminosugars and new approaches towards iminosugar libraries. In *Iminosugars: From synthesis to therapeutic applications*, Compain, P.; Martin, O. R., Eds. John Wiley & Sons Ltd: Chichester, 2007; pp 25-61.

9. (a) Compain, P., Chapter 4: Iminosugar *C*-glycosides: synthesis and biological activity. In *Iminosugars: From synthesis to therapeutic applications*, Compain, P.; Martin, O. R., Eds. John Wiley & Sons Ltd: Chichester, 2007; pp 63-86; (b) Cipolla, L.; la Ferla, B.; Nicotra, F., General methods for iminosugar synthesis. *Curr. Top. Med. Chem.* **2003**, *3*, 485-511.

10. (a) Watson, A.; Fleet, G.; Asano, N.; Molyneux, R.; Nash, R., Polyhydroxylated alkaloids - natural occurrence and therapeutic applications. *Phytochemistry* **2001**, *56*, 265-295; (b) Asano, N., Chapter 2: Naturally occurring iminosugars and related alkaloids: structure, activity and applications. In *Iminosugars: From synthesis to therapeutic applications*, Compain, P.; Martin, O. R., Eds. John Wiley & Sons Ltd: Chichester, 2007; pp 7-24.

11. Welter, A.; Jadot, J.; Dardenne, G.; Marlier, M.; Casimir, J., 2,5-Dihydroxymethyl 3,4-dihydroxypyrrolidine dans les feuilles de Derris elliptica. *Phytochemistry* **1976**, *15*, 747-749.

12. Nash, R. J.; Fellows, L. E.; Dring, J. V.; Fleet, G. W. J.; Derome, A. E.; Hamor, T. A.; Scofield, A. M.; Watkin, D. J., Isolation from Alexa leiopetala and X-ray crystal structure of alexine, (1R,2R,3R,7S,8S)-3-hydroxymethyl-1,2,7-trihydroxypyrrolizidine [(2R,3R,4R,5S,6S)-2-hydroxymethyl-1-azabicyclo[3.3.0]octan-3,4,6- triol], a unique pyrrolizidine alkaloid. *Tetrahedron Lett.* **1988**, *29*, 2487-2490.

13. Colegate, S.; Dorling, P.; Huxtable, C., A spectroscopic investigation of swainsonine: an α-mannosidase inhibitor isolated from Swainsona canescens. *Aust. J. Chem.* **1979**, *32*, 2257-2264.

14. Tepfer, D.; Goldmann, A.; Pamboukdjian, N.; Maille, M.; Lepingle, A.; Chevalier, D.; Dénarié, J.; Rosenberg, C., A plasmid of Rhizobium meliloti 41 encodes catabolism of two compounds from root exudate of Calystegium sepium. *J. Bacteriol.* **1988**, *170*, 1153-1161.

15. Compain, P.; Martin, O. R., Design, synthesis and biological evaluation of iminosugar-based glycosyltransferase inhibitors. *Curr. Top. Med. Chem.* **2003**, *3*, 541-560.

16. Schramm, V. L.; Tyler, P. C., Imino-sugar-based nucleosides. *Curr. Top. Med. Chem.* **2003**, *3*, 525-540.

17. (a) Asano, N., Glycosidase inhibitors: update and perspectives on practical use. *Glycobiology* **2003**, *13*, 93R-104R; (b) Asano, N., Sugar-mimicking glycosidase inhibitors: bioactivity and application. *Cell. Mol. Life Sci.* **2009**, *66*, 1479-1492.

18. Varrot, A.; Tarling, C. A.; Macdonald, J. M.; Stick, R. V.; Zechel, D. L.; Withers, S. G.; Davies, G. J., Direct observation of the protonation state of an imino sugar glycosidase inhibitor upon binding. *J. Am. Chem. Soc.* **2003**, *125*, 7496-7497.

19. Gloster, T. M.; Davies, G. J., Glycosidase inhibition: Assessing mimicry of the transition state. *Org. Biomol. Chem.* **2010**, *8*, 305-320.

20. Koshland, D., Stereochemistry and the mechanism of enzymatic reactions. *Biol. Rev. Camb. Philos. Soc.* **1953**, *28*, 416-436.

21. Parenti, G., Treating lysosomal storage diseases with pharmacological chaperones: From concept to clinics. *EMBO Molecular Medicine* **2009**, *1*, 268-279.

22. Butters, T.; Dwek, R.; Platt, F., Inhibition of glycosphingolipid biosynthesis: Application to lysosomal storage disorders. *Chem. Rev.* **2000**, *100*, 4683-4696.

23. Butters, T. D., Chapter 11: Iminosugar inhibitors for substrate reduction therapy for the lysosomal glycosphingolipidoses. In *Iminosugars: From synthesis to therapeutic applications*, Compain, P.; Martin, O. R., Eds. John Wiley & Sons Ltd: Chichester, 2007; pp 249-268.

24. (a) Fan, J.; Ishii, S.; Asano, N.; Suzuki, Y., Accelerated transport and maturation of lysosomal alpha-galactosidase A in Fabry lymphoblasts by an enzyme inhibitor. *Nat. Med.* **1999**, *5*, 112-115; (b) Fan, J.-Q.; Ishii, S., Active-site-specific chaperone therapy for Fabry disease: Yin and Yang of enzyme inhibitors. *FEBS J.* **2007**, *274*, 4962-4971.

25. Open-Label Phase 3 Long-Term Safety Study of Migalastat (MGM116041); further information available under: http://www.clinicaltrials.gov/.

26. Norton, P. A.; Gu, B.; Block, T. M., Chapter 9: Iminosugars as antiviral agents. In *Iminosugars: From synthesis to therapeutic applications*, Compain, P.; Martin, O. R., Eds. John Wiley & Sons Ltd: Chichester, 2007; pp 209-224.

27. Wrodnigg, T. M.; Steiner, A. J.; Ueberbacher, B. J., Natural and synthetic iminosugars as carbohydrate processing enzyme inhibitors for cancer therapy. *Anti-Cancer Agents Med. Chem.* **2008**, *8*, 77-85.

28. Nishimura, Y., Chapter 12: Iminosugar-based antitumoural agents. In *Iminosugars: From synthesis to therapeutic applications*, Compain, P.; Martin, O. R., Eds. John Wiley & Sons Ltd: Chichester, 2007; pp 269-294.

29. Shaheen, P. E.; Stadler, W.; Elson, P.; Knox, J.; Winquist, E.; Bukowski, R. M., Phase II study of the efficacy and safety of oral GD0039 in patients with locally advanced or metastatic renal cell carcinoma. *Invest. New Drugs* **2005**, *23*, 577-581.

30. Horne, G.; Wilson, F. X.; Tinsley, J.; Williams, D. H.; Storer, R., Iminosugars past, present and future: Medicines for tomorrow. *Drug Discov. Today* **2011**, *16*, 107-118.

31. Cox, T. M.; Platt, F. M.; Aerts, J. M. F. G., Chapter 13: Medicinal use of iminosugars. In *Iminosugars: From synthesis to therapeutic applications*, Compain, P.; Martin, O. R., Eds. John Wiley & Sons Ltd: Chichester, 2007; pp 295-326.

32. CRUK; Key facts on Cancer - all cancers combined cancer statistics; http://publications.cancerresearchuk.org/downloads/Product/CS_KF_ALLCANCERS.pdf.

33. Boyle, P.; Levin, B., World Cancer Report 2008. World Health Organization.

34. Macmillan Cancer support; BBC News article: Half of UK population 'will get cancer in lifetime'; 07.06.2013; http://www.macmillan.org.uk/Home.aspx

35. Bene, N. I.; Healy, C.; Coldiron, B. M., Mohs micrographic surgery is accurate 95.1% of the time for melanoma in situ: A prospective study of 167 cases. *Dermatol. Surg.* **2008**, *34*, 660-664.

36. Weinberg, R. A., The Rational Treatment of Cancer. In *The Biology of Cancer*, Jeffcock, E.; Zayatz, E.; Mickey, R. K., Eds. Garland Science, Taylor & Francis Group, LLC: New York, 2007.

37. Camidge, D. R.; Jodrell, D. I., Chemotherapy. In *Introduction to the Cellular and Molecular Biology of Cancer*, Fourth ed.; Knowles, M.; Selby, P., Eds. Oxford University Press: Oxford, 2005.

38. Druker, B. J.; Tamura, S.; Buchdunger, E.; Ohno, S.; Segal, G. M.; Fanning, S.; Zimmermann, J.; Lydon, N. B., Effects of a selective inhibitor of the Ab1 tyrosine kinase on the growth of Bcr-Ab1 positive cells. *Nat. Med.* **1996**, *2*, 561-566.

39. Druker, B. J.; Talpaz, M.; Resta, D. J.; Peng, B.; Buchdunger, E.; Ford, J. M.; Lydon, N. B.; Kantarjian, H.; Capdeville, R.; Ohno-Jones, S.; Sawyers, C. L., Efficacy and safety of a specific inhibitor of the BCR-ABL tyrosine kinase in chronic myeloid leukemia. *N. Engl. J. Med.* **2001**, *344*, 1031-1037.

40. Nagar, B.; Bornmann, W. G.; Pellicena, P.; Schindler, T.; Veach, D. R.; Miller, W. T.; Clarkson, B.; Kuriyan, J., Crystal structures of the kinase domain of c-Abl in complex with the small molecule inhibitors PD173955 and imatinib (STI-571). *Cancer Res.* **2002**, *62*, 4236-4243.

# 2 PIPERIDINES – 6 MEMBERED IMINOSUGARS

## 2.1 Introduction to piperidines and pipecolic amides

### 2.1.1 Overview

The aim of the work described in this chapter was to synthesize the pipecolic amide **10** in order to confirm its biological activity, which had previously been shown to be very potent against β-*N*-acetyl-hexosaminidase (Figure 2.1).[1] During this synthetic effort, further stereochemistries of pipecolic amides were explored and as the routes proceeded *via* azido-lactones, the usefulness of these lactones as intermediates in the synthesis of iminosugars is discussed. Using molecular modeling a comparison in terms of β-*N*-acetyl-hexosaminidase inhibitory activity between 6-ring and 5-ring iminosugars is drawn and based on the results an activity prediction for 4-membered ring azetidine iminosugars is performed.

### 2.1.2 Pipecolic acid – early synthesis, natural occurrence and biosynthesis

The lead pipecolic amide **10** is a simple peptide derivative of a polyhydroxylated pipecolic acid scaffold **11** with the substituents in α-D-mannose configuration around the piperidine ring (Figure 2.1). The pipecolic or pipecolinic acid **11**, which is the ring expanded analogue of the α-amino acid proline **12L**, was first synthesized as a racemic mixture in 1891.[2] Despite the shortcomings of his students, Ladenburg was able to successfully reduce picolinic acid **13** to pipecolic acid **11** using sodium in ethanol and 5 years later, one of his coworkers was able to separate the enantiomers using cocrystallisation with tartaric acid.[3]

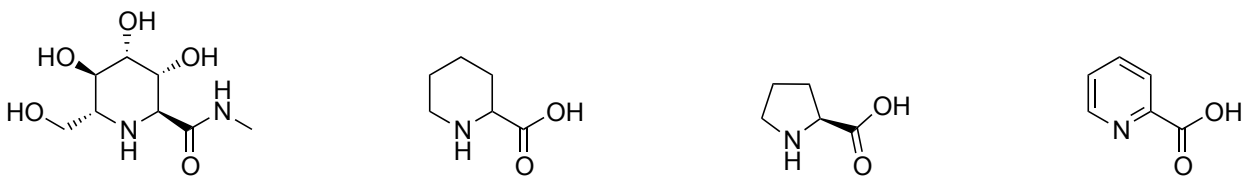


**10** **11 (D/L)** **12L** **13**

**Figure 2.1** Lead pipecolic amide and introduction of the pipecolic acid schaffold.

It took until 1952 for this nonproteinogenic α-amino acid to be found as a natural product, both in white clover (*Trifolium repens*)[4] and green beans (*Phaseolus vulgaris*).[5] It was later discovered in a variety of other plants in both its parent- and derivatized form, carrying hydroxyl-, amino- or keto-groups.[6] Pipecolic acid is also present in microbes[7] and mamals as part of the catabolism of lysine.[8] So it can be found e.g. in the fungus *Rhizoctonia leguminicola* where often more complex secondary metabolites like the alkaloids slaframine and swainsonine are derived from it.[9] Figure 2.2 indicates the molecular details of the breakdown of lysine **14L** as it has been shown in studies involving rats.[10] As this breakdown process is shared with humans, pipecolic acid **11L** can be found in blood plasma (5 µmol/L) and is used as a biomarker for peroxisome biogenesis disorders like the Zellweger syndrome, where it is found to be elevated 8-fold or higher.[11]

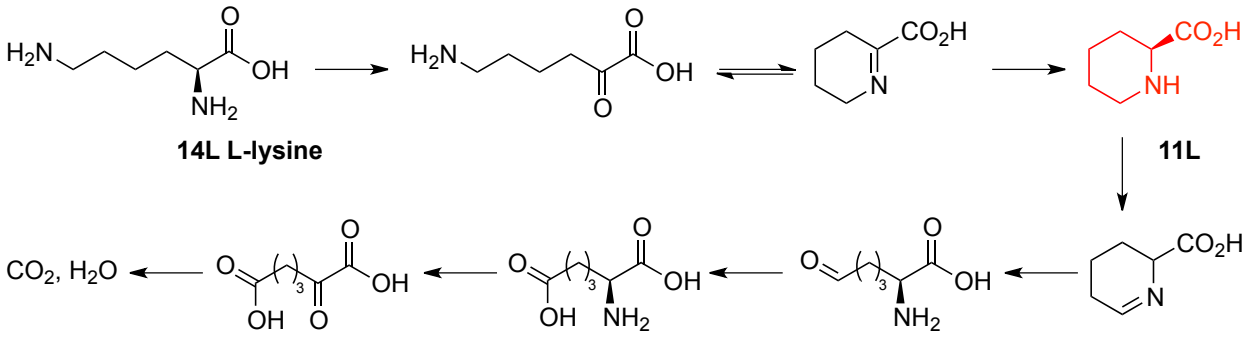


**Figure 2.2** Lysine degradation in mammalian systems *via* pipecolic acid.

### 2.1.3 Pharmacological active compounds containing the pipecolic acid scaffold

As already mentioned pipecolic acid scaffolds become incorporated into secondary metabolites in microbes and these complex alkaloids often have interesting pharmacological activities against pathogens and tumors.[12] Some representative examples are given below.

Rapamycin **15**, now sold by Pfizer under the trade name Sirolimus, was initially discovered as an antifungal antibiotic in *Streptomyces hygroscopicus* (Figure 2.3).[13] It could also be shown to be a powerful immunosuppressant when used in monotherapy in rats and pigs which had received organ transplants.[14] In a phase III clinical trial involving the reduction of kidney transplant

rejections Sirolimus was used in combination with ciclosporin and at a 5 mg dose was able to reduce the failure rate from 32.3% to 16.8%.[15] As a result Sirolimus is now in clinical use to reduce occurrence and severity of kidney transplant rejections. The total synthesis of this complex macrocylce was performed by Smith III et al. in 1997 and is published in a two part account in the Journal of the American Chemical Society.[16] The structure was broken down into 5 subunits which were synthesized in a convergent approach with the longest sequence including 14 steps and the macrocycle was assembled using a palladium mediated Stille coupling.

The symmetric alkaloid sandramycin **16** is produced by the microbe *Nocardioides* sp. found in a Mexican soil sample (Figure 2.3).[17] The molecular structure was determined using detailed NMR analysis of the fragments following acid hydrolysis.[18] The structural and absolute stereochemical assignment was confirmed following its total synthesis in 1996,[19] which allowed for a late introduction of the heteroaromatic chromophore. As a result the sequence selective DNA bis-intercalation properties of sandramycin could be finely tuned, which allowed for the identification of an even more potent analogue showing 1 pM cytotoxicity activity against several cancer cell lines.[20]

The importance of stereochemistry is impressively demonstrated by the direct thrombin inhibitor (DTI) Argatroban **17**, which is marketed as Novastan (Figure 2.3). The structure was first synthesized in 1981 around a central arginine-residue and it was noticed that while the here shown (2*R*, 4*R*)-configuration of the pipecolic acid fragment inhibited thrombin with a $K_i$ of 19 nM the (2*S*, 4*S*)-configuration reduced the activity nearly 15000 fold to 280 μM.[21] In general DTIs are believed to be more predictable in their response than unfractionated heparin and should be more effective at the same time then the low-molecular-weight heparins.[22] More specifically argatroban **17**, unlike heparin, inhibits thrombin *via* interaction with an active-site serine and as a result inhibits all thrombin-mediated effects, which includes platelet aggregation, activation of factor XIII(a) and fibrin formation.[23] Argatroban is given intravenously, has a

plasma half-live of 45 min and has been approved by the FDA for treatment of heparin-induced thrombocytopenia. Its specificity for thrombin against trypsin has been shown,[24] and more recently a shorter seven step synthesis from (±)-4-methylpiperidine has been devised.[25]

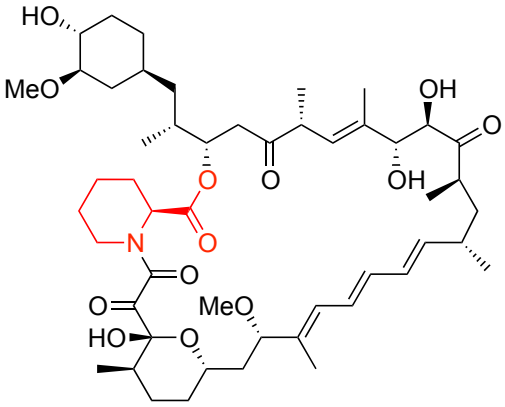

(-)-Rapamycin **15**

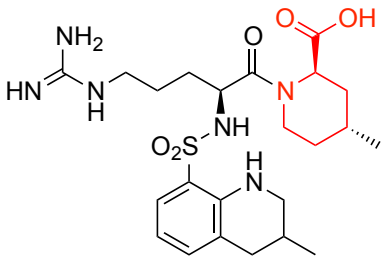

Argatroban **17**

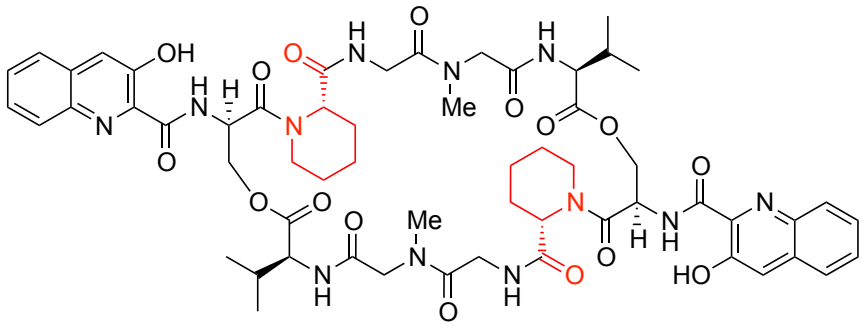

Sandramycin **16**

**Figure 2.3** Pipecolic acid scaffold containing complex alkaloids with pharmacological properties.

### 2.1.4 Synthetic aspects on pipecolic acids and derivatives

Two main reviews cover the asymmetric synthesis of pipecolic acid and its derivatives. The work performed in the field prior to 1997 was covered by Couty, who broke up the synthetic strategy into three approaches: i) from the chiral pool, ii) using a chiral auxiliary, or iii) via asymmetric catalysis.[26] More recent developments up to 2004 are in turn reviewed by Kadouri-Puchot and Comesse.[12]

#### 2.1.4.1 7 carbon carbohydrate scaffolds and sugar lactones as intermediates

For the synthesis of iminosugars in general, including 7 carbon derivatives like the lead pipecolic amide **10**, azido-lactones have been shown to be very useful intermediates time and time again.

As an example azido-δ-lactone **18** has successfully been used for the synthesis of several Homonojirimycin (HNJ) analogues like Homomannojirimycin (HMJ) **19** following its transformation into an azidoheptitol and manipulations using the biotechnology approach of Izumoring (Figure 2.4 A).[27] This powerful approach has been deployed both for the synthesis of branched[28] and deoxy[29] sugars and in this particular case gives access to 8 of the total 16 possible isomers of HNJ from D-mannose, the remaining 8 would be available from D-glucose.

Similarly the synthesis of the highly potent β-*N*-acetyl-hexosaminidase inhibitior LABNAc **21** also was performed *via* an azido-lactone **20** in this case a five ring derivative (Figure 2.4 A).[30] The azido-γ-lactone **20**, in which the nitrogen group is in a *trans* arrangement to the remaining substituents, was obtained under kinetic conditions from the azide displacement on 3,5-*O*-benzylidene protected D-lyxonolactone. Under prolonged reaction time the thermodynamic azide with an all *cis* arrangement is obtained instead.

This behavior is a more general feature of this type of compound and dependent on the reaction conditions employed the configuration of the azide carbon centre can be tightly controlled (Figure 2.4 B).[31] Also the interconversion of the isolated kinetic product **22** to its thermodynamic derivative **24** is possible under equilibration conditions involving pyridinium toluene-*p*-sulfonate (PPTS).

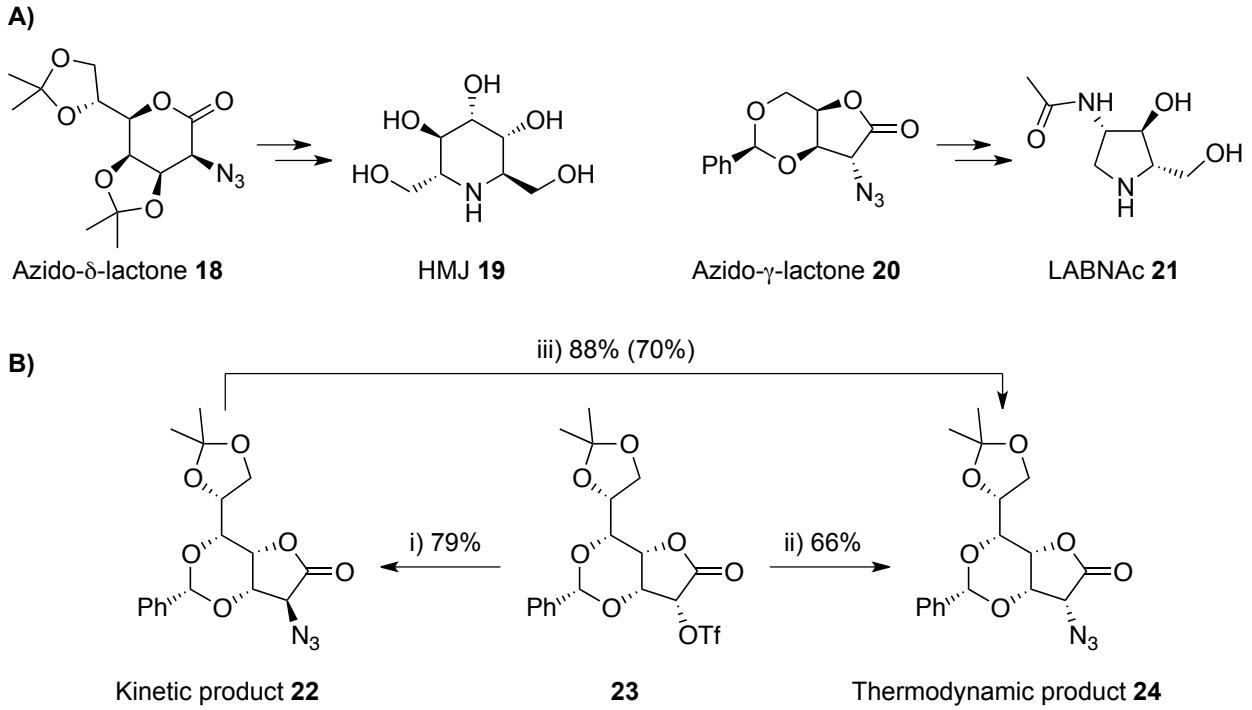


**Figure 2.4** A) Azido-lactones as intermediates in the synthesis of bioactive compounds; B) Production of kinetic and thermodynamic azides and their equilibration[31] i) $NaN_3$, DMF, RT, 1 h; ii) $NaN_3$, DMF, RT, 22 h; iii) $NaN_3$, PPTS, DMF.

### 2.1.4.2 Prior synthetic efforts of pipecolic acids and amides

Although as can be seen above very complex natural products incorporating the pipecolic acid scaffold exist, the synthesis of enantiopure L-pipecolic acid **11L** is still of current interest and many synthetic approaches have been devised. In analogy to the biosynthesis Fujii et al. started their synthesis from L-lysine **14L** (Figure 2.5).[32] In the α-*N*-tosyl derivative **25** the ε-amine was brominated to give acid **26**, which on ester protection to **27** was cyclized using sodium hydride to the cyclic ester **28L**, which gave L-pipecolic acid **11L** on deprotection. Pal et al. have developed an intriguing one-step photocatalytic conversion also starting from L-lysine **14L** to pipecolic acid **11L** using platinum loaded titanium dioxide powder *via* imine **29L**.[33] However the reaction requires further optimization due to epimerization because of competing α-deamination. In an alternative synthesis Ross et al. started from phenylglycinol **30** to form chrial auxiliary **31**, which upon alkylation could be cyclized under reductive conditions to give L-pipecolic acid **11L**.[34]

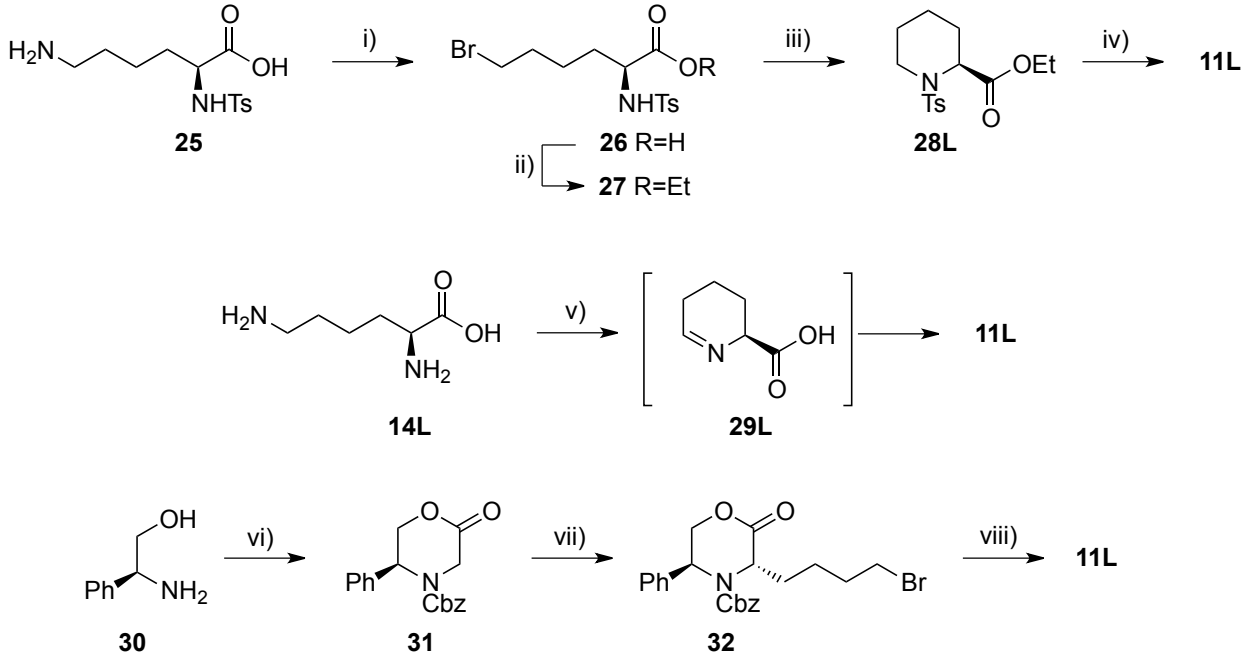


**Figure 2.5** Literature synthesis of pipecolic acid. Reagents and conditions: i) KBr, HBr, $NaNO_2$, $H_2O$, 50-55 °C, 1 h; ii) HCl, EtOH, 60-70 °C, 1 h; iii) NaH, DMF, 10-15 °C, 1 h; iv) NaOH, MeOH, 4h then 0.5 M $H_2SO_4$, EtOAc; v) hγ, $Pt/TiO_2$; vi) $BrCH_2CO_2Et$, $Et_3N$, THF, 3 h then CbzCl, $NaHCO_3$, $CH_2Cl_2$, 1 h then PhMe, 5% pTSA; vii) $Br(CH_2)_4OTf$, NaHMDS, THF; viii) $H_2$, Pd/C, TFA, MeOH.

### *2.1.4.2.1 Polyhydroxylated pipecolic acids synthesis*

The synthesis of polyhydroxylated analogues of pipecolic acids on the other hand is much rarer. Figure 2.6 shows all the stereochemistries of such compounds that are available in the literature which are structurally related to lead pipecolic amide **10**. Pipecolic acid **33** was synthesised in the same study as **10** by Shilvock and was shown to be a moderate inhibitor of β-glucosidase (almond, 690 μM).[1] The C6 epimer **34** was synthesized by Bruce et al. however no attempt was made to assess its glycosidase inhibition.[35] The remaining two scaffolds **35** & **36** were generated recently in a study on immunosuppression.[36]

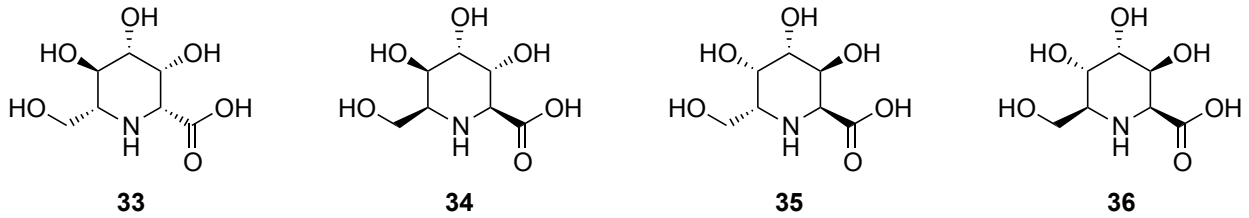


**Figure 2.6** Literature examples of polyhydroxylated pipecolic acids of different stereochemistries.

The synthesis of pipecolic acid **36** began from benzyl protected D-galactose **37** and, following a Wittig reaction, the only free secondary alcohol was converted into an oxime (Figure 2.7). Reduction and Cbz protection gave secondary amine **38**, which could be cyclized on treatment with mercury acetate to give a separable mixture of epimeric alcohols. Sequential oxidation, using pyridinium chlorochromate and sodium chlorite, of primary alcohol **39** gave the corresponding carboxylic acid, which on deprotected gave the desired pipecolic acid **36**. Its C6 epimer **35** was synthesized in similar sequence but from the C6-epimer to alcohol **39**. In an *in vitro* assay, pipecolic acid **36** had a strong suppressing effect on IL-4 and while being an effective immunosupressor it was less cytotoxic then the known drug cyclosporine A.

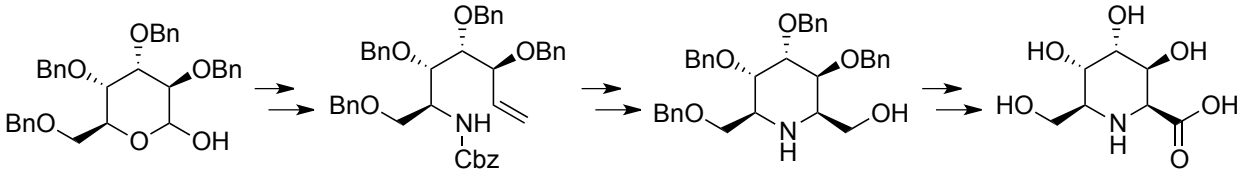


**37** **38** **39** **36**

**Figure 2.7** Synthesis of polyhydroxylated pipecolic acid for study on immunosupression.[36]

*2.1.4.2.2 Previous synthesis of pipecolic amide **10***

As already mentioned Shilvock et al. devised the original synthesis of lead pipecolic amide **10** and its strong β-*N*-acetyl-hexosaminidase inhibition was discovered in the same study.[1] The earlier part of the synthesis in this thesis follows the work of Bruce et al. up to bicycle **42**.[35, 37] Improvements and changes to these literature procedures are outlined throughout the discussion section of this chapter.

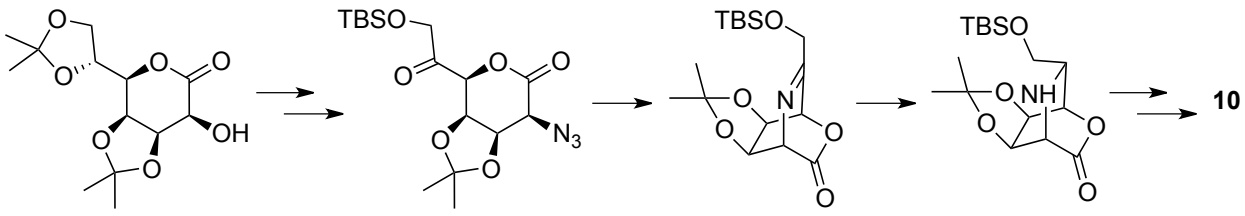


**40** **41** **42** **43**

**Figure 2.8** Literature procedures used for synthesis of lead compound **10.**[1, 35]

## 2.2 Resynthesis of pipecolic amide 10

The Kiliani process gave access to the 7-carbon starting material for the synthetic sequence to lead pipecolic acid **10** (Scheme 2.1). The Kiliani ascension is the process of adding cyanide to the reducing terminus of an aldose followed by subsequent hydrolysis with loss of ammonia resulting in the formation of the corresponding carboxylic acid, which is converted into the lactone on work up.[38] Such treatment of diacetone-D-mannose gives a C2 epimeric mixture of corresponding δ-lactones in 39% yield, which only have OH2 free, as OH5 forms the lactone bond.[39] The major epimer was the starting point of my synthesis and an azide at C2 is readily introduced into the structure with retention to give azido-δ-lactone **18** (Scheme 2.1). Ring closing cyclisation onto C6 either with retention or inversion gives the corresponding bicyclic intermediates, which on lactone opening with methylamine and complete deprotection gives access to the lead compound **10** along with its C6 epimer **44**.[1]

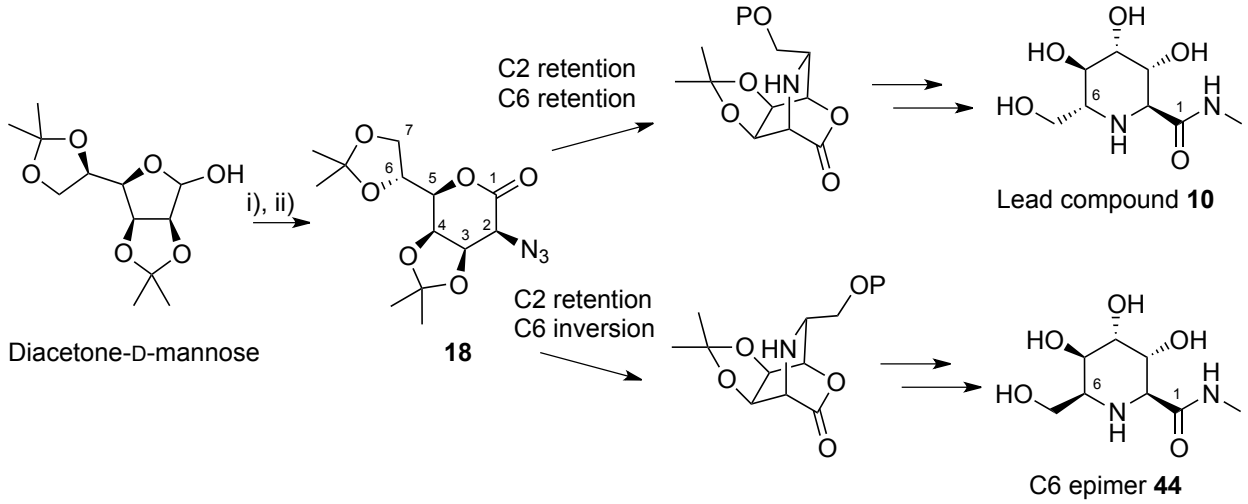


**Scheme 2.1** General synthetic approach for lead compound pipecolic amide **10** *via* azido-δ-lactone **18**. Reagents and conditions: according to lit.[39] i) $H_2O$, NaCN, $NaHCO_3$, then $H_2SO_4$; ii) azide introduced with retention.

### 2.2.1 Reduction of bicycle with Copper based reducing agent

Lactone **40** was therefore converted into the triflate ester and treatment with sodium azide in dimethylformamide gave the azido-δ-lactone **18** with retention in an excellent yield of 94% over two steps (Scheme 2.2).[39] In order to close the bicycle onto C6 it needed to be differentiated

from C7. Selective acetonide removal using aqueous acetic acid gave access to the desired diol **45**, which was protected on the primary alcohol with *tert*-butyldimethylsilyl chloride to give alcohol **46**. Oxidation using pyridinium chlorochromate gave ketone **41**, which is set up for an intramolecular Staudinger-type reaction using triethyl phosphite to give the bridged imine **42**.[40] Chemo- and stereoselective reduction from the less hindered face of the bicycle, avoiding the acetonide protection, and concomitant protection of the created amine functionality with carboxybenzyl chloride gave bicycle **47** in an excellent yield of 90%. In order to give the free amine directly a selective reduction using sodium cyanoborohydride had been attempted, however despite the literature report of 70%, in our hands the yield for this reaction was limited to 32%.[1] Bicycle **47** was then treated with methylamine in order to open the lactone to the corresponding amide **48**. Hydrogenation under acidic conditions allowed for the removal of all three protecting groups simultaneously and gave the lead pipecolic amide **10** in an overall yield of 38% over 9 steps. Proton and carbon NMR compared favorably to the literature sample.[1]

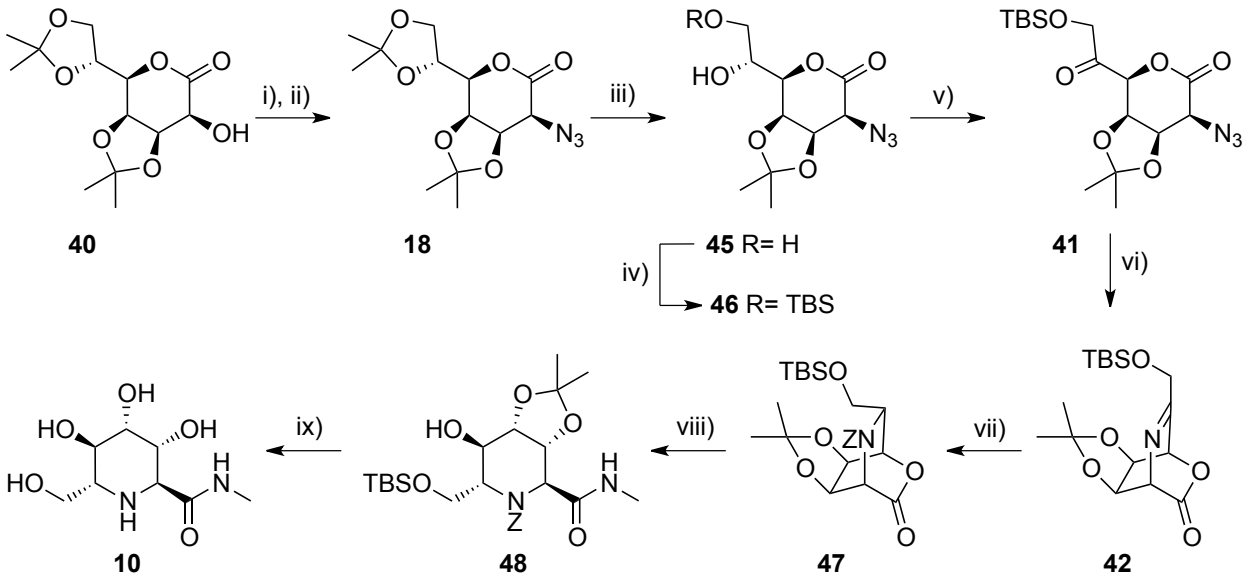


**Scheme 2.2** Synthetic sequence to pipecolic amide **10**. Reagents and conditions: i) $Tf_2O$, Pyridine, DCM, -30°C to -10°C, 40 min; ii) $NaN_3$, DMF, 18 h, 94% over two steps; iii) aq. AcOH, 2.5 h, quant; iv) $Me_2{}^tBuSiCl$, imidazole, DMF, RT, 18 h, 92%; v) PCC, 3Å sieves, DCM, 18 h, 86% vi) $(EtO)_3P$, THF, 18 h, quant; vii) $(Ph_3P)_2CuBH_4$, CbzCl, $HCCl_3$, 5 h, 90%; viii) $MeNH_2$, THF, 18 h, 59%; ix) MeOH/HCl then Pd/C and $H_2$, 22 h, 95%.

The bis(triphenylphosphine) copper(I) tetrahydroborate reducing agent **49**, used in the reduction of the unstable imine bicycle **42**, presents a very mild reagent for converting acetyl chlorides like **50** into aldehydes like **51** in excellent yields, while further reduction to the alcohol requires much prolonged reaction times (Scheme 2.3).[41] It is an easy to handle, bench stable, crystalline white solid which can be readily prepared from copper(I) chloride, triphenylphosphine and sodium tetrahydroborate on scales larger than 200 g.[42] Direct reductive aminations like aldehyde **51** with anilin **52** to give amine **53** can be achieved using sodium cyanoborohydride[43] or triacetoxyborohydride[44] but are also possible with **49** if a proton source is added, in this case a sulfamic acid; the reaction tolerates a whole range of alkyl- and aryl aldehydes and ketones.[45] In absence of acid imines are not reduced by **49**, however iminium salts like *N*-methylquinolinium iodide **54** is reduced to the tertiary amine **55**.[42] Therefore the proposed mechanism for the reduction of imine **42** is *via* initial reaction with carboxybenzyl chloride to give charged intermediate **56** which is then activated for the reduction with **49** to give bicycle **47**, rather then prior production of the secondary amine and subsequent carbamate protection.

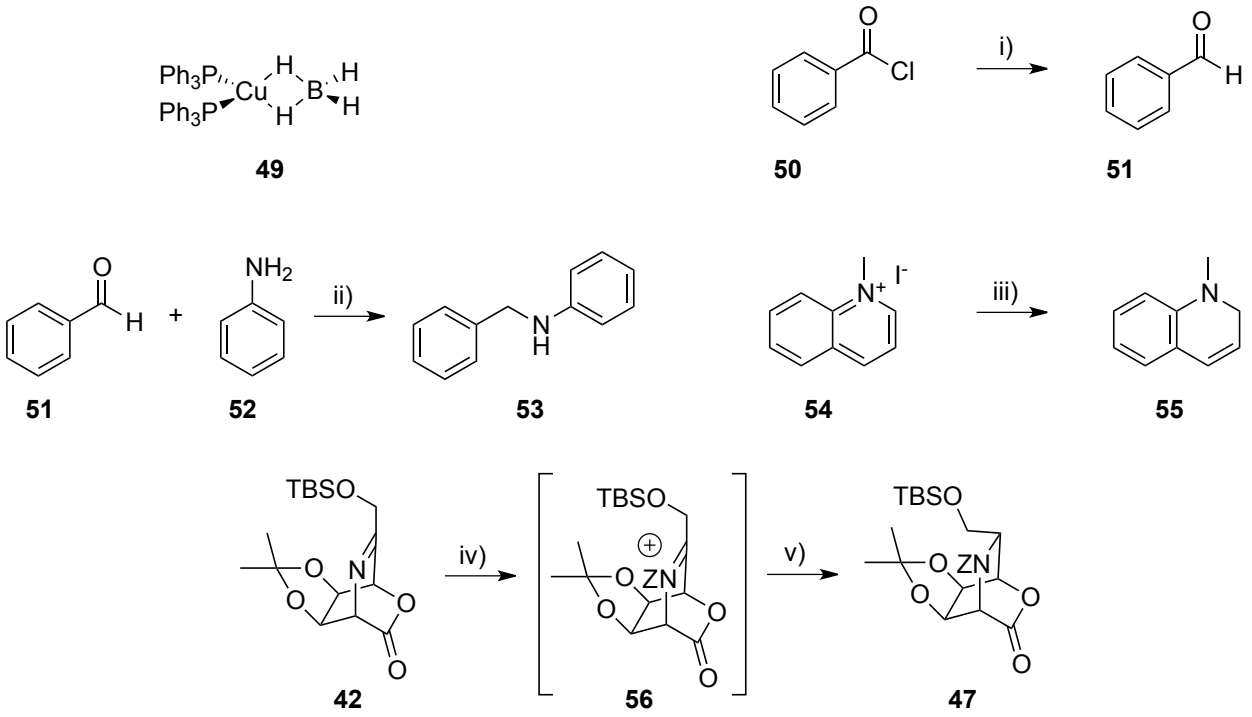


**Scheme 2.3** Bis(triphenylphosphine) copper(I) tetrahydroborate **49** literature reactions; Reagents and conditions: i) **49**, $Ph_3P$, acetone, 76%;[41a] ii) **49**, $NH_2SO_3H$, MeOH, 1.5 h, 94%;[45] iii) **49**, $Ph_3P$, acetone;[42] iv) reaction with CbzCl to generate iminium salt; v) reduction of charged intermediate with **49**.

### 2.2.2 Alternative cyclization to give the C6 epimer

In order to generate the C6 epimer **44** of lead compound **10**, alcohol **46** was activated using triflic anhydride to give triflate **57** (Scheme 2.4). Hydrogenation conditions in presence of a base allowed for reduction of the azide group to a primary amine, which subsequently closed with inversion onto C6 in order to give bicycle **58** in a good yield of 87%. Analogous to its epimer treatment with methylamine opened the lactone to give amide **59**, which could be deprotected under acidic conditions in order to give pipecolic amide **44** in a 33% yield over 8 steps.

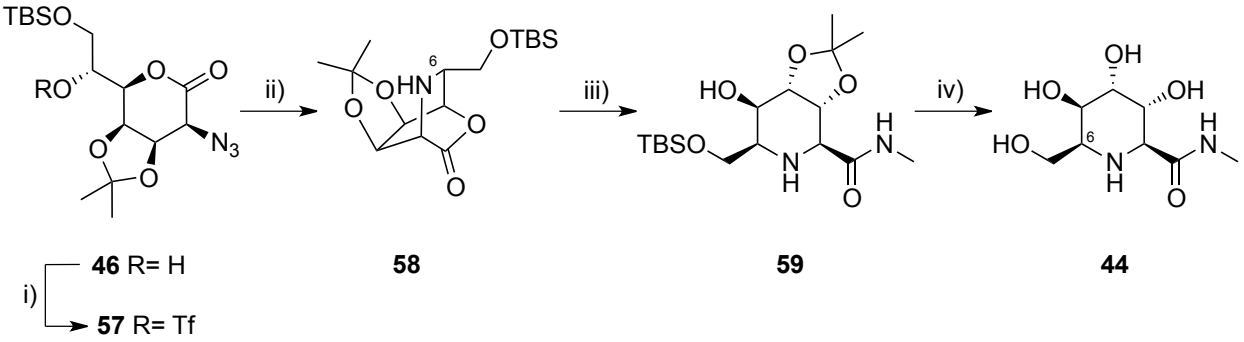


**Scheme 2.4** Synthesis of C6 epimer **44**. Reagents and conditions: i) $Tf_2O$, Pyridine, DCM, -20 °C to -10 °C, 1.5 h, 97%; ii) Pd/C, $H_2$, NaOAc, EtOAc, 16 h, 87%; iii) $MeNH_2$, THF, RT, 18 h, 75%; iv) MeOH/HCl, RT, 18 h, 60%.

## 2.3 Exploration of further pipecolic amide scaffolds

Encouraged by the success of the first pipecolic amide sequence we were interested in exploring further routes towards different stereochemistries. More specifically, by starting from D-glucose instead of D-mannose, the C3 epimers (red) would be obtained as the final products (Scheme 2.5). The general approach therefore is similar to the previous synthesis, however azido-γ-lactone **60** is the key intermediate in this case, which in its all *cis* configuration epimerizes C2 (green) in the final product, and overall two stereocentres are epimerized in comparison to the previous synthesis. If the C2 epimer of **60** were to be used only one of the stereocentres would be changed and overall these synthetic routes would give access to 4 further pipecolic amides.

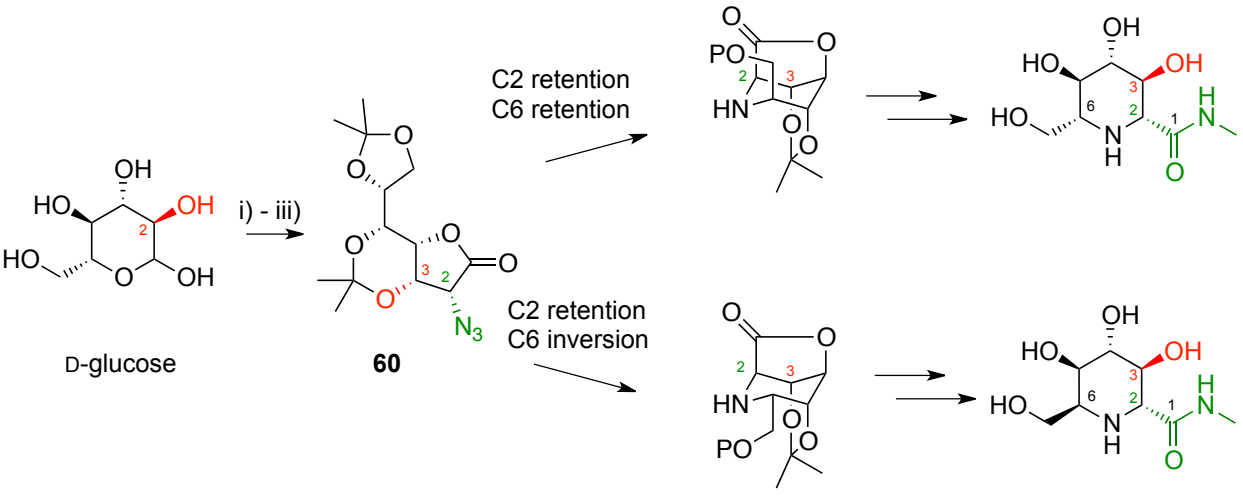


**Scheme 2.5** General synthetic approach to further pipecolic amide scaffolds. Reagents and conditions: i) lit.[46] $H_2O$, NaCN, anh. $CaCl_2$; ii) lit.[47] Acetone, cat. $I_2$; iii) Nitrogen introduced with retention.

### 2.3.1 Kinetic vs Thermodynamic azides

The synthesis started with 3,5:6,7-di-*O*-isopropylidene-D-*glycero*-D-*gulo*-heptono-1,4-lactone **61**, which can be readily synthesized *via* a Kiliani ascension[38] from D-glucose[46] on scales up to 200 kg.[48] Subsequent acetonide protection has equally been performed on scales of up to 500 g in the literature.[47] Careful optimization of the reaction conditions was necessary to obtain acceptable yields for the epimeric azides in the *ido*- **62** and *gulo*-configuration **60** (Scheme 2.6). Treatment of the starting alcohol in the *gulo* configuration with triflic-anhydride yielded the corresponding triflate, which upon treatment with sodium azide at low temperatures over 16 h gave the *ido*-azide **62** quantitatively. In order to obtain its C2 epimer, the *gulo*-azide **60**, two different routes were tried. When the triflate of *gulo*-alcohol **61** was treated with trifluoro-acetate, the C2 inverted *ido*-alcohol **63** could be obtained in 62% over two steps. Esterification of this *ido*-alcohol **63** with triflic-anhydride and subsequent treatment with sodium azide gave the gulo-azide **60** with overall retention with respect to starting alcohol **61**, in 58% over two steps. Alternatively subjecting the *ido*-azide **62** to epimerization conditions involving PPTS gave the *gulo*-azide **60** in 96% yield after 4 days. So despite longer reaction times the equilibration route improves the yield of the *gulo*-azide **60** significantly. Starting from the alcohol **61** the *gulo*-azide **60** is obtained in 96% over three steps rather then in 36% over 4 steps. The thermodynamic *gulo*-azide **60** can therefore be added to the list of examples of azido-lactones that can be equilibrated successfully in the presence of PPTS from their kinetic counterpart, in this case the *ido*-azide **62**.[31]

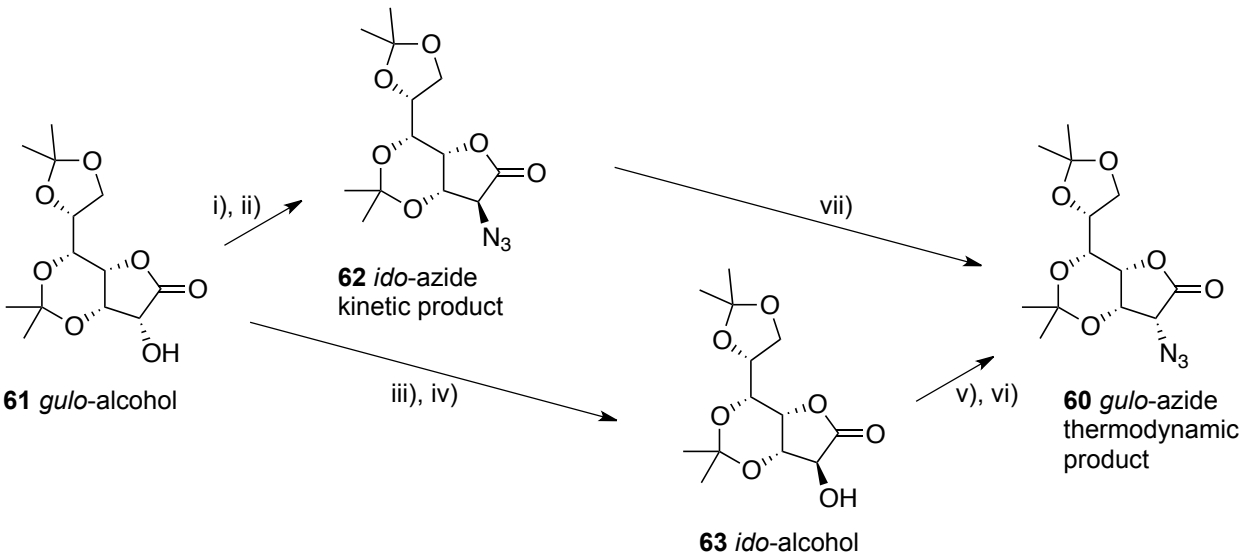


**Scheme 2.6** Thermodynamic and kinetic azido-γ-lactones. Reagents and conditions: i) $Tf_2O$, DCM, Pyridine, -30 °C, 30 min; ii) $NaN_3$ (1.5 eq.), DMF, -15 to +6 °C, 15.5 h, quant over 2 steps; iii) $Tf_2O$, DCM, Pyridine, -40 to -20 °C, 70 min; iv) $CF_3COONa$ (3 eq.), DMF, 60 °C, 72 h then MeOH 16 h, 62% over two steps; v) $Tf_2O$, DCM, Pyridine, -30 °C, 30 min; vi) $NaN_3$ (1.1 eq.), DMF, -18 to +5 °C, 17 h, 58% over two steps; vii) $NaN_3$ (1.4 eq.), PPTS (1.1 eq), DMF, RT, 4d, 94%.

The epimeric azides in the *ido*- **62** and *gulo*-configuration **60** were both crystalline and using X-ray analysis the configuration at C2 could be irrevocably assigned (Figure 2.9). For both structures a chair-configuration is adopted by the six-ring acetonide, while an envelope can be observed for the 5-ring. For *ido*-azide **62** the absolute configuration was confirmed using a Flack parameter.[49] The X-ray data was collected and refined by a coworker.[50]

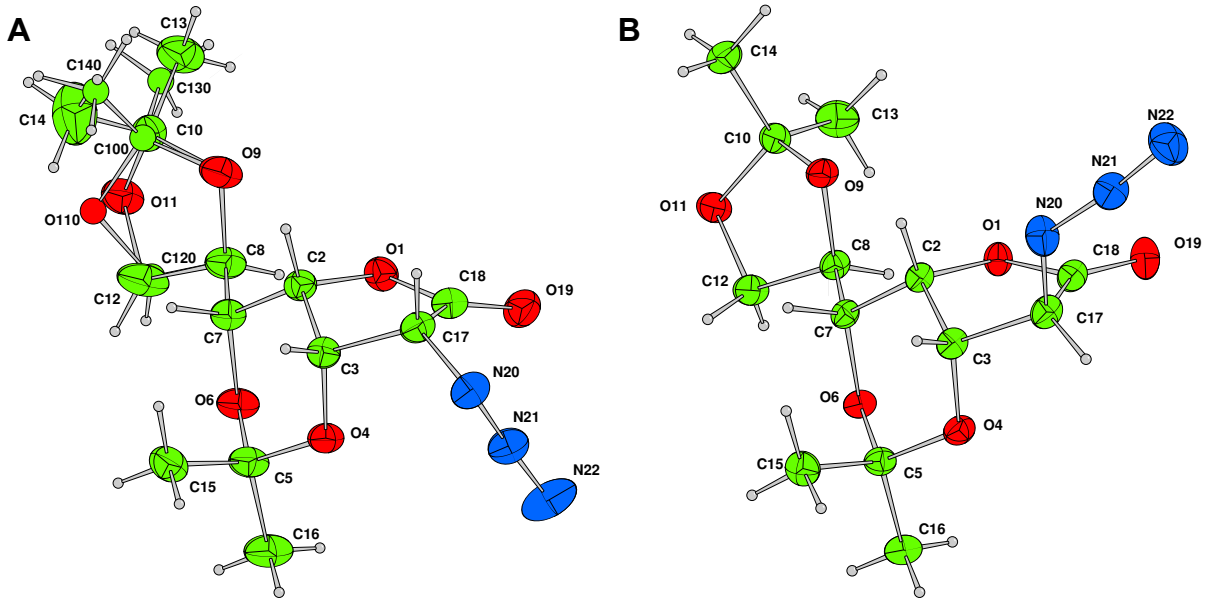


**Figure 2.9** X-ray crystal structures of A) D-*gulo*-γ-lactone **60** (CCDC 917202) and B) D-*ido*-γ-lactone **62** (CCDC 917203) with displacement ellipsoids drawn at the 50% probability level; Hydrogen atoms are shown as spheres of arbitrary radius.

### 2.3.2 Challenges of selective de- and reprotection

With the *gulo*-azide **60** in hand, selective removal of the terminal acetonide was required in order to proceed and, analogously to the previous synthesis, aqueous acetic acid was tried for this purpose (Scheme 2.7). 58% of the desired diol **64** could be isolated, however 25% of the material had eliminated across C2-C3 as well, forming a conjugated system with the lactone carbonyl (Table 2.1 entry 1.). Addition of 1,4-dioxane to the reaction mixture seemed to lower the amount of elimination product, however the yield of the isolated diol was still poor, 51% (Table 2.1 entry 2.). Milder deprotection conditions were sought and found in the form of catalytic iodine in acetonitrile.[51] At low scales this reaction was very high yielding giving a 95% yield of the desired diol **64** with only trace amounts of elimination (Table 2.1 entry 3-4). Unfortunately on an 8 fold scale up to 400 mg, the reaction proceeded sluggishly and only on addition of additional iodine and mild heating could it be driven to completion. As a result the yield dropped considerably to 65% and an increased amount of elimination product was

produced. Nonetheless sufficient material was isolated to proceed further in the synthesis. NMR analysis confirmed the removal of the terminal acetonide with the six ring still in place.[52]

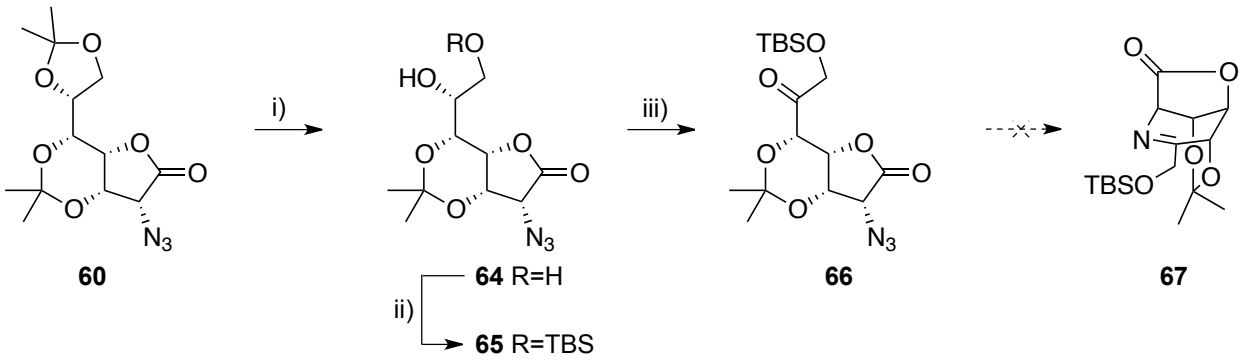


**Scheme 2.7** Synthesis towards further pipecolic amide schaffolds; Reagents and conditions: i) $I_2$, $H_2O$, acetonitrile, RT, 16 h, 95%; ii) $^tBuMe_2SiCl$, imidazole, 3Å sieves, DMF, 31 h, 84%; iii) DMP, DCM, 0 °C – RT, 91%;

The selective protection of the primary alcohol in diol **64** with *tert*-butyldimethylsilyl chloride was prone to overprotection, while consumption of the starting material was often slow and elimination across C2-C3 was frequently observed. When the reaction was performed on a 250 mg scale, the desired alcohol **65** was the major compound in 35% isolated yield, while the di-silylated compound constituted 32% and the eliminated product 11% of the material. The best yield of 84% was obtained with crude diol starting material and rigorous exclusion of moisture using 3Å molecular sieves, however overall the reaction was unreliable. Oxidation using Dess Martin periodinane (DMP), which had been produced in house,[53] on alcohol **65** proceeded in excellent yields of up to 91%. The azido-ketone **66** was subjected to the Staudinger conditions described earlier to close the nitrogen onto C6, however it was impossible to form bicycle **67**. Due to its four axial substituents bicycle **67** might be simply be too strained to form. Therefore a swap of the six-ring azetonide for benzyl protection could aid its formation, and would remove the selective deprotection issue simultaneously, albeit adding an additional four steps to the synthesis.[54] Due to lack of further material and favoring other projects, further work on this sequence had to be abandoned.

| Table 2.1 Conditions for selective removal of terminal acetonide from azido-γ-lactone 60. | | | | |
|---|---|---|---|---|
| **Entry** | **Scale** | **Conditions** | **Elimination** | **Diol** |
| 1. | 100 mg | 70% aqu. AcOH, RT, 48 h | 25% | 58% |
| 2. | 100 mg | 40%-70% aqu. AcOH, 1,4-dioxane, RT, 30 h | 2% | 51% |
| 3. | 28 mg | $I_2$ 30 mol%, $H_2O$, acetonitrile, RT, 3 h | ≤ 2% | 74% |
| 4. | 58 mg | $I_2$ 30-60 mol%, $H_2O$, acetonitrile, RT, 16 h | ≤ 2% | 93% |
| 5. | 400 mg | $I_2$ 40-100 mol%, $H_2O$, acetonitrile, RT - 40°C, 48 h | 10% | 65% |

## 2.4 Biological evaluation and molecular modelling

With authentic samples of the lead pipecolic amide **10** along with its C6 epimer **44** in hand we proceeded to evaluate their glycosidase inhibition. For reasons of comparison between the piperidine and pyrrolidine ring systems the biological evaluation of several 5-ring systems is shown as well, giving a more complete picture of the structure activity relationships overall. Although I was involved in the biological evaluation of these compounds, all 16 stereomers of pyrrolidine amides like **68** were synthesized by coworkers.[55]

### 2.4.1 Enzymatic activity of pipecolic amides and comparison to 5-ring analogues

The enzymatic inhibition data against a set of β-*N*-acetyl-glucosaminidases, β-*N*-acetyl-galactosaminidases and α-*N*-acetyl-galactosamindases for pipecolic amides **10** and **44** is shown in a side by side comparison with their ring contracted pyrrolidine analogues **68** and **69** in Table 2.2. The measurements of the large glycosidase panel was performed by our collaborator Professor Atsushi Kato (University of Toyama),[56] while the *Charonia lampas* α-*N*-acetyl-galactosamindase data and the $K_i$ measurements using HL60 β-*N*-acetyl-glucosaminidase were collected in house.

**Table 2.2 Iminosugars giving 50% inhibition of various glycosidases; $IC_{50}$ given in μM.**

| | 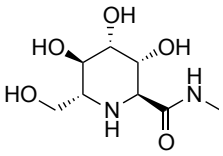 | 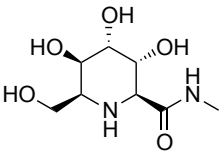 | 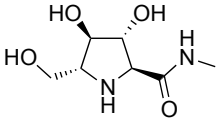 | 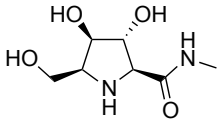 |
|---|---|---|---|---|
| Enzyme | **10** | **44** | **68** | **69** |
| β-*N*-Acetyl-glucosaminidase | | | | |
| Human placenta | 0.14 [0.01]$^{\$,1}$ | NI$^{\S}$ (24.7%) | 0.20 | 5.3 |
| Bovine kidney | 0.27 | NI$^{\S}$ (28.9%) | 0.22 | 4.8 |
| Jack beans | 0.29 | NI$^{\S}$ (21.3%) | 0.033 | 1.2 |
| HL60 | 0.36 | NI$^{\S}$ (14.5%) | 0.20 [0.027]$^{\$}$ | 6.1 [14.9]$^{\$}$ |
| *Aspergillus oryzae* | 49 | NI$^{\S}$ (0%) | 0.30 | 6.6 |
| α-*N*-Acetyl-galactosaminidase | | | | |
| Chicken liver | NI$^{\S}$ (0%) | NI$^{\S}$ (0%) | NI$^{\S}$ (0%) | NI$^{\S}$ (0%) |
| *Charonia lampas* | NI$^{\#}$ (0%) | NI$^{\#}$ (14.4%) | NI$^{\#}$ (1.1%) | NI$^{\#}$ (9.0%) |
| β-*N*-Acetyl-galactosaminidase | | | | |
| HL60 | 1.8 | NI$^{\S}$ (10.6%) | 1.0 | 26 |
| *Aspergillus oryzae* | 26 | NI$^{\S}$ (8.7%) | 0.35 | 7.3 |

§ No inhibition at 1000 μM (% inhibition); # No inhibition at 500 μM (% inhibition); $ [$K_i$ in μM]; Assay details described in Section 2.6.4 (p. 63).

The enzymatic evaluation of pipecolic amide **10** confirmed the high activity levels against β-hexosaminidases (human placeta, bovine kidney, jack bean, HL60, Table 2.2) previously reported by Shilvock et al. ($K_i$ 0.01 μM, human placenta).[1] An exception was the enzyme derived from the fungus *aspergillus oryzae*, against which pipecolic amide **10** seemed less effective ($IC_{50}$ 49 μM). What influence the change of a single stereocenter can have is shown by the C6 epimer **44**, which is inactive against the entire panel of enzymes investigated. The 5-ring analogue **68** of lead compound **10** on excision of C4 demonstrates comparable and in some cases even higher levels of inhibition against β-hexosamindases. A $K_i$ of 27 nM was measured against β-*N*-acetyl-glucosamindase derived from HL60 cell homogenate, demonstrating the impressive inhibition activity of compound **68** (Figure 2.10). Based on the $K_i$ measurements the C5 epimer

**69** (14.9 μM, Figure 2.11), the C4 excision product of pipecolic amide **44**, was more then 500 fold less inhibitory than **68**, therefore showing a similar trend to the 6-ring analogue, albeit less pronounced.

In order to probe its specificity pipecolic amide **44** was also tested against α-glucosidase (yeast), β-glucosidase (almond, bovine liver), α-galactosidase (coffee beans, human lysosome), β-galactosidase (bovine liver), α-mannosidase (jack beans), β-mannosidase (snail), α-L-rhamnosidase (*Penicillium decumbens*), α-L-fucosidase (bovine epididymis) and no inhibition was found. For iminosugars **10** and **68** this panel was extended further with α-glucosidase (rice, *Aspergillus niger*), β-glucosidase (aspergillus niger), α-L-fucosidase (bovine kidney), β-glucuronidase (*Escherichia coli*, bovine liver), α,α-trehalase (porcine kidney) and amyloglucosidase (*Aspergillus niger*, *Rhizopus sp.*) but no inhibition was found, proving the extremely high specificity of these iminosugars.

Table 2.3 shows the corresponding enzymatic evaluation data for the enantiomers **72** and **73** of the pyrrolidines **68** and **69** from the preceding table. Also shown are the five carbon analogues **70** and **71**, which correspond to the hydroxymethyl deletion analogues of **68** and **72** respectively. It should be noted that the deletion of the hydroxymethyl group from **68** reduces its ability to inhibit β-hexosaminidases by three orders of magnitude. Pyrrolidine **70** therefore displays a $K_i$ against β-*N*-acetyl-glucosaminidase of 42.5 μM (Figure 2.12), while its enantiomer **71** is inactive at the highest inhibitor concentration tested. The five carbon analogue **71** can also be interpreted as hydroxymethyl deletion compound of **72** which is still a reasonable inhibitor with a $K_i$ of 75.1 μM (Figure 2.13). As a result comparing the five carbon analogues with their non-hydroxymethyl-deleted derivatives, a three orders of magnitude loss of activity is observed on cut down. In general on moving from **68** and **69** to their respective mirror images **72** and **73** a reduction of inhibition activity of two orders of magnitude or higher is observed.

**Table 2.3 Iminosugars giving 50% inhibition of various glycosidases; $IC_{50}$ given in μM.**

| | 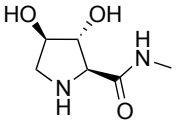 | 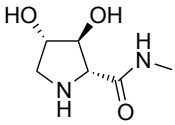 | 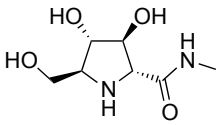 | 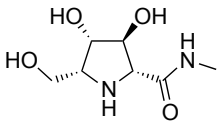 |
|---|---|---|---|---|
| Enzyme | **70** | **71** | **72** | **73** |
| β-*N*-Acetylglucosaminidase | | | | |
| Human placenta | 13 | NI§ (3.3%) | 41 | 584 |
| Bovine kidney | 9.7 | NI§ (5.2%) | 32 | 566 |
| Jack beans | 47 | NI§ (0.4%) | 7.3 | 119 |
| HL60 | 16 [42.5] | NI# (2.7%) | 50 [75.1] | 849 |
| *Aspergillus oryzae* | 9.1 | NI§ (8.3%) | 53 | NI§ (9.3%) |
| α-*N*-Acetylgalactosaminidase | | | | |
| Chicken liver | NI§ (5.1%) | NI§ (3.1%) | NI§ (9.6%) | NI§ (10.0%) |
| *Charonia lampas* | NI# (5.4%) | NI# (3.5%) | NI# (0%) | NI# (4.7%) |
| β-*N*-Acetylgalactosaminidase | | | | |
| HL60 | 22.3 | NI§ (0%) | 206 | NI§ (30.2%) |
| *Aspergillus oryzae* | 57 | NI§ (0.4%) | 84 | NI§ (9.6%) |

§ No inhibition at 1000 μM (% inhibition); # No inhibition at 500 μM (% inhibition); $ [$K_i$ in μM]; Assay details described in Section 2.6.4 (p. 63).

None of the eight iminosugars shown in Table 2.2 and Table 2.3 inhibited α-*N*-acetyl-galactosaminidase (chicken liver, *charonia lampas*) at the highest concentration tested.

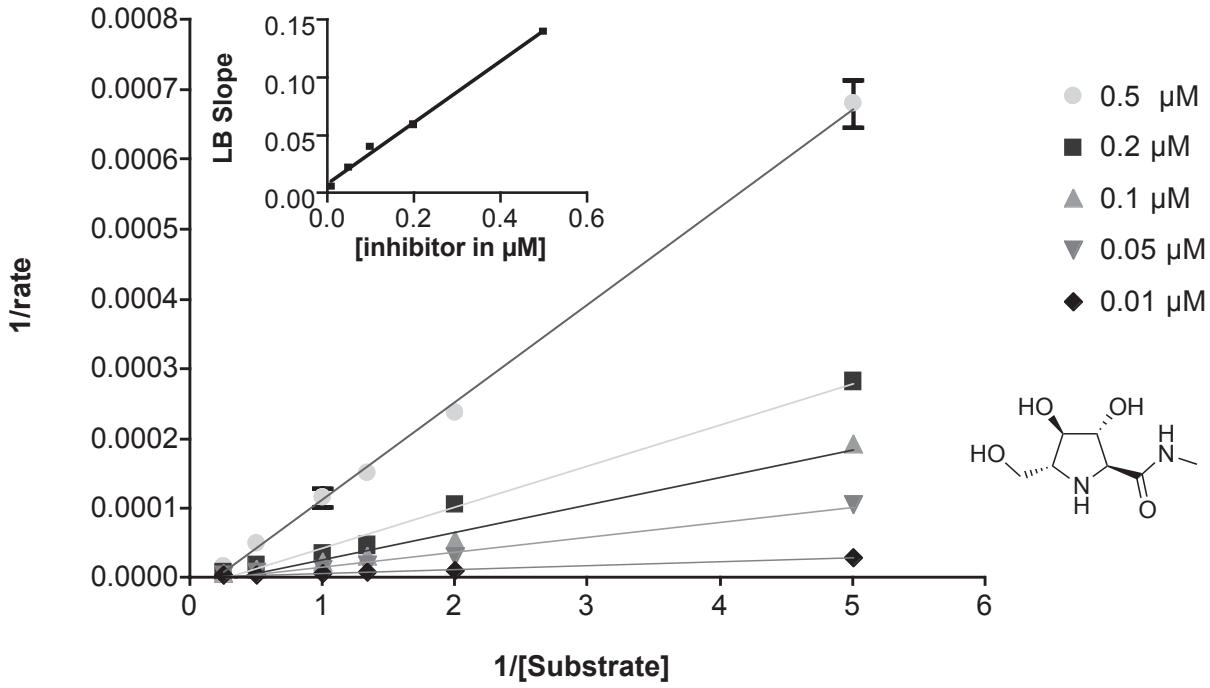


**Figure 2.10** Lineweaver Burk (LB) plot of pyrrolidine amide **68** against β-*N*-acetylglucosaminidase derived from HL60 cell homogenate; Ki = 27 nM based on X-intercept of insert graph (LB slope vs Inhibitor concentration, $R^2$= 0.9946).

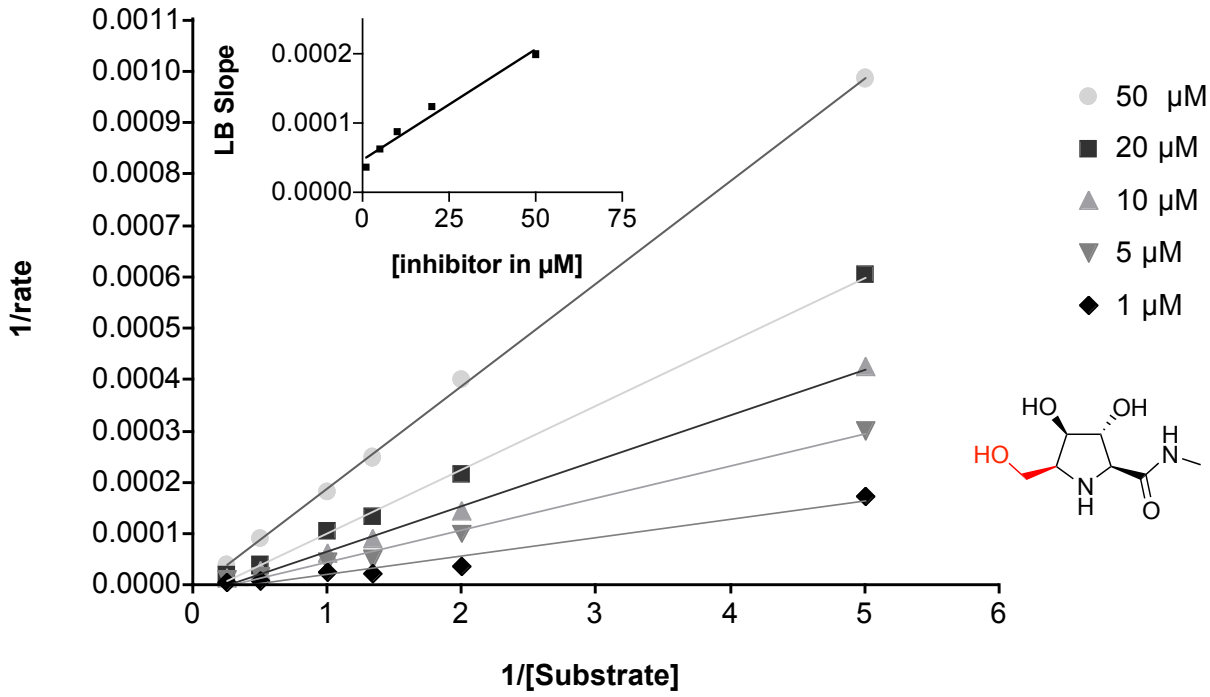


**Figure 2.11** Lineweaver Burk (LB) plot of pyrrolidine amide **69** against β-*N*-acetylglucosaminidase derived from HL60 cell homogenate; Ki = 14.9 μM based on X-intercept of insert graph (LB slope vs Inhibitor concentration, $R^2$= 0.9683).

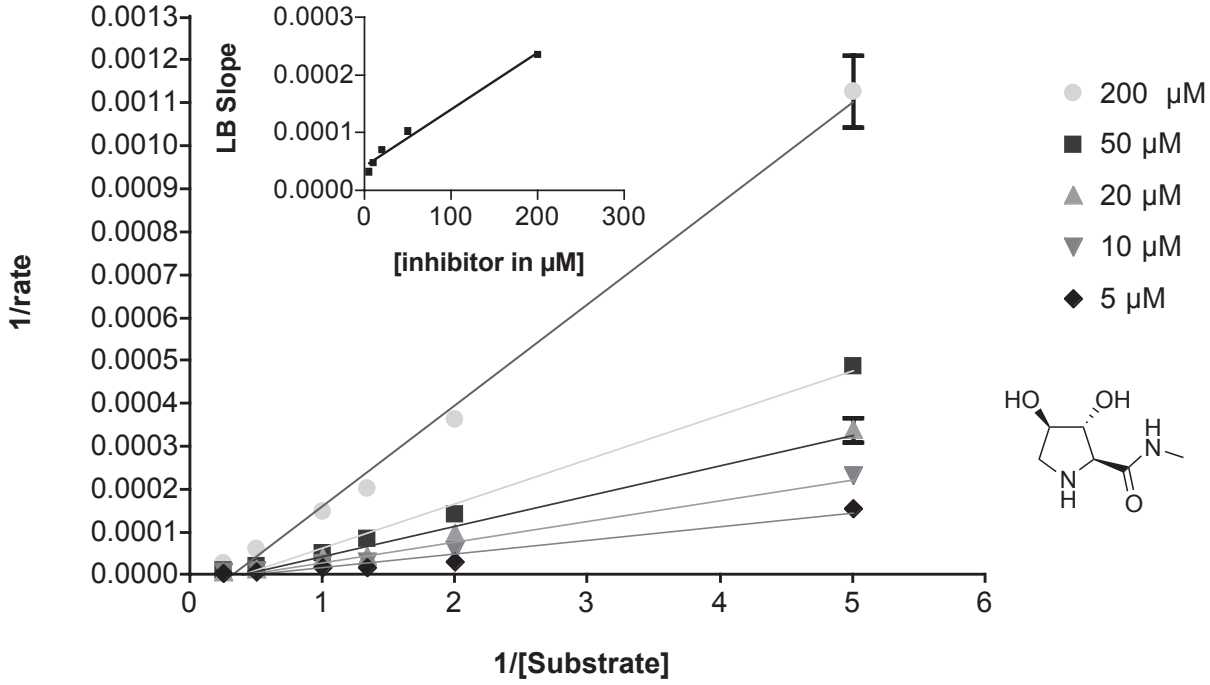


**Figure 2.12** Lineweaver Burk (LB) plot of pyrrolidine amide **70** against β-*N*-acetylglucosaminidase derived from HL60 cell homogenate; Ki = 42.5 μM based on X-intercept of insert graph (LB slope vs Inhibitor concentration, $R^2$= 0.9825).

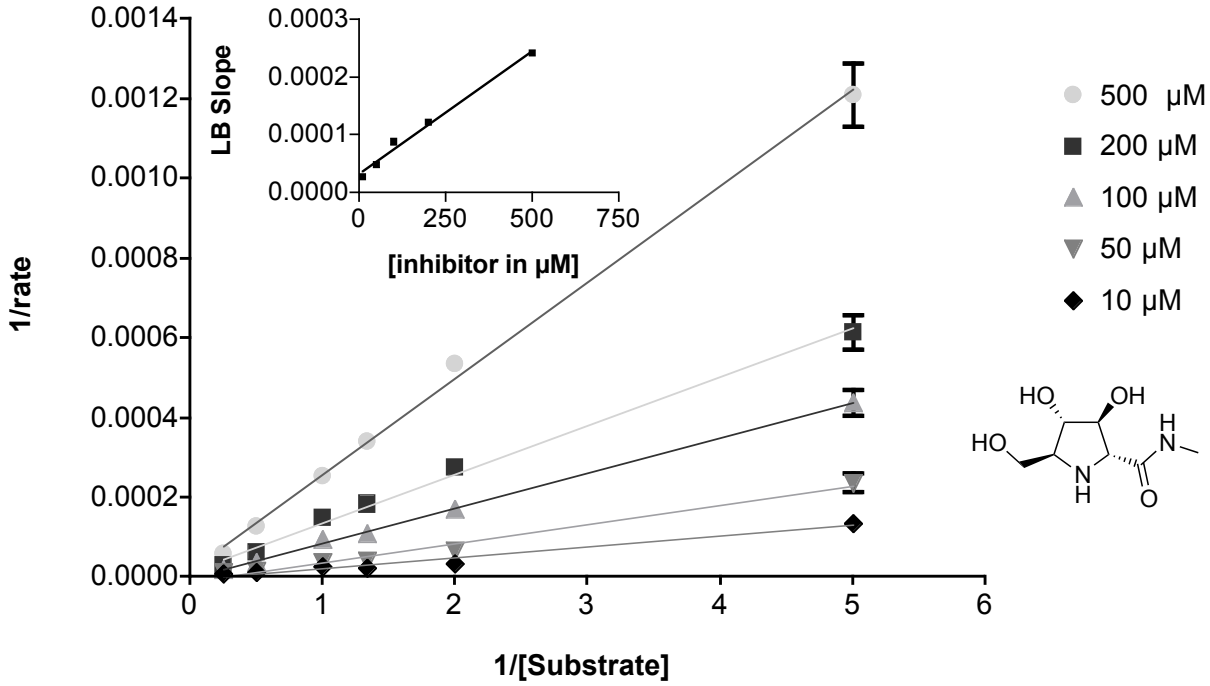


**Figure 2.13** Lineweaver Burk (LB) plot of pyrrolidine amide **72** against β-*N*-acetylglucosaminidase derived from HL60 cell homogenate; Ki = 75.1 μM based on X-intercept of insert graph (LB slope vs Inhibitor concentration, $R^2$= 0.9887).

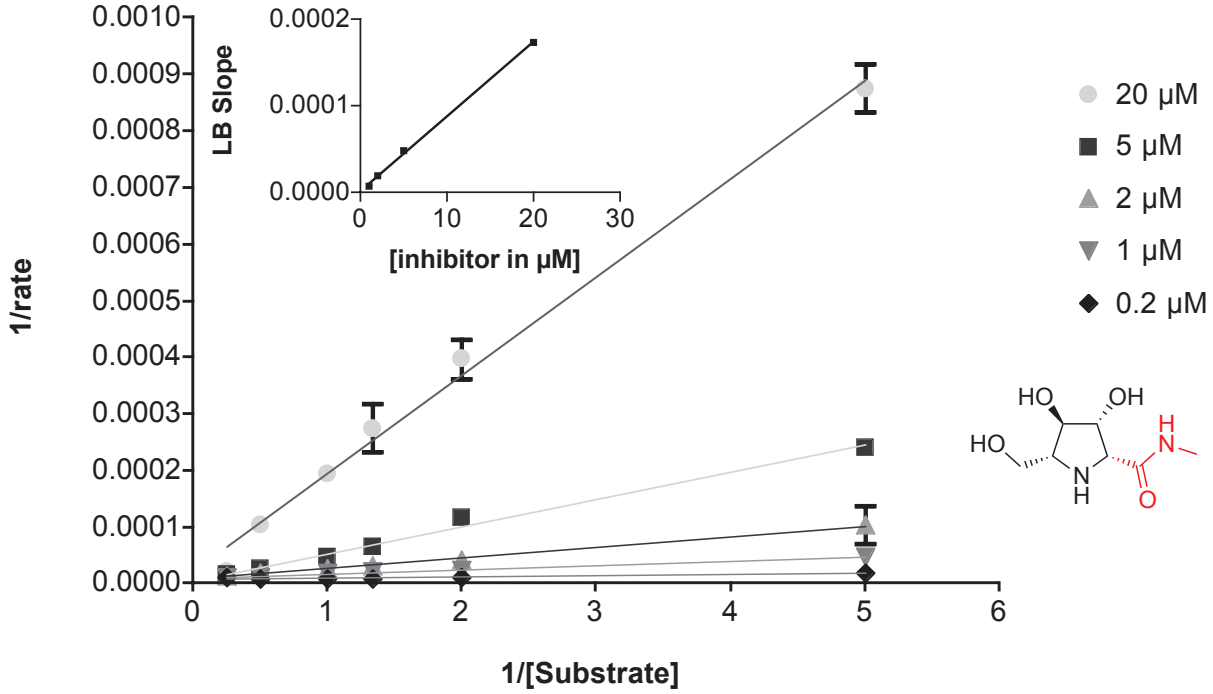


**Figure 2.14** Lineweaver Burk (LB) plot of pyrrolidine amide **74** against β-*N*-acetylglucosaminidase derived from HL60 cell homogenate; Ki = 174 nM based on X-intercept of insert graph (LB slope vs Inhibitor concentration, $R^2$= 0.9989).

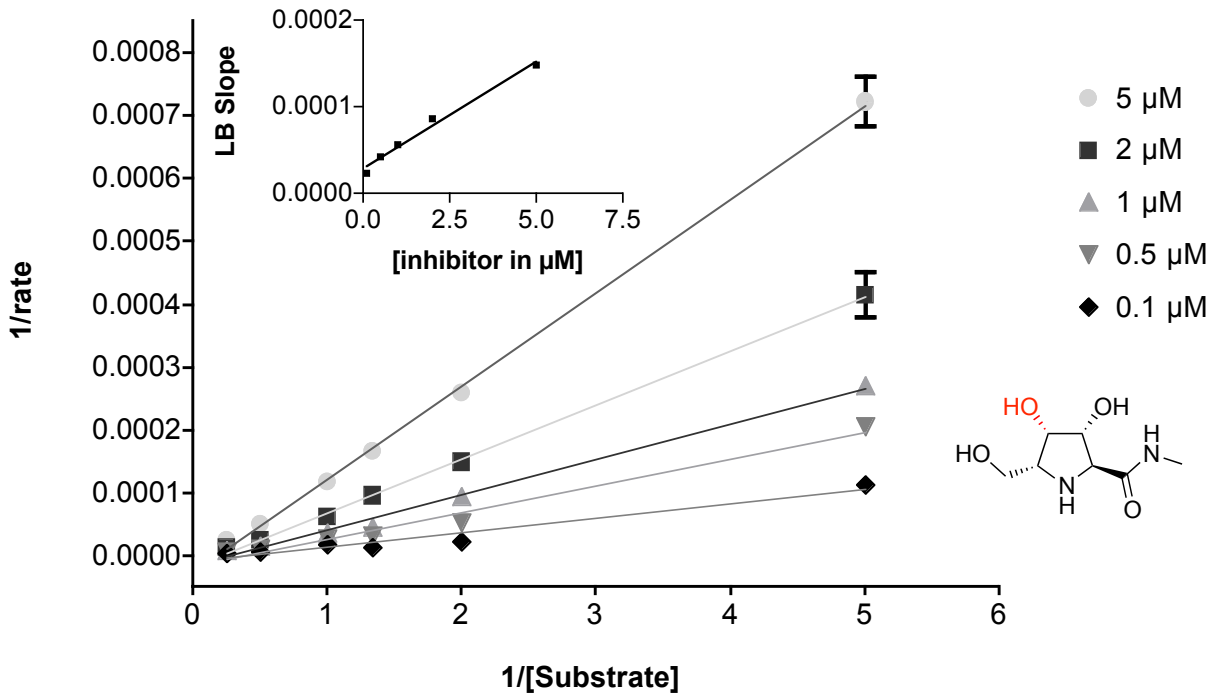


**Figure 2.15** Lineweaver Burk (LB) plot of pyrrolidine amide **75** against β-*N*-acetylglucosaminidase derived from HL60 cell homogenate; Ki = 1.18 μM based on X-intercept of insert graph (LB slope vs Inhibitor concentration, $R^2$= 0.9839).

In order to complete the structure activity investigation of the pyrrolidines the $K_i$ against β-*N*-acetyl-glucosamindase from HL60 cell homogenate was also obtained for the C2 epimer **74** and the C4 epimer **75** of **68**, which gave 174 nM (Figure 2.14) and 1.18 μM (Figure 2.15) respectively. The C3 epimer **76** of **68** was excluded from the $K_i$ evaluation as it had been completely inactive against β-*N*-acetyl-hexosaminidases in the extended glycosidase panel. A summary of the influence on β-*N*-acetyl-glucosaminidase inhibition activity by epimerization of any the 4 stereocentres of pyrrolidine amide **68** is shown in Figure 2.16.

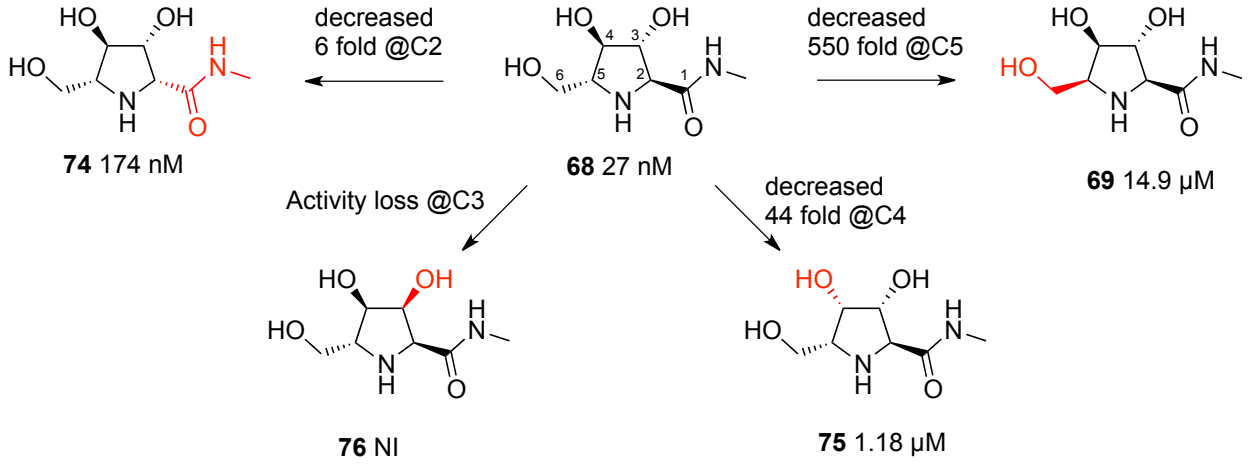


**Figure 2.16** Activity loss on epimerization of ring carbon atoms in potent β-*N*-acetylhexosamindase inhibitor **68** in terms of measured $K_i$ against β-*N*-acetylglucosaminidase from HL60 cell homogenate.

Based on the most potent pyrrolidine β-*N*-acetylhexosaminidase inhibitor **68**, we can therefore conclude that the configuration at C3 is crucial for activity, while changes in stereochemistry at C2 and C4 are relatively well tolerated and inversion at C5 is of intermediate importance.

### 2.4.2 Introduction to molecular modeling

With an increasing body of enzymatic inhibition data available on the 6-ring pipecolic amides and the 5-ring pyrrolidine amides it was of interest, if molecular modeling could be used to rationalize the inhibition data obtained and if predictions of inhibition activity of iminosugar scaffolds synthetically still unavailable were possible. Molecular modeling is a versatile tool used to complement experimental studies and can generally be divided into three areas of

application: 1. Calculating the energy of a molecule at a given conformation; 2. Optimizing the geometry of a system; 3. Calculating the vibrational frequencies from intramolecular motion.[57] We were interested in the second area, which would allow us to visualize the molecular structure in more detail and to draw shape based comparison between inhibitor structures. The methods for performing these calculations can be divided into two main fields: molecular mechanics and electronic structure theory, where the former relies on the laws of classical physics, while the latter is based on quantum mechanics and solutions to the Schrödinger equation. There are numerous approaches to molecular modeling *via* electronic structure theory, including *ab initio* and density functional theory (DFT) methods. Though not as accurate as higher levels of *ab initio* theory for computing relative energies, DFT methods have been used extensively for structural prediction, affording a compromise between accuracy and computational effort. In more detail in order to predict the molecular structure of gas phase iminosugars, DFT calculations were performed in this study at the M06-2X[58] level of theory, which has shown excellent performance for main group chemistry and represents an improvement over the popular B3LYP method.[59] The calculations were run in collaboration with Dr. Fernando Martínez.[60]

### 2.4.3 Shape based approach to molecular modeling

Molecular modeling has been used to successfully calculate structures and molecular shapes for iminosugars. For example DFT calculations were used to predict the structure of azetidine **77** in Araújo et al., which was found to compare very favorably to the structure obtained using X-ray crystallography.[61] The overlap of the two structures shows that molecular modeling is a reliable method for estimating the conformation of iminosugars generally and of azetidines specifically (Figure 2.17).

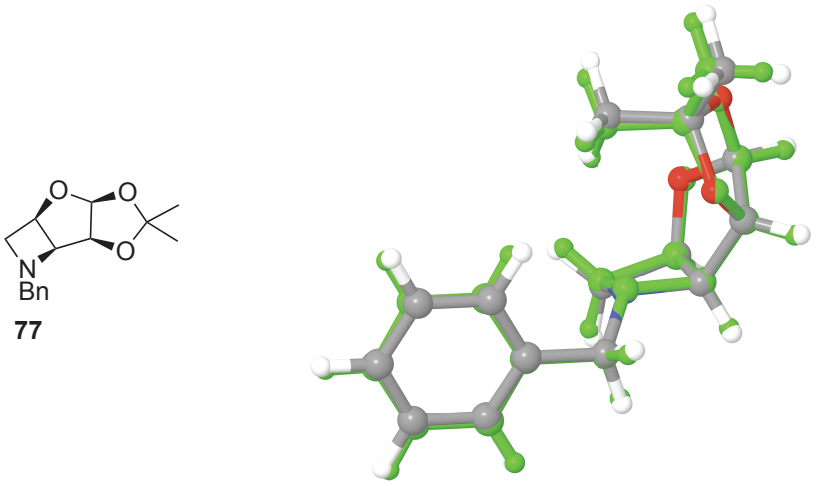


**77**

**Figure 2.17** Overlay of molecular structures of azetidine **77** derived from X-ray crystallography (green) with the molecular modeling (colour).

With the reliability of molecular modeling established, the general idea was to calculate the molecular structure of known β-*N*-acetyl-hexosaminidase inhibitors in different ring sizes and to see if shape-based similarities could be found. The focus lies especially on the favourable overlap of the heteroatoms in the structure (hydroxyl- amide- and ring nitrogen functionality), which are presumed to be the important points of interaction with the active site of the glycosidase enzyme.

### 2.4.4 Favourable comparison of 6- to 5-ring system

The very potent β-*N*-acetyl-hexosaminidase inhibitors **10** and **68** (Table 2.2) were chosen in order to see if an analogy between the six and five-membered rings could be drawn (Figure 2.18). Based on the stereochemistry, the pyrrolidine **68** can be viewed as the C4 excision product of the higher progenitor and therefore OH4 was not overlayed in the comparison. As can be seen in Figure 2.18 the two structures overlay closely and based on the enzymatic acitivity data we can conclude that the interaction of OH4 in **10** with the active site must be less important for inhibitory activity. The less potent analogues of both ring sizes **44** and **69** were subjected to a similar comparison again with an excision of C4 taking us from the six-ring system to the five-

ring analogue (Figure 2.19). Overall it can be concluded that a shape-based comparison of inhibition activity between the different ring sizes is possible.

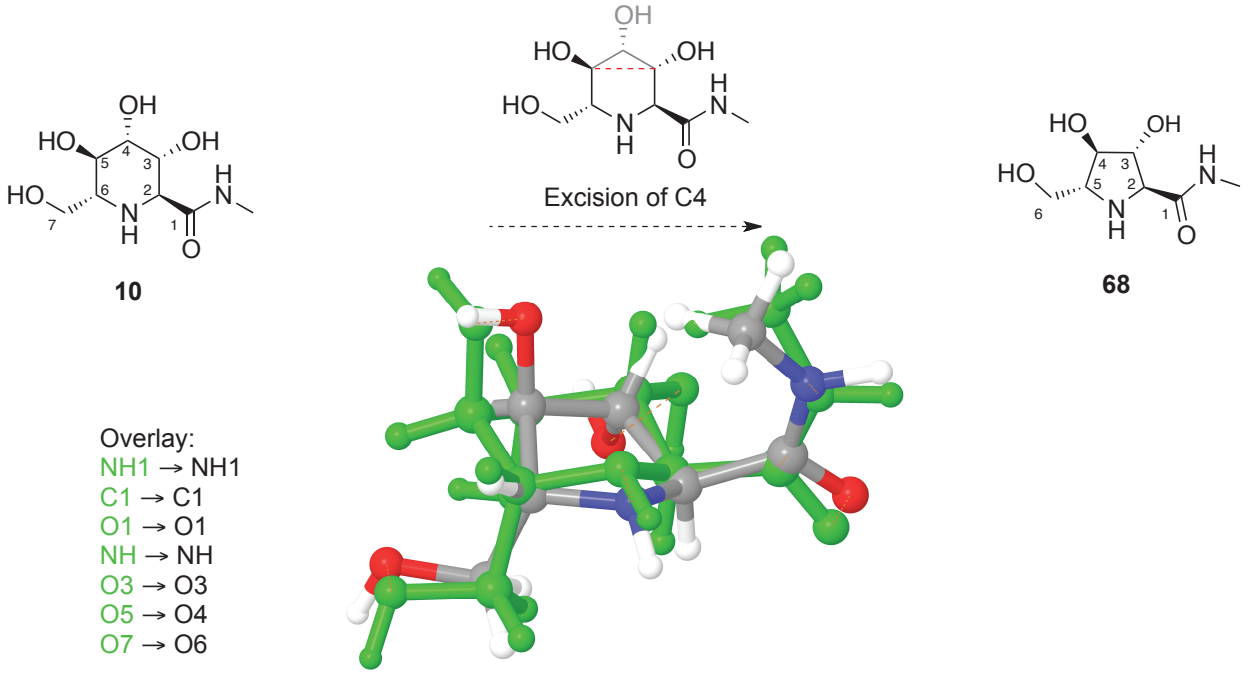


**Figure 2.18** Overlay of pyrrolidine **68** (colour) with pipecolic amide **10** (green) corresponds to excision of the C4 group from the piperidine ring.

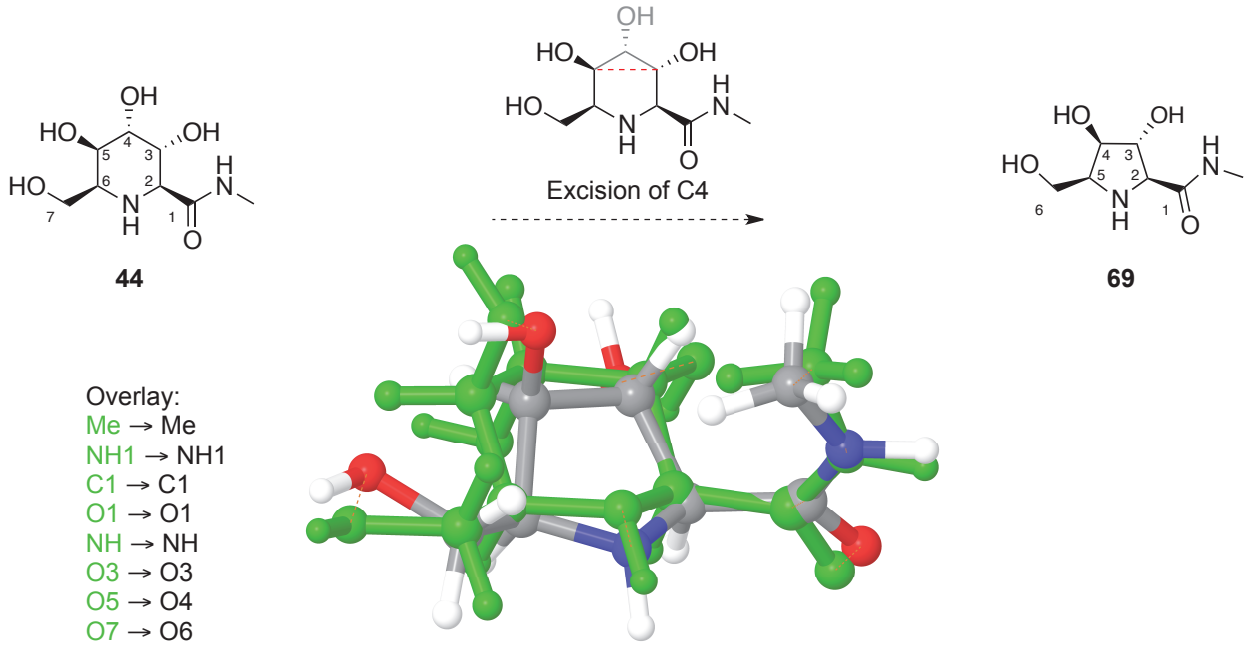


**Figure 2.19** Overlay of pyrrolidine **69** (colour) with pipecolic amide **44** (green) corresponds to excision of the C4 group from the piperidine ring.

### 2.4.5 Predictions for the 4 ring activity based on 5 ring overlays

With the activity comparison between six- and five-membered ring systems established, we were wondering if it would be possible to make prediction on the relative inhibitory activity of 4-membered iminosugars with an azetidine core. In order to develop an inhibitor against β-*N*-acetyl-hexosaminidase, the potent inhibitor **68** was used as a basis for molecular modeling.

*Cis*-azetidine **78L** (*cis* with respect to C1 and C5) with the L-*ribo* configuration overlays well with pyrrolidine **68** [$K_i$ 27 nM, Figure 2.10] (Figure 2.20). The same would be true for its enantiomer **78D** in the D-*ribo* configuration with the pyrrolidine enantiomer **72** [$K_i$ 75.1 μM, Figure 2.13] and as a result we would predict the L-*ribo* derivative to be a good inhibitor of the target enzyme, while its enantiomer D-*ribo* would be of reduced activity. In order to obtain close overlap between these two structures, the primary alcohol of the azetidine **78L** was overlayed with the OH4 of the pyrrolidine **68**. This leads to the excision of C5 and as result of the hydroxmethyl from the pyrrolidine. The inhibition displayed by azetidine **78L** would provide direct evidence of the importance of the interaction of OH6 in the pyrrolidine inhibitor with the enzyme. Possible hints to the outcome of this question are provided by the inhibitory activity of the hydroxymethyl deletion analogue **70** [$K_i$ 42.5 μM, Figure 2.12] (Table 2.3) of pyrrolidine **68** and the negative influence epimerization of C5 to give pyrrolidine **69** [$K_i$ 14.9 μM, Figure 2.11] has on the inhibition activity (Figure 2.16). Based on these facts, we would predict **78L** to be a good but arguably not outstanding inhibitor like pyrrolidine **68**. With the methodology to form *cis*-azetidines currently available in the group,[62] an extension encompassing the synthesis of azetidine **78L** and its enantiomer would be feasible. Synthesis of a *trans*-azetidine would require a substantial extension of the current methodology, nonetheless we were interested in the quality of the overlays of such structures with pyrrolidine **68**.

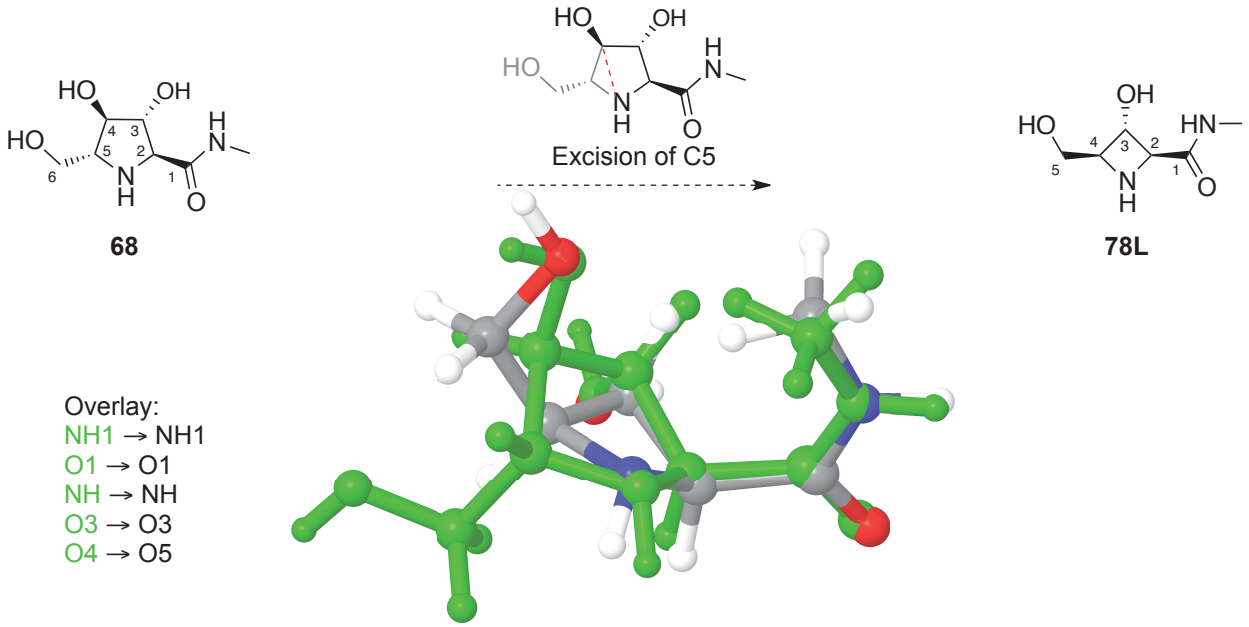


**Figure 2.20** *Cis*-azetidine **78L** (L-ribo) (colour) overlay on **68** (green) corresponds to excision of the C5 group in the pyrrolidine ring.

The epimerization of C4 in pyrrolidine **68** had relatively little influence on the enzymatic inhibition in comparison to changes of stereochemistry at C5 and C3 (Figure 2.16). Therefore performing the ring-contraction *via* excision of C4 gave the *trans*-azetidine **79D**, which can be seen to overlap very favorably with the pyrrolidine inhibitor **68** (Figure 2.21). As a result, comparing the enzyme inhibition data of *cis*-azetidine **78L** with its C4 epimer *trans*-azetidine **79D** could answer the relative importance of the OH6 vs OH4 in pyrrolidine **68**. If the OH6 interaction is indeed more important, then we would expect *trans*-azetidine **79D** to be a potent inhibitor of β-*N*-acetyl-hexosaminidases.

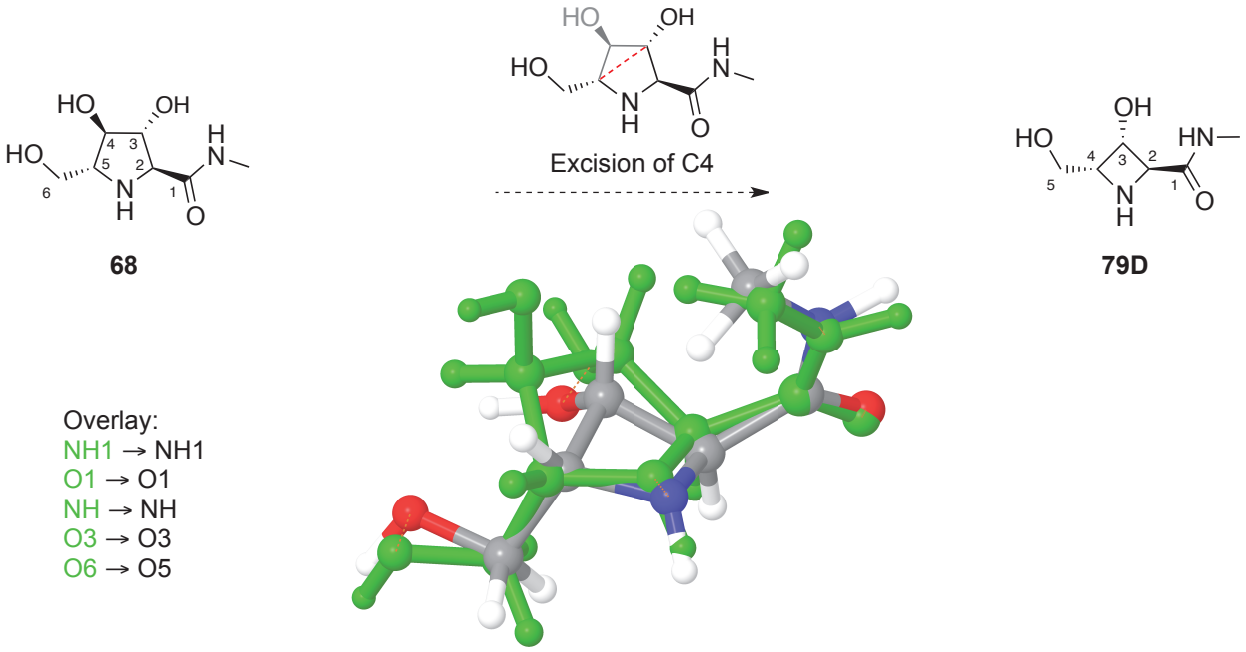


**Figure 2.21** *Trans*-azetidine **79D** (D-lyxo) (colour) overlay on **68** (green) corresponds to excision of the C4 group in the pyrrolidine ring.

As we presumed the amide functionality is vital for enzyme inhibition, an excision at C2 didn't seem feasible, leaving only the excision of C3 from pyrrolidine **68** to be explored. This gave *trans*-azetidine **80D**, the C3 epimer of **79D**, which did not overlap very well with pyrrolidine inhibitor **68** (Figure 2.22). The azetidine ring nitrogen is displaced, the secondary hydroxyls seem distant and the amide functional group is twisted into co-planarity with the azetidine ring rather then remaining perpendicular to it. The latter is presumably due to the steric interaction of OH3 and the amide group, which are in a *cis*-conformation rather then a *trans*-relationship as in the other two azetidine scaffolds investigated. Paired with the fact that epimerization of pyrrolidine **68** at C3 was detrimental to enzyme inhibition, we would predict *trans*-azetidine **80D** to be a weak inhibitor of β-*N*-acetyl-hexosaminidases. We can conclude that of the four azetidines modeled in this study, two (**78L** and **79D**) would be good inhibitors of β-*N*-acetly-hexosaminidase, with some evidence pointing towards **79D** being the candidate for the strongest inhibition, while the other two (**78D** and **80D**) would be weaker inhibitors.

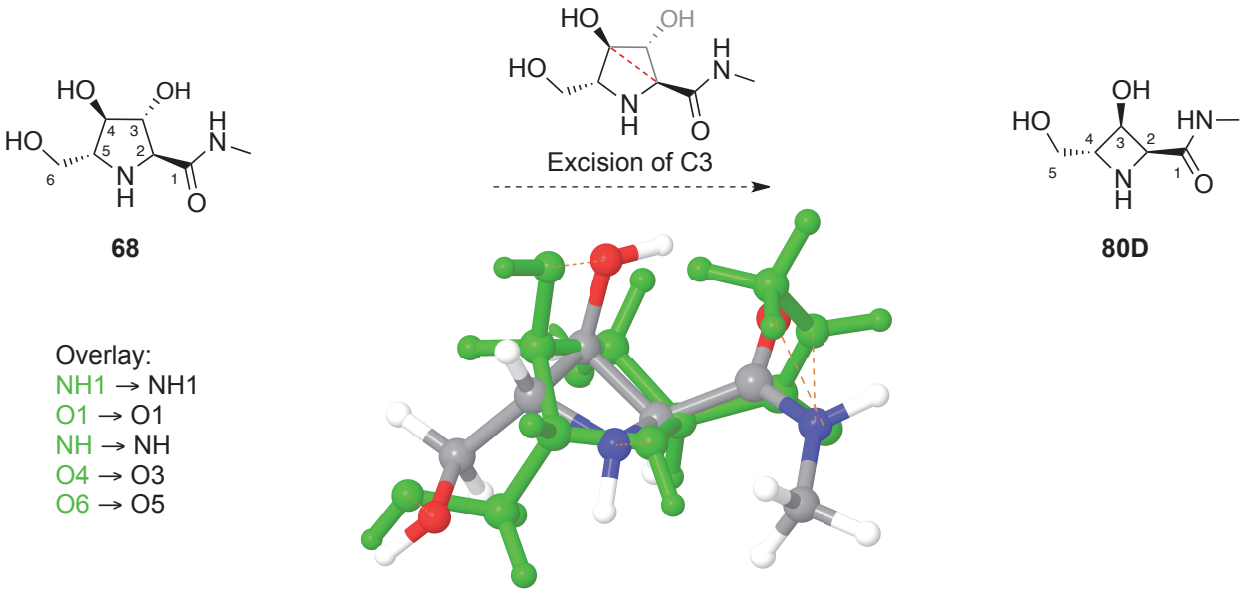


**Figure 2.22** *Trans*-azetidine **80D** (D-arabino) (colour) overlay on **68** (green) corresponds to excision of the C3 group in the pyrrolidene ring.

## 2.5 Conclusion Chapter 2

This chapter saw the synthesis of lead compound pipecolic amide **10** and its impressive inhibition of β-*N*-acetyl-hexosaminidase reported in the literature was confirmed with a $IC_{50}$ of 140 nM (human placenta). Furthermore, its C6 epimer **44** was successfully generated and subjected to enzymatic inhibition evaluation, stressing the extreme impact a single stereocentre change can have on biological activity.

Further pipecolic amide stereochemistries were to be explored, however the work had to be abandoned due to several complications in terms of selectivity of protecting group chemistry. However, very high yielding and robust pathways to epimeric azido-γ-lactones **60** & **62** derived form D-glucose were developed, which are useful synthetic intermediates e.g. towards 8 of possible 16 HNJ epimers.

Besides the biological data on six membered iminosugars, five membered rings, including the highly potent pyrrolidine **68** ($K_i$ 27 nM, HL60 cell homogenate), were evaluated leading to a rich set of structure activity data regarding β-*N*-acetyl-hexosaminidase inibitors. Based on this data, DFT calculations were performed to glean a shape based comparison of these inhibitors

weighing the importance of individual hydroxyl group interactions against each other. With this knowledge in mind, predictions for the inhibition activity against β-*N*-acetyl-hexosamindase of 4-ring iminosugar in novel chemical space have been performed; the synthesis of some of which will be the topic of Chapter 3.

## 2.6 6-ring experimental section

### 2.6.1 General experimental

All commercial reagents were used as supplied. Methanol, pyridine and *N*,*N*-dimethylformamide was purchased dry from Sigma-Aldrich (Dorset, U.K.) in Sure/Seal™ bottles over molecular sieves. All other solvents were used as supplied (Analytical or HPLC grade), without prior purification. Water used was Milli-Q™ grade. Reactions were performed under an atmosphere of argon, unless stated otherwise and maintained by an inflated balloon. Thin layer chromatography (TLC) was performed on aluminium sheets coated with 60 $F_{254}$ silica supplied by Merck (Darmstadt, Germany). Sheets were visualised using a spray of 0.2% w/v cerium (IV) sulfate and 5% ammonium molybdate in 2 M sulfuric acid, or a spray of 1% w/v potassium permanganate (VII), 5% w/v potassium carbonate and 0.1 % Sodium hydroxide in water. Flash chromatography was performed on Sorbsil C60 40/60 silica. Ion exchange chromatography was performed using Dowex® (50W-X8, $H^+$), eluted with 2 M ammonium hydroxide or Amberlite® (IR-120, $H^+$), eluted with 1.0 M ammonium hydroxide. Melting points were recorded on a Kofler hot block and are uncorrected. Optical rotations were recorded on a Perkin-Elmer 241 polarimeter with a path length of 1 dm. Concentrations are quoted in g 100 /mL. Infrared spectra were recorded on a Perkin-Elmer 1750 IR Fourier Transform spectrophotometer using thin films or a Bruker Tensor 27 FT IR spectrophotometer using thin films on either sodium chloride or germanium plates. Only the characteristic peaks are quoted. Low resolution mass spectra (*m/z*) were recorded on a Waters LCT Premier spectrometer, and high resolution mass spectra (HRMS

*m/z*) on a Waters ZMD spectrometer. The ionisation technique used was electrospray ionisation (ESI). Nuclear magnetic resonance (NMR) spectra were recorded on Bruker AMX 500 ($^1$H: 500 MHz and $^{13}$C: 125.7 MHz) and Bruker DPX 400 and DQX 400 spectrometers ($^1$H: 400 MHz and $^{13}$C: 100.6 MHz) in the deuterated solvent stated. All chemical shifts (δ) are quoted in ppm and coupling constants (*J*) in Hz. Residual signals from the solvents were used as an internal reference except in the case of $D_2O$, where acetonitrile was used as an internal reference.

### 2.6.2 Synthesis of literature β-*N*-acetylhexoxamindase inhibitor

**2-*O*-Azido-2-deoxy-3,4:6,7-di-*O*-isopropylidene-D-*glycero*-D-*talo*-heptono-1,5-lactone 18**

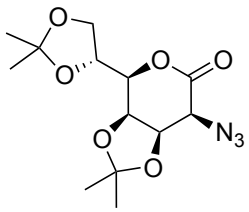

Lactone **40** (5.00 g, 17.34 mmol) was dissolved in dichloromethane (100 mL) and cooled to -30 °C and pyridine (5.3 mL, 65.9 mmol) was added. Trifluoromethanesulfonic anhydride (4.1 mL, 24.28 mmol) was added dropwise and the reaction stirred at -30 °C to -10 °C. After 40 min TLC analysis (1:1 ethyl acetate/cyclohexane) showed that the starting material ($R_f$ 0.25) had been completely converted into a single product ($R_f$ 0.60). The reaction was then quenched *via* addition of 1 M aq. hydrochloric acid (80 mL), the organic layer was washed with brine (2 x 80 mL), dried (magnesium sulfate) and evaporated to dryness to afford the crude reaction product as a crystalline solid (7.47g, quant.), which was used without further purification.

To a solution of crude triflate (7.29 g, 17.34 mmol) in *N*,*N*-dimethylformamide (30 mL) sodium azide (1.41 g, 21.68 mmol) was added and the mixture was stirred at RT for 18 h. After this time TLC analysis (1:1 ethyl acetate/cyclohexane) showed that the starting material ($R_f$ 0.60) had been completely converted to one major product ($R_f$ 0.55). The crude reaction was concentrated *in vacuo* and the residue was partitioned between dichloromethane (100 mL) and brine (100

mL). The organic layer was washed with water (100 mL), dried (magnesium sulfate) and evaporated to dryness to afford the crude product. Purification *via* flash column chromatography (3:1 cyclohexane/ethyl acetate, $R_f$ 0.25) yielded azide **18** as a white crystalline solid (5.10 g, 94%). M.p. 99-101 °C [lit. m.p. 103-104 °C];[39] $[\alpha]_D^{25}$ +94.8 (*c* 1.33 in $CHCl_3$) [lit. $[\alpha]_D^{25}$ +96.7 (*c* 1.13 in $CHCl_3$)];[39] $\nu_{max}$ (thin film): 2119 (s, $N_3$), 1764 (s, C=O); $\delta_H$ (400 MHz, $CDCl_3$): 4.87 (1 H, dd, H3, $J_{3,4}$ 7.8, $J_{2,3}$ 3.4), 4.70 (1 H, dd, H4, $J_{3,4}$ 7.8, $J_{4,5}$ 1.6), 4.41 (1 H, ddd, H6, $J_{5,6}$ 8.5, $J_{6,7}$ 6.0, $J_{6,7'}$ 3.6), 4.15 (1 H, dd, H7 $J_{7,7'}$ 9.4, $J_{6,7}$ 6.0), 4.07 (1 H, dd, H7' $J_{7,7'}$ 9.4, $J_{6,7'}$ 3.6), 3.97 (1 H, dd, H5, $J_{5,6}$ 8.5, $J_{4,5}$ 1.6), 3.84 (1 H, d, H2, $J_{2,3}$ 3.4), 1.47 (3 H, s, $C\underline{H}_3$), 1.44 (3 H, s, $C\underline{H}_3$), 1.39 (3 H, s, $C\underline{H}_3$), 1.37 (3 H, s, $C\underline{H}_3$); $\delta_C$ (100.6 MHz, $CDCl_3$): 166.3 (C1), 111.4, 110.1 (2 x $\underline{C}(CH_3)_2$), 76.8 (C5), 75.5 (C3), 72.5 (C6), 72.4 (C4), 66.6 (C7), 59.3 (C2), 27.1, 25.9, 25.0, 24.5 (2 x $C(\underline{C}H_3)_2$); *m/z* (ESI+ve): 649 ($[2M+Na]^+$, 100%); HRMS (ESI+ve): Found 336.1163 ($[M+Na]^+$); $C_{13}H_{19}N_3NaO_6$ requires 336.1166.

**2-Azido-2-deoxy-3,4-*O*-isopropylidene-D-*glycero*-D-*talo*-heptono-1,5-lactone 45**

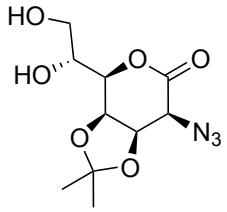


Azide **18** (0.55 g, 1.77 mmol) was stirred in 80% aq. acetic acid (5 mL) at 50 °C. After 2.5 h TLC (3:1 ethyl acetate/cyclohexane) showed that all the starting material ($R_f$ 0.70) had been converted to a major product ($R_f$ 0.15). The solvent was removed and the crude material purified *via* flash column chromatography (4:1 ethyl acetate/cyclohexane) to yield title compound **45** as a white crystalline solid (0.44 g 91%). M.p. 125-127 °C [lit. m.p. 126-127 °C];[35] $[\alpha]_D^{25}$ +122.7 (*c* 1.07 in MeOH) [lit. $[\alpha]_D^{20}$ +131.5 (*c* 1.08 in MeOH)];[35] $\nu_{max}$ (thin film): 3417 (br, O-H), 2121 (s, $N_3$), 1759 (s, C=O); $\delta_H$ (400 MHz, MeOD): 4.90 (1 H, dd, H3, $J_{3,4}$ 7.8, $J_{2,3}$ 3.4), 4.83 (1 H, dd, H4, $J_{3,4}$ 7.8, $J_{4,5}$ 1.3), 4.28 (1 H, dd, H5, $J_{5,6}$ 9.2, $J_{4,5}$ 1.3), 4.23 (1 H, d, H2, $J_{2,3}$ 3.4), 3.89 (1 H,

ddd, H6, $J_{5,6}$ 9.2, $J_{6,7'}$ 4.4, $J_{6,7}$ 2.4), 3.78 (1 H, dd, H7, $J_{7,7'}$ 11.8, $J_{6,7}$ 2.4), 3.69 (1 H, dd, H7', $J_{7,7'}$ 11.8, $J_{6,7'}$ 4.5), 1.41 (3 H, s, C$\underline{H}_3$), 1.39 (3 H, s, C$\underline{H}_3$); $\delta_C$ (100.6 MHz, MeOD): 168.3 (C1), 110.6 ($\underline{C}(CH_3)_2$), 76.1 (C3), 75.6 (C5), 72.8 (C4), 68.9 (C6), 62.7 (C7), 59.6 (C2), 25.3 ($\underline{C}H_3$), 23.5 ($\underline{C}H_3$); *m/z* (ESI+ve): 569 ([2M+Na]$^+$, 100%); HRMS (ESI+ve): Found 296.0853 ([M+Na]$^+$); $C_{10}H_{15}N_3NaO_6$ requires 296.0853.

**2-Azido-7-*O*-*tert*-butyldimethylsilyl-2-deoxy-3,4-*O*-isopropylidene-D-*glycero*-D-*talo*-heptono-1,5-lactone 46**

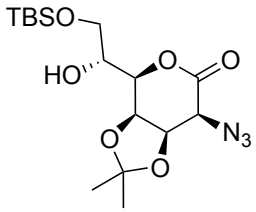


To a solution of diol **45** (500 mg, 1.83 mmol) in dry pyridine (9 mL) was added *tert*-butyldimethylsilyl chloride (414 mg, 2,74 mmol). The reaction was followed by TLC (1:1 cyclohexane/ethyl acetate $R_f$ 0.60) and left to react for 18 h. On completion the solvent was removed and the crude reaction product was co-evaporated with toluene (2 x 10 mL) followed by purification *via* flash column chromatography (4:1 cyclohexane/ethyl acetate) and the title compound **46** was isolated as a white crystalline solid (645 mg, 91%). M.p. 135-137 °C, [lit. m.p. 138-139 °C];[35] $[\alpha]_D^{25}$ +113.1 (*c* 0.99 in $CHCl_3$) [lit. $[\alpha]_D^{20}$ +109.6 (*c* 0.99 in $CHCl_3$)];[35] $\nu_{max}$ (thin film): 3366 (m, br, O-H), 2135 (s, $N_3$), 1770 (s, C=O); $\delta_H$ (400 MHz, $CDCl_3$): 4.87 (1 H, dd, H3, $J_{3,4}$ 7.8, $J_{2,3}$ 3.2), 4.83 (1 H, dd, H4, $J_{3,4}$ 7.8, $J_{4,5}$ 1.1), 4.06 (1 H, H5, m), 4.03 – 3.94 (1 H, m, H6), 3.87 (1 H, dd, H7, $J_{7,7'}$ 10.4, $J_{6,7}$ 3.0), 3.81 (1 H, dd, H7', $J_{7,7'}$ 10.4, $J_{6,7'}$ 3.9), 3.81 (1 H, d, H2, $J_{2,3}$ 3.2), 2.68 (1 H, d, OH, $J_{OH,6}$ 6.1), 1.47 (3 H, s, Me), 1.40 (3 H, s, Me), 0.90 (9 H, s, SiC(C$\underline{H}_3$)$_3$), 0.10 (3 H, s, SiC$\underline{H}_3$), 0.09 (3 H, s, SiC$\underline{H}_3$); $\delta_C$ (100.6 MHz, $CDCl_3$): 166.3 (C1), 111.3 ($\underline{C}(CH_3)_2$), 75.5, 75.4 (C3, C5), 72.4 (C4), 68.4 (C6), 62.8 (C7), 59.3 (C2), 26.0 (SiC($\underline{C}H_3$)$_3$, 1 x C($\underline{C}H_3$)$_2$) 24.5 (1 x C($\underline{C}H_3$)$_2$), 18.4 (Si$\underline{C}$(CH$_3$)$_3$), -5.3 (2 x Si$\underline{C}$H$_3$); *m/z* (ESI+ve):

797 ([2M+Na]$^+$, 100%); HRMS (ESI+ve): Found 410.1713 ([M+Na]$^+$); $C_{16}H_{29}N_3NaO_6Si$ requires 410.1718.

**2-Azido-7-*O*-*tert*-butyldimethylsilyl-2-deoxy-3,4-*O*-isopropylidene-D-*talo*-6-heptulosono-1,5-lactone 41**

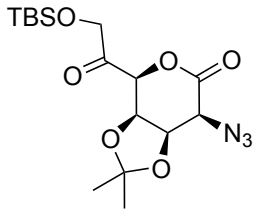


Pyridinium chlorochromate (416 mg, 1.94 mmol) was added to a flame dried flask containing powdered 3 Å molecular sieves (250 mg) along with azido-alcohol **46** (250 mg, 0.65 mmol) and dichloromethane (7 mL) was added. The reaction was stirred for 18 h at RT and the disappearance of the starting material ($R_f$ 0.25) could be observed *via* TLC analysis (3:1 cyclohexane/ethyl acetate) along with formation of a new species ($R_f$ 0.35). On completion the product was purified *via* a celite topped silica flash column (4:1 cyclohexane/ethyl acetate) to give ketone **41** as a white crystalline solid (215 mg, 0.56 mmol, 86%). M.p. 130-132 °C, [lit. m.p. 120-122 °C (ether)];[35] $[\alpha]_D^{25}$ +4.85 (*c* 1.0 in $CHCl_3$), [lit. $[\alpha]_D^{20}$ +5.4 (*c* 1.0 in $CHCl_3$)];[35] $\nu_{max}$ (thin film): 2119 (s, $N_3$), 1771 (s, OC=O), 1744 (s, C=O); $\delta_H$ (400 MHz, $CDCl_3$): 4.90 (1 H, dd, H4, $J_{3,4}$ 7.7, $J_{4,5}$ 1.5), 4.87 (1 H, dd, H3, $J_{3,4}$ 7.7, $J_{2,3}$ 3.0), 4.75 – 4.72 (1 H, H5, m), 4.71 (2 H, m, H7, H5), 4.61 (1 H, d, H7', $J_{7,7'}$ 19.9), 3.83 (1 H, d, H2, $J_{2,3}$ 3.0), 1.46 (3 H, s, C$\underline{H}_3$), 1.33 (3 H, s, C$\underline{H}_3$), 0.91 (9 H, s, SiC(C$\underline{H}_3$)$_3$), 0.10 (3 H, s, SiC$\underline{H}_3$), 0.08 (3 H, s, SiC$\underline{H}_3$); $\delta_C$ (100.6 MHz, $CDCl_3$): 201.7 (C6), 165.2 (C1), 111.9 (C(CH$_3$)$_2$), 80.3 (C5), 75.3, 74.3 (C3, C4), 69.0 (C7), 59.6 (C2), 25.9 (SiC(CH$_3$)$_3$), 25.8 (C(CH$_3$)$_2$), 24.3 (C(CH$_3$)$_2$), 18.6 (SiC(CH$_3$)$_3$), -5.2 (SiCH$_3$) -5.4 (SiCH$_3$); *m/z* (ESI+ve): 793 ([2M+Na]$^+$, 100%), 825 ([2M+Na+MeOH]$^+$, 100%); HRMS (ESI+ve): Found 408.1558 ([M+Na]$^+$); $C_{16}H_{27}N_3NaO_6Si$ requires 408.1561.

**7-*O*-*tert*-Butyldimethylsilyl-2,6-deoxy-2,6-imino-3,4-*O*-isopropylidene-D-*talo*-6-heptulosono-1,5-lactone 42**

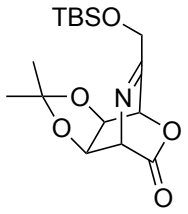


To a solution of ketone **41** (400 mg, 1.04 mmol) in dry tetrahydrofuran (3.3 mL) was added triethylphosphite (0.33 ml, 2.08 mmol). The reaction was left to stir at RT for 18 h and the reaction progress was monitored *via* TLC (3:1 cyclohexane/ethyl acetate, starting material $R_f$ 0.40, product $R_f$ 0.45). On completion the solvent was removed *in vacuo* and the residue was purified *via* flash column chromatography (5:1 cyclohexane/ethyl acetate) and imine **42** was isolated as a clear oil (374 mg, 1.09 mmol, quant.). $[\alpha]_D^{25}$ +106.6 (*c* 0.99 in $CHCl_3$); [lit. $[\alpha]_D^{20}$ +98.3 (*c* 1.0 in $CHCl_3$)];[35] $\nu_{max}$ (thin film): 1781 (s, OC=O), 1650 (w, N=C); $\delta_H$ (400 MHz, $CDCl_3$): 5.49 (1 H, d, H5, $J_{4,5}$ 4.2), 5.19 (1 H, d, H2, $J_{2,3}$ 2.5), 4.69 (1 H, dd, H4, $J_{3,4}$ 7.0, $J_{4,5}$ 4.2), 4.62 (1 H, dd, H3, $J_{3,4}$ 7.0, $J_{2,3}$ 2.5), 4.52 (1 H, d, H7 $J_{7,7'}$ 14.9), 4.42 (1 H, d, H7', $J_{7,7'}$ 14.9), 1.33 (3 H, s, C$\underline{H}_3$), 1.31 (3 H, s, C$\underline{H}_3$), 0.92 (9 H, s, SiC(C$\underline{H}_3$)$_3$), 0.10 (6 H, a-d, Si(C$\underline{H}_3$)$_2$, *J* 9.4); $\delta_C$ (100.6 MHz, $CDCl_3$): 177.4 (C1), 168.0 (C6), 114.2 (C(CH$_3$)$_2$), 74.4 (C4), 73.2 (C3), 71.7 (C5), 65.4 (C7), 62.5 (C2), 25.9 (SiC(CH$_3$)$_3$), 25.5 (C(CH$_3$)$_2$), 24.9 (C(CH$_3$)$_2$), 18.4 (SiC(CH$_3$)$_3$), -5.2 (SiCH$_3$), -5.4 (SiCH$_3$); *m/z* (ESI+ve): 705 ([2M+Na]$^+$, 100%); HRMS (ESI+ve): Found 364.1547 ([M+Na]$^+$); $C_{16}H_{27}N_1NaO_5Si$ requires 364.1551.

**2,6-((benzyloxy)carbonyl)Amino-7-*O*-*tert*-butyldimethylsilyl-2,6-deoxy-3,4-*O*-isopropylidene-D-*glycero*-D-*talo*-heptono-1,5-lactone 47**

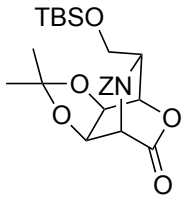


Benzylchloroformate (88 mg, 0.52 mmol, 0.07 mL) in chloroform (1 mL) was added dropwise to a stirred solution of bicyclic imine **42** (88 mg, 0.26 mmol) and bis(triphenylphosphine) copper(I) tetrahydroborate (187 mg, 0.31 mmol) in chloroform (2 mL) and left to react at RT for 5 h. The reaction was followed *via* TLC (3:1 cyclohexane/ethyl acetate, starting material $R_f$ 0.35, product, $R_f$ 0.55) and on completion diethyl ether (30 mL) was added. Scratching of the reaction vessel walls lead to formation of a white precipitate on standing. The precipitate was filtered off and washed with diethyl ether (2 x 25 mL) and the combined organic fractions were evaporated to dryness to yield the crude reaction mixture (405 mg). The crude reaction product **47** was purified *via* flash column chromatography (6:1 ⇒ 5:1 cyclohexane/ethyl acetate) and was isolated as a clear oil (111 mg, 0.232 mmol, 90%). $[\alpha]_D^{25}$ -14.1 (*c* 1.25 in $CHCl_3$); $\nu_{max}$ (thin film): 1787 (s, OC=O), 1715 (s, NC=O); $\delta_H$ (400 MHz, $CDCl_3$): 7.49 – 7.19 (5 H, m, Ph), 5.22 (1 H, d, H8, $J_{8,8'}$ 12.3), 5.14 (1 H, d, H8', $J_{8,8'}$ 12.4), 5.11 (1 H, a-s, H5), 5.06 (1 H, a-s, H2), 4.59 – 4.53 (1 H, m, H4), 4.50 (1 H, dd, H3, $J_{3,4}$ 7.8, $J_{2,3}$ 2.5), 4.39 (1 H, a-s, H7), 4.18 (1 H, a-t, H7', $J_{7,7'} = J_{6,7'}$ = 9.6), 3.97 (1 H, a-s, H6), 1.57 (3 H, s, C$\underline{H}_3$), 1.38 (3 H, s, C$\underline{H}_3$), 0.89 (9 H, s, SiC(C$\underline{H}_3$)$_3$), 0.04 (6 H, s, 2 x SiC$\underline{H}_3$); $\delta_C$ (100.6 MHz, $CDCl_3$): 167.5 (C1), 156.0 (NC=O), 134.1, 134.0 (*ipso*-Ph), 130.0, 128.7, 128.4 (Ph), 113.9 (C(CH$_3$)$_2$), 73.8 (C5), 72.1 (C3), 71.7 (C4), 68.1 (C$\underline{H}_2$Ph), 60.5 (C7), 58.5 (C6), 54.4 (C2), 25.9 (SiC(C$\underline{H}_3$)$_3$), 24.9 (C(C$\underline{H}_3$)$_2$), 23.9 (C(C$\underline{H}_3$)$_2$), 18.3 (Si$\underline{C}$(CH$_3$)$_3$), -5.3 (SiCH$_3$), -5.4 (SiCH$_3$); *m/z* (ESI+ve): 977 ([2M+Na]$^+$, 100%); HRMS (ESI+ve): Found 500.2073 ([M+Na]$^+$); $C_{24}H_{35}NNaO_7Si$ requires 500.2075.

**2,6-((benzyloxy)carbonyl)Amino-7-*O-tert*-butyldimethylsilyl-2,6-deoxy-3,4-*O*-isopropylidene-D-*glycero*-D-*talo*-heptono-methylamide 48**

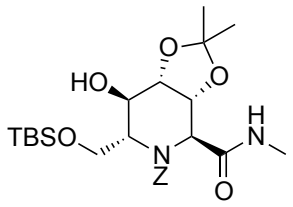


To a solution of bicycle **47** (40 mg, 0.084 mmol) in dry tetrahydrofuran (1 mL) was added methylamine (33% w/w solution in industrial methylated spirit, 0.25 mmol, 0.03 mL). The reaction was followed by TLC analysis (1:1 cyclohexane/ethyl acetate, starting material $R_f$ 0.80, product $R_f$ 0.35) and on completion of the reaction after 18 h, the solution was concentrated to dryness and purified *via* column chromatography (1:1 cyclohexane/ethyl acetate). The title compound **48** was obtained as a white crystalline solid (25 mg, 0.050 mmol, 59%). M.p. 148-152 °C; $[\alpha]_D^{25}$ + 10.34 (*c* 0.99 in $CHCl_3$); $\nu_{max}$ (thin film): 3312 (br, OH), 1702 (s, NC=OO), 1663 (s, amide I), 1570 (w, amide II); $\delta_H$ (400 MHz, $CDCl_3$): 7.34 (5 H, a-s, Ph), 6.75 (1 H, s, NH), 6.06 (1 H, d, OH, $J_{5,OH}$ 11.5), 5.22 (1 H, d, H8', $J_{8,8'}$ 12.5), 5.06 (1 H, d, H8', $J_{8,8'}$ 12.5), 4.60 (1 H, a-s, H2), 4.54 (1 H, d, H3, $J_{3,4}$ 7.5), 4.39 (1 H, d, H4, $J_{3,4}$ 7.5), 4.21 (2 H, a-d, H5, H6, *J* 10.5), 3.80 (1 H, t, H7, $J_{6,7} = J_{7,7'} = 9.7$), 3.67 (1 H, a-s, H7'), 2.81 (3 H, s, NHC$\underline{H}_3$), 1.47 (3 H, s, C$\underline{H}_3$), 1.31 (3 H, s, C$\underline{H}_3$), 0.83 (9 H, s, SiC(C$\underline{H}_3$)$_3$), -0.08 (6 H, s, Si(C$\underline{H}_3$)$_2$); $\delta_C$ (126 MHz, $CDCl_3$): 173.1 (C1), 157.3 (NC=OO), 135.8 (*ipso*-Ph), 128.7, 128.6, 128.5, 128.4, 128.1 (Ph), 107.7 (C$\underline{C}$(CH$_3$)$_2$), 73.5 (C4), 72.1 (C3), 68.1 (C8), 65.2 (C5), 62.0 (C7), 59.7 (C6), 57.7 (C2), 26.8 (C(C$\underline{H}_3$)$_2$), 25.9 (SiC(C$\underline{H}_3$)$_3$), 25.0 (C(C$\underline{H}_3$)$_2$), 22.8 (NHC$\underline{H}_3$), 18.3 (Si$\underline{C}$(CH$_3$)$_3$), -5.2 (SiCH$_3$), -5.3 (SiCH$_3$); *m/z* (ESI+ve): 531 ([M+Na]$^+$, 100%); HRMS (ESI+ve): Found 531.2495 ([M+Na]$^+$); $C_{25}H_{40}N_2NaO_7Si$ requires 531.2497.

**2,6-Dideoxy-2,6-imino-D-*glycero*-D-*talo*-heptono-methylamide 10**

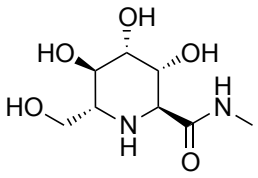

Carbamate **48** (17 mg, 0.03 mmol) was put in 3% methanolic hydrochloric acid and the disappearance of the starting material was monitored *via* TLC (1:1 cyclohexane/ethyl acetate, starting material $R_f$ 0.25, product baseline). The starting material had been completely converted after 4 h and 10% palladium on charcoal (10% by weight, 2 mg) was added, the reaction vessel purged with argon, put under hydrogen and followed by mass spectrometry. After 18 h the reaction mixture was filtered through a glass fibre pad and subjected to ion exchange chromatography (Amberlite IR120, $H^+$ form, eluting with 1.0 M aq. ammonium hydroxide), to give the product **10** as a clear oil (7 mg, 95%). $[\alpha]_D^{25}$ -7.13 (*c* 0.59 in $H_2O$); [lit. $[\alpha]_D^{22}$ -10.0 (*c* 0.66 in $H_2O$)];[1] $\nu_{max}$ (thin film): 3383 (br, NH, OH), 1651 (s, amide I), 1539 (m, amide II); $\delta_H$ (400 MHz, $D_2O$): 4.43 (1 H, a-t, H3, $J_{2,3}$=$J_{3,4}$= 2.9), 3.81 (1 H, dd, H7, $J_{7,7'}$ 11.6, $J_{6,7}$ 3.1), 3.77 – 3.67 (2 H, m, H7', H2), 3.59 (1 H, a-t, H5, $J_{4,5}$=$J_{5,6}$= 9.4), 3.47 (1 H, dd, H4, $J_{4,5}$ 9.5, $J_{3,4}$ 2.9), 2.77 (3 H, s, C<u>H</u>$_3$), 2.65 (1 H, ddd, H6, $J_{5,6}$ 9.3, $J_{6,7'}$5.4, $J_{6,7}$ 3.1); $\delta_C$ (100.6 MHz, $D_2O$): 173.4 (C1), 72.9 (C4), 70.3 (C3), 68.4 (C5), 61.7 (C7), 60.9 (C2), 58.1 (C6), 26.3 (<u>C</u>H$_3$); *m/z* (ESI+ve): 243 ($[M+Na]^+$, 100%); HRMS (ESI+ve): Found 221.1131 ($[M+H]^+$); $C_8H_{17}N_2O_5$ requires 221.1132.

**7-*O*-*tert*-Butyldimethylsilyl-2,6-dideoxy-2,6-imino-3,4-*O*-isopropylidene-L-*glycero*-D-*talo*-heptono-1,5-lactone 58**

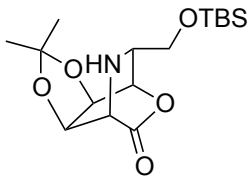


To as stirred solution of alcohol **46** (321 mg, 0.83 mmol) in dichloromethane (10 mL) at -30°C was added pyridine (0.18 mL, 1.08 mmol) and trifluoromethanesulfonic anhydride (0.2 mL, 2.48 mmol). The reaction mixture was allowed to warm to -20°C and after 1.5h TLC analysis (4:1 cyclohexane/ethyl acetate) indicated conversion of the starting material ($R_f$ 0.15) to one major product ($R_f$ 0.45). The reaction mixture was diluted with dichloromethane (13 mL) and washed with dilute aq. hydrochloric acid (2 x 5 mL), brine (60 mL) and dried (magnesim sulfate). The organic layer was evaporated to dryness and the crude reaction product was used without further purification in the next reaction step. The crude triflate **57** (0.43 g, 0.83 mmol) in ethyl acetate (15 mL) was stirred vigorously at RT under hydrogen in the presence of anhydrous sodium acetate (0.27 g, 3.31 mmol) and 10% palladium on charcoal (10% by weight, 45 mg). After 16 h the mixture was filtered through celite, washed with ethyl acetate (15 mL) and evaporated to dryness. The crude product **58** was purified *via* flash column chromatography (1:1 cyclohexane/ethyl acetate) and isolated as a clear oil (246 mg, 0.72 mmol, 87%). $[\alpha]_D^{25}$ -7,00 (*c* 1.3 in $CHCl_3$); $\nu_{max}$ (thin film): 3514 (br, O-H), 1770 (s, C=O); $\delta_H$ (400 MHz, $CDCl_3$): 4.83 (1 H, d, H5, $J_{4,5}$ 4.3), 4.51 (1 H, dd, H4, $J_{3,4}$ 8.0, $J_{4,5}$ 4.3), 4.38 (1 H, dd, H3, $J_{3,4}$ 8.0, $J_{2,3}$ 3.0), 3.67 (1 H, d, H2, $J_{2,3}$ 3.0), 3.53 – 3.45 (3 H, H6, H7, H7', m), 1.60 (3 H, s, C$\underline{H}_3$), 1.40 (3 H, s, C$\underline{H}_3$), 0.88 (9 H, s, SiC(C$\underline{H}_3$)$_3$), 0.05 (6 H, Si$(CH_3)_2$); $\delta_C$ (100.6 MHz, $CDCl_3$): 170.6 (C1), 113.9 (C$(CH_3)_2$), 74.9 (C5), 72.7 (C3), 71.5 (C4), 62.8 (C7), 54.3 (C2), 48.6 (C6), 26.1 (C($\underline{C}H_3)_2$), 26.0 (SiC($\underline{C}H_3)_3$), 24.6 (C($\underline{C}H_3)_2$), 18.4 Si$\underline{C}(CH_3)_3$, -5.3 (SiC$\underline{H}_3$), -5.4 (SiC$\underline{H}_3$); *m/z* (ESI+ve): 709

([2M+Na]$^+$, 100%); HRMS (ESI+ve): Found 366.1704 ([M+Na]$^+$); $C_{16}H_{29}NNaO_5Si$ requires 366.1707.

**Methyl 7-*O*-*tert*-butyldimethylsilyl-2,6-dideoxy-2,6-imino-3,4-*O*-isopropylidene-L-*glycero*-D-*talo*-heptonamide 59**

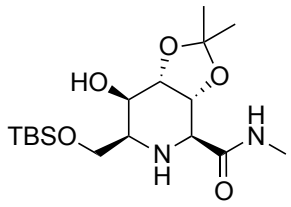


To as solution of bicycle **58** (111 mg, 0.323 mmol) in dry tetrahydrofuran (2 mL) under nitrogen, methylamine (33% w/w solution in industrial methylated spirit, 0.12 mL) was added. By TLC analysis (ethyl acetate, starting material $R_f$ 0.90, product $R_f$ 0.30) the reaction had gone to completion after 18 h and the mixture was concentrated to dryness. The residue was purified *via* flash column chromatography (5:1 ethyl acetate/cyclohexane) and title compound **59** was isolated as colourless oil (91 mg, 0.242 mmol, 52%). $[\alpha]_D^{25}$ +48.5 (*c* 0.63 in $CHCl_3$); $\nu_{max}$ (thin film): 3344 (br, OH, NH), 1657 (s, amide I), 1545 (m, amide II); $\delta_H$ (400 MHz, $CDCl_3$): 6.50 (1 H, NH, br. a-d, $J_{NH,Me}$ 3.6), 4.25 (1 H, dd, H4, $J_{3,4}$ 5.1, $J_{4,5}$ 2.4), 4.22 (1 H, dd, H3, $J_{2,3}$ 8.4, $J_{3,4}$ 5.1), 3.94 (1 H, H5, a-s), 3.83 (1 H, dd, H7, $J_{7,7'}$ 10.0, $J_{6,7}$ 4.3), 3.79 (1 H, dd, H7', $J_{7,7'}$ 10.0, $J_{6,7'}$ 6.6), 3.28 (1 H, d, H2, $J_{2,3}$ 8.4), 3.13 (1 H, d, OH, $J_{OH,5}$ 6.2), 3.03 (1 H, a-t, H6, *J* 5.1), 2.84 (3 H, d, NHC$\underline{H}_3$, $J_{NH,CH3}$ 4.8), 1.54 (3 H, s, C$\underline{H}_3$), 1.39 (3 H, s, C$\underline{H}_3$), 0.90 (9 H, s, SiC(C$\underline{H}_3$)$_3$), 0.08 (6 H, a-d, Si$(CH_3)_2$ *J* 1.8); $\delta_C$ (100.6 MHz, $CDCl_3$): 172.2 (C1), 110.1 (C(CH$_3$)$_2$), 77.3 (C4), 73.4 (C3), 67.3 (C5), 64.5 (C7), 61.0 (C2), 56.7 (C6), 28.4 (C(C$\underline{H}_3$)$_2$), 26.2 (C(C$\underline{H}_3$)$_2$, NHC$\underline{H}_3$), 26.0 (SiC(C$\underline{H}_3$)$_3$), 18.4 (SiC(CH$_3$)$_3$), -5.3 (Si$(CH_3)_2$); *m/z* (ESI+ve): 771 ([2M+Na]$^+$, 100%); HRMS (ESI+ve): Found 397.2115 ([M+Na]$^+$); $C_{17}H_{34}N_2NaO_5Si$ requires 397.2129.

**Methyl 2,6-dideoxy-2,6-imino-L-*glycero*-D-*talo*-heptonamide 44**

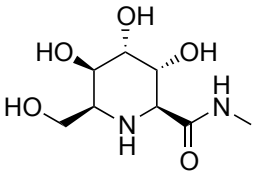

Amide **59** (53 mg, 0.14 mmol) was stirred in 3% methanolic hydrochloric acid (generated from acetyl chloride 0.3 mL with 9.7 mL methanol at 0 °C) at RT for 18 h. The solution was concentrated *in vacuo* and coevaporated with methanol (3 x 10 mL). The residue was purified by ion exchange chromatography (Amberlite IR-120, $H^+$ form, eluting with 1.0 M aq. ammonium hydroxide). TLC analysis showed a single spot (14:3:1:1:1 ethanol/pyridine/n-butanol/acetic acid/water $R_f$ 0.50). Amide **44** was isolated as a colourless oil (18 mg, 0.084 mmol, 60%). $[\alpha]_D^{25}$ +27.3 (*c* 0.75 in $H_2O$); $\nu_{max}$ (thin film): 3316 (br, O-H), 1650 (s, amide I), 1562 (m, amide II); $\delta_H$ (400 MHz, $D_2O$): 3.92 (1 H, a-t, H4, *J* 3.4), 3.87 – 3.77 (2 H, m, H3, H5), 3.55 (1 H, dd, H7, $J_{7,7'}$ 9.4, $J_{6,7}$ 5.0), 3.51 (1 H, dd, H7', $J_{7,7'}$ 9.4, $J_{6,7'}$ 4.9), 3.32 (1 H, d, H2, $J_{2,3}$ 10.4), 3.23 (1 H, N<u>H</u>, s), 2.98 (1 H, a-t, H6, *J* 6.5), 2.67 (3 H, s, $CH_3$); $\delta_C$ (100.6 MHz, $D_2O$): 173.5 (C1), 70.9 (C4), 69.2 (C5), 67.4 (C3), 61.2 (C7), 59.0 (C2), 53.7 (C6), 26.2 (<u>C</u>$H_3$); *m/z* (ESI+ve): 243 ($[M+Na]^+$, 100%); HRMS (ESI+ve): Found 243.0951 ($[M+Na]^+$); $C_8H_{16}N_2NaO_5$ requires 243.0951.

### 2.6.3 Synthesis of epimeric azido-γ-lactones towards pipepcolic amides

**3,5:6,7-Di-*O*-isopropylidene-D-*glycero*-D-*ido*-heptono-1,4-lactone 63**

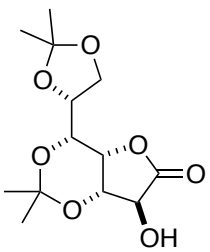

3,5:6,7-Di-*O*-isopropylidene-D-*glycero*-D-*gulo*-heptono-1,4-lactone **61** (1.5 g, 5.21 mmol) was dissolved in dichloromethane (15 mL), pyridine (13.0 mmol, 1.05 mL) was added and the

mixture was cooled to -40 °C. Trifluoromethanesulfonic anhydride (7.3 mmol, 1.2 mL) was added dropwise and the reaction was stirred vigorously as it warmed to -20 °C. After 70 min TLC analysis (1:2 ethyl acetate/cyclohexane) showed all the starting material ($R_f$ 0.10) had been consumed and a single product ($R_f$ 0.50) had been formed. The reaction mixture was diluted with DCM (135 mL) and washed with 2 M aq. hydrochloric acid (45 mL). The aqueous layer was extracted with dichloromethane (60 mL) and the combined organic layers were washed with brine (80 mL), dried (magnesium sulfate), filtered and concentrated *in vacuo* at RT. The crude triflate (2.39 g) was dissolved in *N*,*N*-dimethylformamide (30 mL) and sodium trifluoroacetate (2.12 g, 15.6 mmol) was added and the reaction mixture stirred at 60 °C. After 72 h MeOH (1.5 mL) was added to the reaction and the mixture was stirred for another 16 h. After this time TLC analysis (1:3 ethyl acetate/cyclohexane) indicated a major product ($R_f$ 0.15) and the reaction mixture was diluted with ethyl acetate (200 mL) and washed with 50% brine (3 x 90 mL). The organic layer was dried (magnesium sulfate), filtered and evaporated to dryness. NMR analysis of the crude product still indicated the presence of *N*,*N*-dimethylformamide and hence the crude was redissolved in ethyl acetate (20 mL) and extracted with 50% brine (3 x 20 mL), dried ($MgSO_4$), filtered and evaporated to dryness to yield the crude product as a off white solid (1.10 g, 3.82 mmol, 74%). The crude was purified *via* flash column chromatography (1:4 ethyl acetate/cyclohexane) to yield title compound **63** as white crystalline solid (0.931 g, 3.23 mmol, 62%). M.p. 160-162 °C (ethylacetate/cyclohexane), [lit. m.p. 180 °C (ethylacetate/cyclohexane)];[63] $[\alpha]_D^{25}$ -123.2 (*c* 1.1 in $CHCl_3$), [lit. $[\alpha]_D^{20}$ -99.0 (c 1.07 in $CHCl_3$)];[63] $\nu_{max}$ (thin film): 3376 (m, br, OH), 1783 (s, C=O); $\delta_H$ (400 MHz, $CDCl_3$) 4.67 (1 H, a-t, H4, $J_{3,4}$ 2.2 $J_{4,5}$ 2.2), 4.42 (1 H, dd, H3, $J_{3,4}$ 2.4, $J_{2,3}$ 0.6), 4.31 (1 H, ddd, H6, $J_{5,6}$ 8.4, $J_{6,7}$ 6.2, $J_{6,7'}$ 4.0), 4.16 (1 H, d, H2, $J_{2,OH}$ 2.9), 4.10 (1 H, dd, H7, $J_{7,7'}$ 8.9, $J_{6,7}$ 6.2), 3.94 (1 H, dd, H7, $J_{7,7'}$ 8.9, $J_{6,7}$ 4.0), 3.86 (1 H, dd, H5, $J_{5,6}$ 8.4, $J_{4,5}$ 2.0), 3.36 (1 H, d, OH, $J_{2,OH}$ 3.3), 1.47 (3 H, s, C$\underline{H}_3$), 1.44 (3 H, s, C$\underline{H}_3$), 1.36 (3 H, s, C$\underline{H}_3$), 1.35 (3 H, s, C$\underline{H}_3$); $\delta_C$ (101 MHz, $CDCl_3$) 175.3 (C1),

109.6 (6,7-$\underline{C}(CH_3)_2$), 98.2 (3,5-$\underline{C}(CH_3)_2$), 73.9 (C6), 73.5 (C2), 72.4 (C4), 72.1 (C3), 69.5 (C5), 67.0 (C7), 28.9 (C($\underline{C}H_3)_2$), 27.0 (C($\underline{C}H_3)_2$), 25.0 (C($\underline{C}H_3)_2$), 19.5 (C($\underline{C}H_3)_2$); *m/z* (ESI+ve): 311 ($[M+Na]^+$, 82%), 599 ($[2M+Na]^+$, 100%); HRMS (ESI+ve): Found 311.1107 ($[M+Na]^+$); $C_{13}H_{20}NaO_7$ requires 311.1101.

**2-Azido-2-deoxy-3,5:6,7-di-*O*-isopropylidene-D-*glycero*-D-*ido*-heptono-1,4-lactone 62**

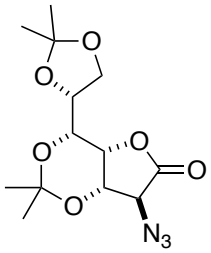

3,5:6,7-Di-*O*-isopropylidene-D-*glycero*-D-*gulo*-heptono-1,4-lactone **61** (1g, 3.47 mmol) was dissolved in dichloromethane (10 mL) and pyridine (0.8 mL, 9.9 mmol) and cooled to -30 °C. Trifluoromethanesulfonic anhydride (0.8 mL, 4.86 mmol) was added dropwise and the reaction was stirred vigorously at -30°C. After 30 min TLC analysis (1:2 ethyl acetate/cyclohexane) indicated the conversion of the starting material ($R_f$ 0.10) into a major product ($R_f$ 0.50). The reaction was diluted in dichloromethane (100 mL) and washed with 2 M aq. hydrochloric acid (30 mL). The aqueous layer was extracted with dichloromethane (2 x 40 mL) and the combined organic fractions were washed with 50% brine (60 mL), dried (magnesium sulfate) and concentrated *in vacuo* at 14 °C to yield the crude triflate as a white crystalline solid (1.48 g, quant) which was used without further purification in the following reaction. The triflate was dissolved in *N*,*N*-dimethylformamide (6 mL, 240 mg/mL), cooled to -15 °C in an ice/salt bath and sodium azide (329 mg 5.1 mmol) was added portionwise. Over 15.5 h the reaction warmed to +6°C and TLC analysis (1:2 ethyl acetate/cyclohexane) showed that the starting material **61** ($R_f$ 0.50) had been converted into a major species **62** ($R_f$ 0.60) with trace amounts of the *gulo*-azide **60** ($R_f$ 0.40) being present. The reaction mixture was diluted with ethyl acetate (120 mL) which had been cooled to +4°C, washed quickly with 50% aq brine (4x 120 mL), dried ($MgSO_4$)

and evaporated to dryness to give the crude product as an off white solid (1.106 g, quant). Column chromatography (8:1 cyclohexane/ethyl acetate) was used to purify the crude reaction residue to yield the title compound **62** as a white crystalline solid (1.01 g, quant) along with a trace of the *gulo*-azide **60** (29 mg, 3%). M.p. 102-104 °C (Diethylether/cyclohexane), [lit. m.p. 102 °C][54], $[\alpha]_D^{25}$ -216.0 (*c* 1.78 in $CHCl_3$), [lit. $[\alpha]_D^{22}$ -224 (*c* 1.0 in $CHCl_3$)][64]; $\nu_{max}$ (thin film): 2116 (s, $N_3$), 1787 (s, C=O); $\delta_H$ (400 MHz, $CDCl_3$) 4.51 (1 H, a-t, H4, $J_{3,4}$=$J_{4,5}$=2.2), 4.33 – 4.25 (2 H, m, H3, H6), 4.09 (1 H, dd, H7, $J_{7,7'}$ 8.9, $J_{6,7}$ 6.2), 4.06 (1 H, s, H2), 3.92 (1 H, dd, H7', $J_{7,7'}$ 8.9, $J_{6,7'}$ 4.0), 3.81 (1 H, dd, H5, $J_{5,6}$ 8.5, $J_{4,5}$ 2.0), 1.45 (3 H, s, C$\underline{H}_3$), 1.44 (3 H, s, C$\underline{H}_3$), 1.36 (3 H, s, C$\underline{H}_3$), 1.35 (3 H, s, C$\underline{H}_3$); $\delta_C$ (101 MHz, $CDCl_3$) 171.1 (C1), 109.9 (6,7-$\underline{C}(CH_3)_2$), 98.8 (3,5-$\underline{C}(CH_3)_2$), 73.8 (C6), 72.4 (C4), 70.8 (C3), 69.5 (C5), 67.1 (C7), 63.4 (C2), 29.0 (C($\underline{C}H_3)_2$), 27.1 (C($\underline{C}H_3)_2$), 25.0 (C($\underline{C}H_3)_2$), 19.6 (C($\underline{C}H_3)_2$); *m/z* (ESI+ve): 336 ($[M+Na]^+$, 100%), 649 ($[2M+Na]^+$, 80%); HRMS (ESI+ve): Found 336.1167 ($[M+Na]^+$); $C_{13}H_{19}N_3NaO_6$ requires 336.1166.

**2-Azido-2-deoxy-3,5:6,7-di-*O*-isopropylidene-D-*glycero*-D-*gulo*-heptono-1,4-lactone 60**

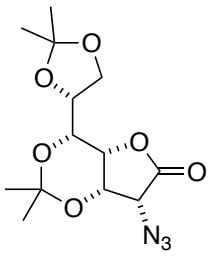


**Method A** (*via* inverted alcohol): 3,5:6,7-Di-*O*-isopropylidene-D-*glycero*-D-*ido*-heptono-1,4-lactone **63** (500 mg, 1.73 mmol) was dissolved in dichloromethane (5 mL) and pyridine (0.35 mL, 4.33 mmol) and cooled to -30 °C. Trifluoromethanesulfonic anhydride (0.41 mL, 2.43 mmol) was added dropwise and the reaction was stirred vigorously at -30 °C. After 30 min TLC analysis (1:2 ethyl acetate/cyclohexane) indicated the conversion of the starting material ($R_f$ 0.20) into a major product ($R_f$ 0.65). The reaction was diluted in dichloromethane (850 mL) and

washed with 2 M aq. hydrochloric acid (20 mL). The aqueous layer was extracted with dichloromethane (2 x 30 mL) and the combined organic fractions were washed with 50% brine (100 mL), dried (magnesium sulfate) and concentrated *in vacuo* to yield the crude triflate as a white crystalline solid (726 mg, quant) which was used without further purification in the following reaction. The triflate (727 mg, 1.72 mmol) was redissolved in dimethylformamide (5 mL) and cooled to -18 °C in an ice/salt bath. Sodium azide (124 mg, 1.90 mmol) was added to the reaction and it was left to react for 17 h at -18 to +5 °C. TLC analysis (1:2 ethyl acetate/cyclohexane) indicated complete consumption of starting triflate ($R_f$ 0.65) and the presence of two major species and a minor impurity. The major spots are the *ido*-azide **62** ($R_f$ 0.60) and the title compound *gulo*-azide **60** ($R_f$ 0.40) with minor amounts of *gulo*-triflate ($R_f$ 0.50). The reaction mixture was diluted with ethyl acetate (50 mL) and extracted with 50% aq. brine (4x 50 mL). The organic fraction was dried (magnesium sulfate) and evaporated to dryness on a rotary evaporator at RT. Purification by column chromatography (5:1 cyclohexane/ethyl acetate) yielded the *ido*-azide **62** (201 mg, 0.64 mmol, 37%) along with the title compound *gulo*-azide **60** (313 mg, 1.0 mmol, 58%).

**Method B** (*via* equilibration): Pyridinium *p*-toluenesulfonate (201 mg, 0.80 mmol) and sodium azide (62 mg, 0.96 mmol) was added to a stirred solution of 2-*O*-azido-2-deoxy-3,5:6,7-di-*O*-isopropylidene-D-*glycero*-D-*ido*-heptono-1,4-lactone **62** (220 mg, 0.70 mmol) in dry *N*,*N*-dimethylformamide (2 mL, 100 mg/mL) at RT and stirred vigorously. The reaction was monitored *via* TLC (1:2 ethyl acetate/cyclohexane) and after 97.5 h the major species was the title compound **60** ($R_f$ 0.40) with trace amounts of the starting epimer remaining **62** ($R_f$ 0.60). The reaction mixture was diluted with ethyl acetate (20 mL) and washed with 50% brine (4x 20 mL). The organic layer was dried (magnesium sulfate) and evaporated to dryness to yield the crude product (227 mg, quant). Column chromatography (6:1 → 3:1 cyclohexane/ethyl acetate) yielded the title compound **60** (206 mg, 0.66 mmol, 94%) along with some retained azide **62** (16

mg, 0.05 mmol, 6%). M.p. 153-155 °C (Isopropyl alcohol/cyclohexane); $[\alpha]_D^{25}$ -91.8 (*c* 1.09 in $CHCl_3$); $\nu_{max}$ (thin film): 2115 (s, $N_3$), 1777 (s, C=O); $\delta_H$ (400 MHz, $CDCl_3$) 4.70 (1 H, dd, H3, $J_{2,3}$ 3.9, $J_{3,4}$ 2.1), 4.35 (1 H, a-t, H4, $J_{4,5}$=$J_{3,4}$= 2.1), 4.32 (1 H, ddd, H6, $J_{5,6}$ 8.6, $J_{6,7}$ 6.0, $J_{6,7'}$ 3.8), 4.11 (1 H, dd, H7, $J_{7,7'}$ 9.0, $J_{6,7}$ 6.0), 3.95 (1 H, d, H2, $J_{2,3}$ 3.9), 3.93 (1 H, dd, H7', $J_{7,7'}$ 9.0, $J_{6,7'}$ 3.8), 3.83 (1 H, dd, H5, $J_{5,6}$ 8.6, $J_{4,5}$ 2.1), 1.50 (3 H, s, C$\underline{H}_3$), 1.43 (6 H, s, 2x C$\underline{H}_3$), 1.35 (3 H, s, C$\underline{H}_3$); $\delta_C$ (101 MHz, $CDCl_3$) 170.6 (C1), 109.9 (6,7-$\underline{C}(CH_3)_2$), 99.1 (3,5-$\underline{C}(CH_3)_2$), 73.3 (C6), 70.1 (C4), 70.0 (C3), 69.7 (C5), 67.1 (C7), 61.7 (C2), 28.8 (C($\underline{C}H_3)_2$), 27.1 (C($\underline{C}H_3)_2$), 25.0 (C($\underline{C}H_3)_2$), 19.6 (C($\underline{C}H_3)_2$); *m/z* (ESI+ve): 336 ($[M+Na]^+$, 100%), 649 ($[2M+Na]^+$, 99%); HRMS (ESI+ve): Found 336.1162 ($[M+Na]^+$); $C_{13}H_{19}N_3NaO_6$ requires 336.1166.

**2-Azido-2-deoxy-3,5-*O*-isopropylidene-D-*glycero*-D-*gulo*-heptono-1,4-lactone 64**

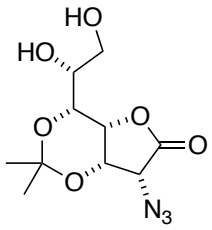


Iodine (30 mol%, 12 mg) was added to a solution of *gulo*-azide **60** (58 mg, 0.19 mmol) in acetonitrile (1 mL) and after addition of water (23 μL) the reaction was stirred at RT for 5 h. After this reaction time TLC analysis (3:1 ethyl acetate/cyclohexane) indicated that the starting material ($R_f$ 0.75) and the title product were present ($R_f$ 0.10) in a 1:1 ratio. More iodine (12 mg, now 60 mol%) was added to the reaction and it was left to stir for 16 h. TLC analysis indicated now complete disappearance of the starting material and the title compound was the major species of the reaction. Sat. aqu. sodium thiosulphate (5 mL) was added to the reaction mixture and the solution was extracted with ethyl acetate (3 x 20 mL). The organic layer was dried (magnesium sulphate), filtered and evaporated to dryness to yield the crude reaction product **64** as a off white crystalline solid (49 mg, 0.18 mmol, 95%) which was used without prior purification in the next reaction step. M.p. 171-173°C; $[\alpha]_D^{25}$ -81.6 (*c* 0.53 in MeOH); $\nu_{max}$ (thin

film): 3400 (m, br, OH), 2120 (s, $N_3$), 1775 (s, C=O); $\delta_H$ (400 MHz, MeOD) 4.82 (1 H, dd, H3, $J_{2,3}$ 3.9, $J_{3,4}$ 2.1), 4.53 (1 H, a-t, H4 $J_{3,4}$=$J_{4,5}$ 2.1), 4.31 (1 H, d, H2, $J_{2,3}$ 3.9), 4.09 (1 H, dd, H5, $J_{5,6}$ 9.1, $J_{4,5}$ 1.8), 3.78 (1 H, ddd, H6, $J_{5,6}$ 9.1, $J_{6,7'}$ 4.8, $J_{6,7}$ 2.5), 3.72 (1 H, dd, H7, $J_{7,7'}$ 11.5, $J_{6,7}$ 2.5), 3.59 (1 H, dd, H7', $J_{7,7'}$ 11.5, $J_{6,7'}$ 4.8), 1.53 (3 H, s, C$\underline{H}_3$), 1.38 (3 H, s, C$\underline{H}_3$); $\delta_C$ (101 MHz, MeOD) 173.5 (C1), 100.1 (C(CH$_3$)$_2$), 72.0, 71.9 (C3, C4), 70.7 (C6), 69.0 (C5), 63.7 (C7), 63.0 (C2), 29.2 (C(CH$_3$)$_2$), 19.6 (C(CH$_3$)$_2$); *m/z* (ESI+ve): 296 ([M+Na]$^+$, 100%), 569 ([2M+H]$^+$, 56%); HRMS (ESI+ve): Found 296.0853 ([M+Na]$^+$); $C_{10}H_{15}N_3NaO_6$ requires 296.0853.

**2-Azido-7-*O*-*tert*-butyldimethylsilyl-2-deoxy-3,5-*O*-isopropylidene-D-*glycero*-D-*gulo*-heptono-1,4-lactone 65**

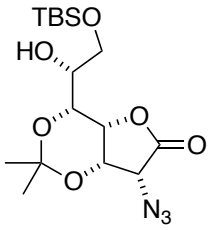


A solution of *tert*-butyldimethylsilylchloride (35 mg, 0.23 mmol) and imidazole (18 mg, 0.27 mg) in dry dimethylformamide (1 mL) was added to a stirred solution of diol **64** (49 mg, 0.18 mmol) in dimethylformamide (2 mL) at 0 °C. Over the course of 31 h an additional 7 eq. of both *tert*-butyldimethylsilylchloride and imidazole along with 3 Å sieves were added and after this time TLC analysis (1:1 cyclohexane/ethyl acetate) showed no remaining starting material ($R_f$ 0.10) and formation of a new species ($R_f$ 0.60). The reaction mixture was filtered through a glass fibre pad and washed with ethyl acetate (30 mL) and 50% brine (30 mL). The biphasic filtrate was transferred to a separation funnel and the organic layer was washed with 50% brine (2 x 30 mL). The organic layer was dried (magnesium sulfate), filtered and evaporated to dryness. The crude reaction product was purified using flash column chromatography (3:1 cylcohexane/ethyl acetate) and the title compound **65** was isolated as a clear oil (57 mg, 0.15 mmol, 84%). $[\alpha]_D^{25}$ -34.1 (*c* 2.63 in $CHCl_3$); $\nu_{max}$ (thin film): 2118 (s, $N_3$), 1789 (s, C=O); $\delta_H$ (400 MHz, $CDCl_3$) 4.70

(1 H, dd, H3, $J_{2,3}$ 3.9, $J_{3,4}$ 2.2), 4.47 (1 H, a-t, H4, $J_{3,4}$=$J_{4,5}$ 2.0), 4.00 (1 H, d, H2, $J_{2,3}$ 3.9), 3.97 (1 H, dd, H5, $J_{5,6}$ 9.0, $J_{4,5}$ 1.9), 3.87 (1 H, a-dt, H6, $J_{5,6}$ 9.0, $J_{6,7}$ 3.1), 3.74 (2 H, a-d, H7, H7', $J_{6,7}$ 3.1), 1.47 (3 H, s, C$\underline{H}_3$), 1.40 (3 H, s, C$\underline{H}_3$), 0.89 (9 H, s, SiC(C$\underline{H}_3$)$_3$), 0.07 (3 H, s, SiCH$_3$), 0.06 (3 H, s, SiCH$_3$); $\delta_C$ (101 MHz, $CDCl_3$) 171.1 (C1), 98.9 ($\underline{C}(CH_3)_2$), 70.4, 70.2 (C3,C4), 69.1 (C6), 67.5 (C5), 62.4 (C7), 61.8 (C2), 28.8 (C($\underline{C}H_3)_2$), 25.9 (SiC$\underline{Me}_3$), 19.4 (C($\underline{C}H_3)_2$), 18.4 (Si$\underline{C}Me_3$), -5.3 (Si$\underline{C}H_3$), -5.4 (Si$\underline{C}H_3$); *m/z* (ESI+ve): 410 ([M+Na]$^+$, 78%), 798 ([2M+H]$^+$, 100%); HRMS (ESI+ve): Found 410.1711 ([M+Na]$^+$); $C_{16}H_{29}N_3NaO_6Si$ requires 410.1718.

**2-Azido-7-*O*-*tert*-butyldimethylsilyl-2-deoxy-3,5-*O*-isopropylidene-D-*gulo*-6-heptulosono-1,4-lactone 66**

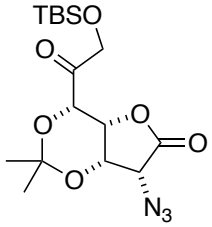


Alcohol **65** (127 mg, 0.33 mmol) was dissolved in dichloromethane (3 mL) and Dess Martin Periodinane (210 mg, 0.5 mmol) was added whilst cooled to 0 °C. After 10 min the reaction was allowed to heat to RT whilst being stirred vigorously. After 18 h TLC (9:1 toluene/acetone, product streaks) all the starting material had been consumed ($R_f$ 0.20) and the reaction showed a major product ($R_f$ 0.35). The milky white reaction mixture was diluted with ethyl acetate (15 mL) and stirred vigorously with sat. aq. sodium bicabonate/sodium thiosulfate (10g / 100 ml) (15 mL) until it cleared with the aqueous layer turning a light yellow. The organic layer was washed twice with sat. aq. sodium bicabonate/sodium thiosulfate (10g / 100 ml) (15 mL), dried (magnesium sulfate) and evaporated to dryness to yield the crude product **66** as a white crystalline solid (116 mg, 0.30 mmol, 91%). M.p. 138-140 °C (phase change: 115 °C); $[\alpha]_D^{25}$ -148.2 (*c* 2.07 in $CHCl_3$); $\nu_{max}$ (thin film): 2118 (s, $N_3$), 1792 (s, OC=O), 1743 (m, C=O); $\delta_H$ (400 MHz, $CDCl_3$) 4.74 (1 H, dd, H3, $J_{2,3}$ 3.9, $J_{3,4}$ 2.2), 4.65 (1 H, d, H5, $J_{4,5}$ 2.2), 4.62 (2 H, a-d, H7,

H7', *J* 3.7), 4.56 (1 H, a-t, H4, $J_{4,5}$=$J_{3,4}$ 2.2), 3.95 (1 H, d, H2, $J_{2,3}$ 3.9), 1.54 (3 H, s, C$\underline{H}_3$), 1.52 (3 H, s, C$\underline{H}_3$), 0.92 (9 H, s, SiC(C$\underline{H}_3$)$_3$), 0.11 (3 H, s, SiC$\underline{H}_3$), 0.10 (3 H, s, SiC$\underline{H}_3$); $\delta_C$ (101 MHz, $CDCl_3$) 204.3 (C6), 170.0 (C1), 99.4 (C(CH$_3$)$_2$), 73.5 (C5), 70.2 (C4), 70.0 (C3), 68.3 (C7), 61.4, (C2) 28.7 (C(CH$_3$)$_2$), 25.9 (SiC(CH$_3$)$_3$), 19.1 (C(CH$_3$)$_2$), 18.52 (SiC(CH$_3$)$_3$), -5.13 (SiCH$_3$), -5.40 (SiCH$_3$); *m/z* (ESI+ve): 793 ([2M+Na]$^+$, 100%), 1027 ([2M+Na+MeOH]$^+$, 91%); HRMS (ESI+ve): Found 408.1559 ([M+Na]$^+$); $C_{16}H_{27}N_3NaO_6Si$ requires 408.1561.

### 2.6.4 Biological evaluation and molecular modeling

#### 2.6.4.1 In house enzymatic evaluation

##### *2.6.4.1.1 Cell culture*

Tissue culture media and supplies were purchased from PAA (Pashing, Austria). The human acute amyloid leukemia cell line HL-60 (ATCC, Cat. No. CCL-240) was cultured in RPMI 1640 medium containing 10% fetal calf serum, 100 units/mL of penicillin and 100 μg/mL streptomycin (PAA) at 37 °C and 5% $CO_2$. The suspension cell line was maintained at a subculture ration of 1:10. Cell viability was checked using Trypan Blue (Sigma Aldrich).

##### *2.6.4.1.2 Materials and methods enzymatic evaluation*

Before use, enzyme solutions were thawed at RT, then put on ice. The solutions were stored at -20 °C. Inhibitors were dissolved in deionized water to a stock concentration of 50 mM. These solutions were stored at RT. Enzyme substrate solutions were generated by dissolving the appropriate mass in 50 mM citrate/citric acid buffer, pH 5.0 at a concentration of 4 mM. These were stored at 4 °C. Assays were carried out in triplicate, using water in place of the inhibitor as a positive control and both enzyme and inhibitor replaced with water were used as blank to determine the background of the experiment. Linearity over the time course of the reaction was confirmed using a series of incubation times.

**α-*N*-Acetyl-D-galactosaminidase assay:**

Materials: Enzyme α-*N*-acetyl-D-galactosaminidase (*Charonia lampas*) purified from the natural sources (Oxford Glycobiology Institute) in 50 mM citrate–phosphate buffer at pH 5 containing 1 mg/mL bovine serum albumin (BSA) and 0.02% sodium azide. Substrate *p*-nitrophenyl-2-acetamido-2-deoxy-α-D-galactopyranoside (Koch-Light Ltd.). Method: Enzyme (5μL) and inhibitor solution (5μL) were added to a 96-well microtitre plate which was pre-incubated at 37 °C for 5 min before starting the reaction by addition of 40 μL of the substrate solution. After a further 40 min of incubation at 37 °C the reaction was quenched by the addition of 200 μL of 0.5 M sodium carbonate (aq.). Absorbance at 405 nm was measured immediately using a microtitre plate reader (Molecular Devices UVmax kinetic microplate reader and SOFTmax 2.35 software).

**β-*N*-Acetyl-D-hexosaminidase assay:**

Material: β-*N*-acetyl-D-hexosaminidase activity in a HL-60 cell homogenate was used. The homogenate was generated from washed cells (human promyelocytic leukemia cells), which were centrifuged into a pellet from phosphate buffered saline. The cell pellet was then lysed in deionized $H_2O$ (1.5 mL) using a glass dounce homogeniser and following centrifugation at 500 x g for 5 min at 4 °C, the supernatant was removed and used as enzyme source. Sodium azide was added to a final concentration of 0.02%. Substrate 4-methylumbelliferyl-*N*-acetyl-β-D-glucosaminide (Sigma). Method: A similar protocol as described above was used but fluorescence was measured using a microtitre plate reader (Molecular Devices SPECTRAmax M5 Rom v2.1.35, Ex. 355 nm, Em. 460 nm, Cutoff 455 nm).

#### *2.6.4.1.3 Data analysis – $IC_{50}$ and Ki*

$IC_{50}$ values: Percentage inhibition was plotted against the log of the inhibitor concentration, and the data set was fitted to a four parameter Hill plot with a bottom restraint of zero using Prism 4.0a for Mac. $K_i$ values: Data sets in triplicate were subjected in Prism 4.0a to a Lineweaver–Burk analysis (1/rate against 1/[Substrate concentration]) using a suitable range of substrate

solutions (4, 2, 1, 0.75, 0.5, 0.2 mM) and five or three inhibitor concentrations. The obtained slopes were plotted against the inhibitor concentration and the $K_i$ obtained from the X-axis intercept. Graphs for plotted data is shown Figure 2.10 to Figure 2.15.

#### 2.6.4.2 Glycosidase panel analysis performed by collaborators

The data for the large panel glycosidase inhibition was collected by a collaborator Prof. Atsushi Kato (University of Toyama).[56] The evaluation was performed according to the following protocol: The enzymes α-glucosidases (from rice, yeast and *Aspergillus niger*), β-glucosidases (from almond, *Aspergillus niger,* and bovine liver), α-galactosidase (from coffee bean), β-galactosidase (from bovine liver), α-mannosidase (from jack beans), α-mannosidase (from snail), α-L-fucosidase (from bovine kidney and bovine epididymis), trehalase (from porcine kidney), α-L-rhamnosidase (from *Penicillium decumbens*), amyloglucosidase (from *Aspergillus niger* and *Rhizopus* sp.), β-*N*-acetyl-glucosaminidases (from human placenta, bovine kidney, *Aspergillus oryzae*, and jack beans), α-*N*-acetyl-galactosaminidase (from chicken liver), β-*N*-acetyl-galactosaminidase (from *Aspergillus oryzae*) and *p*-nitrophenyl glycosides were purchased from Sigma Aldrich Co. The cell lysate of human acute amyloid leukemia cell line HL60 was used as the source of β-*N*-acetyl-glucosaminidase and β-*N*-acetyl-galactosaminidase. For the activity of rice α-glucosidase the reaction mixture (0.2 mL) contained 25 mM maltose and the appropriate amount of enzyme, and the incubations were performed for 10-30 min at 37 °C. The reaction was stopped by heating at 100 °C for 3 min. After centrifugation (600 g; 10 min), 0.05 mL of resulting reaction mixture was added to 3 mL of Glucose CII-test Wako (Wako Pure Chemical Ind., Osaka, Japan). The absorbance at 505 nm was measured to determine the amount of the released D-glucose. Other glycosidase activities were determined using an appropriate *p*-nitrophenyl glycoside as substrate at optimum pH of each enzyme. The reaction mixture (1 mL) contained 2 mM of the substrate and the appropriate amount of enzyme. The

reaction was stopped by adding 2 mL of 400 mM $Na_2CO_3$. The released *p*-nitrophenol was measured spectrometrically at 400 nm.

### 2.6.5 Molecular modeling

DFT calculations at the M06-2X/6-311++G** level of theory using Gaussian 09[65] were performed to evaluate the gas-phase geometries of pipecolic amides, pyrrolidines and azetidines in this chapter. Structures were rendered and overlayed as indicated in the corresponding figure description using the Maestro 9.3.5 software of the Schrödinger Suite 2012.

### 2.6.6 X-ray crystallography experimental

X-Ray diffraction data was collected on either a Nonius Kappa-CCD Diffractometer[66] (**60**) or a Oxford Diffraction/Agilent SuperNovae A[67] (**62**) using molybdenum or copper radiation respectively. The crystals were placed in the cold stream of an Oxford Cryosystems open-flow nitrogen cryostat[68] with a nominal stability of 0.1K. Cell refinement and data reduction was performed using either Denzo/scalepack[69] or CrysAlis RED.[70] The SIR92[71] program was used to solve the structures and the structures were refined in CRYSTALS.[72] For the *gulo* **60** compound in the absence of significant anomalous scattering, Friedel pairs were merged and the absolute configuration was assigned from the use of D-glycero-D-gulo-heptonolactone as the starting material. In the case of the *ido* **62** compound the absolute configuration was determined by refinement of the Flack parameter.[49, 73] The H-atoms were all located in a difference map, but those attached to carbon were repositioned geometrically. The H-atoms were initially refined with soft restraints on the bond lengths and angles to regularize their geometry (C-H in the range 0.93-0.98 A) and $U_{iso}$(H) (in the range 1.2-1.5 times $U_{eq}$ of the parent atom) after which the positions were refined with riding constraints.[74] Optimisation of weights was carried out using a Chebychev polynomial[75] for the *gulo* **60** structure and a modified Sheldrick auto-statistical method for the *ido* **62** structure. An extinction correction[76] was applied for the *gulo* **60** structure. The graphics were prepared using CAMERON.[77] Crystallographic Data (excl structure factors)

have been deposited with the Cambridge Crystallographic Data Centre (CCDC 917202 *gulo*-azide **60**, 917203 *ido*-azide **62**) and copies of the data can be obtained free of charge via www.ccdc.cam.ac.uk/data_request/cif.

## 2.7 References Chapter 2


1. Shilvock, J. P.; Nash, R. J.; Lloyd, J. D.; Winters, A. L.; Asano, N.; Fleet, G. W. J., Intermediates for incorporation of tetrahydroxypipecolic acid analogues of α- and β-D-mannopyranose into combinatorial libraries: Unexpected nanomolar-range hexosaminidase inhibitors. Synthesis of α- and β-homomannojirimycin. *Tetrahedron: Asymmetry* **1998**, *9*, 3505-3516.

2. Ladenburg, A., Ueber die Piperidincarbonsäuren. *Chem. Ber.* **1891**, *24*, 640-643.

3. Mende, F., Spaltung der Pipecolinsäure in ihre beiden optischen Componenten. *Chem. Ber.* **1896**, *29*, 2887-2889.

4. Morrison, R. I., Naturally occurring L-pipecolinic acid. *Biochem. J.* **1952**, *50*, xiv-xv.

5. Zacharius, R. M.; Thompson, J. F.; Steward, F. C., The detection, isolation and identification of (-)-pipecolic acid as a constituent of plants [11]. *J. Am. Chem. Soc.* **1952**, *74*, 2949.

6. Fowden, L., The Chemistry and Metabolism of recently isolated Amino Acids. *Annu. Rev. Biochem.* **1964**, *33*, 173-204.

7. He, M., Pipecolic acid in microbes: Biosynthetic routes and enzymes. *J. Ind. Microbiol. Biotechnol.* **2006**, *33*, 401-407.

8. Broquist, H. P., Lysine-pipecolic acid metabolic relationships in microbes and mammals. *Annu. Rev. Nutr.* **1991**, *11*, 435-448.

9. Broquist, H. P., The indolizidine alkaloids, slaframine and swainsonine: contaminants in animal forages. *Annu. Rev. Nutr.* **1985**, *5*, 391-409.

10. Rothstein, M.; Miller, L. L., The conversion of lysine to pipecolic acid in the rat. *J. Biol. Chem.* **1954**, *211*, 851-858.

11. Steinberg, S. J.; Dodt, G.; Raymond, G. V.; Braverman, N. E.; Moser, A. B.; Moser, H. W., Peroxisome biogenesis disorders. *BBA-Mol. Cell. Res.* **2006**, *1763*, 1733-1748.

12. Kadouri-Puchot, C.; Comesse, S., Recent advances in asymmetric synthesis of pipecolic acid and derivatives. *Amino Acids* **2005**, *29*, 101-130.

13. Singh, K.; Sun, S.; Vezina, C., Rapamycin (AY-22,989), a new antifungal antibiotic. IV. Mechanism of action. *J. Antibiot.* **1979**, *32*, 630-645.

14. Calne, R. Y.; Collier, D. S.; Lim, S.; Pollard, S. G.; Samaan, A.; White, D. J.; Thiru, S., Rapamycin for immunosuppression in organ allografting. *Lancet* **1989**, *2*, 227.

15. Kahan, B. D., Efficacy of sirolimus compared with azathioprine for reduction of acute renal allograft rejection: A randomised multicentre study. *Lancet* **2000**, *356*, 194-202.

16. (a) Smith III, A. B.; Condon, S. M.; McCauley, J. A.; Leazer Jr., J. L.; Leahy, J. W.; Maleczka Jr., R. E., A unified total synthesis of the immunomodulators (-)-rapamycin and (-)-27-demethoxyrapamycin: Construction of the C(21-42) perimeters. *J. Am. Chem. Soc.* **1997**, *119*, 947-961; (b) Smith III, A. B.;

Condon, S. M.; McCauley, J. A.; Leazer Jr., J. L.; Leahy, J. W.; Maleczka Jr., R. E., A unified total synthesis of the immunomodulators (-)-rapamycin and (-)-27-demethoxyrapamycin: Assembly of the common C(1-20) perimeter and final elaboration. *J. Am. Chem. Soc.* **1997**, *119*, 962-973.

17. Matson, J. A.; Bush, J. A., Sandramycin, a novel antitumor antibiotic produced by a Nocardioides sp. Production, isolation, characterization and biological properties. *J. Antibiot.* **1989**, *42*, 1763-1767.

18. Matson, J. A.; Colson, K. L.; Belofsky, G. N.; Bleiberg, B. B., Sandramycin, a novel antitumor antibiotic produced by a nocardioides sp. II. Structure determination. *J. Antibiot.* **1993**, *46*, 162-166.

19. Boger, D. L.; Chen, J.-H.; Saionz, K. W., (-)-Sandramycin: Total synthesis and characterization of DNA binding properties. *J. Am. Chem. Soc.* **1996**, *118*, 1629-1644.

20. Boger, D. L.; Chen, J.-H., An exceptionally potent analog of sandramycin. *Bioorg. Med. Chem. Lett.* **1997**, *7*, 919-922.

21. Okamoto, S.; Hijikata, A.; Kikumoto, R.; Tonomura, S.; Hara, H.; Ninomiya, K.; Maruyama, A.; Sugano, M.; Tamao, Y., Potent inhibition of thrombin by the newly synthesized arginine derivative No. 805. The importance of stereo-structure of its hydrophobic carboxamide portion. *Biochem. Biophys. Res. Commun.* **1981**, *101*, 440-446.

22. Di Nisio, M.; Middeldorp, S.; Büller, H. R., Direct thrombin inhibitors. *New Engl. J. Med.* **2005**, *353*, 1028-1040.

23. Bush, L. R., Argatroban, a selective, potent thrombin inhibitor. *Cardiovasc. Drug Rev.* **1991**, *9*, 247-263.

24. Kikumoto, R.; Tamao, Y.; Tezuka, T.; Tonomura, S.; Hara, H.; Ninomiya, K.; Hijikata, A.; Okamoto, S., Selective inhibition of thrombin by (2R,4R)-4-methyl-1-[N 2-[(3-methyl-1,2,3,4-tetrahydro-8-quinolinyl)sulfonyl]-L-arginyl]-2- piperidinecarboxylic acid. *Biochemistry* **1984**, *23*, 85-90.

25. Cossy, J.; Belotti, D., A short synthesis of argatroban: A potent selective thrombin inhibitor. *Bioorg. Med. Chem. Lett.* **2001**, *11*, 1989-1992.

26. Couty, F., Asymmetric syntheses of pipecolic acid and derivatives. *Amino Acids* **1999**, *16*, 297-320.

27. Lenagh-Snow, G. M. J.; Jenkinson, S. F.; Newberry, S. J.; Kato, A.; Nakagawa, S.; Adachi, I.; Wormald, M. R.; Yoshihara, A.; Morimoto, K.; Akimitsu, K.; Izumori, K.; Fleet, G. W. J., Eight Stereoisomers of Homonojirimycin from D-Mannose. *Org. Lett.* **2012**, *14*, 2050-3.

28. (a) Jones, N. A.; Rao, D.; Yoshihara, A.; Gullapalli, P.; Morimoto, K.; Takata, G.; Hunter, S. J.; Wormald, M. R.; Dwek, R. A.; Izumori, K.; Fleet, G. W. J., Green syntheses of new 2-C-methyl aldohexoses and 5-C-methyl ketohexoses: D-tagatose-3-epimerase (DTE)-a promiscuous enzyme. *Tetrahedron: Asymmetry* **2008**, *19*, 1904-1918; (b) Rao, D.; Yoshihara, A.; Gullapalli, P.; Morinioto, K.; Takata, G.; da Cruz, F. P.; Jenkinson, S. F.; Wormald, M. R.; Dwek, R. A.; Fleet, G. W. J.; Izumori, K., Towards the biotechnological isomerization of branched sugars: D-tagatose-3-epimerase equilibrates both enantiomers of 4-C-methyl-ribulose with both enantiomers of 4-C-methyl-xylulose. *Tetrahedron Lett.* **2008**, *49*, 3316-3321.

29. (a) Gullapalli, P.; Yoshihara, A.; Morimoto, K.; Rao, D.; Akimitsu, K.; Jenkinson, S. F.; Fleet, G. W. J.; Izumori, K., Conversion of L-rhamnose into ten of the sixteen 1-and 6-deoxyketohexoses in water with three reagents: D-tagatose-3-epimerase equilibrates C3 epimers of deoxyketoses. *Tetrahedron Lett.* **2010**, *51*, 895-898; (b) Rao, D.; Best, D.; Yoshihara, A.; Gullapalli, P.; Morimoto, K.; Wormald, M. R.; Wilson, F. X.; Izumori, K.; Fleet, G. W. J., A concise approach to the synthesis of all twelve 5-deoxyhexoses: D-tagatose-3-epimerase-a reagent that is both specific and general. *Tetrahedron Lett.* **2009**, *50*, 3559-3563.

30. Rountree, J. S. S.; Butters, T. D.; Wormald, M. R.; Dwek, R. A.; Asano, N.; Ikeda, K.; Evinson, E. L.; Nash, R. J.; Fleet, G. W. J., Efficient synthesis from D-lyxonolactone of 2-acetamido-1,4-imino-1,2,4-trideoxy-L-arabinitol LABNAc, a potent pyrrolidine inhibitor of hexosaminidases. *Tetrahedron Lett.* **2007**, *48*, 4287-4291.

31. Krulle, T.; Davis, B.; Ardron, H.; Long, D.; Hindle, N.; Smith, C.; Brown, D.; Lane, A.; Watkin, D.; Marquess, D.; Fleet, G., Kinetic and thermodynamic azides from alpha-triflates of gamma-lactones: Intermediates for the incorporation of polyhydroxylated D- and L-alpha-aminoacids into combinatorial libraries. *Chem. Commun.* **1996**, 1271-1272.

32. Fuji, T.; Miyoshi, M., A Novel Synthesis of L-pipecolic acid. *Bull. Chem. Soc. Jpn.* **1975**, *48*, 1341-1342.

33. Pal, B.; Ikeda, S.; Kominami, H.; Kera, Y.; Ohtani, B., Photocatalytic redox-combined synthesis of L-pipecolinic acid from L-lysine by suspended titania particles: Effect of noble metal loading on the selectivity and optical purity of the product. *J. Catal.* **2003**, *217*, 152-159.

34. Roos, G. H. P.; Dastlik, K. A., Highly diastereoselective alkylation of the Dellaria oxazinone template with bifunctional electrophiles. *Synth. Commun.* **2003**, *33*, 2197-2208.

35. Bruce, I.; Fleet, G.; Dibello, I.; Winchester, B., Iminoheptitols as glycosidase inhibitors - Synthesis of alpha-Homomannojirimycin, 6-epi-alpha-Homomannojirimycin and of a highly substituted pipecolic acid. *Tetrahedron* **1992**, *48*, 10191-10200.

36. Ye, X.-S.; Sun, F.; Liu, M.; Li, Q.; Wang, Y.; Zhang, G.; Zhang, L.-H.; Zhang, X.-L., Synthetic iminosugar derivatives as new potential immunosuppressive agents. *J. Med. Chem.* **2005**, *48*, 3688-3691.

37. Bruce, I.; Fleet, G.; Dibello, I.; Winchester, B., Iminoheptitols as glycosidase inhibitors - synthesis of, and mannosidase and fucosidase inhibition by, alpha-Homomannojirmycin and 6-epi-Homomannojirmycin. *Tetrahedron Lett.* **1989**, *30*, 7257-7260.

38. Kiliani, H., Ueber die Einwirkung von Blausäure auf Dextrose. *Chem. Ber.* **1886**, *19*, 767-772.

39. Bruce, I.; Fleet, G.; Girdhar, A.; Haraldsson, M.; Peach, J.; Watkin, D., Retention and apparent inversion during azide displacement of alpha-triflates of 1,5-lactones. *Tetrahedron* **1990**, *46*, 19-32.

40. Kürti, L.; Czakó, B., Staudinger Reaction. In *Strategic Applications of Named Reactions in Organic Synthesis*, Elsevier Academic Press: 2005; pp 428-429.

41. (a) Fleet, G.; Fuller, C.; Harding, P., Bis(triphenylphosphine) copper(I) tetrahydroborate in reduction of acid-chlorides to aldehydes. *Tetrahedron Lett.* **1978**, 1437-1440; (b) Sorrell, T.; Pearlman, P., Preparation of aldehydes from acid-chlorides using copper tetrahydroborate complexes. *J. Org. Chem.* **1980**, *45*, 3449-3451; (c) Sorrell, T., Correction to Preparation of aldehydes from acid-chlorides using copper tetrahydroborate complexes. *J. Org. Chem.* **1981**, *46*, 2603-2603.

42. Fleet, G.; Harding, P., Convenient Synthesis of bis(triphenylphosphine) copper(I) tetrahydroborate and reduction of acid-chlorides to aldehydes. *Tetrahedron Lett.* **1979**, 975-978.

43. Borch, R. F.; Bernstein, M. D.; Durst, H. D., The cyanohydridoborate anion as a selective reducing agent. *J. Am. Chem. Soc.* **1971**, *93*, 2897-2904.

44. Abdel-Magid, A. F.; Carson, K. G.; Harris, B. D.; Maryanoff, C. A.; Shah, R. D., Reductive amination of aldehydes and ketones with sodium triacetoxyborohydride. Studies on direct and indirect reductive amination procedures. *J. Org. Chem.* **1996**, *61*, 3849-3862.

45. Bhanushali, M. J.; Nandurkar, N. S.; Bhor, M. D.; Bhanage, B. M., Direct reductive amination of carbonyl compounds using bis(triphenylphosphine) copper(I) tetrahydroborate. *Tetrahedron Lett.* **2007**, *48*, 1273-1276.

46. Hudson, C.; Hartley, O.; Purves, C. B., A Convenient Modification of the Kiliani Synthesis of Higher Carbon Acids (or their Lactones) from Reducing Sugars1. *J. Am. Chem. Soc.* **1934**, *56*, 1248-1249.

47. Kinder, F.; Wattanasin, S.; Versace, R.; Bair, K.; Bontempo, J.; Green, M.; Lu, Y.; Marepalli, H.; Phillips, P.; Roche, D.; Tran, L.; Wang, R.; Waykole, L.; Xu, D.; Zabludoff, S., Total syntheses of bengamides B and E. *J. Org. Chem.* **2001**, *66*, 2118-2122.

48. Gomory, J.; Kacina, R.; Antalova, S.; Major, M. Method of producing α-D-glucoheptonic acid lactone. CS257827B1, Jun 15, 1988.

49. Thompson, A.; Watkin, D., CRYSTALS enhancements: absolute structure determination. *J. Appl. Cryst.* **2011**, *44*, 1017-1022.

50. The X-ray crystallgraphy was performed by Dr. S. Jenkinson at Chemical Crystallography, Chemistry Research Laboratory, 12 Mansfield Road, Oxford, OX1 3TA.

51. Yadav, J.; Satyanarayana, M.; Raghavendra, S.; Balanarsaiah, E., Chemoselective hydrolysis of terminal isopropylidene acetals in acetonitrile using molecular iodine as a mild and efficient catalyst. *Tetrahedron Lett.* **2005**, *46*, 8745-8748.

52. Buchanan, J. G.; Chacón-Fuertes, M. E.; Edgar, A. R.; Moorhouse, S. J.; Rawson, D. I.; Wightman, R. H., Assignment of ring size in isopropylidene acetals by 13C N.M.R. *Tetrahedron Lett.* **1980**, *21*, 1793-1796.

53. (a) Ireland, R. E.; Liu, L., An improved procedure for the preparation of the Dess-Martin periodinane. *J. Org. Chem.* **1993**, *58*, 2899; (b) Frigerio, M.; Santagostino, M.; Sputore, S., A user-friendly entry to 2-iodoxybenzoic acid (IBX). *J. Org. Chem.* **1999**, *64*, 4537-4538.

54. Lee, R.; Smith, M.; Nash, R.; Griffiths, R.; McNeil, M.; Grewal, R.; Yan, W.; Besra, G.; Brennan, P.; Fleet, G., Inhibition of UDP-Gal mutase and mycobacterial galactan biosynthesis by pyrrolidine analogues of galactofuranose. *Tetrahedron Lett.* **1997**, *38*, 6733-6736.

55. Mr. B. Ayers, Dr. S. Jenkinson, Dr. F. Martínez, Mr. M. Hollas, Mr. N. Ngo are acknowledged for the work on the synthesis of the pyrrolidine structures in this chapter. Chemistry Research Laboratory, 12 Mansfield Road, Oxford, OX1 3TA.

56. Prof. A. Kato, Department of Hospital Pharmacy, University of Toyama, 2630 Sugitani, Toyama 930-0194, Japan.

57. Foresman, J. B.; Frisch, Æ., Computational Models & Model Chemistries. In *Exploring Chemistry with Electronic Structure Methods*, Gaussian, Inc. : Pittsburgh, PA, 1996; pp 3-11.

58. (a) Zhao, Y.; Truhlar, D. G., The M06 suite of density functionals for main group thermochemistry, thermochemical kinetics, noncovalent interactions, excited states, and transition elements: Two new functionals and systematic testing of four M06-class functionals and 12 other functionals. *Theor. Chem. Acc.* **2008**, *120*, 215-241; (b) Zhao, Y.; Truhlar, D. G., Density functionals with broad applicability in chemistry. *Acc. Chem. Res.* **2008**, *41*, 157-167.

59. (a) Becke, A. D., Density-functional thermochemistry. III. The role of exact exchange. *J. Chem. Phys.* **1993**, *98*, 5648-5652; (b) Lee, C.; Yang, W.; Parr, R. G., Development of the Colle-Salvetti correlation-energy formula into a functional of the electron density. *Phys. Rev. B* **1988**, *37*, 785-789; (c) Stephens, P. J.; Devlin, F. J.; Chabalowski, C. F.; Frisch, M. J., Ab Initio calculation of vibrational absorption and circular dichroism spectra using density functional force fields. *J. Phys. Chem.* **1994**, *98*, 11623-11627.

60. (a) Dr. R. F. Martínez, Chemistry Research Laboratory, 12 Mansfield Road, Oxford, OX1 3TA; (b) The Research & Technological Innovation and Supercomputing Center of Extremadura (CenitS) is gratefully acknowledged for permitting the use of the super-computer LUSITANIA.

61. Araújo, N.; Jenkinson, S. F.; Martínez, R. F.; Glawar, A. F. G.; Wormald, M. R.; Butters, T. D.; Nakagawa, S.; Adachi, I.; Kato, A.; Yoshihara, A.; Akimitsu, K.; Izumori, K.; Fleet, G. W. J., Synthesis from D-altrose of (5 R,6 R,7 R,8 S)-5,7-dihydroxy-8- hydroxymethylconidine and 2,4-dideoxy-2,4-imino-D-glucitol, azetidine analogues of swainsonine and 1,4-dideoxy-1,4-imino-D-mannitol. *Org. Lett.* **2012**, *14*, 4174-4177.

62. Lenagh-Snow, G. M. J.; Araujo, N.; Jenkinson, S. F.; Martinez, R. F.; Shimada, Y.; Yu, C.-Y.; Kato, A.; Fleet, G. W. J., Azetidine Iminosugars from the Cyclization of 3,5-Di-O-triflates of alpha-Furanosides and of 2,4-Di-O-triflates of beta-Pyranosides Derived from Glucose. *Org. Lett.* **2012**, *14*, 2142-2145.

63. Bichard, C.; Brandstetter, T.; Estevez, J.; Fleet, G.; Hughes, D.; Wheatley, J., Complex tetrahydrofurans from carbohydrate lactones: Easy access to epimeric C-glycosides of glucofuranose from D-glycero-D-gulo-heptono-1,4-lactone. *J. Chem. Soc. Perk. T. 1* **1996**, 2151-2156.

64. De La Fuente, C.; Krülle, T. M.; Watson, K. A.; Gregoriou, M.; Johnson, L. N.; Tsitsanou, K. E.; Zographos, S. E.; Oikonomakos, N. G.; Fleet, G. W. J., Glucopyranose spirohydantoins: Specific inhibitors of glycogen phosphorylase. *Synlett* **1997**, 485-487.

65. Frisch, M. J.; Trucks, G. W.; Schlegel, H. B.; Scuseria, G. E.; Robb, M. A.; Cheeseman, J. R.; Scalmani, G.; Barone, V.; Mennucci, B.; Petersson, G. A.; Nakatsuji, H.; Caricato, M.; Li, X.; Hratchian, H. P.; Izmaylov, A. F.; Bloino, J.; Zheng, G.; Sonnenberg, J. L.; Hada, M.; Ehara, M.; Toyota, K.; Fukuda, R.; Hasegawa, J.; Ishida, M.; Nakajima, T.; Honda, Y.; Kitao, O.; Nakai, H.; Vreven, T.; Montgomery, J., J. A.; Peralta, J. E.; Ogliaro, F.; Bearpark, M.; Heyd, J. J.; Brothers, E.; Kudin, K. N.; Staroverov, V. N.; Kobayashi, R.; Normand, J.; Raghavachari, K.; Rendell, A.; Burant, J. C.; Iyengar, S. S.; Tomasi, J.; Cossi, M.; Rega, N.; Millam, N. J.; Klene, M.; Knox, J. E.; Cross, J. B.; Bakken, V.; Adamo, C.; Jaramillo, J.; Gomperts, R.; Stratmann, R. E.; Yazyev, O.; Austin, A. J.; Cammi, R.; Pomelli, C.; Ochterski, J. W.; Martin, R. L.; Morokuma, K.; Zakrzewski, V. G.; Voth, G. A.; Salvador, P.; Dannenberg, J. J.; Dapprich, S.; Daniels, A. D.; Farkas, Ö.; Foresman, J. B.; Ortiz, J. V.; Cioslowski, J.; Fox, D. J. *Gaussian 09, Revision C.01*, Gaussian, Inc.: Wallingford CT, 2010.

66. Nonius, B. V. *COLLECT*, Delft, the Netherlands, 2001.

67. *Gemini User Manual*, Oxford Diffraction Ltd: Abingdon, UK, 2006.

68. Cosier, J.; Glazer, A., A nitrogen-gas-stream cryostat for general X-ray diffraction studies. *J. Appl. Cryst.* **1986**, *19*, 105-107.

69. Otwinowski, Z.; Minor, W., Processing of X-ray diffraction data collected in oscillation mode. *Methods Enzymol.* **1997**, *276*, 307-326.

70. *CrystAlis RED*, Oxford Diffraction Ltd: Abingdon, UK, 2002.

71. Altomare, A.; Cascarano, G.; Giacovazzo, C.; Guagliardi, A.; Burla, M.; Polidori, G.; Camalli, M., SIRPOW.92 - a program for automatic solution of crystal structures by direct methods optimized for powder data. *J. Appl. Cryst.* **1994**, *27*, 435-436.

72. Betteridge, P.; Carruthers, J.; Cooper, R.; Prout, K.; Watkin, D., CRYSTALS version 12: software for guided crystal structure analysis. *J. Appl. Cryst.* **2003**, *36*, 1487.

73. (a) Flack, H., On enantiomorph-polarity estimation. *Acta Crystallogr. Sect. A: Found. Crystallogr.* **1983**, *39*, 876-881; (b) Flack, H. D.; Bernardinelli, G., Reporting and evaluating absolute-structure and absolute-configuration determinations. *J. Appl. Cryst.* **2000**, *33*, 1143-1148; (c) Thompson, A. L.; Watkin, D. J.; Gal, Z. A.; Jones, L.; Hollinshead, J.; Jenkinson, S. F.; Fleet, G. W. J.; Nash, R. J., The absolute configuration of 1-epialexine hemihydrate. *Acta Crystallogr. Sect. C: Cryst. Struct. Commun.* **2008**, *64*, o649-o652; (d) Thompson, A. L.; Watkin, D. J., X-ray crystallography and chirality: understanding the limitations. *Tetrahedron: Asymmetry* **2009**, *20*, 712-717.

74. Cooper, R.; Thompson, A.; Watkin, D., CRYSTALS enhancements: dealing with hydrogen atoms in refinement. *J. Appl. Cryst.* **2010**, *43*, 1100-1107.

75. (a) Watkin, D., The control of difficult refinements. *Acta Crystallogr. Sect. A: Found. Crystallogr.* **1994**, *50*, 411-437; (b) Prince, E., *Mathematical Techniques in Crystallography and Material Science*. Springer-Verlag: New York, 1982.

76. Larsen, A. C., *Crystallographic Computing*. Munksgaard: Copenhagen, 1970; p 291-294.

77. Watkin, D. J.; Prout, C. K.; Pearce, L. J. *CAMERON*, Oxford, UK, 1996.

# 3 AZETIDINES – 4 MEMBERED IMINOSUGARS

## 3.1 Introduction to Azetidine systems

### 3.1.1 Overview

This chapter focuses on azetidines, 4-membered heterocycles containing nitrogen. L-Azetidine-2-carboxylic acid L-Aze or Aze **83L** represents the lower homologue of proline. The aim of the work described in this project was to explore novel chemical space by devising synthetic routes to polyhydroxylated analogues of Aze and to test these iminosugars for glycosidase inhibition. Figure 3.1 shows all 8 possible stereoisomers of the scaffold in question and based on the molecular modeling presented in the preceeding chapter the enantiomeric pair in the *ribo*-configuration **78** along with the D-*lyxo* derivative **79D** were chosen as synthetic targets.

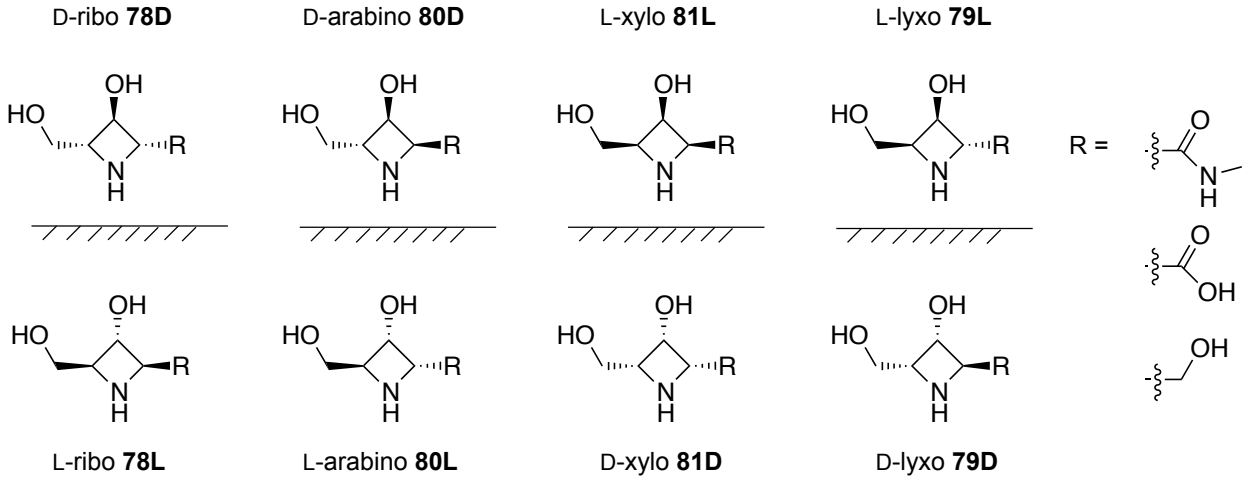


**Figure 3.1** All possible stereoisomers of polyhydroxylated aztidine-2-carboxylic acid. Numbering refers to methyl amide derivative.

There are many excellent reviews, which have investigated the synthesis of azetidines and therefore I have focused on giving an overview of the biological properties of azetidines, which encompases both natural products and synthetic agents. I will however cover some synthetic approaches towards azetidines and azetidine containing peptides.

### 3.1.2 Physical properties of azetidines

Azetidines, like the most simple derivative **82**, are rigid, slightly puckered heterocycles (Figure 3.2).[1] Depending on the substitution pattern the pucker can deviate between 10-20° from planarity and Aze **83L** e.g. shows a pucker of 11° between the two planes defined by C3-C4-N and C3-C2-N as determined by X-ray crystallography.[2] The ring strain in the azetidine ring has been experimentally estimated to be 25.2 kcal/mol, while the 5-membered and 6-membered analogues are 5.8 kcal/mol and 0 kcal/mol respectively.[1] Despite this difference the $pK_a$ of an azetidine (11.29) is quite similar to that of a pyrrolidine (11.31) and azetidines behave like secondary amines in many reactions. Similarly the $pK_a$ of Aze is 1.76 for the carboxylic acid and 10.25 for the imino group[3] and therefore quite comparable to proline with 1.99 and 10.60.[4]

When the ring nitrogen is involved in an amide bond the ring conformation becomes practically planar. This can be the case if the carbonyl is part of the ring system like in β-lactam **84** or if the carbonyl is exocyclic as for the Boc protected analogue of Aze **85L**.[5] The same planarity has been observed in NMR studies of *N*-acetyl-Aze.[6] This result is important to keep in mind, when Aze and derivatives are part of protein structures, as the ring puckering observed in the monomer will be lost on polymer formation.

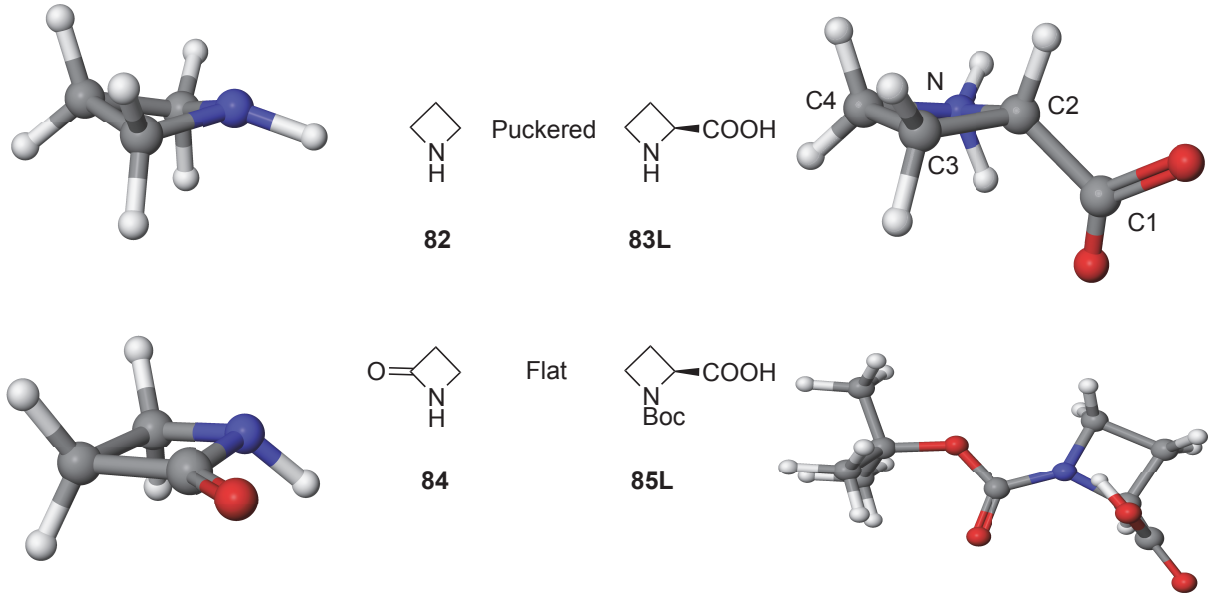


**Figure 3.2** Ring conformation of four membered ring heterocycles.

### 3.1.3 Biological aspects

The azetidine motif occurs in a rich set of biologically active molecules ranging from iron sequestering enzymes in plants for the synthesis of chlorophyll, to their presence as β-lactam antibiotics like penicillin and are part of many structures in clinical trials by major pharmaceutical firms.

#### 3.1.3.1 L-Azetidine-2-carboxylic acid – biosynthesis and misincorporation

In 1955 Fowden discovered a novel four-membered ring amino acid in *Convallaria majalis* **L**. (lily-of-the-valley, a white flowering plant used commonly at weddings e.g. the royal wedding in 2011) which by analysis methods he described as the structure of L-azetidine-2-carboxylic acid (Aze) **83L**.[7] This finding came shortly after the already mentioned first biological isolation of pipecolic acid **11L**, which had been discovered in 1952.[8] Further investigations by Fowden confirmed the structure of Aze *via* comparison to synthesised samples and discovered this amino acid in further plants of the families Liliaceae, Agavaeae and Amarylidaceae.[9] He also noticed that Aze, the lower homologue of proline **12L**, was readily misincorporated into proteins, and was able to show that nearly 50% of the newly synthesized protein in *Escherichia coli* in the

presence of Aze contained the four ring amino acid.[10] Final proof of the structure came in form of the X-ray crystal structure revealing that the compound crystallised in its zwitterionic form.[2]

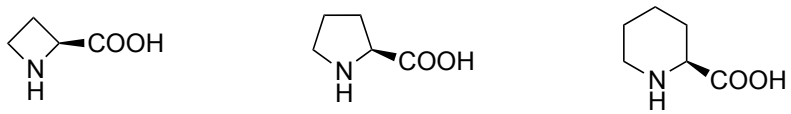


**83L** **12L** **11L**

**Figure 3.3** 6-, 5- and 4-ring amino acids

In recent times a comprehensive review on Aze was published by Couty and Evano covering both synthesis and reactivity of Aze **83L** and its derivatives.[11] The biosynthetic pathway was first probed in 1964 by Leete and using various radiolabelling experiments it was established that Aze **83L** was indeed derived from L-methionine **86L** via $S_N2$ displacement on an adenosinyl intermediate **87** (Figure 3.4).[12]

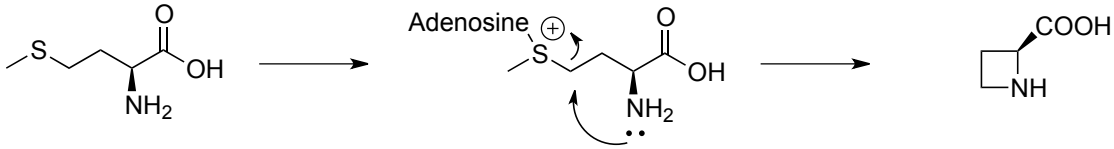


**86L** **87** Aze **83L**

**Figure 3.4** Biosynthetic pathway of Aze in *Convallaria Majalis.*

Besides the already mentioned plants, which are not fit for human consumption, Aze has also been discovered in more common food materials and routes into the human food chain. Sugar beet, required for 30% of the world's supply of sucrose, is not consumed directly by humans, but the sugar production waste products are fed in various forms to livestock, which in turn are. Relative to proline **12L**, Aze **83L** constituted up to 1.6% of these waste products and could be incorporated into protein, thus entering the food chain.[13] Furthermore Aze **83L** was discovered in rhizomes of the species *Plygonatum* which is used as food supplement e.g. in tea at concentrations of 9.23 mg/g.[14] Most prominently Aze **83L** has been revealed to be contained in beetroots at rates of up to 20% relative to proline.[15] Although the analysis method probably

requires further refinement, it should be noted that a non-protein amino acid is contained in a widely eaten food.

#### *3.1.3.1.1 Incorporation of Aze into protein triggers the heat shock response*

This is especially true as Aze **83L**, as already mentioned previously, is readily incorporated into proteins instead of proline **12L** leading to changes in conformation and often loss of function. The incorporation of Aze **83L** and other non-protein amino acids into proteins and the various resulting biological effects have been reviewed by Rubenstein.[16] It should be noted that plants presumably generate these non-protein amino acids as a method of self-defense against predators and in the case of Aze **83L** to avoid autotoxicity, they are equipped with a proline activating enzyme that is able to reject Aze **83L** and hence does not lead to Aze **83L** containing tRNA, hence avoiding protein misincorporation.[17] As early as 1973 it was noticed that Aze **83L** could be incorporated into mammalian protein, more specifically hemoglobin, in rabbit reticulocytes *in vitro*.[18] Since then it has been noted, that *Escherichia coli* recombinant protein becomes conformationally altered, if the bacteria is grown in the presence of Aze **83L**.[19] Similarly the function of the Hypoxia-inducible Transcription factor (HIF) was lost on incorporation of Aze **83L** into the protein structure in place of proline.[20] Different isoforms of HIF are constitutively expressed but quickly degraded under normoxic conditions, however replacement of a critical proline residue, the hydroxylation of which usually targets HIF for degradation via the von Hippel-Lindau E3 ubiquitin ligase complex, by Aze **83L** gave a very high rate of uncoupled 2-oxoglutarate decarboxylation. In a study probing the underlying molecular mechanisms of neurodegenerative diseases like Alzheimer's disease and Parkinson's disease Aze **83L** was used as a tool to simulate increased levels of abnormal protein in aging cells.[21] Treatment of rat neuronal and astrocyte cultures with Aze **83L** revealed an increase in TAR DNA-binding protein of 43-kDa (TDP-43), which has been implicated in protein misfolding and neural toxicity. This protein could be a novel addition to the already established upregulation of heat shock proteins

in response to Aze **83L** treatment, which has been shown amongst others in *Saccharomyces cerevisiae*.[22] Trotter et al. found that genes related to heat shock were upregulated 27-fold by treatment with Aze **83L**, when he was investigating this theory, that detection of missfolded proteins cause the heat shock response even in absence of temperature changes. In a more recent study the signaling network involved in the heat shock response, induction of cellular stress and changes in phosphorylation patterns involving the mammalian target of rapamycin complex 1 (mTORC1) were probed by Qian et al.[23]

#### *3.1.3.1.2 Incorporation of Aze into collagen*

Misincorporation of Aze **83L** instead of proline **12L** into protein leads to loss of function in some cases and stimulates the heat shock response due to presence of misfolded proteins in the cells. Such misincorporations have also been noticed for the most abundant protein in animals: collagen.[24] Collagen is a fibrous, structural protein which adopts a left handed polyproline type-II (PPII) helix structure and three individual strands coil together to form a right handed triple helix overall (Figure 3.5). This structural motif dictates every third amino acid residue in collagen to be glycine (Gly) and this results in the general repeating sequence XaaYaaGly where Xaa and Yaa can be any amino acid, however the most common ones found are proline (Pro **12L**, 28%) and (2*S*,4*R*)-4-hydroxyproline (Hyp **88**, 38%).[24] As a result the most common observed repeating triplet is ProHypGly and 22% of all residues found in human collagen are either Pro **12L** or Hyp **88**. The PPII helix was first described in 1955 based on a polymer of L-proline **12L**, has *trans*-amide bonds between all its constituent amino acids and hydrogen bonds to maintain the triple helix superstructure.[25]

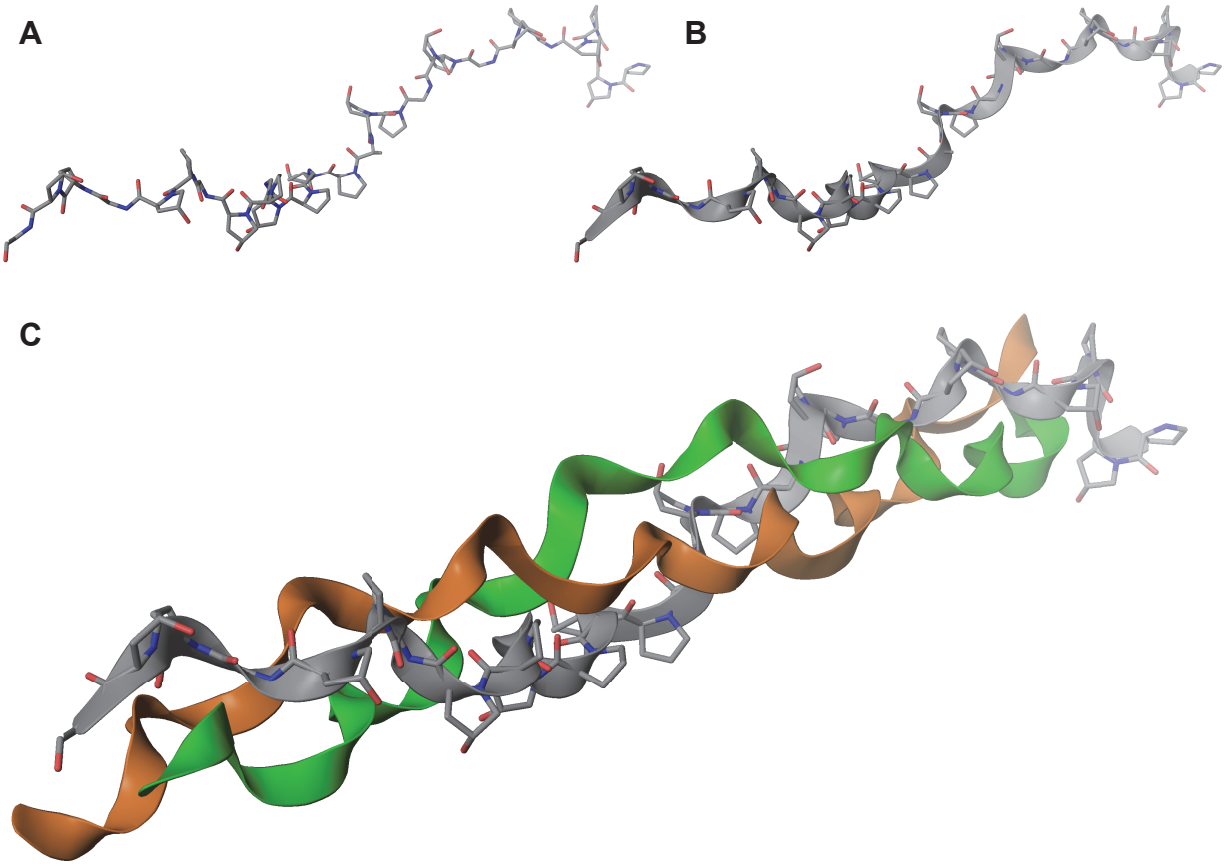


**Figure 3.5** Crystal structure representation of a collagen-like molecule at 1.9 Å according to PDB entry 1CAG: A) Left handed poly proline II helix (PPII) in tube representation; B) Ribbon representation of same helix overlayed on tube representation; C) Three PPII helixes complex together to form a left handed triple helix.

In general substituents on the proline ring can help the triple helix formation process by preorganization of the helix. In the Yaa position C*γ-exo* ring pucker of Pro **12L** is preferred, whilst the Xaa position requires Pro **12L** to adopt the C*γ-endo* ring pucker (Figure 3.6). The C*γ-endo* conformation is preferred by Pro **12L** roughly two fold over C*γ-exo* and this effect is strongly increased by the introduction of fluorine in a *cis* position at C4. On the other hand a hydroxyl group in a *trans* position at C4 favours the C*γ-exo* conformation. The underlying rationale for the adoption of these conformations by the proline derivatives are believed to be stereoelectronic effects. One of the possible explanation is hyperconjugation e.g. in the case of *trans*-4-hydroxyproline the donation of the σ(Cβ–H) and σ(Cδ–H) into the σ∗(Cγ–O).[26]

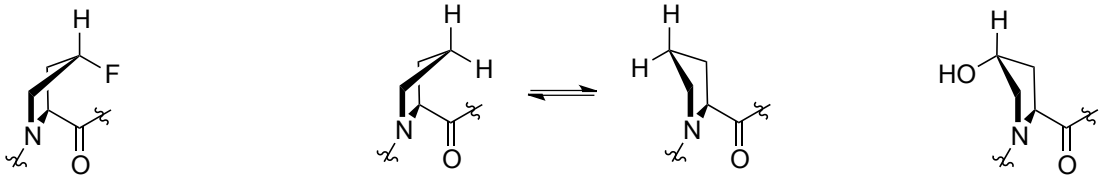


*cis*-4-fluoroproline prefers the *endo* conformation | Cγ-*endo* pucker preferred in Xaa | Cγ-*exo* pucker preferred in Yaa | *trans*-4-hydroxyproline prefers the *exo* conformation

**Figure 3.6** Ring puckering observed in proline and ring substituted derivatives of proline.

With such strict stereochemical and puckering requirements for successful assembly of the triple helix replacement of Pro **12L** with Aze **83L** would lead to disruption of correct collagen formation and this phenomenon has been investigated experimentally. Using $^{14}C$ radiolabelled Aze **83L**, the incorporation into collagen produced by chick embryonic cartilage has been proven and this incorporation in place of Pro **12L** reduced the ability of prolyl hydroxylases to convert Pro **12L** into Hyp **88**.[27] As a result the cartilage cells seem to be unable to extrude the abnormal collagen to the same degree as they would with unmodified polymer to form the extracellular matrix.[28] These *in vitro* studies were followed up by treatment of chick embyos for a 5 day period with 500 μg of Aze **83L** a day; it was found that the proline analogue arrested the accumulation of collagen and led to a significant increase in the fragility of the embryos.[29] Analysis *via* electron microscopy showed a marked decrease in cross-straited collagen fibrils in tendons of the treated embryos and analysis of the collagen composition showed an incorporation of about 4 Aze **83L** per 1000 amino acid residues.[30] In follow-on studies in cells derived from chick embryos and human skin fibroblasts, the underlying reason for the decreased collagen hydroxylation and secretion was identified as the inability of the abnormal collagen incorporating Aze to form a stable triple helix.[31] Due to the subtle conformational changes imposed by Aze incorporation, the supermolecular assembly of the polypeptides is disrupted and the abnormal collagen is preferentially degraded.

It should be noted at this stage that Pro **12L** residues contained in collagen are modified by prolyl hydroxylases which belong to the group of 2-oxoglutarate and Fe(II)-dependent

dioxygenases. Pro in the Yaa position are hydroxylated by prolyl 4-hydroxylase to form (2*S*,4*R*)-4-hydroxyproline (*trans*-4-hydroxyproline, Hyp or 4Hyp, **88**) (Figure 3.7 B), which favours the Cγ-*exo* pucker of the 5 membered ring causing a preassembly and hence stabilization of the collagen triple helix. To a lesser extend but also found naturally is (2*S*,3*S*)-3-hydroxyproline (*trans*-3-hydroxyproline, 3Hyp, **89**) as Xaa in the triplet –Xaa4HypGly- especially in basement membrane collagen IV which is introduced by prolyl 3-hydroxylase (P3H) (Figure 3.7 C).[32] The first mammalian P3H, termed P3H1, has recently been isolated from embrionic chicks, which showed 3-hydroxylase activity on a procollagen substrate.[33] Previously a P3H had been purified from *Streptomyces* sp. strain TH1 and its structural gene was identified as well,[34] which at the time was only the second hydroxylase that accepts free L-proline **12L** as a substrate following the P4H discovered in *Streptomyces griseoviridus* P8648.[35] The molecular mechanism of P3H from *Steptomyces* sp TH1 has been established in detail, including its X-ray structure, and it was found to hydroxylate Pro **12L** to *cis*-3-hydroxyproline **90** (Figure 3.7 D).[36] Similarly, Aze **83L** was found in a study investigating the substrate promiscuity of proline hydroxylases to be hydroxylated to *cis*-3-hydroxy-azetidine-2-carboxylic acid **91**.[37] The same study showed that a proline 4-hydroxylase from *Dactylosporangium* sp. RH1 would not accept Aze as a substrate.

Therefore it has been experimentally established, that hydroxylases, although from bacterial origin, are also able to accept Aze as a substrate and can, possibly even when integrated into protein structures, undergo hydroxylation. Such hydroxylations could have detrimental effects on protein structure when viewed in the light of the relative instability of such hydroxylated compounds in terms of their susceptiblity to retro-aldol reactions, which are discussed later on in this chapter.

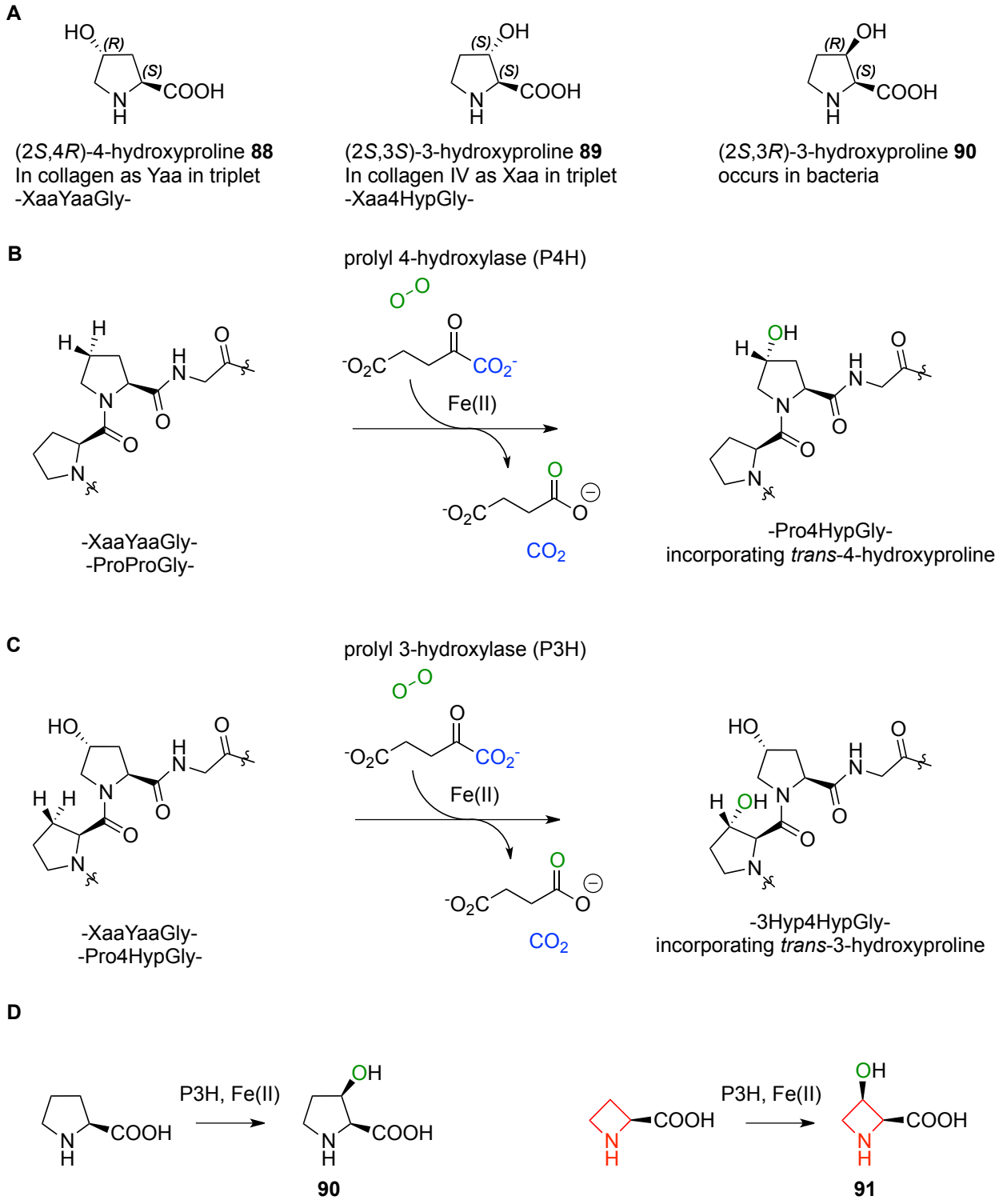


**Figure 3.7** A) Examples of different hydroxylated prolines and their natural occurrence; B) Mechanism of action of mammalian prolyl 4-hydroxylase; C) Proposed mechanism of action of mammalian prolyl 3-hydroxylase; D) Proline 3-hydroxylase derived from *Streptomyces* sp. TH1 acting on proline and Aze.

#### 3.1.3.1.3 Biological consequences of Aze incorporation into collagen

There are multiple biological results of the disruption to correct collagen biosynthesis. Ameloblasts of mouse tooth buds treated with Aze **83L** *in vitro* have been studied and it was found that the proline analogue prevents collagen excretion and as a result disrupts the differentiation of ameloblasts.[38] In a similar study *in vivo* odontoblasts of mice showed severe morphological changes to the collagen secreting golgi apparatus.[39] Another *in vivo* study investigated the interruption of the collagen layer in the cornea of chick embryos due to Aze **83L** treatment.[40] The wound healing progress is also influenced by the aberrant collagen formation as could be shown in a trial involving Yorkshire pigs. In the days following the skin wound infliction, there usually is a sharp increase in Hyp **88** concentration in the underlying dermis. However, consistent with previous findings on reduced conversion of Pro **12L** to Hyp **88**, on treatment with Aze **83L** the Hyp **88** concentration was markedly reduced and wound healing was retarded by 78% in comparison to untreated controls.[41] In hamster fetuses teratogenic effects were recorded upon Aze **83L** treatment, which involved external malformations, growth retardation and high frequency of anomalies of the skeleton.[42] Again the underlying molecular origin of these adverse biological effects was attributed to disrupted collagen formation.

Both theoretical and experimental studies have been performed in order to investigate the molecular origin of how even such low incorporation of Aze into collagen could have such pronounced biological consequences. Scheraga and coworkers undertook a series of theoretical investigations of Pro **12L** substitutions by Aze **83L** with collagen like polymers of increasing length.[43] From the modeling comparison of Pro **12L** and Aze **83L** containing dipeptides, the following could be concluded about the conformational differences of these amino acids when incorporated into collagen:[43a] 1) There is increased flexibility of the Aze **83L** containing analogue due to a higher number of accessible low energy conformations while the Pro **12L** derivative prefers the F-conformation,[44] which is relatively higher in energy for Aze **83L**; 2) The

*trans* peptide bonds of Aze **83L** analogues are more extended displaying ψ between 175° and 180° while ψ for Pro derivatives is 164-168°, which again is consistent with the collagen triple helix requirement of *trans* peptide bonds for an F-conformation of $\psi < 170°$; 3) There is additional increased flexibility due to decreased steric bulk of the Aze **83L** ring structure in comparison to Pro **12L**. Although further theoretical studies were unable to show significant differences in conformational energies of collagen like polymers; an increased flexibility of the structure was noticed, which could be responsible for disrupting the preassembly of the single strands due to correct proline puckering and overall destabilize the collagen triple helix.[43b, 43d] Experimental investigations into poly-Aze in analogy with poly-Pro have been performed and the circular dichroism (CD)[45] and NMR[46] spectra obtained. The CD spectra of poly-Aze in water seemed to not have any similarity with the PPII structure that is observed for poly-Pro in the same solvent.[45] NMR data seemed to give evidence of a mixture of *cis* and *trans* peptide bonds in water, while the PPII helix would only allow for *trans* bonds.[47] Tsai et al. were able to improve the synthesis of the key intermediate *N*-benzhydryl-2-carbobenzyloxy azetidine which allowed for Aze **83L** to be generated on a larger scale and hence they were able to create, amongst others, the polymer Boc-$(Pro)_3$-Aze-Opcp [Opcp pentachlorophenyl].[48] They were able to experimentally confirm the increased flexibility on Aze **83L** incorporation and by NMR the ratio of *cis* and *trans* peptide bonds in the structure was assigned to be 2:1. Therefore it can be concluded that incorporation of Aze **83L** into collagen at a frequency as low as 4 per 1000 residues can increase the chain flexibility due to the appearance of *cis* peptide bond conformations, which disrupt the preassembly of the collagen mono-helixes blocking it from forming the triple helix required for correct collagen function.

With it established that Aze **83L** can be incorporated into proteins with often detrimental biological consequences and a possible entrance of Aze **83L** into the human foodchain, a connection to multiple sclerosis has been proposed by Rubenstein.[49] The theory, though so far

based mostly on circumstantial evidence, is fueled by events like 60 out of 100 newborn lambs dying of a neurological disorder after having been fed sugar beet waste products.[50] He proposed the disease was caused by incorporation of Aze **83L** into meylin basic protein (MBP), a protein containing a proline rich segment, which is crucial for function and would be particularly vulnerable to conformational changes. Both experimental[51] and theoretical[52] investigations of MBP incorporating Aze **83L** are currently being undertaken to test this hypothesis.

This possible implication in human disease stresses the need for the synthesis of Aze **83L** and its analogues as monomers for incorporation into peptides, in order to understand the molecular basis of the conformational changes of such incorporations and to gain insight into the resulting biological consequences.

### 3.1.3.2 Azetidines in natural products

#### *3.1.3.2.1 Penaresidines and further azetidine alkaloids*

From marine sponges of the species *penares* several azetidine containing alkaloids with structural similarities to sphingosine and varied biological activity have been isolated (Figure 3.8). From a sponge found in Okinawa, Kobayashi and coworkers were able to isolate penaresidin A and B, **93** and **94**, and the mixture of these two sphingosine **92** related alkaloids was able to increase the ATPase activity of myofibrils from rabbit skeletal musle by 81% relative to a control and these alkaloids were implicated as possible chemical tool for the investigation of the actin-myosin contractile system.[53] To allow complete assignment of penaresidins A and B including the stereochemistry of the hydroxyl at C15 both synthesis of **93**[54] and **94**[55] and derivatization with Mosher's acid (alpha-methoxy-alpha-trifluoromethylphenylacetic acid, MTPA) was necessary.[56]

Penazetidine A **95** in turn was isolated 3 years later from a marine sponge found in Papua New Guinea and could be shown to be an inhibitor of protein kinase C.[57] Similar to staurosporine,[58]

azetidine **95** could be used as potential anti-cancer agent via the interruption of the kinase dependent signaling cascade leading to uncontrolled cellular proliferation. Despite both stereoisomers at the chiral carbon of the long alkyl side-chain having been synthesized, the comparison of the optical rotation relative to the natural product, which had been recorded at a very low concentration of *c* 0.04, was unable to determine the actual configuration in the natural derivative.[59]

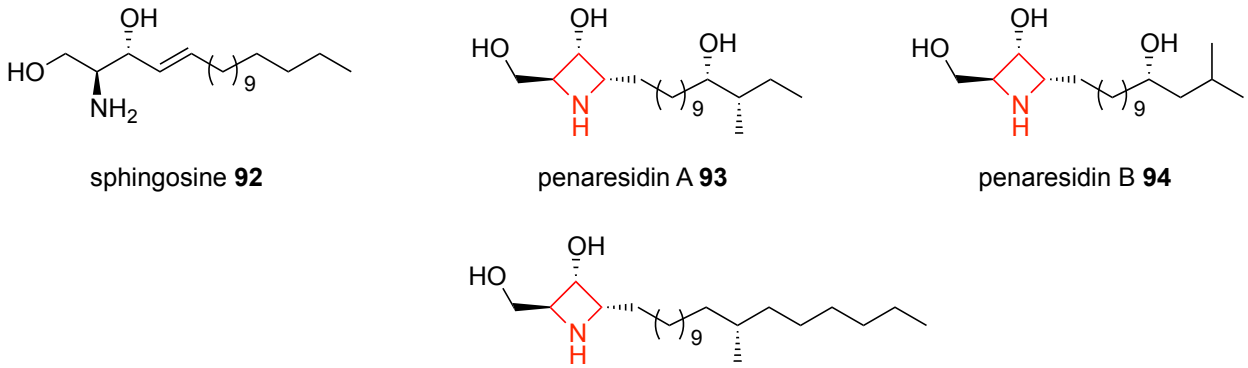


**Figure 3.8** Examples of sphingosine-like azetidine containing alkaloids.

The work done on the azetidine alkaloid class of Polyoxins is very nicely summarized in the manuscript by Isono et al.[60] Out of the 10 peptide nucleosides identified from a culture broth of *Streptomyces cacaoi* var. *asoensis*, four were found to contain an azetidine ring **96-99** (Figure 3.9). The anti-fungal activity of this set of compounds was attributed to its structural similarity to uridine diphosphate *N*-acetylglucosamine and therefore its possible interruption of chitin synthase.

More recently the highly complex alkaloids Gelsemoxonine **100** and calydaphninone **101** have been identified (Figure 3.9). In 2003 Kitajima et al.[61] suggested a revised structure for oxindole **100** isolated from *Gelsemium elegans*, a plant that has been used as chinese medicine more then 1250 years ago.[62] The presence of the azetidine ring structure was confirmed using heteronuclear multiple-bond correlation spectroscopy (HMBC) recorded in deuterated pyridine at -30 °C

revealing the interaction of the hydrogen on the nitrogen with two rather then just one carbon atom(s). Additional evidence was provided by X-ray crystallography. The hexacyclic alkaloid **101**, which in turn was isolated from *Daphiphyllum calycillum*, features three quaternary carbon centers, one of which is located in the azetidine ring.[63] Again extensive NMR studies and X-ray crystallography were required in order to solve the structure of compound **101**. Additional computational studies were performed in order to investigate the solution phase behaviour of this alkaloid, which indicated at least two low energy conformations of this molecule. Therefore a whole range of azetidine alkaloids with increasing complexity have been discovered in nature.

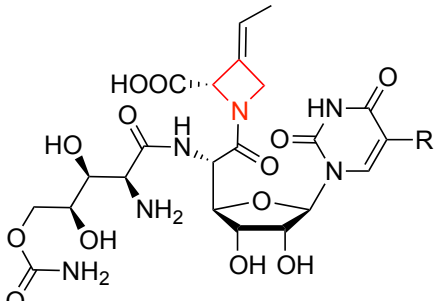


Polyoxin A **96** R= $CH_2OH$
F **97** COOH
H **98** $CH_3$
K **99** H

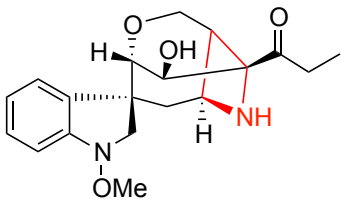


Gelsemoxonine **100**

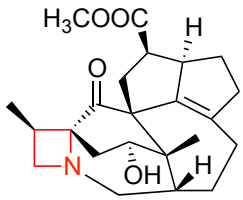


calydaphninone **101**

**Figure 3.9** Further examples of azetidine containing alkaloids.

### *3.1.3.2.2 Phytosiderophores – Iron chelators in plants*

Mugineic acid (MA) **102** was the first phytosiderophore to be discovered in barley in 1978 (Figure 3.10).[64] This iron chelating molecule, along with closely related MAs which vary in hydroxylation pattern like **103**, **104** and **105**, are secreted by the roots of graminaceous plants e.g. rye, wheat and beer barley.[65] This allows for uptake of the important cofactor $Fe^{3+}$ from the ground, which - despite being present in abundance - is otherwise unavailable to the plant due to the poor solubility of the ions in alkaline ground in the presence of oxygen.[66] In using this chelation principle these strategy II plants stand in contrast to strategy I plants which alter the pH of their environment to allow for iron uptake. If plants are unable to sequester enough iron they succumb to a disease called chlorosis, as this cofactor is required in many important processes in

the plant like photosynthesis, nitrogen fixation and chlorophyll synthesis.[67] Especially the latter explains the phenotype of this disease, which leads to loss of the green colour in stem and leaves and results in low crop production in orchards and vineyards.[68]

The biosynthesis of these MAs was majorly deciphered by Mori et al. and is performed *via* the formation of nicotianamine (NA) **106**, which in turn is generated from three L-methionine **86L** molecules.[37, 69] NA **106**, which was first isolated from green tabacco leaves of *Nicotiana tabacum L.*, is believed to be present as an iron transporter in all plants but, unlike the MAs in strategy II organisms, it is not secreted.[70] Nicotianamine aminotransferase however is responsible for the conversion of NA **106** into 2'-deoxy mugineic acid **105** which can then be hydroxylated to form the remaining set of MAs **102**, **103** and **104**. This biosynthetic pathway shows the evolutionary connection between strategy I and II plants. Therefore azetidine containing compounds play a crucial role the transport of iron in many plants, which is required for some of their most fundamental functions, especially photosynthesis.

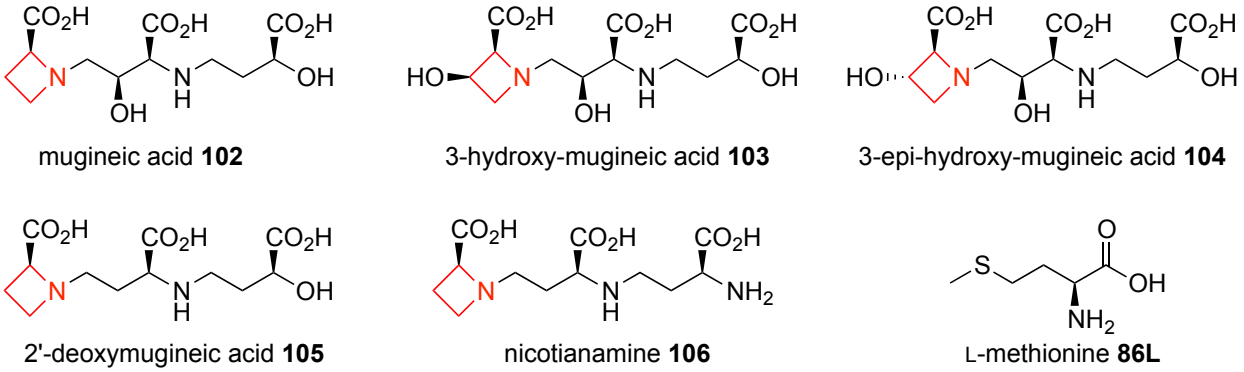


**Figure 3.10** Examples of iron chelators in plants.

### *3.1.3.2.3 Azetidines in antibiotics*

Another extremely important type of azetidine found in nature is the special case of the azetidine-2-one; better known as β-lactams, which are present most prominently in antibiotics like pencillins and cephalosporins. Although the anti-bacterial power of the *penicillium* fungus had been recognized before, Fleming's recordings of the ability of *penicillium rubrum* to lyse

*staphylococcus* bacteria was what prompted a team of scientist at the Sir William Dunn School of Pathology in Oxford, including Howard Florey, Ernst Chain and Norman Heatley, to investigate its properties as an antibiotic *in vivo*.[71] But it was Dorothy Hodgkin's work on X-ray crystallography which allowed for the structure of penicillin including the β-lactam to be elucidated and it was for this work she was awarded the nobel prize in 1964.[72] These discoveries sparked the development of the rich variety of different β-lactam containing antibiotics we have today, some representative examples of which can be seen in Figure 3.11.

Today penicillins **107** are usually generated *via* a semi-synthetic approach, where large scale fermentation produces the Penicllin-G or -V core, which is then further modified at the $R^1$ group to yield the desired pharmacokinetics.[73] The cephalosporins **108** can be obtained *via* oxidative rearrangements of penicillins[74] however they were first isolated as natural products from *cephalosporium acremonium*.[75] The first antibiotic with a carbapenem core **109**, which is similar to penicillin but has the sulfur atom replaced by a carbon, was isolated from *Streptomyces catteya*.[76] The monocyclic β-lactams, called monobactams **110**, were first discovered in *pseudomonas acidophila*[77] and then developed into more potent antibiotics like Aztreonam.[78] The biomolecular pathways leading to the production of β-lactams in nature, including a special focus on the enzymes involved, can be found in the excellent review by Schofield and coworkers.[79]

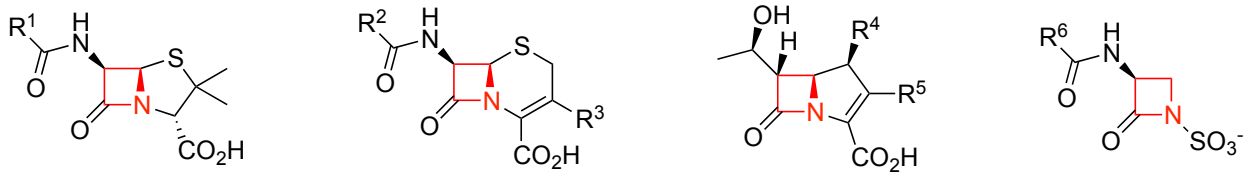


Penicillins **107** Cephalosporins **108** Carbapenems **109** Monobactams **110**

**Figure 3.11** Representative classes of β-lactam antibiotics.

In early 2010 the total market of β-lactam antibiotics was estimated to be $18 billion, $10 billion of which fell to cephalosporins and about $8 billion on penicillins indicating the relative

importance of these antibiotics for world health.[80] Overall β-lactams hold 65% of the world antibiotics market.[73] Although the interest of pharmaceutical companies in antibiotics has been waning, due to shrinking of possible revenues, there is a constant need for novel antibiotics due to the adaptability of bacteria and the resulting emergence of resistance.[81]

The mechanism of action of β-lactam antibiotics is exemplified by the action of penicillin on bacteria *Staphylococcus aureus* in Figure 3.12.[82] The strain of the β-lactam ring system is of crucial importance for the bactericidal effect and an increase in ring strain can be found to correlate with activity.[74] This behaviour can be explained by the reaction of penicillin with a transpeptidase of the bacterium, which is responsible for cross-linking peptides of the proteoglycan network that makes up the cell wall of the bacterium. A serine residue contained in the active site of the transpeptidase enzyme forms a covalent bond following nucleophilic attack on the β-lactam carbonyl, which increases in reactivity with ring-strain. The adduct is relatively stable to hydrolysis and as a result stops the crosslinking activity of the enzyme.[83] This disruption results in an incomplete cell wall formation and hence lysis of the bacterium.

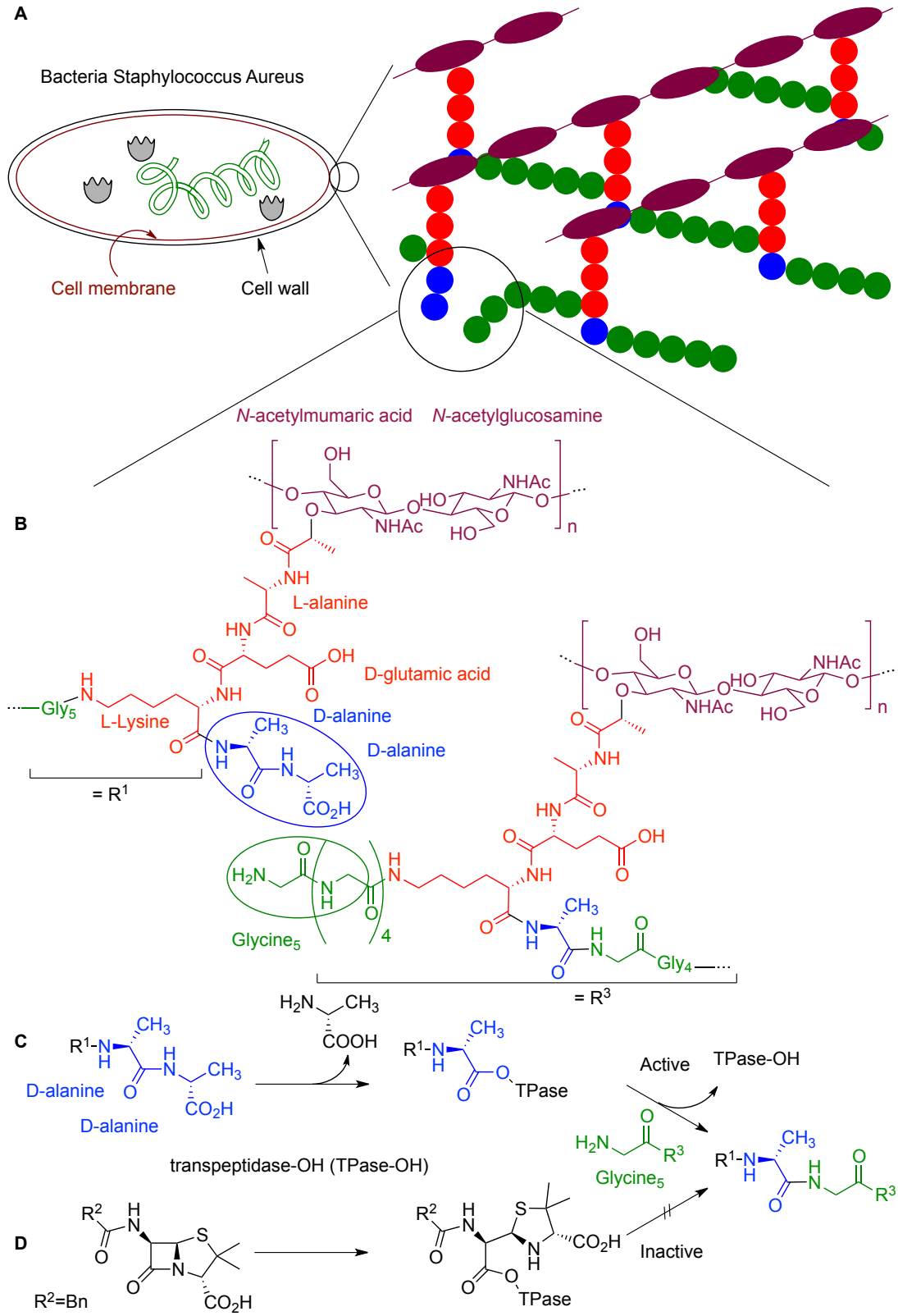


**Figure 3.12** Mechanism of action of penicillin A) Systematic representation of the bacterium *staphylococcus aureus* with enlarged view of peptidoglycan network of the cell wall; B) Molecular description of peptidoglycan network with point of action of penicillins; C) Regular cross-linking action of transpetidase; D) Mechanism of action of penicillins *via* irreversible reaction of azetidine β-lactam with serine hydroxyl group of active site of transpeptidase, inhibiting bacterial cell wall formation.

One of the two main modes of bacterial resistance has a molecular mechanism highly related to the regular mode of action of β-lactams. The strained β-lactam ring is opened to form either an adduct, which is subsequently readily hydrolysed or, as in the case of the metallo-β-lactamases, is hydrolysed directly.[84] The other resistance method is to limit the presence of the drug inside the bacterium either *via* limiting drug penetration or active expulsion.[81b] In order to overcome these developing resistances a variety of β-lactam antibiotics needed to be developed (Figure 3.11). In particular to overcome the β-lactamases new inhibitors of these enzymes have been investigated in order to be co-administered alongside the antibiotics. Three β-lactamases inhibitors are shown in Figure 3.13 which are now commercially available in combination with antibiotics:[85] Augmentin™ (amoxicillin/clavulanic acid **111**),[86] Unasyn™ (ampicillin/sulbactam **112**)[87] and Zosyn™ (Piperacillin/tazobactam **113**).[88]

Therefore the emergence of resistant bacteria against the available antibiotics shows that β-lactams are certainly not a topic of the past but remain important today in the continued battle against bacterial pathogens.

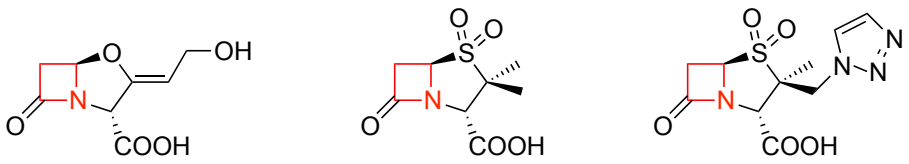


Clavulanic acid **111** Sulbactam **112** Tazobactam **113**

**Figure 3.13** β-lactamase inhibitors base on the β-lactam core.

### 3.1.3.3 Azetidines in synthetic products

Besides the β-lactams other azetidine containing pharmacologically active compounds have emerged over the last decade. This increased interest in azetidines can be seen by the fact that many major pharmaceutical companies have a lead compound containing an azetidine in their research pipelines.[11]

In a study looking at the inhibition of angiotensin-converting enzyme (ACE) for the treatment of hypertension by the Squibb Institute, several mercaptoacyl amino acids including azetidine **114** were trialed (Figure 3.14).[89] Although azetidine **114** was a good inhibitor of ACE with an $IC_{50}$ of 1.7 μM, proline **115** turned out to be even more powerful ($IC_{50}$ 0.25 μM) which could be further improved by inclusion of a methyl branch α to the amide carbonyl to give Captopril **116** with a 10 fold improvement ($IC_{50}$ 0.02 μM). Captopril **116** went on to gain approval by the Food and Drug Administration (FDA) in 1981. Aziridine **118** and azetidine **117** were compared in terms of their ability as a radiosensitizer and selective toxins to hypoxic cells (Figure 3.14).[90] **117** retained its ability as radiosensitizers, presumable due to the presence of the 2-nitro-imidazole moity, which is known to infer radiosensitization[91] and hypoxic cytotoxicity.[92] However, azetidine **117** has no alkylating activity in contrast to aziridine **118**, which overall limited the toxicity of **117** to hypoxic cells. Similar combinations of radiosensitizing and DNA crosslinking properties are still the subject of more recent work, where the radiation triggered release of phosphoramidate mustard conjugates from 2-nitroimdazoles are investigated.[93]

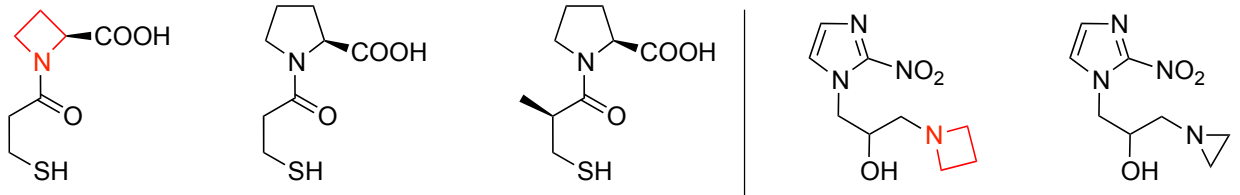


**114** **115** Captopril **116** **117** **118**

**Figure 3.14** Left: Captopril and related structures; Right: Azetidine and aziridine radiosensitizers.

In more recent times research at GlaxoSmithKline is being performed towards a cathepsin K inhibitor.[94] Cathepsin K, a cysteine protease, is able to rapidly hydrolyze type I collagen and hence has been implicated for the treatment of osteoporosis. In this particular study azetidine **120** is nearly forty fold more active then pyrrolidine **119** and is a picomolar inhibitor of cathepsin K, being overall the most active compound evaluated (Figure 3.15). Similarly Merck is working on very late activating antigen-4 (VLA-4), which is a cell surface integrin, that promotes leukocyte

attachment and extravasation from the vasculature and hence regulates inflammation. As a result it is thought to be important in diseases like asthma, rheumatoid arthritis and multiple sclerosis. If only marginally, azetidine **122** was again a more potent inhibitor of target enzyme VLA-4 in comparison to the 5-membered ring derivative **121**, displaying an $IC_{50}$ of 0.08 rather than 0.09 nM.[95] In a follow-on study substitution of the amide functionality with an amidine further improved the pharmacokinetic profile of **122** whilst retaining potency.[96]

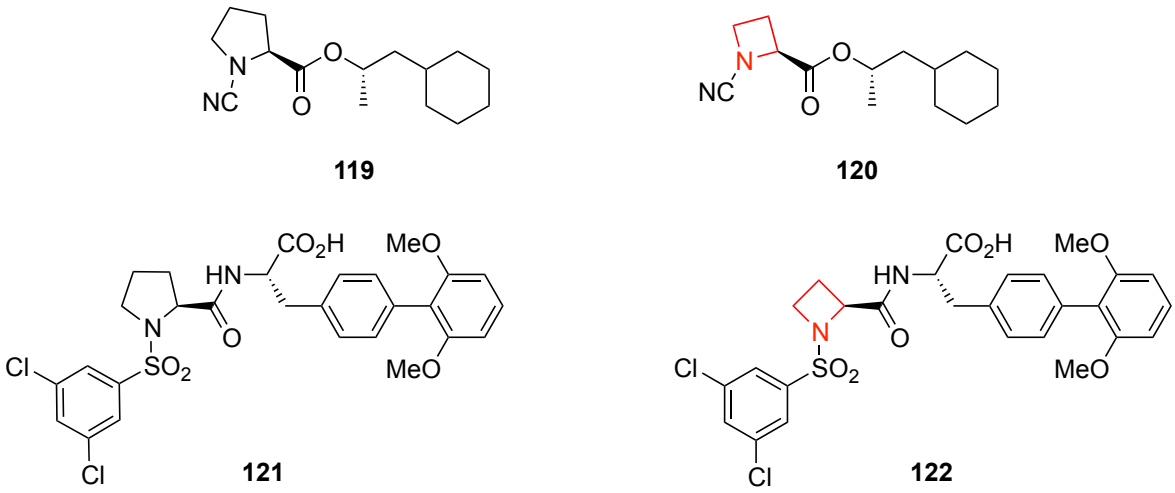


**Figure 3.15** 5 and 4 ring analogues of a cathepsin K inhibitor (**119**/**120**) and an antagonist of VLA-4 (**121**/**122**)

AstraZeneca is developing an orally available anticoagulant thrombin inhibitor, which would require no monitoring, as a replacement to warfarin. Earlier development led to the azetidine containing Exanta **123** (marketed as Ximelagatran), which is a prodrug to Melagatran **124**, the active species in the body (Figure 3.16). Altough Exanta **123** was shown to be as effective an anti-coagulant as a combination of enoxaparin/warfarin, elevated liver enzymes prompted the development of this particular compound to be discontinued.[97] Hence work was initiated on AZD0837 **125** another azetidine-2-carboxy amide.[98] The prodrug AZD0837 **125** again is metabolically converted into its active form via action of cytochrome P450 leading to demethylation and formation of **126**. On further action of *N*-hydroxylamine reductase **126** is converted into the active agent **127**, which showed promise in animal bleeding trials (Figure 3.16).[99] A phase I clinical trial involving 44 caucasian males AZD0837 **125** was well tolerated in

oral doses ranging from 15-750 mg and the selected biomarkers showed the efficacy of **125** with the drug being well tolerated overall.[100] These promising results are supporting further clinical development.

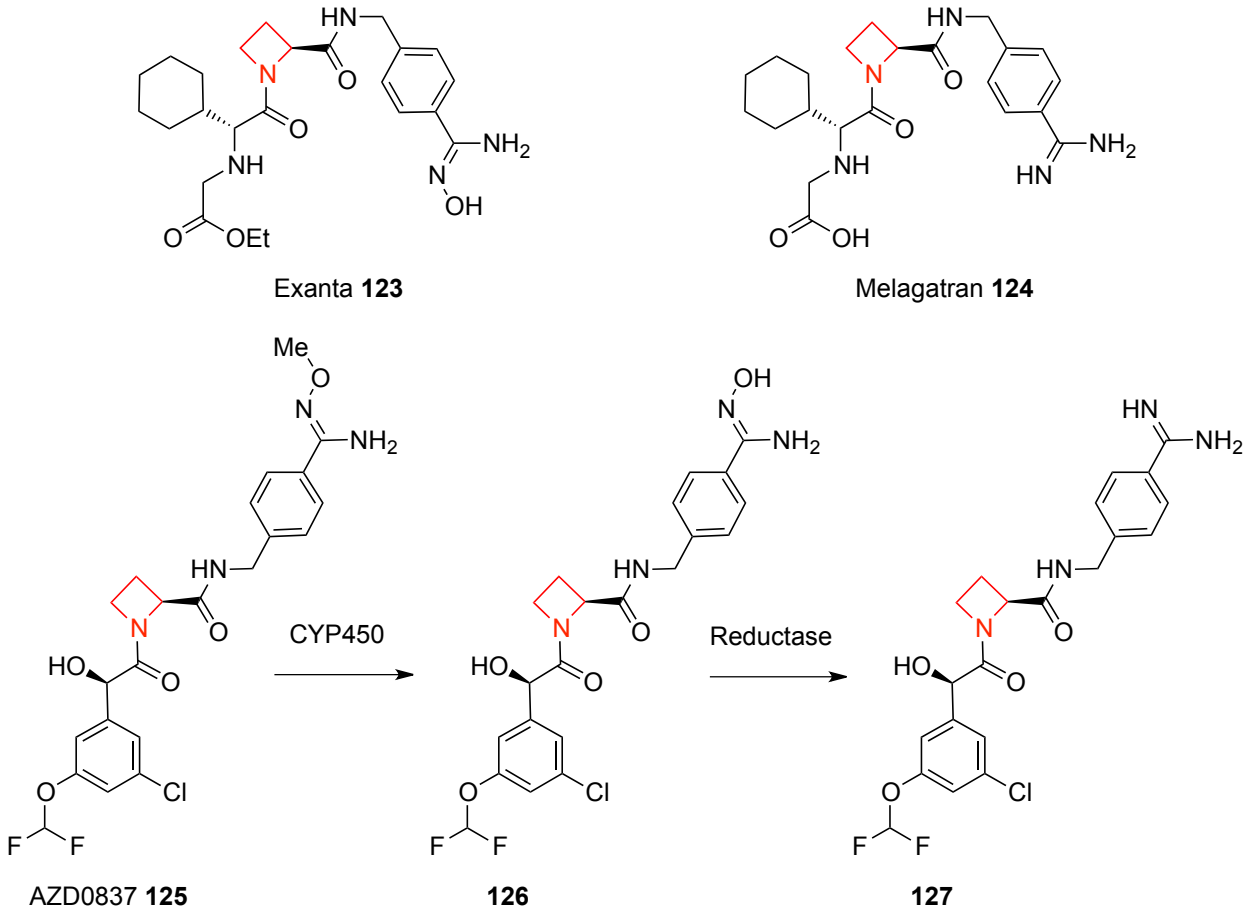


**Figure 3.16** Development of thrombin inhibitor AZD0837 and metabolism of prodrug into active derivative.

A current effort by the drug discovery unit of Johnson&Johnson is less far along the development pipeline and is on the structure activity relationship (SAR) study on a selective inhibitor of monocyte chemotactic protein-1 (MCP-1), which is of interest due to its potential treatment application towards inflammatory diseases like asthma and multiple sclerosis.[101] Azetidine **128** showed an $IC_{50}$ of 5 nM against MCP-1 and was more then 500 fold selective over the potassium channel hERG, which is associated with cardiovascular complications (Figure 3.17). In a similar study the G protein-coupled receptor MCHR1 for the melanin-concentrating hormone (MCH) is being investigated. It is thought that a small molecule

antagonist of the MCH1 receptor could be a treatment for mood disorder and obesity. Lu et al. aimed to tune the compound's properties for optimizing CNS penetration and dihydroindolyl azetidine **129** was developed.[102]

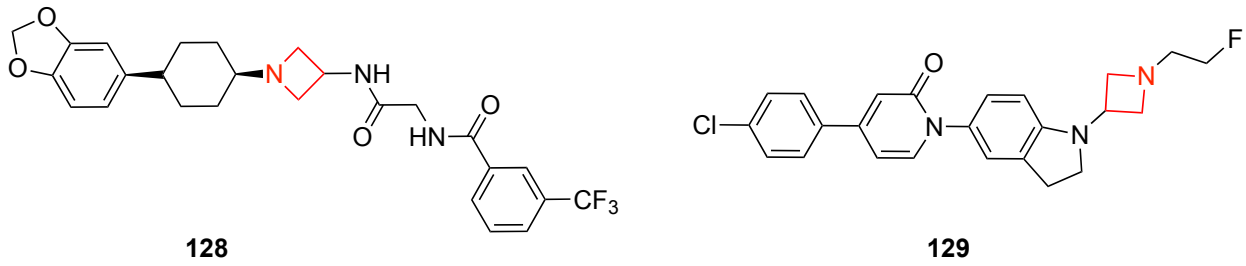


**128** **129**

**Figure 3.17** Current SAR studies on azetidine containing lead compounds.

In most recent times a series of SAR studies on α- and β-amino acids azetidine containing compounds have been published. In an effort to improve the water-solubility of cisplatin related compounds like carboplatin as a potential anti-cancer treatment azetidine-3,3-dicarboxylate ligands were developed.[103] Azetidine **130** emerged as a more selective agent then carboplatin, showing increased cytotoxicity against four cancer cell lines in direct comparison, whilst reducing acute toxicity (Figure 3.18). Similarly in a quest for a human cytomegalovirus (HCMV), a β-herpes virus inhibitor, Pérez-Faginas et al. synthesized a series of α-amino acid azetidine containing dipeptides.[104] Their work is based on a β-lactam structure from which they omitted the 2-carboxyl group in order to generate a non-covalent inhibitor and dipeptide **131** emerged as one of the most active compounds in an *in vitro* assay against HCMV. A small molecule selective $M_1$ muscarinic receptor inhibitor for treatment of diseases like Pakinson and fragile X syndrome was investigated for the inclusion of a cyclic constraint in the lead structure.[105] Amino-sulfone **132** was found, amongst others, to display improved activity whilst maintaining the desired selectivity for the $M_1$ type of the possible 5 subtypes of the muscarinic receptor. Nakamura et al. are currently exploring the optimization of a selective inhibitor of modulators of sphingosine phosphate receptor-1 ($S1P_1$) as a possible anti-autoimmune agent based on an initial lead compound developed by Merck.[106] The result of this effort is 4-ethyl

thiophene **133** termed CS-2100 which is more then 5000 fold selective for receptor $S1P_1$ over $S1P_3$, which is associated with bradycardic side-effects in rodents.

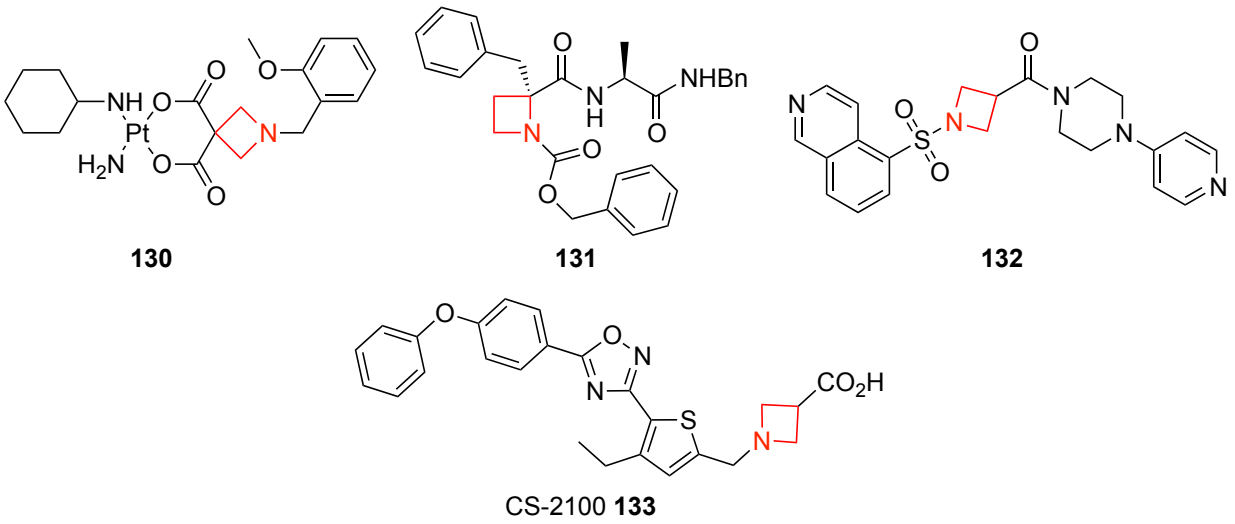


**Figure 3.18** α and β-amino acids in recent SAR studies.

Overall it can be observed that several large pharmaceutical companies have lost their reservation towards the supposedly unstable azetidine functional group and especially in recent time an increased number of pharmaceutical agents containing this moiety are being developed.

### 3.1.4 The synthesis of azetidines

There have been several excellent reviews scrutinizing synthetic approaches towards azetidine containing structures. Couty and Evano focused on Aze and covered both natural occurrence, synthesis and reactivity of this particular azetidine.[11] A review focusing on the variety of different synthetic strategies in a very well structured manner towards generating azetidines was peformed by Brandi et al..[107] Concentrated on [2+2] cycloyadditions and anti-biotic synthesis[5a] Yoda et al. did, while Rousseau and Robin looked at azetidine synthesis apart from β-lactams.[108] Most recently Bott and West reviewed not only the synthesis but also synthetic applications of azetidines as intermediates.[1]

### 3.1.4.1 General methodologies for azetidine synthesis

The azetidine ring is inherently more strained (25.2 kcal/mol) than its five and particular six ring analogues. Due to this energetic penalty it is one of the most challenging ring systems to form of the common nitrogen containing heterocycles (5>3>6>7≈4).[1] Despite this challenge several approaches towards azetidine ring formation have been devised which can be broken up into three main categories: 1) C-N bond formation; 2) C-C bond formation; 3) [2+2] cylcoadditions (Figure 3.19). One of the oldest and best-established approaches to azetidines is either the inter- or intramolecular displacement of a leaving group (LG) by a suitable amine (Figure 3.19 a, b). This route tolerates a large variety of substituents and typically involves halides or activated hydroxyls as LG. The C-C bond forming approach is particularly applicable to forming Aze and derivatives with $R^4$=COOH, however often suffers from formation of epimeric mixtures (Figure 3.19 e). Recently improved conditions for [2+2] cylcoadditions were found that now allow for yields that enhance the applicability of this approach (Figure 3.19 f). Some representative examples will be discussed below.

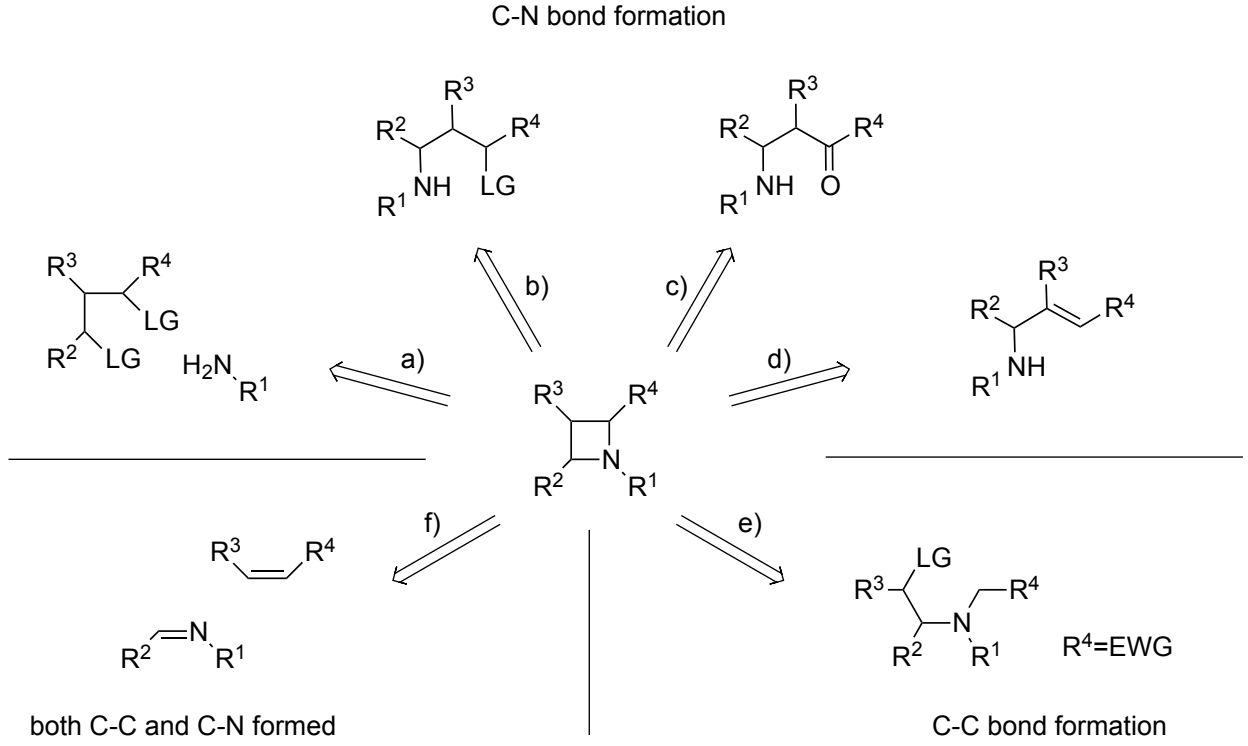


**Figure 3.19** Synthetic access to azetidines via: a) addition of amine to 1,3-dielectrophile; b) ring closure of an amine onto a γ-leaving group; c) reductive amination of a β-ketone/aldehyde; d) cylization of an activated allyl-amine; e) intramolecular alkylation; f) intermolecular [2+2] cylcoaddition.

One of the examples of the reaction of an amine with a 1,3-dielectrophile is the displacement of a ditriflate with benzylamine on a multi kg scale in order to give azetidine-3-carboxylic acids **137**.[109] The process used in this case was a one-pot procedure which involved esterification of the corresponding diol **134** derived from diethylmalonate with triflic anhydride followed by subsequent displacement with benzylamine to give azetidine **136** (Scheme 3.1).

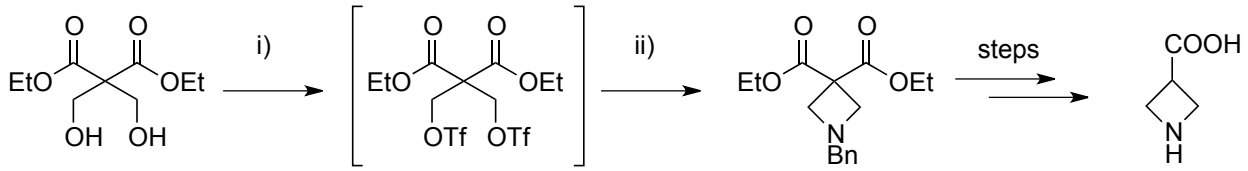


**Scheme 3.1** Addition of amine to 1,3-dielectrophile. Reagents and conditions: i) $Tf_2O$, DIPEA, -20° to -10°, MeCN, 2.5 h; ii) $BnNH_2$, DIPEA, -10° then reflux, 2h.

A similar methodology involving ditriflates has been used by our group in order to generate 5- and 6-ring fused bicyclic azetidine compounds from glucose in order to investigate their inhibition profile against a panel of glycosidases.[110]

Equally starting from a sugar starting material, in this case D-arabinose, Yoda et al. performed a synthesis of penaresidin B (Scheme 3.2).[55] The protected γ-lactam **139** was formed *via* addition of the corresponding acetylide to an amine derivative of sugar **138** followed by oxidative degradation with PCC and reduction. Following differential protection the lactam was reduced and the terminal alcohol protected with chloromethyl methyl ether. Reductive conditions removed the benzyl protecting group and mesylation set up alcohol **140** for azetidine formation under basic conditions to give **142**. Acid catalyzed hydrolysis removed all protecting groups and yielded Penaresidin B **94**.

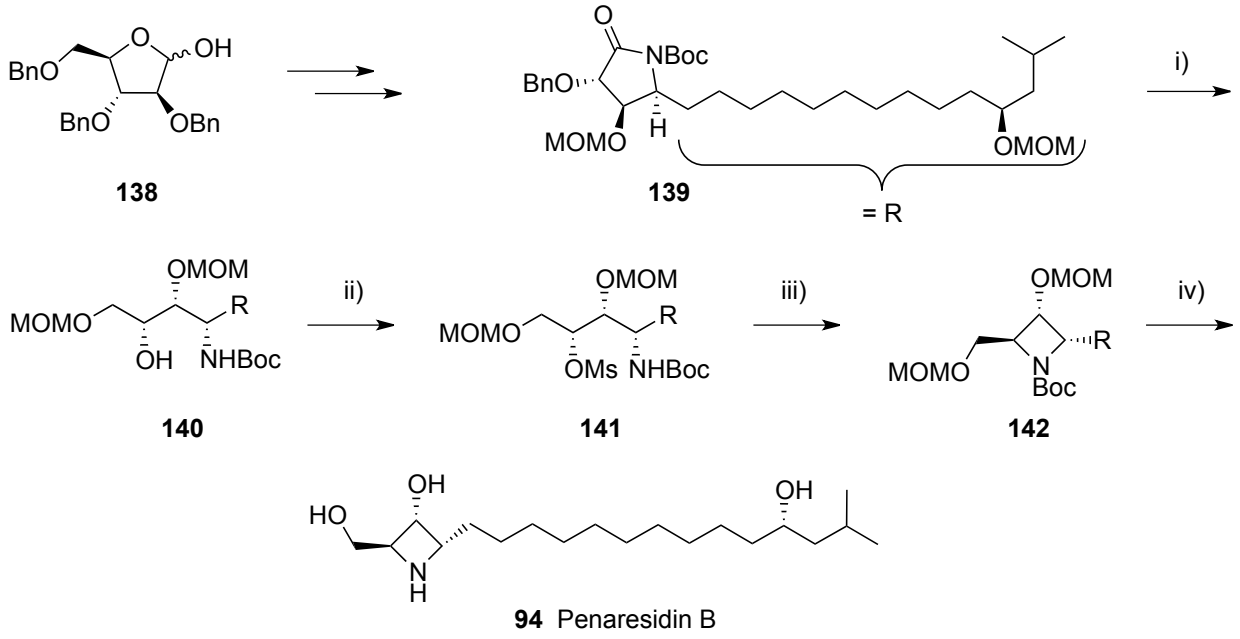


**Scheme 3.2** Intramolecular closure of amine onto γ-leaving group. Reagents and conditions: i) $NaBH_4$, MeOH, quant then MOMCl, DIPEA, $CH_2Cl_2$, quant then Pd (black), 4.4% HCOOH-MeOH, quant; ii) MsCl, $Et_3N$, $CH_2Cl_2$; iii) NaH, THF, 50% (two steps); iv) conc. HCl, MeOH.

A short and efficient synthesis of both enantiomers of Aze was devised by Couty et al. which features a C-C bond formation to close the azetidine ring (Scheme 3.3).[111] While more syntheses of Aze are discussed in their review,[11] in this case amine **143** was alkylated using benzyl bromoacetate and the resulting alcohol **144** was converted into the corresponding chloride. The protected amino acid **145** was then set up for deprotonation adjacent to the carbonyl and

intramolecular nucleophilic displacement to give azetidines **146** and **147**. Following separation hydrogenolysis gave both enantiomers of Aze **83**.

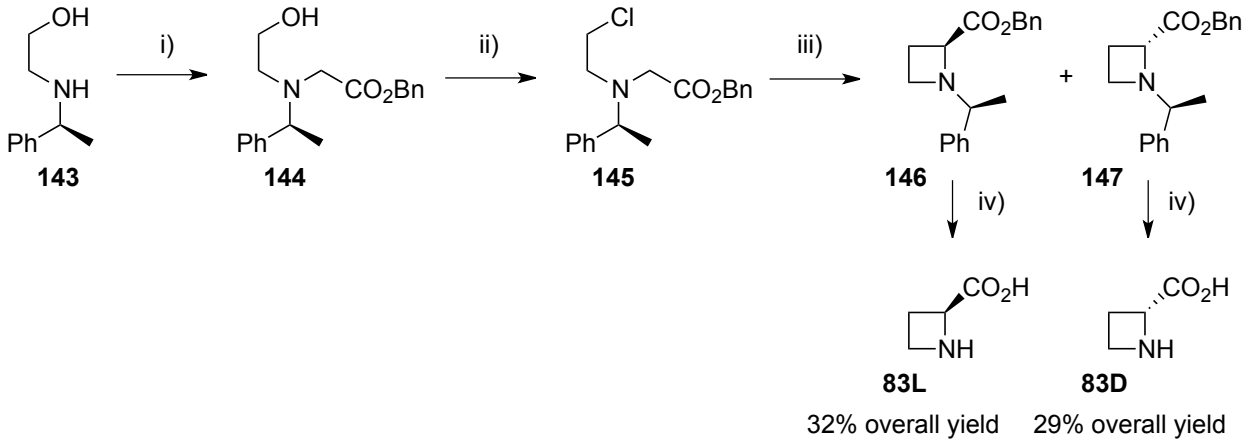


**Scheme 3.3** C-C bond formation. Reagents and conditions: i) $BrCH_2CO_2Bn$, NaI, $NaHCO_3$, DMF, RT, 74%; ii) $SOCl_2$, $CH_2Cl_2$, reflux, quant; iii) LiHMDS, THF, -78 °C to -20 °C, 82%; iv) $H_2$, Pd/C, MeOH, quant.

An intriguing methodology to generate azetidines with excellent enantiomeric excesses involves a copper catalyzed [2+2] cycloaddition using a chiral ligand (Scheme 3.4).[112] 1-methoxyallenylsilane **148** was reacted with α-imino-ester **149** to yield the highly substituted azetidine **150**.

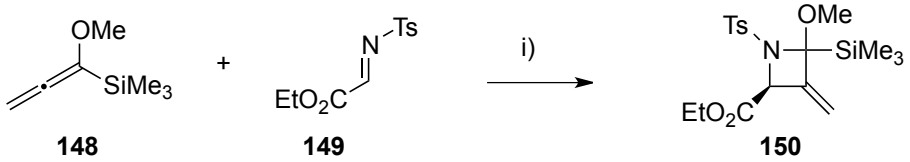


**Scheme 3.4** [2+2] cylcoaddition. Reagents and conditions: i) 10 mol% $[Cu^{+}(MeCN)_4]BF_4^{-}$, (R)-Tol-BINAP, -78 °C, MS 4Å, THF, 90%, ee 97%.

### 3.1.4.2 Azetidine-2-carboxylic acids in peptides

In section 3.1.3.1 the misincorporation of azetidine-2-carboxylic acid into peptides and its structural consequences were explained and section 3.1.3.3 presented some synthetic products containing α- and β-amino acids of azetidines. With the preceding section presenting some monomeric synthesis of azetidines, the following one focuses on the synthesis of peptides integrating Aze **83L** and its derivatives.

Poly-L-proline **152** has been synthesized[113] and the helical structure it forms has been investigated, leading to the identification of the already mentioned poly-proline II helix containing only *trans* peptide bonds (Figure 3.20 A).[25] Similarly a polymer of L-azetidine-2-carboxylic acids **151** has been explored using self-condensation of the penta-chlorophenyl esters of the L-azetidine-2-carboxylic acid hydrochloride.[47] The solution conformation of this polymer was investigated using NMR spectroscopy and although a regular helical structure was formed, evidence for *cis* and *trans* peptide bonds was found, unlike in the PPII structure.[46]

Further peptides like model tetramer **153** were synthesized more recently by Baeza et al. in a series of investigations into the structural motifs induced by azetidine incorporation (Figure 3.20 B).[114] Evidence for γ-turn[115] induction using rigorous conformational analysis including X-ray analysis was found by the peptides incorporating 2-alkyl-2-carboxy-azetidines.[116] Similarly δ-amino acids incorporating an oxetane ring, an oxygen 4 ring analogue of an azetidine, can be viewed as a dipeptide isosteres, which induce β-turns[115] into tetramers and higher homo-polymers as determined by NMR NOE analysis (**154**, Figure 3.20 B).[117]

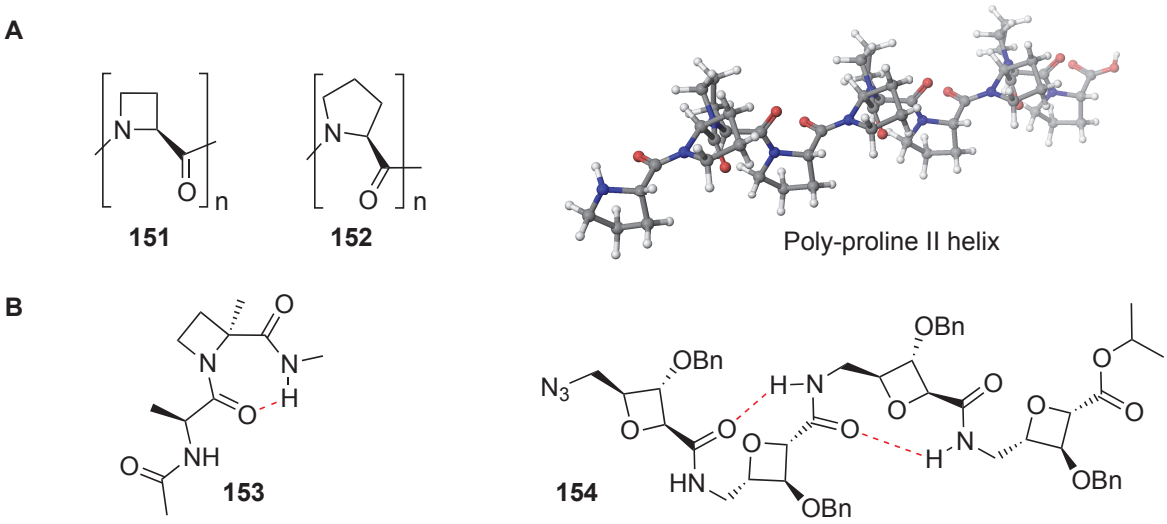


**Figure 3.20** A) Peptide polymers based on Aze and Pro monomer and Poly-proline II structure resulting from all-*trans* peptide bonds; B) γ-turn induced by 2-alkyl-azetidine and β-turn induced by oxetane-δ-amino acids.

### 3.1.4.3 Related previous synthetic efforts

As far as we are aware there has been no syntheses of a scaffold containing a 2-carboxy-3-hydroxy-azetidine functionality, where both the ring nitrogen and the C3 oxygen are unprotected. The closest synthetic effort in the literature is a sequence for the formation of 3-epi-hydroxymugineic acid **104** (Figure 3.21).[118] However the fully deprotected amino acid was never formed in the synthesis, but this was attempted by Dureault et al., who produced the differentially protected amino esters **155** and **156**.[119] Efforts to deprotect these structures to the free amino acid were equally unsuccessful and amino acid **157** could only be formed with a methyl protecting group on OH3, while oxidation of the primary alcohol to the carboxylic acid was impossible with OH3 unprotected.[120] In an effort to synthesise aziridins azetidine **158** was formed instead, however once again no deprotection was attempted.[121] Biohydroxylation of azetidines is possible[122] and the Aze has been biohydroxylated to its *cis* analogue **91**, but only in an isolated yield of 2.5 mg.[37]

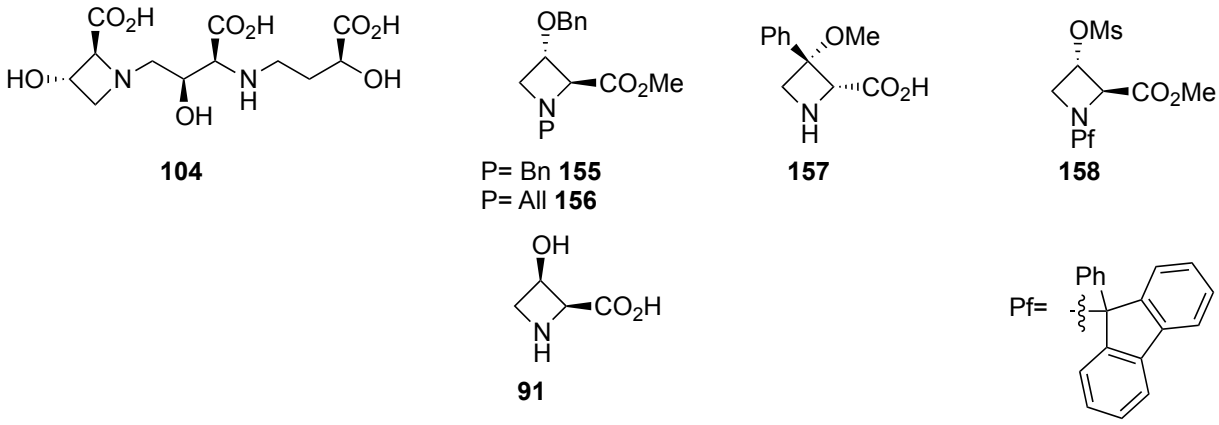


**Figure 3.21** Closely related synthetic efforts from the literature.

Overall there is a need for synthesis and further biological evaluation of hydroxylated azetidine-2-carboxylic acids, both as monomeric compounds and for incorporation into peptide polymers. Especially as the only synthesis of the unprotected amino acids are *via* biohydroxylation.[37]

## 3.2 D- and L-*ribo* azetidine synthesis

Both synthetic routes to the enantiomeric pair of polyhydroxylated azetidine amides **78L** and **78D** in the *ribo*-configuration were started from D-glucose **2**. For the L-*ribo* amide **78L** early cleavage in the synthetic sequence of the C5-C6 carbon bond in this sugar gave the carbohydrate in the xylose configuration, which upon suitable protection and esterification with trifluoroaceticanhydride gave key intermediate **159** (Scheme 3.5 top branch). Ring closure between C2 and C4 with benzylamine formed the azetidine and yielded bicycle **160,** which upon adjustment of oxidation state of C1 from +I to +III gave the desired L-*ribo* amide **78L**. On the other hand for the D-*ribo* amide **78D** the azetidine ring was formed prior to degradation of the carbon chain (Scheme 3.5 bottom branch). Protection of all hydroxyls bar OH-2 and OH-4 in D-glucose **2** allowed for the same ring closure with benzylamine to form the azetidine from intermediate **161**. Reduction of the C1 carbon gives triol **162**. Periodate cleavage of the diol, which corresponds to the C5-C6 bond in D-glucose **2**, gives an aldehyde at C5, which upon further oxidation can be elaborated into D-*ribo* amide **78D**. Therefore based on the C5-C6 degraded D-glucose **2** with the azetidine ring formed between C2 and C4, either C1 or C5 were oxidized to the carboxylic acid level to yield the enantiomeric *ribo*-amides.

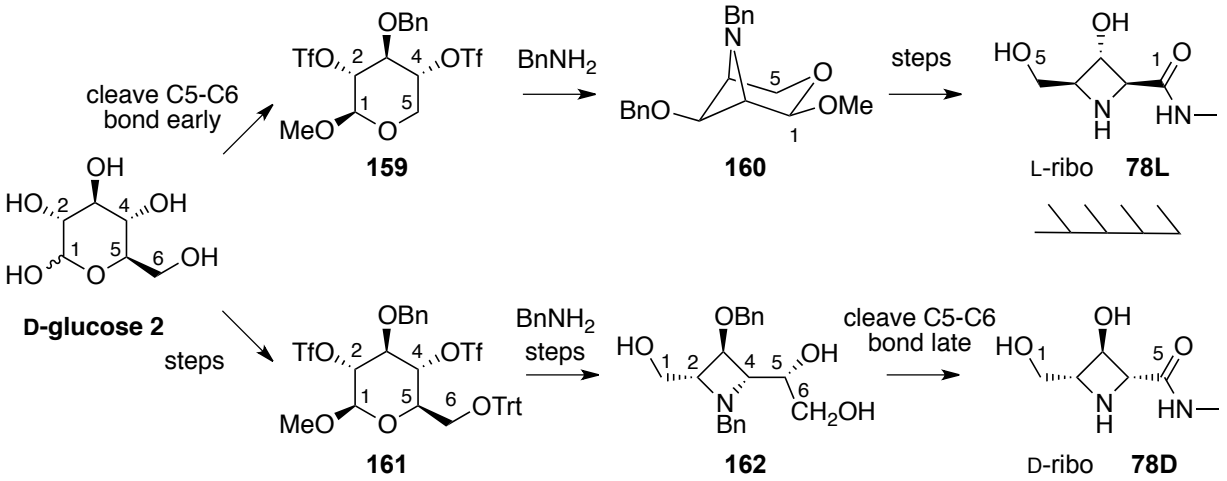


**Scheme 3.5** Overview of synthetic strategies towards the enantiomeric azetidine-ribo-amides. Compound numbering based on D-glucose.

### 3.2.1 Synthesis of bicyclic azetidine towards L-*ribo* configuration- early cut down series

The L-*ribo* amide synthesis began from tri-acetate **164**, which is readily available *via* literature procedures from di-acetone-D-glucose **163** featuring benzyl protection, selective acetonide cleavage and oxidative degradation with periodate followed by reduction, complete acid hydrolysis and acetylation (Scheme 3.6).[123] Treatment of **164** with HBr in acetic acid yielded the anomeric bromide, which was subjected crude to action of $AgCO_3$ in methanol to give the β-methyl-glycoside **165** in 61% according to the Koenig-Knorr reaction conditions.[124] Previous experience in the group had shown that in related systems only the β-glycosides were able to form the bicyclic structures containing azetidines, while the corresponding α-glycoside would show no reaction.[110b] In hindsight the methyl-glycoside step turned out to be the lowest yielding of the entire sequence, possibly due to the instability of the anomeric halide. This step could possibly be improved using Bi(III)halide catalysis,[125] which has been applied in high yields to highly related systems (87% over three steps to give the deacetylated methyl glycoside).[126] Under base catalysis the methyl glycoside **165** was deacetylated to give diol **166** in quantitative yield. Esterification of the free hydroxyls with triflic-anhydride set up compound **159** for azetidine ring closure with benzylamine between carbon C2 and C4, giving key bicycle **160** in a very good yield of 85%.

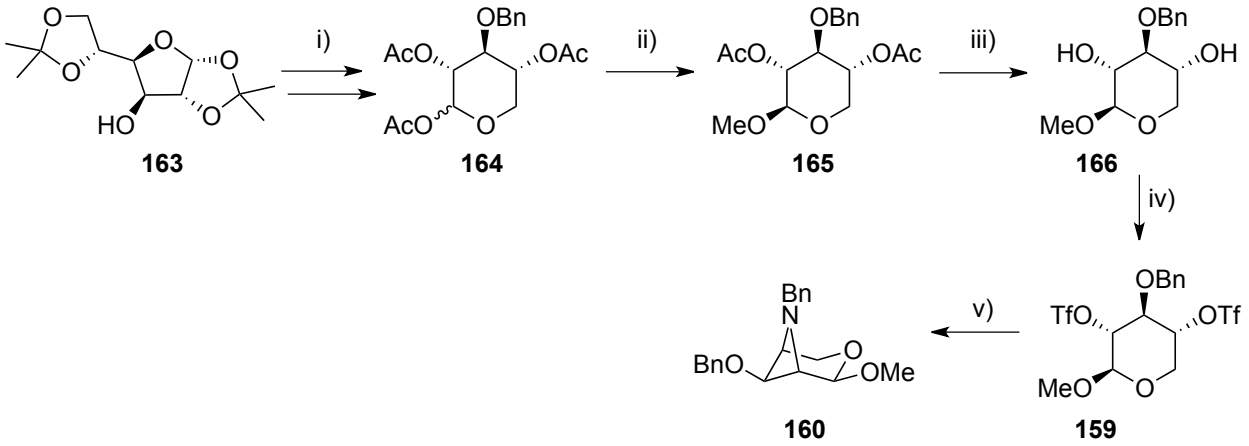


**Scheme 3.6** Reagents and conditions: i) Literature procedure[123] ii) HBr, 5-10 °C, 7:3 MeCOOH/$H_2O$, 4 h then $AgCO_3$, MeOH, RT, 18 h, 61% over two steps; iii) NaOMe, MeOH, RT, 18 h, quant; iv) $Tf_2O$, Pyridine, $CH_2Cl_2$, -20 to -10 °C, 4 h, quant; v) $BnNH_2$, MeCN, 70 °C, 2 h, 85%.

### 3.2.2 Initial lactone route – solution via a methyl ester

With the bicyclic azetidine **160** in hand the acid catalyzed hydrolysis of the methyl-glycoside to lactol **167L** proceeded in excellent yield (Scheme 3.7). Originally it was envisioned that the lactol **167L** could be oxidized to lactone **168**, which would then be readily opened by a suitable nucleophile like methylamine to the protected amide **169L**. Initial conditions attempted involved halogen based oxidation using molecular iodine in *tert*-butanol at 50 °C.[127] However TLC analysis of the reaction indicated the formation of a complex mixture of products in which the lactol, lactone and even the *tert*-butyl ester were able to be identified by mass spectrometry. With such an unlikely product being formed gave evidence of the extremely strained nature of the formed bicyclic lactone **168**. In order to force the reaction to completion, the iodine oxidation was repeated under reflux conditions, but although the starting material was consumed completely the reaction again yielded a complex mixture of products after workup. As the lactol **167L** had been found to be unstable to heating, and as a workup involving water might lead to opening the formed lactone **168** to the corresponding carboxylic acid to further complicate isolation of the product, reaction conditions were sought, that avoided both predicaments.

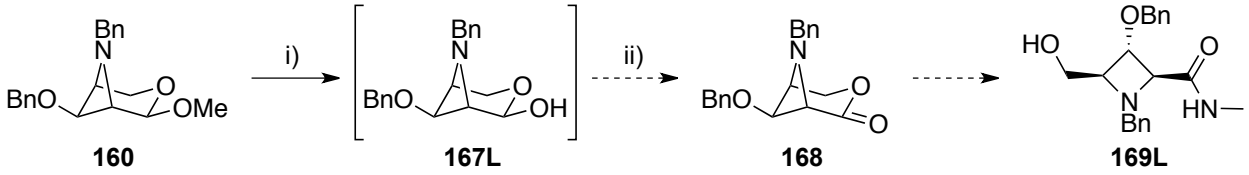


**160** **167L** **168** **169L**

**Scheme 3.7** Lactone bicycle approach. Reagents and conditions: i) 1:5 dioxane/ 2M HCl, 50 °C, 21 h, quant; ii) $I_2$, $K_2CO_3$, $^tBuOH$, 50 °C or reflux, 1.5 -2.5 h.

A Swern oxidation at -60°C to RT with a non-aqueous work up was therefore next attempted.[128] The reaction was performed on a test scale of 20 mg, and following column chromatography it was possible to isolate a sample, which was identified as the lactone **168** using mass spectrometry. However the yield of the reaction was poor and insufficient amounts were isolated for proton-NMR analysis. Dess-Martin oxidation with a non-aqueous workup generated a complex mixture from which it was impossible to isolate the desired lactone **168**.[129]

Having obtained the rather surprising evidence of the formation of the *tert*-butyl ester in the iodine oxidation and with the isolation of the lactone **168** being hampered by its instability due to the inherent ring strain, the synthetic strategy was changed to ring opening the lactone *in situ* with a suitable nucleophile in order to isolate the resulting product for further elaboration. As a result it was decided to replace the solvent with anhydrous methanol and to lower the reaction temperature to 0°C according to an adapted procedure by Yamada et al. (Scheme 3.8).[130] This reaction gave the methyl ester **170L** in reliably high yield (77-81%) following column chromatography but was also clean enough to be used without purification in the subsequent step (96% crude).

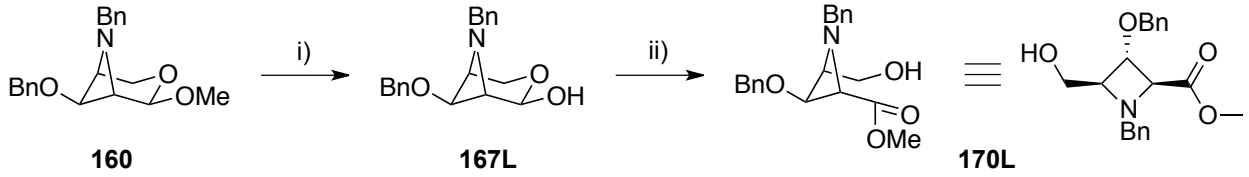


**160** **167L** **170L**

**Scheme 3.8** Isolation of the methyl ester. Reagents and conditions: i) 1:5 dioxane/ 2M HCl, 50 °C, 21 h, quant; ii) $I_2$, $K_2CO_3$, anh. MeOH, 0°C, 1 h, 81%.

### 3.2.3 Amide synthesis – ionic catalysis

Although the direct conversion of a carboxylic ester to an amide is a frequently undertaken transformation in organic chemistry, it often suffers from low yields and long reaction times and sometimes has to be performed in a three step sequence of ester hydrolysis, activation and aminolysis.[131] As a result Ley and coworkers published a manuscript in 2008 that used $Mg_3N_2$ in methanol as an *in situ* source of ammonia in order to convert alkyl esters, including methyl and *tert*-butyl derivatives, into primary amides.[132] Although their protocol allows a way to generate precise amounts of ammonia, especially on a small scale, safety concerns were raised about the exothermic nature of this reaction and the associated pressure build up, which can lead to explosions. It was however noticed, that this reaction produced the amide product in higher yields than commercial solutions of ammonia under the same conditions. Therefore additional factors had to be important possibly involving the $Mg(OMe)_2$ which is generated as a side product.

To explore this aspect of the reaction Bundesmann et al. investigated the amidation of alkyl esters in the presence of a range of ionic salts together with commercial ammonia solutions in methanol.[133] From this study $Mg(OMe)_2/NH_3$ and $CaCl_2/NH_3$ emerged as the reagent combinations of choice and a large range of ester substrates were successfully converted into primary amides including the ethyl ester of protected proline **171L** (Scheme 3.9 A). Usually employed as a desiccating agent, $CaCl_2$ is readily available in the laboratory and because the degree of epimerization was considerably lower for the conversion of ester **171L** to amide **172L** with $CaCl_2$ rather then using $Mg(OMe)_2$, it was chosen for the reaction with azetidine **170L**. Taking the strained nature of the azetidine ring into account the temperature was adjusted to 45°C and ammonia was substituted with methylamine to give amide **169L** (Scheme 3.9 B). TLC analysis indicated that the reaction had gone to completion in 1-3 h and amide **169L** could be formed in 72% yield over the three steps starting from azetidine bicycle **160**. When the reaction

was performed in absence of $CaCl_2$, it was exceedingly slow. Heated to 45°C with 20 eq. of $MeNH_2$ only traces of the desired amide could be seen *via* TLC analysis after 5 days.

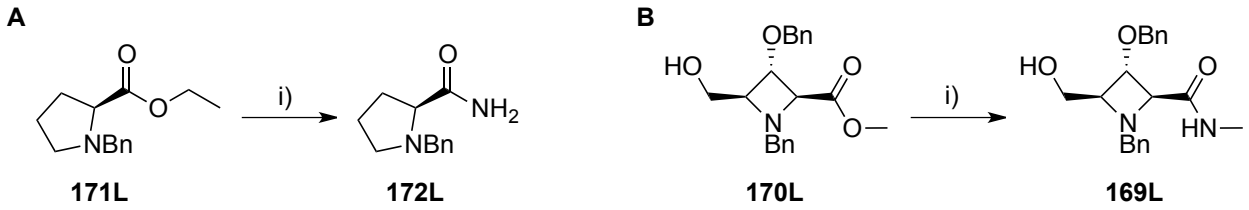


**Scheme 3.9** Amidation of alkyl ester. Reagents and conditions: A) i) 10 eq. $NH_3$ in MeOH, 1 eq. anh. $CaCl_2$, MeOH, sealed tube, 80 °C, 24 h, 82%; B) i) 20 eq. $MeNH_2$ in EtOH, $CaCl_2$, anh. MeOH, 45 °C in sealed tube, 1 h, 70%.

Although the role of the divalent cation is not fully understood, Bundesmann proposes coordination of the magnesium or calcium to the carbonyl group of the ester **173** predisposing it to nucleophilic attack (Scheme 3.10). Furthermore in a similar fashion to the mechanism of amidation of esters by formamide under basic catalysis with NaOMe the reaction[134] is autocatalytic in the formed amide **175**, which could be proven by isolation of imide **174** as an intermediate. Overall the adapted protocol is a very mild and quick way of converting azetidine esters into their corresponding primary amides in good yields.

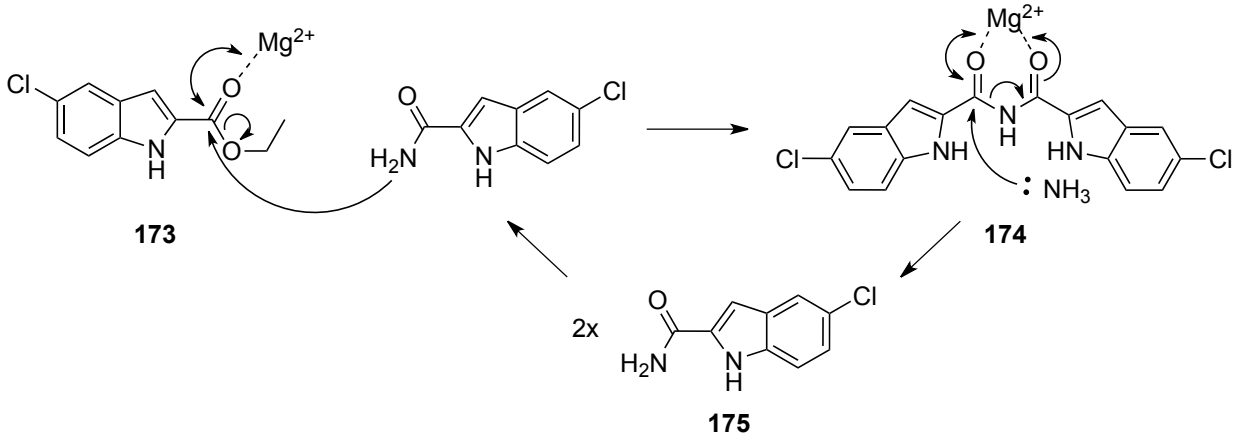


**Scheme 3.10** Proposed autocatalytic mechanism for amidation. Reagents and conditions: 10 eq. $NH_3$ in MeOH, 1 eq. $Mg(OCH_3)_2$, MeOH, sealed tube, 80 °C, 24 h, **174** 2%, **175** 72%.

### 3.2.4 Challenges of deprotection due to the retro-aldol reaction

The final step in the reaction sequence towards azetidine amide **78L** was the removal of the *N*-benzyl and *O*-benzyl protection in order to yield the free amino acid (Scheme 3.11). Initially

transfer hydrogenation, using ammonium formate as the hydrogen source, was attempted as the established conditions for deprotecting azetidines in our group. However TLC analysis revealed the reaction to be quite slow and only went to completion after 6.5 h, which is relatively long in comparison to the usual reaction time of 30 min (Table 3.1 entry 1). NMR analysis indicated a complex mixture of compounds being formed following work up of the reaction. A possible reason for the slow reaction progress might have been insufficient heating. Therefore the reaction was repeated under vigorous reflux conditions and TLC analysis after 30 min indicated a single product was formed (Table 3.1 entry 2). However following Dowex purification the NMR analysis of the resulting product was again very complex. Alternative deprotection procedures were sought and a Pd/C hydrogenation in the presence of HCl (generated *in situ via* reaction of AcCl with EtOH) in EtOH as a solvent was attempted (Table 3.1 entry 3). NMR analysis of the crude reaction product, which had been obtained *via* filtration through a glass fibre pad, yielded a clean spectra of what was presumed to be the dissolved HCl salt. In order to generate a free base spectra, purification using Dowex was attempted and it was at this stage that the susceptibility of 3-hydroxy-azetidine-2-amides to retro-aldol reactions was seen (Scheme 3.12). The aqueous ammonia solution used for elution purposes in this purification step was sufficiently basic to cause irreversible ring cleavage *via* deprotonation at OH3. This instability to Dowex purification precluded the further use of transfer hydrogenation conditions and therefore it was decided to repeat the hydrogen gas based reduction (Table 3.1 entry 4). Unfortunately partial alkalytion was observed on this repeat, which is discussed further in section 3.2.7. The solvent was therefore switched to water, which was mixed 2:1 with 1,4-dioxane to assist the solvation of the starting material **169L**. The reaction was followed by mass spectrometry and seemed to indicate the prolonged persistence of the mono-benzyl species despite TLC analysis indicating completion of the reaction and therefore the reaction time was increased to 27 h (Table 3.1 entry 5). The prolonged reaction conditions however led to epimerization of 20% of

the final product. The reaction was thus repeated and this time the reaction progress was solely judged by TLC analysis and stopped after 10 h. These conditions gave the 3-hydroxy-azetidine-2-amide **78L** in quantitative yield and starting from **164** it was obtained in an overall yield of 34% (Table 3.1 entry 6).

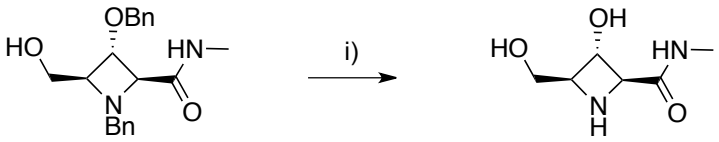


**169L** **78L**

**Scheme 3.11** Debenzylation challenges. Reagents and conditions: i) see Table 3.1.

**Table 3.1 Removal of *N*-benzyl and *O*-benzyl group from Azetidine 169L.**

| Entry | Conditions | Solvent | Purification | Outcome |
|---|---|---|---|---|
| 1(451) | $HCOONH_4$, Pd/C, 65°C, 6.5 h | Anh. MeOH | Dowex | Decomp. |
| 2(456) | $HCOONH_4$, Pd/C, reflux, 45 min | Anh. MeOH | Dowex | Decomp. |
| 3(460) | $H_2$, AcCl, Pd/C, RT, 8 h | EtOH | Dowex | Decomp. |
| 4(462) | $H_2$, AcCl, Pd/C, RT, 11 h | EtOH | Glass fibre | Alkylation |
| 5(512) | $H_2$, HCl, Pd/C, RT, 27 h | 2:1 $H_2O$, 1,4-dioxane | Glass fibre | Epimerization |
| 6(517) | $H_2$, HCl, Pd/C, RT, 10 h | 2:1 $H_2O$, 1,4-dioxane | Glass fibre | quantitative |

The decomposition of unprotected azetidine **78L** *via* a retro-aldol mechanism forms aldehyde **176**, which can rearrange to amide **177** and closes back to the anomeric pair of six ring hydroxy-lactams **178** (Scheme 3.12). The reaction is presumably driven by the release of the ring strain of the 4-membered system and results in the strain free 6-ring. Using NMR spectroscopy it was possible to assign the mixture of hydroxy-lactams **178** and the desired azetidine **78L**, the details of which are shown in Figure 3.22 (A and B are the *cis* and *trans* epimeric hydroxy-lactams **178** respectively and C is the azetidine **78L**). The assignment thus performed compares favorably to data that is available in the literature. The crystal structure of compound **179** has been obtained (CCDC 719613) and in the same publication **181** was formed from precursor aldehyde **180** which is a piperidine analogue of the piperazine in our study.[135] As shown in this study the amide closes the ring *via* the nitrogen onto the aldehyde. The anomeric proton of simple

hydroxyl-lactam **182** derived from glutarimide was assigned a shift of 4.91 ppm, very similar to the shifts observed for the anomeric products in this case.[136] The carbon spectrum of the compound mixture, albeit quite weak, showed the anomeric carbons at 79.7 and 79.2 ppm which is consistent with a hemiaminal rather then a hemiacetal. A similar rearrangement to a six-ring mixture of anomers from a β-lactam containing an hydroxyl group at C2 was noticed by Jäger and coworkers.[137]

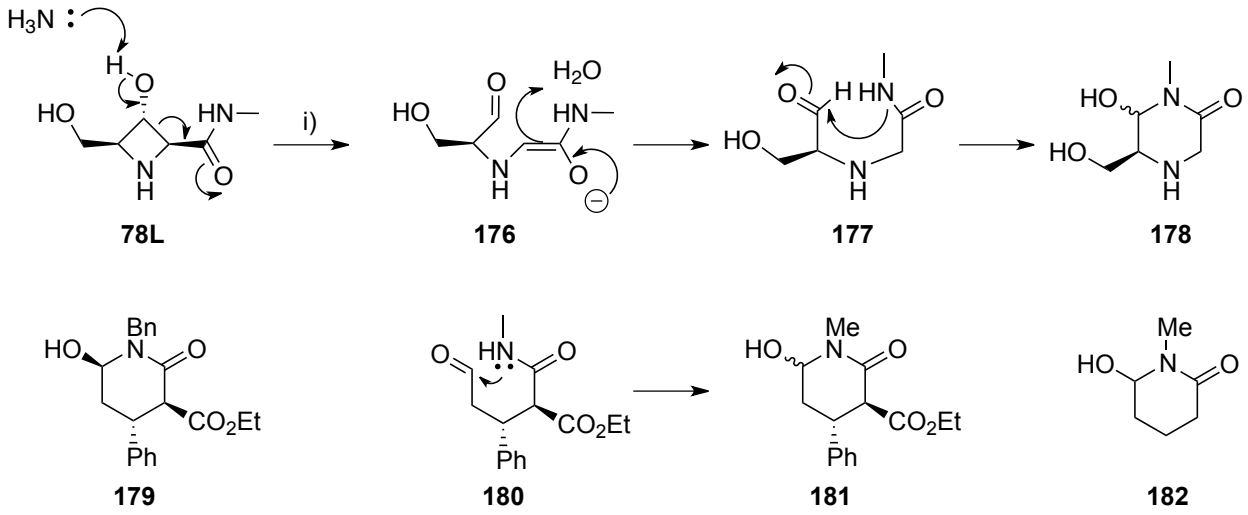


78L 176 177 178 179 180 181 182

**Scheme 3.12** Proposed retro-aldol mechanism and literature examples of related structures containing a hydroxy-lactam.

The azetidine amides formed in this work are therefore vulnerable to retro-aldols at high pH, but were completely stable at room temperature under neutral or acidic conditions. Analysis of a six month old sample, which had been stored at RT, showed no decomposition.

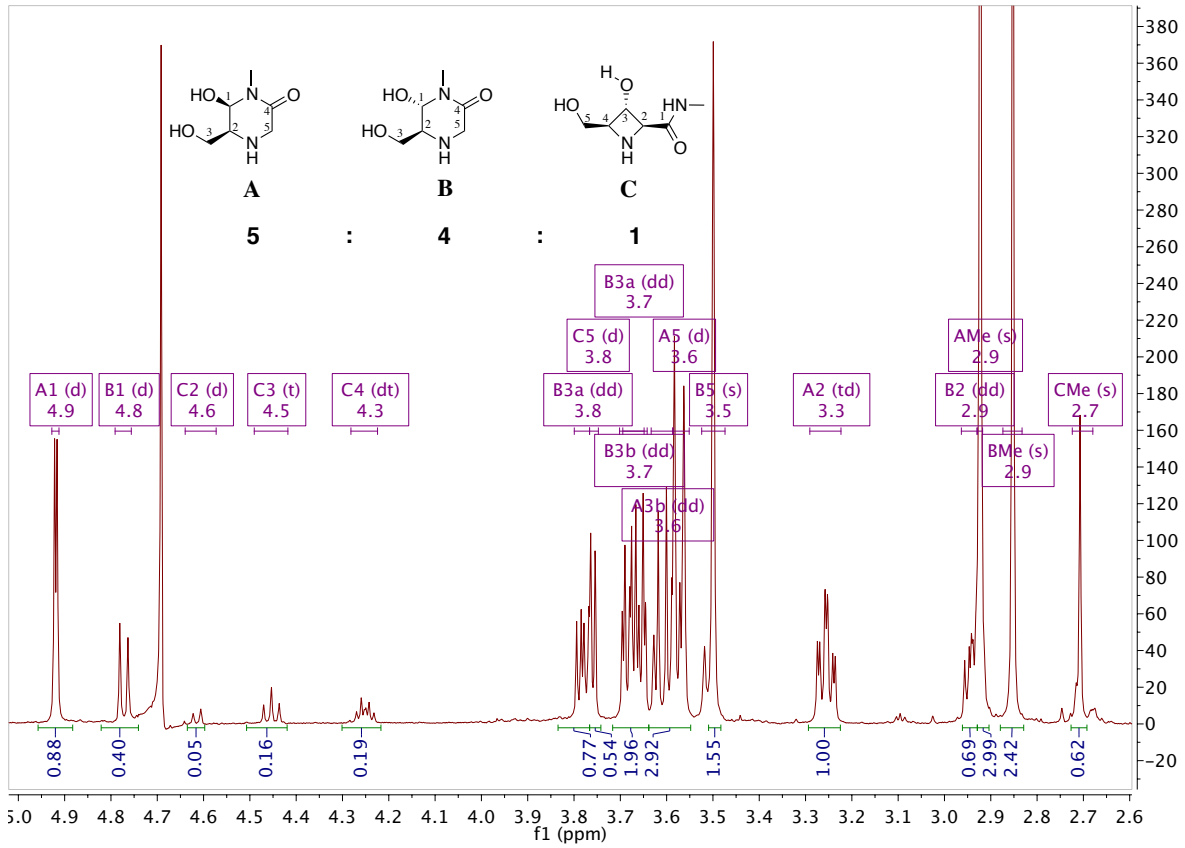


**Figure 3.22** $^{1}$H spectrum of retro-aldol products formed on Dowex purification. In the assignment the capital letter refer to the three compounds involved, with the corresponding carbon skeleton numbering detailed in the figure. The lower case letters a and b denote the pair of protons of a $CH_2$ and the splitting pattern is given in brackets.

Retro-aldol ring cleavage mechanisms have been observed in the literature for other four membered ring systems. The cycloalkane **183**, formed *via* a [2+2] cycloaddition, undergoes a retro-aldol reaction in order to give the corresponding diketone **184** (Figure 3.23) and this can be rationalized by release of the ring strain of about 26.3 kcal/mol (azetidine 25.2 kcal/mol).[138] This reaction has been used in a study of taxane diterpenes, where ring opening was induced using a lewis acid,[139] while in the total synthesis of (±)-Ingenol the retro-aldol was base triggered.[140] Ring cleavage was also observed with the related oxetane system in which 3-hydroxy-oxetane-2-carboxylate ester **185** decomposed to the open chain aldehyde derivative **186** under basic conditions.[141] Azetidines have previously been found to undergo the related retro-Dieckmann reactions when they contain a ketone or a methyl acetal at C3. Ketone **187** was unstable to

purification *via* silica gel and opened to the symmetric diester in the presence of methanol,[142] while amino acid **188** was extremely unstable on Dowex purification even decomposed on standing at room temperature.[143] Wessig et al. were unable to oxidize the primary alcohol in azetidine **189** in presence of an unprotected hydroxyl at C3.[120] The reason the desired carboxylic acid could not be formed in this oxidation was presumably due to the instability of the intermediate aldehyde, which would also be susceptible to a retro-aldol reaction.

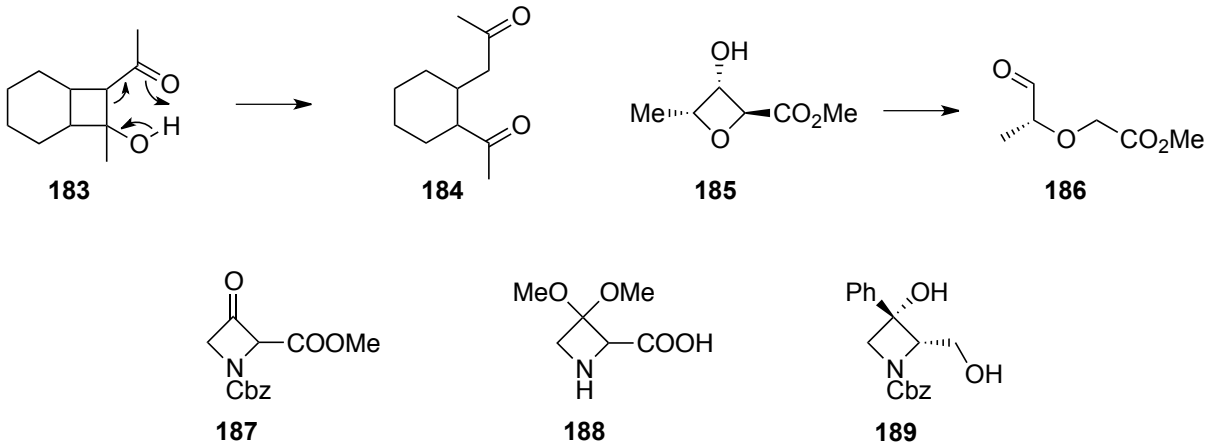


**Figure 3.23** Literature examples undergoing retro-aldols and unstable azetidines as a result.

During the hydrogenation in 2:1 water/1,4-dioxane in the presence of HCl it was possible to stop the reaction for NMR analysis at the stage where exactly 1 benzyl group had been removed (reaction time 6h). Analysis of the spectra revealed that the *N*-benzyl group had been removed prior to the *O*-benzyl. In general *N*-benzyl bonds are cleaved with more difficulty then *O*-benzyl groups and therefore can be deprotected selectively.[144] However Czech and Bartsch were able to show that the *N*-benzyl group in **190** can be removed selectively in the presence of *O*-benzyl group as the resulting amine poisons the catalyst. They were also able to selectively reduce a double bond in the presence of an *O*-benzyl via addition of *n*-butylamine to the reaction mixture (Scheme 3.13 A).[145] Similarly the *N*-benzyl group for piperidine **192** under hydrogenation conditions was removed prior to the *O*-benzyl, which was subsequently removed *via* dissolving metal conditions to give piperidine **194** (Scheme 3.13 B).[146] But during the synthesis of deoxymannonojirimycin **196** both *N*-benzyl and *O*-benzyl groups were removed simultaneously

*via* hydrogenation in the presence of HCl as a source of protons (Scheme 3.13 C).[147] This procedure is very similar to the one used in this study with exception to the solvent – ethanol, which was avoided due to the prior mentioned complications of alkylation with alcoholic solvents.

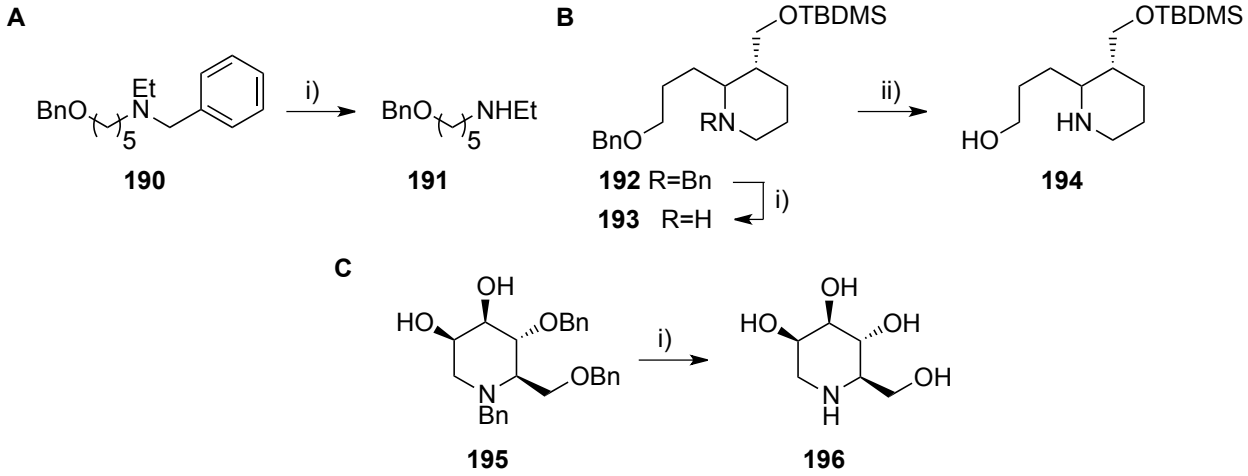


**Scheme 3.13** Selectivity of *O*-benzyl and *N*-benzyl deprotection. Reagents and conditions: A) i) 3 atm. $H_2$, 10% Pd/C, EtOH, RT, 20 h, quant.;[145] B) i) 3 atm. $H_2$, 10% Pd/C, MeOH, RT, 24h, ii) Li, liq. $NH_3$, THF, -78 °C to -33 °C, 2 h, 66%;[146] C) $H_2$, Pd/C, HCl, EtOH, RT, 14 h, 52%.[147]

### 3.2.5 Details of assignment of NMR bicycle

The NMR analysis of bicycle **160** in the L-ribo early cut down series revealed three interesting phenomenona and the assigned spectra can be seen Figure 3.24.

The first unusual feature that is apparent when analyzing the spectra is that there appears to be no coupling between the proton pairs H2/H3 and also H3/H4. As a result H3 appears as a sharp singlet. Molecular modeling was performed in order to obtain insights into the dihedral angle between the pair of protons involved and were found to be $\phi$ = -98.2 and $\phi$ = 99.5 (Figure 3.25). When plotting the Karplus equation[148] in its quadratic form[149] which describes the mathematical relationship between the dihedral angle $\phi$ with the coupling constant $J_{HCCH} = A \cos^2\phi + B \cos\phi + C$ with A = 9.0, B = -0.5, C = -0.3 it should be noted that $J_{HCCH} = 0$ at $\phi$ = 77.7° and 99.0°. Although this is a very rough analysis of the results, this angle dependence gives a possible explanation, why the coupling to H3 is exceedingly small.

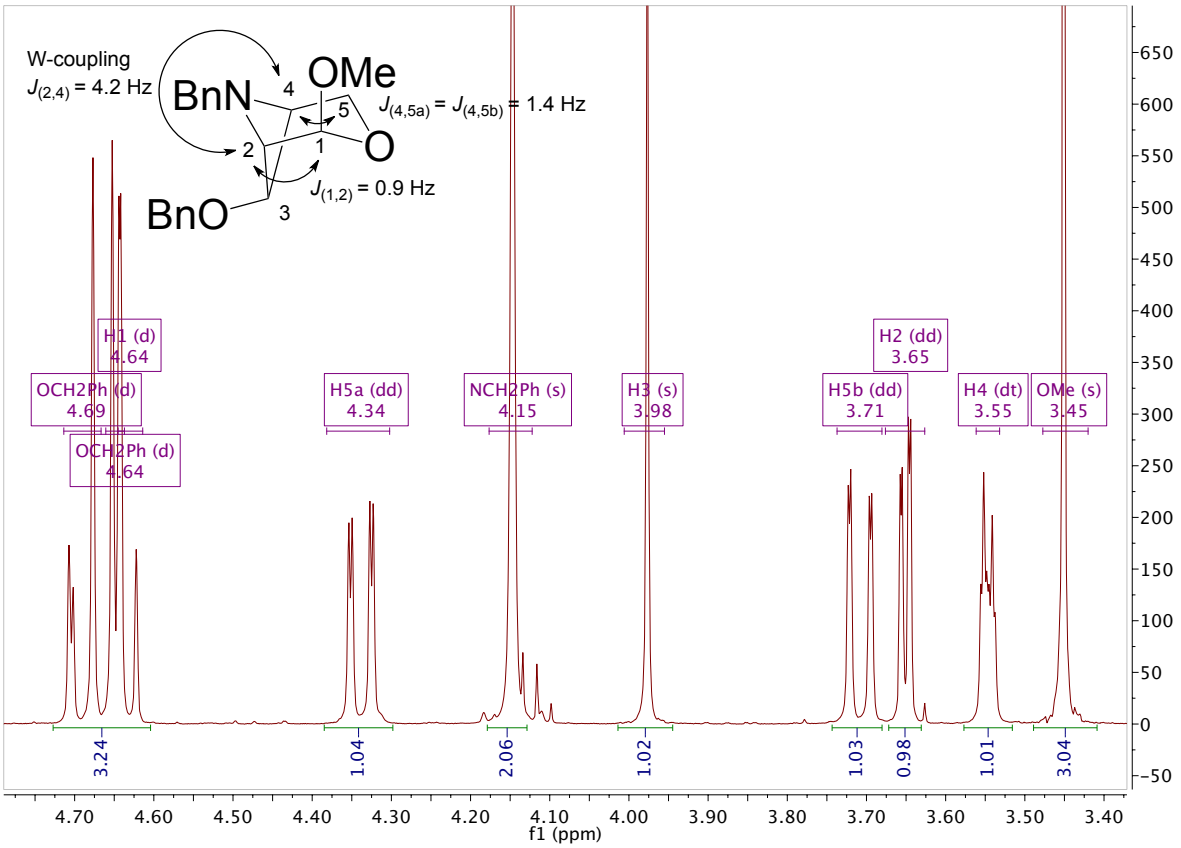


**Figure 3.24** $^{1}$H spectrum of bicycle **160**. The COSY coupling pattern with corresponding coupling constants is indicated on the bicycle representation.

Secondly the molecule displays an interesting long-range coupling between H2 and H4. This W-coupling between bridgehead protons is comparable to that one found in the all carbon scaffold bicyclo[3.1.1]heptane. In that system the W-coupling for the bridgeheads was estimated using theoretical calculations at 4.57 Hz[150] and experimental observations confirmed this at 5.4 Hz.[151] Therefore the coupling is quite comparable to the $J_{HCCH}$ = 4.2 Hz found in this study (Figure 3.24).

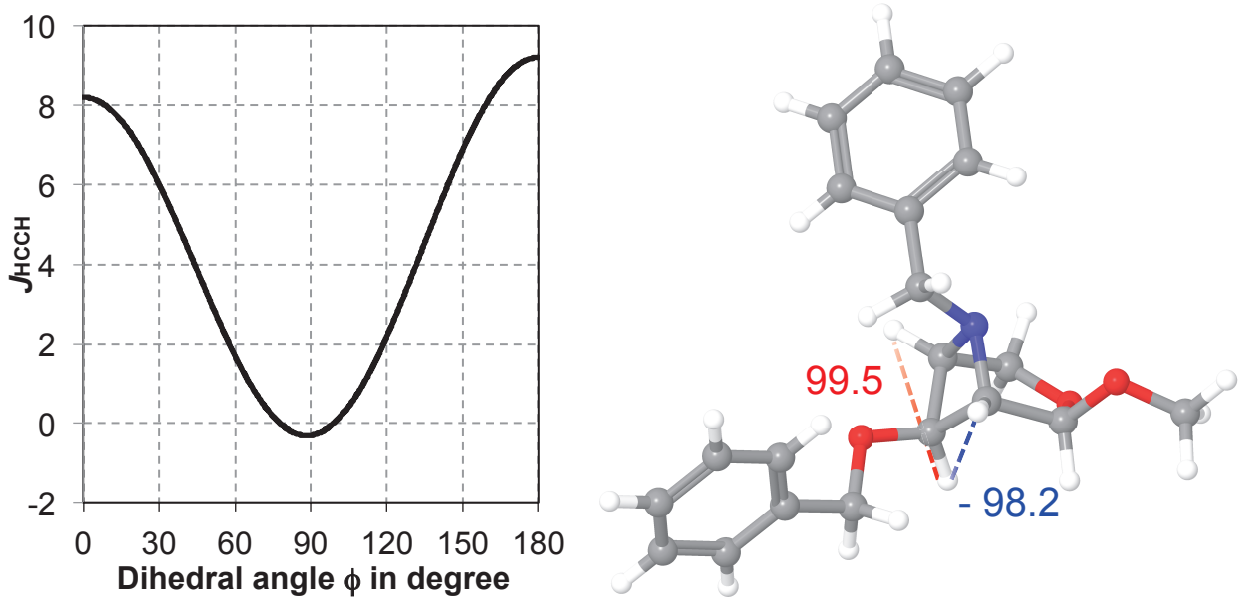


**Figure 3.25** Karplus curve of the formula: $J_{HCCH}$ = A $\cos^2\phi$ + B $\cos\phi$ + C with A = 9.0, B = -0.5, C = -0.3 and $\phi$ the dihedral angle;[148-149] DFT calculations at the M06-2X/6-311++G** level of theory were used to model bicycle **160** providing dihedral angles HCCH between H2 and H3 (blue) and H3 and H4 (red).

Nuclear Overhauser enhancement (NOE) NMR experiments were performed in order to check if a chair conformation is adopted by C1-C2-C3-C4-C5-O as found in bicycle **197**,[152] or by C1-C2-N-C4-C5-O as observed for bicycle **198** (Figure 3.26).[153] In the first case the protons H1 and H5 adopt a diaxial arrangement as in conformation **160-ax**, while in the latter the same protons are diequatorial as shown in **160-eq**. As no NOE interaction was observed for H1 and H5 it can be concluded that the conformation adopted by bicycle **160** is predominantly that of **160-eq** and therefore analogous to the one observed in the NBn containing bicycle **198**.

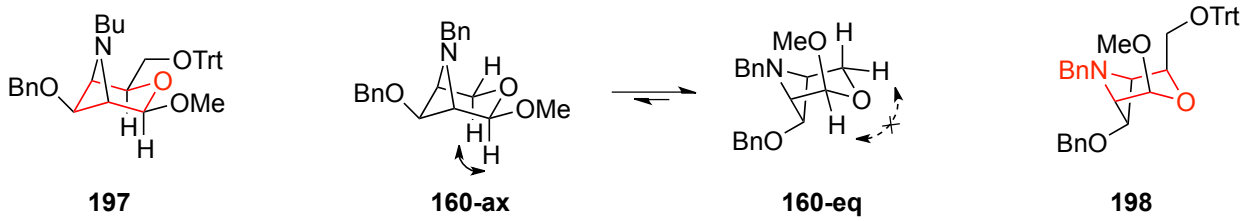


**Figure 3.26** Adopted conformation of bicycle **160**. Representative examples of each bicycle conformation are shown flanking.

### 3.2.6 Synthesis of the *meso*-iminoribitol

In a divergent synthesis again starting from bicyclic intermediate **160** meso-iminoribitol **200** was formed. This triol is of interest as it has very recently been shown, in a study on reversible male contraceptives, that the *N*-nonyl derivative of **200** is a potent inhibitor of α-glucosidase (*Saccharomyces cerevisiae*, 0.6 μM).[154] Therefore, in this case after removal of the methyl glycoside, bicycle **167L** was reduced with sodium borohydride and then subjected to purification *via* an acetylation/deacetylation sequence in order to give diol **199** in 74% yield over 4 steps (Scheme 3.14). Removal of the benzyl protection was achieved using hydrogenation conditions, which yielded triol **200** in quantitative yield.

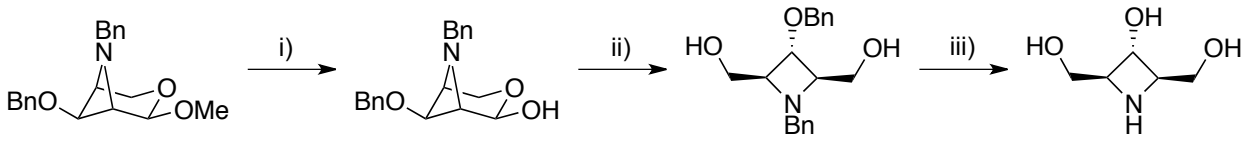


**160** **167** **199** **200**

**Scheme 3.14** Synthesis of *meso*-iminoribitol**.** Reagents and Conditions: i) 1:5 dioxane/ 2M HCl, 50 °C, 21 h, quant; ii) $NaBH_4$, MeOH, RT, 1.5 h then 1:1 $Ac_2O$, Pyridine, RT, 20 h then NaOMe, MeOH, RT, 47 h, 74% over 4 steps; iii) $H_2$, Pd/C, HCl, 2:1 $H_2O$/1,4-dioxane, 72 h, quant.

### 3.2.7 Alkylations of azetidine amides

As described previously in the attempt to completely remove the benzyl groups from the protected precursor **78L** (Scheme 3.11, page 110) in ethanol as a solvent partial alkylation to **201** of the desired azetidine **78L** was observed (Scheme 3.15). As the two azetidines proved to be inseparable, it was decided to subject the mixture to reductive amination conditions in the presence of ethanal in order to drive the alkylation to completion.

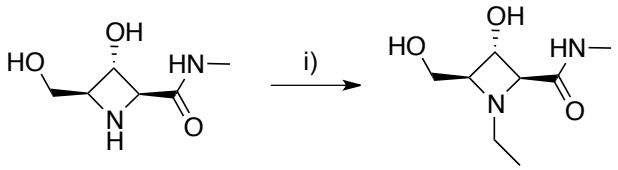


**78L** **201**

**Scheme 3.15** Alkylation *via* reductive amination. Reagents and Conditions: i) Ethanal, $H_2$, Pd/C, EtOH, 2 h, quant.

In the literature synthesis of (-)-Suaveoline methylations in high yields have been recorded for Pd/C reductions of *N*-benzyl groups in methanol, while they were avoided when ethanol was used instead with the HCl salt of the starting material.[155] It is known that commercial solutions of methanol and ethanol can contain formaldehyde and ethanal respectively.[156] Further possibilities to the source of ethanal in the reaction conditions of this study could be considered.

In order to affect reduction of both the *O*-benzyl and *N*-benzyl groups in a system a proton source is usually needed.[147] In a study on structurally related azetidines the benzyl group of the ring nitrogen was removed using hydrogenation conditions in presence of a proton source.[157] Therefore similar conditions were employed in this study and in order to produce a known amount of hydrogen chloride, acetyl chloride was reacted with ethanol prior to subjecting the reaction to the reducing conditions (Scheme 3.16 I).[158] However in the presence of trace amounts of water in the reaction mixture (Sigma-Aldrich data sheet of ethanol solutions quotes water content as up to 0.2%, which equates to 0.33 mmol present) direct reaction with acetyl chloride or hydrolysis of ethyl acetate would be feasible avenues for acetic acid formation (Scheme 3.16 II and III). In presence of a transition metal catalyst under reducing conditions acetic acid can be converted to ethanol *via* ethanal (Scheme 3.16 IV), which could alkylate any free amine in the reaction mixture (Scheme 3.16 V).[159] Alternatively the ethanal could be formed *via* subsequent oxidative addition and β-hydride elimination of palladium to ethanol (Scheme 3.16 VI) This reaction scheme was proposed by Sydnes et al. following the discovery that the prolonged exposure of nitro aryls to reducing conditions involving palladium on charcoal in ethanol yielded 41% of the secondary amine along with 47% of the desired amine. Therefore we can conclude that reductions of compounds forming amines in alcoholic solvents should be undertaken with caution due to the high risk of unwanted alkylation of the formed amine.

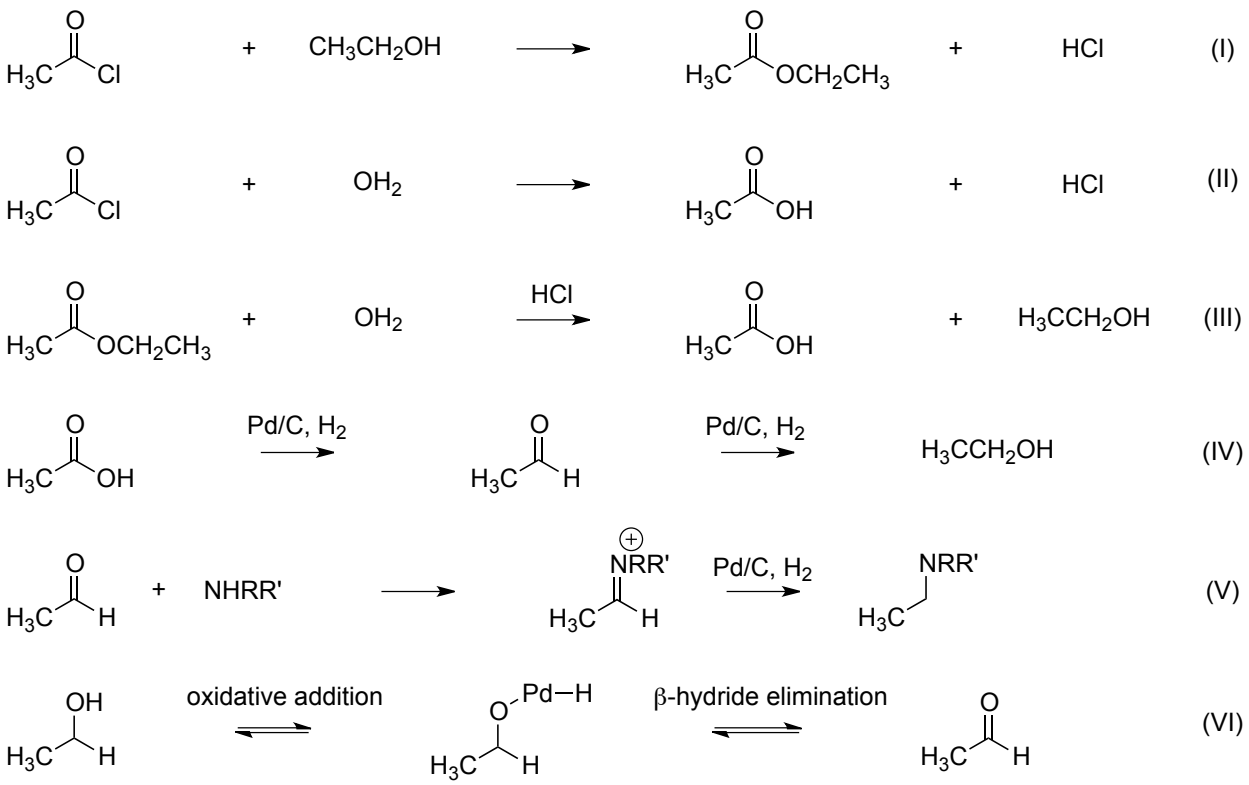


**Scheme 3.16** (I) *In situ* production of HCl; (II) + (III) Possible ways of forming acetic acid; (IV) Reduction of acetic acid to ethanol via ethanal;[159] (V) Reductive amination with ethanal; (VI) Alternative method of oxidizing ethanol to ethanol in the presence of palladium.[160]

Although the alkylation in this case was not desired, this sequence shows nonetheless, that azetidine iminosugars with free NH groups can be retrospectively derivatised to their alkylated analogues using reductive amination with the corresponding aldehyde.

### 3.2.8 Synthesis of the D-ribo enantiomer via the late cut down sequence

The enantiomeric D-ribo compound was accessed *via* the reaction sequence featuring the carbon-chain cutdown after the azetidine ring closure (Scheme 3.5, page 103). Therefore following the procedure established in the group[110b] the synthesis was started from tetra-acetate **202**, which is readily available from diacetone-D-glucose **163** (Scheme 3.17). The Koenig-Knorr reaction gave the methyl-glycoside **203** in the β-configuration in a good yield of 77%. Following deacetylation under catalytic basic conditions triol **204** was obtained, which was readily protected at the primary alcohol with a trityl ether to give diol **205**. This compound was then set up for

esterification with trifluoromethanesulfonic anhydride and azetidine formation with benzylamine to give the key bicyclic intermediate **198** in 76% yield.

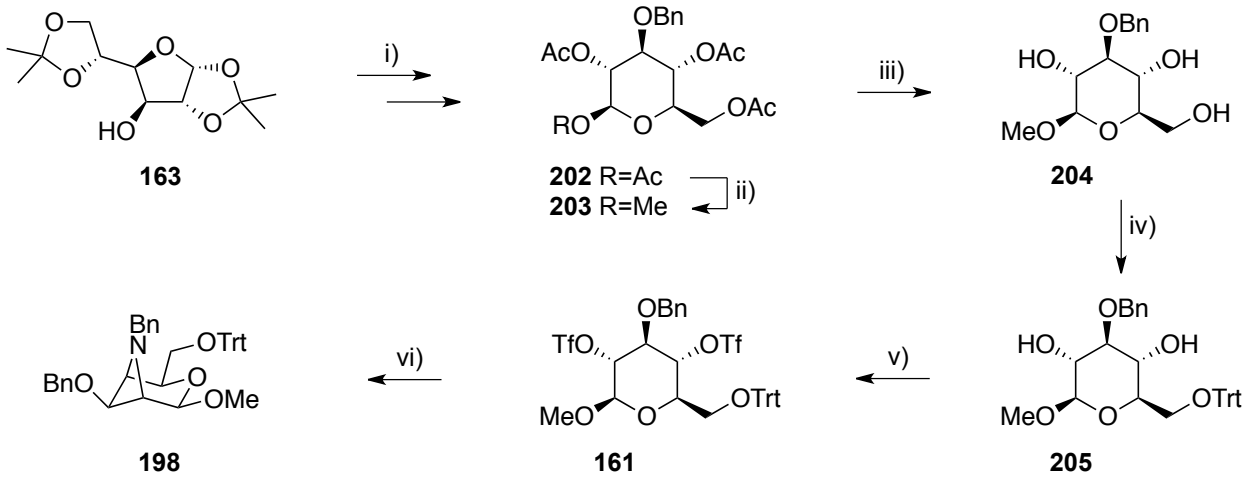


**Scheme 3.17** Synthesis of bicycle **198** towards azetidines in the D-ribo configuration. Reagents and conditions: i) Literature procedure[110b] ii) HBr, 7:3 MeCOOH/$H_2O$, 5 to 10 °C, 5 h then MeOH, 18 h, 77%; iii) NaOMe, MeOH, 18 h; iv) TrtCl, Pyridine, 18 h, 92% over two steps; v) $Tf_2O$, Pyridine, DCM, -20 to -10 °C, 4 h, 95%; vi) $BnNH_2$, MeCN, 70 °C, 2 h, 76%.

Bicycle **198** was deprotected under acidic conditions to lactol **206** and then readily reduced to triol **162**, which required purification via an acetylation/deacetylation sequence to allow for the removal of boron salts and gave the desired triol **162** in 78% over 4 steps (Scheme 3.18). Treatment with sodium periodate allowed for the oxidative degradation of the diol functionality to yield aldehyde/lactol **167D**, which was subjected crude to the oxidative conditions described for the enantiomer **167L** to give the intermediate ester **170D**. The best overall yields were obtained when the ester was converted directly into the corresponding amide giving **169D** in 78% over 3 steps. The previously identified hydrogenation conditions in the presence of hydrogen chloride gave the azetidine amide **78D** (29% over 14 steps starting from tetra-acetate **202**).

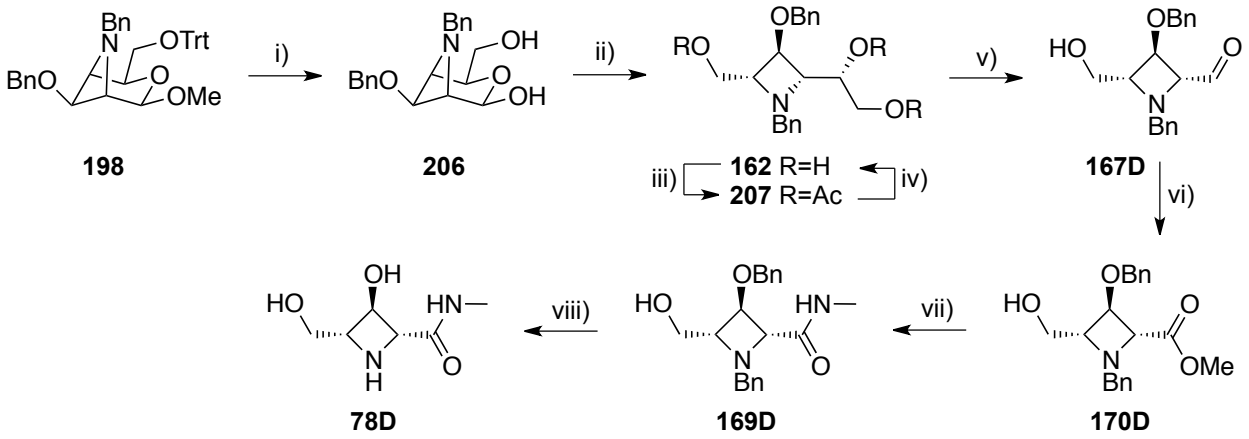


**Scheme 3.18** Synthesis of D-ribo azetidine amide **78D**. Reagents and conditions: i) 1:1 2M HCl/1,4-dioxane, 50 °C, 48 h; ii) $NaBH_4$, MeOH, RT, 1 h; iii) $Ac_2O$, Pyridine, 18 h iv) NaOMe, MeOH, 48 h, 78% over four steps v) $NaIO_4$, 2:1 $H_2O$/acetone, 1.5 h vi) $I_2$, $K_2CO_3$, anh. MeOH, 1 h; vii) $CaCl_2$, $MeNH_2$, MeOH, 45 °C in sealed tube, 1 h, 73% over three steps; viii) $H_2$, Pd/C, HCl, 2:1 $H_2O$/1,4-dioxane, 11.5 h, quant.

### 3.2.9 Polyhydroxylated azetidine-2-carboxylic acids

With the enantiomeric pair of methyl esters **170D/L** in hand hydrolysis to the corresponding α-amino acid was attempted (Scheme 3.19). In the light of the instability of the deprotected analogues to basic condition the hydrolysis of the methyl esters was performed under acidic conditions, which gave the protected amino acids **208D/L**. Despite the long reaction times required (3-7d), the hydrolyses occurred in very good yields and purification of the resultant material was not required.

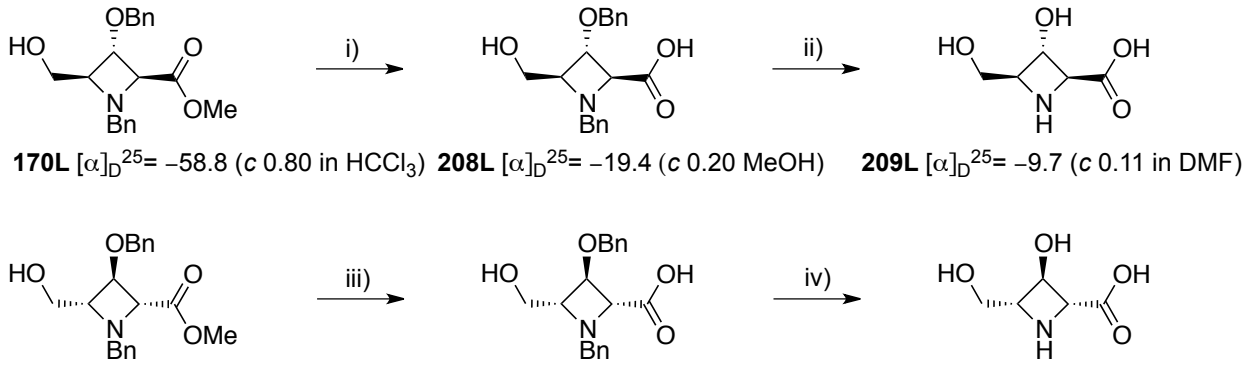

**170L** $[\alpha]_D^{25}$= –58.8 (*c* 0.80 in $HCCl_3$) **208L** $[\alpha]_D^{25}$= –19.4 (*c* 0.20 MeOH) **209L** $[\alpha]_D^{25}$= –9.7 (*c* 0.11 in DMF)

**170D** $[\alpha]_D^{25}$= +55.5 (*c* 0.51 in $HCCl_3$) **208D** $[\alpha]_D^{25}$= +25.1 (*c* 0.66 in MeOH) **209D**$[\alpha]_D^{25}$= +6.6 (c 0.19 in DMF)

**Scheme 3.19** Enantiomeric azetidine amino acid synthesis. Reagents and conditions: i) HCl, 2:1 $H_2O$/1,4-dioxane, 70°C, 3 d, 81%; ii) Pd/C, $H_2$, HCl, 2:1 $H_2O$/1,4-dioxane, 15 h, quant; iii) HCl, 2:1 $H_2O$/1,4-dioxane, RT to 70 °C, 7 d, 96%; iv) Pd/C, $H_2$, HCl, 2:1 $H_2O$/1,4-dioxane, 18 h, quant.

The X-ray crystal structure of the protected carboxylic acid **208D** was obtained and it was found to crystalize as the zwitterionic species with one molecule of water in the unit cell (Figure 3.27). Debenzylation of the enantiomers **208D/L** was performed with the same conditions as used for amides **169D/L** and proceeded with excellent yields. It should be noted that α-amino acids **209D/L**, in contrast to the amides **78D/L**, were stable to purification by DOWEX® ion exchange chromatography, indicating that the reactivity of the carboxylic acid group was low enough to exert resistance to retro-aldol type reactions induced by the dilute ammonia solution. Following debenzylation of **208D** NOE studies confirmed, that the stereochemistry (all *trans*) was unaffected by the deprotection. As amino acid **208D** is derived from intermediate **170D**, which is the precursor for amide **169D**, this gives confidence in the structure of amide **78D** as well as their enantiomers **169L** and **78L**. Several attempts at obtaining a mass spectrum of the amino acids **209D/L** however were unsuccessful. Several different spectrometers and techniques were trailed: Waters LCT Premier (electrospray ionization), Micromass LCT (electrospray ionization), Bruker μTOF (electrospray ionization) and field ionization, but the compound was found not well suited to mass spectrometry possibly due to its zwitterionic character and very low molecular weight.[161] The synthetic investigations towards azetidine acids **209D/L**, amides **78D/L** and triol **200** have recently been published.[162]

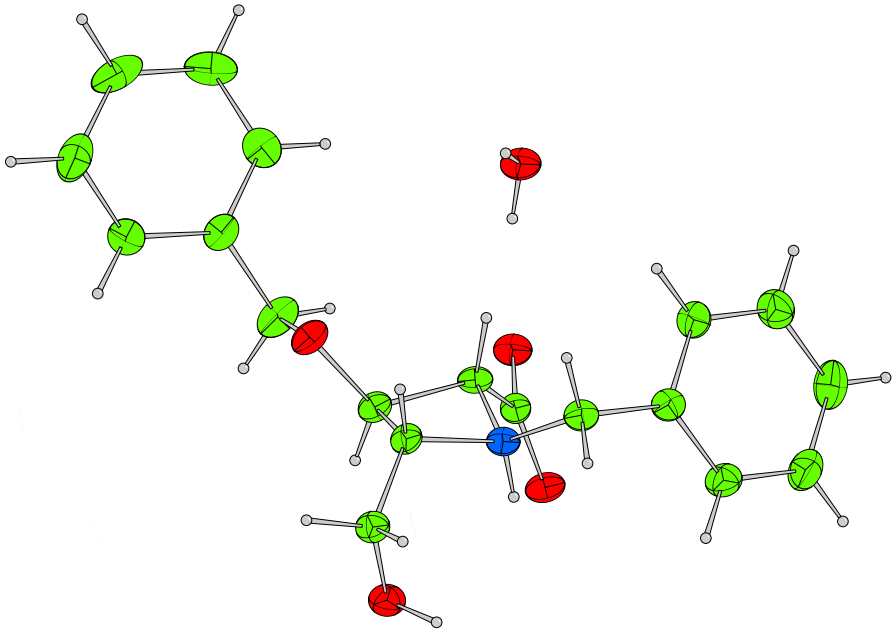

**Figure 3.27** X-ray structure of azetidine carboxylic acid **208D** with displacement ellipsoids drawn at the 50% probability level (CCDC 924224); Hydrogen atoms are shown as spheres of arbitrary radius.[162]

## 3.3 Route towards D-Lyxo azetidine

Encouraged by the synthetic success in the *Ribo* series we were curious if the methodology could be modified to move away from bicyclic systems towards open chain closures of azetidines. This approach would not only allow access to the desired D-*lyxo* compound, which had been predicted as candidate for β-*N*-acetyl-hexosaminidase inhibition in the molecular modeling Section 2.4.5 (page 40), but in future open the avenue to further trans-azetidines shown in Figure 3.1 (page 72).

In order to obtain the correct stereochemistry of azetidine amide **79D** the synthesis was started from D-gulose **210**, which is epimeric to D-glucose **2** at C3 and C4 (Scheme 3.20). Although the synthesis strategy mimics the late cut down series of the D-ribo synthesis, OH2 and OH4 are in a *trans* configuration preventing the formation of a bicyclic intermediate. Therefore the synthetic strategy involved an open chain cyclization to form the azetidine from a suitable intermediate featuring orthogonal protection to allow for the diol functionality ($P_b$) to be unmasked in the presence of a protected C3 hydroxy and ring nitrogen ($P_a$). The same chemistry as used

previously would allow for the cut down of the carbon-chain and oxidation of C5 to the correct oxidation level to allow formation of the methyl amide. The overall result is the *trans*-azetidine amide **79D** (with respect to the hydroxymethyl and amide chain), which is epimeric to the L-*ribo* derivative at the hydroxylmethyl group.

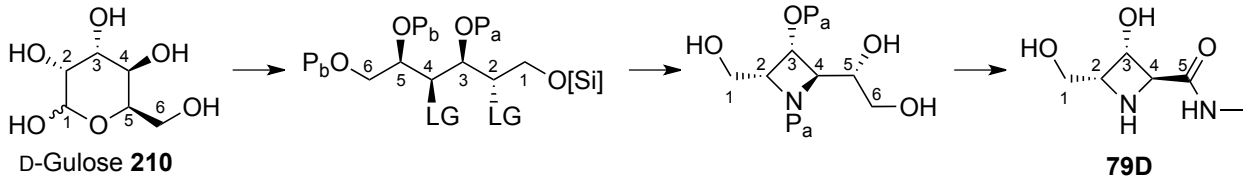


**Scheme 3.20** Synthesis strategy for azetidine in D-*lyxo* configuration. Numbering refers to the D-gulose starting material.

### 3.3.1 Challenges in the starting material synthesis – reduction of a double bond

Synthesis of the starting material 1,2:5,6-di-acetone-D-gulose **214** was performed from the readily available di-acetone-D-glucose **163** (Scheme 3.21). Alcohol **163** was therefore oxidized to the corresponding ketone **211** using Dess-Martin reagent, which had been prepared according to the combined protocols of Frigerio and Ireland.[163] There are a variety of conditions in the literature for the synthesis of D-gulose **214**, all of which proceed *via* the acetyl-captured enolate **212**, which is subsequently reduced from the less hindered face of the molecule to give acetate **213** as the protected analogue of **214**. Ketone **211** was therefore treated with acetic-anhydride in order to yield alkene **212**. A variety of conditions were subsequently trialed for the reduction of the double bond in the system by varying the catalyst, pressure and reaction time of the hydrogenation (Table 3.2 Entry 1-4).[164] However all attempts returned starting material **212**, therefore more forcing conditions were employed involving Adam's catalyst, protic solvents and transfer-hydrogentations (Table 3.2 Entry 5-8). In this case the major product of the reaction was deoxy analogue **216**, although following deacetylation it was possible for the first time to isolate alcohol **214** (The deoxy compound **216** and acetyl **213** cospot by TLC). Reductions involving sodium borohydride gave D-gulose **214** directly, however only in unacceptably low yields of 17-25% (Table 3.2 Entry 9-10). The real improvement in this reaction was only obtained after the

catalyst loading was shifted to 50% by weight and the solvent was changed to diethyl-ether (Table 3.2 Entry 11).[165] Fortunately it was possible to obtain even better yields, when the catalyst was changed from palladium black to the more economical 10% palladium on charcoal, and on scale up of 3 g acetyl **213** was isolated in an excellent yield of 97%. Deacetylation gave the suitably protected D-gulose **214** with only the C3 hydroxyl group free, which was subsequently protected using benzyl bromide in order to give starting material **215** for the azetidine **79D**.

**Table 3.2 Reductive conditions trialed for synthesis of D-gulose. Compounds from Scheme 3.21.**

| Entry | Scale | Cat | Load | *P* | Solvent | *t* | **212** | **216** | **213** |
|---|---|---|---|---|---|---|---|---|---|
| 1(526) | 500 mg$ | Pd black | 5% b.w. | 1 | EtOAc | 3 d | 52% | | |
| 2(534) | 521 mg | Pd black | 5% b.w. | 1 | EtOAc | 14 h | 92% | | |
| 3(533) | 262 mg | $PtO_2$ | 10% b.w. | 1 | EtOAc | 14 h | 94% | | |
| 4(535) | 506 mg | 10% Pd/C | 15% b.w. | 4 | EtOAc | 16 h | 95% | | |
| 5(537) | 57 mg | $PtO_2$ | 10% b.w. | 1 | THF | 2 d | | 70%# | 30%# |
| 6(538) | 48 mg | $PtO_2$ | 10% b.w. | 1 | EtOH | 18 h | Complex mixture | | |
| 7(536) | 106 mg | Pd/C $HCOONH_4$ | 70% b.w. | - | MeOH | 30 min | | 70%# | 30%# |
| 8(539) | 54 mg | Pd/C $HCOONH_4$ | 70% b.w. | - | MeOH | 30 min | | 61% | 25%§ |
| 9(541) | 56 mg | $NaBH_4$ | 2 Eq. | - | EtOH | 2 h | | | 17%§ |
| 10(542) | 91 mg | $NaBH_4$ | 2 Eq. | - | EtOH | 1 h | | | 25%§ |
| 11(540) | 60 mg | Pd black | 50% b.w. | 1 | $Et_2O$ | 14 h | | | 78%# |
| 12(544) | 46 mg | 10% Pd/C | 50% b.w. | 1 | $Et_2O$ | 2 d | | | 93% |
| 13(545) | 3 g | 10% Pd/C | 50% b.w. | 1 | $Et_2O$ | 17 h | | | 97% |

# conversion based on NMR data; § based on isolation of **214**; $ crude starting material.

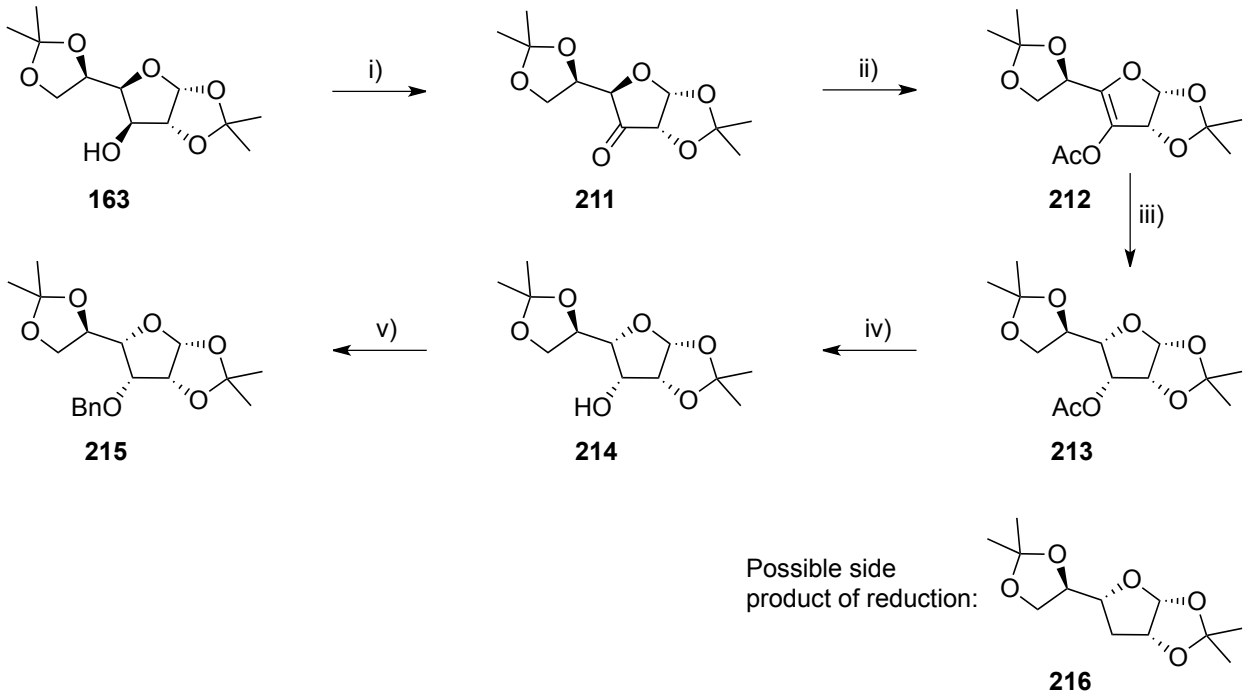


**Scheme 3.21** Synthesis of the D-gulose configured starting material **214**. Reagents and conditions: i) Dess-Martin-Periodate, DCM, 0 °C → RT, 22 h, 97%; ii) $Ac_2O$, Pyridine, reflux, 10 h, 96%; iii) $H_2$, Pd/C 50% b.w., $Et_2O$, 97%; iv) MeOH, $H_2O$, $Et_3N$, 81%; v) BnBr, NaH, DMF, 0 °C → RT, 95%.

### 3.3.2 Selective acetonide deprotection

Although the selective removal of the primary acetonide with acetic acid on scales up to 52 g in diacetone-D-glucose **163** is well established and proceeds in very good yields,[166] the only report of a similar reaction on a carbohydrate in the *gulo* configuration **214** has a crude yield of 58% following treatment with 80% aq. acetic acid with the remaining material isolated as the completely deprotected tetrol.[167] Furthermore selective deprotections involving acetic acid can be unrealiable on scale up, as the reaction continues during removal of the reagent under reduced pressure, making it difficult to control. Therefore a variety of conditions to affect the synthesis of diol **217** were tried, initially starting with 1% sulfuric acid in a water/1,4-dioxane mixture (Table 3.3, Scheme 3.22). Although the reaction initially showed formation of diol **217** by TLC and mass spectrometry, after 23 h only the completely deprotected derivative could be isolated. Similarly any conditions involving acetic acid were prone to overdeprotection, leading to poor yields of diol **217** (Table 3.3 Entry 1-3). Milder deprotection conditions were discovered in form

of the lewis acid bismuth-trichloride in acetonitrile or dichloromethane.[168] Due to its heterogeneous character the reaction was difficult to follow in dicholoromethane, however in acetonitrile on a large scale of ~2 g the desired diol **217** could be obtained in purified form in an excellent conversion of 86%.

**Table 3.3 Selective acetonide deprotection conditions compared.**

| Entry | Scale | Reagent | Solvent | T in °C | t | **215** | **217** | Conv |
|---|---|---|---|---|---|---|---|---|
| 1 | 60 mg | 1 % $H_2SO_4$ | $H_2O$/1,4-dioxane | RT | 23 h | - | - | - |
| 2 | 52 mg | 80% aq. AcOH | $H_2O$ | RT to 50 °C | 5 h | - | 42%§ | 42% |
| 3 | 55 mg | 50% aq. AcOH | $H_2O$ | 45-50 °C | 1.5 h | - | 55% | 55% |
| 4 | 52 mg | $BiCl_3$ | MeCN | RT to 60 °C | 2.5 h | 10%# | 62%# | 70% |
| 5 | 52 mg | $BiCl_3$ | DCM/$H_2O$ | RT | 9 h | Rxn very slow | | |
| 6 | 51 mg | $BiCl_3$ | DCM | RT | 2 h | Complex mixture | | |
| 7 | 52 mg | $BiCl_3$ | MeCN | RT | 35 min | 60%# | 40%# | 100% |
| 8 | 200 mg | $BiCl_3$ | MeCN | RT | 1.8 h | 31% | 55% | 79% |
| 9 | 1.79 g | $BiCl_3$ | MeCN | RT | 2 h | 32% | 58% | 86% |

§ crude yield; # conversion based on NMR data.

With sufficient amounts of diol **217** in hand allyl protection preceded smoothly to give tetrahydrofuran **218** in a 95% yield. With selectivity no longer required the previously tried sulfuric acid conditions were employed to remove the remaining acetonide to give lactol **219**.

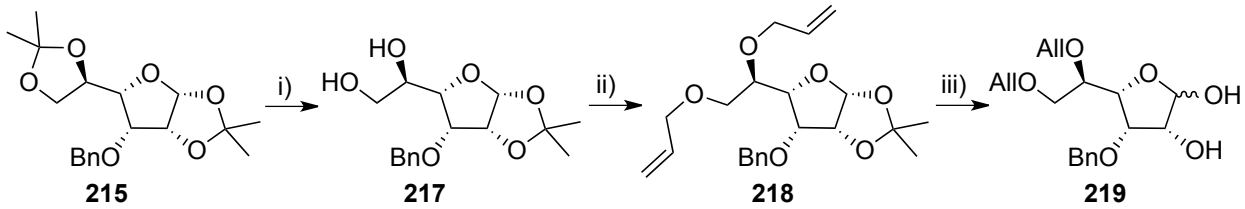


**215** **217** **218** **219**

**Scheme 3.22** Selective acetonide cleavage and orthogonal protection. Reagents and conditions: i) $BiCl_3$, MeCN, $H_2O$, 2 h, 58%, 86% conv.; ii) AllylBr, NaH, DMF, 0 °C → RT, 95%; iii) 1% $H_2SO_4$, $H_2O$, 1,4-dioxane, 40 °C, 5 h, 98%.

### 3.3.3 Stability of di-triflate vs di-mesylate for open chain azetidine cyclization

In order to set up the compound for cylization to the corresponding *trans*-azetidine all alcohols groups bar the hydroxyls at C2 and C4 needed to be protected. As a result lactol **219** was reduced to the corresponding triol **220** and silyl ether formation at the primary acohol yields diol

**221**. The conversion of the free hydroxyls yielded an extremely unstable ditriflate **222**, which decomposed both on silica and on standing at room temperature. Time restrictions precluded me personally to perform further synthesis on this system at this stage.

However a co-worker developed an open chain azetidine cyclization on a related system involving the activation of a diol with mesyl-chloride. As diol **221** had been generated on a scale of 670 mg, sufficient material was available for the co-worker to apply the conditions to form dimesylate **223** in quantitative yield.[169] On treatment of the dimesylate **223** with benzylamine under prolonged heating the formation of azetidine **224,** along with the mono-allyl derivative, was observed. Removal of the remaining allyl groups led to formation of a complex mixture of products. Microwave conditions were attempted for the closure but again the two main products observed were the desired product **224** along with a mono-allyl derivative as identified by mass spectrometry. Further work on the formation of *trans*-azetidines including this scaffold is ongoing in the group.

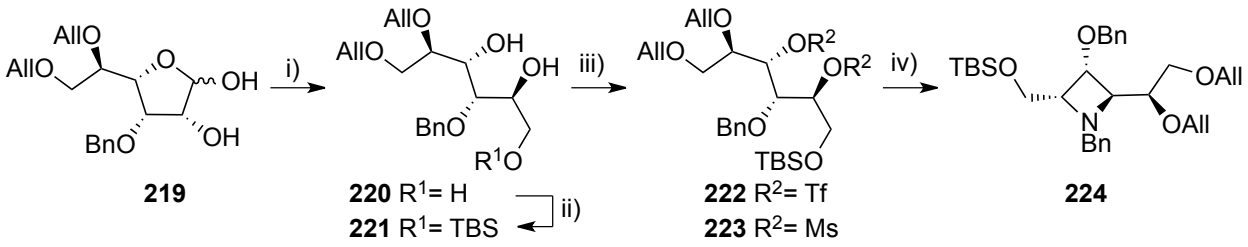


**Scheme 3.23** Azetidine ring closure. Reagents and conditions: i) $NaBH_4$, EtOH, 1h, 99%; ii) TBDMSCl, imidazole, DMF, -30°C → -20°C, 45 min, 92%; iii) $Tf_2O$, pyridine, DCM, -30 °C, 3h or MsCl, pyridine, DCM, RT, 18h, quant. iv) $BnNH_2$, 110-140 °C, 4d or $BnNH_2$, 180 °C, microwave, 2h.

## 3.4 Biological evaluations

Tests of the methyl amides **78D/L** and **201L**, carboxylic acids **209D/L** and the *meso* alcohol **200** for their biological activity were performed. The measurements of the large glycosidase panel were performed by collaborator Atsushi Kato (University of Toyama),[170] while the HL60 β-*N*-acetyl-glucosaminidase and *charonia lampas* α-*N*-acetyl-galactosaminidase data (incl. $K_i$ measurements) was collected in house.

### 3.4.1 Azetidine iminosugar glycosidase panel inhibition results

With exception of **78D** all azetidine iminosugars were subjected to a panel of 26 glycosidases with a selection of the results listed in Table 3.4.

**Table 3.4 Azetidine iminosugars giving 50% inhibition of various gylcosidases; $IC_{50}$ given in μM.**

| | 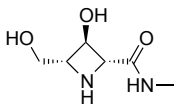 | 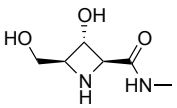 | 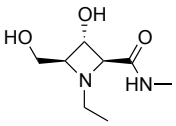 | 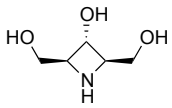 |
|---|---|---|---|---|
| Enzyme | **78D** | **78L** | **201L** | **200** |
| α-Glucosidase | | | | |
| Rice | ND[#] | NI[§] (0%) | NI (0%) | 83 |
| Yeast | ND | NI (23.2%) | NI (0%) | **9.5** |
| Aspergillus niger | ND | NI (7.8%) | NI (7.1%) | 693 |
| β-Glucuronidase | | | | |
| E. coli | **59** | NI (22.8%) | NI (45.1%) | NI (10.3%) |
| Bovine liver | NI (12.1%) | NI (0%) | NI (0%) | NI (2.6%) |
| α,α-Trehalase | | | | |
| Porcine kidney | ND | NI (3.0%) | NI (0%) | 30 |
| Amyloglucosidase | | | | |
| *Aspergillus niger* | ND | NI (0%) | NI (0%) | 758 |
| *Rhizopus sp.* | ND | NI (0%) | NI (0%) | 274 |
| β-*N*-Acetylglucosaminidase | | | | |
| Human placenta | NI (42.8%) | 4.3 | 46 | NI (7.4%) |
| Bovine kidney | NI (46.8%) | 2.7 | 21 | NI (8.9%) |
| Jack beans | 797 | 4.2 | 36 | NI (14.8%) |
| HL60 | NI (34.7%) | **5.2 [0.892][$]** | **45 [6.93]** | NI (5.1%) |
| *Aspergillus oryzae* | NI (21.4%) | 64 | 927 | NI (0%) |
| α-*N*-Acetylgalactosaminidase | | | | |
| Chicken liver | NI (12.5%) | NI (0%) | NI (0%) | NI (2.2%) |
| *Charonia lampas* | NI (13.9%) | NI (15.3%) | NI (18.2%) | NI (31.4%) |
| β-*N*-Acetylgalactosaminidase | | | | |
| HL60 | NI (11.3%) | 20 | 240 | NI (2.1%) |
| *Aspergillus oryzae* | NI (26.0%) | 36 | 556 | NI (5.8%) |

# Not determined; § No inhibition at 1000 μM (% inhibition); $ [$K_i$ in μM]; Details in Section 2.6.4 (p. 63).

Excluded from the result set of Table 3.4 as none of the compounds (for **78D/L**, **201L**, **200**) showed any inhibition ($IC_{50}$ > 1000 μM) were: β-glucosidase (almond, bovine liver, *Aspergillus niger*), α-galactosidase (coffee beans), β-galactosidase (bovine liver), α-mannosidase (jack beans), β-mannosidase (*Helix pomatia*), α-L-rhamosidase (Penicillium decumbens), α-L-fucosidase (bovine kidney). The amino acids **209D/L** although tested against the full panel showed no inhibition against any of the enzymes tested and therefore were equally excluded from the table of results.

### 3.4.2 Discussion on azetidine iminosugar glycosidase inhibition profiles

Although there are many glycosidase inhibition studies involving iminosugars with piperidine and pyrrolidine ring structures, the only glycosidase inhibition study in the literature on a polyhydroxylated azetidine is that of a triol in the L-*xylo* configuration **225L** (Figure 3.28).[137] The activity of this compound against amyloglucosidases was confirmed by us recently and the L-arabino analogue **226L** was found to be an inhibitor of amyloglucosidases and α-glucosidases as well, albeit less specifically.[110a] The 6-carbon tetrol analogues **227D/L**, which have the same configuration around the azetidine ring as the D-*ribo* and L-*ribo* compounds in this study respectively were also subjected to a glycosidase panel of 15 enzymes.[110b] Tetrol **227L** turned out to be a weak inhibitor of α-glucosidase (176 μM, rat intestinal maltase), while its enantiomer **227D** was inactive against the entire glycosidase panel. Bicyclic azetidines have also been studied for their inhibition profiles, but none showed significant inhibition.[171]

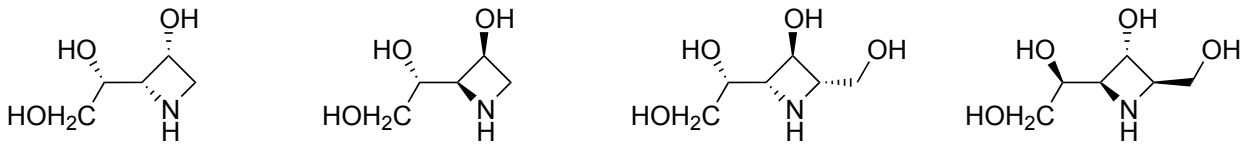


**Figure 3.28** Glycosidase inhibition from literature azetidine compounds.

The D-*ribo* azetidine **78D** turned out to be a weak inhibitor of β-*N*-acetyl-glucosaminidase (797 μM, Jack beans, Table 3.4). Often the enantiomers of iminosugars turn out to be more potent inhibitors than their natural analogues, as in the case for the pyrrolidine DMDP.[172] Furthermore it is noteworthy that amide **78D** was a specific inhibitor of bacterial β-glucuronidase, as it has been noticed that the β-glucuronidase of a gut resident symbiotic bacterium is responsible for the dose limiting toxicity of the common colorectal cancer treatement CPT-11.[173] The enantiomer L-ribo azetidine **78L** inhibited the set of hexosaminidases under investigation e.g. with $IC_{50}$ of 4.3 μM (β-*N*-acetyl-glucsoaminidase, human placenta) and 5.2 μM (β-*N*-acetyl-glucosaminidase, HL60); the $K_i$ was determined to be 0.892 μM (Figure 3.29, β-*N*-acetyl-gluccosaminidase, HL60). Its inhibition was very selective as well, as none of the other 19 glycosidases that were tested showed any significant inhibition by this amide. Its *N*-ethyl analogue **201L** was about an order of magnitude less active, with a $K_i$ of 6.93 μM (Figure 3.30, β-*N*-acetyl-gluccosaminidase, HL60), but was similarly selective. Other properties of iminosugars, like cell penetration, can be crucially influenced by *N*-alkylation and will be explored further in Chapter 4.

The triol **200** is the parent compound of the *N*-nonyl derivative, which has been shown to be a very potent α-glucosidase inhibitor (0.6 μM, *Saccharomyces cerevisiae*, yeast) and good β-glucosidase inhibitor (20 μM, almond).[154] It should be mentioned that the *N*-butyl derivative was completely inactive in the same study, however triol **200** turned out to be a potent inhibitor of α-glucosidase (9.5 μM, yeast) but showed no inhibition against β-glucosidase. In this context the ER α-glucosidase I inhibition was also tested but triol **200** turned out to have no inhibitory activity against this enzyme. It was, however, a good inhibitior of α,α-trehalase (30 μM, procine kidney) and a weak inhibitor of amyloglucosidases (274 μM, *Rhizopus* mold; 758 μM, *Aspergillus niger*) and in this respect is similar to triols **225L** and **226L**. None of the azetidines that were investigated in this study were inhibitors of α-*N*-acetylgalactosamindase.

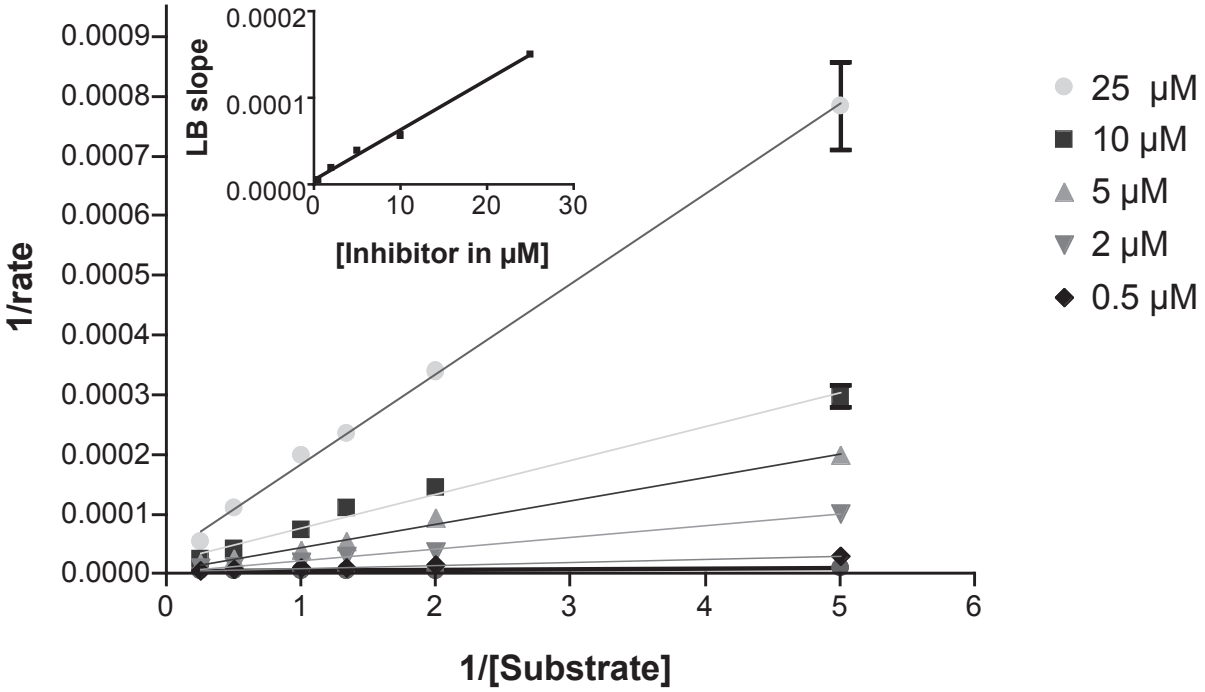


**Figure 3.29** Lineweaver Burk (LB) plot of azetidine amide **78L** against β-*N*-acetylglucosaminidase derived from HL60 cell homogenate; $K_i$ = 0.892 μM based on X-intercept of insert graph (LB slope vs Inhibitor concentration, $R^2$= 0.9940)

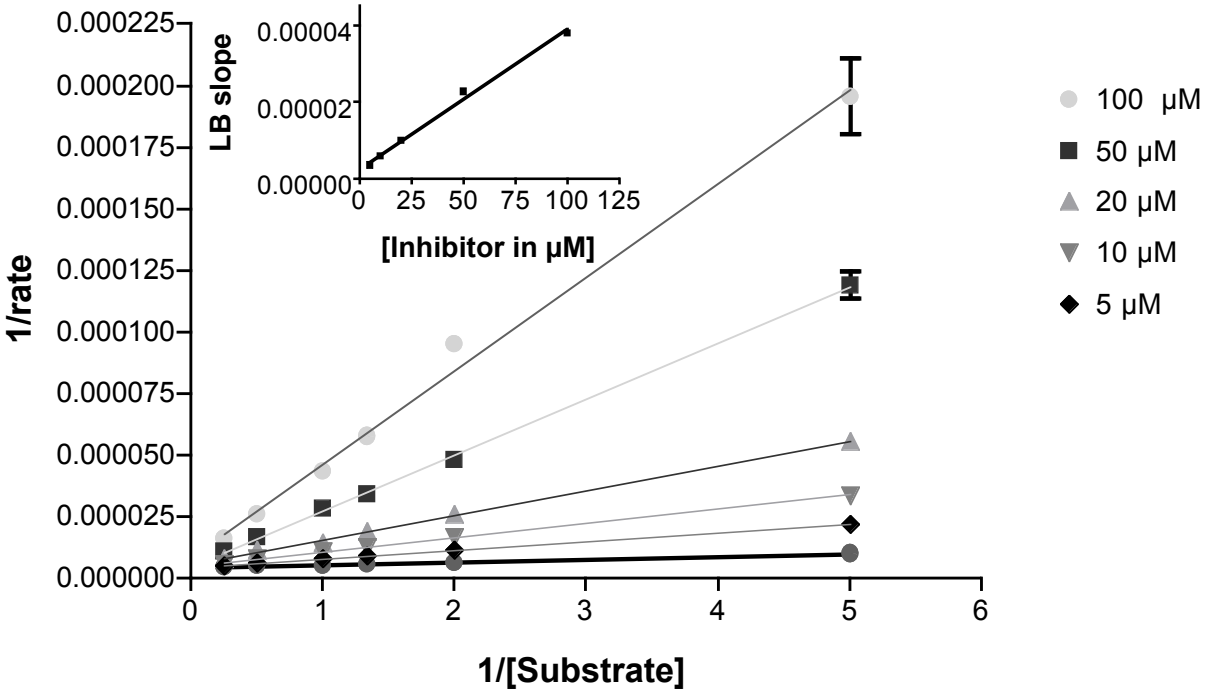


**Figure 3.30** Lineweaver Burk (LB) plot of azetidine amide **201L** against β-*N*-acetylglucosaminidase derived from HL60 cell homogenate; $K_i$ = 6.93 μM based on X-intercept of insert graph (LB slope vs Inhibitor concentration, $R^2$=0.9932)

### 3.4.3 Comparison of molecular modeling predictions with observed activity

In Section 2.4.5 (page 40) a comparison using molecular modeling between β-*N*-acetylglucosaminidase inhibitors of various ring sizes was drawn. The understanding was developed that the 5-ring pyrrolidine **68** is a ring-contracted version of pipecolic amide **10**, rationalizing their similar high level of inhibition. In turn L-*ribo* azetidine **78L** was a ring-contracted version of the 5-ring **68**, and was predicted to be an inhibitor of β-*N*-acetylglucosaminidase, which was now confirmed with an $IC_{50}$ of 5.2 μM (HL60). Albeit against the same enzyme from the same source both the pipecolic amide **10** (0.36 μM) and the pyrrolidine **68** (0.20 μM) were a magnitude more active, however this represents one of the rare examples where molecular modeling was able to successfully predict the activity of an iminosugar inhibitor. The inhibition study on the D-*lyxo* azetidine **79D** is anticipated to solve the relative importance of OH3 vs OH5 in the enzyme inhibition displayed by pyrrolidine **68** and due to time constrictions was not part of this study.

## 3.5 Conclusion Chapter 3

Overall in terms of synthetic aspects and enzymatic evaluation of the azetidine iminosugars the following can be concluded:

The synthesis route developed in our group towards *cis*-azetidines *via* bicyclic intermediates was successfully expanded with an oxidative protocol, which allowed the formation of the enantiomeric pairs of *ribo* azetidine carboxylic acids and amides. As far as we are aware this synthesis for the first time provides access to a 3-hydroxy-2-carboxy-azetidine with no protection on the ring nitrogen and the OH3. It also furnishes suitable intermediate monomers for the inclusion into polymeric structures and peptides. The synthetic methodology explored towards the *trans*-azetidine in the D-lyxo conformation in future should allow access to all 8 possible stereoisomers of the azetidine iminosugars investigated in this chapter.

The enzymatic evaluation of the azetidines confirmed the α-glucosidase inhibition of the *meso*-triol **200**, although not as potent as the inhibition potential of its nonyl derivative, and revealed the surprisingly selective inhibition of β-glucuronidase of the D-ribo amide **78D**. The L-ribo amide **78L**, a simple azetidine peptide, turned out to be a very potent and highly selective inhibitor of the possible new anti-cancer target β-*N*-acetyl-hexosamindase. This inhibitor in novel chemical space is one of the rare examples of a successful inhibition activity prediction in the field of iminosugars using molecular modeling.

## 3.6 4-ring experimental section

General chemical experimental found in Chapter 2 (p. 44).

### 3.6.1 L-*ribo* amide synthesis

Synthesis started from 1,2,4-tri-*O*-acetyl-3-*O*-benzyl-β-D-xylopyranose **164** which can be prepared according to literature procedures[123, 174] from D-glucose.

**Methyl 2,4-di-*O*-acetyl-3-*O*-benzyl-β-D-xylopyranoside 165**

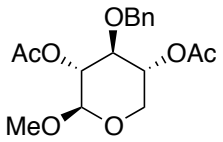


Hydrobromic acid (33% wt, in acetic acid, 0.63 mL, 3.67 mmol) was added dropwise over a 20 min period to a stirred solution of the triacetate **164** (500 mg, 1.36 mmol) in 7:3 acetic acid /dichloromethane (5 mL) at 10 °C, and the reaction mixture then cooled to 5 °C. TLC analysis (1:1 cylcohexane/ethyl acetate) after 5 h indicated disappearance of the starting material ($R_f$ 0.65) and formation of a major product ($R_f$ 0.80). The solution was diluted with dichloromethane (25 mL) and poured into ice water (25 mL). The organic layer was washed with cold saturated sodium bicarbonate (2 x 25 mL), water (25 mL), dried (magnesium sulphate), filtered and evaporated at 20 °C. The crude bromide was dissolved in methanol (8 mL) in a foil-wrapped

flask in the presence of silver carbonate (637 mg, 2.31 mmol) and stirred in the dark at RT for 14 h. TLC analysis (1:1 cyclohexane/ethyl acetate) indicated the formation of a major product ($R_f$ 0.60); the reaction mixture was filtered through a glass fibre pad and washed with methanol. The combined filtrates were evaporated and the residue (384 mg, 83%) purified by flash column chromatography (8:1→7:1 cylcohexane/ethyl acetate) to afford the β-pyranoside **165**, as a white crystalline solid (280 mg, 61%). M.p. 93-95 °C (ethylacetate/cyclohexane), [lit. m.p. 95.5-96 °C];[123a] $[\alpha]_D^{25}$ -56.5 (*c* 1.3 in $CHCl_3$), [lit. $[\alpha]_D^{22}$ -57 (c 1.00 in $CHCl_3$)];[123a] $\nu_{max}$ (thin film): 1745 (s, C=O); $\delta_H$ (400 MHz, $CDCl_3$) 7.37 – 7.26 (Ar, 5 H, m), 4.96 (H2, 1 H, dd, $J_{2,3}$ 7.3, $J_{1,2}$ 5.6), 4.92 (H4, 1 H, td, $J_{3,4}$=$J_{4,5}$ 7.1, $J_{4,5}$ 4.4), 4.68 (C$\underline{H}_2$Ph, 2 H, s), 4.40 (H1, 1 H, d, $J_{1,2}$ 5.6), 4.15 (H5, 1 H, dd, $J_{5,5'}$ 12.0, $J_{4,5}$ 4.4), 3.66 (H3, 1 H, t, $J_{2,3}$=$J_{3,4}$ 7.2), 3.45 (OC$\underline{H}_3$, 3 H, s), 3.35 (H5', 1 H, dd, $J_{5,5'}$ 12.0, $J_{4,5}$ 7.1), 2.04 (COC$\underline{H}_3$, 6 H, s); $\delta_C$ (101 MHz, $CDCl_3$) 170.0 (C=O), 169.6 (C=O), 138.0 (ipso-Ph), 128.5, 127.9, 127.8 (Ph), 101.3 (C1), 77.0 (C3), 73.4 (C$\underline{H}_2$Ph), 70.9 (C2), 70.3 (C4), 61.2 (C5), 56.4 (OC$\underline{H}_3$), 21.1 (C=OC$\underline{H}_3$); *m/z* (ESI+ve): 361 ($[M+Na]^+$, 32%), 699 ($[2M+Na]^+$, 100%); HRMS (ESI+ve): Found 361.1257 ($[M+Na]^+$); $C_{17}H_{22}NaO_7$ requires 361.1258.

**Methyl 3-*O*-benzyl-β-D-xylopyranoside 166**

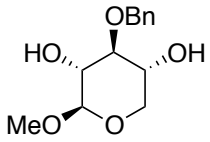


A solution of the protected β-pyranoside **165** (239 mg, 0.70 mmol) and sodium methoxide (3.8 mg, 0.07 mmol) in methanol (4 mL) was stirred at 40 °C. After 14 h, TLC analysis (1:1 cylcohexane/ethyl acetate) indicated complete disappearance of the starting material ($R_f$ 0.70) and formation of a single product ($R_f$ 0.30). The reaction mixture was evaporated to dryness and the residue was taken up in ethyl acetate (25 mL), washed with water (2 x 25 mL) and brine (25 mL). The aqueous phase was extracted with ethyl acetate (2 x 50 mL) and the combined organic

solutions were dried (magnesium sulfate) and evaporated to dryness to yield the methyl pyranoside **166** as a white crystalline solid (203 mg, 100%). M.p. 102-104 °C, [lit. m.p. 103-104°C];[123a] $[\alpha]_D^{25}$ -79.8 (*c* 1.0 in $CHCl_3$), [lit. $[\alpha]_D^{22}$ -71.5 (c 1.00 in $CHCl_3$)];[123a] $\nu_{max}$ (thin film): 3409 (m, OH); $\delta_H$ (400 MHz, $CDCl_3$) 7.41 – 7.28 (Ar, 5 H, m), 4.98 (C$\underline{H}_2$Ph, 1 H, d, $J_{gem}$ 11.7), 4.74 (C$\underline{H}_2$Ph', 1 H, d, $J_{gem}$ 11.7), 4.17 (H1, 1 H, d, $J_{1,2}$ 7.1), 4.01 (H5, 1 H, dd, $J_{5,5'}$ 11.6, $J_{4,5}$ 5.2), 3.72 (H4, 1 H, dddd, $J_{4,5'}$ 9.7, $J_{3,4}$ 8.4, $J_{4,5}$ 5.2, $J_{4,OH}$ 3.1), 3.54 (OC$\underline{H}_3$, 3 H, s), 3.51 (H2, 1H, ddd, $J_{2,3}$ 8.8, $J_{1,2}$ 7.2, $J_{2,OH}$ 2.6), 3.37 (H3, 1 H, a-t, $J_{2,3}$=$J_{3,4}$ 8.5), 3.26 (H5', 1 H, dd, $J_{5,5'}$ 11.6, $J_{4,5'}$ 9.8), 2.47 (2-OH, 1 H, d, $J_{2,OH}$ 2.7), 2.24 (4-OH, 1 H, d, $J_{4,OH}$ 3.1); $\delta_C$ (101 MHz, $CDCl_3$) 138.6 (*ipso*-Ph), 128.8, 128.2 (3 x Ph), 104.5 (C1), 83.4 (C3), 74.6 (C$\underline{H}_2$Ph), 74.0 (C2), 69.4 (C4), 65.3 (C5), 57.3 (OC$\underline{H}_3$); *m/z* (ESI+ve): 377 ($[M+Na]^+$, 100%), 531 ($[2M+Na]^+$, 32%); HRMS (ESI+ve): Found 277.1045 ($[M+Na]^+$); $C_{13}H_{18}NaO_5$ requires 277.1046.

**Methyl 3-*O*-benzyl-2,4-di-*O*-triflouromethanesulfonyl-β-D-*xylo*-pyranoside 159**

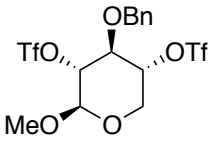


Trifluoromethanesulfonic anhydride (0.95 mL, 5.6 mmol) was added slowly to a stirred solution of the pyranoside **166** (357 mg, 1.4 mmol) and pyridine (0.68 mL, 8.4 mmol) in dichloromethane (10 mL) at -20 °C under nitrogen. The reaction mixture was stirred at -10 °C; after 1.5 h TLC analysis (1:1 cylcohexane/ethyl acetate) indicated complete consumption of the starting material ($R_f$ 0.30) and formation of a major species ($R_f$ 0.80). The reaction mixture was diluted with dichloromethane (10 mL), washed with aqueous hydrochloric acid (2M, 3 x 20 mL), dried (magnesium sulfate), filtered and concentrated to dryness to afford the crude ditriflate **159** as a clear yellow oil (729 mg, 100%). $[\alpha]_D^{25}$ -38.2 (*c* 1.29 in $CHCl_3$); $\nu_{max}$ (thin film): fingerprint region only; $\delta_H$ (400 MHz, $CDCl_3$) 7.45 – 7.29 (Ph, 5 H, m), 4.85 (H4, 1 H, a-td, $J_{3,4}$=$J_{4,5'}$ 7.7, $J_{4,5}$ 4.7), 4.80 (C$\underline{H}_2$Ph, 1 H, d, $J_{gem}$ 10.4), 4.76 (C$\underline{H}_2$Ph', 1 H, d, $J_{gem}$ 10.4), 4.64 (H2, 1 H, dd, $J_{2,3}$

7.6, $J_{1,2}$ 6.2), 4.53 (H1, 1 H, d, $J_{1,2}$ 6.1), 4.27 (H5, 1 H, dd, $J_{5,5'}$ 12.4, $J_{4,5}$ 4.6), 3.91 (H3, 1 H, a-t, $J_{2,3}$=$J_{3,4}$ 7.6), 3.62 (H5', 1 H, dd, $J_{5,5'}$ 12.4, $J_{4,5'}$ 8.0), 3.53 (OC$\underline{H}_3$, 3 H, s); $\delta_C$ (101 MHz, $CDCl_3$) 135.7 (*ipso*-Ph), 128.7, 128.7, 128.6 (3 x Ph), 100.5 (C1), 82.2 (C2), 81.6 (C4), 76.6 (C3), 75.5 ($\underline{C}H_2Ph$), 61.4 (C5), 57.4 (O$\underline{C}H_3$); *m/z* (ESI+ve): 541 ($[M+Na]^+$, 25%), 1059 ($[2M+Na]^+$, 100%); HRMS (ESI+ve): Found 541.0034 ($[M+Na]^+$); $C_{15}H_{16}F_6NaO_9S_2$ requires 541.0032.

**Methyl *N*,3-*O*-dibenzyl-2,4-dideoxy-2,4-imino-β-L-*ribo*-pyranoside 160**

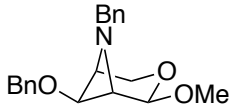


Benzylamine (0.77 mL, 7.0 mmol) was added to the crude ditriflate **159** (729 mg, 1.4 mmol) in acetonitrile (7 mL); the reaction mixture was stirred at 65-70 °C for 2 h when TLC analysis (2:1 cyclohexane/ethyl acetate) indicated complete disappearance of the starting material ($R_f$ 0.70) and formation of a major species ($R_f$ 0.55). The reaction mixture was left to cool, concentrated *in vacuo* and the residue purified by flash column chromatography (7:1 cyclohexane/ethyl acetate) to afford the bicyclic azetidine **160** as a light yellow oil (388 mg, 85%). $[\alpha]_D^{25}$ -30.7 (*c* 1.21 in $CHCl_3$); $\nu_{max}$ (thin film): fingerprint region only; $\delta_H$ (400 MHz, $CDCl_3$) 7.45 – 7.18 (Ar, 10 H, m), 4.69 ($OCH_2Ph$, 1 H, d, $J_{gem}$ 12.1), 4.64 (H1, 1 H, d, $J_{1,2}$ 0.8), 4.64 ($OCH_2Ph$, 1 H, d, $J_{gem}$ 12.1), 4.34 (H5, 1 H, dd, $J_{5,5'}$ 10.6, $J_{4,5}$ 1.7), 4.15 ($NCH_2Ph$, 2 H, s), 3.98 (H3, 1 H, s), 3.71 (H5', 1 H, dd, $J_{5,5'}$ 10.6, $J_{4,5'}$ 1.1), 3.65 (H2, 1 H, dd, $J_{2,4}$ 4.2, $J_{1,2}$ 0.9), 3.55 (H4, 1 H, dt, $J_{2,4}$ 4.2, $J_{4,5}$=$J_{4,5'}$ 1.4), 3.45 (OC$\underline{H}_3$, 3 H, s); $\delta_C$ (101 MHz, $CDCl_3$) 139.4, 137.8 (*ipso*-Ph), 128.6, 128.4, 128.3, 128.1, 128.0, 126.7 (Ph), 100.9 (C1), 79.9 (C3), 71.6 (O$\underline{C}H_2Ph$), 66.2 (C2), 63.3 (C4), 62.4 (C5), 55.9 (O$\underline{C}H_3$), 51.6 (N$\underline{C}H_2Ph$); *m/z* (ESI+ve): 326 ($[M+H]^+$, 100%), 348 ($[M+Na]^+$, 26%), 673 ($[2M+Na]^+$, 64%); HRMS (ESI+ve): Found 326.1750 ($[M+Na]^+$); $C_{20}H_{24}NO_3$ requires 326.1751.

**Methyl *N*,3-*O*-dibenzyl-2,4-dideoxy-2,4-imino-L-ribonate or (2*S*,3*S*,4*S*)-methyl 1-benzyl-3-(benzyloxy)-4-(hydroxymethyl)azetidine-2-carboxylate 170L**

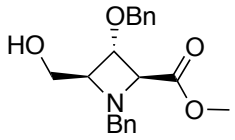


A solution of the bicyclic azetidine **160** (136 mg, 0.42 mmol) in 1,4-dioxane/aqueous hydrochloric acid (2 M, 1:5, 6 mL) was stirred at 40 °C for 17.5 h, after which TLC analysis (2:1 cyclohexane/ethyl acetate; sample quenched with triethylamine) indicated the absence of starting material ($R_f$ 0.50) and the formation of a major product ($R_f$ 0.10). The reaction mixture was diluted with dichloromethane (30 mL), washed with sat. aq. sodium bicarbonate (25 mL). The aqueous fraction was extracted with dichloromethane (2 x 30 mL). The combined organic fractions were washed with brine (40 mL) and dried (magnesium sulfate). Evaporation to dryness yielded bicyclic lactol **167L** (147 mg, 100%) as an unstable colourless glass, which was used without further purification. A solution of the crude lactol **167L** (102 mg, 0.30 mmol) and potassium carbonate (124 mg, 0.90 mmol) in anhydrous methanol (4 mL) was stirred at 0 °C under an atmosphere of nitrogen. Iodine, (99 mg, 0.39 mmol) dissolved by sonication in anhydrous methanol (4 mL), was added dropwise to the stirred reaction mixture at 0 °C. Mass spectrometry indicated the formation of the desired product after 1 h of reaction time and TLC analysis (ethyl acetate) showed consumption of the starting material ($R_f$ 0.60) and formation of a single compound ($R_f$ 0.80). The reaction was quenched by addition of sat. aq. sodium sulfite (8 mL). The resultant white precipitate was dissolved in water (32 mL) and the aqueous fraction was extracted with diethyl ether (4 x 50 mL). The combined organic fractions were dried (magnesium sulfate), filtered and evaporated *in vacuo* to yield the title compound **170L** (98 mg, 96%). The highest yield was obtained when the ester **170L** was used without further purification in the following hydrolysis. However on one occasion the ester was isolated as follows: In this

case the lactol **167L** (147 mg, 0.42 mmol) reacted in the same way as above gave the crude methyl ester **170L** (136 mg, 95%). Purification using flash column chromatography (cyclohexane/ethyl acetate/triethylamine 80:19:1 → 66:32:1) gave the methyl ester **170L** (116 mg, 81%) as a clear colourless oil. $[\alpha]_D^{25}$ -58.8 (*c* 0.80 in $CHCl_3$); $\nu_{max}$ (thin film): 3445 (w, OH), 1737 (s, C=O); $\delta_H$ (400 MHz, $CDCl_3$) 7.37 – 7.24 (Ar, 10 H, m), 4.62 ($OCH_2Ph$, 1 H, d, $J_{gem}$ 11.6), 4.47 ($OCH_2Ph$, 1 H, d, $J_{gem}$ 11.6), 4.20 (H3, 1 H, a-t, $J_{2,3}$=$J_{3,4}$ 5.3), 3.93 ($NCH_2Ph$, 1 H, d, $J_{gem}$ 12.4), 3.70 ($NCH_2Ph$, 1 H, d, $J_{gem}$ 12.5), 3.67 (H2, 1 H, d, $J_{2,3}$ 5.3), 3.66 ($OC\underline{H}_3$, 3 H, s), 3.31 – 3.22 (H4, H5, 2 H, m), 3.08 (H5', 1 H, dd, $J_{5,5'}$ 11.9, $J_{4,5'}$ 2.8), 2.54 (OH-5, 1 H, d, $J_{OH,5}$ 8.5); $\delta_C$ (101 MHz, $CDCl_3$) 171.7 (C=O), 137.5, 136.7 (2 x *ipso*-Ph), 129.4, 128.6, 128.1, 128.0, 127.9 (6 x Ph), 72.8 (C3), 71.9 ($O\underline{C}H_2Ph$), 70.6 (C4), 69.7 (C2), 60.9 ($N\underline{C}H_2Ph$), 60.6 (C5), 52.1 ($O\underline{C}H_3$); *m/z* (ESI+ve): 342 ($[M+H]^+$, 56%), 364 ($[M+Na]^+$, 100%), 705 ($[2M+Na]^+$, 88%); HRMS (ESI+ve): Found 364.1512 ($[M+Na]^+$); $C_{20}H_{23}NNaO_4$ requires 364.1519.

**Methyl *N*,3-*O*-dibenzyl-2,4-dideoxy-2,4-imino-L-ribonamide or (2*S*,3*S*,4*S*)-1-benzyl-3-(benzyloxy)-4-(hydroxymethyl)-*N*-methylazetidine-2-carboxamide 169L**

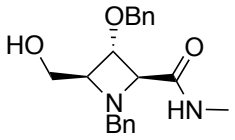


To a 15 mL screw cap vial was added the methyl ester **170L** (51 mg, 0.15 mmol) along with calcium chloride (17 mg, 0.15 mmol) and anhydrous methanol (5 mL). Methylamine in absolute ethanol (0.37 mL, 3.0 mmol) was added and the reaction vessel flushed with a stream of nitrogen before being heated to 45 °C for 2 h. TLC analysis (1:1 cyclohexane/ethyl acetate) indicated the complete consumption of the starting material ($R_f$ 0.45) and the formation of a single new product ($R_f$ 0.10) along with mass spectrometry showing only the desired product in the positive. The reaction mixture was evaporated to dryness and the residue dissolved in saturated aqueous ammonium chloride/water (1:3, 4 mL). The resultant mixture was adjusted to pH 5 with aqueous

hydrogen chloride (2 M) and stirred at RT for 20 min. Ethyl acetate (5 mL) was then added to the mixture and stirred for an additional 10 min. The aqueous layer was extracted with ethyl acetate (3 x 10 mL) and the combined organic fractions were dried (magnesium sulfate), filtered and evaporated to give the crude reaction product (51 mg, 100%). The crude was loaded in dichloromethane/triethylamine (99:1) and purified via flash column chromatography (cyclohexane/ethyl acetate/triethylamine 66:33:1 → 0:99:1) to yield the methyl amide **169L** as white crystalline solid (36 mg, 70%). M.p. 97-99 °C; $[\alpha]_D^{25}$ -57.3 (*c* 0.43 in $HCCl_3$); $\nu_{max}$ (thin film): 3343 (m, OH), 1651 (s, C=O, amide I), 1540 (m, C=O, amide II); $\delta_H$ (400 MHz, $CDCl_3$) 7.38 – 7.24 (Ar, 10 H, m), 6.54 (NH, 1 H, br. d, $J_{NH,Me}$ 4.1), 4.83 ($OCH_2Ph$, 1 H, d, $J_{gem}$ 11.7), 4.45 ($OCH_2Ph$, 1 H, d, $J_{gem}$ 11.6), 3.92 (H3, 1 H, a-t, $J_{2,3}$=$J_{3,4}$ 5.1), 3.77 ($NCH_2Ph$, 1 H, d, $J_{gem}$ 12.2), 3.73 ($NCH_2Ph$, 1 H, d, $J_{gem}$ 12.2), 3.65 (H2, 1 H, d, $J_{2,3}$ 5.1), 3.44 – 3.30 (H4, H5, H5', 3 H, m), 2.63 ($NHC\underline{H}_3$, 3 H, d, $J_{NH,Me}$ 5.0), 1.73 (OH, 1 H, s); $\delta_C$ (101 MHz, $CDCl_3$) 171.5 (C1), 137.7 , 136.9 (ipso-Ph), 129.3, 128.9, 128.5, 128.1, 128.1, 127.9 (8 x Ph), 73.9 (C3), 72.6 (C2), 71.4 ($O\underline{C}H_2Ph$), 70.9 (C4), 61.9 ($N\underline{C}H_2Ph$), 61.6 (C5), 25.7 ($NH\underline{C}H_3$); *m/z* (ESI+ve): 341 ($[M+H]^+$, 100%), 363 ($[M+Na]^+$, 73%), 703 ($[2M+Na]^+$, 57%; (ESI-ve): 375 ($[M+Cl]^-$, 100%); HRMS (ESI+ve): Found 363.1679 ($[M+Na]^+$); $C_{20}H_{24}N_2NaO_3$ requires 363.1679.

**Methyl 2,4-dideoxy-2,4-imino-L-ribonamide or (2*S*,3*S*,4*S*)-3-hydroxy-4-(hydroxymethyl)-*N*-methylazetidine-2-carboxamide 78L**

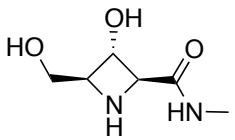


Concentrated hydrochloric acid (11.6 M, 8 µL, 0.10 mmol) was diluted with water (2 mL), premixed with 1,4-dioxane (1 mL) and added to the protected methyl amide **169L** (16 mg, 0.05 mmol). To this solution was added 10% palladium on charcoal (40% b.w., 6 mg) and the reaction vessel was degassed and charged with hydrogen. After 10 h of vigorous stirring, TLC

analysis (14:3:1:1:1 ethanol/pyridine/n-butanol/acetic acid/water) indicated the presence of a single product ($R_f$ 0.70). The reaction mixture was filtered (GF/A glass microfibre), washed with methanol and the solvent removed *via* lyophilisation to yield the methyl amide **78L** as a clear colourless glass (11 mg, 100%). $[\alpha]_D^{25}$ -12.2 (*c* 0.42 in MeOH); $\nu_{max}$ (thin film): 3273 (m, OH), 1673 (s, C=O, amide I), 1570 (m, C=O, amide II); $\delta_H$ (500 MHz, MeOD) 4.62 (H2, 1 H, d, *J* 6.6), 4.53 (H3, 1 H, t, *J* 6.7), 4.28 (H4, 1 H, dt, *J* 7.2, 3.9), 3.83 (H5, 2 H, d, *J* 4.0), 2.82 (NHC$\underline{H}_3$, 3 H, s); $\delta_C$ (126 MHz, MeOD) 167.2 (C1), 69.6 (C4), 68.6 (C3), 66.1 (C2), 58.9 (C5), 26.5 (NH$\underline{C}H_3$); *m/z* (ESI+ve): 102 (100%), 161 ($[M+H]^+$, 80%), 183 ($[M+Na]^+$, 57%); HRMS (ESI+ve): Found 183.0742 ($[M+Na]^+$); $C_6H_{12}N_2NaO_3$ requires 183.0740.

### 3.6.2 *Meso*-ribitol synthesis

**N,3-*O*-dibenzyl-2,4-dideoxy-2,4-imino-*meso*-ribitol 199**

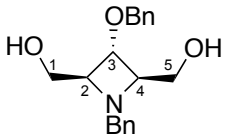


Bicyclic azetidine **160** (56 mg, 0.17 mmol) was dissolved in 1,4-dioxane/aqueous hydrochloric acid (2 M, 1:5, 6 mL) and stirred at 40 °C for 5 h, after which TLC analysis (2:1 cyclohexane/ethyl acetate; sample quenched with triethylamine) indicated the consumption of the starting material ($R_f$ 0.50) and the presence of a major compound ($R_f$ 0.10). The reaction mixture was diluted with dichloromethane (30 mL), washed with sat. aq. sodium bicarbonate (25 mL) and the aqueous fraction extracted with dichloromethane (2 x 30 mL). Evaporation to dryness at 30 °C of the combined organic fractions yielded the lactol **167L** (60 mg, 100%) as a colourless glass, which was used without further purification. The crude lactol **167L** was dissolved in methanol/1,4-dioxane (3:1, 4 mL), sodium borohydride (8 mg, 0.20 mmol) was added and the reaction mixture stirred at RT for 1.5 h. At this point TLC analysis (ethyl acetate) indicated the disappearance of the lactol ($R_f$ 0.65) and the formation of a new major compound

($R_f$ 0.40, streaks to baseline) and mass spectrometry (ESI+ve) indicated the sole presence of the desired compound. The reaction mixture was quenched by addition of a few drops of acetic acid and was evaporated to dryness to give the crude diol **199** (97 mg, 100%). The residue was dissolved in pyridine/acetic anhydride (1:1, 4 mL) and stirred at RT for 19 h. TLC analysis (3:1 cyclohexane/ethyl acetate) indicated disappearance of the starting material ($R_f$ 0.0) and appearance of a new major compound ($R_f$ 0.65) which was identified using mass spectrometry (ESI+ve) as the diacetylated intermediate and the reaction was, on dilution with toluene (4 mL), evaporated to dryness and coevaporated with toluene (2 x 4 mL). The residue was dissolved in ethyl acetate (30 mL), washed with water (2 x 25 mL), sat. aq. sodium bicarbonate (25 mL), brine (25 mL), dried (magnesium sulfate), filtered and concentrated *in vacuo* to yield the crude diacetate as colourless oil (65 mg, 0.16 mmol, 96%). The residue was dissolved in anhydrous methanol (2 mL), sodium methoxide (4 mg, 0.07 mmol) was added and the reaction mixture stirred at RT for 20 h. TLC analysis (ethyl acetate) indicated consumption of starting material ($R_f$ 0.95) and formation of a major product ($R_f$ 0.55) along with an additional species ($R_f$ 0.85) which was tentatively identified as the mono-acetate (using mass spectrometry) and an additional quantity of sodium methoxide (4 mg, 0.07 mmol) was added to the reaction mixture. TLC analysis (1:1 cyclohexane/ethyl acetate) after a total reaction time of 45 h indicated formation of a major species ($R_f$ 0.20) with only traces of the intermediate ($R_f$ 0.65) remaining and the reaction mixture was concentrated *in vacuo*. The crude was dry loaded from methanol/triethylamine (99:1) and flash column chromatography (cylcohexane/ethyl acetate/triethylamine 75:29:1 → 0:99:1) yielded dibenzyl diol **199** as a clear colourless oil (39 mg, 0.13 mmol, 74%). $[\alpha]_D^{25}$ +0.23 (*c* 1.05 in $CHCl_3$); $\nu_{max}$ (thin film): 3405 (m, br, OH); $\delta_H$ (400 MHz, $CDCl_3$) 7.40 – 7.24 (Ar, 10 H, m), 4.50 ($OCH_2Ph$, 2 H, s), 4.02 (H3, 1 H, t, $J_{2,3}$=$J_{3,4}$ 5.4), 3.75 ($NCH_2Ph$, 2 H, s), 3.34 (H1, H5, 2 H, dd, $J_{5,5'}$=$J_{1,1'}$ 11.8, $J_{1,2}$=$J_{4,5}$ 3.0), 3.29 (H1', H5', 1 H, dd, $J_{5,5'}$=$J_{1,1'}$ 11.8, $J_{1',2}$=$J_{4,5'}$ 3.4), 3.23 (H2, H4, 1 H, dt, $J_{2,3}$=$J_{3,4}$ 6.1, $J_{1,2}$=$J_{1',2}$=$J_{4,5}$=$J_{4,5'}$ 3.2),

2.17 (OH, 2 H, br. s); $\delta_C$ (101 MHz, $CDCl_3$) 138.0, 137.9 (2 x ipso-Ph), 129.1, 128.8, 128.7, 128.1, 128.0, 127.9 (10 x Ph), 72.1 (O<u>C</u>$H_2$Ph), 71.7 (C3), 71.6 (C2, C4), 61.9 (C1, C5), 61.4 (N<u>C</u>$H_2$Ph); *m/z* (ESI+ve): 314 ($[M+H]^+$, 100%), 336 ($[M+Na]^+$, 98%), 649 ($[2M+Na]^+$, 77%); *m/z* (ESI-ve): 312 ($[M-H]^-$, 100%); HRMS (ESI+ve): Found 314.1745 ($[M+H]^+$); $C_{19}H_{24}NO_3$ requires 314.1751.

**2,4-dideoxy-2,4-imino-*meso*-ribitol 200**

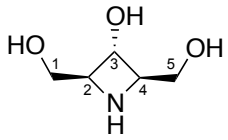


Concentrated hydrochloric acid (11.6 M, 11 μL, 0.13 mmol) was diluted with water (2 mL), premixed with 1,4-dioxane (1 mL) and added to diol **199** (20 mg, 0.07 mmol). To this solution was added 10% palladium on charcoal (40% b.w., 8 mg) and the reaction vessel was degassed and charged with hydrogen. After 5 h of vigorous stirring TLC analysis (4:1 ethyl acetate/methanol) indicated a trace of remaining starting material ($R_f$ 0.80) along with a major species on the base line and an intermediate compound ($R_f$ 0.35) and similarly TLC analysis (14:3:1:1:1 ethanol/pyridine/n-butanol/acetic acid/water) indicated the presence of a major product ($R_f$ 0.80) along with a minor component ($R_f$ 0.90). Mass spectrometry still showed evidence of the starting material along with a mono-benzyl intermediate. After having been resubjected to the reaction conditions for an additional 18 h, only a trace of the mono-benzyl species remained by TLC analysis, however mass spectrometry still indicated its presence until a total of 72 h had passed. The reaction mixture was then filtered (GF/A glass microfibre), washed with methanol (2 mL), concentrated *in vacuo* and loaded onto a short column of Dowex® (50W-X8, $H^+$) in which the resin had been pre-treated by washing with water (until eluent was neutral). The crude was loaded (water/1,4-dioxane 2:1) and washed sequentially with water, 1,4-dioxane, ethanol and water again. The product was eluted with aqueous ammonia (2 M) and the

ammoniacal fractions concentrated *in vacuo* at RT to yield triol **200** as a viscous gum (11 mg, 100%). $[\alpha]_D^{25}$ +0.68 (*c* 0.29 in MeOH); $\nu_{max}$ (thin film): 3271 (m, br, OH); $\delta_H$ (400 MHz, $D_2O$) 4.27 (H3, 1 H, t, $J_{2,3}$=$J_{3,4}$ 7.1), 4.05 (H2 and H4, 2 H, dt, $J_{2,3}$=$J_{3,4}$ 7.1, $J_{1,2}$=$J_{4,5}$ 4.4), 3.62 (H1 and H5, 4 H, dd, $J_{1,2}$=$J_{4,5}$ 4.4, *J* 1.4); $\delta_C$ (63 MHz, $D_2O$) 66.9 (C2, C4), 64.0 (C3), 58.2 (C1, C5); *m/z* (ESI-ve): 312 ($[M+Cl]^-$, 72%), 362 (100%); HRMS (ESI+ve): Found 134.0807 ($[M+H]^+$); $C_5H_{12}NO_3$ requires 134.0812.

### 3.6.3 Alkylation of L-*ribo* azetidine amide

**Methyl 2,4-dideoxy-2,4-imino-*N*-ethyl-L-ribonamide 201L**

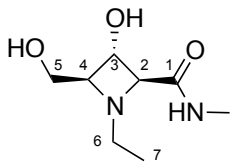


L-ribo amide **78L** (18 mg, 0.11 mmol) was dissolved in ethanol (3 mL) and ethanal (0.13 mL, 2.25 mmol) was added. To this solution was added 10% palladium on charcoal (40% b.w., 7 mg) and the reaction vessel was degassed and charged with hydrogen. After 2 h of vigorous stirring TLC analysis (4:1 ethyl acetate/methanol) indicated the disappearance of the starting material ($R_f$ 0.15) and the presence of a new compound ($R_f$ 0.45). The reaction mixture was then filtered (GF/A glass microfibre), washed with ethanol (3 mL), concentrated *in vacuo*, resuspended in water (2 mL) and the solvent removed *via* lyophilisation to yield the alkylated methyl amide **201L** as an orange gum (22 mg, 100%). $[\alpha]_D^{25}$ -10.6 (*c* 0.78 in MeOH); $\nu_{max}$ (thin film): 3243 (m, br, OH), 1674 (s, amide I), 1570 (w, amide II); $\delta_H$ (500 MHz, MeOD) 4.68 (H2, 1 H, d, $J_{2,3}$ 6.5), 4.43 (H3, 1 H, t, $J_{2,3}$=$J_{3,4}$ 6.7), 4.26 (H4, 1 H, ddd, $J_{3,4}$ 7.0, $J_{4,5'}$ 4.8, $J_{4,5}$ 3.1), 3.93 (H5, 1 H, dd, $J_{5,5'}$ 13.3, $J_{4,5}$ 3.0), 3.87 (H5', 1 H, dd, $J_{5,5'}$ 13.3, $J_{4,5'}$ 4.9), 3.49 (H6, 1 H, a-dq, $J_{6,6'}$ 14.4, $J_{6,7}$ 7.2), 3.35 (H6', 1 H, dq, $J_{6,6'}$ 12.6, $J_{6',7}$ 7.2), 2.83 (NHC$\underline{H}_3$, 3 H, s), 1.24 (H7, 3 H, t, $J_{6,7}$=$J_{6',7}$ 7.2); $\delta_C$ (126 MHz, MeOD) 166.8 (C1), 77.5 (C4), 73.2 (C2), 66.2 (C3), 58.6 (C5), 52.2 (C6),

26.6 ($NH\underline{C}H_3$), 9.95 (C7); *m/z* (ESI+ve): 189 ($[M+H]^+$, 81%), 211 ($[M+Na]^+$, 100%), 399 ($[2M+Na]^+$, 62%); HRMS (ESI+ve): Found 211.1052 ($[M+Na]^+$); $C_8H_{16}N_2NaO_3$ requires 211.1053.

### 3.6.4 D-*ribo* azetidine amide synthesis

This reaction sequence was started from 1,2,4,6-tetra-*O*-acetyl-3-*O*-benzyl-β-D-glucopyranose **202**, which is readily available from D-glucose according to literature procedures.[110b]

**Methyl 2,4,6-tri-*O*-acetyl-3-*O*-benzyl-β-D-*gluco*-pyranoside 203**

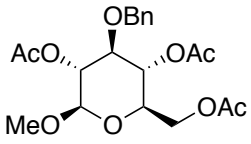


Hydrobromic acid (33% wt, in acetic acid, 1.6 mL, 9.24 mmol) was added drop-wise over a period of 20 min to tetra-acetate **202** (1.5 g, 3.42 mmol) in 7:3 acetic acid/dichloromethane (10 mL) at 10 °C and the resultant mixture was stirred at 5 °C. TLC analysis (1:1 cyclohexane/ethyl acetate) after 5 h indicated the formation of a new species ($R_f$ 0.75) with a faint spot remaining ($R_f$ 0.65), running very similar to the starting material ($R_f$ 0.60). The reaction mixture was then diluted with dichloromethane (50 mL) and poured into ice water (50 mL). The organic layer was washed with aqueous sodium bicarbonate (2 x 50 mL), water (50 mL), dried (magnesium sulfate), filtered and concentrated *in vacuo* at 25°C. The crude bromide was then redissolved in methanol (25 mL) and stirred in a foil wrapped flask with silver carbonate (1.6 g, 5.81 mmol) at RT for 12 h. TLC analysis (1:1 cyclohexane/ethyl acetate) indicated formation of a major species ($R_f$ 0.45) along with three minor components ($R_f$ 0.65, 0.30, 0.15). The reaction mixture was filtered through celite, washed with methanol (20 mL) and concentrated *in vacuo* to yield the crude title compound (1.30 g, 93%). Purification *via* flash column chromatography (5:1 cyclohexane/ethyl acetate) yielded β-pyranoside **203** as a clear oil (1.08 g, 2.63 mmol, 77%),

which crystallized on standing. M.p. 87-90 °C, [lit. M.p. 90 °C];[175] $[\alpha]_D^{25}$ -26.8 (*c* 1.1 in $HCCl_3$), [lit. $[\alpha]_D^{22\text{-}24}$ -25 (*c* 1.0 in $HCCl_3$)];[175] $\nu_{max}$ (thin film): 1744 (s, C=O); $\delta_H$ (400 MHz, $CDCl_3$) 7.36 – 7.20 (Ph, 5 H, m), 5.13 (H4, 1 H, t, $J_{3,4}$=$J_{4,5}$ 9.6), 5.05 (H2, 1 H, dd, $J_{2,3}$ 9.2, $J_{1,2}$ 8.1), 4.62 ($CH_2$Ph, 1 H, d, $J_{gem}$ 11.7), 4.58 ($CH_2$Ph, 1 H, d, $J_{gem}$ 11.6), 4.35 (H1, 1 H, d, $J_{1,2}$ 7.9), 4.23 (H6, 1 H, dd, $J_{6,6'}$ 12.2, $J_{5,6}$ 5.0), 4.13 (H6', 1 H, dd, $J_{6,6'}$ 12.2, $J_{5,6'}$ 2.5), 3.70 (H3, 1 H, t, $J_{2,3}$=$J_{3,4}$ 9.3), 3.60 (H5, 1 H, ddd, $J_{4,5}$ 9.9, $J_{5,6}$ 4.9, $J_{5,6'}$ 2.5), 3.49 (OC<u>H</u>$_3$, 3 H, s), 2.08 (COC<u>H</u>$_3$, 3 H, s), 2.02 (COC<u>H</u>$_3$, 3 H, s), 1.98 (COC<u>H</u>$_3$, 3 H, s); $\delta_C$ (101 MHz, $CDCl_3$) 170.9, 169.5, 169.4 (3x C=O), 137.9 (ipso-Ph), 128.6, 128.0, 127.9 (Ph), 101.9 (C1), 80.2 (C3), 73.9 (<u>C</u>$H_2$Ph), 72.5, 72.2 (C2 and C5), 69.7 (C4), 62.4 (C6), 56.9 (O<u>C</u>$H_3$), 21.0, 20.9 (3 x C=O<u>C</u>$H_3$); *m/z* (ESI+ve): 433 ($[M+Na]^+$, 48%), 843 ($[2M+Na]^+$, 100%); HRMS (ESI+ve): Found 433.1468 ($[M+Na]^+$); $C_{20}H_{26}NaO_9$ requires 433.1469.

**Methyl 3-*O*-benzyl-6-*O*-trityl-β-D-*gluco*-pyranoside 205**

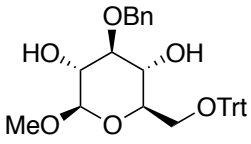


Sodium methoxide (14 mg, 0.25 mmol) was added to diacetate **203** (1.03 g, 2.51 mmol) in methanol (15 mL) and stirred at 40 °C for 20 h. At this stage TLC analysis (ethyl acetate) indicated complete consumption of the starting material ($R_f$ 0.75) and the formation of a major product ($R_f$ 0.25) along with a minor component ($R_f$ 0.40), which was tentatively identified as the mono-acetate. Additional sodium methoxide (14 mg, 0.25 mmol) was added and the reaction mixture was resubjected to 40 °C for an additional 17.5 h at which point TLC indicated only the desired product. *In vacuo* removal of the solvent gave triol **204** as off-white foam (0.750 g, 2.64 mmol, quant), which was redissolved in dry pyridine (10 mL). 4-Dimethylaminopyridine (31 mg, 0.25 mmol) was added along with trityl chloride (2.01 g, 7.53 mmol) and stirred at RT under nitrogen for 8 h. TLC analysis (ethyl acetate) indicated a newly formed product ($R_f$ 0.70) along

with remaining starting material, therefore additional trityl chloride was added (1.4 g, 5.02 mmol) and the reaction stirred for an additional 16 h. During the reaction a precipitate crashed out of solution and additional dry pyridine (5 mL) was added to redissolve the reaction mixture. TLC analysis showed, that no starting material remained and methanol (8mL) was added to quench any remaining trityl chloride. The solvent was removed *in vacuo* and the resulting residue was co-evaporated with toluene (3x 20 mL). The crude reaction product was redissolved in ethyl acetate (100 mL), washed with water (2x 100 mL) and brine (100 mL), dried (magnesium sulfate), filtered and the solvent removed *in vacuo* to give the crude product as a clear thick oil. The residue was purified by flash column chromatography (11:1→2:1 cylcohexane/ethyl acetate) to afford the title compound **205**, as a white crystalline solid (1.21 g, 92%). M.p. 180-181 °C, [lit. M.p. 176-177 °C (toluene)];[110b] $[\alpha]_D^{25}$ -37.7 (*c* 1.0 in $HCCl_3$), [lit. $[\alpha]_D^{25}$ -33.3 (*c* 1.0 in $HCCl_3$)];[110b] $\nu_{max}$ (thin film): 3459 (m, br, OH); $\delta_H$ (400 MHz, $C_6D_6$) 7.68 – 7.57, 7.37 – 7.29, 7.20 – 6.99 (Ph, 20 H, 3x m), 5.02 ($C\underline{H}_2Ph$, 1 H, d, $J_{gem}$ 11.8), 4.78 ($C\underline{H}_2Ph$, 1 H, d, $J_{gem}$ 11.8), 4.01 (H1, 1 H, d, $J_{1,2}$ 7.7), 3.69 (H4, 1 H, dd, *J* 8.8, $J_{4,OH}$ 2.5), 3.64 (H2, 1 H, dd, $J_{1,2}$ 7.5, $J_{2,OH}$ 2.0), 3.54 (H6, 1 H, dd, $J_{6,6'}$ 9.8, $J_{5,6}$ 3.1), 3.48 (H6', 1 H, dd, $J_{6,6'}$ 9.9, $J_{5,6'}$ 5.1), 3.43 – 3.34 (H3, H5, 2 H, m), 3.33 ($OC\underline{H}_3$, 3 H, s), 2.31 (OH2, 1 H, d, $J_{2,OH}$ 2.3), 2.20 (OH4, 1 H, d, $J_{4,OH}$ 2.9); $\delta_C$ (101 MHz, $C_6D_6$) 144.7, 139.6 (2x ipso-Ph), 129.2, 128.6, 128.3, 128.3, 127.8, 127.3 (6x Ph), 104.3 (C1), 87.2 ($\underline{C}Ph_3$), 84.3 (C3), 75.2, 75.2 (C2 and C5), 74.7 ($\underline{C}H_2Ph$), 71.2 (C4), 64.3 (C6), 56.4 ($O\underline{C}H_3$); *m/z* (ESI+ve): 549 ($[M+Na]^+$, 67%), 1075 ($[2M+Na]^+$, 100%); HRMS (ESI+ve): Found 549.2242 ($[M+Na]^+$); $C_{33}H_{34}NaO_6$ requires 549.2248.

**Methyl 3-*O*-benzyl-2,4-*O*-ditrifluoromethanesulfonate-6-*O*-trityl-β-D-*gluco*-pyranoside 161**

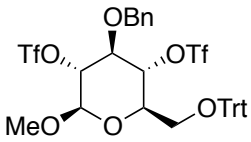


Trifluoromethanesulfonic anhydride (1.28 mL, 7.6 mmol) was added slowly to a stirred solution of the pyranoside **205** (1 g, 1.9 mmol) and pyridine (1.23 mL, 15.2 mmol) in dichloromethane (20 mL) at -30 °C under nitrogen. The reaction mixture was stirred at -10 °C; after 5 h TLC analysis (2:1 cylcohexane/ethyl acetate) indicated complete consumption of the starting material ($R_f$ 0.40) and formation of a major species ($R_f$ 0.65). The reaction mixture was diluted with dichloromethane (20 mL), washed with aqueous hydrochloric acid (2 M, 2 x 40 mL), dried (magnesium sulfate), filtered and concentrated to dryness to afford the crude ditriflate **161** as a clear yellow syrup (1.54 g, 100%). Purification using flash column chromatography (8:1 cylcohexane/ethyl acetate) followed by co-evaporation with dichloromethane (2 x 15 mL) afforded the title compound **161**, as a white solid foam (1.43 g, 95%). M.p. 49-51 °C, [lit. m.p. 49-51 °C];[110b] $[\alpha]_D^{25}$ -12.9 (*c* 1.1 in $HCCl_3$), [lit. $[\alpha]_D^{25}$ -11.6 (*c* 0.85 in $HCCl_3$)];[110b] $\nu_{max}$ (thin film): fingerprint region only; $\delta_H$ (400 MHz, $CDCl_3$) 7.42-7.48, 7.40 – 7.22 (Ph, 20 H, 2x m), 4.99 (H4, 1 H, t, $J_{3,4}$=$J_{4,5}$ 9.2), 4.85 ($CH_2$Ph, 1 H, d, $J_{gem}$ 9.7), 4.81 ($CH_2$Ph, 1 H, d, $J_{gem}$ 9.4), 4.78 (H2, 1 H, dd, $J_{2,3}$ 9.0, $J_{1,2}$ 7.8), 4.55 (H1, 1 H, d, $J_{1,2}$ 7.8), 3.93 (H3, 1 H, a-t, $J_{2,3}$=$J_{3,4}$ 9.0), 3.72 (H5, 1 H, ddd, $J_{4,5}$ 9.6, $J_{5,6'}$ 5.5, $J_{5,6}$ 2.3), 3.67 (OC$\underline{H}_3$, 3 H, s), 3.51 (H6, 1 H, dd, $J_{6,6'}$ 10.7, $J_{5,6}$ 2.2), 3.33 (H6', 1 H, dd, $J_{6,6'}$ 10.7, $J_{5,6'}$ 5.5); $\delta_C$ (101 MHz, $CDCl_3$) 143.3, 135.9 (2x ipso-Ph), 128.9, 128.5, 128.3, 128.1, 128.0, 127.4 (6x Ph), 100.5 (C1), 87.3 ($\underline{C}Ph_3$), 84.5(C2), 80.5 (C4), 79.2 (C3), 75.9 ($\underline{C}H_2$Ph), 73.2 (C5), 61.8 (C6), 57.4 (O$\underline{C}H_3$); *m/z* (ESI+ve): 813 ($[M+Na]^+$, 100%), 1603 ($[2M+Na]^+$, 64%); *m/z* (ESI-ve): 825 ($[M+Cl]^-$, 12%), 1615 ($[2M+Cl]^-$, 100%); HRMS (ESI+ve): Found 813.1231 ($[M+Na]^+$); $C_{35}H_{32}F_6NaO_{10}S_2$ requires 813.1233.

**Methyl *N*-benzyl-3-*O*-benzyl-2,4-dideoxy-2,4-imino-6-*O*-trityl-β-D-*talo*-pyranoside 198**

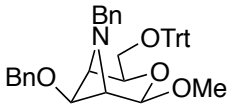


Benzylamine (0.47 mL, 4.33 mmol) was added to ditriflate **161** (685 mg, 0.87 mmol) in acetonitrile (7 mL) and stirred at 70 °C. TLC analysis (3:1 cyclohexane/ethyl acetate) indicated complete disappearance of the starting material ($R_f$ 0.65) after 4 h and formation of a major species ($R_f$ 0.55) and the reaction mixture was left to cool to RT. The reaction mixture was then concentrated to dryness and purified *via* flash column chromatography (98:2 → 19:1 cyclohexane/ethyl acetate) in order to yield the title compound **198** as a white foam and after coevaporation with dichloromethane (3 x 10 mL) as a clear glass (425 mg, 82 %). $[\alpha]_D^{25}$ -20.1 (*c* 1.95 in $CHCl_3$), [lit. $[\alpha]_D^{25}$ -24.4 (c 0.54 in $CHCl_3$)];[110b] $\nu_{max}$ (thin film): fingerprint region only; $\delta_H$ (400 MHz, $C_6D_6$) 7.61 – 6.98 (Ar, 25 H, m), 4.47 (H1, 1 H, d, $J_{1,2}$ 0.9), 4.42 ($NCH_2Ph$, 1 H, d, $J_{gem}$ 14.2), 4.30 ($NCH_2Ph$, 1 H, d, $J_{gem}$ 14.2), 4.27 ($OCH_2Ph$, 2 H, s), 3.99 (H5, 1 H, a-td, $J_{5,6}$=$J_{5,6'}$ 6.5, $J_{4,5}$ 0.9), 3.82 (H3, 1 H, a-s), 3.79 (H6, 1 H, dd, $J_{6,6'}$ 9.2, $J_{5,6}$ 6.8), 3.52 (H6', 1 H, dd, $J_{6,6'}$ 9.2, $J_{5,6}$ 6.5), 3.50 (H4, 1 H, dd, $J_{2,4}$ 5.3, $J_{4,5}$ 1.2), 3.35 (H2, 1 H, dd, $J_{2,4}$ 5.3, $J_{1,2}$ 0.8), 3.28 ($OC\underline{H}_3$, 3 H, s); $\delta_C$ (126 MHz, $C_6D_6$) 144.8, 140.3, 138.6 (5 x ipso-Ph), 129.3, 128.8, 128.7, 128.4, 128.4, 128.2, 128.0, 127.2, 126.8 (25 x Ph), 101.5 (C1), 87.1 ($O\underline{C}Ph_3$), 84.3 (C3), 76.4 (C5), 70.9 ($O\underline{C}H_2Ph$), 66.7 (C2), 65.3 (C6), 64.8 (C4), 56.0 ($NCH_2Ph$), 55.8 ($O\underline{C}H_3$); *m/z* (ESI+ve): 598 ($[M + H]^+$, 100%); HRMS (ESI+ve): Found 598.2953 ($[M + H]^+$); $C_{40}H_{40}NO_4$ requires 598.2952.

**1,5,6-tri-*O*-Acetyl-*N*-benzyl-3-*O*-benzyl-2,4-dideoxy-2,4-imino-D-talitol 207**

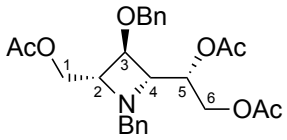


Bicylic azetidine **198** (402 mg, 0.67 mmol) was dissolved in 1:1 1,4-dioxane/aq. hydrochloric acid (2 M, 10 mL) and stirred at 50 °C for 17 h. TLC analysis (sample quenched with triethylamine, ethyl acetate as mobile phase) indicated complete consumption of the starting material ($R_f$ 0.90) and appearance of a single new species ($R_f$ 0.15). The reaction mixture was diluted with dichloromethane (30 mL) and washed with saturated aqueous sodium bicarbonate (30 mL). The aqueous phase was extracted then extracted with dichloromethane (3 x 30 mL) and the combined organic fractions were dried *in vacuo* to give the crude lactol **206** as a viscous oil (456 mg). The residue was redissolved in methanol (10 mL) and sodium borohydride (33 mg) was added and the reaction stirred at RT for 2.5 h at which point TLC analysis (ethyl acetate) indicated the disappearance of the starting material (streaky up to $R_f$ 0.30) and appearance of a major product (baseline streaking to $R_f$ 0.15) along with an impurity ($R_f$ 0.85). Mass spectrometry confirmed the formation of the triol **162** and the reaction mixture was quenched by addition of 10 drops of acetic acid and evaporated to dryness to yield the crude triol **162** as a white solid. The residue was redissolved in 1:1 pyridine/acetic anhydride (24 mL) and stirred at RT for 14 h. At this point TLC analysis (2:1 cylcohexane/ethyl acetate) showed, that the starting material (baseline) had completely disappeared and a new major species ($R_f$ 0.50) had formed along with an impurity ($R_f$ 0.70). The reaction mixture was concentrated *in vacuo* and following co-evaporation with toluene (2 x 40 mL) the residue was redissolved in ethyl acetate (80 mL) and washed with water (2 x 80 mL), saturated aqueous bicarbonate (80 mL) and brine (80 mL), then dried (magnesium sulphate), filtered and concentrated to dryness to give the crude product as a off white solid (449 mg). Purification using flash column chromatography (95:5 → 4:1

cylcohexane/ethyl acetate) afforded the title compound **207**, as a clear colourless oil (259 mg, 82%). $[\alpha]_D^{25}$ +28.7 (*c* 1.1 in $CHCl_3$), [lit. $[\alpha]_D^{25}$ +28.4 (c 0.56 in $CHCl_3$)];[110b] $\nu_{max}$ (thin film): 1740 (s, C=O); $\delta_H$ (400 MHz, $CDCl_3$) 7.39 – 7.21 (Ph, 10 H, m), 4.96 (H5, 1 H, a-td, $J_{4,5}$=$J_{5,6'}$ 6.5, $J_{5,6}$ 2.8), 4.47 ($OCH_2Ph$, 2 H, s), 4.33 (H6, 1 H, dd, $J_{6,6'}$ 12.1, $J_{5,6}$ 2.7), 4.05 (H6', 1 H, dd, $J_{6,6'}$ 12.0, $J_{5,6'}$ 6.8), 3.89 (H1, 1 H, dd, $J_{1,1'}$ 11.7, $J_{1,2}$ 5.2), 3.80 (H3, 1 H, a-dd, $J$ 9.5, $J_{2,3}$ 4.0), 3.80 ($NCH_2Ph$, 1 H, d, $J_{gem}$ 13.4), 3.72 (H1', 1 H, dd, $J_{1,1'}$ 11.3, $J_{1',2}$ 5.0), 3.69 ($NCH_2Ph$, 1 H, d, $J_{gem}$ 12.9), 3.35 (H4, 1 H, a-t, $J_{3,4}$=$J_{4,5}$ 6.0), 3.21 (H2, 1 H, a-q, $J_{1,2}$=$J_{1',2}$=$J_{2,3}$ 4.9), 2.00 ($C=OC\underline{H}_3$, 3 H, s), 1.99 ($C=OC\underline{H}_3$, 3 H, s), 1.94 ($C=OC\underline{H}_3$, 3 H, s); $\delta_C$ (101 MHz, $CDCl_3$) 170.8, 170.3 (3x C=O), 137.9, 137.5 (2x ipso-Ph), 129.1, 128.7, 128.5, 128.2, 127.8, 127.6 (6x Ph), 72.9 (C3), 72.4 (C5), 71.5 ($O\underline{C}H_2Ph$), 69.1 (C4), 68.8 (C2), 64.7 (C1), 62.7 (C6), 61.9 ($N\underline{C}H_2Ph$), 21.0, 20.9 (3x $C=O\underline{C}H_3$); *m/z* (ESI+ve): 492 ($[M+Na]^+$, 84%), 961 ($[2M+Na]^+$, 100%); HRMS (ESI+ve): Found 492.1987 ($[M+Na]^+$); $C_{26}H_{31}NNaO_7$ requires 492.1993.

**_N_-Benzyl-3-_O_-benzyl-2,4-dideoxy-2,4-imino-D-talitol 162**

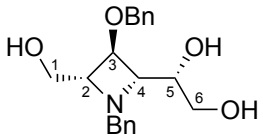


Triacetate **207** (249 mg, 0.53 mmol) was dissolved in methanol (5 mL), sodium methoxide (11.5 mg, 0.21 mmol) was added and the reaction mixture heated to 45 °C under stirring. After 18 h TLC analysis (ethyl acetate) indicated consumption of starting material ($R_f$ 0.90) and formation of a single new product ($R_f$ 0.20). The reaction mixture was evaporated to dryness and the residue purified using flash column chromatography (1:1 cylcohexane/ethyl acetate → 1:9 methanol/ethyl acetate) to yield the triol **162** as a clear colourless oil (165 mg, 91%). $[\alpha]_D^{25}$ +31.1 (*c* 1.7 in $CHCl_3$), [lit. $[\alpha]_D^{25}$ +17.7 (c 0.35 in $CHCl_3$)];[110b] $\nu_{max}$ (thin film): 3386 (m, br, OH); $\delta_H$ (400 MHz, MeOD) 7.39 – 7.23 (10 H, m), 4.52 ($OCH_2Ph$, 1 H, d, $J_{gem}$ 11.8), 4.48 ($OCH_2Ph$, 1 H, d, $J_{gem}$ 11.8), 3.98 ($NCH_2Ph$, 1 H, d, $J_{gem}$ 12.5), 3.91 (H3, 1 H, a-t, $J_{2,3}$=$J_{3,4}$ 4.7),

3.63 ($NCH_2Ph$, 1 H, d, $J_{gem}$ 12.5), 3.57 (H5, 1 H, a-dd, $J$ 10.8, $J_{4,5}$ 5.4), 3.51 (H6, 1 H, dd, $J_{6,6'}$ 10.9, $J_{5,6}$ 5.2), 3.43 (H6', 1 H, dd, $J_{6,6'}$ 10.9, $J_{5,6'}$ 6.7), 3.24 (H4, 1 H, a-t, $J_{3,4}$=$J_{4,5}$ 5.0), 3.17 – 3.05 (H2, H1, H1', 3 H, m); $\delta_C$ (101 MHz, MeOD) 139.6, 139.1 (2x ipso-Ph), 130.8, 129.4, 129.0, 128.7, 128.5 (6x Ph), 74.1, 73.7 (C3 and C5), 72.5 (C2), 72.3 ($O\underline{C}H_2Ph$), 72.2 (C4), 64.6 (C6), 63.5 ($N\underline{C}H_2Ph$), 63.2 (C1); *m/z* (ESI+ve): 344 ($[M+H]^+$, 100%), 366 ($[M+Na]^+$, 34%), 709 ($[2M+Na]^+$, 95%); HRMS (ESI+ve): Found 344.1856 ($[M+H]^+$); $C_{20}H_{26}NO_4$ requires 344.1856.

**Methyl *N*,3-*O*-dibenzyl-2,4-dideoxy-2,4-imino-D-ribonate or (2R,3R,4R)-methyl 1-benzyl-3-(benzyloxy)-4-(hydroxymethyl)azetidine-2-carboxylate 170D**

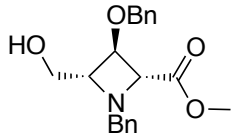


Sodium periodate (117 mg, 0.55 mmol) was added to a solution of the triol **162** (159 mg, 0.46 mmol) in aqueous acetone (water/acetone, 2:1, 6 mL) and the reaction mixture was stirred at RT for 1 h. TLC analysis (ethyl acetate) indicated consumption of the starting material ($R_f$ 0.30) and formation of a single new compound ($R_f$ 0.65). Ethanol (24 mL) was added, the reaction stirred for 45 min and the resultant precipitate was removed by filtration (GF/A glass microfibre). The filtrate was concentrated *in vacuo* (only careful heating) to yield the lactol **167D** as a clear glass (163 mg, 100%), which was used directly without further purification. The lactol **167D** (70 mg, 0.23 mmol) was dissolved in anhydrous methanol (3 mL) along with potassium carbonate (95 mg, 0.69 mmol) and stirred at 0 °C under an atmosphere of nitrogen. Iodine (76 mg, 0.30 mmol) was dissolved, under sonication, in anhydrous methanol (3 mL) and added dropwise to the stirred reaction mixture at 0 °C. Mass spectrometry indicated the formation of the desired product after 45 min of reaction time and TLC analysis (ethyl acetate) showed the consumption of the starting material ($R_f$ 0.60) and formation of a single compound ($R_f$ 0.80). The reaction was quenched by addition of sat. aq. sodium sulfite (6 mL). The resultant white precipitate was

dissolved in water (16 mL) and the aqueous fraction was extracted with diethyl ether (4 x 30 mL). The organic layer was dried (magnesium sulfate), filtered and evaporated to dryness to yield the crude title compound **170D** (84 mg, 100%). Purification using flash column chromatography (80:19:1 → 66:32:1 cyclohexane/ethyl acetate/triethylamine) gave the methyl ester **170D** (60 mg, 77%) as a clear colourless oil. $[\alpha]_D^{25}$ +55.5 (*c* 0.51 in $CHCl_3$).

**Methyl *N*,3-*O*-dibenzyl-2,4-dideoxy-2,4-imino-D-ribonamide or (2*R*,3*R*,4*R*)-1-benzyl-3-(benzyloxy)-4-(hydroxymethyl)-*N*-methylazetidine-2-carboxamide 169D**

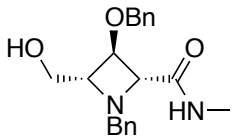


Starting from *N*-Benzyl-3-*O*-benzyl-2,4-dideoxy-2,4-imino-D-talitol **162** (75 mg, 0.22 mmol), the methyl amide **169D** was isolated as white crystalline solid (54 mg, 72%) without intermediate purification. $[\alpha]_D^{25}$ +58.5 (*c* 1.04 in $HCCl_3$).

**Methyl 2,4-dideoxy-2,4-imino-D-ribonamide or (2*R*,3*R*,4*R*)-3-hydroxy-4-(hydroxymethyl)-*N*-methylazetidine-2-carboxamide 78D**

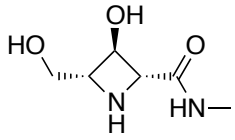


The methyl amide **78D** was isolated as a clear colourless glass (33 mg, 100%). $[\alpha]_D^{25}$ +7.7 (*c* 1.29 in MeOH).

### 3.6.5 L-ribo acid synthesis:

***N*,3-*O*-dibenzyl-2,4-dideoxy-2,4-imino-L-ribonic acid or (2*S*,3*S*,4*S*)-1-benzyl-3-(benzyloxy)-4-(hydroxymethyl)azetidine-2-carboxylic acid 208L**

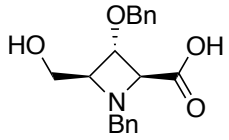


Concentrated hydrochloric acid (11.6 M, 11 μL, 0.13 mmol) was diluted with water (4 mL), premixed with 1,4-dioxane (2 mL), added to the methyl ester **170L** (22.5 mg, 0.066 mmol) and stirred at 70 °C without a condenser, open to air for 3 d. The reaction progress was following using mass spectrometry (Starting material found in the +ve, title compound in the -ve; on completion the title compound is found in both). Furthermore TLC analysis (ethyl acetate) indicated the complete disappearance of the starting material ($R_f$ 0.80) and appearance of a new compound ($R_f$ 0.0). On completion the reaction mixture was concentrated *in vacuo*. The residue was loaded onto a short column of Dowex® (50W-X8, $H^+$) where the resin had been pre-treated by sequential washing with water (until eluent was neutral), 1,4-dioxane and water again. The crude was loaded (water/1,4-dioxane 2:1) and washed sequentially with water, 1,4-dioxane and water again. The product was eluted with aqueous ammonia (2 M) and the ammoniacal fractions concentrated *in vacuo* to afford the carboxylic acid **208L** as white crystalline solid (18 mg, 81%). M.p. 172-174 °C; $[\alpha]_D^{25}$ -19.4 (*c* 0.16 in MeOH); $\nu_{max}$ (thin film): 3326 (w, OH), 1634 (s, C=O); $\delta_H$ (400 MHz, Pyr-$d_5$) 7.57 – 7.48 (Ar, 4 H, m), 7.39 – 7.24 (Ar, 6 H, m), 4.95 ($OCH_2Ph$, 1 H, d, $J_{gem}$ 11.9), 4.85 ($OCH_2Ph$, 1 H, d, $J_{gem}$ 11.9), 4.72 (H3, 1 H, a-t, $J_{2,3}$=$J_{3,4}$ 5.4), 4.30 ($NCH_2Ph$, 1 H, d, $J_{gem}$ 12.9), 4.10 (H2, 1 H, d, $J_{2,3}$ 5.5), 3.97 ($NCH_2Ph$, 1 H, d, $J_{gem}$ 12.9), 3.76 (H5 and H5', 2 H, d, $J_{4,5}$ 4.7), 3.61 (H4, 1 H, a-q, $J_{3,4}$=$J_{4,5}$ 4.8); $\delta_C$ (126 MHz, Pyr-$d_5$) 174.9 (C=O), 139.4, 138.7 (2 x ipso-Ph), 130.56, 129.1, 129.0, 128.6, 128.3, 128.1 (10 x Ph), 76.1 (C3), 72.1 (C4), 71.8 ($O\underline{C}H_2Ph$), 70.9 (C2), 63.5 (C5), 62.0 ($N\underline{C}H_2Ph$); *m/z* (ESI+ve): 328

([M+H]$^+$, 45%), 350 ([M+Na]$^+$, 100%); (ESI-ve): 326 ([M-H]$^-$, 100%); HRMS (ESI+ve): Found 350.1356 ([M+Na]$^+$); $C_{19}H_{21}NNaO_4$ requires 350.1363.

**2,4-dideoxy-2,4-imino-L-ribonic acid or (2*S*,3*S*,4*S*)-3-hydroxy-4-(hydroxymethyl)azetidine-2-carboxylic acid 209L**

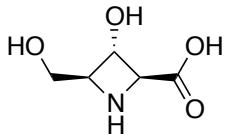


Concentrated hydrochloric acid (11.6 M, 7 μL, 0.08 mmol) was diluted with water (2 mL), premixed with 1,4-dioxane (1 mL) and added to the protected amino acid **208L** (15 mg, 0.04 mmol). To this solution was added palladium on charcoal (40% b.w., 6 mg) and the reaction vessel was degassed and charged with hydrogen. After 15 h of vigorous stirring TLC analysis (14:3:1:1:1 ethanol/pyridine/n-butanol/acetic acid/water) indicated the presence of a single product ($R_f$ 0.60). The reaction mixture was filtered (GF/A glass microfibre), concentrated *in vacuo* at RT and loaded onto a short column of Dowex® (50W-X8, $H^+$) in which the resin had been pre-treated by sequential washing with water (until eluent was neutral), 1,4-dioxane and water again. The crude was loaded (water/1,4-dioxane 2:1) and washed sequentially with water, 1,4-dioxane and water again. The product was eluted with aqueous ammonia (2 M) and the ammoniacal fractions concentrated *in vacuo* at RT to yield the amino acid **209L** as a viscous gum (7 mg, 100%). Data for HCl salt: $[\alpha]_D^{25}$ – 9.7 (*c* 0.11 in DMF); $\nu_{max}$ (thin film): 3209 (m, br, OH, NH), 1733 (s, C=OOH), 1604 (m, anti. sym.-stretch, $CO_2^-$), 1420 (m, sym.-stretch, $CO_2^-$); $\delta_H$ (500 MHz, MeOD) 4.73 (H2, 1 H, d, $J_{2,3}$ 6.6), 4.66 (H3, 1 H, a-t, $J_{2,3}$=$J_{3,4}$ 6.6), 4.28 (H4, 1 H, dt, $J_{3,4}$ 6.7, $J_{4,5}$=$J_{4,5'}$ 3.5), 3.83 (H5 and H5', 2 H, d, $J_{4,5}$=$J_{4,5'}$3.6); $\delta_C$ (126 MHz, MeOD) 168.8 (C=O), 69.5 (C4), 68.4 (C3), 65.3 (C2), 58.8 (C5).

### 3.6.6 D-ribo acid synthesis:

**_N_,3-_O_-dibenzyl-2,4-dideoxy-2,4-imino-D-ribonic acid or (2_R_,3_R_,4_R_)-1-benzyl-3-(benzyloxy)-4-(hydroxymethyl)azetidine-2-carboxylic acid 208D**

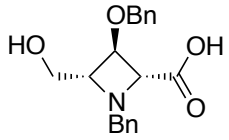


The protected amino acid **208D** was isolated as a white solid (32 mg, 96%). M.p. 177-178 °C; $[\alpha]_D^{25}$ +25.1 (*c* 0.66 in MeOH).

**2,4-dideoxy-2,4-imino-D-ribonic acid or (2_R_,3_R_,4_R_)-3-hydroxy-4-(hydroxymethyl)azetidine-2-carboxylic acid 209D**

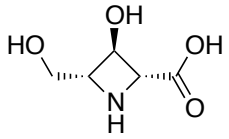


The amino acid **209D** was isolated as off white viscous gum (15.1 mg, 100%). Data for HCl salt: $[\alpha]_D^{25}$ +6.6 (*c* 0.19 in DMF).

### 3.6.7 Towards D-lyxo amide synthesis:

**1,2-5,6-Di-_O_-ispropylidene-α-D-_ribo_-hexofuranos-3-ulose 211**

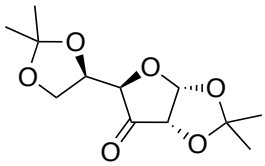


Diacetone-D-glucose **163** (6 g, 23.1 mmol) was dissolved, under sonication, in dichloromethane (60 mL) and Dess Martin periodate (12.7 g, 30 mmol) was added to the solution at 0 °C. After 15 min the ice bath was removed and the reaction mixture was allowed to warm to RT. After 22 h mass spectrometry analysis indicated the complete consumption of starting material and

formation of the title compound. The reaction mixture was diluted with dichloromethane (90 mL) and stirred vigorously with saturated aqueous sodium bicarbonate containing sodium thiosulfate (0.12 g/mL) until both phases cleared. After separation of the layers the organic fraction was washed with more of the same solution (50 mL). The combined aqueous fraction was extracted with dichloromethane (90 mL) and the combined organic fractions were dried (magnesium sulfate) and evaporated to dryness to yield ketone **211** as a clear oil (5.76 g, 97%). $[\alpha]_D^{25}$ +31.1 (*c* 1.99 in $CHCl_3$), [lit. $[\alpha]_D^{20}$ +39 ($CHCl_3$)];[176] $\nu_{max}$ (thin film): 1632 (s, C=O); $\delta_H$ (400 MHz, $CDCl_3$) 6.12 (H1, 1 H, d, $J_{1,2}$ 4.5), 4.37 (H2, 1 H, dd, $J_{1,2}$ 4.5, $J$ 0.8), 4.36 – 4.31 (H4, H5, 2 H, m), 4.03 – 3.99 (H6, H6', 2 H, m), 1.43 ($C\underline{H}_3$, 3 H, s), 1.41 ($C\underline{H}_3$, 3 H, s), 1.31 ($C\underline{H}_3$, 6 H, s); $\delta_C$ (101 MHz, $CDCl_3$) 209.0 (C=O), 114.4, 110.4 (2x $\underline{C}(CH_3)_2$), 103.2 (C1), 79.0 (C4 or C5), 77.3 (C2), 76.4 (C4 or C5), 64.4 (C6), 27.6, 27.2, 26.1, 25.4 (4x $\underline{C}H_3$); *m/z* (ESI+ve): 313 ($[M+MeOH+Na]^+$, 100%); HRMS (ESI+ve): Found 313.1257 ($[M+MeOH+Na]^+$); $C_{13}H_{22}NaO_7$ requires 313.1258.

**3-*O*-Acetyl-1,2-5,6-di-*O*-ispropylidene-α-D-*erythro*-hex-3-enofuranose 212**

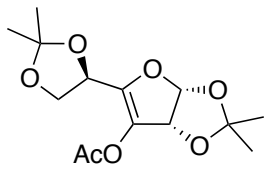


The ketone **211** (4.56g, 17.64 mmol) was dissolved in 1:1 pyridine/acetic anhydride (50 mL) and stirred under reflux. The reaction mixture turned very dark during reaction progression and after 12.5 h TLC analysis (1:1 ethyl acetate/cyclohexane) indicated complete consumption of the starting material ($R_f$ 0.45) and formation of a major product ($R_f$ 0.65). The reaction mixture was diluted with toluene (45 mL) and evaporated to dryness. The crude was coevaporated with toluene (3 x 30 mL) and purified using column chromatography (1% acetone in toluene) to yield the title compound **212** as a clear oil which crystalizes on standing (5.07g, 96%). M.p. 50-52 °C, [lit. m.p. 62-63 °C];[177] $[\alpha]_D^{25}$ -37.3 (*c* 0.95 in $CHCl_3$), [lit. $[\alpha]_D^{20}$ -33.0 (*c* 1.0 $CHCl_3$)];[177] $\nu_{max}$

(thin film): 1769 (s, C=O); $\delta_H$ (400 MHz, $CDCl_3$) 6.02 (H1, 1 H, d, $J_{1,2}$ 5.5), 5.38 (H2, 1 H, dd, $J_{1,2}$ 5.5, $J_{2,Me}$ 0.4), 4.69 (H5, 1 H, t, $J_{5,6}$=$J_{5,6'}$ 6.4), 4.05 (H6, H6', 2 H, qd, $J_{6,6'}$ 8.5, $J_{5,6}$=$J_{5,6'}$ 6.4), 2.20 (C=OC$\underline{H}_3$, 3 H, s), 1.52 (C$\underline{H}_3$, 3 H, s), 1.46 (C$\underline{H}_3$, 3 H, s), 1.43 (C$\underline{H}_3$, 3 H, s), 1.36 (C$\underline{H}_3$, 3 H, d, $J_{2,Me}$ 0.4); $\delta_C$ (101 MHz, $CDCl_3$) 169.1 (C=O), 145.4 (C4), 129.1 (C3), 113.6, 110.5 (2x $\underline{C}(CH_3)_2$), 104.1 (C1), 80.9 (C2), 68.7 (C5), 66.0 (C6), 28.0, 28.0, 25.9, 25.7 (4x C($\underline{C}H_3)_2$), 20.6 (C=O$\underline{C}H_3$); *m/z* (ESI+ve): 323 ($[M+Na]^+$, 100%); HRMS (ESI+ve): Found 323.1098 ($[M+Na]^+$); $C_{14}H_{20}NaO_7$ requires 323.1101.

**3-deoxy-1,2-5,6-di-*O*-ispropylidene-α-D-*ribo*-hexofuranose 216**

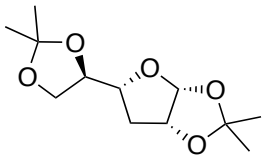

Thoroughly dried enol **212** (54 mg, 0.18 mmol) along with 10% palladium on charcoal (10 mol%, 42 mg, 0.04 mmol) and ammonium formate (227 mg, 3.6 mmol) was dissolved in anhydrous methanol (5 mL) and refluxed strongly under argon. After 30 min TLC analysis (9:1 toluene/acetone) indicated the consumption of the starting material ($R_f$ 0.50) and the formation of the deoxy derivative **216** ($R_f$ 0.35) along with acetate **213** ($R_f$ 0.30). In order to allow for separation of the two reaction products the solvent was evaporated to dryness and the residue was redissolved in anhydrous methanol (3 mL), sodium methoxide (4.3 mg, 0.08 mmol) was added and the reaction stirred at RT for 5 h. At this stage TLC analysis still indicated remaining acetate **213** and additional sodium methoxide (6.4 mg) was added and the reaction stirred for further 18.5 h. As the reaction was still incomplete, the mixture was heated to 50 °C for 24 h at which stage additional sodium methoxide was added (10 mg) and the temperature increased to 60 °C for an extra 24 h. However only after addition of water (3 mL) and triethylamine (0.6 mL) and heating to 60 °C for 5.5 h did TLC analysis (9:1 toluene/acetone) indicate the complete consumption of acetate **213** ($R_f$ 0.30) and formation of diacetone-D-gulose **214** ($R_f$ 0.20). The

reaction mixture was evaporated to dryness and flash column chromatography (3:1 → 1:1 cyclohexane/ethyl acetate) allowed for the separation of the deoxy title compound **216** (27 mg, 61%, white solid) and diacetone-D-gulose **214** (12 mg, 25%, white solid). The data of the deoxy compound **216** is given. M.p. 72-74 °C, [lit. m.p. 78-80 °C];[178] $[\alpha]_D^{25}$ -28.0 (*c* 0.91 in $CHCl_3$), [lit. $[\alpha]_D^{25}$ -28.4 (*c* 1.1 in $CHCl_3$)];[178] $\nu_{max}$ (thin film): fingerprint reagion only; $\delta_H$ (400 MHz, $CDCl_3$) 5.79 (H1, 1 H, d, $J_{1,2}$ 3.8), 4.72 (H2, 1 H, ddd, $J_{2,3}$ 6.1, $J_{1,2}$ 3.9, $J_{2,3'}$ 1.4), 4.42 (H5, 1 H, dt, $J_{4,5}$ 8.3, $J_{5,6}$=$J_{5,6'}$ 6.7), 4.10 (H4, 1 H, td, $J_{3,4}$=$J_{4,5}$ 8.4, $J_{3',4}$ 3.9), 4.04 (H6, 1 H, dd, $J_{6,6'}$ 8.2, $J_{5,6}$ 6.6), 3.60 (H6', 1 H, dd, $J_{6,6'}$ 8.2, $J_{5,6'}$ 6.9), 2.20 (H3, 1 H, ddd, $J_{3,3'}$ 14.5, $J_{3,4}$ 8.5, $J_{2,3}$ 6.2), 1.81 (H3', 1 H, ddd, $J_{3,3'}$ 14.3, $J_{3',4}$ 4.0, $J_{2,3'}$ 1.3), 1.56 ($C\underline{H}_3$, 3 H, s), 1.44 ($C\underline{H}_3$, 3 H, s), 1.36 ($C\underline{H}_3$, 3 H, s), 1.31 ($C\underline{H}_3$, 3 H, s); $\delta_C$ (101 MHz, $CDCl_3$) 112.9, 110.1 (2x $\underline{C}(CH_3)_2$), 106.6 (C1), 81.7 (C4), 80.6 (C2), 77.8 (C5), 66.2 (C6), 33.7 (C3), 27.4, 26.9, 26.4, 25.4 (4 x $C(\underline{C}H_3)_2$); *m/z* (ESI+ve): 267 ($[M+Na]^+$, 100%); HRMS (ESI+ve): Found 267.1201 ($[M+Na]^+$); $C_{12}H_{20}NaO_5$ requires 267.1203.

**3-*O*-Acetyl-1,2-5,6-di-*O*-ispropylidene-α-D-*gulo*-furanose 213**

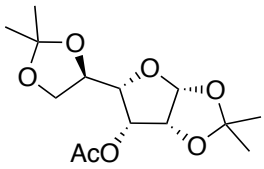


The enol **212** (3.02 g, 10.1 mmol) was dissolved in diethylether (60 mL) and 10% palladium on charcoal (50% b.w., 1.5 g) was added and the mixture degassed. The reaction vessel was then purged with hydrogen and stirred vigorously for 17 h at RT. At this point TLC analysis (9:1 toluene/acetone) indicated complete consumption of starting material ($R_f$ 0.50) and formation of a single new product ($R_f$ 0.30) and the reaction mixture was filtered through celite and the filter cake washed with dichloromethane. The combined organic fractions were evaporated to dryness to yield the title compound **213** as a white crystalline solid (2.96 g, 97%). M.p. 57-59 °C, [lit.

m.p. 73-74 °C (ethanol)];[165] $[\alpha]_D^{25}$ +67.6 (*c* 2.0 in $CHCl_3$), [lit. $[\alpha]_D^{20}$ +66.0 (*c* 0.36 in $CHCl_3$)];[165] $\nu_{max}$ (thin film): 1747 (s, C=O); $\delta_H$ (400 MHz, $CDCl_3$) 5.80 (H1, 1 H, d, $J_{1,2}$ 4.1), 5.05 (H3, 1 H, dd, $J_{3,4}$ 6.7, $J_{2,3}$ 5.6), 4.79 (H2, 1 H, dd, $J_{2,3}$ 5.6, $J_{1,2}$ 4.1), 4.60 (H5, 1 H, ddd, $J_{4,5}$ 9.3, $J_{5,6'}$ 7.2, $J_{5,6}$ 6.7), 4.09 (H6, 1 H, dd, $J_{6,6'}$ 8.5, $J_{5,6}$ 6.5), 4.06 (H4, 1 H, dd, $J_{4,5}$ 9.4, $J_{3,4}$ 6.7), 3.51 (H6', 1 H, dd, $J_{6,6'}$ 8.4, $J_{5,6'}$ 7.4), 2.11 (C=OC$\underline{H}_3$, 3 H, s), 1.56 (C$\underline{H}_3$, 3 H, s), 1.42 (C$\underline{H}_3$, 3 H, s), 1.37 (C$\underline{H}_3$, 3 H, s), 1.33 (C$\underline{H}_3$, 3 H, s); $\delta_C$ (101 MHz, $CDCl_3$) 169.7 ($\underline{C}$=O), 114.6, 109.3 (2x $\underline{C}(CH_3)_2$), 105.1 (C1), 81.4 (C4), 78.6 (C2), 75.2 (C5), 71.8 (C3), 66.4 (C6), 26.8, 26.7, 25.3 (4x C($\underline{C}H_3)_2$), 20.7 (C=O$\underline{C}H_3$); *m/z* (ESI+ve): 325 ($[M+Na]^+$, 100%); HRMS (ESI+ve): Found 325.1255 ($[M+Na]^+$); $C_{14}H_{22}NaO_7$ requires 325.1258.

**1,2-5,6-Di-*O*-ispropylidene-α-D-*gulo*-furanose 214**

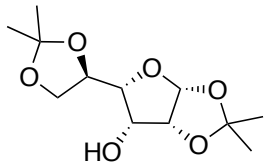


The starting acetate **213** (2.94 mg, 9.72 mmol) was dissolved in a 5:5:1 mixture of methanol/water/triethylamine and stirred at RT. TLC analysis (1:1 ethyl acetate/cylcohexane) after 3 h indicated the disappearance of the starting material ($R_f$ 0.50) and formation of a single product ($R_f$ 0.30). The reaction mixture was evaporated to dryness and the crude was purified using column chromatography (3:1 → 1:1 cyclohexane/ethyl acetate), which yielded the alcohol **214** as a white crystalline solid (2.05 g, 81%). M.p. 100-102 °C, [lit. m.p. 103 °C];[165] $[\alpha]_D^{25}$ +10.2 (*c* 0.88 in $CHCl_3$), [lit. $[\alpha]_D^{25}$ +10.0 (*c* 0.4 in $CHCl_3$)];[165] $\nu_{max}$ (thin film): 3492 (OH); $\delta_H$ (400 MHz, $CD_3CN$) 5.69 (H1, 1 H, d, $J_{1,2}$ 4.0), 4.58 (H2, 1 H, dd, $J_{2,3}$ 5.8, $J_{1,2}$ 4.0), 4.47 – 4.40 (H5, 1 H, m), 4.24 (H3, 1 H, q, $J_{2,3}$=$J_{3,4}$=$J_{3,OH}$ 6.4), 4.09 (H6, 1 H, dd, $J_{6,6'}$ 8.7, *J* 6.6), 3.85 (H4, 1 H, dd, *J* 9.3, $J_{3,4}$ 6.6), 3.57 (H6', 1 H, dd, $J_{6,6'}$ 8.7, *J* 7.3), 3.08 (OH3, 1 H, d, $J_{3,OH}$ 6.7), 1.54 (C$\underline{H}_3$, 3 H, s), 1.34 (C$\underline{H}_3$, 3 H, d, *J* 0.5), 1.33 (C$\underline{H}_3$, 3 H, d, *J* 0.5), 1.29 (C$\underline{H}_3$, 3 H, d, *J* 0.5); $\delta_C$

(101 MHz, $CD_3CN$) 114.5, 108.9 (2x $\underline{C}(CH_3)_2$), 105.9 (C1), 84.8 (C4), 80.7 (C2), 76.5 (C5), 71.1 (C3), 67.2 (C6), 27.1, 26.9, 26.8, 25.5 (4x $\underline{C}H_3$); *m/z* (ESI+ve): 283 ($[M+Na]^+$, 100%); HRMS (ESI+ve): Found 283.1151 ($[M+Na]^+$); $C_{12}H_{20}NaO_6$ requires 283.1152.

**3-*O*-Benzyl-1,2-5,6-di-*O*-ispropylidene-α-D-*gulo*-furanose 215**

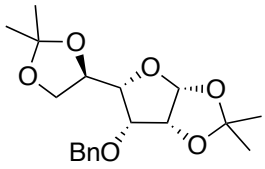


Starting alcohol **214** (2.0 g, 7.68 mmol) was dissolved in anhydrous dimethylformamide (20 mL) under argon in a flame dried flask. Benzylbromide (2.74 mL, 23.1 mmol) was added and the mixture stirred at RT for 20 min. Then the reaction mixture was cooled to 0 °C and sodium hydride (616 mg, 15.4 mmol) was added and the reaction was stirred at 0 °C for 2 h. The ice bath was then removed and the reaction stirred at RT for another 1 h at which point TLC analysis (1:1 ethyl acetate/cyclohexane) indicated the consumption of starting material ($R_f$ 0.30) and the formation of a major new species ($R_f$ 0.60) along with an additional spot ($R_f$ 0.90). The reaction was then quenched *via* the addition of water (5 mL) and the crude reaction mixture was diluted with ethyl acetate (100 mL) and washed with 50% aqueous brine (3x 80 mL). The organic phase was dried (magnesium sulfate) and evaporated to dryness. The crude reaction product mixture was purified using column chromatography (5:1 → 3:1 cyclohexane/ethyl acetate) and the title compound **215** was yielded as a white crystalline solid (2.56 g, 95%). M.p. 133-135 °C, [lit. m.p. 128.5-129.5 °C];[179] $[\alpha]_D^{25}$ +42.2 (*c* 0.94 in $CHCl_3$), [lit. $[\alpha]_D^{20}$ + 42.5 (*c* 1.5 in $CHCl_3$)];[179] $\nu_{max}$ (thin film): fingerprint region only; $\delta_H$ (400 MHz, $CD_3CN$) 7.42 – 7.29 (Ph, 5 H, m), 5.71 (H1, 1 H, d, $J_{1,2}$ 3.9), 4.73 (H2, 1 H, dd, $J_{2,3}$ 5.0, $J_{1,2}$ 4.0), 4.68 ($OCH_2Ph$, 1 H, d, $J_{gem}$ 11.5), 4.55 (H5, 1 H, dt, *J* 9.6, $J_{5,6'}$ 6.9), 4.48 (OCH2Ph, 1 H, d, J 11.5), 4.16 (H3, 1 H, dd, $J_{3,4}$ 7.3, $J_{2,3}$ 5.0), 3.98 (H4 and H6, 2 H, m), 3.55 (H6', 1 H, dd, *J* 8.7, $J_{5,6'}$ 7.2), 1.53 ($C\underline{H}_3$, 3 H, s), 1.33 ($C\underline{H}_3$, 3 H, s), 1.32 – 1.30 ($C\underline{H}_3$, 3 H, m), 1.29 – 1.26 ($C\underline{H}_3$, 3 H, m); $\delta_C$ (101 MHz, $CD_3CN$): 138.9 (ipso-Ph),

129.3, 128.7, 128.6 (3x Ph), 114.2, 108.8 (2x $\underline{C}(CH_3)_2$), 106.0 (C1), 83.5 (C4), 79.0 (C2), 78.7 (C3), 76.4 (C5), 73.0 ($O\underline{C}H_2Ph$), 67.6 (C6), 27.1, 27.0, 26.6, 25.4 (4x $C(\underline{C}H_3)_2$); *m/z* (ESI+ve): 373 ($[M+Na]^+$, 100%); HRMS (ESI+ve): Found 373.1618 ($[M+Na]^+$); $C_{19}H_{26}NaO_6$ requires 373.1622.

**3-*O*-Benzyl-1,2-*O*-ispropylidene-α-D-*gulo*-furanose 217**

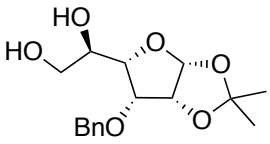


Diacetonide **215** (1.79 g, 5.13 mmol) was dissolved in acetonitrile (72 mL) and was treated with bismuth trichloride (162 mg, 0.51 mmol) along with 18 drops of water and stirred at RT. TLC analysis (ethyl acetate) indicated the starting material ($R_f$ 0.90) becoming fainter, while a new species appeared ($R_f$ 0.45), with the fully deprotected derivative appearing closer to the baseline ($R_f$ 0.05). After 2 h the reaction was quenched with sat. aq. sodium bicarbonate (10 mL) and the solvent removed *in vacuo*. The residue was partitioned between water (100 mL) and dichloromethane (200 mL), the aqueous layer was washed with additional dichloromethane (2x 150 mL) and the combined organic fractions were washed with brine (200 mL), dried (magnesium sulfate), filtered and evaporated to dryness. The crude reaction product mixture was separated using column chromatography (1:1 → 5:2 ethyl acetate/cyclohexane) and the title compound **217** was found as clear oil (926 mg, 58%, 86% brsm). Starting material **215** (577 mg, 32%) was also recovered. $[\alpha]_D^{25}$ +44.1 (*c* 0.26 in $CHCl_3$); $\nu_{max}$ (thin film): 3461 (m, br, OH); $\delta_H$ (400 MHz, $CDCl_3$) 7.41 – 7.28 (Ph, 5 H, m), 5.76 (H1, 1 H, d, $J_{1,2}$ 4.0), 4.78 ($OCH_2Ph$, 1 H, d, $J_{gem}$ 11.8), 4.64 (H2, 1 H, a-t, $J_{1,2}$=$J_{2,3}$ 4.5), 4.56 ($OCH_2Ph$, 1 H, d, $J_{gem}$ 11.9), 4.27 (H5, 1 H, dt, $J$ 7.7, $J_{5,6}$=$J_{5,6'}$ 4.0), 4.20 – 4.12 (H3 and H4, 2 H, m), 3.80 (H6, 1 H, dd, $J_{6,6'}$ 11.5, $J_{5,6}$ 3.6), 3.67 (1 H, dd, $J_{6,6'}$ 11.5, $J_{5,6'}$ 4.5), 2.99 (OH, 1H, br-s), 2.32 (OH, 1H, br-s), 1.63 ($C\underline{H}_3$, 3 H, s), 1.35 ($C\underline{H}_3$, 3 H, s); $\delta_C$ (101 MHz, $CDCl_3$) 137.2 (ipso-Ph), 128.7, 128.2, 127.9 (3x Ph), 114.2

($\underline{C}(CH_3)_2$), 104.9 (C1), 79.0, 78.0, 77.7 (C2, C3, C4), 72.7 ($O\underline{C}H_2Ph$), 69.3 (C5), 63.7 (C6), 26.5, 26.2 (2x $C(\underline{C}H_3)_2$); *m/z* (ESI+ve): 333 ($[M+Na]^+$, 100%); HRMS (ESI+ve): Found 333.1309 ($[M+Na]^+$); $C_{16}H_{22}NaO_6$ requires 333.1309.

**5,6-Di-*O*-allyl-3-*O*-benzyl-1,2-*O*-ispropylidene-α-D-*gulo*-furanose 218**

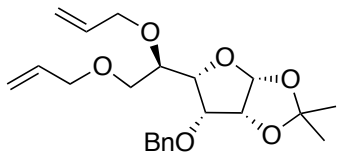


The thoroughly dried diol **217** (282 mg, 0.91 mmol) was dissolved in *N*,*N*-dimethylformamide (3 mL), allyl bromide (0.3 mL, 3.64 mmol) was added and the reaction stirred at RT under argon for 20 min. The reaction mixture was then cooled to 0 °C and sodium hydride (73 mg, 1.82 mmol) was added and after 10 min the cool bath was removed and the reaction allowed to warm to RT. After 2 h TLC analysis (1:1 cyclohexane/ethyl acetate) indicated the consumption of the starting material **217** ($R_f$ 0.20) and formation of a major species ($R_f$ 0.80) along with two spots of intermediate $R_f$ (0.40 and 0.55), which were tentatively identified as the mono-allyl derivatives using mass spectrometry. Additional allyl bromide (0.15 mL, 1.82 mmol) and sodium hydride (46 mg, 0.91 mmol) were added and after further 2 h only a single compound was observable using TLC analysis. Therefore the reaction was quenched after a total time of 4 h with water (1.5 mL) and the resulting mixture diluted with ethyl acetate (15 mL) and washed with 50% aq. brine (3 x 10 mL). The organic phase was dried (magnesium sulfate), filtered and evaporated to dryness. The residue was purified using flash column chromatography (5:1 hexane/ethyl acetate) to give the di-allyl compound **218** as a clear oil (338 mg, 95%). $[\alpha]_D^{25}$ + 63.1 (*c* 1.17 in $CHCl_3$); $\nu_{max}$ (thin film): fingerprint region only; $\delta_H$ (400 MHz, $CDCl_3$) 7.39 – 7.28 (Ph, 5 H, m), 5.96 (allyl-A: $CH_2C\underline{H}=CH_2$, 1 H, ddt, $J_{trans}$ 17.1, $J_{cis}$ 10.5, $J_{CH,H}=J_{CH,H'}$ 5.7), 5.84 (allyl-B: $CHH'C\underline{H}=CH_2$, 1 H, ddt, $J_{trans}$ 17.3, $J_{cis}$ 10.4, $J_{CH,H}=J_{CH,H'}$ 5.6), 5.71 (H1, 1 H, d, $J_{1,2}$ 4.6), 5.27 (allyl-A: *trans*-$CHH'CH=C\underline{H}_2$, 1 H, ddd, $J_{trans}$ 17.3, *J* 3.3, *J* 1.6), 5.20 (*trans*-$CHH'CH=C\underline{H}_2$, 1

H, ddd, $J_{trans}$ 17.2, $J$ 3.3, $J$ 1.6), 5.15 – 5.10 (2x *cis*-CHH'CH=C$\underline{H}_2$, 2 H, m), 4.84 (OC$\underline{H}_2$Ph, 1 H, d, $J_{gem}$ 11.6), 4.74 (H2, 1 H, a-t, $J_{1,2}$=$J_{2,3}$ 5.0), 4.42 (OCH$_2$Ph, 1 H, d, $J_{gem}$ 11.6), 4.29 (allyl-A: C$\underline{H}$H'CH=CH$_2$, 1 H, ddt, $J_{gem}$ 12.8, $J_{CH,H}$ 5.5, $J_{=CH2,H}$ 1.4), 4.19 (allyl-A: CH$\underline{H}$'CH=CH$_2$, 1 H, ddt, $J_{gem}$ 12.9, $J_{CH,H'}$ 5.9, $J_{=CH2,H'}$ 1.3), 4.02 – 3.90 (H3, H4, H5, C$\underline{H}$H'CH=CH$_2$, 4 H, m), 3.83 (allyl-B: CH$\underline{H}$'CH=CH$_2$, 1 H, ddt, $J_{H,H'}$ 12.9, $J_{CH,H'}$ 5.7, $J_{=CH2,H'}$ 1.3), 3.60 (H6, 1 H, dd, $J_{6,6'}$ 10.6, $J_{5,6}$ 2.0), 3.53 (H6', 1 H, dd, $J_{6,6'}$ 10.6, $J_{5,6'}$ 3.9), 1.59 (C$\underline{H}_3$, 3 H, s), 1.43 (C$\underline{H}_3$, 3 H, s); $\delta_C$ (101 MHz, $CDCl_3$) 137.9 (ipso-Ph) , 135.7, 135.0 (2x CH$_2$C$\underline{H}$=CH$_2$), 128.5, 128.1, 127.9 (3x Ph), 116.9, 116.7 (2x CH$_2$CH=C$\underline{H}_2$), 115.2 (C$\underline{(CH_3)_2}$), 105.0 (C1), 81.5 (C2), 80.5, 77.7, 76.6 (C3, C4, C5), 72.9 (OC$\underline{H}_2$Ph), 72.5, 72.3 (2x C$\underline{H}_2$CH=C$\underline{H}_2$), 70.1 (C6), 27.8, 27.1 (2x C(C$\underline{H}_3$)$_2$); *m/z* (ESI+ve): 413 ([M+Na]$^+$, 100%); HRMS (ESI+ve): Found 413.1932 ([M+Na]$^+$); $C_{22}H_{30}NaO_6$ requires 413.1935.

**5,6-Di-*O*-allyl-3-*O*-benzyl-D-*gulo*-furanose 219**

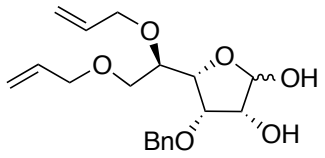


Diallyl **218** (680 mg, 1.74 mmol) was dissolved in 1:2 1% aq. sulfuric acid/1,4-dioxane (12 mL) and stirred at 40 °C for 5 h. At this stage TLC analysis (1:1 cyclohexane/ethyl acetate) indicated complete consumption of starting material ($R_f$ 0.80) and formation of a new species ($R_f$ 0.55). The reaction was quenched with the addition of solid sodium bicarbonate until a neutral pH was reached. The resulting mixture was diluted with ethyl acetate (10 mL), dried (magnesium sulfate) and filtered. The filter-cake was washed with ethyl acetate (2x 10 mL) and the combined organic fractions were concentrated *in vacuo* and co-evaporated with dichloromethane (2x 10 mL) to yield the crude product **219** as a clear oil (595 mg, 98%), which was used without further purification in the subsequent step. Selected data for diol **219**: $[\alpha]_D^{25}$ -44.1 (*c* 0.21 in $CHCl_3$ following 24 h of equilibration); $\nu_{max}$ (thin film): 3376 (m, br, OH); *m/z* (ESI+ve): 373

([M+Na]$^+$, 100%); HRMS (ESI+ve): Found 373.1610 ([M+Na]$^+$); $C_{19}H_{26}NaO_6$ requires 373.1622.

**5,6-Di-*O*-allyl-3-*O*-benzyl-D-gulitol (1,2-Di-*O*-allyl-4-*O*-benzyl-L-glucitol)[180] 220**

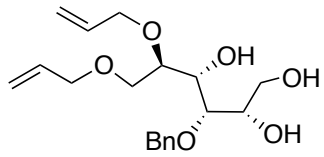


Lactol **219** (595 mg, 1.7 mmol) was dissolved in ethanol (12 mL), sodium borohydride (129 mg, 3.4 mmol) was added and the reaction mixture stirred at RT. After 1 h TLC analysis (1:1 cylcohexane/ethyl acetate) indicated complete consumption of starting material ($R_f$ 0.45) and the formation of a single new compound ($R_f$ 0.10 streaks to baseline). The reaction was quenched by addition of a few drops of acetic acid and the mixture was evaporated to dryness followed by coevaporation with methanol (3x 10 mL). The residue was partitioned between dicholoromethane (30 mL) and brine (10 mL) and the organic fraction was dried (magnesium sulfate), filtered and concentrated *in vacuo* to yielded the crude triol **220** as a clear oil (593 mg, 99%), which required no further purification. $[\alpha]_D^{25}$ -27.3 (*c* 1.2 in $CHCl_3$); $\nu_{max}$ (thin film): 3416 (OH); $\delta_H$ (400 MHz, $CDCl_3$) 7.39 – 7.27 (Ph, 5 H, m), 5.89 ($CH_2C\underline{H}=CH_2$, 2 H, m), 5.35 – 5.25 (*trans*-$CH_2CH=C\underline{H}_2$, 2 H, m), 5.24 – 5.16 (*cis*- $CH_2C\underline{H}=CH_2$, 2 H, m), 4.68 ($OC\underline{H}_2Ph$, 1 H, d, $J_{gem}$ 11.4), 4.61 ($OC\underline{H}_2Ph$, 1 H, d, $J_{gem}$ 11.4), 4.26 ($C\underline{H}H'CH=CH_2$, 1 H, ddt, $J_{gem}$ 12.4, *J* 5.6, *J* 1.3), 4.06 ($CH\underline{H}'CH=CH_2$, 1 H, ddt, $J_{gem}$ 12.4, *J* 6.1, *J* 1.2), 4.01 – 3.90 ($C\underline{H}_2CH=CH_2$, H2, H4, 4 H, m), 3.81 – 3.60 (H1, H1', H3, H5, H6, 5 H, m), 3.46 (H6', 1 H, dd, *J* 10.4, *J* 4.6), 3.12 (OH, 3 H, br-s); $\delta_C$ (101 MHz, $CDCl_3$) 137.9 (ipso-Ph), 134.4 (2x $CH_2\underline{C}H=CH_2$), 128.6, 128.3, 128.1 (3x Ph), 117.9, 117.5 (2x $CH_2CH=\underline{C}H_2$), 77.7 (C3), 77.5 (C5), 73.2 ($O\underline{C}H_2Ph$), 72.5 ($\underline{C}H_2CH=CH_2$), 72.4, 71.7 (H2, H4, $\underline{C}H_2CH=CH_2$), 69.6 (C6), 63.9 (C1); *m/z* (ESI+ve): 353 ([M+H]$^+$, 100%), 375 ([M+Na]$^+$, 73%); HRMS (ESI+ve): Found 375.1766 ([M+Na]$^+$); $C_{19}H_{28}NaO_6$ requires 375.1778.

**5,6-Di-*O*-allyl-3-*O*-benzyl-6-*O*-*tert*-butyl-di-methyl-silyl-D-gulitol (5,6-Di-*O*-allyl-3-*O*-benzyl-6-*O*-*tert*-butyl-di-methyl-silyl-L-glucitol)[180] 221**

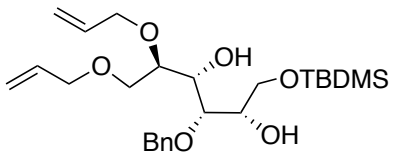


Triol **220** (552 mg, 1.57 mmol) was dissolved in anhydrous dimethylformamide (6 mL), imidazole (326 mg, 4.71 mmol) was added and the reaction mixture was stirred under argon at -30°C. *tert*-butyldimethylsilyl chloride (306 mg, 2.04 mmol) was added to the mixture and stirring continued at -20°C. TLC analysis (ethyl acetate) after 45 min indicated complete consumption of starting material **220** ($R_f$ 0.55) and formation of a single new species ($R_f$ 0.90). The reaction mixture was diluted with ethyl acetate (30 mL), washed with 50% aq. brine (2x 20 mL) and brine (20 mL). The organic layer was dried (magnesium sulfate), filtered and concentrated to dryness. The residue was purified using flash column chromatography (9:1 → 5:1 cyclohexane/ethyl acetate) to give title silyl compound **221** as a clear oil (670 mg, 92%). $[\alpha]_D^{25}$ -7.8 (*c* 1.3 in $CHCl_3$); $\nu_{max}$ (thin film): 3442 (m, br, OH); $\delta_H$ (400 MHz, $CDCl_3$) 7.36 – 7.27 (Ph, 5 H, m), 5.89 ($CH_2C\underline{H}=CH_2$, 2 H, a-dtdd, *J* 17.0, *J* 16.0, *J* 10.6, *J* 5.7), 5.33 – 5.20 (*trans*-$CH_2CH=\underline{C}H_2$, 2 H, m), 5.16 (*cis*-$CH_2CH=C\underline{H}_2$, 2 H, d, *J* 10.4), 4.71 ($OC\underline{H}_2Ph$, 1 H, d, $J_{gem}$ 11.4), 4.61 ($OC\underline{H}_2Ph$, 1 H, d, $J_{gem}$ 11.4), 4.32 – 4.23 ($C\underline{H}H'CH=CH_2$, 1 H, m), 4.07 ($CH\underline{H}'CH=CH_2$, 1 H, dd, *J* 12.5, *J* 6.0), 4.01 – 3.95 (H2, H4, 2 H, m), 3.93 ($C\underline{H}_2CH=CH_2$, 2 H, d, *J* 5.6), 3.81 – 3.75 (H1, H1', 2 H, m), 3.72 (H5, 1 H, a-dd, *J* 10.3, *J* 5.1), 3.66 (H3, 1 H, dd, *J* 5.8, *J* 3.0), 3.54 (H6, 1 H, dd, $J_{6,6'}$ 10.3, $J_{5,6}$ 4.6), 3.42 (H6', 1 H, dd, $J_{6,6'}$ 10.3, $J_{5,6'}$ 5.1), 3.09 (OH, 2 H, br-s), 0.90 ($SiC(C\underline{H}_3)_3$, 9 H, s), 0.07 (2x $SiC\underline{H}_3$, 6 H, s); $\delta_C$ (101 MHz, $CDCl_3$) 138.2 (ipso-Ph), 134.9, 134.7 (2x $CH_2\underline{C}H=CH_2$), 128.5, 128.3, 128.0 (3x Ph), 117.4, 117.2 (2x $CH_2CH=\underline{C}H_2$), 78.3 (C5), 77.1 (C3), 72.9 ($OCH_2Ph$), 72.4 ($\underline{C}H_2CH=CH_2$), 72.3 (C2 or C4), 72.0 ($\underline{C}H_2CH=CH_2$), 71.2 (C2 or C4), 69.7 (C6), 64.1 (C1), 26.0 ($C(\underline{C}H_3)_3$), 18.4 ($\underline{C}(CH_3)_3$), -5.2 (2x

$CH_3$); *m/z* (ESI+ve): 489 ($[M+Na]^+$, 100%); HRMS (ESI+ve): Found 489.2641 ($[M+Na]^+$); $C_{25}H_{42}NaO_6Si$ requires 489.2643.

### 3.6.8 Molecular modelling and NOE experiment on bicycle 160

DFT calculations at the M06-2X/6-311++G** level of theory using Gaussian 09[181] were performed to evaluate the gas-phase geometries of bicycle **160**. Structures were rendered using the Maestro 9.3.5 software of the Schrödinger Suite 2012. The NOE spectra of the bicycle **160** was recorded in order to determine its confirmation. The irradiated proton is indicated on right hand axis with the reference spectrum of the compound shown at the bottom.

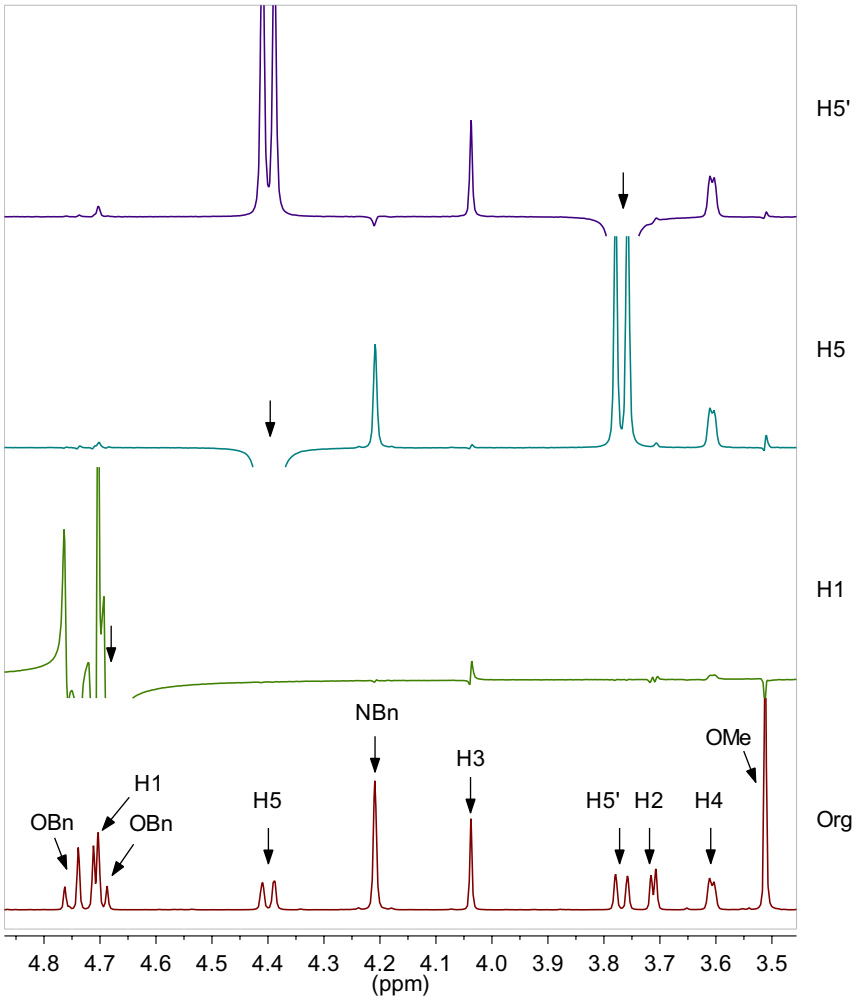


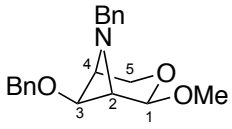


**160**

### 3.6.9 X-ray crystallography experimental and NOE experiment on amino acid 209D

Benzyl protected amino acid **209D** was recrystallised from toluene/acetone/pyridine. M.p. 177-178 °C. Data were collected using synchrotron radiation on I19 (EH1) at Diamond Light Source[182] at low temperature[183] and the structure was solved with SuperFlip[184] and refined with the CRYSTALS software suite.[185] CCDC 924224 contains the supplementary crystallographic data for this compound. These data can be obtained free of charge from The Cambridge Crystallographic Data Centre *via* www.ccdc.cam.ac.uk/data_request/cif. Following debenzylation, nuclear Overhauser effect (NOE) enhancements for 2,4-dideoxy-2,4-imino-L-ribonic acid **209D** showed the all *trans* relationship of the compound. The irradiated proton is indicated on right hand axis with the reference spectrum of the compound shown at the bottom.

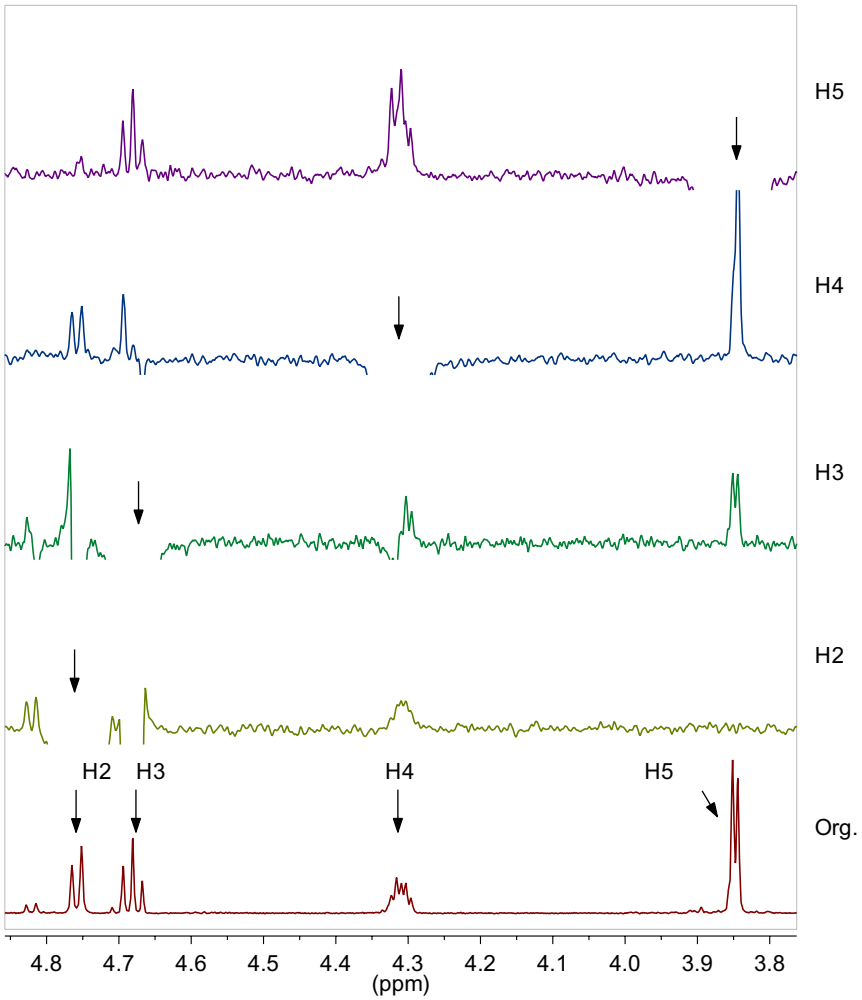


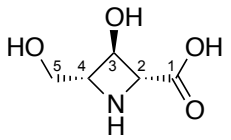


**209D**

### 3.6.10 Enzymatic inhibition assays

Assays were performed analogously to protocols in Chapter 2 (Section 2.6.4, p. 63).

## 3.7 References Chapter 3


1. Bott, T. M.; West, F. G., Preparation and synthetic applications of azetidines. *Heterocycles* **2011**, *84*, 223-264.

2. Berman, H. M.; McGandy, E. L.; Burgner II, J. W.; VanEtten, R. L., The crystal and molecular structure of L-azetidine-2-carboxylic acid. A naturally occurring homolog of proline. *J. Am. Chem. Soc.* **1969**, *91*, 6177-6182.

3. Anderegg, G.; Ripperger, H., Correlation between metal complex formation and biological activity of nicotianamine analogues. *J. Chem. Soc., Chem. Commun.* **1989**, 647-650.

4. Campbell, M. K.; Farrell, S. O., Amino Acids and Peptides. In *Biochemistry*, Lockwood, L.; White, A., Eds. Brooks/Cole, Cengage Learning: Belmont, 2008; pp 65-86.

5. (a) Yoda, H.; Takahashi, M.; Sengoku, T., Azetidine and Its Derivatives. In *Heterocycles in Natural Product Synthesis*, Majumdar, K. C.; Chattopadhyay, S. K., Eds. Wiley-VCH Verlag GmbH & Co. KGaA.: Weinheim, 2011; pp 41-61; (b) Cesari, M.; D'Ilario, L.; Giglio, E.; Perego, G., The Crystal and Molecular Structure of N-(t-Butyloxycarbonyl)-L-azetidine-2-carboxylic Acid and Conformational Analysis of Poly-(L-Azetidinecarboxylic Acid). *Acta Crystallogr. B* **1975**, *31*, 49-55.

6. Thomas, W.; Williams, M., Conformational effects in cyclic imino acids-I: The NMR spectra and conformations of L‐azetidine‐2‐carboxylic acid and its *N*‐acetyl derivative. *Org. Magn. Resonance* **1972**, *4*, 145-152.

7. Fowden, L., Azetidine-2-carboxylic acid: A new constituent of plants. *Nature* **1955**, *176*, 347-348.

8. Morrison, R. I., Naturally occurring L-pipecolinic acid. *Biochem. J.* **1952**, *50*, xiv-xv.

9. Fowden, L., Azetidine-2-carboxylic acid: a new cyclic imino acid occurring in plants. *Biochem. J.* **1956**, *64*, 323-332.

10. Fowden, L.; Richmond, M. H., Replacement of proline by azetidine-2-carboxylic acid during biosynthesis of protein. *Biochim. Biophys. Acta* **1963**, *71*, 459-461.

11. Couty, F.; Evano, G., Azetidine-2-carboxylic acid. From lily of the valley to key pharmaceuticals. A jubilee review. *Org. Prep. Proced. Int.* **2006**, *38*, 427-465.

12. (a) Leete, E., The biosynthesis of azetidine-2-carboxylic acid. *J. Am. Chem. Soc.* **1964**, *86*, 3162; (b) Leete, E.; Davis, G. E.; Hutchinson, C. R.; Woo, K. W.; Chedekel, M. R., Biosynthesis of azetidine-2-carboxylic acid in *Convallaria majalis*. *Phytochemistry* **1974**, *13*, 427-433; (c) Leete, E.; Louters, L. L.; Prakash Rao, H. S., Biosynthesis of azetidine-2-carboxylic acid in *Convallaria majalis*: Studies with N-15 labelled precursors. *Phytochemistry* **1986**, *25*, 2753-2758.

13. Rubenstein, E.; McLaughlin, T.; Winant, R. C.; Sanchez, A.; Eckart, M.; Krasinska, K. M.; Chien, A., Azetidine-2-carboxylic acid in the food chain. *Phytochemistry* **2009**, *70*, 100-104.

14. Beak, S.-H.; Lee, G. L.; Park, S. Y.; Piao, X.-L.; Kim, H. Y.; Bae, O.-N.; Park, J. H., Gas chromatographic determination of azetidine-2-carboxylic acid in rhizomes of *Polygonatum sibiricum* and *Polygonatum odoratum*. *J. Food Comp. Anal.* **2012**, *25*, 137-141.

15. Rubenstein, E.; Zhou, H.; Krasinska, K. M.; Chien, A.; Becker, C. H., Azetidine-2-carboxylic acid in garden beets (*Beta vulgaris*). *Phytochemistry* **2006**, *67*, 898-903.

16. Rubenstein, E., Biologic effects of and clinical disorders caused by nonprotein amino acids. *Medicine* **2000**, *79*, 80-89.

17. Peterson, P. J.; Fowden, L., Different specificities of proline-activating enzymes from some plant species. *Nature* **1963**, *200*, 148-151.

18. Baum, B. J.; Troxler, R. F.; Kagan, H. M.; Grasso, J. A.; Faris, B.; Franzblau, C., Incorporation of L-azetidine-2-carboxylic acid into hemoglobin in rabbit reticulocytes. *Biochem. Biophys. Res. Commun.* **1973**, *53*, 1350-1356.

19. Deming, T. J.; Fournier, M. J.; Mason, T. L.; Tirrell, D. A., Structural modification of a periodic polypeptide through biosynthetic replacement of proline with azetidine-2-carboxylic acid. *Macromolecules* **1996**, *29*, 1442-1444.

20. Li, D.; Hirsilä, M.; Koivunen, P.; Brenner, M. C.; Xu, L.; Yang, C.; Kivirikko, K. I.; Myllyharju, J., Many amino acid substitutions in a hypoxia-inducible transcription factor (HIF)-1α-like peptide cause only minor changes in its hydroxylation by the HIF prolyl 4-hydroxylases: Substitution of 3,4-dehydroproline or azetidine-2-carboxylic acid for the proline leads to a high rate of uncoupled 2-oxoglutarate decarboxylation. *J. Biol. Chem.* **2004**, *279*, 55051-55059.

21. Dasuri, K.; Ebenezer, P. J.; Uranga, R. M.; Gavilán, E.; Zhang, L.; Fernandez-Kim, S. O.; Bruce-Keller, A. J.; Keller, J. N., Amino acid analog toxicity in primary rat neuronal and astrocyte cultures: Implications for protein misfolding and TDP-43 regulation. *J. Neurosci. Res.* **2011**, *89*, 1471-1477.

22. (a) Shang, J., Quantitative measurement of events in the mammalian unfolded protein response. *Methods* **2005**, *35*, 390-394; (b) Trotter, E. W.; Kao, C. M.-F.; Berenfeld, L.; Botstein, D.; Petsko, G. A.; Gray, J. V., Misfolded proteins are competent to mediate a subset of the responses to heat shock in *Saccharomyces cerevisiae*. *J. Biol. Chem.* **2002**, *277*, 44817-44825.

23. Qian, S.-B.; Zhang, X.; Sun, J.; Bennink, J. R.; Yewdell, J. W.; Patterson, C., mTORC1 links protein quality and quantity control by sensing chaperone availability. *J. Biol. Chem.* **2010**, *285*, 27385-27395.

24. Shoulders, M. D.; Raines, R. T., Collagen structure and stability. *Annu. Rev. Biochem.* **2009**, *78*, 929-958.

25. (a) Cowan, P. M.; McGavin, S., Structure of poly-L-proline. *Nature* **1955**, *176*, 501-503; (b) Arnott, S.; Dover, S. D., The structure of poly-L-proline II. *Acta Crystallogr. B* **1968**, *24*, 599-601.

26. Taylor, C. M.; Hardré, R.; Edwards, P. J. B., The impact of pyrrolidine hydroxylation on the conformation of proline-containing peptides. *J. Org. Chem.* **2005**, *70*, 1306-1315.

27. Takeuchi, T.; Prockop, D. J., Biosynthesis of abnormal collagens with amino acid analogues. I. Incorporation of L-azetidine-2-carboxylic acid and cis-4-fluoro-L-proline into protocollagen and collagen. *BBA - Protein Structure* **1969**, *175*, 142-155.

28. Takeuchi, T.; Rosenbloom, J.; Prockop, D. J., Biosynthesis of abnormal collagens with amino acid analogues. II. Inability of cartilage cells to extrude collagen polypeptides containing L-azetidine-2-carboxylic acid or cis-4-fluoro-L-proline. *BBA - Protein Structure* **1969**, *175*, 156-164.

29. Lane, J. M.; Dehm, P.; Prockop, D. J., Effect of the proline analogue azetidine-2-carboxylic acid on collagen synthesis in vivo I. Arrest of collagen accumulation in growing chick embryos. *BBA - Protein Structure* **1971**, *236*, 517-527.

30. Lane, J. M.; Parkes, L. J.; Prockop, D. J., Effect of the proline analogue azetidine-2-carboxylic acid on collagen synthesis in vivo II. Morphological and physical properties of collagen containing the analogue. *BBA - Protein Structure* **1971**, *236*, 528-541.

31. (a) Uitto, J.; Prockop, D. J., Incorporation of proline analogues into collagen polypeptides. Effects on the production of extracellular procollagen and on the stability of the triple helical structure of the molecule. *BBA - Protein Structure* **1974**, *336*, 234-251; (b) Tan, E. M. L.; Ryhanen, L.; Uitto, J., Proline analogues

inhibit human skin fibroblast growth and collagen production in culture. *J. Invest. Dermatol.* **1983**, *80*, 261-267.

32. (a) Gryder, R. M.; Lamon, M.; Adams, E., Sequence position of 3-hydroxyproline in basement membrane collagen. Isolation of glycyl-3-hydroxyprolyl-4-hydroxyproline from swine kidney. *J. Biol. Chem.* **1975**, *250*, 2470-2474; (b) Jenkins, C. L.; Bretscher, L. E.; Guzei, I. A.; Raines, R. T., Effect of 3-hydroxyproline residues on collagen stability. *J. Am. Chem. Soc.* **2003**, *125*, 6422-6427.

33. Vranka, J. A.; Sakai, L. Y.; Bächinger, H. P., Prolyl 3-hydroxylase 1, enzyme characterization and identification of a novel family of enzymes. *J. Biol. Chem.* **2004**, *279*, 23615-23621.

34. Mori, H.; Shibasaki, T.; Yano, K.; Ozaki, A., Purification and cloning of a proline 3-hydroxylase, a novel enzyme which hydroxylates free L-proline to cis-3-hydroxy-L-proline. *J. Bacteriol.* **1997**, *179*, 5677-5683.

35. Lawrence, C. C.; Sobey, W. J.; Field, R. A.; Baldwin, J. E.; Schofield, C. J., Purification and initial characterization of proline 4-hydroxylase from Streptomyces griseoviridus P8648: A 2-oxoacid, ferrous-dependent dioxygenase involved in etamycin biosynthesis. *Biochem. J.* **1996**, *313*, 185-191.

36. Clifton, I. J.; Hsueh, L.-C.; Baldwin, J. E.; Harlos, K.; Schofield, C. J., Structure of proline 3-hydroxylase: Evolution of the family of 2-oxoglutarate dependent oxygenases. *Eur. J. Biochem.* **2001**, *268*, 6625-6636.

37. Shibasaki, T.; Sakurai, W.; Hasegawa, A.; Uosaki, Y.; Mori, H.; Yoshida, M.; Ozaki, A., Substrate selectivities of proline hydroxylases. *Tetrahedron Lett.* **1999**, *40*, 5227-5230.

38. Ruch, J. V.; Fabre, M.; Karcher Djuricic, V.; Staubli, A., The effects of L-azetidine-2-carboxylic acid (analogue of proline) on dental cytodifferentiations *in vitro*. *Differentiation* **1974**, *2*, 211-220.

39. Cho, M.-I.; Garant, P. R., Comparative radioautographic study of the effects of L-azetidine-2-carboxylic acid on matrix secretion and Golgi of the mouse incisor. *Calcified Tissue Int.* **1984**, *36*, 409-420.

40. Coulombre, A. J.; Coulombre, J. L., Corneal development. IV. Interruption of collagen excretion into the primary stroma of the cornea with L-azetidine-2-carboxylic acid. *Dev. Biol.* **1972**, *28*, 183-190.

41. Alvarez, O. M.; Mertz, P. M.; Eaglstein, W. H., The effect of the proline analogue L-azetidine-2-carboxylic acid (LACA) on epidermal and dermal wound repair. *Plast. Reconstr. Surg.* **1982**, *69*, 284-289.

42. Joneja, M. G., Teratogenic effects of proline analogue L-azetidine-2-carboxylic acid in hamster fetuses. *Teratology* **1981**, *23*, 365-372.

43. (a) Zagari, A.; Nemethy, G.; Scheraga, H. A., The effect of the L-azetidine-2-carboxylic acid residue on protein conformation. I. Conformations of the residue and of dipeptides. *Biopolymers* **1990**, *30*, 951-959; (b) Zagari, A.; Nemethy, G.; Scheraga, H. A., The effect of the L-azetidine-2-carboxylic acid residue on protein conformation. II. Homopolymers and copolymers. *Biopolymers* **1990**, *30*, 961-966; (c) Zagari, A.; Nemethy, G.; Scheraga, H. A., The effect of the L-azetidine-2-carboxylic acid residue on protein conformation. III. Collagen-like poly (tripeptide)s. *Biopolymers* **1990**, *30*, 967-974; (d) Zagari, A.; Palmer, K. A.; Gibson, K. D.; Nemethy, G.; Scheraga, H. A., The effect of the L-azetidine-2-carboxylic acid residue on protein conformation. IV. Local substitutions in the collagen triple helix. *Biopolymers* **1994**, *34*, 51-60.

44. Zimmerman, S. S.; Pottle, M. S.; Némethy, G.; Scheraga, H. A., Conformational analysis of the 20 naturally occurring amino acid residues using ECEPP. *Macromolecules* **1977**, *10*, 1-9.

45. Boni, R.; Verdini, A. S., Optical properties of poly(L-azetidinecarboxylic acid) in solution. *Macromolecules* **1973**, *6*, 517-520.

46. Boni, R.; Di Blasi, R.; Verdini, A. S., Conformational properties of poly(L-azetidine-2-carboxylic acid) in solution as studied by carbon-13 and proton nuclear magnetic resonance spectroscopy. *Macromolecules* **1975**, *8*, 140-145.

47. Boni, R.; Verdini, A. S., Synthesis of poly-(L-azetidine-2-carboxylic acid). *J. Chem. Soc., Perkin Trans. 1* **1974**, 2173-2177.

48. Tsai, F.-H.; Overberger, C. G.; Zand, R., Synthesis and peptide bond orientation in tetrapeptides containing L-azetidine-2-carboxylic acid and L-proline. *Biopolymers* **1990**, *30*, 1039-1049.

49. (a) Rubenstein, E., Misincorporation of the proline analog azetidine-2-carboxylic acid in the pathogenesis of multiple sclerosis: A hypothesis. *J. Neuropath. Exp. Neur.* **2008**, *67*, 1035-1040; (b) Sobel, R. A., Editorial: A novel unifying hypothesis of multiple sclerosis. *J. Neuropath. Exp. Neur.* **2008**, *67*, 1032-1034.

50. Chalmers, G. A., Swayback (enzootic ataxia) in Alberta lambs. *Can. J. Comp. Med.* **1974**, *38*, 111-117.

51. Bessonov, K.; Bamm, V. V.; Harauz, G., Misincorporation of the proline homologue Aze (azetidine-2-carboxylic acid) into recombinant myelin basic protein. *Phytochemistry* **2010**, *71*, 502-507.

52. Bessonov, K.; Vassall, K. A.; Harauz, G., Parameterization of the proline analogue Aze (azetidine-2-carboxylic acid) for molecular dynamics simulations and evaluation of its effect on homo-pentapeptide conformations. *J. Mol. Graphics Modell.* **2013**, *39*, 118-125.

53. Kobayashi, J.; Cheng, J.-F.; Ishibashi, M.; Wälchli, M. R.; Yamamura, S.; Onizumi, Y., Penaresidin A and B, two novel azetidine alkaloids with potent actomyosin ATPase-activating activity from the Okinawan marine sponge *Penares* sp. *J. Chem. Soc., Perkin Trans. 1* **1991**, 1135-1137.

54. (a) Takikawa, H.; Maeda, T.; Mori, K., Synthesis of penaresidin A, an azetidine alkaloid with actomyosin ATPase-activating property. *Tetrahedron Lett.* **1995**, *36*, 7689-7692; (b) Knapp, S.; Dong, Y., Stereoselective synthesis of penaresidin A and related azetidine alkaloids. *Tetrahedron Lett.* **1997**, *38*, 3813-3816.

55. Yoda, H.; Uemura, T.; Takabe, K., Novel and practical asymmetric synthesis of an azetidine alkaloid, penaresidin B. *Tetrahedron Lett.* **2003**, *44*, 977-979.

56. Kobayashi, J.; Tsuda, M.; Cheng, J.-F.; Ishibashi, M.; Takikawa, H.; Mori, K., Absolute stereochemistry of penaresidins A and B. *Tetrahedron Lett.* **1996**, *37*, 6775-6776.

57. Alvi, K. A.; Jaspars, M.; Crews, P.; Strulovicia, B.; Oto, E., Penazetidine A, an alkaloid inhibitor of protein kinase C. *Bioorg. Med. Chem. Lett.* **1994**, *4*, 2447-2450.

58. Tamaoki, T.; Nomoto, H.; Takahashi, I.; Kato, Y.; Morimoto, M.; Tomita, F., Staurosporine, a potent inhibitor of phospholipid Ca++dependent protein kinase. *Biochem. Biophys. Res. Commun.* **1986**, *135*, 397-402.

59. Yajima, A.; Takikawa, H.; Mori, K., Synthesis of sphingosine relatives, XVIII: Synthesis of penazetidine A, an alkaloid inhibitor of protein kinase C isolated from the marine sponge *Penares sollasi*. *Liebigs Ann.* **1996**, 1083-1089.

60. Isono, K.; Asahi, K.; Suzuki, S., Studies on polyoxins, antifungal antibiotics. XIII. The structure of polyoxins. *J. Am. Chem. Soc.* **1969**, *91*, 7490-7505.

61. Kitajima, M.; Kogure, N.; Yamaguchi, K.; Takayama, H.; Aimi, N., Structure reinvestigation of gelsemoxonine, a constituent of *Gelsemium elegans*, reveals a novel, azetidine-containing indole alkaloid. *Org. Lett.* **2003**, *5*, 2075-2078.

62. Kitajima, M.; Arai, Y.; Takayama, H.; Aimi, N., A chemical study on "Yakatsu" stored in Shosoin repository: Isolation and characterization of four indole alkaloids from a 1250 year-old sample of the Chinese toxic medicine. *P. Jpn. Acad. B-Phys.* **1998**, *74*, 159-163.

63. Di, Y.-T.; He, H.-P.; Wang, Y.-S.; Li, A.-B.; Lu, Y.; Gong, J.-B.; Fang, X.; Kong, N.-C.; Li, S.-N.; Zhu, H.-J.; Hao, X.-J., Isolation, X-ray crystallography, and computational studies of calydaphninone, a new alkaloid from *Daphniphyllum calycillum*. *Org. Lett.* **2007**, *9*, 1355-1358.

64. Takemoto, T.; Nomoto, K.; Fushiya, S.; Ouchi, R.; Kusano, G.; Hikino, H.; Takagi, S.; Matsuura, Y.; Kakudo, M., Structure of mugineic acid, a new amino acid possessing an iron-chelating activity from roots washings of water-cultured *Hordeum vulgare* L. *P. Jpn. Acad. B-Phys.* **1978**, *54*, 469-473.

65. Ma, J. F.; Nomoto, K., Effective regulation of iron acquisition in graminaceons plants. The role of mugineic acids as phytosiderophores. *Physiol. Plant.* **1996**, *97*, 609-617.

66. Curie, C.; Briat, J.-F., Iron Transport and Signaling in Plants. *Annu. Rev. Plant Biol.* **2003**, *54*, 183-206.

67. Briat, J.-F.; Fobis-Loisy, I.; Grignon, N.; Lobreaux, S.; Pascal, N.; Savino, G.; Thoiron, S.; Von Wiren, N.; Van Wuytswinkel, O., Cellular and molecular aspects of iron metabolism in plants. *Biol. Cell* **1995**, *84*, 69-81.

68. Tagliavini, M.; Rombolà, A. D., Iron deficiency and chlorosis in orchard and vineyard ecosystems. *Eur. J. Agron.* **2001**, *15*, 71-92.

69. (a) Shojima, S.; Nishizawa, N.-K.; Fushiya, S.; Nozoe, S.; Irifune, T.; Mori, S., Biosynthesis of phytosiderophores: *In vitro* biosynthesis of 2'-deoxymugineic acid from L-methionine and nicotianamine. *Plant Physiol.* **1990**, *93*, 1497-1503; (b) Negishi, T.; Nakanishi, H.; Yazaki, J.; Kishimoto, N.; Fujii, F.; Shimbo, K.; Yamamoto, K.; Sakata, K.; Sasaki, T.; Kikuchi, S.; Mori, S.; Nishizawa, N. K., cDNA microarray analysis of gene expression during Fe-deficiency stress in barley suggests that polar transport of vesicles is implicated in phytosiderophore secretion in Fe-deficient barley roots. *Plant J.* **2002**, *30*, 83-94.

70. (a) Noma, M.; Noguchi, M.; Tamaki, E., A new amino acid, nicotianamine, from tobacco leaves. *Tetrahedron Lett.* **1971**, *12*, 2017-2020; (b) Von Wirén, N.; Klair, S.; Bansal, S.; Briat, J.-F.; Khodr, H.; Shioiri, T.; Leigh, R. A.; Hider, R. C., Nicotianamine chelates both Fe(III) and Fe(II) implications for metal transport in plants. *Plant Physiol.* **1999**, *119*, 1107-1114.

71. (a) Fleming, A., On the antibacterial action of cultures of a penicillium, with special reference to their use in the isolation of *B. influenzae*. *Brit. J. Exp. Pathol.* **1929**, *10*, 226-236; (b) Abraham, E. P.; Chain, E.; Fletcher, C. M.; Gardner, A. D.; Heatley, N. G.; Jennings, M. A.; Florey, H. W., Further Observations on Penicillin. *Lancet* **1941**, *238*, 177-189.

72. Hodgkin, D. C., The X-ray analysis of the structure of penicillin. *Advancement of science* **1949**, *6*, 85-89.

73. Elander, R. P., Industrial production of β-lactam antibiotics. *Appl. Microbiol. Biotechnol.* **2003**, *61*, 385-392.

74. Morin, R. B.; Jackson, B. G.; Mueller, R. A.; Lavagnino, E. R.; Scanion, W. B.; Andrews, S. L., Chemistry of cephalosporin antibiotics. XV. Transformations of penicillin sulfoxide. A synthesis of cephalosporin compounds. *J. Am. Chem. Soc.* **1969**, *91*, 1401-1407.

75. Abraham, E.; Newton, G., Purification and some properties of cephalosporin N, a new penicillin. *Biochem. J.* **1954**, *58*, 94-102.

76. Birnbaum, J.; Kahan, F. M.; Kropp, H.; MacDonald, J. S., Carbapenems, a new class of beta-lactam antibiotics. Discovery and development of imipenem/cilastatin. *Am. J. Med.* **1985**, *78*, 3-21.

77. Imada, A.; Kitano, K.; Kintaka, K.; Muroi, M.; Asai, M., Sulfazecin and isosulfazecin, novel β-lactam antobiotics of bacterial origin. *Nature* **1981**, *289*, 590-591.

78. Sykes, R. B.; Bonner, D. P., Aztreonam: The first monobactam. *Am. J. Med.* **1985**, *78*, 2-10.

79. Hamed, R. B.; Gomez-Castellanos, J. R.; Henry, L.; Ducho, C.; McDonough, M. A.; Schofield, C. J., The enzymes of β-lactam biosynthesis. *Nat. Prod. Rep.* **2013**, *30*, 21-107.

80. Schmidt, F.-R., The β-Lactam Antibiotics: Current Situation and Future Prospects in Manufacture and Therapy. In *The Mycota X Industrial Applications*, 2nd Edition ed.; Hofrichter, M., Ed. Springer-Verlag Berlin Heidelberg: 2010; pp 101-121.

81. (a) Freire-Moran, L.; Aronsson, B.; Manz, C.; Gyssens, I. C.; So, A. D.; Monnet, D. L.; Cars, O., Critical shortage of new antibiotics in development against multidrug-resistant bacteria - Time to react is now. *Drug Resist. Update* **2011**, *14*, 118-124; (b) Walsh, C. T.; Wright, G., Introduction: Antibiotic resistance. *Chem. Rev.* **2005**, *105*, 391-393.

82. Waxman, D. J.; Strominger, J. L., Penicillin-binding proteins and the mechanism of action of β-lactam antibiotics. *Annu. Rev. Biochem.* **1983**, *Vol. 52*, 825-869.

83. Wilmouth, R. C.; Westwood, N. J.; Anderson, K.; Brownlee, W.; Claridge, T. D. W.; Clifton, I. J.; Pritchard, G. J.; Aplin, R. T.; Schofield, C. J., Inhibition of elastase by *N*-sulfonylaryl β-lactams: Anatomy of a stable acyl-enzyme complex. *Biochemistry* **1998**, *37*, 17506-17513.

84. (a) Page, M. I.; Laws, A. P., The mechanism of catalysis and the inhibition of β-lactamases. *Chem. Commun.* **1998**, 1609-1617; (b) Wang, Z.; Fast, W.; Valentine, A. M.; Benkovic, S. J., Metallo-β-lactamase: Structure and mechanism. *Curr. Opin. Chem. Biol.* **1999**, *3*, 614-622.

85. Buynak, J. D., Understanding the longevity of the β-lactam antibiotics and of antibiotic/β-lactamase inhibitor combinations. *Biochem. Pharmacol.* **2006**, *71*, 930-940.

86. White, A. R.; Kaye, C.; Poupard, J.; Pypstra, R.; Woodnutt, G.; Wynne, B., Augmentin® (amoxicillin/clavulanate) in the treatment of community-acquired respiratory tract infection: A review of the continuing development of an antimicrobial agent. *J. Antimicrob. Chemother.* **2004**, *53*, i3-i20.

87. Lode, H., Role of sultamicillin and ampicillin/sulbactam in the treatment of upper and lower bacterial respiratory tract infections. *Int. J. Antimicrob. Ag.* **2001**, *18*, 199-209.

88. Sanders Jr., W. E.; Sanders, C. C., Piperacillin/tazobactam: A critical review of the evolving clinical literature. *Clin. Invect. Dis.* **1996**, *22*, 107-123.

89. Condon, M. E.; Petrillo Jr., E. W.; Ryono, D. E.; Reid, J. A.; Neubeck, R.; Puar, M.; Heikes, J. E.; Sabo, E. F.; Losee, K. A.; Cushman, D. W.; Ondetti, M. A., Angiotensin-converting enzyme inhibitors: Importance of the amide carbonyl of mercaptoacyl amino acids for hydrogen bonding to the enzyme. *J. Med. Chem.* **1982**, *25*, 250-258.

90. Suto, M. J.; Stier, M. A.; Werbel, L. M.; Arundel-Suto, C. M.; Leopold, W. R.; Elliott, W. E.; Sebolt-Leopold, J. S., A new class of analogues of the bifunctional radiosensitizer α-(1-aziridinylmethyl)-2-nitro-1H-imidazole-1-ethanol (RSU 1069): The cycloalkylaziridines. *J. Med. Chem.* **1991**, *34*, 2484-2488.

91. Stratford, I. J., Mechanisms of hypoxic cell radiosensitization and the development of new sensitizers. *Int. J. Radiat. Oncol.* **1982**, *8*, 391-398.

92. (a) Brown, J. M., The mechanisms of cytotoxicity and chemosensitization by misonidazole and other nitroimidazoles. *Int. J. Radiat. Oncol.* **1982**, *8*, 675-682; (b) Rauth, A. M., Pharmacology and toxicology of sensitizers: Mechanism studies. *Int. J. Radiat. Oncol.* **1984**, *10*, 1293-1300.

93. Duan, J.-X.; Jiao, H.; Kaizerman, J.; Stanton, T.; Evans, J. W.; Lan, L.; Lorente, G.; Banica, M.; Jung, D.; Wang, J.; Ma, H.; Li, X.; Yang, Z.; Hoffman, R. M.; Ammons, W. S.; Hart, C. P.; Matteucci, M., Potent and highly selective hypoxia-activated achiral phosphoramidate mustards as anticancer drugs. *J. Med. Chem.* **2008**, *51*, 2412-2420.

94. Deaton, D. N.; Hassell, A. M.; McFadyen, R. B.; Miller, A. B.; Miller, L. R.; Shewchuk, L. M.; Tavares, F. X.; Willard Jr., D. H.; Wright, L. L., Novel and potent cyclic cyanamide-based cathepsin K inhibitors. *Bioorg. Med. Chem. Lett.* **2005**, *15*, 1815-1819.

95. Hagmann, W. K.; Durette, P. L.; Lanza, T.; Kevin, N. J.; De Laszlo, S. E.; Kopka, I. E.; Young, D.; Magriotis, P. A.; Li, B.; Lin, L. S.; Yang, G.; Kamenecka, T.; Chang, L. L.; Wilson, J.; MacCoss, M.; Mills, S. G.; Van Riper, G.; McCauley, E.; Egger, L. A.; Kidambi, U.; Lyons, K.; Vincent, S.; Stearns, R.; Colletti, A.; Teffera, J.; Tong, S.; Fenyk-Melody, J.; Owens, K.; Levorse, D.; Kim, P.; Schmidt, J. A.;

Mumford, R. A., The discovery of sulfonylated dipeptides as Potent VLA-4 antagonists. *Bioorg. Med. Chem. Lett.* **2001**, *11*, 2709-2713.

96. Kamenecka, T. M.; Park, Y.-J.; Lin, L. S.; De Laszlo, S.; McCauley, E. D.; Van Riper, G.; Egger, L.; Kidambi, U.; Mumford, R. A.; Tong, S.; Tang, W.; Colletti, A.; Teffera, Y.; Stearns, R.; MacCoss, M.; Schmidt, J. A.; Hagmann, W. K., Amidines as amide bond replacements in VLA-4 antagonists. *Bioorg. Med. Chem. Lett.* **2004**, *14*, 2323-2326.

97. Fiessinger, J.-N.; Huisman, M. V.; Davidson, B. L.; Bounameaux, H.; Francis, C. W.; Eriksson, H.; Lundström, T.; Berkowitz, S. D.; Nyström, P.; Thorsén, M.; Ginsberg, J. S., Ximelagatran vs low-molecular-weight heparin and warfarin for the treatment of deep vein thrombosis: A randomized trial. *J. Am. Med. Assoc.* **2005**, *293*, 681-689.

98. Kallabis, H.; Thielemann, W.; Perzborn, E.; Rohrig, S.; Kubitza, D.; Spiro, T.; Haskell, L.; Mahal, J. Oxazolidinones For the Treatment and/or Prophylaxis of Heart Failure. US20110003804, 2011.

99. Pehrsson, S.; Johansson, K.; Kjaer, M.; Elg, M., Evaluation of AR-H067637, the active metabolite of the new direct thrombin inhibitor AZD0837, in models of venous and arterial thrombosis and bleeding in anaesthetised rats. *Tromb. Haemostasis* **2010**, *104*, 1242-1249.

100. Johansson, S.; Cullberg, M.; Eriksson, U. G.; Elg, M.; Dunér, K.; Jensen, E.; Wollbratt, M.; Wåhlander, K., Single-dose pharmacokinetics, pharmacodynamics and safety of AZD0837, a novel oral direct thrombin inhibitor, in young healthy male subjects. *Int. J. Clin. Pharm. Th.* **2011**, *49*, 258-267.

101. Zhang, X.; Hufnagel, H.; Markotan, T.; Lanter, J.; Cai, C.; Hou, C.; Singer, M.; Opas, E.; McKenney, S.; Crysler, C.; Johnson, D.; Sui, Z., Overcoming hERG activity in the discovery of a series of 4-azetidinyl-1-aryl-cyclohexanes as CCR2 antagonists. *Bioorg. Med. Chem. Lett.* **2011**, *21*, 5577-5582.

102. Lu, K.; Jiang, Y.; Chen, B.; Eldemenky, E. M.; Ma, G.; Packiarajan, M.; Chandrasena, G.; White, A. D.; Jones, K. A.; Li, B.; Hong, S.-P., Strategies to lower the Pgp efflux liability in a series of potent indole azetidine MCHR1 antagonists. *Bioorg. Med. Chem. Lett.* **2011**, *21*, 5310-5314.

103. Sun, Y.; Gou, S.; Yin, R.; Jiang, P., Synthesis, antiproliferative activity and DNA binding study of mixed ammine/cyclohexylamine platinum(II) complexes with 1-(substituted benzyl) azetidine-3,3-dicarboxylates. *Eur. J. Med. Chem.* **2011**, *46*, 5146-5153.

104. Pérez-Faginas, P.; Aranda, M. T.; García-López, M. T.; Snoeck, R.; Andrei, G.; Balzarini, J.; González-Muñiz, R., Synthesis and SAR studies on azetidine-containing dipeptides as HCMV inhibitors. *Bioorg. Med. Chem.* **2011**, *19*, 1155-1161.

105. Melancon, B. J.; Utley, T. J.; Sevel, C.; Mattmann, M. E.; Cheung, Y.-Y.; Bridges, T. M.; Morrison, R. D.; Sheffler, D. J.; Niswender, C. M.; Scott Daniels, J.; Jeffrey Conn, P.; Lindsley, C. W.; Wood, M. R., Development of novel M1 antagonist scaffolds through the continued optimization of the MLPCN probe ML012. *Bioorg. Med. Chem. Lett.* **2012**, *22*, 5035-5040.

106. (a) Nakamura, T.; Asano, M.; Sekiguchi, Y.; Mizuno, Y.; Tamaki, K.; Nara, F.; Kawase, Y.; Yabe, Y.; Nakai, D.; Kamiyama, E.; Urasaki-Kaneno, Y.; Shimozato, T.; Doi-Komuro, H.; Kagari, T.; Tomisato, W.; Inoue, R.; Nagasaki, M.; Yuita, H.; Oguchi-Oshima, K.; Kaneko, R.; Nishi, T., Synthesis and evaluation of CS-2100, a potent, orally active and S1P3-sparing S1P1 agonist. *Eur. J. Med. Chem.* **2012**, *51*, 92-98; (b) Nakamura, T.; Asano, M.; Sekiguchi, Y.; Mizuno, Y.; Tamaki, K.; Kimura, T.; Nara, F.; Kawase, Y.; Shimozato, T.; Doi, H.; Kagari, T.; Tomisato, W.; Inoue, R.; Nagasaki, M.; Yuita, H.; Oguchi-Oshima, K.; Kaneko, R.; Watanabe, N.; Abe, Y.; Nishi, T., Discovery of CS-2100, a potent, orally active and S1P3-sparing S1P1 agonist. *Bioorg. Med. Chem. Lett.* **2012**, *22*, 1788-1792.

107. Brandi, A.; Cicchi, S.; Cordero, F. M., Novel syntheses of azetidines and azetidinones. *Chem. Rev.* **2008**, *108*, 3988-4035.

108. Rousseau, G.; Robin, S., Four-Membered Heterocycles: Structure and Reactivity. In *Modern Heterocyclic Chemistry*, First ed.; Alvarez-Builla, J.; Vaquero, J. J.; Barluenga, J., Eds. Wiley-VHC Verlag GmbH & Co. KGaA: 2011; pp 163-268.

109. Miller, R. A.; Lang, F.; Marcune, B.; Zewge, D.; Song, Z. J.; Karady, S., A practical process for the preparation of azetidine-3-carboxylic acid. *Synth. Commun.* **2003**, *33*, 3347-3353.

110. (a) Lenagh-Snow, G. M. J.; Araujo, N.; Jenkinson, S. F.; Rutherford, C.; Nakagawa, S.; Kato, A.; Yu, C.-Y.; Weymouth-Wilson, A. C.; Fleet, G. W. J., Inhibition of nonmammalian glycosidases by azetidine iminosugars derived from stable 3,5-Di-O-triflates of pentoses. *Org. Lett.* **2011**, *13*, 5834-5837; (b) Lenagh-Snow, G. M. J.; Araujo, N.; Jenkinson, S. F.; Martinez, R. F.; Shimada, Y.; Yu, C.-Y.; Kato, A.; Fleet, G. W. J., Azetidine Iminosugars from the Cyclization of 3,5-Di-O-triflates of alpha-Furanosides and of 2,4-Di-O-triflates of beta-Pyranosides Derived from Glucose. *Org. Lett.* **2012**, *14*, 2142-2145.

111. Couty, F.; Evano, G.; Vargas-Sanchez, M.; Bouzas, G., Practical asymmetric preparation of azetidine-2-carboxylic acid. *J. Org. Chem.* **2005**, *70*, 9028-9031.

112. Akiyama, T.; Daidouji, K.; Fuchibe, K., Cu(I)-catalyzed enantioselective [2 + 2] cycloaddition of 1-methoxyallenylsilane with α-imino ester: Chiral synthesis of α,β-unsaturated acylsilanes. *Org. Lett.* **2003**, *5*, 3691-3693.

113. Berger, A.; Kurtz, J.; Katchalski, E., Poly-L-proline. *J. Am. Chem. Soc.* **1954**, *76*, 5552-5554.

114. (a) Baeza, J. L.; Gerona-Navarro, G.; Pérez de Vega, M. J.; García-López, M. T.; González-Muñiz, R.; Martín-Martínez, M., 2-Alkyl-2-carboxy-azetidines as scaffolds for the induction of γ-turns. *Tetrahedron Lett.* **2007**, *48*, 3689-3693; (b) Baeza, J. L.; Gerona-Navarro, G.; De Vega, M. J. P.; García-Lopez, M. T.; González-Muñiz, R.; Martín-Martínez, M., Azetidine-derived amino acids versus proline derivatives. Alternative trends in reverse turn induction. *J. Org. Chem.* **2008**, *73*, 1704-1715.

115. Némethy, G.; Printz, M. P., The γ turn, a possible folded conformation of the polypeptide chain. Comparison with the β turn. *Macromolecules* **1972**, *5*, 755-758.

116. Baeza, J. L.; Gerona-Navarro, G.; Thompson, K.; De Vega, M. J. P.; Infantes, L.; García-López, M. T.; González-Muñiz, R.; Martín-Martínez, M., Further evidence for 2-alkyl-2-carboxyazetidines as γ-turn inducers. *J. Org. Chem.* **2009**, *74*, 8203-8211.

117. Claridge, T. D. W.; Lopez-Ortega, B.; Jenkinson, S. F.; Fleet, G. W. J., Secondary structural investigations into homo-oligomers of δ-2,4-cis oxetane amino acids. *Tetrahedron: Asymmetry* **2008**, *19*, 984-988.

118. (a) Matsuura, F.; Hamada, Y.; Shioiri, T., Efficient synthesis of phytosiderophores, 3-epi-hydroxymugineic acid and distichonic acid A. *Tetrahedron Lett.* **1992**, *33*, 7921-7924; (b) Matsuura, F.; Hamada, Y.; Shioiri, T., Total syntheses of phytosiderophores, 3-epi-hydroxymugineic acid, distichonic acid A, and 2'-hydroxynicotianamine. *Tetrahedron* **1994**, *50*, 265-274.

119. Dureault, A.; Portal, M.; Carreaux, F.; Depezay, J. C., Synthesis of highly functionalized homochiral azetidines and azetidine-2-carboxylic esters. *Tetrahedron* **1993**, *49*, 4201-4210.

120. Wessig, P.; Schwarz, J., Enantioselective Preparation of (2R)- and (2S)-Azetidine-2-carboxylic Acids. *Helv. Chim. Acta* **1998**, *81*, 1803-1814.

121. Fernández-Megía, E.; Montaos, M. A.; Sardina, F. J., A short, efficient, and stereoselective procedure for the synthesis of cis-3-hydroxymethyl-aziridine-2-carboxylic acid derivatives, important intermediates in the synthesis of mitomycinoids. *J Org Chem* **2000**, *65*, 6780-6783.

122. Chang, D.; Feiten, H.-J.; Engesser, K.-H.; Van Beilen, J. B.; Witholt, B.; Li, Z., Practical Syntheses of N-Substituted 3-Hydroxyazetidines and 4-Hydroxypiperidines by Hydroxylation with Sphingomonas sp. HXN-200. *Org. Lett.* **2002**, *4*, 1859-1862.

123. (a) Kovac, P.; Alföldi, J., Alternative syntheses of methylated sugars. XVIII.* Synthesis of methyl 2,4-di-O-acetyl-β-D-xylopyranoside. *Chemicke Zvesti* **1979**, *33*, 785-791; (b) Mandal, S.; Sharma, N.; Mukhopadhyay, B., Synthesis of a tetrasaccharide related to the triterpenoid saponin Bellisoside isolated from *Bellis perennis* (compositae). *Tetrahedron: Asymmetry* **2010**, *21*, 2172-2176.

124. Koenigs, W.; Knorr, E., Ueber einige Derivate des Traubenzuckers und der Galactose. *Chem. Ber.* **1901**, *34*, 957-981.

125. Montero, J.-L.; Winum, J.-Y.; Leydet, A.; Kamal, M.; Pavia, A. A.; Roque, J.-P., A convenient synthesis of peracetylated glycosyl halides using bismuth(III) halides as catalysts. *Carbohydr. Res.* **1997**, *297*, 175-180.

126. Jain, R.; Kamau, M.; Wang, C.; Ippolito, R.; Wang, H.; Dulina, R.; Anderson, J.; Gange, D.; Sofia, M. J., 3-Azido-3-deoxy-glycopyranoside derivatives as scaffolds for the synthesis of carbohydrate-based universal pharmacophore mapping libraries. *Bioorg. Med. Chem. Lett.* **2003**, *13*, 2185-2189.

127. Mori, N.; Togo, H., Facile oxidative conversion of alcohols to esters using molecular iodine. *Tetrahedron* **2005**, *61*, 5915-5925.

128. Paquette, L. A.; Oplinger, J. A., Synthesis of a Structurally Modified Glycal. (-)-(2*R*,4*S*)-2-Methyl-2-vinyl-4-(benzyloxy)-3,4-dihydro-2*H*-pyran. *J. Org. Chem.* **1988**, *53*, 2953-2959.

129. Tojo, G., Dess-Martin Periodinane In *Oxidation of Alcohols to Aldehydes and Ketones: a Guide to Current Common Practice*, Fernandez, M., Ed. Springer: 2006; pp 182-189.

130. Yamada, S.; Morizono, D.; Yamamoto, K., Mild Oxidation of Aldehydes to the Corresponding Carboxylic-Acids and Esters - Alkaline Iodine Oxidation Revisisted. *Tetrahedron Lett.* **1992**, *33*, 4329-4332.

131. Patiño-Molina, R.; Cubero-Lajo, I.; Pérez de Vega, M. J.; García-López, M. T.; González-Muñiz, R., Chiral 1,3,6-trisubstituted 2,4-dioxohexahydropyrimidines: a convenient stereoselective synthesis from aspartic acid derivatives. *Tetrahedron Lett.* **2007**, *48*, 3613-3616.

132. Veitch, G. E.; Bridgwood, K. L.; Ley, S. V., Magnesium nitride as a convenient source of ammonia: Preparation of primary amides. *Org. Lett.* **2008**, *10*, 3623-3625.

133. Bundesmann, M. W.; Coffey, S. B.; Wright, S. W., Amidation of esters assisted by Mg(OCH3)(2) or CaCl2. *Tetrahedron Lett.* **2010**, *51*, 3879-3882.

134. Allred, E. L.; Hurwitz, M. D., Amidation of esters with amides in the presence of methoxide ion. *J. Org. Chem.* **1965**, *30*, 2376-2381.

135. Valero, G.; Schimer, J.; Cisarova, I.; Vesely, J.; Moyano, A.; Rios, R., Highly enantioselective organocatalytic synthesis of piperidines. Formal synthesis of (-)-Paroxetine. *Tetrahedron Lett.* **2009**, *50*, 1943-1946.

136. Thomas, E. W.; Rynbrandt, R. H.; Zimmermann, D. C.; Bell, L. T.; Muchmore, C. R.; Yankee, E. W., Reaction of novel imide reducing reagents with pyrrolizidinediones. *J. Org. Chem.* **1989**, *54*, 4535-4543.

137. Krämer, B.; Franz, T.; Picasso, S.; Pruschek, P.; Jäger, V., Glycono-1,3-lactams, Xylo Series: Stereoselective Access by [2+2] Cycloaddition, Exploratory Transformations, and Discovery of a New, Highly Selective Inhibitor of Glucoamylases. *Synlett* **1997**, *1997*, 295-297.

138. De Mayo, P.; Takeshita, H.; Sattar, A. B. M. A., The photochemical synthesis of 1,5-diketones and their cyclisation: A new annulation process. *Proc. Chem. Soc.* **1962**, 119.

139. Benchikh Le-Hocine, M.; Do Khac, D.; Fetizon, M., Model studies in taxane diterpene synthesis. Part III. *Synth. Commun.* **1992**, *22*, 245-255.

140. Winkler, J. D.; Rouse, M. B.; Greaney, M. F.; Harrison, S. J.; Jeon, Y. T., The first total synthesis of (±)-ingenol. *J. Am. Chem. Soc.* **2002**, *124*, 9726-9728.

141. Jenkinson, S. F.; Harris, T.; Fleet, G. W. J., Oxetane cis- and trans β-amino-acid scaffolds from D-xylose by efficient SN2 reactions in oxetane rings: Methyl and hydroxymethyl analogues of the antibiotic oxetin, an oxetane β-amino-acid. *Tetrahedron: Asymmetry* **2004**, *15*, 2667-2679.

142. Moyer, M. P.; Feldman, P. L.; Rapoport, H., Intramolecular N-H, O-H, and S-H insertion reactions. Synthesis of heterocycles from α-diazo β-keto esters. *J. Org. Chem.* **1985**, *50*, 5223-5230.

143. Mangelinckx, S.; Boeykens, M.; Vliegen, M.; Van Der Eycken, J.; De Kimpe, N., Synthesis of new 3,3-dimethoxyazetidine-2-carboxylic acid derivatives. *Tetrahedron Lett.* **2005**, *46*, 525-529.

144. Smith, G. V.; Notheisz, F., *Heterogenous Catalysis in Organic Chemistry*. 1999; Vol. Academic Press, p 160-171.

145. Czech, B. P.; Bartsch, R. A., Effect of amines on O-benzyl group hydrogenolysis. *J. Org. Chem.* **1984**, *49*, 4076-4078.

146. Paulvannan, K.; Stille, J. R., Heterocycle formation through aza-annulation: Stereochemically controlled syntheses of (±)-5-epitashiromine and (±)-tashiromine. *J. Org. Chem.* **1994**, *59*, 1613-1620.

147. Cook, G. R.; Beholz, L. G.; Stille, J. R., Construction of hydroxylated alkaloids (±)-mannonolactam, (±)-deoxymannojirimycin, and (±)-prosopinine through aza-annulation. *J. Org. Chem.* **1994**, *59*, 3575-3584.

148. Karplus, M., Vicinal proton coupling in nuclear magnetic resonance [22]. *J. Am. Chem. Soc.* **1963**, *85*, 2870-2871.

149. Coxon, B., Developments in the Karplus Equation as they Relate to the NMR Coupling Constants of Carbohydrates. In *Advances in Carbohydrate Chemistry and Biochemistry*, First Edition ed.; Horton, D., Ed. Elsevier Academic Press: 2009; Vol. 62, pp 17-82.

150. Krivdin, L., Non-empirical calculations of NMR indirect carbon-carbon coupling constants. Part 4: Bicycloalkanes. *Magn. Reson. Chem.* **2003**, *41*, 417-430.

151. Barfield, M.; Della, E.; Pigou, P., Nuclear Spin-Spin Coupling via Nonbonded Interactions. 6. The Importance of Bridgehead Interactions on 1H-1H, 1H-13C, and 13C-13C Coupling Constants in Bicycloalkanes. *J. Am. Chem. Soc.* **1984**, *106*, 5051-5054.

152. Dr. R. F. Martínez, Unpublished results; Chemistry Research Laboratory, 12 Mansfield Road, Oxford, OX1 3TA.

153. Lenagh-Snow, G. M. J. D. Phil. Thesis: The Synthesis of Azetidine and Piperidine Iminosugars form Monosaccharides. University of Oxford, 2012.

154. Lee, J. C.; Francis, S.; Dutta, D.; Gupta, V.; Yang, Y.; Zhu, J.-Y.; Tash, J. S.; Schönbrunn, E.; Georg, G. I., Synthesis and evaluation of eight- and four-membered iminosugar analogues as inhibitors of testicular ceramide-specific glucosyltransferase, testicular β-glucosidase 2, and other glycosidases. *J. Org. Chem.* **2012**, *77*, 3082-3098.

155. (a) Fu, X.; Cook, J. M., Enantiospecific total synthesis of the ajmaline related alkaloids (-)-suaveoline, (-)-raumacline, and (-)-*N*(b)-methylraumacline. *J. Am. Chem. Soc.* **1992**, *114*, 6910-6912; (b) Fu, X.; Cook, J. M., General approach for the synthesis of ajmaline-related alkaloids. Enantiospecific total synthesis of (-)-suaveoline, (-)-raumacline, and (-)-*N*b-methylraumacline. *J. Org. Chem.* **1993**, *58*, 661-672.

156. Marcus, Y.; Glikberg, S., Recommended Methods for the Purification of Solvents and Tests for Impurities. Methanol and Ethanol. *Pure Appl. Chem.* **1985**, *57*, 855-864.

157. Brauner-Osborne, H.; Bunch, L.; Chopin, N.; Couty, F.; Evano, G.; Jensen, A.; Kusk, M.; Nielsen, B.; Rabasso, N., Azetidinic amino acids: stereocontrolled synthesis and pharmacological characterization as ligands for glutamate receptors and transporters. *Org. Biomol. Chem.* **2005**, *3*, 3926-3936.

158. Nudelman, A.; Bechor, Y.; Falb, E.; Fischer, B.; Wexler, B. A.; Nudelman, A., Acetyl chloride-methanol as a convenient reagent for: A) quantitative formation of amine hydrochlorides; B) carboxylate ester formation; C) mild removal of *N*-t-Boc-protective group. *Synth. Commun.* **1998**, *28*, 471-474.

159. Olcay, H.; Xu, L.; Xu, Y.; Huber, G. W., Aqueous-Phase Hydrogenation of Acetic Acid over Transition Metal Catalysts. *Chemcatchem* **2010**, *2*, 1420-1424.

160. Sydnes, M. O.; Kuse, M.; Isobe, M., Reductive monoalkylation of nitro aryls in one-pot. *Tetrahedron* **2008**, *64*, 6406-6414.

161. Sparrow, C., Personal Communication. Mass spectrometry Department, Oxford University, 2012.

162. Glawar, A. F. G.; Jenkinson, S. F.; Thompson, A. L.; Nakagawa, S.; Kato, A.; Butters, T. D.; Fleet, G. W. J., 3-Hydroxyazetidine Carboxylic Acids: Non-Proteinogenic Amino Acids for Medicinal Chemists. *ChemMedChem* **2013**, *8*, 658-666.

163. (a) Frigerio, M.; Santagostino, M.; Sputore, S., A user-friendly entry to 2-iodoxybenzoic acid (IBX). *J. Org. Chem.* **1999**, *64*, 4537-4538; (b) Ireland, R. E.; Liu, L., An improved procedure for the preparation of the Dess-Martin periodinane. *J. Org. Chem.* **1993**, *58*, 2899.

164. (a) Elhalabi, J.; Rice, K., Synthesis of Uridine 5'-[2-S-Pyridyl-3-thio-α-D-galactopyranosyl Diphosphate]: Precursors of UDP-Thiogal Sugar Nucleotide Donor Substrate for β-1,4-Galactosyltransferase. *Nucleosides* **2004**; (b) Raju, R.; Castillo, B. F.; Richardson, S. K.; Thakur, M.; Severins, R.; Kronenberg, M.; Howell, A. R., Synthesis and evaluation of 3"- and 4"-deoxy and -fluoro analogs of the immunostimulatory glycolipid, KRN7000. *Bioorg. Med. Chem. Lett.* **2009**, *19*, 4122-5.

165. Slessor, K.; Tracey, A., 1,2: 5,6-Di-O-isopropylidene-D-hexofuranoses and their 3-keto derivatives. *Can. J. Chem.* **1969**.

166. Gavard, O.; Hersant, Y.; Alais, J.; Duverger, V.; Dilhas, A.; Bascou, A.; Bonnaffé, D., Efficient preparation of three building blocks for the synthesis of heparan sulfate fragments: Towards the combinatorial synthesis of oligosaccharides from hypervariable regions. *Eur. J. Org. Chem.* **2003**, 3603-3620.

167. Reckendorf, W.; Schultz, N.; Kreimeier, R., Synthese, Strukturaufklärung und Reaktionen trans-verknüpfter 3,6-Anhydro-1,2-O-isopropyliden-α-D-hexofuranosen. *Liebigs Ann. Chem.* **1994**, 337-346.

168. Swamy, N. R.; Venkateswarlu, Y., A mild and efficient method for chemoselective deprotection of acetonides by bismuth(III) trichloride. *Tetrahedron Lett.* **2002**, *43*, 7549-7552.

169. Dr. S. Jenkinson and Dr. N. Araújo performed the attempts on the *trans*-azetidine ring closure. Chemistry Research Laboratory, 12 Mansfield Road, Oxford, OX1 3TA.

170. Prof. A. Kato, Department of Hospital Pharmacy, University of Toyama, 2630 Sugitani, Toyama 930-0194, Japan.

171. (a) Araújo, N.; Jenkinson, S. F.; Martínez, R. F.; Glawar, A. F. G.; Wormald, M. R.; Butters, T. D.; Nakagawa, S.; Adachi, I.; Kato, A.; Yoshihara, A.; Akimitsu, K.; Izumori, K.; Fleet, G. W. J., Synthesis from D-altrose of (5R,6R,7R,8S)-5,7-dihydroxy-8-hydroxymethylconidine and 2,4-dideoxy-2,4-imino-D-glucitol, azetidine analogues of swainsonine and 1,4-dideoxy-1,4-imino-D-mannitol. *Org. Lett.* **2012**, *14*, 4174-4177; (b) Sanap, S. P.; Ghosh, S.; Jabgunde, A. M.; Pinjari, R. V.; Gejji, S. P.; Singh, S.; Chopade, B. A.; Dhavale, D. D., Synthesis, computational study and glycosidase inhibitory activity of polyhydroxylated conidine alkaloids - A bicyclic iminosugar. *Org. Biomol. Chem.* **2010**, *8*, 3307-3315.

172. Yu, C.-Y.; Asano, N.; Ikeda, K.; Wang, M.-X.; Butters, T. D.; Wormald, M. R.; Dwek, R. A.; Winters, A. L.; Nash, R. J.; Fleet, G. W. J., Looking glass inhibitors: L-DMDP, a more potent and specific inhibitor of α-glucosidases than the enantiomeric natural product DMDP. *Chem. Commun.* **2004**, *10*, 1936-1937.

173. (a) Patel, A. G.; Kaufmann, S. H., Targeting bacteria to improve cancer therapy. *Science* **2010**, *330*, 766-767; (b) Wallace, B. D.; Wang, H.; Lane, K. T.; Scott, J. E.; Orans, J.; Koo, J. S.; Venkatesh, M.; Jobin, C.; Yeh, L.-A.; Mani, S.; Redinbo, M. R., Alleviating cancer drug toxicity by inhibiting a bacterial enzyme. *Science* **2010**, *330*, 831-835; (c) Rasmussen, T. S.; Koldsø, H.; Nakagawa, S.; Kato, A.; Schiøtt, B.; Jensen, H. H., Synthesis of uronic-Noeurostegine - A potent bacterial β-glucuronidase inhibitor. *Org. Biomol. Chem.* **2011**, *9*, 7807-7813.

174. Paquette, L. A.; Barriault, L.; Pissarnitski, D.; Johnston, J. N., Stereocontrolled elaboration of natural (-)-polycavernoside A, a powerfully toxic metabolite of the red alga *Polycavernosa tsudai*. *J. Am. Chem. Soc.* **2000**, *122*, 619-631.

175. Finan, P. A.; Warren, C. D., 596. 2,4,6-tri-O-acetyl-3-O-benzyl-α-D-glucopyranosyl bromide: A new intermediate for the Koenigs-Knorr synthesis of glycosides. *J. Chem. Soc.* **1962**, 3089-3092.

176. Legler, G.; Pohl, S., Synthesis of 5-amino-5-deoxy-d-galactopyranose and 1,5-dideoxy-1,5-imino-D-galactitol, and their inhibition of α- and β-D-galactosidases. *Carbohydr. Res.* **1986**, *155*, 119-129.

177. Meyer zu Reckendorf, W., Synthesis of D-gulose from D-glucose. *Angew. Chem. Int. Ed.* **1967**, *6*, 177.

178. Yadav, J.; Prathap, I.; Tadi, B., Formal synthesis of fostriecin by a carbohydrate-based approach. *Tetrahedron Lett.* **2006**.

179. Kishimoto, H.; Ohrui, H.; Meguro, H., An enantioselective synthesis of bengamide E. *J. Org. Chem.* **1992**, *57*, 5042-5044.

180. Naming according to IUPAC nomenclature for carbohydrates 1996, but for consitency of NMR data the original sugar denominator is retained.

181. Frisch, M. J.; Trucks, G. W.; Schlegel, H. B.; Scuseria, G. E.; Robb, M. A.; Cheeseman, J. R.; Scalmani, G.; Barone, V.; Mennucci, B.; Petersson, G. A.; Nakatsuji, H.; Caricato, M.; Li, X.; Hratchian, H. P.; Izmaylov, A. F.; Bloino, J.; Zheng, G.; Sonnenberg, J. L.; Hada, M.; Ehara, M.; Toyota, K.; Fukuda, R.; Hasegawa, J.; Ishida, M.; Nakajima, T.; Honda, Y.; Kitao, O.; Nakai, H.; Vreven, T.; Montgomery, J., J. A.; Peralta, J. E.; Ogliaro, F.; Bearpark, M.; Heyd, J. J.; Brothers, E.; Kudin, K. N.; Staroverov, V. N.; Kobayashi, R.; Normand, J.; Raghavachari, K.; Rendell, A.; Burant, J. C.; Iyengar, S. S.; Tomasi, J.; Cossi, M.; Rega, N.; Millam, N. J.; Klene, M.; Knox, J. E.; Cross, J. B.; Bakken, V.; Adamo, C.; Jaramillo, J.; Gomperts, R.; Stratmann, R. E.; Yazyev, O.; Austin, A. J.; Cammi, R.; Pomelli, C.; Ochterski, J. W.; Martin, R. L.; Morokuma, K.; Zakrzewski, V. G.; Voth, G. A.; Salvador, P.; Dannenberg, J. J.; Dapprich, S.; Daniels, A. D.; Farkas, Ö.; Foresman, J. B.; Ortiz, J. V.; Cioslowski, J.; Fox, D. J. *Gaussian 09, Revision C.01*, Gaussian, Inc.: Wallingford CT, 2010.

182. Nowell, H.; Barnett, S. A.; Christensen, K. E.; Teat, S. J.; Allan, D. R., I19, the small-molecule single-crystal diffraction beamline at Diamond Light Source. *J. Synchrotron Radiat.* **2012**, *19*, 435-441.

183. Cosier, J.; Glazer, A., A nitrogen-gas-stream cryostat for general X-ray diffraction studies. *J. Appl. Cryst.* **1986**, *19*, 105-107.

184. Palatinus, L.; Chapuis, G., SUPERFLIP - A computer program for the solution of crystal structures by charge flipping in arbitrary dimensions. *J. Appl. Cryst.* **2007**, *40*, 786-790.

185. (a) Betteridge, P.; Carruthers, J.; Cooper, R.; Prout, K.; Watkin, D., CRYSTALS version 12: software for guided crystal structure analysis. *J. Appl. Cryst.* **2003**, *36*, 1487; (b) Cooper, R.; Thompson, A.; Watkin, D., CRYSTALS enhancements: dealing with hydrogen atoms in refinement. *J. Appl. Cryst.* **2010**, *43*, 1100-1107.

# 4 BIOLOGICAL EVALUATION OF IMINOSUGARS IN AN ANTI-CANCER SETTING

## 4.1 Introduction to glycosidase inhibition in an anti-cancer setting

### 4.1.1 Overview

Having explored and developed inhibitors for β-*N*-acetyl-hexosamindase in the preceding chapters, the modification of the highly potent α-*N*-acetyl-galactosaminidase inhibitor 2-acetamido-1,2-dideoxy-D-*galacto*-nojirimycin (DGJNAc) will be subject of this section. Furthermore, with inhibitors for both cancer targets established, the attention will shift to developing robust and meaningful *in vitro* assays to explore if these inhibitors and glycosidase targets are indeed useful to anti-cancer therapy development.

### 4.1.2 α-*N*-acetyl-galactosaminidase and the macrophage activation factor

Having been implicated in immunosuppression in advanced cancer patients α-*N*-acetyl-galactosaminidase and its relation to vitamin $D_3$ binding protein (DBP) will be explored first.

#### 4.1.2.1 Vitamin $D_3$-binding protein

In 1959 Hirschfeld at al. discovered an inheritance maker he called group-specific component (GC protein), a globular protein present in the blood plasma of all humans, also known as GC globulin.[1] It was discovered shortly after, that GC protein is the carrier of Vitamin D and its metabolites in the plasma and hence was renamed vitamin D-binding protein (DBP).[2] Although more then 120 mutants of the *GC* gene have been described there are three main alleles found in 99% of all individuals, which are GC*1F, GC*1S and GC*2.[3] These alleles can give rise to six GC phenotypes with GC 1f-1f, GC 1s-1s, GC 2-2, GC 1f-1s, GC 1f-2, GC 1s-2 and were differentiated by their electrophoretic pattern following isoelectric focussing.[4] In their homozygous form GC 2-2 gives rise to a single band [p*I* of 5.1], while both GC 1-1 phenotypes

give rise to a double band closer to the anode. The double band [GC1a, anodal, p*I* of 4.84; GC1c, cathodal, p*I* of 4.94] of GC 1f-1f (f for fast) is closer to the anode then GC 1s-1s [s for slow; GC1a, anodal, p*I* of 4.85; GC1c, cathodal, p*I* of 4.95] and the two observed spots are believed to differ in glycosylation, more precisely in sialic acid content.[3, 5] As an aside, it should be noted that although there is no difference in vitamin D binding potential between the different phenotypes, a recent study has shown that the *GC2* allel is associated with a reduced risk of postmenopausal breast cancer.[6] The plasma concentration of DBP has been found to be 300-600 μg/mL and it is produced at a mean rate of 10.1 mg/kg per day in healthy humans.[7]

In 1986 the complete GC2 protein was sequenced (UniProtKB database entry P02774) and established as a 458 amino acid protein with extensive homology to human serum albumin and human-α-fetoprotein.[8] The sequences of the other two main alleles were determined using DNA sequence analysis.[9] In comparison to GC2 both the GC1 phenotypes have a threonine instead of lysine residue at amino acid position 420 and GC1s has an additional substitution of glutamic acid instead of aspartic acid at position 416. The human gene structure for DBP was fully elucidated in 1993 and it is located on the long arm of chromosome 4.[10] A X-ray crystal structure of DBP in complex with the vitamin D metabolite 25-hydroxyvitamin $D_3$ has been obtained,[11] along with three crystal structures of DBP in complex with actin.[12]

Besides the already mentioned Vitamin D binding, DBP is able to associate with further molecules of biological importance. It was found to form a tight 1:1 complex with actin *in vitro*.[13] The binding constant with monomeric actin (G-actin) was measured ($K_d = 10^{-9}$ M) and it is believed that its biological function is the rapid clearance of, otherwise harmful, free actin from the circulation.[14] Similarly DBP like albumin can bind to fatty acids.[15] The association constant of palmitic acid and arachidonic acid with DBP was measured to be $K_a = 7 \times 10^5\ M^{-1}$ and $K_a = 6 \times 10^5\ M^{-1}$ respectively. It should also be noted that DBP is able to significantly

increase the chemotactic activity of C5a and $C5a^{desArg}$ and this process is mediated *via* the glycoprotein CD44 and annexin A2.[16]

For further details on biological and physiological properties of DBP, very good reviews have been written by Cooke and Haddad,[17] and more recently by Speeckaert et al. in 2006.[18]

#### 4.1.2.2 Discovery of MAF and its immunoregulatory properties

In 1985 Yamamoto and Ngwenya noticed mixed cultures of mouse peritoneal adherent (macrophages) and nonadherent (lymphocytes) cells treated with lysophosphatidylcholine (lyso-PC) to display increased ingestion activity of IgG-coated cells by the macrophages.[19] Treatment of macrophages with lyso-Pc in absence of the nonadherent cells didn't trigger this phenomenon. When they investigated this finding further they discovered that the lymphocytes only had this effect in the presence of a certain serum factor, which they identified to be DBP.[20] Encouraged by these findings they investigated DBP further and found it to be the precursor of a potent macrophage activating factor *via* the action of membrane bound glycosidases of B- and T-cells.[21] In the same study using a phagocytosis assay they were able to show that *in vitro* treatment of *GC1* DBP with neuraminidase and β-galactosidase and of *GC2* DBP with β-galactosidase alone gave the same macrophage activating effect. Yamamoto concluded when working with a mixture of *GC1S* and *GC1F* that the proteins carry a branched trisaccharide, which is trimmed in a stepwise process by β-galactosidase of B-cells and neuraminidase of T-cells leaving a single α-*N*-acetly-galactosamine residue on the DBP protein, which is the structure that represents the macrophage activating factor (MAF).[22] This branched glycan structure on MAF was confirmed when DBP was incubated with solid phase immobilized glycosidases and the intermediates isolated using solid bound lectins, as the application of the two glycosidases in either order were able to give the potent activating factor.[23] A comprehensive summary of Yamamoto's findings on macrophage activation and especially the in vitro generation of MAF using glycosidases can

be found in the US patent US5326749.[24] In 1996 this theory was extended when he noticed that only 30% of cancer patients displayed macrophage activation comparable to control, while 25% showed severely depressed activity.[25] After observing that there was no difference in DBP protein content between cancer patients and healthy humans, the reason for the immunosuppression was traced to glycosylation differences on DBP instead. Yamamoto postulated the presence of an endo-α-*N*-acetylgalactosaminidase in the plasma of cancer patients, which would be able to remove the glycan from both the precursor DBP and MAF itself. He was able to show α-*N*-acetyl-galactosaminidase activity to be elevated in cancer patients in comparison to healthy controls (2.1-5.2 nmol/mg/min vs. 0.2-0.4 nmol/mg/min), however, using an exo-substrate (therefore was able to confirm the presence of exo-enzyme activity). The endo-enzyme would cleave the glycan off DBP rendering it inactive as a MAF precursor and this model of immune suppression by α-*N*-acetylgalactosaminidase is presented in Figure 4.1.

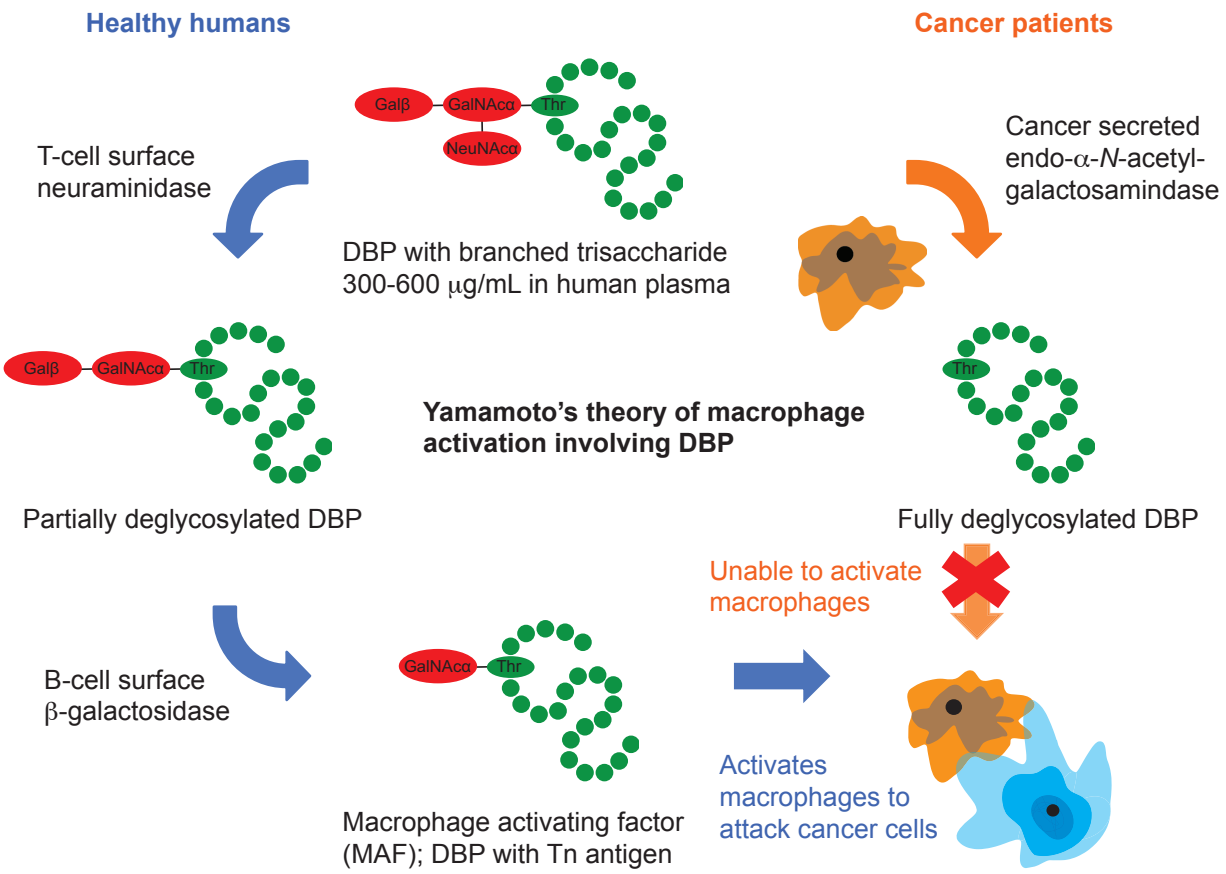


**Figure 4.1** Formation of MAF from DBP in healthy humans (blue pathway) and immunosuppresion in cancer patients due to DBP deglycosylation (organe pathway).

With the MAF theory by Yamamoto established, Hori and coworkers were interested in taking a more scrutinizing look at the phenotypical differences in DBP and how it would influence the ability to generate MAF. In 2004 they stated that only the GC1f phenotype was able to generate a macrophage activating signal, with the other two phenotypes being unable to generate a response in a phagocytosis assay.[26] However, more recently they revoked this statement and have established that all three major phenotypes of DBP can be used to generate MAF.[27]

Other groups have investigated the way that the macrophages attack the tumor cells in more detail. Macrophages are believed to kill target cells *via* induction of apoptosis and mainly three mediators have been implicated in signal transduction involved: tumor necrosis factor α (TNF-α), reactive nitrogen species like nitric oxide (NO) and reactive oxygen intermediates (ROI) like hydrogen peroxide and the superoxide anion ($O_2^{\cdot-}$).[28] In a detailed study it was shown that

monocytes brought in contact with tumour cells produce ROI, which leads to spontaneous cytotoxicity in tumour cells.[29] In an earlier study of Yamamoto involving the stimulation of macrophages using lyso-PC the superoxide generating capacity of the monocytes was recorded.[30] Following this discovery, Hori and coworkers developed a spectrometric assay for superoxide production by mouse peritoneal macrophages and were able to show the release of this ROI on treatment with MAF.[31] It was also shown that the stimulation of macrophages with MAF does not lead to NO or TNF-α release and therefore the response of such treated monocytes is limited to superoxide production and phagocytosis.[32]

Several animal tests were successfully performed involving MAF. It had been noticed that in BALB/c mice bearing Ehrlich ascites tumors that α-*N*-acetyl-galactosaminidase activity (exo-substrate) increased linearly with tumor burden.[33] When mice were administered MAF following tumor transplantation, the mean survival time of the animals was increased from 16 ± 2 to 35 ± 4 days. Upon moving the administration to regular intervals every 4 days the survival could be increased beyond 90 days and after 30 days the α-*N*-acetyl-galactosaminidase level had returned to the level of healthy controls. In another trial involving the same type of mouse and tumor but a changed dose regime these positive results could be confirmed.[34] Similarly when a 9,10-dimethyl-1,2-benzanthracene (DMBA)-induced hamster cheek pouch cancer model was used, MAF treatment was able to extend the mean survival time of the animals significantly, showing its effectiveness for oral cancer.[35] However only 2 out of 14 animals did not eventually succumb to the tumor burden, which is rationalized by the fact that MAF therapy is less effective for well differentiated tumor cells, like those found in the cheek pouch carcinoma, but more effective against undifferentiated adenocarcinomas like breast and prostate cancer. In 2012 in an animal trial with severe combined immunodeficiency (SCID) mice and transplanted HepG2 cells (human hepatocellular carcinoma (HCC), liver carcinoma cell line), MAF treated animals (n = 10/ group) were compared with untreated controls.[36] MAF treatment successfully inhibited

tumor growth (treatment group: 126 ± 18 $mm^3$; untreated group: 1691.5 ± 546.9 $mm^3$) and representative examples of removed tumors are shown in Figure 4.2.

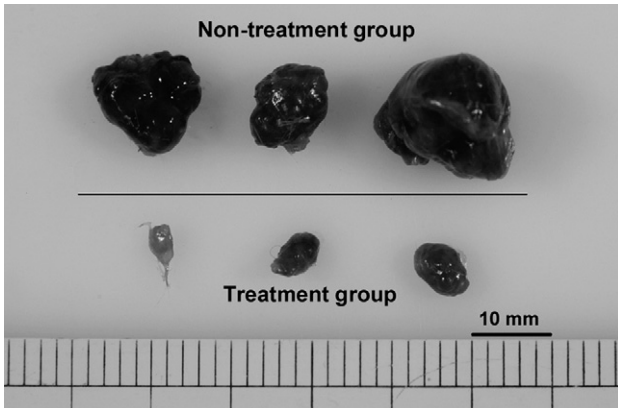


**Figure 4.2** Figure reproduced with permission from Elsevier from an article in the *Journal of Surgical Research* by Nonaka et al.[36] Representative tumors removed after 21 days from untreated controls and MAF treated animals (40 ng/kg/d).

To show the applicability of immunotherapy involving MAF to human anti-cancer treatment three clinical trials were performed in 2008 by Yamamoto and coworkers featuring patients with metastatic breast cancer,[37] with metastatic colorectal cancer[38] and prostate cancer.[39] In all three cases the patients had undergone tumor resections before MAF monotherapy was initiated at a weekly regime of 100 ng and tumor burden and therapy progression was monitored by measuring blood serum α-*N*-acetyl-galactosaminidase acitvity. For the breast cancer patients (n = 16) enzyme activity dropped from 2.32-6.25 nmol/min/mg protein to 0.38-0.63 nmol/min/mg protein following treatment and no recurrence was recorded for four years. In the case of metastatic colorectal cancer (n = 8) annual CT scans were added to the follow up, but the more established tumor markers carcinoembryonic antigen (CEA) and carbohydrate antigen 19-9 (CA19-9) were ruled out as too insensitive for monitoring therapy progression. All treated patients remained disease free for over seven years in both the colorectal and the prostate cancer trial. In the latter study (n = 16) serum α-*N*-acetyl-galactosaminidase activity had returned to the level of healthy controls within 14 to 25 weeks but prostate-specific antigen (PSA) levels were unable to show a difference between the treatment group and controls and hence were not

assessed. A similar trail was also performed on HIV-infected patients.[40] Although the clinical trials of Yamamoto have been very successful they have been criticized for the small sample groups, pre-selection of patients and rarely using standard tumor markers.

#### 4.1.2.3 Further anti-cancer properties of MAF

Besides its immune-modulatory effects further anti-cancer properties have been ascribed to MAF including anti-angiogenesis and cancer cell cytotoxicity. Gumireddy et al. were able to reproduce the production of ROI by RAW 264.7 macrophages with MAF at concentrations of 1 μg/mL/well, while at higher concentrations of 15-100 μg/mL/well apoptosis could be observed in the macrophage cell line.[41] They concluded that ERK1/2, p38 and JNK1/ MAPK pathways are involved in the up-regulation of caspase-3, -8 and -9 which leads to apoptosis. In a more recent study involving human prostate cancer cell lines LNCaP and PC3 a macrophage independent anti-proliferative effect was recorded upon MAF treatment.[42] Anti-migratory properties were noticed as well along with a reduction in uPAR expression, which is a factor associated with tumor metastasis.

Another property influenced by MAF as noticed by Yamamoto was angiogenesis or the formation of new blood vessels. Angiogenesis is one of the hallmarks of cancer and the blood vessel growth is required by the tumor in order to expand beyond its nutrient dependent growth limit.[43] Hence a variety angiogenic factors like FGF-2, VEGF-A and Ang2 are produced by the tumor, which were all successfully suppressed by MAF in the two endothelial cell lines (IBE and PAE cells) investigated.[44] Evidence seemed to point towards the p38 MAPK signaling pathway through CD36, however the activation of the full signaling pathway could not be confirmed. Besides these *in vitro* results the inhibitory effect on FGF-2 by MAF was confirmed in a *in vivo* model using a mouse cornea micropocket assay. Kisker et al. were able to confirm these anti-angiogensis properties of MAF in a chick chorioallantoic membrane (CAM) assay and then

moved on to *in vivo* experiments using SCID mice and transplants of human pancreatic cancer cell lines BxPC-3 and SU88.86.[45] At low doses (4 ng/kg per day) they found MAF to effectively inhibit further growth of transplanted tumors, while at higher doses (4 μg/kg) regression of the tumors was observed. Histological examinations of the tumors revealed decreased micro-vessel formation and massive macrophage infiltration for the treated tumor specimen in comparison to untreated controls. In a follow on study, the aim was to understand the mechanism of angiogenesis inhibition by MAF as exerted on human endothelial cells (HEC).[46] It was noticed that MAF inhibited HEC proliferation *via* inhibition of DNA synthesis ($IC_{50}$ = 7.8 ± 0.15 μg/mL), which resulted in S-and $G_0/G_1$-phase arrest. Furthermore it could suppress cell migration, tube formation and displayed potent anti-angiogenesis properties in an aortic ring sprouting assay. The inhibition of VEGFR-2 autophosphorylation and the downstream ERK1/2 in the presence of VEGF, could be identified as the underlying signaling mechanism of action of MAF. In recent times the signaling cascade triggered by MAF stimulation has been extended further by 3'-5'-cylic adenosine monophosphate (cAMP) formation as a secondary messenger molecule in work by Pacini et al.[47] They were also able to confirm the previously reported results of MAF inhibitory action in CAM assays and extended this methodology to function as a screen of the quality of commercially available MAF (www.gcmaf.eu). Using the same assay they were also able to show that MAF negates the angiogenesis effect of the human breast cancer cell line MCF-7.[48]

Overall we can conclude that there are three distinct effects caused by MAF: a) a macrophage mediated immune response to destroy cancer cells, b) anti-angiogenesis properties on a variety of cell lines and c) direct cytotoxicity to several cancer cell lines.

#### 4.1.2.4 Development of α-*N*-acetyl-galactosaminidase as cancer biomarker

In the previously mentioned clinical trial involving MAF, disease status and therapy progression was assessed using serum α-*N*-acetyl-galactosaminidase activity measurements and several groups have developed this enzyme into a more generally applicable biomarker for cancer. Yamamoto had shown that there was an inverse relationship between MAF precursor activity and blood serum derived α-*N*-acetyl-galactosaminidase activity in a study involving 46 oral cancer patients with squamous cell carcinoma.[33] In the same study he showed the tumor burden in BALB/c mice to be directly proportional to the serum α-*N*-acetyl-galactosaminidase activity. A patent was filed by the same author for a general method of detecting α-*N*-acetyl-galactosaminidase activity in cancer and HIV patients using a colorimetric evaluation of ammonium sulfate precipitations of plasma samples.[49] Another patent extends the measurement method for α-*N*-acetyl-galactosaminidase in blood plasma to using an antibody-sandwich enzyme-linked immunosorbent assay (ELISA) kit in order to further improve the diagnostic/prognostic use of this enzyme.[50] In an animal study involving C3H/HeN and BALB/c mice bearing murine squamous cell carcinoma SCCVII the utility of serum α-*N*-acetyl-galactosamindase as a diagnostic marker was extended to gauging the success of radio- and photodynamic therapy.[51] Following a single dose of radiation to the tumor body (20 Gy at 3.33 Gy/min) serum α-*N*-acetyl-galactosaminidase decreased over 10 days before starting to rise again, while treatment with photodynamic therapy indicated more rapid tumor cell death and α-*N*-acetyl-galactosamindase did not increase once a curative dose had been administered. This method was found to be more sensitive and showed changes in tumor fate more rapidly then the more established postate-specific antigen (PSA) measurement and in mice regrowth of a carcinoma was detectable by this method 8 days prior to visible recurrence.

Groups independent of Yamamoto adopted the idea of α-*N*-acetyl-galactosaminidase as a prognostic/diagnostic marker and in 2000 a study involving 210 patients with squamous cell carcinoma (SCC) of the uterine cervix was undertaken.[52] They confirmed α-*N*-acetyl-galactosaminidase activity correlated with tumor burden and aggressiveness of the disease. While age-matched healthy controls showed very low activity in their blood (0.26 ± 0.1 nmol/mg per min), cancer patients showed a 3-19 fold elevation over these levels and this increase was cancer stage dependent (Figure 4.3). Following radiotherapy α-*N*-acetyl-galactosaminidase levels declined significantly, reflecting the destruction of cancer cells, which are believed to be the source of this enzyme in the blood circulation.

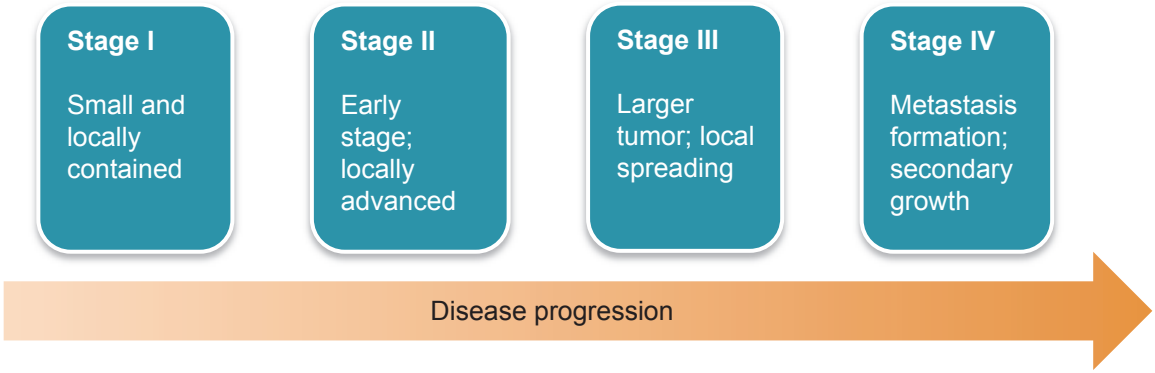


**Figure 4.3** Definition of cancer stage division. Based on CRUK definition.[53]

In 2009 Greco et al. took a holistic proteomic approach to identify novel non-invasive serum biomarkers for cutaneous malignant melanoma.[54] The blood serum of 50 individuals about to undergo surgery for a suspected melanoma was analysed and one of the three proteins that showed a significant change in the proteomic profile was DBP. Hence they moved on to investigate the serum α-*N*-acetyl-galactosaminidase activity and similarly found that the levels increased with tumor thickness and decreased following surgical removal. However, in melanoma, α-*N*-acetyl-galactosaminidase activity is only useful as a diagnostic tool at stage III of the disease, as no significant difference to controls in stage I and II could be found. It can therefore be concluded that in certain cancer types α-*N*-acetyl-galactosaminidase activity in the

blood can indeed be a useful diagnostic and prognostic biomarker for disease stage and aggressiveness.

#### 4.1.2.5 Structural aspects of the glycan present in MAF

As could be gleaned from the discourse given above, the precise structure of the glycan present on DBP is of crucial importance for the macrophage activation theory and several studies have been dedicated to elucidating this structural aspect of DBP. However, despite these efforts there is still some dispute in the literature about the connectivity of the glycan (branched vs linear), the attachment site, the degree of glycosylation and inter-phenotype heterogeneity.

##### *4.1.2.5.1 Early investigations of the glycan on DBP*

At an early stage structural elucidations on DBP were mainly performed by two groups: Viau & Constans and Svasti & Bowman. Although frequently cited as structural evidence, especially by Yamamoto, some of the conclusions drawn by Svasti & Bowman were later identified not to be correct. In 1978 they stated that GC1f protein can be converted into GC1s *via* neuraminidase digestion, suggesting that the difference between these two proteins is only post-translational in nature.[55] A follow on publication repeats this statement, but they concede there to be one amino acid difference between GC1f and GC1s.[56] While their 1983 publication corrects the earlier statements by detailing that the difference in the two bands produced each by the *GC1f* and *GC1s* gene differ in neuraminic acid content, it however, confusingly still refers to the anodal and cathodal bands as "fast" and "slow".[57] They therefore confirm the findings of Cleve & Patutschnick, that had made the same observation in 1979 (Figure 4.4),[5] but they are able to show that GC1 protein contains an α-*N*-acetyl-galactosamine residue and that GC2 differs from GC1 by a threonine to lysine substitution, which is the attachment site of the glycan in GC1.

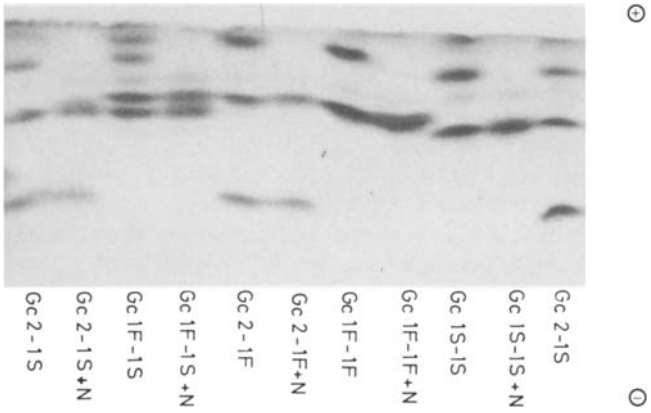


**Figure 4.4** Isoelectric focussing pattern of neuraminidase digest of the three common Gc isoforms GC1f, GC1s and GC2. Figure reproduced with permission from Springer from an article in *Human Genetics* by Cleve et al.[5]

One of the best early structural accounts of the glycan present on DBP is given by Viau and Constans in 1983.[58] In their study they purified DBP protein of the GC1s and GC2 phenotype using three successive chromatographies: blue sepharose, immuno affinity (IgG anti DBP) and DEAE Tris Acryl column. According to their claims, only this level of purification along with rigorous purity control using SDS electrophoresis and isoelectric focusing will allow for reliable results and might account for the discrepancies reported in the literature. Using gas liquid chromatography they were able to detect no glycans on GC2 but three carbohydrate residues on GC1s, which they identified as galactose, *N*-acetyl-galactosamine and *N*-acetyl-neuraminic acid. The molar composition they detected was consistent with a trisaccharide and TLC analysis of the β-elimination product of the released glycan matches in terms of $R_{lactose}$ the ones for glycans released from fetuin.[59] Furthermore the TLC analysis discovered traces of a tetrasaccharide in DBP which is also present on fetuin. Viau et al. assigned the glycan structures according to the literature data for fetuin at the time,[60] which is α-NeuNAc-(2→3)-β-D-Gal-(1→3)-α-D-GalNAc-(1→*O*)-(threonine) **228** and α-NeuNAc-(2→3)-β-D-Gal-(1→3)-[α-NeuNAc-(2→6)]-α-D-GalNAc-(1→*O*)-(threonine) **229** (Figure 4.5). These glycan structures from bovine fetuin have been more recently confirmed by reverse-phase HPLC and 600 Mhz NMR analysis of the pyridylaminated derivatives,[61] in a study using an endo-α-*N*-acetylgalactosaminidase from

*Stretomyces* sp. OH-11242,[62] which is able to release *O*-glycans with the sialic acids still in place. Viau & Constans furthermore confirmed that DBP carries no *N*-glycan and that it doesn't bind to a concanavalin A column, precluding the presence of α-D-mannose and α-D-glucose residues in the structure. The overall amount of glycosylation in the GC1s phenotype was quantified at about 1% of the total protein. Based on the observation noted previously[5] of the double band appearance of GC1s collapsing to a single band on neuraminidase treatment, the glycan containing species was assessed to be present in the top band.

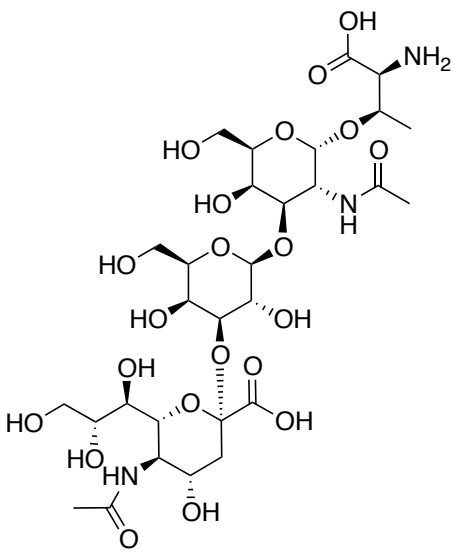

**228**

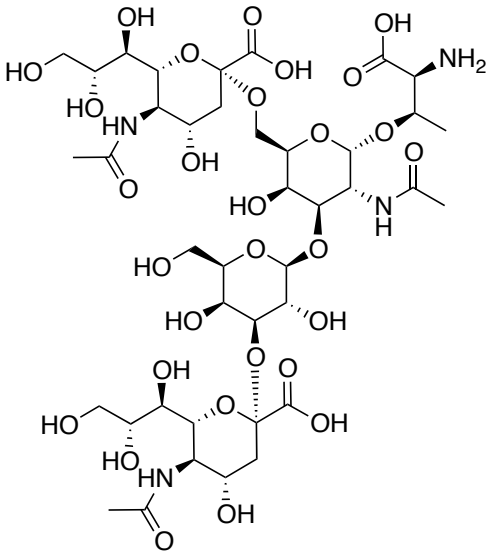

**229**

**Figure 4.5** Trisaccharide **228** and Tetrasaccharide **229** as found on fetuin and DBP.[58]

*4.1.2.5.2 Glycan structural evidence by Yamamoto*

As is apparent from the vast body of literature detailing the use of MAF, Prof. Yamamoto is one of the principle authors on this topic. However, information by him regarding the structural detail of the glycan carried by DBP has been less detailed and can be mainly found in his publication from 1996.[23] In his original publication on MAF in 1991 he detailed that sequential treatment by B-cells carrying β-galactosidase and then solution neuraminidase or solution β-galactosidase followed by T-cell neuraminidase both led to formation of MAF, as shown by a phagocytosis assay.[21] However, this sequence of glycosidase digestion (β-galactosidase then

neuraminidase) would preclude the glycan from being the linear form as described by Viau & Constans as the formation of MAF (DBP with a single GalNAc residue) would require neuraminidase treatment first then β-galactosidase treatment. In the 1996 publication, Yamamoto utilizes immobilized glycosidases and lectins in order to digest the DBP glycan and purify the intermediate products respectively.[23] This detailed approach confirms that the sequence of the employed glycosidases, β-galactosidase and neuraminidase, does not matter for the formation of MAF, which enhances the theory of the dibranched glycan rather then a linear structure. Overall, however, the evidence given by Yamamoto for the branched glycan is circumstantial, as techniques investigating the structure directly have not been used.

#### *4.1.2.5.3 The strict requirement of a single remaining GalNAc residue*

Although little is known on how MAF interacts with the macrophages to activate them on a molecular level, a possible explanation could be offered by the discovery of a calcium dependent lectin in mouse macrophages that was found to specifically bind to D-galactose/*N*-acetyl-D-galactosamine residues by Osawa and coworkers in 1988.[63] The lectin was discovered in OK-432-elicited peritoneal macrophages as a highly *N*-glycosylated protein, which gives a tight band of 35 kDa on SDS-PAGE following deglycosylation. A cDNA clone of the human derivative of this lectin was obtained from IL-2 treated peripheral blood monocytes by the same group and was called human macrophage C-type lectin (HML).[64] The recombinant form of HML was found to bind strongly to octapeptides from human glycophorin A following their glycan digestion to leave a single GalNAc–Ser/Thr residue, which using detailed $^{13}C$ NMR analysis has been shown to carry the same tetraglycan **229** found in fetuin and in traces on DBP.[65] This glycan epitope (GalNAc-Ser/Thr) is known as Tn antigen[66] and this abnormal mucin-type *O*-glycan is associated with different diseases, including cancer.[67] In 1999 the binding mechanism of HML to Tn antigen has been explored further using surface plasmon resonance on recombinant protein with synthetic peptides that had an increasing number of single GalNAc

residues attached to threonine residues.[68] HML was found to be a marker for macrophage differentiation and was renamed in the macrophage galactose/N-acetylgalactosamine (Gal/GalNAc)-specific C-type lectin (MGL) or more specifically in its human form (hMGL).[69] Many further functions have been ascribed to MGL since then including MUC1 recognition in cancer cells and interaction with T-cells *via* CD45 as detailed in a recent review.[70] In 2012 MGL was shown to be present in immature dendritic cells and that binding to Tn antigen triggered homodimerization followed by downstream phosphorylation of ERK1/2 and nuclear factor-κB activation.[71] As mentioned previously, ERK1/2 phosphorylation has also been noticed on MAF activation of RAW 264.7 macrophages.[41]

Although as far as I am aware the binding of MAF to MGL has not been probed, this does however show the signaling potential of a single remaining GalNAc residue. In this context it should be noted that when Kisker et al. recombinantly expressed DBP in *E. coli*, which is expressed devoid of glycosylation, they were unable to elicit a macrophage activating response using this peptide.[45]

#### *4.1.2.5.4 Mass spectrometry studies on DBP and MAF*

With the technical advancement of mass spectrometry, especially of matrix-assisted laser desorption/ionization (MALDI) spectrometric analysis, the investigation of proteins and their posttranslational modifications has become more routine. As a result DBP purified on a large scale from plasma Cohn fraction IV paste was subjected to MALDI mass spectrometry in 2006.[72] A variety of techniques were employed for measuring the degree and nature of the glycosylation on DBP including a commercial glycan detection kit (fetuin glycan detection limit 20 ng), a lectin pulldown using enzyme derived from *Erythrina cristagalli* and *Maackia amurensis*, protein digestion and analysis of resulting peptides *via* MALDI-MS and several others. However they were unable to detect any carbohydrates and concluded that DBP purified on a large scale was devoid of glycosylation. In a follow on study, which focused on

investigating sequence and post-translational modification differences of the major phenotypes of DBP, they were able to confirm the protein sequences that had been deduced earlier based on DNA data.[73] Further fractionation of their large scale purified product using ion exchange chromatography allowed for a trace amount of glycan to be identified, which was consistent with both the Yamamoto[23] and Viau & Constans[58] presented structure of a tri-saccharide, which on neuramindase treatment lost a mass fraction consistent with a single sialic acid unit. A similar result was also obtained using commercial sources of DBP, however no futher glycosidase digestions were attempted that could have solved the question of the branched vs. linear glycan structure. The enormous difficulty in the detection of the glycan might have been derived from their initial large scale purification protocol of DBP[72], which is further detailed in a patent.[74] This purification method could be selectively removing the glycan or be biased against glycosylated proteins. Further convoluting factors could be the starting material used to obtain the DBP, which is the plasma Cohn fraction IV resulting from an ethanol fractionation (40% ethanol at pH 5.9)[75] rather then unchanged donor blood plasma, or the mass spectrometry sample preparation technique employed by the group.[76]

A very clear and detailed investigation of DBP using mass spectrometry was undertaken by Borges et al. in 2008.[77] Using plasma samples of 113 healthy individuals (226 alleles) they performed both whole protein analysis using electron spray ionization time of flight mass spectrometry (ESI-TOF) and MALDI mass spectrometry on peptides of Arg-C digested protein samples. Using these techniques they were able to confirm the sequence data for all three major alleles of DBP GC1f, GC1s and GC2 (UniProtKB database entry P02774). Furthermore they elucidated products of the *GC1* allele to carry a linear trisaccharide NeuNAc-Gal-GalNAc (10-25 mol %) at T420 and in some cases a disaccharide Gal-GalNAc (< 5 mol %) at T418. GC2 proteins are shown not to contain any of the trisaccharide but can contain the disaccharide (2 mol %) and are therefore much less glycosylated then GC1 proteins. Of course because of potential

ionization efficiency differences between the DBP isoforms the exact molar percentages might vary from the presented results. The linearity of the trisaccharide was confirmed using a TOF/TOF spectrum where no evidence of galactose loss alone could be found. Additionally they were able to confirm the absence of *N*-glycosylation and the possible presence of a mannose in the glycan structure, as none of these derivatives could be detected in any of their samples. It should also be noted that in their Arg-C digest peptides they were able to detected traces of GalNAc only glycan carrying protein, which would indicate the presence of MAF to a low degree in the samples. In a follow-on study by Borges and coworkers involving 56 patients with breast, colorectal, pancreatic and prostate cancer, charge state deconvoluted ESI mass spectra of immuno-affinity purified DBP were collected to evaluate the degree of deglycosylation in cancer patients.[78] However, a depletion in the species carrying the trisaccharide, and therefore the direct precursor of MAF, could not be found, nor was the amount of MAF reduced in the serum of cancer patients. On the contrary the concentration of MAF (defined as DBP protein with a single GalNAc residue) present in circulating blood of cancer patients was estimated to be 5-10 mg/L and therefore seems to be in contradiction with Yamamoto's theory and activity measurements.

In a most recent mass spectrometry study by the group that performed the large scale purification they were able to further refine their ion exchange chromatography allowing them to reliably identify a glycosylated protein of the GC1s and GC1f phenotype.[79] Following sequential digestion with endoproteinase AspN (cleaves peptides bonds *N*-terminal to aspartic acid residues) and trypsin including a HILIC enrichment they were able to record an MSMS spectrum for GC1s protein confirming the linearity of the trisaccharide on T420. They were able to corroborate this result further using glycosidase digestion, where the glycan was shown to be unchanged by β-galactosidase treatment alone, however, was successfully converted into MAF on treatment with neuraminidase followed by β-galactosidase. They were however, unable to

confirm the disaccharide found previously on T418 by Borges et al. and estimated the degree of glycosylation to be only 0.5-1%.

Despite the enormous potential that the technique of mass spectrometry holds for structure and post-translational modification elucidation, the inherent difficulty in the purification process of DBP, especially with the glycan intact, has led to inconsistent results. The question of the glycan structure and relative amount of glycosylation on DBP still seems unanswered due to the discrepancies in data obtained across different laboratories.

Based on the discourse above, Figure 4.6 attempts to summarize the current knowledge of amino acid and glycosylation differences between the three main phenotypes of DBP Gc2, Gc1s and Gc1f using a stylised isoelectric focusing pattern.

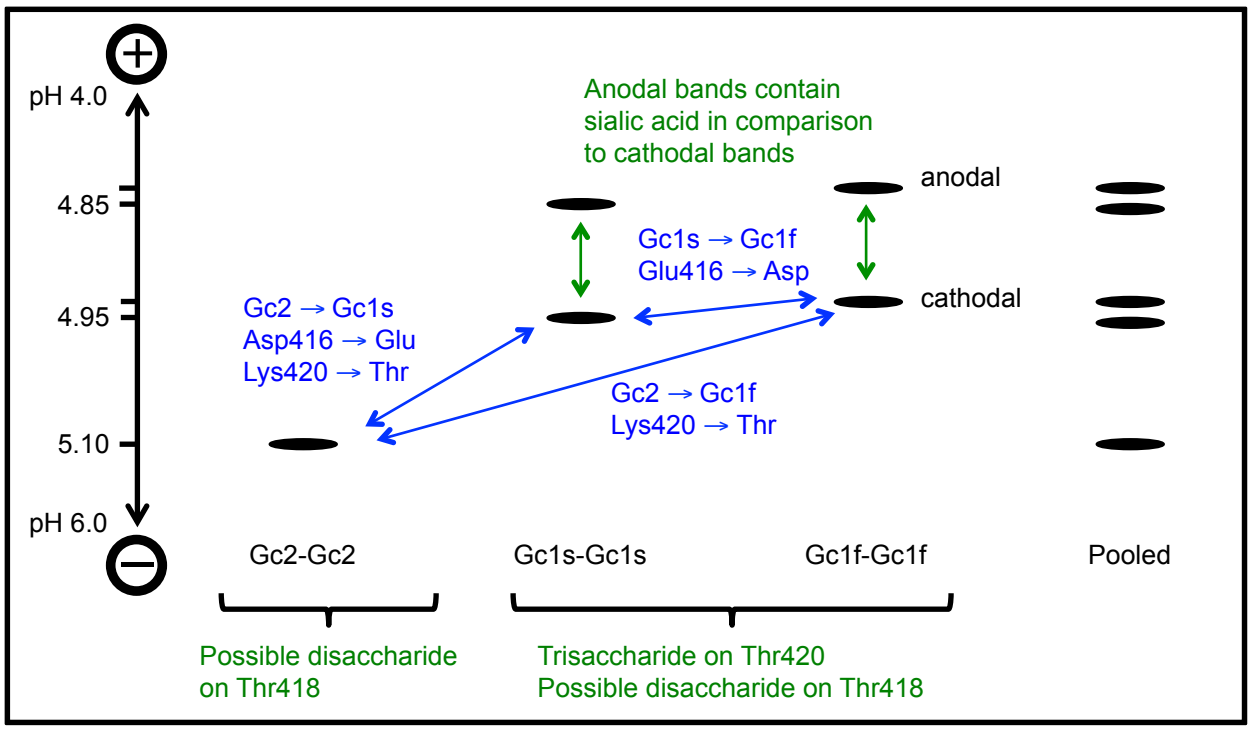


**Figure 4.6** Stylized isoelectric focusing pattern of the three main phenotypes of DBP in homozygous form along with a pooled plasma sample. Amino acid differences in the bands are indicated in blue (UniProtKB database entry P02774),[8-9] glycan differences are indicated in green.[5, 58] Glycan position on sequence indicated below labels.[77]

#### 4.1.2.6 Outline for the potential of α-*N*-acetyl-galactosamindase inhibitors

Based on Yamamoto's theory of macrophage activation (Figure 4.1) α-*N*-acetyl-galactosamindase secreted into extra cellular space by solid tumors is responsible for the deglycosylation of DBP, the precursor of the signaling molecule MAF, which is generated from DBP *via* the sequential action of surface glycosidases from T- and B-cells leaving a single GalNAc residue. Treatment approaches to lift the resulting immunosuppression currently involves *in vitro* generation of MAF by solid bound glycosidases treatment of DBP followed by intra-venous injection. The resulting macrophage activation allows the patients immune system to fight residual cancer cells as monitored by plasma α-*N*-acetyl-galactosaminidase activity.

Here an alternative treatment approach protecting MAF and its precursor *in vivo* from destruction by α-*N*-acetyl-galactosaminidase activity using an iminosugar inhibitor specific to the enzyme, instead of generating MAF *in vitro* is proposed. An iminosugar could be designed to be orally available but preferentially restricted to extra cellular space, the location of the cancer secreted α-*N*-acetyl-galactosaminidase. A non-invasive biomarker for the effectiveness of the therapy in form of serum activity measurements of the same enzyme is already established. The concept could be tested *in vitro* by extending the existing macrophage activation assays to include cancer cell derived α-*N*-acetyl-galactosaminidase enzyme in order to show the deactivation of pregenerated MAF (Figure 4.7). The iminosugar could then be used in the same setup to stop the deglycosylating activity of α-*N*-acetyl-galactosaminidase on MAF. If the concept was to be successful the iminosugar would directly relieve the immunosuppression in cancer patients, which is caused by α-*N*-acetyl-galactosaminidase secretion.

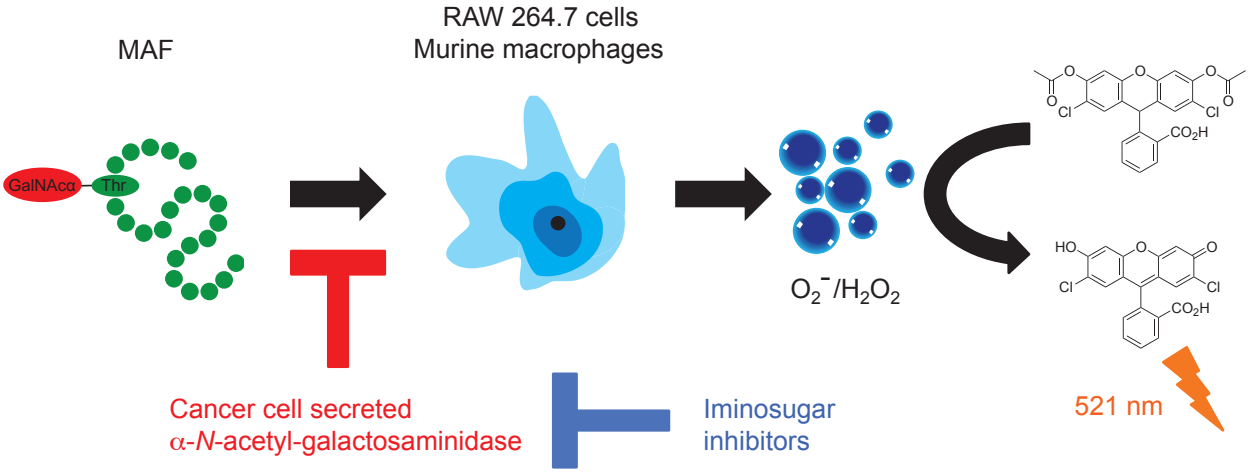


**Figure 4.7** Conceptual setup of macrophage activation assay. Activity of macrophages quantified by measurement of reactive oxygen intermediates *via* oxidation of 2',7'-dichlorofluorescin-diacetate to the fluorescently active 2'-7'-dichlorofluorescein.

### 4.1.3 β-*N*-Acetyl-hexosaminidase and the extra cellular matrix

The other glycosidase that was investigated in more detail in this thesis is β-*N*-acetyl-hexosaminidase, because of its reported involvement in the degradation of the extra cellular matrix (ECM) by cancer cells.[80]

The ECM is a scaffold that gives stability to individual organs and the human body as a whole, especially in its calcified form of bone.[81] It furthermore provides a basis for cells to adhere to and consists of an intricately interwoven network of glycoproteins and polysaccharides. More specifically this complex web consists of fibrous glycoproteins like laminin, type IV collagen and nidogen along with glycosaminoglycans (GAGs) and proteoglycans like perlecan, which are furthermore interlinked by proteins like fibronectin and elastin.[82] The overall structure of the ECM is represented in Figure 4.8, which takes on a layered organization with epithelial cells adhering to the basal lamina, which separates the cells from the underlying connective tissue. The epithelial cells are interconnected with cadherin molecules and are anchored to the basal lamina using integrins. The connective tissue is interspersed by a variety of cells e.g. fibroblasts, which are responsible for secretion of the macromolecules, that constitute the ECM and macrophages, which are recruited to sites of inflammation.

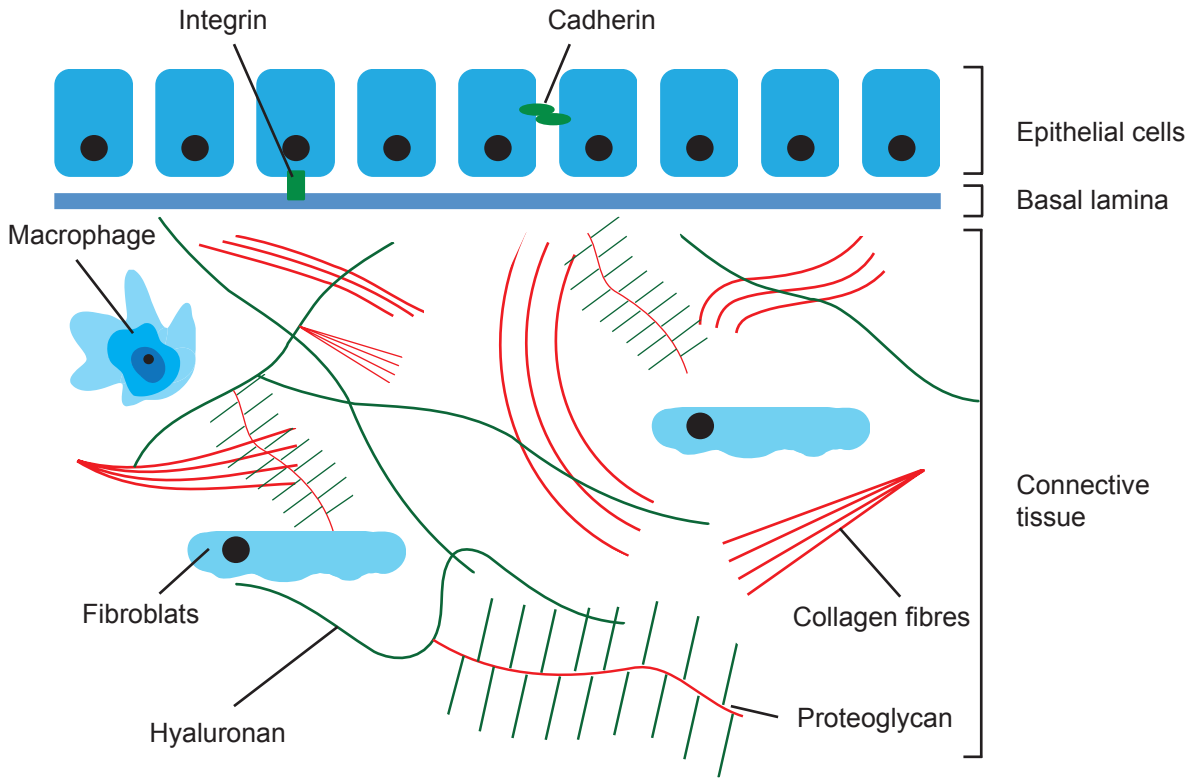


**Figure 4.8** Structure of the extra cellular matrix. Protein fibers are indicated in red and carbohydrate residues in green.

Therefore many of the ECM component macromolecules contain carbohydrates, especially the GaGs, which are polymers of repeating disaccharides. One of the simplest GAGs is hyaluron (also known as hyaluronate or hyaluronic acid) **230**, which is a non-branched polymer of repeating disaccharide subunits (*N*-acetylglucosamine-glucuronic acid) with a chain length up to 25,000 sugar monomers.[81] Unlike many other GAGs, hyaluron is not linked to a core protein (which would make it a proteoglycan), contains no sulfated sugars and its chain length surpasses that found for other proteoglycans. It is however able to absorb a large quantity of water molecules, which makes it occupy a large amount of space and hence plays an important role in organ development and wound healing.

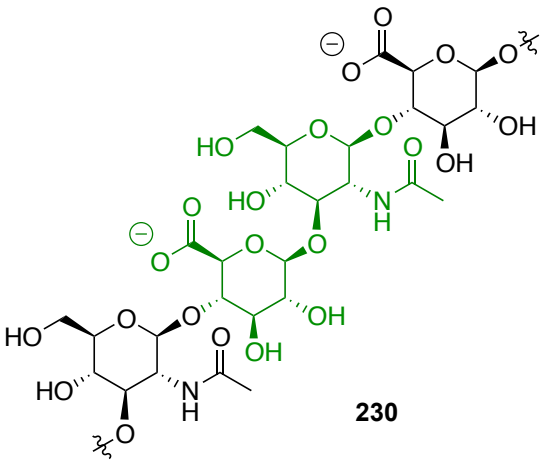

**230**

**Figure 4.9** Structure of Hyaluronan, a carbohydrate polymer with up to 25,000 monomer units. The repeated disaccharide subunit is indicated in green.

Although normal cells produce a variety of hydrolytic enzymes to remodel the ECM, allowing them to pass through the structure or to reshape it if required, the process is tightly regulated in order to not disrupt the delicate balance that rules a multicellular organism. This control is lost in invasive cancer cells and the unregulated release of hydrolytic enzymes allows the cells to break through the extracellular matrix that encapsulates the organ the tumor originates in. These hydrolytic enzymes can be subdivided into four classes: 1) serine proteases; 2) cysteine proteases; 3) metalloproteinases and 4) endo- and exoglycosidases.[83] As the names suggest the first two proteases rely on the respective amino acid residues to perform a nucleophilic attack, while metalloproteinases contain zinc (II) ions in the active site in order to break the peptide bond. Much work has been devoted to developing inhibitors of these proteases in order to limit cancer cell invasion, especially of matrix metallo proteinases (MMPs) and a case-study for one of these will be presented in this chapter. The focus of this thesis, however, will be on glycosidases.

As early as 1969 its was noticed that fibroblasts transformed with an oncogenic virus display a upregulation in hydrolytic activity of seven glycosidases.[84] Since then a whole set of glycosidases and glycosyltransferases have been found to be elevated in cancer patients. Besides the already mentioned α-*N*-acetyl-galactosaminidase other more prominent examples have

emerged like heparase, an endo-β-D-glucoronidase that is capable of degrading heparan sulfate a proteoglycan present in the ECM.[85] In an investigation of human invasive breast and colon tumors, sialyltransferase activity was found to be elevated in comparison to benign tissue.[86] Bernacki et al. wrote an excellent review putting the elevation of various glycosidases and invasiveness of cancer cells into context.[87] Some of these glycosidases and glycosyl transferases are implicated in the aberrant glycosylation that is found on many cancer cells.[88] An example of this aberrant surface glycosylation is the increased β-1,6-GlcNAc branching of *N*-glycans caused by *N*-acetyl-glucosaminyltransferase V, which when overexpressed leads to tumor formation and increased metastatic potential.[88a] Further cell surface glycans associated with malignancy are Lewis A and sialyl Lewis X and these glycosylation profiles have been more recently suggested as useful biomarkers of disease.[89]

Another enzyme out of the set of glycosidases that was found to be elevated in malignant tissue is β-*N*-acetyl-hexosaminidase. This observation was first made in the murine lymphoma cell line L5178Y by Bernacki and Bosmann in 1970.[90] Out of the 11 glycosidases investigated in the cell homogenate β-*N*-acetyl-hexosaminidase showed the highest enzyme activity and a similar observation was made when metastatic and non-metastatic derivatives of the murine C57 cell line (based on ability to cause lung metastasis on tail vain injection) were compared. A three or two fold elevation was found for β-*N*-acetyl-galactosaminidase and β-*N*-acetyl-glucosaminidase respectively in the metastatic derivative.[91] Similar observations were made for mouse tumor tissues from C57BL/6J mice and female Swiss CD-1 white mice. Following the transplant of a highly malignant anaplastic carcinoma, β-*N*-acetyl-glucosaminidase activity doubled between day 14 and day 17.[92] High levels of β-*N*-acetyl-glucosaminidase acitivity was also found in cancer cell homogenate and ascite fluid of samples derived from peritoneal injections of Ehrlich ascites tumor cells, showing that the enzyme was in fact secreted into extra cellular space.[93]

The enzyme is found to be expressed in human cancer tissue as well, as can be seen by a study involving human colonic adenocarcinoma cell lines.[94] Both fetal and cancer cell lines secreted β-*N*-acetyl-glucosaminidase and β-*N*-acetyl-galactosaminidase into the surrounding media.[94] In another study involving several common cancer cell lines including, for example, the human breast carcinoma line MDA-MB-231, an increase in the secreted β-*N*-acetyl-glucosaminidase activity was observed over a 96 h time period.[95]

Similar results were obtained, when human tissue samples were analysed following surgical removal of a tumor. In a study comparing healthy human ovary tissue with that of ovarian adenocarcinoma a highly significant increase in β-*N*-acetyl-hexosaminidase activity was found for the malignant tissue (49 ± 16 rising to 130 ± 64 nmol/min/mg).[96] In the same report it was noticed that the enzyme levels correlated with the degree of differentiation of the tumor, with well-differentiated tumors showing normal activities while poorly differentiated ones showed high levels of activity. The same observation was also made later in a study using lung tissue.[97] The total amount of β-*N*-acetyl-hexosaminidase acitivity was nearly doubled in malignant samples in comparison to normal lung tissue. In 2006 samples from human gliomas were subjected to a similar analysis and again a significant increase in β-*N*-acetyl-hexosaminidase activity was found in malignant tissue in comparison to healthy brain.[98] Activity was found again to correlate well with degree of malignancy and infiltrating primary tumors again showed higher levels then solid primary tumors, stressing the fact that invasive tissue produces the highest degree of secreted glycosidases. The value of β-*N*-acetyl-hexosaminidase activity as a non-invasive biomarker was shown most recently in an investigation of patients with pancreatic adenocarcinoma.[99] Enzyme activity was found to be significantly elevated in blood and urine samples of the 15 cancer patients in comparison to healthy controls and therefore displays the possible utility of β-*N*-acetyl-hexosaminidase as a prognostic and diagnostic marker.

Therefore β-*N*-acetyl-hexosaminidase is established as member of the cocktail of hydrolytic enzymes secreted by cancer cells and it has been previously shown that human lysosomal β-*N*-acetyl-hexosminidase is able to degrade GAGs *in vitro*.[100] With the ECM being rich in GAGs and other heavily glycosylated proteins inhibitors of glycosidases have been proposed as useful additions to existing anti-metastatic agents like protease inhibitors.[101]

#### 4.1.3.1 Cancer metastasis formation – a change for cytostatic agents

90% of cancer deaths are related to metastasis formation.[102] Hence the already mentioned interest in developing anti-metastatic therapies.[101] The process of metastasis formation is a complex process of sequential steps (Figure 4.10).[81] Following the shedding of cells from the primary tumor, the cancer cell needs to break through the basal lamina and stroma making up the ECM in order to enter a capillary and therefore the systematic circulation. Following this intravasation, cancer cells travel through the body until they adhere in the capillary at a secondary site in the body. The cancer cells then leave the blood vessel, a process known as extravasation, and burrow through the ECM in order to set up a micrometastasis, which can grow into a secondary metastasis in a distant organ. As this overall process involves the degradation of the ECM on two occasions, it is a reasonable assumption that protection of ECM could be a viable anti-cancer therapy. Of course in contrast to classic cytotoxic therapy this approach would have the aim of halting disease progression rather then its eradication. The molecules in this approach of disease stabilisation can therefore be termed cytostatic agents.

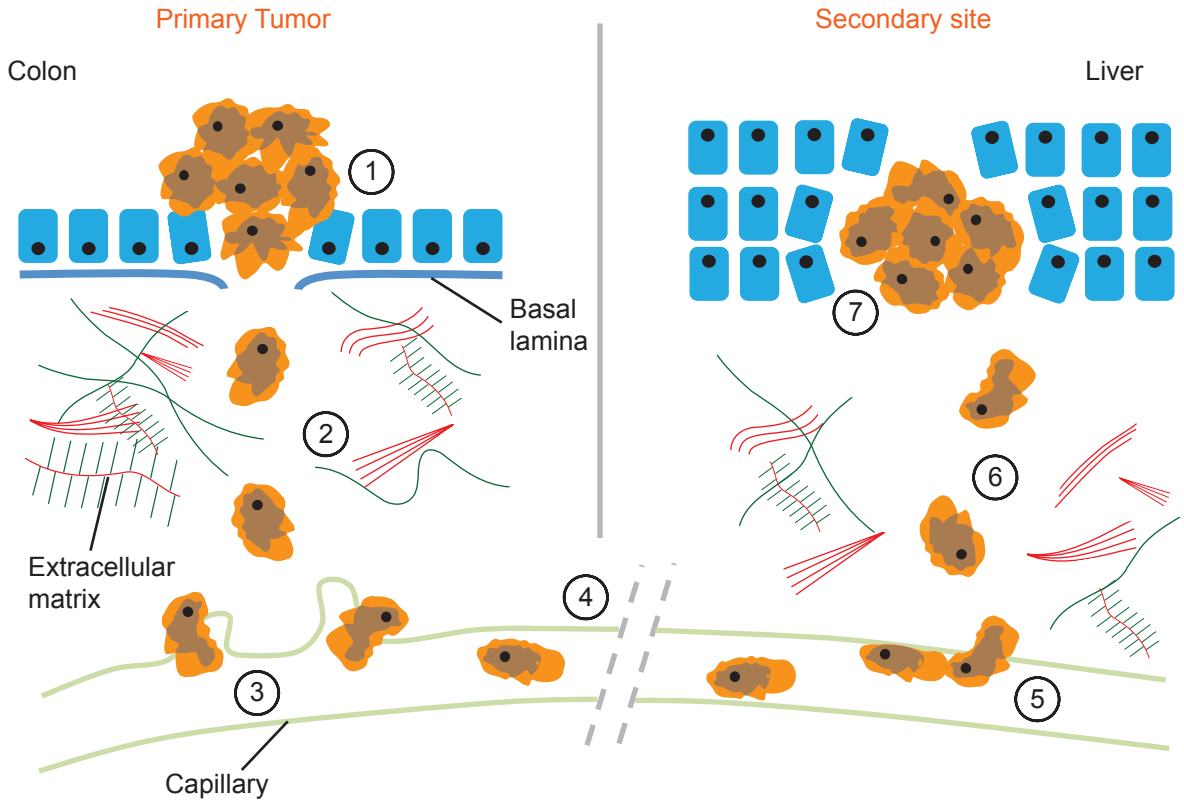


**Figure 4.10** The 7 stages of metastasis formation. Example of colorectal cancer metastasis to the liver. 1) Cancer cell shedding by primary tumor; 2) local invasion of the extra cellular matrix and breaking through the basal lamina; 3) intravasation, entering of the blood vessel assisted by leaky vessels due to stimulated angiogenesis; 4) cancer cell travel through blood stream less then 1 in 1000 cells are successful; 5) blood vessel adhesion and extravasation; 6) local invasion of secondary site; 7) micrometastasis formation, which grows into secondary tumor.

#### 4.1.3.2 Protection of the ECM using β-*N*-acetyl-hexosaminidase inhibitors

With the high degree of β-*N*-acetyl-hexosamindase activity in invasive cancer cells established, the idea was born of using a glycosidase inhibitor as cytostatic agent to protect the ECM. In order to test the viability of this theory Bernacki and coworkers developed an *in vitro* ECM degradation assay.[103] Tritium radiolabelled carbohydrates were integrated into the ECM, which was deposited by bovine corneal endothelial cells on culture dishes. Using cancer cells the ECM could be degraded and the degree of invasiveness quantified by measuring the radiolabel released into the medium. Using this assay system Bernacki et al. were able to show for the first time that a glycosidase inhibitor could indeed be utilized to protect the ECM.[80] The human ovarian carcinoma cell line, which displayed a 5-8 fold overexpression of β-*N*-acetyl-

hexosaminidase in comparison to normal cells, was able to release up to 30% of the radiolabel from the ECM. On addition of glycosidase inhibitor **231**, which is the oxidized version of *N*-acetyl-glucosamine, the enzyme dependent degradation of the ECM was completely suppressed (Figure 4.11). In a follow on study, they were able to differentiate the individual contributions of three intracellular isoenzyme forms to the overall β-*N*-acetyl-hexosaminidase acitivty.[104]

The iminosugar 2-acetamindo-1,5-imino-1,2,5-trideoxy-D-glucitol **232** (Figure 4.11) synthesised by our group,[105] which had been shown to be a potent β-*N*-acetyl-hexosaminidase inhibitor ($IC_{50}$ 6.0 μM, $K_i$ 0.9 μM, human placenta),[106] was tested in the same *in vitro* ECM degradation assay.[107] The iminosugar was able to inhibit the extra cellular secreted enzyme displaying a $K_i$ of 2.7-5.7 μM for the three isoenzymes of β-*N*-acetyl-hexosaminidase and decreased the cancer cell dependent degradation of the ECM by 70-80% when used at a concentration of 1 mM. In a study by Ramessur et al. involving the iminosugar (-)-steviamine **233**, which is a natural product isolated from *Stevia rebaudiana*,[108] it was shown to inhibit β-*N*-acetyl-hexosaminidase activity derived from the medium of the breast cancer cell line MDA-MB-435 at a 1 mM concentration in combination with a protease inhibitor cocktail (2-aminoethyl benzenesulphonyl fluoride, EDTA, bestatin, L-*trans*-epoxysuccinyl-leucylamide-4-guanido-butane, leuceptin, aprotinin).[109] The same mixture of protease and glycosidase inhibitors was able to reduce the invasiveness of the same cell line in a matrigel invasion assay. The inhibition of cancer derived β-*N*-acetyl-hexosaminidase is singular, as (-)-steviamine used in this study, the structure of which has been confirmed by X-ray crystallography,[110] has been shown to be non inhibitory against β-*N*-acetyl-hexosaminidase from other sources at the same concentration (human placenta, jack beans, 1 mM).[111] Although the combined results with protease inhibitors are indicated, the effect of the iminosugar as a single agent on cancer cell invasion was omitted from the study.

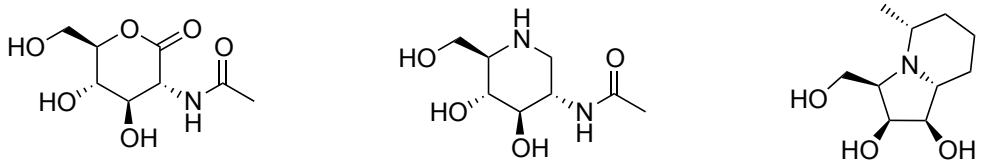

231 232 233

**Figure 4.11** Glycosidase inhibitors investigated in an ECM protective setting

#### 4.1.3.3 ECM protection – the matrix metalloproteinase inhibitor case-study

As described earlier, the idea of protecting the ECM is not a new one, and will be explained in more detail in context of the cytostatic agent marimastat, an orally available matrix metalloproteinase (MMP) inhibitor. Like for many other MMP inhibitors, the preclinical data of marimastat had been very promising and phase I clinical trails showed that the agent was well tolerated in healthy volunteers.[112] Similarly phase II clinical trials involving 113 patients with advanced pancreatic cancer treated with marimastat demonstrated the tumoristatic properties of this anti-metastatic agent and further clinical development was recommended.[113]

Despite the promise held by the early results of these anti-metastasis agents, the outcome of the phase III clinical trials using marimastat were chastening.[114] The trial involved 179 patients with late stage metastatic breast cancer, which had undergone first-line chemotheraphy and investigated improvements to progression-free survival caused by marimastat as single agent therapy in comparison to placebo. Marimastat was unable to prolong progression-free survival and higher levels of musculoskeletal toxicity was noticed in the treatment group. Similar shortcomings were noticed for other MMP inhibitors in advanced clinical trials and are presented in the excellent review by Coussens et al., which also outlining the preclinical promise of these agents.[115]

Possible reasons for the poor performance of the MMP inhibitors can be found in the clinical trial design, lack of reliable biomarkers for MMP inhibition *in vivo* and their application in single agent therapy. The use of classic clinical trial designs, which have been developed for cytotoxic agents, to cytostatic agents like anti-angiogenesis and anti-metastasis therapy has been criticised

before.[116] More specifically the phase III clinical trails of the MMP inhibitors often involved the wrong type of cancer e.g. based on patient availability pancreatic and lung cancer were chosen for clinical trials for which mouse model "proof of principle" was less established and also the wrong stage of the disease for anti-metastatic therapy.[115] Traditionally late stage cancer patients are chosen for clinical trials, however patients with already established metastasis were to see little benefit from anti-metastatic therapy. Also as clinical readout of therapy success, standard endpoints like tumor shrinkage were selected, a poor choice for therapy that aims at disease stabilisation at best when used as single agent. With such standard endpoints removed, however, the need for a reliable biomarkers to follow disease state and progression becomes more pressing, an area which currently still is in need of further research activity.

Therefore with the negative clinical results of the anti-metastasis agents put into context the future of cytostatic therapy might lie in a combination approach. In the absence of a reliable biomarker for evaluating disease stage, classical endpoints of tumor shrinkage could become applicable, if anti-metastatic therapy were to be combined with cytotoxic agents. Phase I clinical trials combining marimastat with carboplatin and paclitaxel have already been performed successfully recording partial response in 57% of patients and disease stabilization in further 19%.[117] Furthermore with the ECM protection state being uncertain due to variations in bioavailablity of the MMP inhibitors, combination with further ECM protecting agents like a selective glycosidase inhibitor could further improve efficacy of these inhibitors *in vivo*.

#### 4.1.3.4 Outline for the potential of β-*N*-acetyl-hexosaminidase inhibitors

As can be seen in Chapter 2 and Chapter 3 a large set of very potent β-hexosaminidase inhibitors ranging in ring size from 4 to 6 has been successfully generated. Some of the structures are in very novel chemical space and it was of interest to determine if these inhibitors were applicable to anti-metastatic treatment as cytostatic agents.

The goal of this aspect of the project was to develop a platform, which would allow for the anti-invasive effects of the β-*N*-acetyl-hexosaminidase inhibitors to be determined reliably in an *in vitro* assay. Ideally this should be based on a cell-line, which could be readily translated into animal experiments, and on a method, which doesn't rely on cell counting. Once established this method would allow for an expansion on the preliminary results, that exist on ECM protection using iminosugars,[107, 109] by exploring the use of iminosugars at physiological relevant concentrations and in combination with protease inhibitors. Especially contrasting single agent treatment with the combination approach would allow us to establish if the combination of glycosidase and protease inhibitors is synergistic or additive. Overall it should be possible to determine if glycosidase inhibitors are worth adding to the arsenal of anti-metastatic treatment approaches.

## 4.2 Investigations of Vitamin $D_3$-binding protein

In order to confirm the signaling effect of MAF, a repetition of the literature *in vitro* macrophage superoxide assay was planned, followed by an expansion to include the use of iminosugars for signaling rescue in the presence of α-*N*-acetyl-galactosaminidase.

### 4.2.1 *In vitro* immune response assay with commercial vitamin $D_3$-binding protein

The initial outset of this work was to repeat and combine two protocols for the macrophage activation assay using MAF generated from commercially available DBP (Sigma Aldrich). The work by Mohamad et al. used peritoneal macrophages derived from BALB/c mice, which had been elicited with 3% thioglycollate and employed lipopolysaccharide (LPS), an endotoxin derived from the membrane of gram negative bacteria, as positive control.[31] Kisker and coworkers on the other hand used the murine macrophage cell line RAW 264.7 as the source of macrophages in their *in vitro* experiments but hadn't used a positive control in their experiments.[45] For ease of scaling up of the experiment to a larger sample set and to avoid

animal work, it was decided to use RAW 264.7 cells but employ the LPS as possible positive control in the experiment. It should be noted that the former manuscript used DBP from a commercial source (Athens Research and Technology Inc), while the latter performed 25-hydroxyvitamin $D_3$ affinity column chromatography in order to isolate DBP from human sera.

The Kisker publication had used the oxidation of dihydrofluoresceine diacetate (DHF-DA) to the fluorescently active fluoresceine in order to quantify the reactive oxygen intermediates (ROI) produced by the macrophage cells.[45] In more detail cellular acetylesterases remove the protecting groups on DHF-DA **234**, giving diol **235** which is then readily oxidized by the ROIs generated from the macrophages to the fluorescently active fluorescein **236**, which can be quantified spectrofluorometrically. This method was chosen for detecting of the oxidative burst of RAW 264.7 cells in this study.

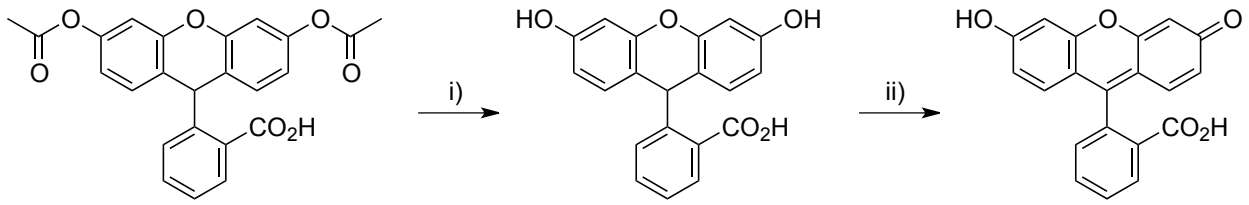


DHF-DA **234** DHF **235** Fluorescein **236**

**Scheme 4.1** Conversion of non fluorescent reduced dihydrofluoresceine diacetate to fluorescent fluorescein. Reagent and conditions: i) Cellular esterases; ii) oxidation *via* ROI.

For the treatment of RAW 264.7 cells, MAF was generated from commercial DBP using sepharose bound glycosidases according to literature procedures,[23] and was used at 1 ng/mL concentration, while LPS was used at 10 μg/mL alongside further controls using only phosphate buffered saline (PBS, negative control), undigested DBP (1 ng/mL) and the glycosidases only. However neither the MAF nor the LPS treated wells indicated a statistically significant increase in ROI species relative to the negative control based on the measurement of fluorescein release.

Therefore it was decided to ensure that ROI detection was working correctly by stimulating DHF-DA directly using hydrogen peroxide in the absence of cells. Following the suggestions in

a publication on assay development involving fluorescein and derivatives by Hempel et al., improvements on the signal to noise ratio of the assay by avoiding light exposure, base pre-treatment and cofactor additions were explored using this method.[118] When comparing the hydrogen peroxide (2 mM final concentration) treated wells with untreated controls, no improvements in signal to noise ratio could be detected for the samples which had not been exposed to light or pretreated with base in order to deacetylate the compound. By employing horseradish peroxidase (HRP) as a cofactor for the reaction it was possible to obtain a significant difference between treated and negative control, however only at very high concentrations of hydrogen peroxide (20 mM, Figure 4.12). The DHF-DA detection of ROI therefore was not sensitive enough in our hands and an alternative method of detecting macrophage activation had to be sought.

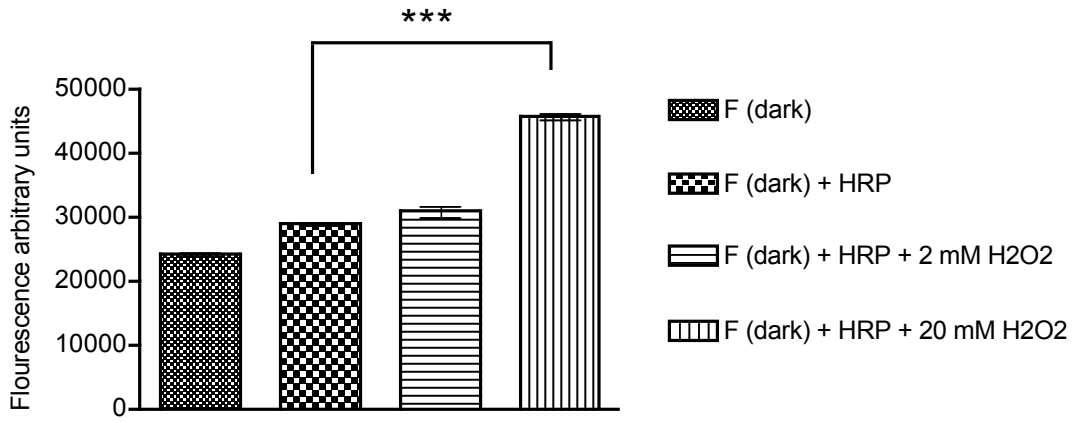


**Figure 4.12** DHF-DA was kept in the dark and treated with varying concentrations of hydrogen peroxide in the presence of horseradish peroxidase (HRP) as a cofactor; incubation time 30 min.

Of the three types of signaling molecules (NO, ROI, TNF-α) usually produced by activated macrophages,[28] two had been noted not to be elicited on stimulation with MAF.[32] A more sensitive method for detecting ROI was therefore employed in the form of the Invitrogen hydrogen peroxide detection kit. Using this method hydrogen peroxide concentration ranging from 100 nM to 10 μM correlated in a linear fashion with the detected fluorescence and this assay was considerably more sensitive then the previously employed DHF-DA method.

With this effective method of detection for ROI in hand it was decided to return to the cell based assays using the RAW 264.7 cell line. But again LPS stimulation at concentrations up to 50 μg/mL was unable to elicit an oxidative response from RAW cells, even when a new batch of LPS was used. It was at this stage that the morphology of the RAW 264.7 cells was investigated more closely. Cells used up to this stage had been grown on bacterial plates, which doesn't allow for the cells to attach to the surface leading to a rounded phenotype and the RAW 264.7 cells behave like a suspension cell line. However when subsequently grown on tissue culture plastic it was noticed that these cells did not revert to the adherent, dendritic phenotype, which was displayed by RAW 264.7 cells freshly obtained from the American Type Culture Collection (ATCC). In order to rule out the possibility that a certain cell population had been preselected by the growth on bacterial plastic, which were incapable of macrophage activation, further work was performed with the newly obtained cell line. However despite these changes no ROI could be elicited on stimulation with increasing concentrations of LPS and MAF (Figure 4.13). As a result it had to be concluded that LPS is unable to serve as a positive control in this *in vitro* macrophage activation assay. This is consistent with the fact that only co-treatment with interferon-γ was able to stimulate •NO release from RAW 264.7 cells when elicited with LPS.[119] Maybe similar co-treatment is required for release of ROI on LPS stimulation from this cell line.

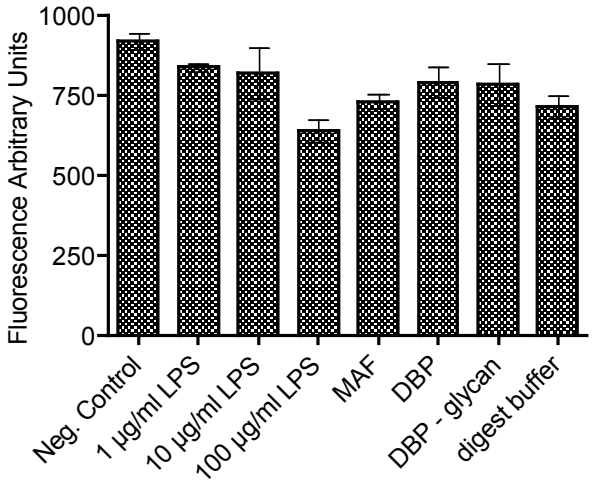


**Figure 4.13** Newly obtained RAW 264.7 cells from ATCC were treated with LPS (1-100 μg/mL) and MAF (1 ng/mL). Negative control with incubation buffer. Further controls DBP, fully deglycosylated DBP and the digestion buffer to create MAF. Incubation time for LPS and MAF 3h. Commercial hydrogen peroxide kit used; 30 min of development time.

To conclude, for the macrophage activation assay the following factors were varied: incubation time (30 min to 24 h), ROI detection method (DHF-DA or hydrogen peroxide detection kit), incubation buffer (PBS or Ringer buffer) and growth method of RAW 264.7 cells (bacterial plates or tissue culture plastic). But with no variation allowing for an oxidative burst on MAF treatment to be detected from RAW 264.7 cells, the focus shifted towards structural elucidation of the nature and quantity of glycosylation present on the precursor DBP.

As outlined in the introduction, in recent times the advances in MALDI mass spectrometry have allowed for more detailed analysis of proteins and their glycosylation and hence this technique was chosen to analyze the glycosylation state of commercial DBP. Several attempts at obtaining a spectrum of the whole protein without broadening were unsuccessful and hence a digestion with an endoproteinase was performed in order to obtain peptide fragments, which were analysed more readily. Following the procedure outlined in Borges et al. the protein was subjected to the endoproteinase Arg-C, which cleaves peptide bonds specifically at the C-terminal end of arginine residues and the resulting peptides were evaluated by mass spectrometry.[77] The MALDI image of Arg-C digested DBP from Aldrich confirmed it to be

derived from a pooled plasma sample containing protein of all three major allels of DBP: GC1F, GC1S and GC2 (Figure 4.14). However unlike the reports in the literature which indicate the GC1 isoforms to carry a trisaccharide, no trace of such glycosylation could be found in our studies.[77, 120] A mass shift corresponding to either a disaccharide or trisaccharide being present on the peptide wasn't detectable in any of the Arg-C digests of DBP, and it had to be concluded that the glycan might have been removed in the commercial purification method, similar to the complications faced in the purification of DBP by Joergensen et al.[72] The glycan is crucial for macrophage activation as has been shown by *in vitro* deactivation of MAF with α-*N*-acetyl-galactosaminidase using cancer patient blood plasma[25] and chicken liver derived enzyme[31] and hence a possible explanation for the inability to activate RAW 264.7 cells in our assay system was found.

With both the activity data and the evaluation by MALDI-MS casting doubt on the presence of the glycan on the commercially obtained DBP two new project goals were defined to be performed by students under my supervision: direct isolation of DBP from human plasma and development for a quantitative quality control methodology for glycan presence on DBP. An affinity column was synthesised based on the commercially more viable vitamin $D_3$ in adaptation from literature procedures, which use 25-hydroxy-vitamin $D_3$.[121] With this column, in combination with gel electrophoresis, it was possible to isolate DBP from human blood plasma. A method of *O*-glycan release[122] in combination with fluorescent labeling for HPLC analysis had been developed by a coworker,[123] which allowed for the identification of the required glycan on DBP in comparison to fetuin.[61] This methodology furthermore confirmed the previous MALDI-MS results, that no glycan is present on commercial DBP. Using the in house purified DBP it was possible to elicit an oxidative response from RAW 264.7 cells on MAF generation. Work on the isolation of α-*N*-acetyl-galactosaminidase from cancer serum, investigation of its

deactivating effect on MAF and its inhibition using iminosugars is currently being explored by our group and will be subject of a future publication.

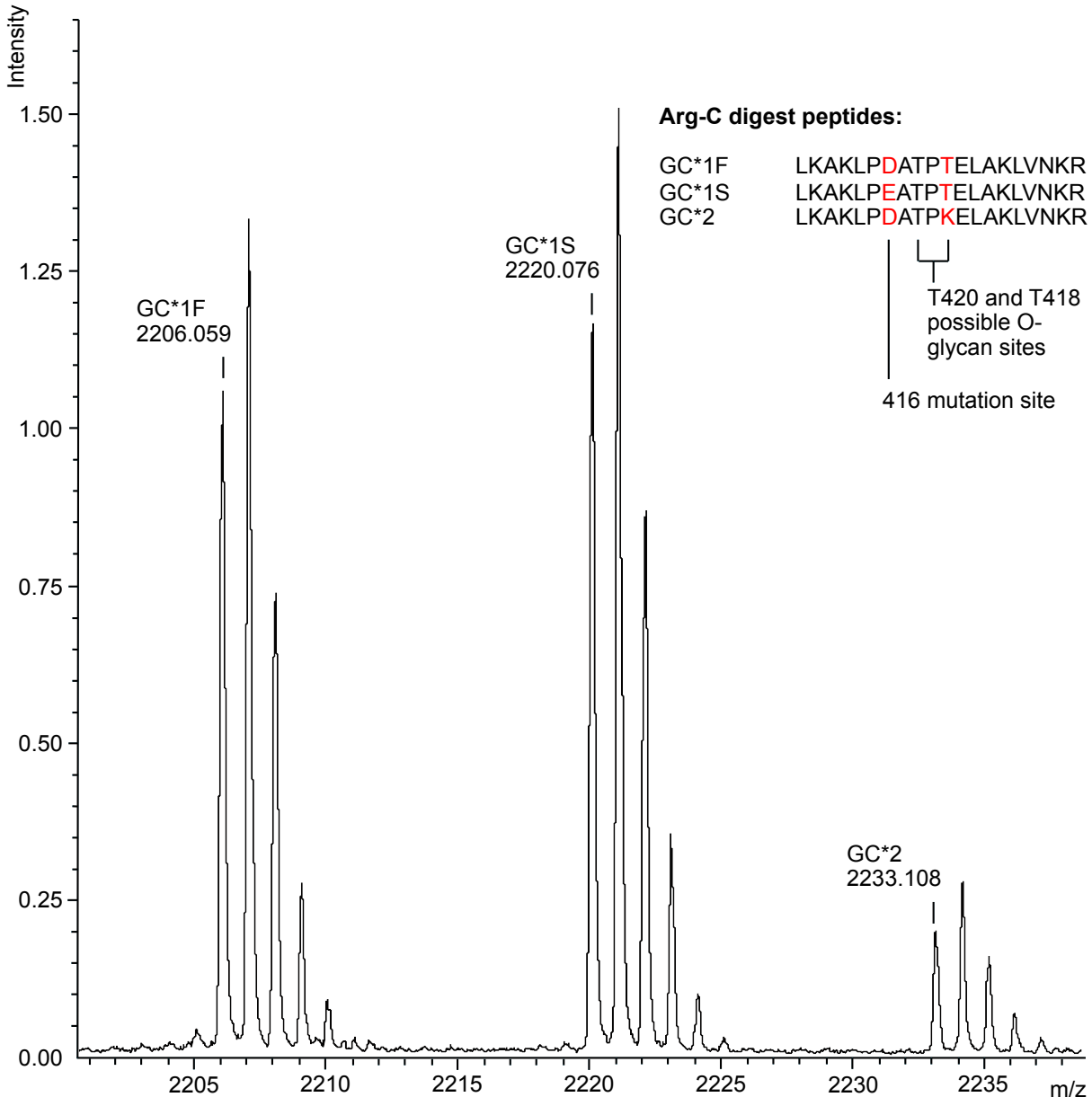


**Figure 4.14** MALDI-TOF mass spectrum of peptides derived from the Arg-C digested DBP (Sigma-Aldrich) obtained from a pooled human plasma source. The monoisotopic peaks are GC*1F 2206.059 (calc. 2206.3281), GC*1S 2220.076 (calc. 2220.3437) and GC*2 2233.108 (calc. 2233.3754). Peptide sequences are indicated in figure insert.

## 4.3 Iminosugars in a cellular environment

As a general principle in medicinal chemistry for drug discovery, once an inhibitor's potency is established on an enzymatic level, several further stages are required before such a molecule can

reach the clinic. This usually involves cell line based assays followed by animal trials. Hence in order to further explore the usefulness of iminosugars in an anti-cancer setting we were interested in the effect of these compounds in a cellular environment.

An HPLC based technique of monitoring free oligosaccharide (FOS) levels has been developed by the group, which allows for the intracellular inhibition of glycosidases to be quantified. By comparing enzymatic inhibition data with cellular inhibition data conclusions over the fate of an iminosugar in a cellular context can be drawn. Especially should the observed inhibitions not correlate, then other factors besides the absolute strength of inhibition must be of importance, like cell or organell penetration.

This concept was applied successfully to *N*-alkyl derivatives of the potent α-*N*-acetyl-galactosaminidase inhibitor 2-acetamido-1,2-dideoxy-D-*galacto*-nojirimycin (DGJNAc) **239** and similar derivatives of the most potent 5-ring β-*N*-acetyl-hexosaminidase inhibitor **68** introduced in chapter 2.

### 4.3.1 Introduction to the free oligosaccharide (FOS) analysis

The FOS assay was originally developed in a study investigating the use of the β-*N*-acetyl-hexosaminidase inhibitor[124] 2-acetamide-1,4-imino-1,2,4-trideoxy-L-arabinitol[125] (LABNAc) as an *in vitro* cellular model of suppressed β-*N*-acetyl-hexosaminidase caused lysosomal storage disorders, to allow for the testing of iminosugars as substrate reduction therapy treatments.[126] The general concept of the assay can be broken down into the five steps as shown in Figure 4.15. First RAW 264.7 cells are grown in the presence of LABNAc leading to inhibition of lysosomal β-*N*-acetyl-hexosamindase enzyme, which causes incomplete degradation of *N*-linked glycoprotein derived FOS. These GlcNAc-terminated species accumulate in the lysosome, causing the observed phenotype and a snapshot of this population of FOSs is conserved, when the cells are homogenised in the second stage. As the third step, in order to separate the cellular

debris from the oligosaccharides a mixed-bed ion-exchange column is performed.[127] The isolated FOS are then fluorescently labeled using anthranilic acid (2-AA) *via* reductive amination in the fourth stage in preparation for HPLC analysis as the final step.[128] Using internal controls in the HPLC profiles, which are unchanged on treatment, the relative degree of intracellular (and intra-lysosomal) inhibition of β-*N*-acetyl-hexosaminidase inhibition can be determined based on integration data of the newly appearing peaks.

In this study the murine RAW 264.7 cells were substituted with HL60 cells, a human leukemia cell line, in order to resemble the target cell for anti-cancer treatment more closely.

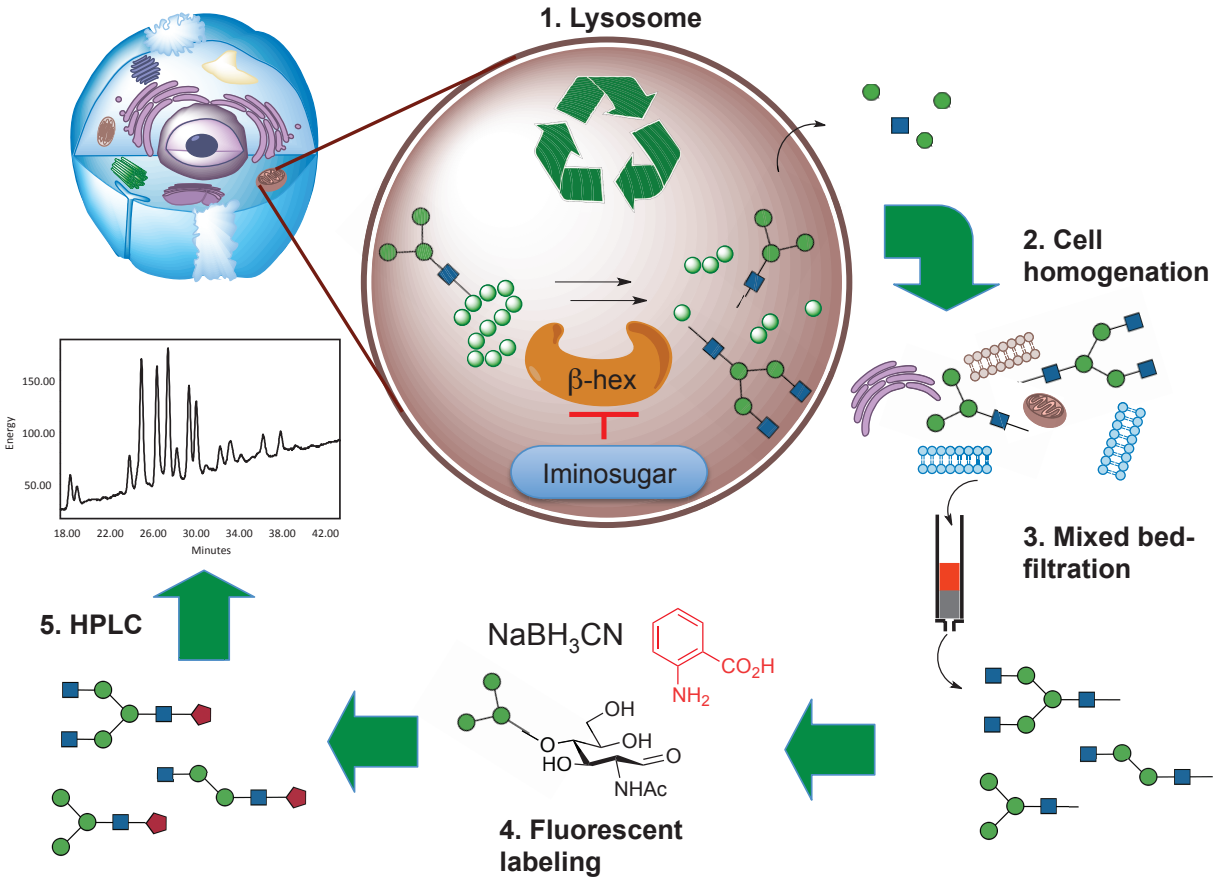


**Figure 4.15** Free oligosaccharide analysis in five stages.

### 4.3.2 The α-*N*-acetyl-galactosaminidase inhibitor DGJNAc and its derivatisation

Although β-*N*-acetyl-hexosaminidase inhibitors are relatively abundant, as shown also by the amount of inhibitors identified in Chapter 2 and 3, inhibitors of α-*N*-acetyl-galactosaminidase

are comparatively rare. An investigation of the literature shows that reported inhibitors are limited to piperidine **237**,[129] the already mentioned (-)-steviamine **233**[111] and pyrrolidine **238** (Figure 4.16).[130] However none of these compounds were as potent as 2-acetamido-1,2-dideoxy-D-*galacto*-nojirimycin (DGJNAc) **239**, which was recently synthesised by a coworker.[131] Like many other iminosugars[132] DGJNAc **239** is derived from D-glucuronolactone and starting from the acetonide protected analog[133] was produced over 19 steps in 20% overall yield. With respect to D-glucuronolactone, nitrogen was introduced with inversion at C5 and the hydroxyl at C3 was inverted followed by ring closure with nitrogen between C2 and C6 both with inversion. The robust synthesis sequence has since been scaled up to 1 g of final compound. Previous synthesis of DGJNAc **239** were performed starting from deoxynojirimycin,[134] or with a racemic mixture as final product.[135]

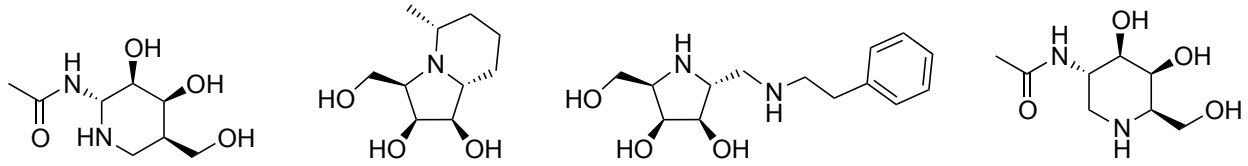


**Figure 4.16** Literature examples of α-*N*-acetyl-galactosaminidase inhibitiors.

Very recently the potential of DGJNAc **239** as a pharmacological chaperone for the treatment of Schindler/Kanzaki disease has been shown.[136] As Schindler/Kanzaki disease is based on a deficiency in lysosomal α-*N*-acetyl-galactosamindase activity,[137] the X-ray crystal structure of the human protein was solved at a 1.4 Å resolution (PDB entry: 4DO4). This included co-crystallisation with DGJNAc **239** showing the snug fit of the inhibitor in the active site (Figure 4.17). Although the question of the source of the extra cellular secreted α-*N*-acetyl-galactosaminidase in cancer has not been answered, it is feasible to be the result of lysosomal exocytosis. Especially as exocytosis of lysosomes for secretion of degradative enzymes[138] and more specifically glycosidases[139] has been shown previously. Should this indeed be the case then future anti-cancer inhibitor design could be based on this crystal structure.

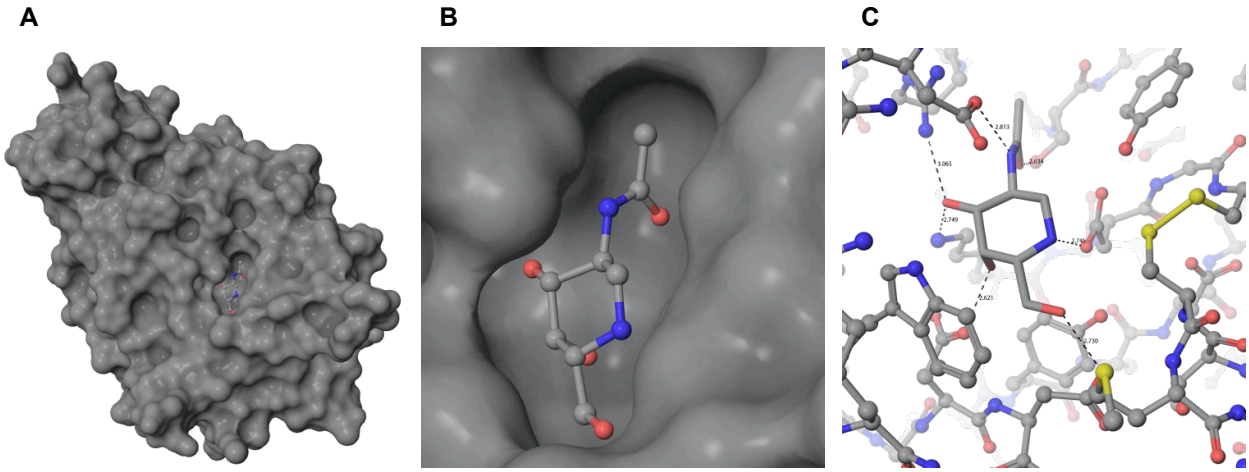


**Figure 4.17** Human α-*N*-acetyl-galactosaminidase with DGJNAc **239** bound in active site according to PDB entry 4DO4.[136] A) Overview of monomer of enzyme with surface modeled. B) Detailed view of actives site including DGJNAc **239**. C) Interactions indicated of ligand with active site.

As can be gleaned from the discourse on Schindler/Kanzaki disease lysosomal α-*N*-acetyl-galactosaminidase activity is required for natural cellular catabolism. This should be kept in mind for the design of a possible anticancer agent and inhibition of this "natural" enzyme activity should be avoided, as a lysosomal storage disorder like phenotype would otherwise be generated. One way of achieving this goal would be to make use of the fact that the enzymes are present in separate biological compartments (lysosome vs. extra cellular space/blood plasma). It was hence of interest, what effect derivatisation would have on the biodistribution and activity levels of DGJNAc **239** with the goal of creating an inhibitor, which is able to target the secreted α-*N*-acetyl-galactosaminidase. In order to determine the degree of lysosomal penetration of the α-*N*-acetyl-galactosaminidase inhibitors, use of their concomitant inhibition of β-*N*-acetyl-hexosaminidase would be made, as this enzyme is equally located in the lysosome. The inhibition of β-*N*-acetyl-hexsoaminidase would hence serve as a readout for the degree of cellular interference caused by the iminosugars and similarly represent an *in vitro* way of estimating side effects of this set of compounds.

#### 4.3.2.1 Synthesis of DGJNAc derivatives

Hence in order to change the biological properties of DGJNAc **239** the endocyclic nitrogen was derivatised. *N*-alkylation on the ring nitrogen is a common way of tuning the biological acitivity of iminosugars,[140] however rather then introducing the alkylation early during synthesis, a late stage modification of DGJNAc using reductive amination with the corresponding aldehyde was chosen (Scheme 4.2). Using palladium catalyzed hydrogenation conditions it was possible to obtain the *N*-methyl **240**, *N*-ethyl **241** and *N*-hydroxyethyl **244** derivatives, while sodium cyanoborohydride reductions were chosen to get access to the *N*-butyl **242** and *N*-benzyl **243** compounds. With exception of the benzylation all modifications proceeded in excellent yields.

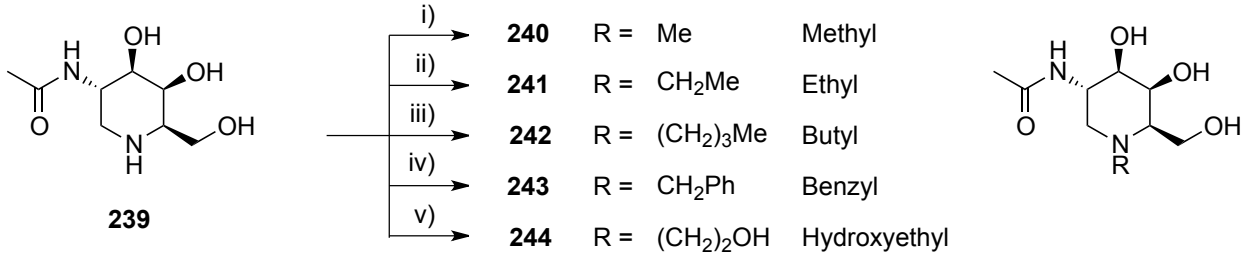


**Scheme 4.2** DGJNAc derivatisation *via* reductive amination. Reagents and conditions: i) HCHO, $H_2$, 10% Pd/C, 1,4-dioxane, $H_2O$, RT, 18 h, 100%; ii) MeCHO, $H_2$, 10% Pd/C, EtOH, RT, 4.5 h, 100%; iii) $MeCH_2CH_2CHO$, $NaBH_3CN$, AcOH, EtOH, RT, 2.5 h, 100%; iv) PhCHO, $NaBH_3CN$, AcOH, EtOH, RT, 3 h, 68%; v) $HOCH_2CHO$, $H_2$, 10% Pd/C, 1,4-dioxane, $H_2O$, RT, 16 h, 95%.

#### 4.3.2.2 Enzymatic inhibition evaluation of DGJNAc derivatives

With the derivatives in hand, the influence of *N*-alkylation on the enzymatic inhibition profiles of these compounds could be probed. The five derivatives **240-244** along with the parent compound DGJNAc **239** were hence subjected to a panel of α-*N*-acetyl-galactosaminidases and β-*N*-acetyl-hexosaminidases from various species by a collaborator Professor Atsushi Kato (University of Toyama)[141] and the results are shown in Table 4.1 and Table 4.2. Additionally the $K_i$s against α-*N*-acetyl-galactosaminidase (*Charonia lampas*) were obtained in house and are included in the tables, with their corresponding Lineweaver-Burk analyses shown in Figure 4.18-Figure 4.23.

**Table 4.1 DGJNAc and derivatives giving 50% inhibition of various glycosidases; $IC_{50}$ given in μM.**

| | 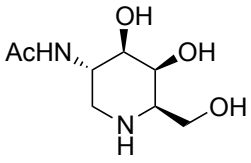 | 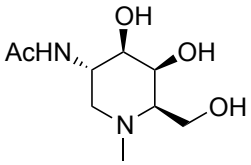 | 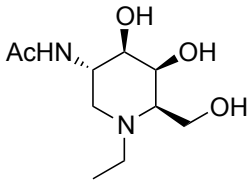 |
|---|---|---|---|
| Enzyme | **239** DGJNAc | **240** *N*-Me DGJNAc | **241** *N*-Et DGJNAc |
| β-*N*-Acetyl-glucosaminidase | | | |
| Human placenta | 8.3 | 5.7 | 7.3 |
| Bovine kidney | 4.2 | 2.1 | 3.1 |
| *Aspergillus oryzae* | NI[§] (8.8%) | NI[§] (22.1%) | NI[§] (26.5%) |
| HL60 | 7.1 | 5.4 | 7.9 |
| Jack Beans | 1.8 | 1.5 | 3.4 |
| α-*N*-Acetyl-galactosaminidase | | | |
| Chicken liver | 0.32 | 107 | 5.6 |
| *Charonia lampas* | [0.17][$] | [0.97][$] | [8.9][$] |
| β-*N*-Acetyl-galactosaminidase | | | |
| *Aspergillus oryzae* | NI[§] (9.6%) | NI[§] (29.4%) | NI[§] (26.3%) |
| HL 60 | 23 | 26 | 44 |

§ No inhibition at 1000 μM (% inhibition); $ [$K_i$ in μM]; Assay details see Section 2.6.4 (p. 63).

Based on the enzymatic data DGJNAc **239** and its derivatives **240-244** were all strong inhibitors (≤ 10 μM) of β-*N*-acetyl-hexosaminidase, with exception of the enzymes derived from *Aspergillus oryzae*. More specifically β-*N*-acetyl-glucosaminidase inhibition seems to be largely unaltered by ring-alkylation. An exception to this trend is the *N*-benzyl derivative **243**, which displays a ten-fold drop in activity. Therefore inhibition of all other derivatives against this enzyme derived from HL60 cells is within 1-10 μM. Against β-*N*-acetyl-galactosaminidase the same trend is observed and bar the *N*-benzyl compound **243** all derivatives show similar levels of inhibition to the parent compound **239**. However the inhibition activity level overall is lowered roughly one order of magnitude for all compounds in comparison to their β-*N*-acetyl-glucosaminidase inhibition.

**Table 4.2 DGJNAc and derivatives giving 50% inhibition of various glycosidases; $IC_{50}$ given in μM.**

| | 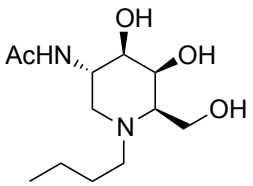 | 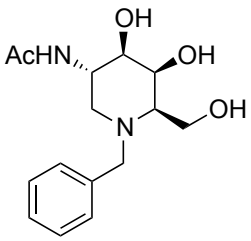 | 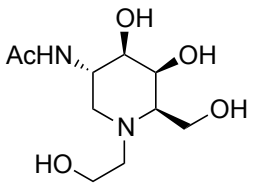 |
|---|---|---|---|
| Enzyme | **242** *N*-Bu DGJNAc | **243** *N*-Bn DGJNAc | **244** *N*-EtOH DGJNAc |
| β-*N*-Acetyl-glucosaminidase | | | |
| Human placenta | 2.7 | 45 | 8.2 |
| Bovine kidney | 1.2 | 40 | 3.7 |
| *Aspergillus oryzae* | NI[§] (22.6%) | NI[§] (11.4%) | NI[§] (46.9%) |
| HL60 | 1.7 | 52 | 8.3 |
| Jack Beans | 2.7 | 22 | 1.9 |
| α-*N*-Acetyl-galactosaminidase | | | |
| Chicken liver | 166 | 11 | 6.3 |
| *Charonia lampas* | [120][$] | [9.6][$] | [3.3][$] |
| β-*N*-Acetyl-galactosaminidase | | | |
| *Aspergillus oryzae* | NI[§] (29.8%) | NI[§] (5.8%) | 926 |
| HL 60 | 14 | 187 | 35 |

§ No inhibition at 1000 μM (% inhibition); $ [$K_i$ in μM]; Assay details see Section 2.6.4 (p. 63).

Looking at the $K_i$ values for α-*N*-acetyl-galactosaminidase (*Charonia lampas*) a clear trend can be noticed on going from *N*-H **239** → *N*-methyl **240** → *N*-ethyl **241** → *N*-butyl **242**. For each iteration one order of magnitude of inhibitory activity is lost seeming to indicate that increasing bulk on the ring nitrogen is not well tolerated by the enzyme. The inhibitor strength of *N*-hydroxyethyl **244** is intermediate between the *N*-methyl and *N*-ethyl inhibitors as one might expect in terms of the bulk argument, however by the same logic *N*-benzyl **243** compound would appear to be too potent. Therefore additional factors must influence the inhibition activity of this compound. With exception of *N*-methyl **240** the same trends are observed for the inhibition of α-*N*-acetyl-galactosaminidase derived from chicken liver.

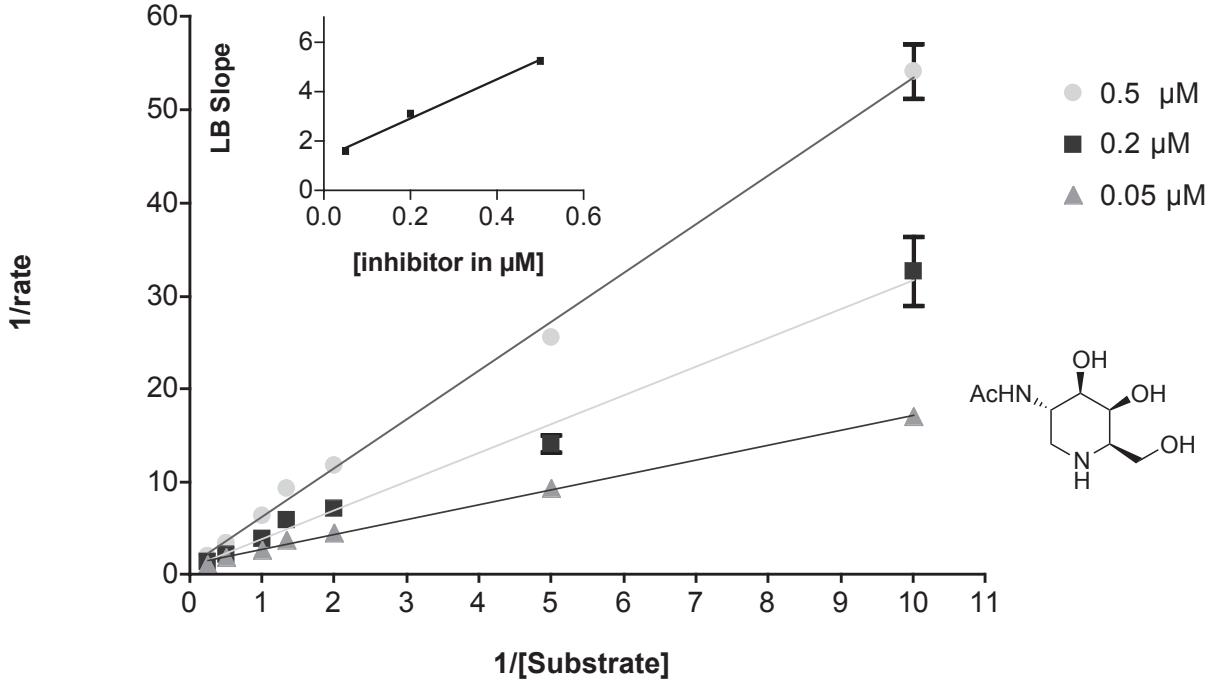


**Figure 4.18** Lineweaver Burk (LB) plot of DGJNAc **239** against α-*N*-acetyl-galactosaminidase derived from *Charonia lampas*; $K_i$ = 167 nM based on X-intercept of insert graph (LB slope vs Inhibitor concentration, $R^2$ = 0.9922).

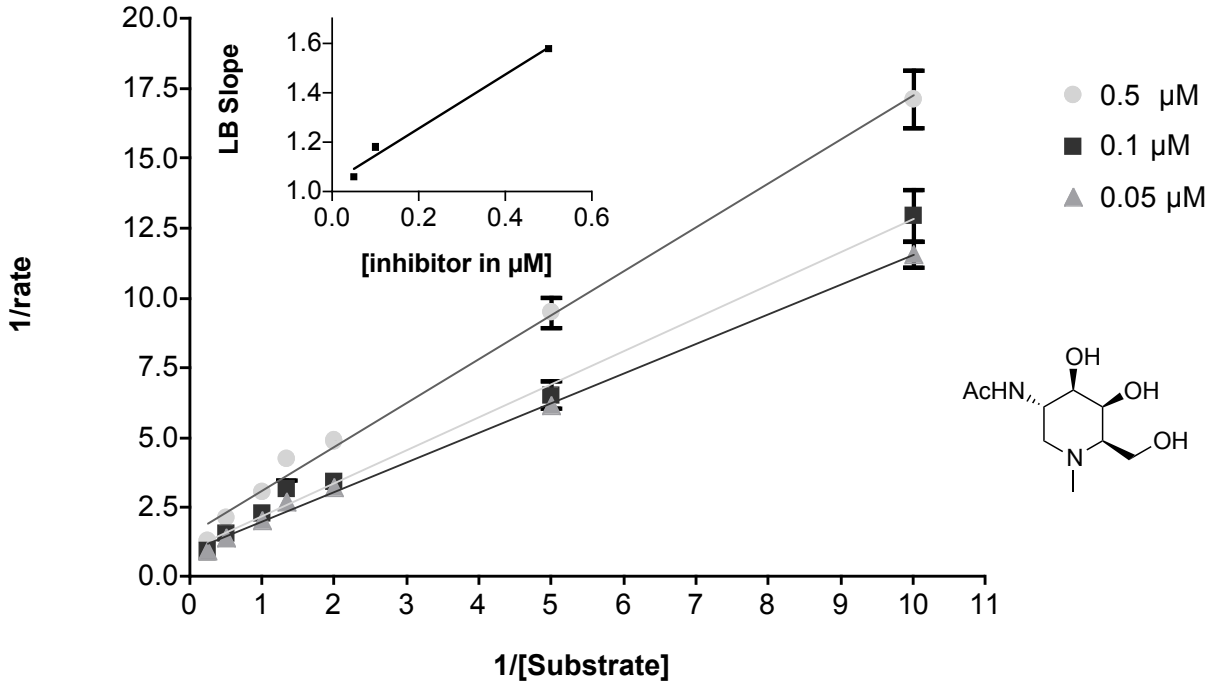


**Figure 4.19** Lineweaver Burk (LB) plot of *N*-Me DGJNAc **240** against α-*N*-acetyl-galactosaminidase derived from *Charonia lampas*; $K_i$ = 0.95 μM based on X-intercept of insert graph (LB slope vs Inhibitor concentration, $R^2$ = 0.9852).

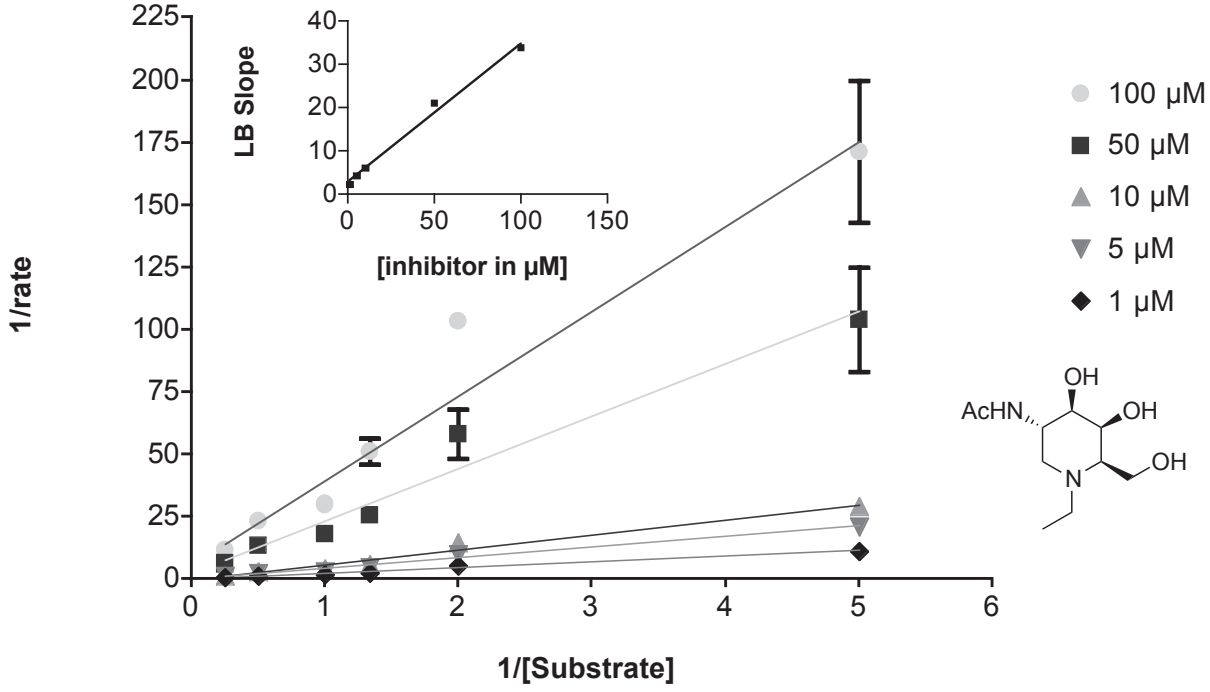


**Figure 4.20** Lineweaver Burk (LB) plot of *N*-Et DGJNAc **241** against α-*N*-acetyl-galactosaminidase derived from *Charonia lampas*; $K_i$ = 8.87 μM based on X-intercept of insert graph (LB slope vs Inhibitor concentration, $R^2$ = 0.9915).

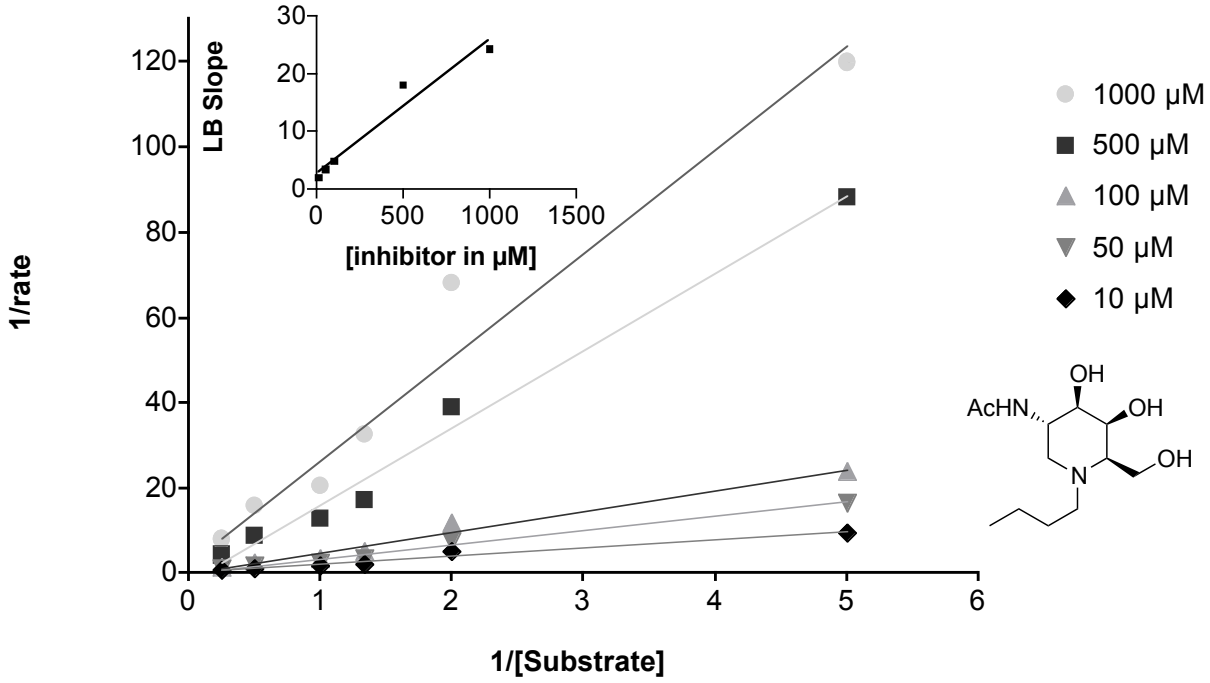


**Figure 4.21** Lineweaver Burk (LB) plot of *N*-Bu DGJNAc **242** against α-*N*-acetyl-galactosaminidase derived from *Charonia lampas*; $K_i$ = 119.5 μM based on X-intercept of insert graph (LB slope vs Inhibitor concentration, $R^2$ = 0.9546).

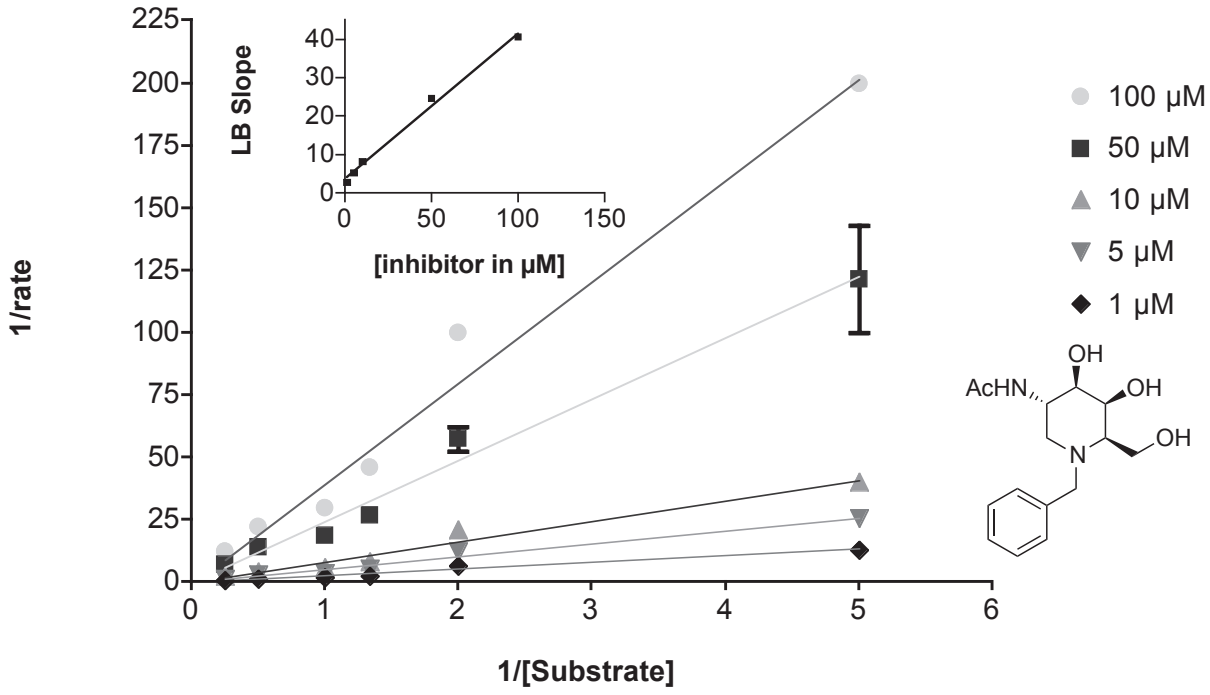


**Figure 4.22** Lineweaver Burk (LB) plot of *N*-Bn DGJNAc **243** against α-*N*-acetyl-galactosaminidase derived from *Charonia lampas*; $K_i$ = 9.57 μM based on X-intercept of insert graph (LB slope vs Inhibitor concentration, $R^2$ = 0.9930).

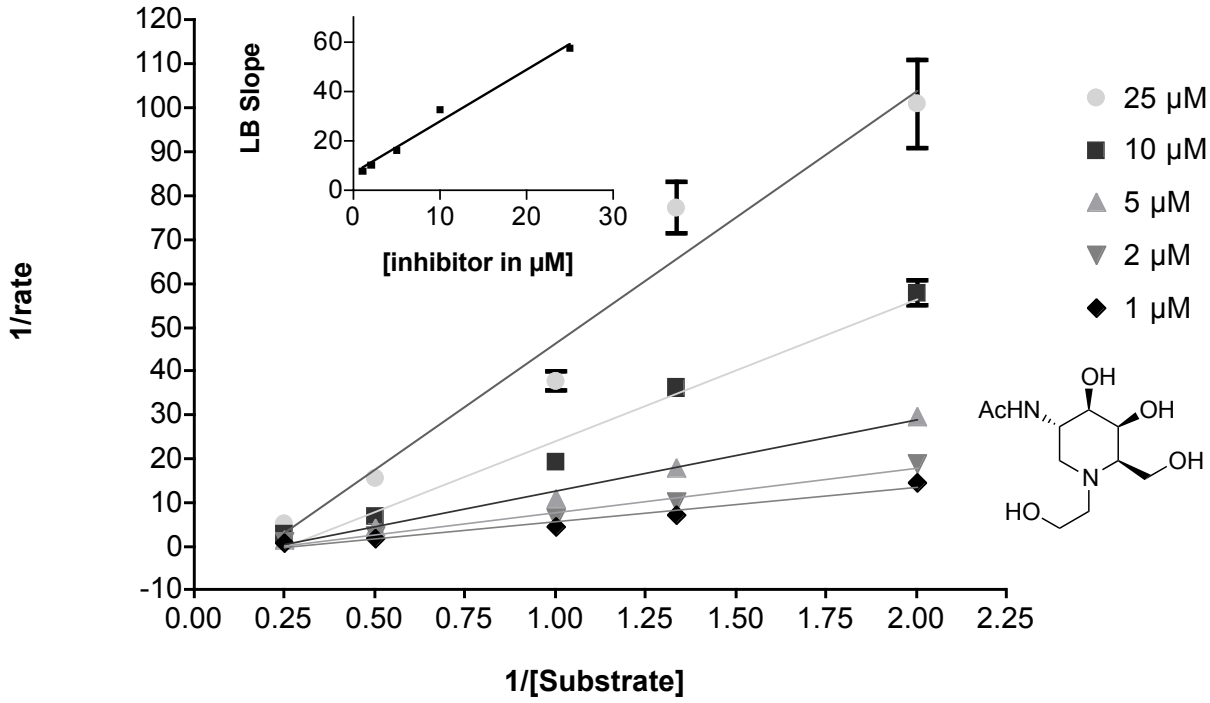


**Figure 4.23** Lineweaver Burk (LB) plot of *N*-EtOH DGJNAc **244** against α-*N*-acetyl-galactosaminidase derived from *Charonia lampas*; $K_i$ = 3.29 μM based on X-intercept of insert graph (LB slope vs Inhibitor concentration, $R^2$ = 0.9835).

### 4.3.3 FOS analysis in HL60 cells with DGJNAc and derivatives

As can be seen from the enzymatic data above iminosugars **239-242**, **244** were very comparable in terms of their inhibition of β-*N*-acetyl-hexosaminidase derived from HL60 cells. It was therefore of interest if the FOS analysis using the same cell line, would reveal the same uniformity in the inhibition for the enzyme located within the lysosome.

HL60 cells were cultured for 24 h in the presence of DGJNAc **239** along with four of its derivatives **240-242**, **244** at three concentrations of 500, 100 and 50 μM. FOS were then extracted from the corresponding cell homogenates and HPLC profiles of untreated in comparison to 500 μM DGJNAc **239** treated cells are shown in Figure 4.24. As can be inferred from this comparison, inhibition of lysosomal glycosidases has caused the incomplete degradation of glycans, which appear as additional peaks in the treated spectrum.

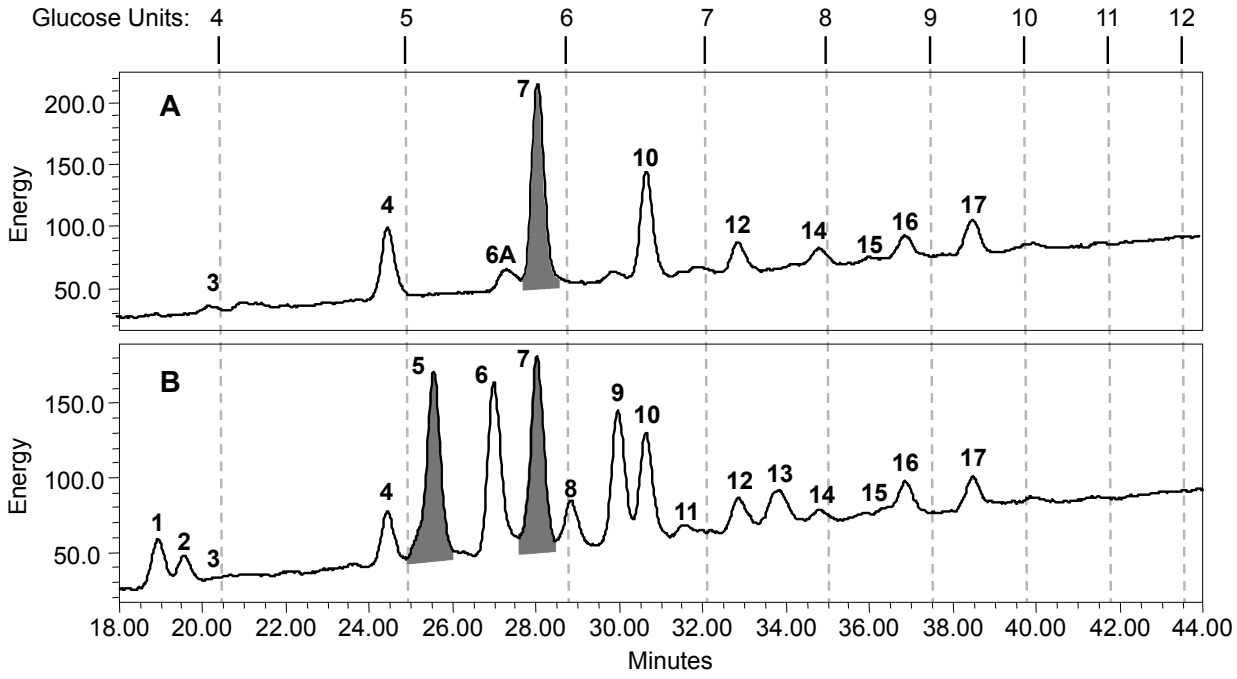


**Figure 4.24** HL60 cells were homogenized and the free oligosaccharides (FOS) extracted as described in the experimental section. After 2-AA labeling the FOS were separated using HPLC. A) Profile of untreated cells. B) Cells treated with 500 μM DGJNAc **239**. Peaks have been numbered and their structure are given in Table 4.3. The ratio of the areas of peak 5 and peak 7 were used to gauge β-*N*-acetyl-hexosaminidase inhibition in Figure 4.27.

The appearance of the new peaks could be shown to be dose dependent and high inter- and intra-experimental reproducibility was given as indicated by the triplicate overlay in Figure 4.25. Digestion with jack bean β-*N*-acetyl-glucosaminidase revealed the new glycans to contain GlcNAc residues at the non-reducing terminus (Figure 4.26) and removal of all non-reducing GlcNAc residues exposed the underlying core mannose structures. This data in combination with a comparison of peak retention times in glucose units (GUs) to literature data,[126] allowed for a structure to be assigned to all the new glycans (Table 4.3). On the grounds of the same considerations structures of peaks 8, 11 and 13 were proposed.

As indicated in Figure 4.24 B the ratio of integration data on the strongest newly appeared peak 5 ($GlcNAc_2Man_3GlcNAc_1$) was used in comparison to the unchanged control peak 7 ($Man_5GlcNAc_1$) to estimate the level of lysosomal inhibition of β-*N*-acetyl-hexosaminidase. Based on this ratio a direct comparison of DGJNAc **239** and its derivatives at 50 μM is shown in Figure 4.27.

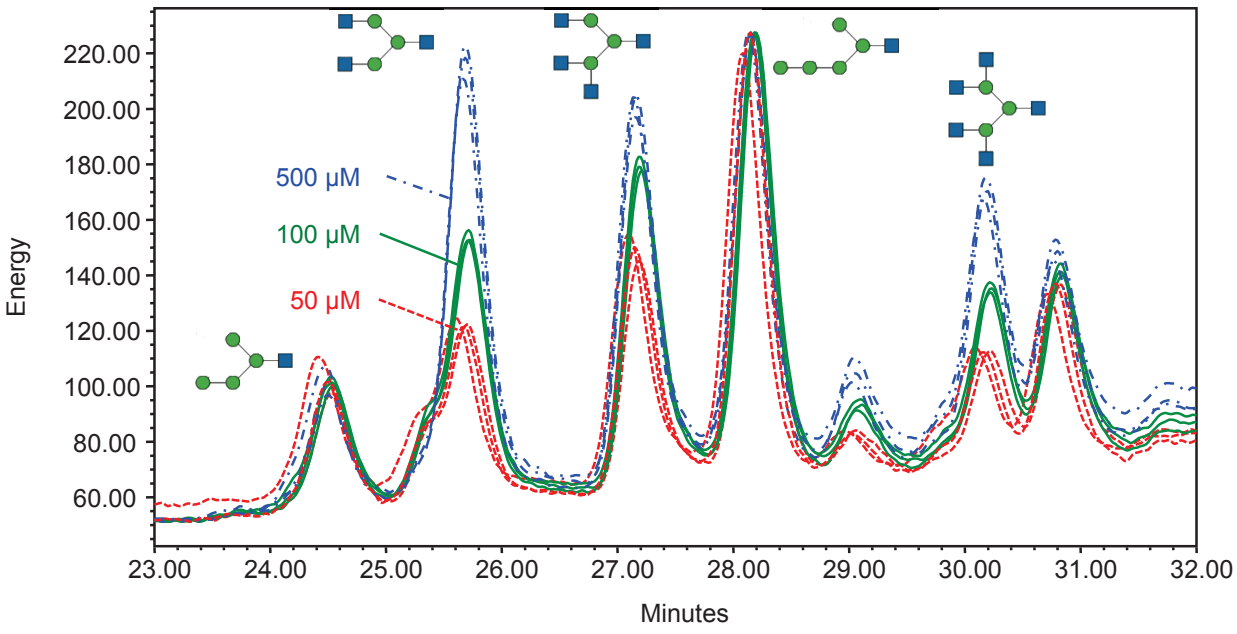


**Figure 4.25** Dose dependence of FOS analysis using DGJNAc **239** in triplication. Nomenclature: ● Mannose; ■ *N*-Acetyl-glucosamine.

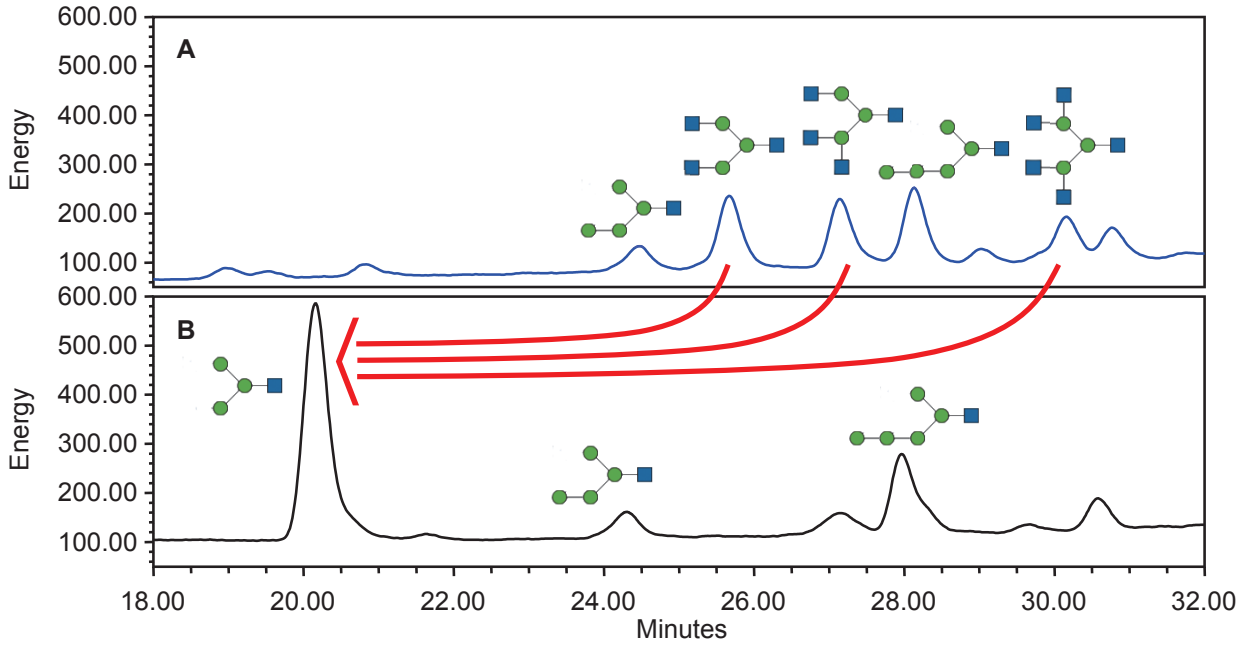


**Figure 4.26** Digestion of FOS with β-*N*-acetyl-hexosaminidase (Jack bean). A) profile before and; B) profile after digest. Nomenclature: ● Mannose; ■ *N*-Acetyl-glucosamine.

**Table 4.3** Structures, retention time in glucose units (GUs) and relative intensity in percent of FOS peaks isolated from a control experiment and 500 μM DGJNAc-treated HL60 cells. Peak IDs labeled according to Figure 4.24. Intensity measurements are the mean value of three independent measurements (±S.D.). The species were assigned according literature values.[126] Labels are as follows: ◇ Glucose; ● Mannose; ⬟ 2-Aminobenzoic acid; ■ *N*-Acetyl-glucosamine; ✻ Proposed structure.

| ID | Untreated GU | Treated GU | Structure name | Structure | Untreated cells [%] | Treated cells [%] |
|---|---|---|---|---|---|---|
| 1 | - | 3.77 | $GlcNAc_1Man_2GlcNAc_1$ |  | - | 2.45 ± 0.10 |
| 2 | - | 3.88 | $GlcNAc_2Man_2GlcNAc_1$ | 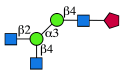 | - | 1.62 ± 0.21 |
| 3 | 4.13 | 4.16 | $Man_3GlcNAc_1$ |  | 3.44 ± 1.16 | 1.66 ± 0.88 |
| 4 | 4.95 | 4.99 | $Man_4GlcNAc_1$ | 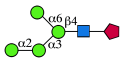 | 14.37 ± 1.67 | 5.20 ± 0.93 |
| 5 | - | **5.28** | $GlcNAc_2Man_3GlcNAc_1$ | 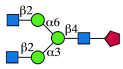 | - | **17.98 ± 0.68** |
| 6 | - | 5.65 | $GlcNAc_3Man_3GlcNAc_1$ | 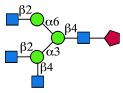 | - | 15.08 ± 0.11 |
| 6A | 5.62 | - | $Man_5GlcNAc_1$ | 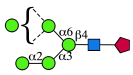 | 4.22 ± 0.45 | - |
| 7 | **5.87** | **5.91** | $Man_5GlcNAc_1$ | 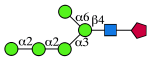 | **38.76 ± 1.06** | **16.81 ± 0.37** |
| 8 | - | 6.16 | $GlcNAc_4Man_3GlcNAc_1$ | 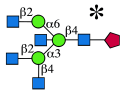 | - | 2.92 ± 0.29 |
| 9 | - | 6.49 | $GlcNAc_4Man_3GlcNAc_1$ | 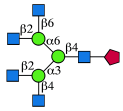 | - | 10.00 ± 0.24 |
| 10 | 6.62 | 6.67 | $Glc_1Man_5GlcNAc_1$ | 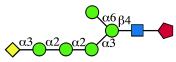 | 14.92 ± 0.13 | 7.37 ± 0.36 |
| 11 | - | 6.96 | $GlcNAc_5Man_3GlcNAc_1$ | 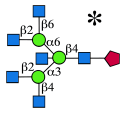 | - | 1.35 ± 0.16 |
| 12 | 7.31 | 7.37 | $Glc_2Man_5GlcNAc_1$ | 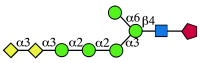 | 6.17 ± 0.35 | 3.24 ± 0.57 |
| 13 | - | 7.73 | $GlcNAc_5Man_3GlcNAc_1$ | 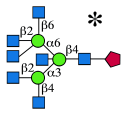 | - | 4.51 ± 0.12 |
| 14 | 7.99 | 8.04 | $Man_7GlcNAc_2$ | 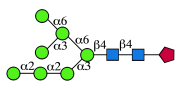 | 2.25 ± 0.81 | 0.88 ± 0.20 |
| 15 | 8.47 | 8.42 | $Man_8GlcNAc_2$ | 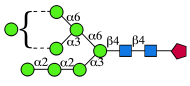 | 1.25 ± 0.12 | 1.03 ± 0.60 |
| 16 | 8.79 | 8.87 | $Man_8GlcNAc_2$ | 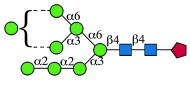 | 5.39 ± 0.58 | 3.88 ± 0.29 |
| 17 | 9.46 | 9.55 | $Man_9GlcNAc_2$ | 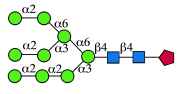 | 9.24 ± 0.54 | 4.05 ± 0.23 |

Despite the *in vitro* enzymatic inhibition of all the iminosugars involved being of comparable strength the cellular based FOS assay reveals pronounced differences between the derivatives in terms of their ability to inhibit lysosomal β-*N*-acetyl-hexosaminidase (Figure 4.27). *N*-Bu DGJNAc **242** displays twice the inhibition strength of the parent compound, with *N*-hydroxyethyl DGJNAc **244** showing a significantly decreased activity in comparison to the same compound. The methyl and ethyl side chains seem to have little influence on the inhibition on a cellular level. Based on these results it can be concluded that increasing alkyl side chain length allows for more effective cell or organelle penetration, while addition of hydrophilic side chains restricts the inhibitor to extra cellular space preferentially. As a result the *N*-butyl derivative **242** is about 5 fold more effective at reaching and hence inhibiting the lysosomal β-*N*-acetyl-hexosaminidase when compared to the *N*-hydroxyethyl variant **244**. This observation correlates well with the reports in the literature that *N*-alk(en)yl derivatives ($C_4$, $C_9$, $C_{18}$) of DNJ **4** are taken up by cells in less then one minute.[142] Another positive correlation of these results is noticed with the body compartment distribution of the two iminosugars currently used in the clinic, which are the *N*-butyl (Miglustat) and *N*-hydroxyethyl (Miglitol) derivatives of DNJ **4**. The apparent volume of distribution ($V_D$), which is defined as the volume required to accommodate the total drug content of the body at the concentration present in the plasma, is a pharmacological indicator for restriction of a drug to blood plasma (≤0.05 L/kg), extracellular compartments (≤0.2 L/kg) or total body water (0.5 L/kg).[143] A $V_D$ larger then the total body water indicates drugs which are able to traverse cell membranes well and distribute into fatty tissue as it is the case for Miglustat, which displays a $V_D$ of 1.04-1.31 L/kg (based on a 80 kg individual).[144] With 0.18 L/kg the $V_D$ of the *N*-hydroxyethyl derivative Miglitol is 5.7-7.3-fold lower then for Miglustat, which is consistent with the restriction of the compound to extra cellular space.[145] The results on the variation of cell and organelle penetration of DGJNAc **239** on *N*-alkylations of the endocylic nitrogen have recently been published.[146]

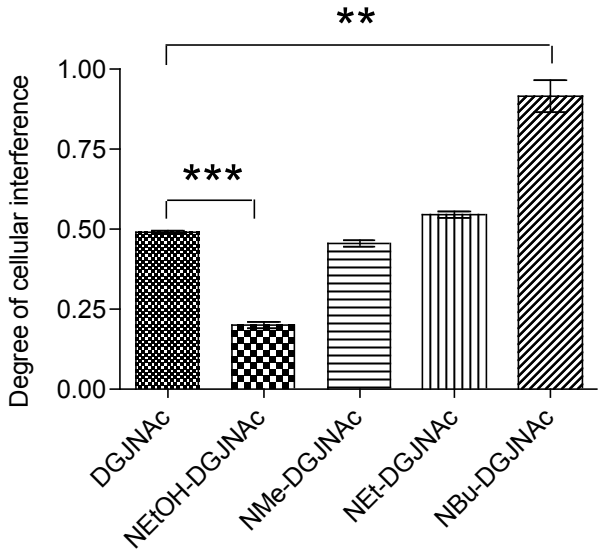


**Figure 4.27** The Ratio of the integration of peak 5 to the control peak 7 is shown for derivatives of DGJNAc **239** (50 μM). With all derivatives having very comparable *in vitro* inhibition of β-*N*-acetyl-hexosaminidase, the variation can be attributed to differences in cell- and organelle-penetration.

### 4.3.4 FOS analysis in HL60 cells with pyrrolidine 68 and derivatives

In order to confirm that this side chain dependent modification of pharmacological properties of DGJNAc derivatives was not unique to this particular parent scaffold, a similar study was performed involving the most potent β-*N*-acetyl-hexosaminidase pyrrolidine inhibitor **68** (Chapter 2) as a parent compound (Table 4.4). Coworkers in the Fleet group were able to successfully synthesis the *N*-butyl **247** and *N*-hydroxyethyl **246** side chain derivatives.[147] Furthermore in order to further expand the range of tested side chains a carboxylic acid derivative **245** was equally generated.[148] The set of four compounds was subjected to the same panel of glycosidases as the DGJNAc derivatives by a collaborator Professor Atsushi Kato (University of Toyama)[141] and the results are listed in Table 4.4. The α-*N*-acetyl-galactosaminidase data (*Charonia lampas*) and the $K_i$s for β-*N*-acetyl-glucosaminidase derived from HL60 cells were performed in house with their Lineweaver-Burk plots given in Figure 4.28-Figure 4.30.

**Table 4.4 Pyrrolidine derivatives giving 50% inhibition of various glycosidases; $IC_{50}$ given in μM.**

| | 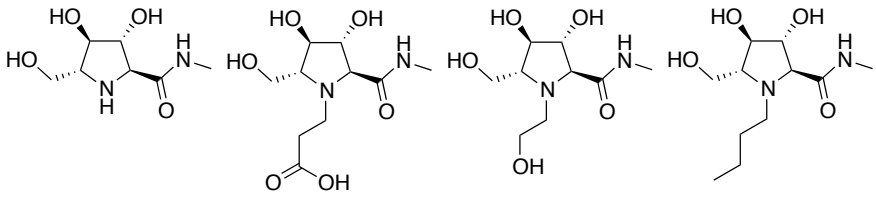 | | | |
|---|---|---|---|---|
| Enzyme | **68** | **245** | **246** | **247** |
| β-*N*-Acetyl-glucosaminidase | | | | |
| Human placenta | 0.20 | 1.9 | 4.8 | ND |
| Bovine kidney | 0.22 | 2.7 | 6.3 | 1.5 |
| Jack beans | 0.033 | 0.41 | 1.8 | 0.35 |
| HL60 | 0.2 [Ki= 0.027] | 1.6 [Ki=1.08] | 4.0 [Ki= 0.72] | 2.50 [Ki=1.31] |
| *Aspergillus oryzae* | 0.30 | 3.4 | 17 | 0.83 |
| α-*N*-Acetyl-galactosaminidase | | | | |
| *Charonia lampas* | NI# (1.1%) | NI§ (15.9%) | NI# (1.6%) | NI# (0%) |
| Chicken liver | NI§ (0%) | NI§ (9.8%) | NI§ (20.8%) | NI§ (7.9%) |
| β-*N*-Acetyl-galactosaminidase | | | | |
| HL60 | 1.0 | 7.9 | ND | ND |
| *Aspergillus oryzae* | 0.35 | 3.7 | 16 | 0.79 |

§ No inhibition at 1000 μM (% inhibition); # No inhibition at 500 μM (% inhibition); $ [$K_i$ in μM].

Just like the parent compound **68** none of the derivatives were inhibitors for α-*N*-acetyl-galactosaminidase. But all five ring compounds were potent inhibitors (≤ 10 μM) of β-*N*-acetyl-hexosaminidase including enzymes derived from *Aspergillus oryzae*. For this particular species the β-*N*-acetyl-galactosaminidase inhibitory activity could be noticed to parallel the β-*N*-acetyl-glucosaminidase activity closely. In terms of the β-*N*-acetyl-glucosaminidase activity from various sources the parent compound **68** displays the strongest level of inhibition, while all derivatisation leads to a 10 fold loss in activity. Therefore it should be noted for the FOS analysis, while the parent compound displays a considerably higher $K_i$ (0.027 μM, Figure 2.10, page 33) against β-*N*-acetylglucosaminidase derived from HL60 cells, all the derivatives **245-247** have very comparable levels of inhibition of around 1 μM (based on $K_i$).

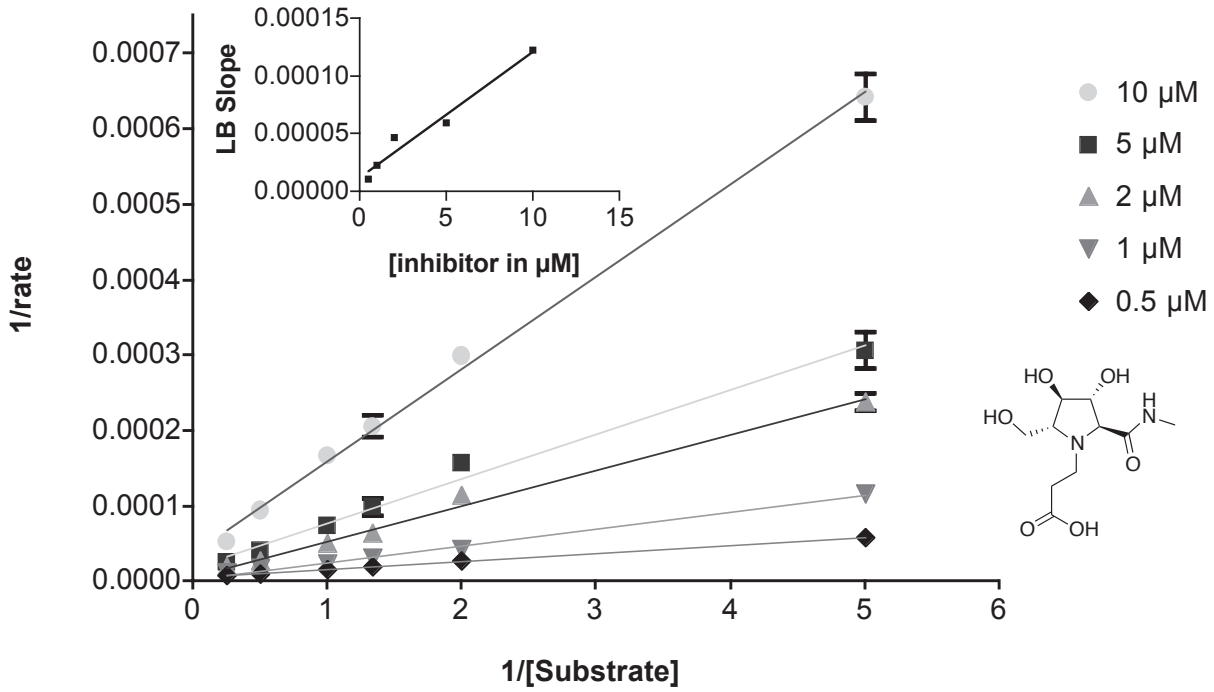


**Figure 4.28** Lineweaver Burk (LB) plot of *N*-EtCOOH pyrrolidine **245** against β-*N*-acetyl-hexosaminidase derived from HL60 cell homogenate; $K_i$ = 1.08 μM based on X-intercept of insert graph (LB slope vs Inhibitor concentration, $R^2$ = 0.9637).

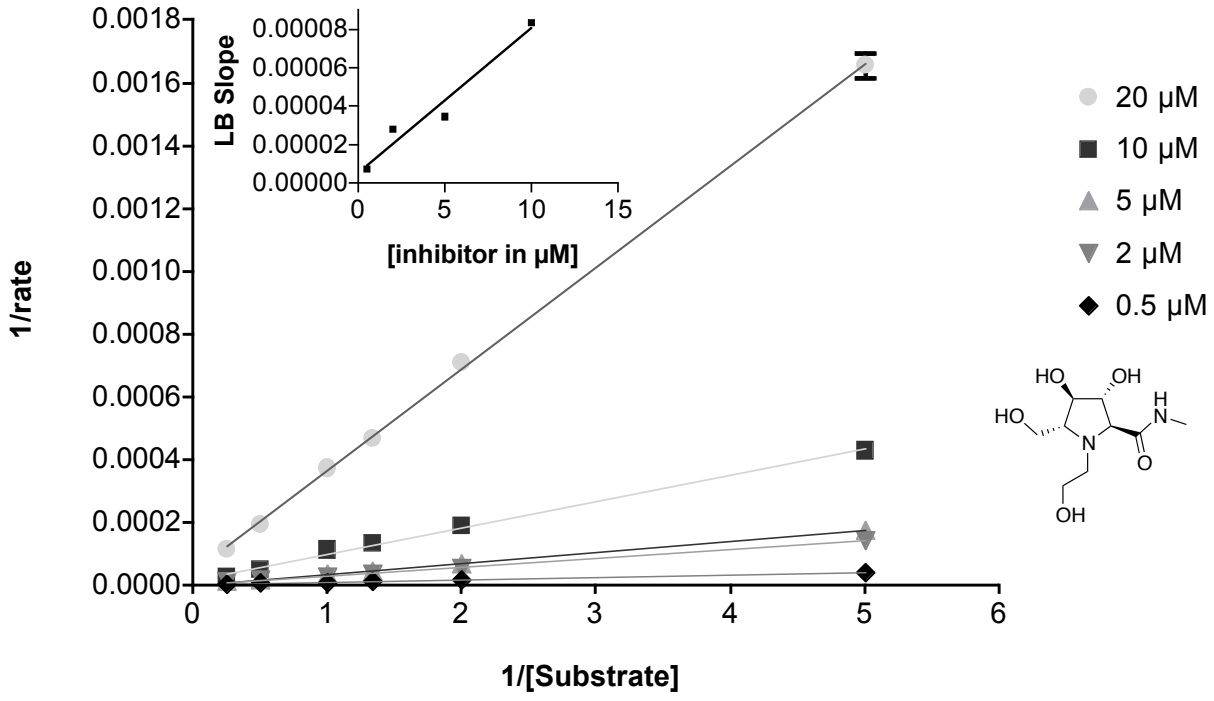


**Figure 4.29** Lineweaver Burk (LB) plot of *N*-EtOH pyrrolidine **246** against β-*N*-acetyl-hexosaminidase derived from HL60 cell homogenate; $K_i$ = 0.718 μM based on X-intercept of insert graph (LB slope vs Inhibitor concentration, $R^2$ = 0.9541).

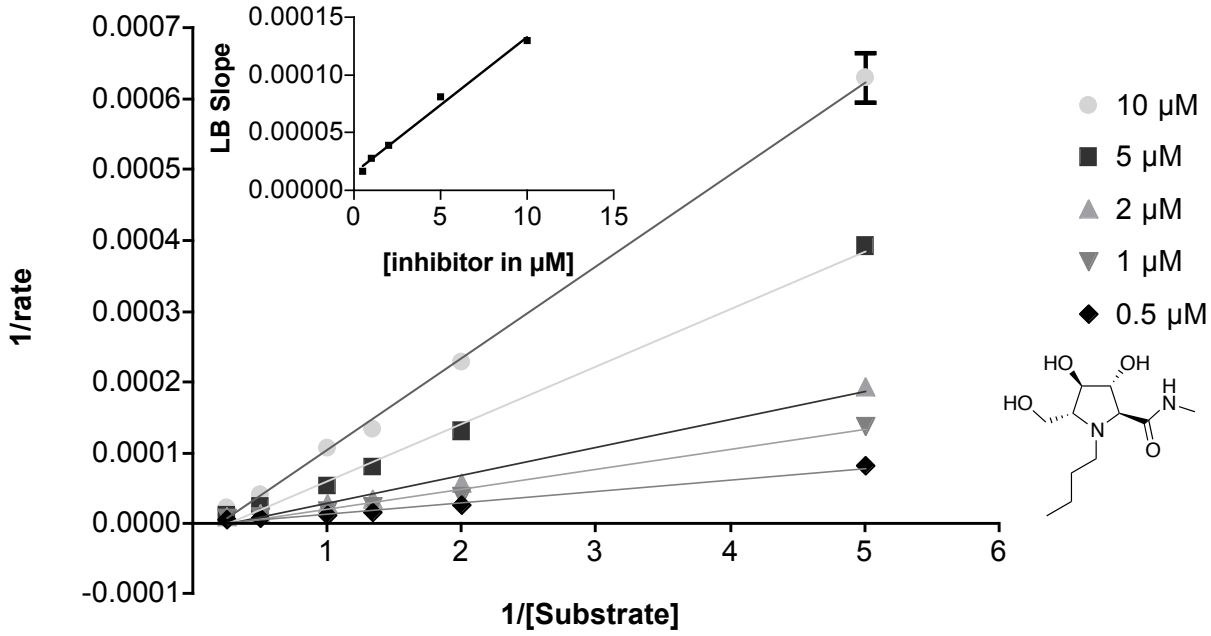


**Figure 4.30** Lineweaver Burk (LB) plot of *N*-Bu pyrrolidine **247** against β-*N*-acetyl-hexosaminidase derived from HL60 cell homogenate; $K_i$ = 1.31 μM based on X-intercept of insert graph (LB slope vs Inhibitor concentration, $R^2$ = 0.9898).

With their enzymatic glycosidase inhibition profiles established, FOS analysis was performed by treating HL60 cells for 24 h with the 4 inhibitors at concentrations of 200, 50 and 5 μM. The same peak assignment was performed in the resulting HPLC profiles as for the FOS study on DGJNAc derivatives (Figure 4.24) and the detailed results in terms of GUs and relative peak intensity for the 200 μM parent iminosugar **68** case are given in Table 4.5. An overlay of the HPLC profiles of all inhibitors at 200 μM is displayed in Figure 4.31 and in combination with Figure 4.32 it can be gleaned that the parent compound **68** was the most potent inhibitor of lysosomal β-*N*-acetyl-hexosaminidase. This is presumably due to its exceptionally high *in vitro* inhibition activity, but it is noteworthy how similar the inhibition strength of the *N*-butyl derivative **247** is in this cellular assay, despite a nearly 50 fold weaker inhibition *in vitro*. In direct comparison to *N*-butyl **247** at 200 and 50 μM concentrations both the hydroxyethyl **246** and carboxylic acid **245** derivative of parent compound **68** showed very significant reductions in inhibition of lysosomal β-*N*-acetyl-hexosaminidase.

**Table 4.5** Structures, retention time in glucose units (GUs) and relative intensity in percent of FOS peaks isolated from a control experiment and 200 μM D-manno amide **68** treated HL60 cells. Peak IDs labeled according to Figure 4.24. Intensity measurements are the mean value of three independent measurements (±S.D.). The species were assigned according literature values.[126] Labels are as follows: ◇ Glucose; ● Mannose; ⬟ 2-Aminobenzoic acid; ■ *N*-Acetyl-glucosamine; ✻ Proposed structure.

| ID | Untreated GU | Treated GU | Structure name | Structure | Untreated cells [%] | Treated cells [%] |
|---|---|---|---|---|---|---|
| 1 | - | 3.71 | $GlcNAc_1Man_2GlcNAc_1$ |  | - | 3.88 ± 0.06 |
| 2 | - | 3.83 | $GlcNAc_2Man_2GlcNAc_1$ | 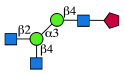 | - | 2.62 ± 0.18 |
| 3 | 4.16 | 4.10 | $Man_3GlcNAc_1$ | 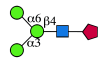 | 2.06 ± 0.25 | 1.12 ± 0.41 |
| 4 | 4.94 | 4.92 | $Man_4GlcNAc_1$ | 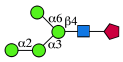 | 13.43 ± 0.15 | 4.40 ± 0.16 |
| 5 | **-** | **5.19** | $GlcNAc_2Man_3GlcNAc_1$ | 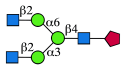 | **-** | **15.85 ± 0.43** |
| 6 | - | 5.57 | $GlcNAc_3Man_3GlcNAc_1$ | 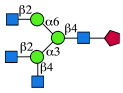 | - | 13.55 ± 0.26 |
| 6A | 5.67 | - | $Man_5GlcNAc_1$ | 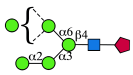 | 4.16 ± 0.82 | - |
| 7 | **5.86** | **5.84** | $Man_5GlcNAc_1$ | 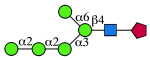 | **36.28 ± 1.20** | **15.67 ± 0.39** |
| 8 | - | 6.06 | $GlcNAc_4Man_3GlcNAc_1$ | 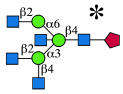 | - | 4.18 ± 0.00 |
| 9 | - | 6.39 | $GlcNAc_4Man_3GlcNAc_1$ | 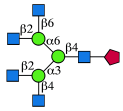 | - | 11.09 ± 0.24 |
| 10 | 6.60 | 6.59 | $Glc_1Man_5GlcNAc_1$ | 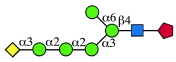 | 19.48 ± 0.89 | 8.43 ± 0.12 |
| 11 | - | 6.86 | $GlcNAc_5Man_3GlcNAc_1$ | 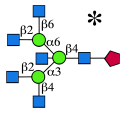 | - | 1.65 ± 0.15 |
| 12 | 7.29 | 7.29 | $Glc_2Man_5GlcNAc_1$ | 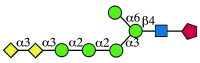 | 6.25 ± 0.20 | 3.20 ± 0.22 |
| 13 | - | 7.60 | $GlcNAc_5Man_3GlcNAc_1$ | 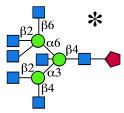 | - | 4.53 ± 0.16 |
| 14 | 7.97 | 7.95 | $Man_7GlcNAc_2$ | 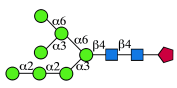 | 3.94 ± 0.23 | 1.86 ± 0.12 |
| 15 | 8.42 | 8.31 | $Man_8GlcNAc_2$ | 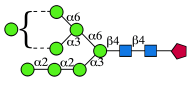 | 1.52 ± 0.66 | 0.83 ± 0.09 |
| 16 | 8.75 | 8.74 | $Man_8GlcNAc_2$ | 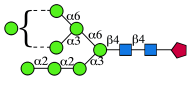 | 5.61 ± 0.21 | 4.12 ± 0.13 |
| 17 | 9.43 | 9.42 | $Man_9GlcNAc_2$ | 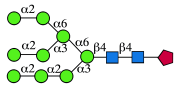 | 7.27 ± 0.16 | 3.01 ± 0.06 |

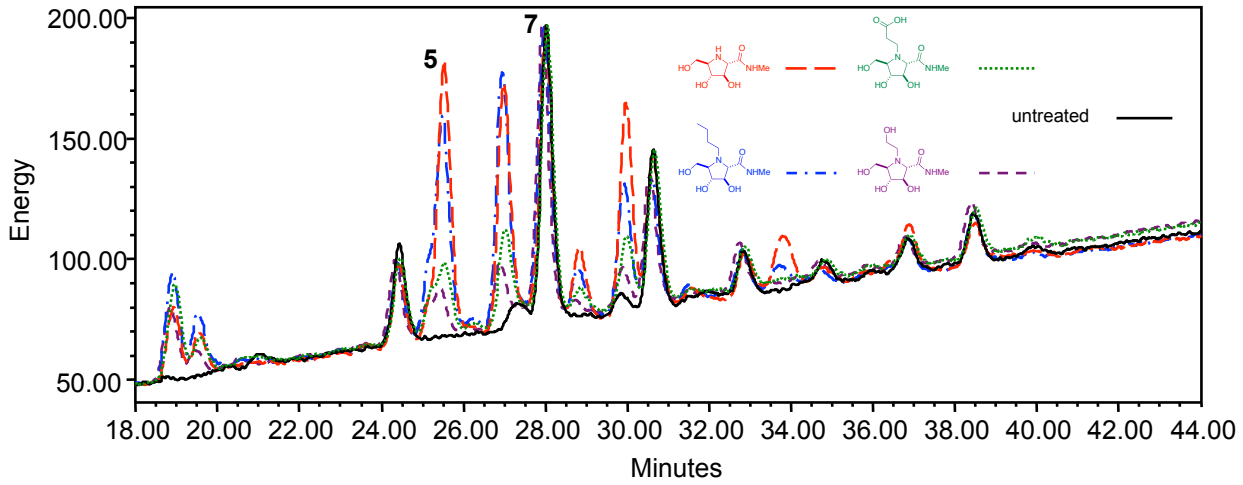


**Figure 4.31** Overlay of HPLC traces with all inhibitors at 200 μM in comparison to untreated cells indicating the variation in peak 5 in comparison to peak 7.

The reduction in activity of *N*-hydroxyethyl derivative **246** is noteworthy, being nearly lower by one order of magnitude in comparison to *N*-butyl **247** at 50 μM and still by 70% at 200 μM (Figure 4.32). At the physiological relevant concentration of 5 μM no inhibition of lysosomal β-*N*-acetly-hexosaminidase was detectable by either the hydroxyethyl **246** or carboxylic acid **245** derivative.

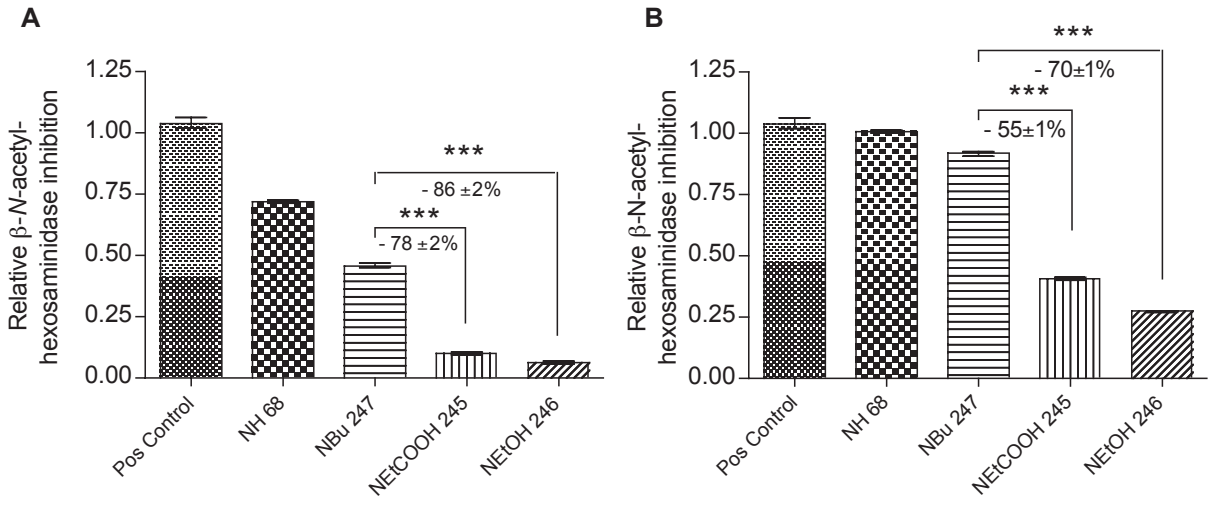


**Figure 4.32** The Ratio of the integration of peak 5 to the control peak 7 are shown for derivatives of D-manno pyrrolidine **68** at A) Inhibitor concentration at 50 μM; B) Inhibitor concentration at 200 μM. The positive control in both cases is DGJNAc at 500 μM corresponding to exhaustive inhibition. With all derivatives having very comparable *in vitro* inhibition of β-*N*-acetyl-hexosaminidase, the variation can be attributed to differences in cell- and organelle-penetration. Decreases in inhibition relative to the butyl derivative **247** are indicated in % with (±S. D.).

To ensure that the observed trends were not due to protein variations in the collected samples a bicinchoninic acid (BCA) assay was performed indicating stable protein levels within error of the technique. Furthermore to rule out cytotoxicity of the iminosugars as a confounding factor their influence on cell proliferation was tested in an assay involving 3-(4,5-dimethylthiazol-2-yl)-5-(3-carboxymethoxyphenyl)-2-(4-sulfophenyl)-2H-tetrazolium (MTS). The assay was performed at the same concentrations used for the FOS assay both at a one and three day timepoint, but none of the iminosugar derivatives **68**, **245**-**247** displayed any cytotoxicity even at the highest concentration of 200 μM (Figure 4.33).

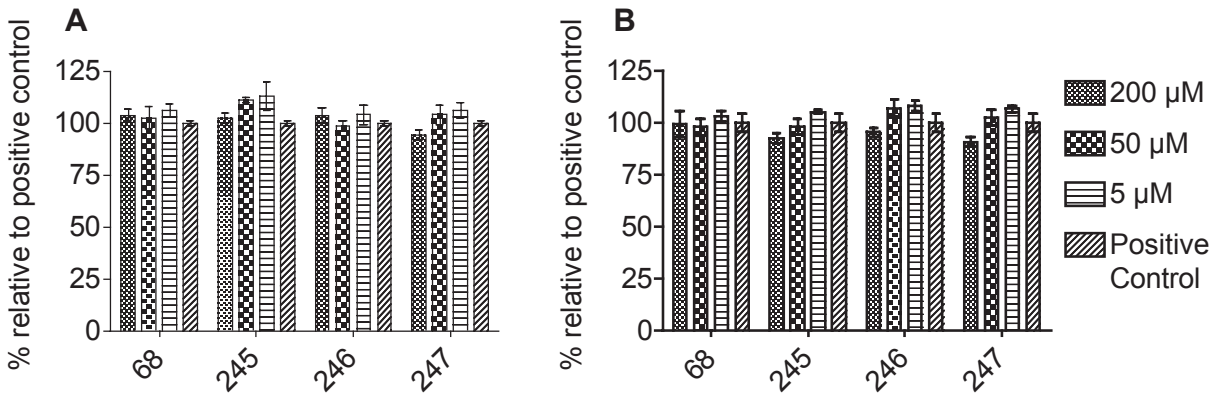


**Figure 4.33** HL60 cell proliferation evaluated using an MTS assay in presence of D-Manno pyrrolidine **68** and derivatives **245-247** relative to untreated control ($H_2O$ instead of inhibitor) with 12500 cells/well. A) 24 h reading. B) 72 h reading.

The results of the 5-ring derivatives therefore confirm the results obtained with the series of DGJNAc analogues and a more general principle emerges: Hydrophobic sidechains (*N*-butyl) on the endocyclic nitrogen of an iminosugar promote cellular uptake, while hydrophilic (hydroxyethyl or carboxylic acid derivatives) modifications restrict the inhibitors to extracellular compartments.

In terms of designing an anti-cancer therapeutic, the latter derivatisation would effectively allow for secreted glycosidases to be targeted, while avoiding the enzymes present in their native cellular compartments. In particular, for targeting secreted α-*N*-acetyl-galactosaminidase, the *N*-hydroxyethyl DGJNAc derivative **244** makes for an interesting candidate, as it is restricted to

extra cellular space, but still a good inhibitor of the target enzyme ($K_i$ 3.3 μM). Obviously a balance of limitation to extra cellular space with oral availability of the inhibitor would have to be struck, which could be addressed in a future animal trial.

## 4.4 Cancer cell invasion assay - an *in vitro* ECM

As the final part of the biological evaluation of iminosugars in an anti-cancer setting, an *in vitro* assay was developed in order to confirm and further progress the idea of β-*N*-acetyl-hexosaminidase inhibitors as cytostatic anti-metastasis agents. As β-*N*-acetyl-hexosaminidase inhibitors to be investigated the two parent scaffolds DGJNAc **239** and pyrrolidine **68** from the preceding section were chosen, which as previously shown can readily be derivatised. A range of cancer cell lines were chosen to be evaluated with special focus on lines derived from breast cancer as the most common cancer in women in the UK constituting more then 30% of all new incidences.[149]

### 4.4.1 The Boyden Chamber setup

A review from 2011 provides an excellent overview of the four main *in vitro* assay techniques for investigating cell migration and invasion.[150] Scratch assays, cell exclusion zone assays, microfluidic devices and transmembrane assays are compared and the last of the four was chosen for this study as it is the only technique that can be adopted for a non optical readout (cell staining and counting) and is less technically challenging to set up then some. The transmembrane assay was developed by Albini et al. and involves malignant cells migrating through filters coated with basement membrane in a boyden-chamber setup.[151] More specifically the basement membrane and therefore model of the ECM was derived from the extracts of Engelbreth Holm-Swarm (EHS) mouse tumor,[152] which has been shown to secrete large amounts of ECM macromolecules including laminin, type IV collagen, heparin sulfate proteoglycans, entactin and nidogen.[153] Albini's method stained the cells, which successfully migrated through

the filter and then quantified by counting the number of cells. It was of interest if an alternative method of cell detection could be combined with the Boyden chamber assay and the solution was found in form of the QCM™ 24-well cell invasion assay (Millipore), which employs a fluorescence based detection method for quantifying the number of invaded cells.[154] A conceptual summary of the assay setup is therefore shown in Figure 4.34. Invasive cancer cells grown under starvation conditions are seeded in fetal calf serum (FCS) free media in an insert, which is placed in a 24 well plate containing medium with FCS as a chemo-attractant. The inserts are separated from the rest of the well by a porous membranes coated in ECM macromolecules derived from EHS. With time the cancer cells migrate through the ECM model system and adhere to the bottom of the insert where they are exposed to the FCS. On completion of the assay the insert is transferred to a well, containing a detachment buffer and the invaded cells are subsequently lysed and their number quantified using the CyQUANT reagent. This fluorescence based method is highly sensitive and allows quantification of cell numbers ranging from as low as 10-50 up to 100.000-250.000.[155] As a result this setup should be relatively free of inaccuracies introduced by the cell staining and optical counting process usually employed in this assay.

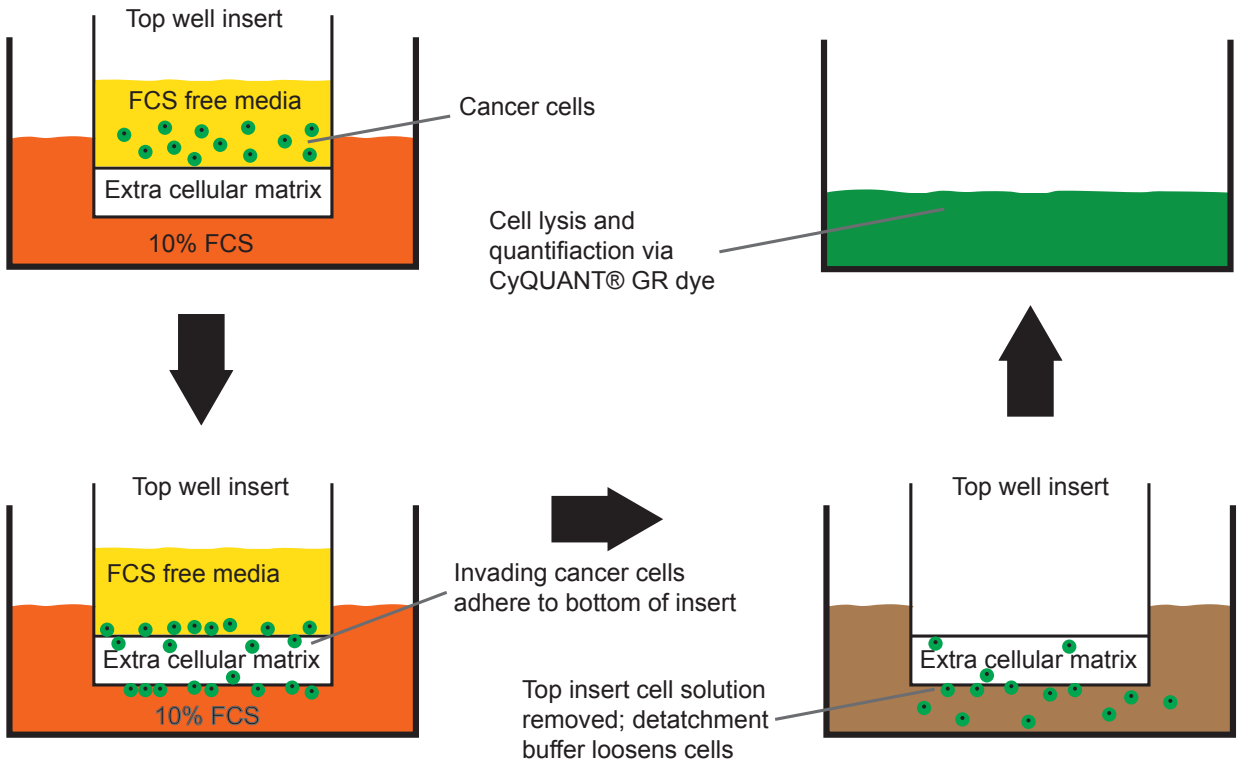


**Figure 4.34** Boyden chamber setup using Merk Millipore ECM554 assay kit.

### 4.4.2 Selection of the cell line

With the assay system established, suitable cell lines needed to be chosen for the iminosugar investigation. Neve et al. performed a detailed comparison of the genetic profile displayed by 51 cancer cell lines with 145 samples from primary breast cancer in order to establish their utility as "model systems" for this heterogenous disease.[156] As part of this investigation 30 breast cancer cell lines were directly compared for their invasiveness in a boyden chamber setup similar to the one used in this thesis. The MDA-MB-231 cell line emerged as the most invasive of the set and was chosen along the less invasive MCF-7 breast cancer cell line to be investigated in this study.

### 4.4.3 Iminosugars and cancer cell invasion

#### 4.4.3.1 Testing of the Boyden chamber setup

To check the commercial assay kit performance the HT1080 cell line (a fibrosarcoma cell line) was used in initial assays, as this cell line had been described previously to give reliable results in the same setup.[157] HT 1080 cells, which had been grown under starvation conditions (no

FCS), were seeded in the top inserts and a significant difference was noticed for the number of invaded cells for the positive control (10% FCS in bottom well) in comparison to the negative control (no FCS) at an invasion time of 24 h (Figure 4.35). The correlation of fluorescence with a standard curve derived with the CyQUANT reagent and this specific cell line allowed for the number of invaded cells to be quantified. The two iminosugars **68** and **239** were used in this initial test as well (both at 500 μM) and although statistically not significant, a trend towards reduced cell invasion seems to be noticeable for the pyrrolidine **68**.

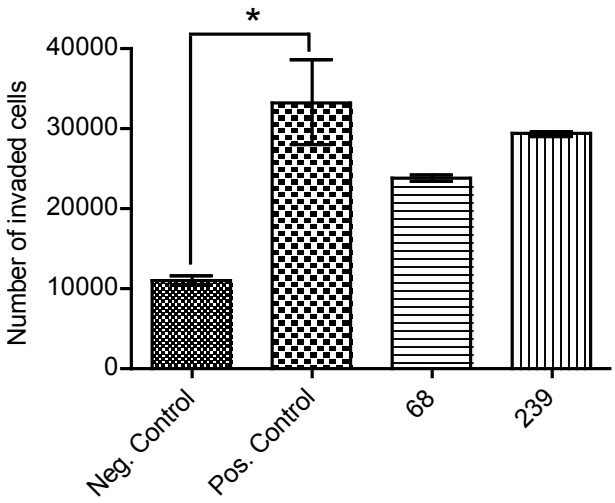


**Figure 4.35** Cell invasion assay using HT1080 cells; 250,000 cells/well; 24 h starvation; 24 h invasion; iminosugars used at concentration of 500 μM; chemo-attractant is 10% FCS; negative control with no FCS.

#### 4.4.3.2 Invasion of MCF-7 and MDA-MB-231 cells

With the function of the assay system established it was decided to move on to the two breast cancer cell lines. The less invasive MCF-7 cell line was seeded at a high density (750,000 cells/well) into the top insert and following 24 h of incubation no difference could be detected in terms of directed migration between the positive and negative control (Figure 4.36). This result might be expected for non-invasive breast cancer and the cells which were gathered from the bottom of the insert were presumably due to random cell migration, independent of the presence of the chemo-attractant (10% FCS) present in the bottom well. It should be noted however

statistical significant decrease was observed for the wells containing pyrrolidine iminosugar **68** (0.2 μM, HL60, Table 4.4) at a 500 μM concentration, meaning that the random motion of cells through the ECM is indeed influenced by inhibition of β-*N*-acetyl-hexosaminidase enzyme. Although not statistically significant to the same degree the same trend was observed for the weaker β-*N*-acetyl-hexosaminidase inhibitor DGJNAc **239** (7.1 μM, HL60, Table 4.1) at the same concentration.

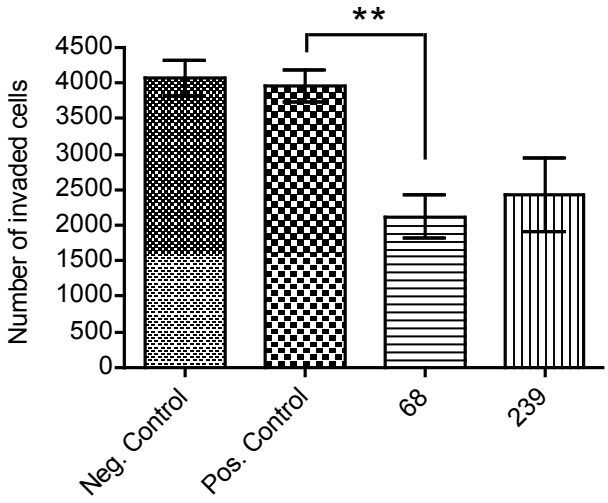


**Figure 4.36** Cell invasion assay using MCF-7 cells; 750,000 cells/well; 24 h starvation; 24 h invasion; iminosugars used at concentration of 500 μM; chemo-attractant is 10% FCS; negative control with no FCS.

When the highly invasive breast cancer cell line MDA-MB-231 was used instead, a statistical significant difference could be established between the wells containing the chemo-attractant FCS and the ones without (Figure 4.37). The same high seeding density (750,000 cells/well) was used as in the case of the MCF-7 cells and following an incubation time of 24 h in the presence of the iminosugars **68** and **239** at 500 μM the same inhibitory trend on cell invasion was noticed. These preliminary results were very encouraging, especially if the very high invasiveness of this particular cell line is kept in mind.

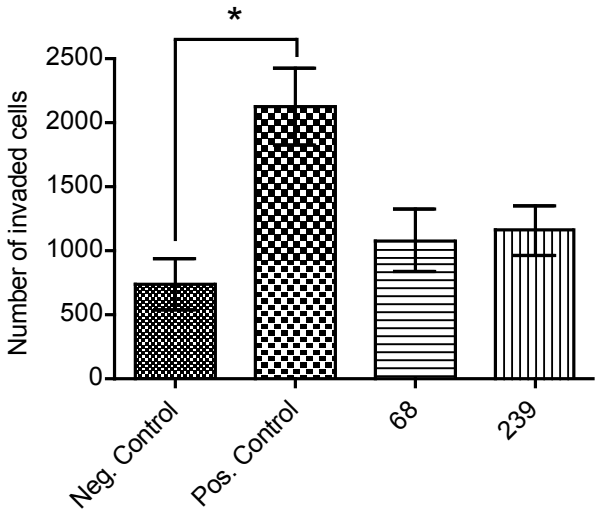


**Figure 4.37** Cell invasion assay using MDA-MB-231 cells; 750,000 cells/well; 30 h starvation; 24 h invasion; iminosugars used at concentration of 500 μM; chemo-attractant is 10% FCS; negative control with no FCS.

In the light of the these positive results MDA-MB-231 cells were equally used in co-treatment experiments of iminosugars with the orally available broadband MMP inhibitor marimastat **248** (Figure 4.38).[158] In a Boyden-chamber assay setup closely related to the one used in this investigation the invasiveness of cells derived from primary gliomas through matrigel was examined and marimastat **248** was found to reduce cell invasion by 80% at a concentration of 0.3 μM.[159]

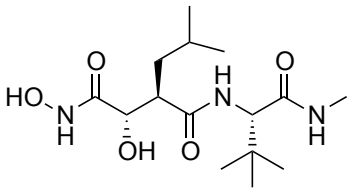


marimastat **248**

**Figure 4.38** Structure of MMP inhibitor marimastat.

In combination with the MDA-MB-231 cells a 10 fold increase in concentration of marimastat to 3 μM was required to obtain comparable levels of inhibition showing a reduction of invasion of 70% when used as a single agent (Figure 4.39 A). Although the combination with the pyrrolidine iminosugar **68** confirmed the very significant decrease in invasion of MDA-MB-231 cells, the contribution of the iminosugar at 500 μM seemed minor when the experiment was incubated for

24 h. However when the incubation time was increased to 64 h, although overall the anti-invasive effects of the inhibitors were reduced, the contribution of the iminosugar seemed to become more pronounced (Figure 4.39 B). After this extended time period the iminosugar and MMP inhibitor as single agent showed a 16% and 25% decrease in invasiveness of the breast cancer cells, while their combination gave a reduction of 41% indicating that the effect of these two inhibitors is additive. This is contrary to the reports in the literature of synergistic effects when β-*N*-acetyl-hexosaminidase iminosugars are combined with protease inhibitors.[109] However the study by Ramessur et al. involved a cocktail of protease inhibitors (2-aminoethyl benzenesulphonyl fluoride, EDTA, bestatin, L-*trans*-epoxysuccinyl-leucylamide-4-guanido-butane, leuceptin, aprotinin) and a synergistic relationship of one of the 6 inhibitors with iminosugars cannot be excluded. Still, an additive effect of β-*N*-acetyl-hexosaminidase inhibitors with MMP inhibitors shows that the in order to provide an answer to the hydrolytic enzyme cocktail produced by invasive cancer cells to degrade the complex meshwork, which constitutes the ECM, a multi-pronged approach will be required.

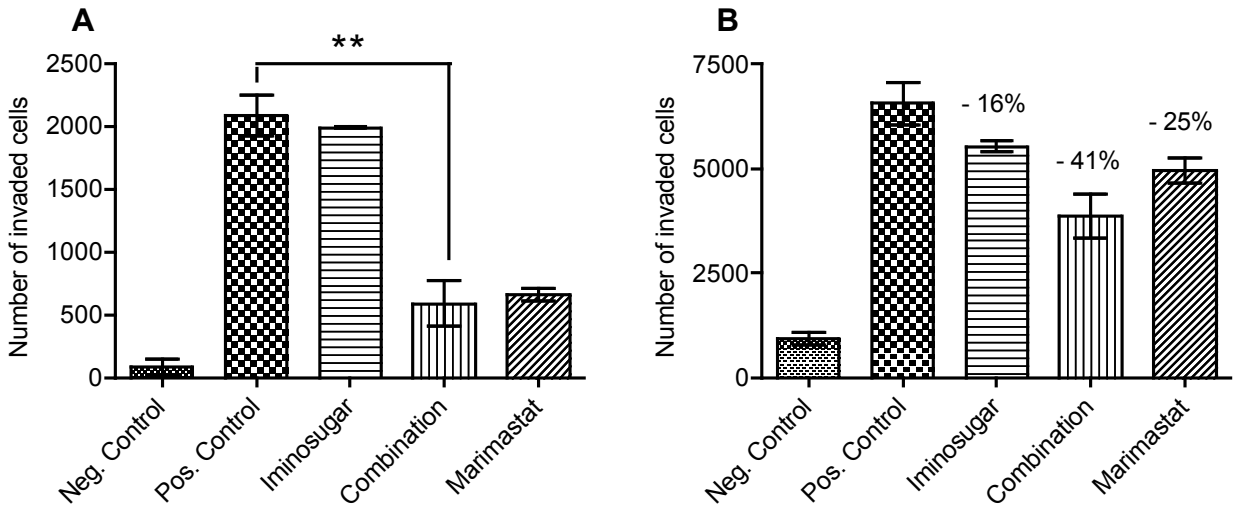


**Figure 4.39** Combination treatment of iminosugar **68** and MMP inhibitor **248** in cell invasion assay using MDA-MB-231 cells show additive effects; 820,000 cells/well; 24 h starvation; iminosugar **68** used at concentration of 500 μM; MMP inhibitor Mariamastat **248** at 3 μM; chemo-attractant is 10% FCS; negative control with no FCS; A) 24 h invasion time; B) 64 h invasion time.

As previous experiments investigating the anti-invasive properties of iminosugars had been performed at 1 mM concentration the substantial concentration of 500 μM was chosen throughout the previous experiments as outlined above.[109] However, the anti-invasive properties exerted by β-*N*-acetyl-hexosaminidase inhibitors at lower concentrations were of interest as well, as they are readily obtainable under physiological relevant conditions. A dose variation of 500 μM, 50 μM and 5 μM was tested with pyrrolidine iminosugar **68** (Figure 4.40), which probes below the concentration obtainable in the blood plasma using iminosugars currently employed in the clinic (maximum plasma concentration of Miglustat in a multiple dose regime is 12.7 μM; Miglitol in a 100 mg oral dose is 8.4 μM).[160] At an incubation time of 48 h pyrrolidine iminosugar **68** at 5 μM was able to reduce the invasiveness of MDA-MB-231 cells by 29%, while the use of higher concentrations provided no further benefit.

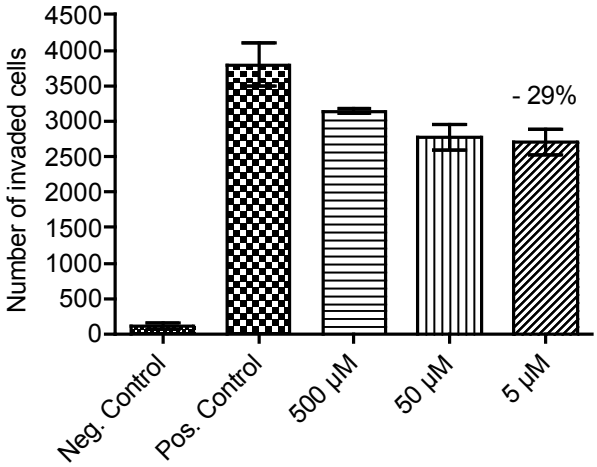


**Figure 4.40** Dose dependence of cell invasion assay using MDA-MB-231 cells; 750,000 cells/well; 24 h starvation; 48 h invasion; iminosugar **68** at 3 concentrations; chemoattractant is 10% FCS; negative control with no FCS.

The lack of a dose response displayed by the iminosugar **68** displayed in this assay setup, might be explained by the fact that glycosidase inhibitors are only able to inhibit part of the hydrolytic cocktail derived from cancer cells. Therefore even at exceedingly high concentrations, complete suppression of cancer cell invasion cannot be accomplished by this agent alone. However the

fact, that invasion of the aggressive breast cancer cell line MDA-MB-231 was suppressed by one third when the inhibitor was used at concentrations as low as 5 μM is impressive.

#### 4.4.3.3 Verification of assay results

In order to rule out the possibility of confounding factors causing the observed anti-invasive activity of iminosugars the following experiments were performed. To test that the CyQUANT agent is not influenced by the addition of the iminosugar a know amount of cells were incubated in the presence and the absence of the two iminosugar **68** and **239** at 500 μM. Despite the exposure of the quantifying agent to much higher concentrations then present in the experiment (as shown in Figure 4.34 the insert is transferred to a new well containing the detachment buffer and therefore no iminosugar), no change in the observed fluorescence was detected in comparison to control ruling out assay interference.

To equally rule out toxicity of the investigated iminosugars **68** and **239** each cell line used in the cell invasion assay was probed with an MTS assay. Therefore HT1080, MCF-7 and MDA-MB-231 cells were incubated for 24 h and 72 h with the iminosugars at range of concentrations from 5 μM to 1 mM and their ability to metabolize MTS was investigated (Figure 4.41). Even at the highest concentration employed no cytotoxicity was detectable for the two iminosugars **68** and **239** for any of the cell lines or time points.

Overall it can be concluded from these preliminary results, that although the combination of iminosugars with a MMP inhibitor is non synergistic, the additive effect provided by a completely non-toxic inhibitor, could make an exciting addition to the arsenal of anti-metastatic agents. In the literature such a combination approach of inhibitors to target a mixture of hydrolytic enzymes has been shown to be fruitful before. Zengel et al. explored the combined use of a MMP inhibitor (galardin) with other agents acting on cyclooxygenase-2 (COX-2,

celecoxib) and urokinase plasminogen activator (uPA, WX-UK1) and found an 80% reduction of invasion in a matrigel assay in contrast to the 50% achieved by single agent therapy.[161]

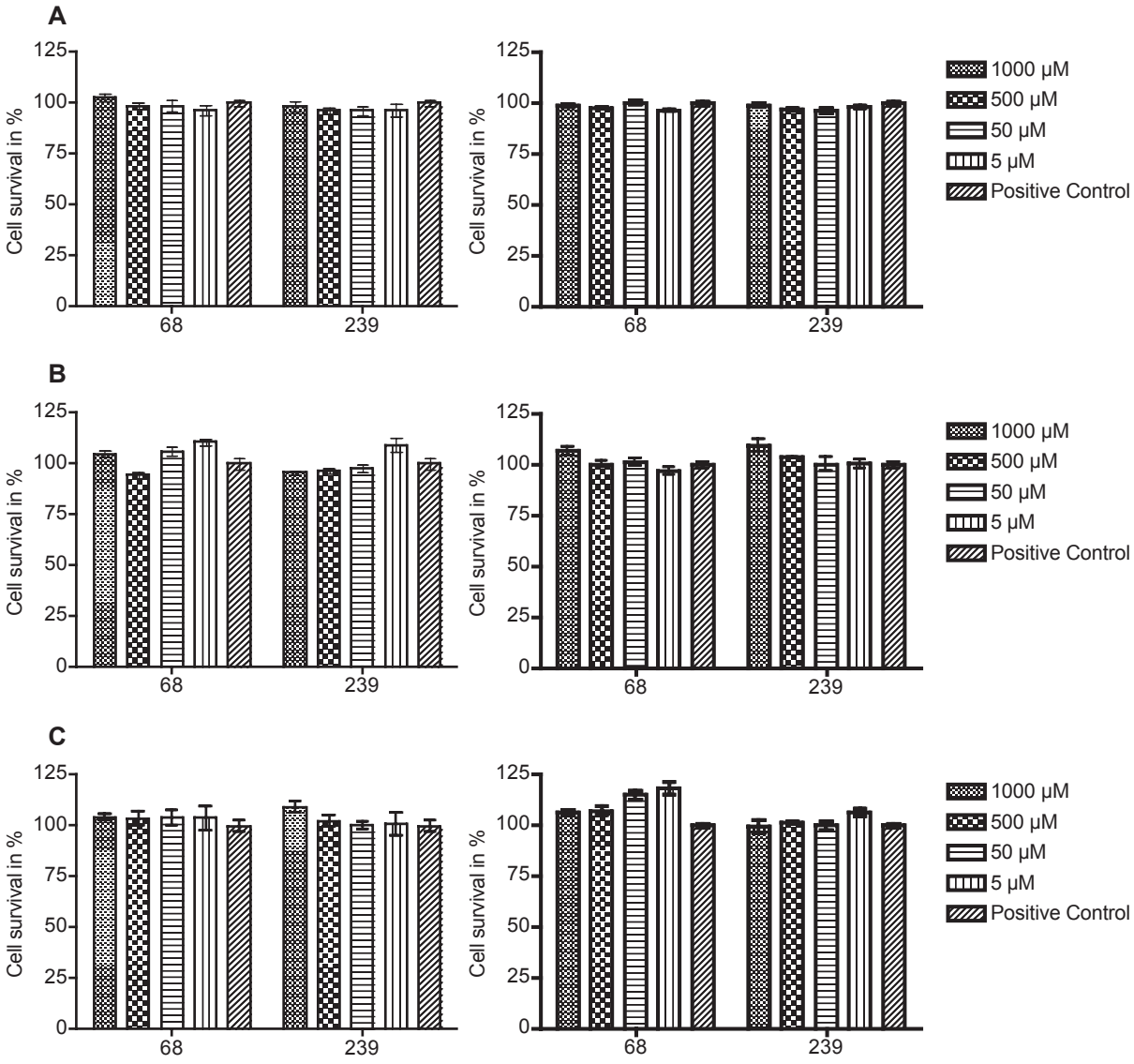


**Figure 4.41** Toxicity investigation of iminosugars **68** and **239** in cell lines used in cancer invasion assay using an MTS assay. To measure metabolic activity incubated with MTS for 4h. Prior incubation with iminosugar for 24 h (left) or 72 h (right). A) HT-1080 cells, 10,000 cells/well; B) MCF-7 cells, 20,000 cells/well; C) MDA-MB-231 cells, 10,000 cells/well.

## 4.5 Conclusion Chapter 4

This chapter saw significant steps towards the development of two *in vitro* assay systems for the novel anti-cancer targets α-*N*-acetyl-galactosaminidase and β-*N*-acetyl-hexosaminidase. Although development on the former assay did not come to completion during the work for this

thesis, the enormous structural importance of the *O*-glycan on MAF for macrophage activation was confirmed in this study and my results have stimulated further research by the Butters group. This has led to the development of a HPLC based quality control system for DBP glycosylation and investigations on the protection of MAF with DGJNAc for lifting immunosuppression are ongoing. For the latter enzyme a Boyden-chamber based cancer cell invasion assay to probe the protective effect of iminosugar inhibitors on the ECM was successfully established. The system was tested with a variety of cancer cell lines and conditions including physiologically relevant iminosugar concentrations and combined application with MMP protease inhibitors. As a result it can be concluded that although the utility of β-*N*-acetyl-hexosaminidase inhibitors as single agent therapy is limited, a 30% reduction in invasiveness of the aggressive breast cancer cell line MDA-MB-231 at 5 μM is still noteworthy. The addition of this non-cytotoxic agent to a cocktail of protease inhibitors would make an interesting proposition as a multipronged anti-metastasis array, in answer to the mixture of hydrolytic enzymes secreted by invading cancer cells. If this addition was to be free of side effects by selectively targeting the biocompartments of interest using sidechain variations of the endocyclic nitrogen, native lysosomal enzymes would be left undisrupted.

Obviously the preliminary nature of the results presented in this chapter have to be kept in mind, but their promising nature will surely warrant the future exploration of iminosugars for selective anti-cancer therapy.

## 4.6 Experimental section of biological evaluation chapter

### 4.6.1 Synthetic experimental

General experimental can be found in Chapter 2 (Section 2.6.1, page 44).

#### 4.6.1.1 Synthesis of DGJNAc derivatives

Spectra and full data on 2-Acetamido-1,2,5-trideoxy-1,5-imino-D-galactitol DGJNAc **239**.[146]

**2-Acetamido-1,2,5-trideoxy-1,5-imino-1-*N*-methyl-D-galactitol, (*N*-methyl-DGJNAc) 240**

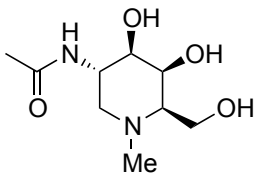


Formaldehyde (37% in water, 0.03 mL, 0.3 mmol) and 10% palladium on charcoal (20% b.w., 6 mg) were added to a solution of DGJNAc **239** (30 mg, 0.15 mmol) in 1:1 1,4-dioxane/water (2 mL). The vessel was degassed and charged with hydrogen, and the reaction mixture stirred at RT for 18 h after which LRMS indicated the absence of the starting material. The reaction mixture was filtered (GF/A glass microfibre) and concentrated *in vacuo*. The residue was loaded in water onto a short column of Dowex® (50W-X8, $H^+$) and the resin washed with water until neutral fractions were obtained. The product was liberated with aq. ammonia (2 M) and the ammoniacal fractions concentrated *in vacuo* to afford *N*-methyl-DGJNAc **240** as a brown, crystalline solid (35 mg, quant.). Free base data: M.p. 203-206 °C; $[\alpha]_D^{22}$ +23.6 (*c* 0.65 in $H_2O$); $\nu_{max}$ (thin film): 3289 (m, br, O-H), 1639 (s, amide I), 1561 (s, amide II); $\delta_H$ (400 MHz, $D_2O$): 4.10 – 3.92 (2 H, m, H2, H4), 3.74 (1 H, dd, H6, $J_{6,6'}$ 11.6, $J_{5,6}$ 4.5), 3.68 (1 H, dd, H6', $J_{6,6'}$ 11.6, $J_{5,6'}$ 6.1), 3.41 (1 H, dd, H3, $J_{3,4}$ 10.6, $J_{2,3}$ 2.1), 2.81 (1 H, dd, H1, $J_{1,1'}$ 11.7, $J_{1,2}$ 4.5), 2.20 (4 H, s, H5, NHMe), 2.04 (1 H, a-t, H1, H1', $J_{1,1'}$=$J_{1',2}$ 11.6), 1.88 (3 H, s, COMe); $\delta_C$ (126 MHz, $D_2O$): 174.5 (C=O), 72.4 , 69.5, 65.4 (C3, C4, C5), 60.6 (C6), 57.7 (C1), 47.2 (C2), 41.0 ($NCH_3$), 22.0 ($CH_3C$=O); *m/z* (ESI+ve): 459 ($[2M+Na]^+$, 100%); HRMS (ESI+ve): Found 241.1158 ($[M+Na]^+$); $C_9H_{18}N_2NaO_4$ requires 241.1159.

**2-Acetamido-1,2,5-trideoxy-1-*N*-ethyl-1,5-imino-D-galactitol, (*N*-ethyl-DGJNAc) 241**

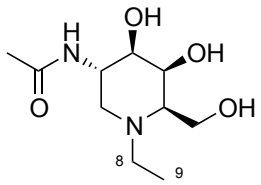


Ethanal (0.01 mL, 0.2 mmol) and 10% palladium on charcoal (40% b.w., 8 mg) were added to a solution of DGJNAc **239** (20.9 mg, 0.10 mmol) in ethanol (1 mL). The vessel was degassed and charged with hydrogen, and the reaction mixture stirred at RT for 4.5 h after which LRMS indicated the absence of the starting material. The reaction mixture was filtered (GF/A glass microfibre) and concentrated *in vacuo*. The residue was loaded in water onto a short column of Dowex® (50W-X8, $H^+$) and the resin washed with water until neutral fractions were obtained. The product was liberated with aqueous ammonia (2 M) and the ammoniacal fractions concentrated *in vacuo* to afford *N*-ethyl-DGJNAc **241** as a colourless oil (24 mg, quant.). Free base data: $[\alpha]_D^{25}$ +18.1 (*c* 1.0 in MeOH); $\nu_{max}$ (thin film, Ge): 3317 (m, br, OH, NH), 1637 (s, amide I), 1560 (m, amide II); $\delta_H$ (400 MHz, $D_2O$): 4.20 – 4.04 (2 H, m, H2, H4), 3.87 (1 H, dd, H6, $J_{6,6'}$ 11.4, $J_{5,6}$ 3.9), 3.80 (1 H, dd, H6', $J_{6,6'}$ 11.4, $J_{5,6}$ 6.4), 3.51 (1 H, br. d, H3, *J* 10.3), 2.98 (1 H, dd, H1, $J_{1,1'}$ 11.5, $J_{1,2}$ 4.0), 2.85 (1 H, dd, H8, $J_{8,8'}$ 13.6, $J_{8,9}$ 6.9), 2.63 (1 H, dd, H8', $J_{8,8'}$ 13.6, $J_{8',9}$ 7.0), 2.58 (1 H, a-s, H5), 2.23 (1 H, a-t, H1', $J_{1,1'} = J_{1,2}$ 11.4), 2.01 (3 H, s, H7), 1.02 (3 H, t, H9, $J_{8,9}$ 6.9); $\delta_C$ (101 MHz, $D_2O$): 175.0 (C=O), 73.0 (C3), 70.0 (C4), 62.8 (C5), 60.8 (C6), 53.3 (C1), 47.8 (C2), 46.6 (C8), 22.7 (C7), 8.6 (C9); *m/z* (ESI+ve): 487 ($[2M+Na]^+$, 100%); HRMS (ESI+ve): Found 233.1495 ($[M+H]^+$); $C_{10}H_{21}N_2O_4$ requires 233.1296.

**2-Acetamido-1-*N*-butyl-1,2,5-trideoxy-1,5-imino-D-galactitol, (*N*-butyl-DGJNAc) 242**

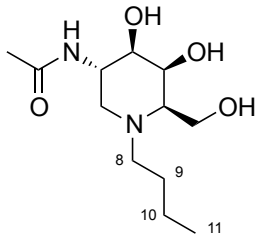


Butyraldehyde (0.01 mL, 0.1 mmol) and sodium cyanoborohydride (6 mg, 0.1 mmol) were added to a solution of DGJNAc **239** (22.4 mg, 0.110 mmol) in 200:1 ethanol/acetic acid (10 mL). The reaction mixture was stirred at RT for 2.5 h after which LRMS indicated the absence of the starting material. The reaction mixture was concentrated *in vacuo* and the crude residue purified by cation-exchange chromatography (Bond Elut SCX 1 cc cartridge, residue loaded in 50 mM HCl and eluted with 3.5% ammonium hydroxide in methanol/water) and reverse-phase chromatography (SepPak $C_{18}$ 1 cc cartridge, residue loaded in water and eluted with methanol) to afford *N*-butyl-DGJNAc **242** as a white crystalline solid (32 mg, quant.). Free base data: M.p. 180-184 °C; $[\alpha]_D^{25}$ +14.4 (*c* 0.62 in MeOH); $\nu_{max}$ (thin film, Ge): 3286 (m, br, OH, NH), 1644 (s, amide I), 1559 (m, amide II); $\delta_H$ (400 MHz, $D_2O$): 4.13 – 4.07 (1 H, m, H2), 4.07 (1 H, dd, H4, $J_{4,5}$ 5.7, $J_{3,4}$ 3.7), 3.86 (1 H, dd, H6, $J_{6,6'}$ 11.4, $J_{5,6}$ 4.6), 3.78 (1 H, dd, H6', $J_{6,6'}$ 11.4, $J_{5,6'}$ 6.7), 3.49 (1 H, dd, H3, $J_{2,3}$ 10.8, $J_{3,4}$ 3.7), 2.95 (1 H, dd, H1, $J_{1,1'}$ 11.7, $J_{1,2}$ 4.6), 2.67 (1 H, ddd, H8, $J_{8,8'}$ 13.5, $J_{8,9}$ 9.7, $J_{8,9'}$ 6.8), 2.52 – 2.43 (2 H, m, H8', H5), 2.18 (1 H, a-t, H1', $J_{1',1} = J_{1',2}$ 11.5), 2.01 (3 H, s, Me), 1.52 – 1.35 (2 H, m, H9), 1.32 – 1.20 (2 H, m, H10), 0.89 (3 H, t, H11 $J_{10,11}$ 7.3); $\delta_C$ (126 MHz, $D_2O$) 175.0 (C=O), 73.4 (C3), 70.1 (C4), 63.1 (C5), 61.0 (C6), 54.4 (C1), 52.4 (C8), 48.0 (C2), 25.9 (C9), 22.7 (C7), 20.7 (C10), 13.8 (C11); *m/z* (ESI+ve): 261 ($[M+H]^+$, 100%); HRMS (ESI+ve): Found 260.1809 ($[M+H]^+$); $C_{12}H_{25}N_2O_4$ requires 261.1809.

**2-Acetamido-1-*N*-benzyl-1,2,5-trideoxy-1,5-imino-D-galactitol, (*N*-benzyl-DGJNAc) 243**

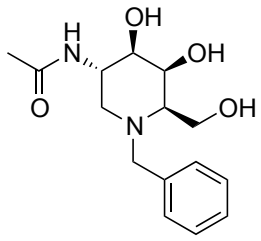

Benzaldehyde (0.01 mL, 0.1 mmol) and sodium cyanoborohydride (6 mg, 0.1 mmol) were added to a solution of DGJNAc **239** (20 mg, 0.10 mmol) in 200:1 ethanol/acetic acid (10 mL). The reaction was stirred at RT for 3 h after which LRMS indicated the absence of the starting material. The reaction mixture was concentrated *in vacuo* and the crude residue purified by cation-exchange chromatography (Bond Elut SCX 1 cc cartridge, residue loaded in 50 mM HCl and eluted with 3.5% ammonium hydroxide in methanol/water). A large proportion of the product was eluted during the wash fractions, which were concentrated and loaded onto a short column of Dowex® (50W-X8, $H^+$) and the resin washed with water. The product was liberated with aqueous ammonia (2 M) and the ammoniacal fractions concentrated *in vacuo*. The products of both columns were combined to afford *N*-benzyl-DGJNAc **243** as a clear oil (20 mg, 68%). Free base data: $[\alpha]_D^{25}$ +17.6 (*c* 0.25 in MeOH); $\nu_{max}$ (thin film, Ge): 3385 (m, br, OH, NH), 1635 (s, amide I), 1558 (m, amide II); $\delta_H$ (400 MHz, $D_2O$): 7.48 – 7.41 (5 H, m, Ph), 4.30 (1 H, d, H8, $J_{8,8'}$ 13.1), 4.25 – 4.11 (3 H, m, H2, H4, H6), 4.06 (1 H, dd, H6' $J_{6,6'}$ 12.1, $J_{5,6'}$ 5.9), 3.83 (1 H, d, H8', $J_{8,8'}$ 13.1), 3.58 (1 H, dd, H3, *J* 10.7, *J* 2.9), 3.02 (1 H, dd, H1, $J_{1,1'}$ 11.7, $J_{1,2}$ 4.2), 2.96 (1 H, app. br. s, H5), 2.30 (1 H, a-t, H1', $J_{1,1'} = J_{1,2}$ = 11.7), 1.95 (3 H, s, Me); $\delta_C$ (126 MHz, $D_2O$): 175.0 (C=O), 136.8 (ipso-Ph), 131.8, 131.3, 129.4, 128.9 (Ph), 72.3 (C3), 70.2 (C4), 64.6 (C5), 60.5 (C6), 56.7 (C8), 52.7 (C1), 46.5 (C2), 22.5 (Me); *m/z* (ESI+ve): 295 ($[M+H]^+$, 100%), 317 ($[M+Na]^+$, 75%); HRMS (ESI+ve): Found 295.1648 ($[M+H]^+$); $C_{15}H_{23}N_2O_4$ requires 295.1652.

**2-Acetamido-1,2,5-trideoxy-1-*N*-hydroxyethyl-1,5-imino-D-galactitol, (*N*-hydroxyethyl-DGJNAc) 244**

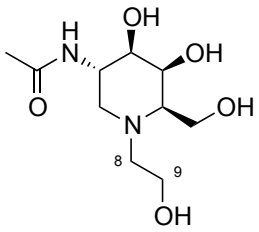


Glycoaldehyde dimer (180 mg, 1.50 mmol) and 10% palladium on charcoal (40% b.w., 12 mg) were added to a solution of DGJNAc **239** (30 mg, 0.15 mmol) in 1:1 1,4-dioxane/water (4 mL). The vessel was degassed, charged with hydrogen, and the reaction mixture stirred at RT for 16 h after which LRMS indicated the absence of the starting material. The reaction mixture was filtered (GF/A glass microfibre) and concentrated *in vacuo*. The residue was loaded onto a short column of Dowex® (50W-X8, $H^+$) and the resin washed with water. The product was liberated with aqueous ammonia (2 M) and the ammoniacal fractions concentrated *in vacuo* to afford *N*-hydroxyethyl-DGJNAc **244** as an off-white, viscous gum (35 mg, 95%). Data for free base: $[\alpha]_D^{25}$ +14.2 (*c* 0.96 in MeOH); $\nu_{max}$ (thin film, Ge): 3318 (s, br, OH), 1638 (s, amide I), 1561 (m, amide II); $\delta_H$ (400 MHz, $D_2O$) 4.12 – 3.96 (2 H, m, H4, H2), 3.85 (1 H, dd, H6, $J_{6,6'}$ 11.5, $J_{6,5}$ 5.1), 3.79 (1 H, dd, H6', $J_{6,6'}$ 11.5, $J_{6',5}$ 5.9), 3.68 (2 H, td, H9, *J* 11.8, 5.7), 3.50 (1 H, dd, H3, *J* 10.5, 2.8), 3.02 (1 H, dd, H1, $J_{1,1'}$ 11.8, $J_{1,2}$ 4.5), 2.96 – 2.85 (1 H, H8, m), 2.71 – 2.52 (2 H, H8', H5, m), 2.21 (1 H, a-t, H1', $J_{1,1'}$ 11.4), 2.00 (3 H, s, H7); $\delta_C$ (101 MHz, $D_2O$) 174.96 (C=O), 73.24 (C3), 70.62 (C4), 64.08 (C5), 61.39 (C6), 58.73 (C9), 54.82 (C1), 53.46 (C8), 48.17 (C2), 22.63 (C7); *m/z* (ESI+ve): 249 ($[M+H]^+$, 27%), 271 ($[M+Na]^+$, 66%), 519 ($[2M+Na]^+$, 100%); HRMS (ESI+ve): Found 271.1256 ($[M+Na]^+$); $C_{10}H_{20}N_2NaO_5$ requires 271.1264.

### 4.6.2 Biological experimental

#### 4.6.2.1 Cell culture

RAW 264.7 cells (obtained from in house cell bank) were cultured on bacterial plate petri dishes in RPMI 1640 medium containing 10% fetal calf serum (FCS), 1% L-glutamine, 100 units/mL of penicillin and 100 μg/mL streptomycin (PAA, Pashing, Austria) at 37 °C and 5% $CO_2$. When grown on petri dishes RAW 264.7 cells adopt a rounded phenotype and behavior of a suspension cell line, are fast growing and require 1:10 splitting every 3 days. Alternatively when RAW 264.7 cells (ATCC, Cat. No. TIB-71) are grown on tissue culture plastic they adopt a dendritic, heterogeneous phenotype and adhere strongly to the surface. In this case a lidocaine (8 mg/mL) and EDTA (5 mM) solution in PBS was generated and sterile filtered (0.2 μM, Merk Millipore) in order to separate the cells from the surface to allow for propagation.

HL60 cells were cultured according to the protocol described in Chapter 2.

HT-1080 cells (ATCC, Cat. No. CCL-121) and MDA-MB-231 cells (obtained from in house cell bank) were grown in the same conditions as RAW 264.7 cells but in DMEM (PAA, Pashing, Austria) and without the FCS in the case of starvation conditions employed. For subculture of a 75 $cm^2$ flask old cell culture medium would be aspirated and discarded, adherent cells washed with PBS (10 mL), 2 mL of Trypsin-EDTA (Sigma-Aldrich, Dorset, U.K., T3924) added and incubated for 5-15 min at 37 °C. Trypsinised cell suspension would be diluted with 8 mL of medium and an aliquot added to a new T75 flask resulting in a subculture ratio of 1:4 in 15 mL of new media.

MCF-7 cells (obtained from in house cell bank) were grown in DMEM or DMEM/F12 (PAA, Pashing, Austria) and with a subculture ratio of 1:3 but otherwise the same conditions as HT-1080.

#### 4.6.2.2 Macrophage activating factor assay development

Human DBP (Gc-globulin) 1 mg of ≥90% purity (SDS-PAGE) along with contained sodium chloride and phosphate buffer salts (Sigma-Aldrich, Dorset, U.K., G8764-1MG) was reconstituted in 1 mL of dist. water. Aliquots of this 1mg/mL solution (90% DBP) were used throughout this thesis.

The protocol for MAF generation using sepharose bound glycosidases was adapted from literature procedures.[23] Neuraminidase from *Arthrobacter ureafaciens* (200 μL, 0.6 U, Oxford GlycoScience, Abinbdon, U.K.) and β-galactosidase from jack bean (200 μL, 2 U, in house purified) were dialyzed in coupling buffer at 4 °C for 18 h (0.1 mM sodium hydrogen carbonate, 0.5 mM sodium chloride, pH 8.3) and coupled to 0.18 and 0.6 g of CNBr-activated Sepharose® 4B (GE Healthcare, Uppsala, Sweden) respectively (4 °C for 18 h), which had previously been swollen with 1 mM hydrochloric acid (washed 6 x with 1 mM HCl and once with coupling buffer). Remaining coupling sites were blocked with incubation with glycine (0.2 M, ph 8.0) and the activity of the sepharose bound enzymes tested with the corresponding methylumbelliferyl fluorescence substrate in accordance with protocols of Chapter 2. DBP (150 μL, 135 μg) along with sepharose bound glycosidases (0.2 U of activity) was incubated in phosphate buffer (50 mM, pH 5.0) for 2 h at 37 °C. Sepharose was pelleted at 2600 x g for 5 min and the supernatant contained glycosidase treated DBP, the potential MAF.

The macrophage activation assay using dihydrofluorescein diacetate (DHF-DA) was adapted from a literature procedure[45] combined with LPS as a positive control.[31] RAW 264.7 cells were cultured for 18 h in a 24-well plate at a density 50.000 cells/well. Following this the medium was replaced with solutions made up in PBS (1 mL/well) or Ringer's buffer (200 μL/well, 155 mM NaCl, 5 mM KCl, 2 mM CaCl2, 1 mM $MgCl_2 \bullet 6H_2O$, 2 mM $NaH_2PO_4 \bullet H_2O$, 10 mM HEPES, 10 mM glucose and 1 mg/mL ovalbumin; sterile filtered) of DBP (1 ng/mL), MAF (1 ng/mL), LPS

(10 μg/mL, positive control, Sigma-Aldrich, L6018), phosphate buffer treated with glycosidases and PBS only as negative control. The treated cells were incubated for 3 h at 37 °C and 5% $CO_2$. DHF-DA dissolved in DMSO (Hybri-max, Sigma-Aldrich, D2650) was then added (20 μL) to the wells to a final concentration of 2 mM, incubated for a further 1 h, spun down (500 x g, 5 °C, 5 min) and then 500 μL transferred to a new 24-well plate for fluorescence reading (Molecular Devices SPECTRAmax M5 Rom v2.1.35, excitation 485 nm, emission 538 nm).

In order to improve the sensitivity of the DHF-DA detection of ROI suggestions from Hempel et al. were investigated.[118] DHF-DA was dissolved in DMSO (0.1 M), diluted in PBS (2 mM) and treated with horseradish peroxidase (30 U, Sigma-Aldrich, P8125) and $H_2O_2$ (30% stock) at a final concentration of 2 mM (1 eq.) and 20 mM (10 eq.). Following incubation at 37°C for 30 min the fluorescence was detected as above.

As an alternative for detection of ROI the Invitrogen Amplex Red hydrogen peroxide/peroxidase assay (Molecular probes, A22188) was employed. Cells were treated with various concentrations of LPS, MAF and DBP in ringer buffer (200 μL/well) and following 3 h of incubation at 37 °C and 5% $CO_2$ 100 μL of supernatant were combined with 100 μL of Amplex Red development solution (10-acetyl-3,7-dihydroxyphenoxazine in DMSO 0.01 M and horseradish peroxidase 0.2 U/mL in 0.25 M sodium phosphate, pH 7.4) in a 96 well plate. Following incubation at RT for 30 min fluorescence was measured (Molecular Devices SPECTRAmax M5 Rom v2.1.35, excitation 544 nm, emission 590 nm).

#### 4.6.2.3 MALDI investigations of DBP

The digestion of DBP with endoproteinase Arg-C from *Closteridium histolyticum* (Roche, Penzberg, Germany, Cat. No. 11 370 529 001) was performed in accordance with an adopted protocol from Borges et al.[77] To 50 μL of reconstituted DBP (45 μg) was added 50 μL of digestion buffer (100 mM Tris-HCl, 10 mM $CaCl_2$, pH 7.6), 10 μL of acetonitrile, 20 μL of

activation solution (50 mM dithiothreitol (DTT), 5 mM EDTA in water) and 10 μL of reconstituted Arg-C (50 mM Tris-HCl, 10 mM $CaCl_2$, pH 8.0, 1 μg Arg-C). The resultant mixture is incubated under shaking (750 rpm) at 37 °C for 2 h. The samples were stored at –20°C until use.

Mass spectrometric analysis was carried out on a Bruker Ultraflex MALDI TOF/TOF mass spectrometer (Bruker Daltonics, Coventry, UK) equipped with a nitrogen laser (wavelength 337 nm, pulse energy 100 μJ, pulse width 1ns). Samples were prepared by mixing 1 μl of protein Arg-C digest and 4 μl of CHCA matrix (α-cyano-hydroxycinnamic acid, saturated solution in 50% acetonitrile, 0.1% trifluoroacetic acid) and depositing 1 μl of the mixture on a steel target plate which was left to dry in air. Spectra were acquired in reflectron mode (mass range 500-4100 m/z) after instrument calibration with peptide calibration standard II (Bruker Daltonics, Coventry, UK). In order to calculate the theoretical mass of the Arg-C digest peptides the online tool PeptideMass from Expasy was used.[162]

#### 4.6.2.4 Enzymatic inhibition

Enzymatic assays were performed in house and by a collaborator Professor Atsushi Kato (University of Toyama)[141] analogous to the descriptions given in section 2.6.4 of Chapter 2.

#### 4.6.2.5 Free oligosaccharide analysis (FOS)

##### *4.6.2.5.1 Materials*

Sodium cyanoborohydride, bicinchoninic acid/copper (II) sulfate reagent, sodium acetate trihydrate and anthranilic acid (2-AA) from Sigma-Aldrich (Dorset, U.K.). Water was Milli-Q$^{TM}$ grade. Acetonitrile HPLC grade from Merk (Darmstadt, Germany), boric acid from BDH and Methanol from VWR (Lutterworth, Leicestershire, U.K.), ion exchange resins AG50-X12 and AG4-X4 from Biorad (Hemel Hampstead, Hertfordshire, U.K.), Spe-ed amide 2 from Applied

Separations (Allentown, Pennsylvania, U.S.), Amicon Ultra centrifugal filter from Millipore (Croxley, Watford, U.K.).

#### *4.6.2.5.2 Inhibition treatment of HL60 cells and FOS isolation*

Protocol was an adapted literature procedure according to Boomkamp et al.[126] Having been propagated at a higher density, HL60 cells were seeded in a 6 well plate at a 5 x $10^5$ cells/mL concentration and treated with 2 mL of fresh medium containing the derivatives of DGJNAc **239** at a concentration of 500 μM, 100 μM and 50 μM for 24 h. NB-DNJ (500 μM) and untreated wells were used as controls. For pyrrolidine **68** and its derivatives HL60 cells were treated at concentrations of 200 μM, 50 μM and 5 μM for 24 h. DGJNAc (500 μM) served as a positive control. Following incubation, cells were centrifuged at 350 g, 10 °C, for 7 min and the pellet was washed three times with PBS (5 mL). Washed cell pellets were stored at -20 °C until use. Following thawing at RT, samples were resuspended in 650 μL of water and Dounce homogenized. An aliquot of 50 μL was removed and treated for 16 h at RT with 2.6 μL NaOH (5 M) solution prior to protein concentration determination in comparison to a standard using bicinchoninic acid/copper(II) sulfate reagent (Sigma Aldrich). For desalting and deproteination, 500 μL of the homogenate was subjected to a mixed-bed ion-exchange column [0.2 mL of AG50-X12, ($H^+$, 100-200 mesh) 0.4 mL of AG4-X4, ($OH^-$, 100-200 mesh)], which had been preequilibrated with water (5 x 1 mL). The homogenate was added to the column and eluted with water (4 x 1 mL). The eluent containing the free oligosaccharides (FOS) was collected and dried by lyophilisation.

#### *4.6.2.5.3 FOS fluorescent labeling*

The lyophilised samples were resuspended in 300 μL total of water and transferred to an Eppendorf tube and evaporated to dryness using a Thermo Savant (SPD121P) SpeedVac system. As previously described[127] anthranilic acid (2-AA) was dissolved at 30 mg/mL in a solution

containing 4% sodium acetate trihydrate (w/v) and 2% boric acid (w/v) in methanol. To this mixture sodium cyanoborohydride was added to a final concentration of 45 mg/mL (labeling buffer). The dried samples were dissolved in 30 μL of water and 80 μL of 2-AA labeling buffer was added followed by incubation at 80 °C for 1 h.

#### *4.6.2.5.4 Purification of the labeled FOS*

After cooling, 1 mL of acetonitrile/water 97:3 was added to the labeled FOS samples, vortexed and added to a Spe-ed amide-2 column, which had been pre-equilibrated as follows: 1 mL acetonitrile, 2 mL water, 2 mL acetonitrile. The eluent was discarded and the column washed with 2 mL of acetonitrile/water 95:5 and discarded. The purified 2-AA labeled FOS were eluted by gravity using two times 0.75 mL water. Samples were stored at -20 °C until analysed by HPLC.

#### *4.6.2.5.5 Carbohydrate analysis by normal phase HPLC*

The Chromatography system used consisted of a Water Alliance 2695 separations module and an in-line Waters 474 fluorescence detector set at Exλ 360 nm and Emλ 425 nm.[128] The gain for the detector was set to 1000 and the emission bandwidth to 40 nm. Chromatography was performed at 30 °C. Solvent A was acetonitrile. Solvent B was water. Solvent C consisted of 800 mM ammonium hydroxide, titrated to pH 3.85 with acetic acid in water and was prepared using a standard ammonium hydroxide solution (5 M, Sigma Aldrich). Data collection and processing was performed using Waters Empower software. Glucose units were derived by comparison to a 2-AA labeled glucose oligomer ladder (obtained by partial digestion of dextran) as external standard. 50 μL of a 1:1 mixture sample/acetonitrile were injected for each run. Separation was performed on a 4.6 x 250 mm TSK gel-Amide 80 column (5 μM) (Anachem, Luton, Beds, U.K.) and the following gradient conditions were used for the analysis of the FOS samples: time = 0 min (t = 0), 71.6% A, 25.9% B, 2.5% C (0.8 mL/min); t = 6, 71.6% A, 25.9% B, 2.5% C (0.8 mL/min); t = 45, 46.2% A, 51.3% B, 2.5% C (0.8 mL/min); t = 46, 35% A, 62.5% B, 2.5% C

(0.8 mL/min); t = 48, 35% A, 62.5% B, 2.5% C (0.8 mL/min); t = 49, 71.6% A, 25.9% B, 2.5% C (0.8 mL/min); t = 51, 71.6% A, 25.9% B, 2.5% C (1.2 mL/min); t = 64, 71.6% A, 25.9% B, 2.5% C (1.2 mL/min); t = 65, 71.6% A, 25.9% B, 2.5% C (0.8 mL/min). Labeled FOS glycans were assigned according to literature GUs[126] for known species, which had been characterized using MALDI-TOF mass spectrometry.[142]

*4.6.2.5.6 Enzyme digest of FOS (Jack Bean β-N-acetyl-hexosaminidase)*

Glycosidase digest using jack bean β-*N*-acetyl-hexosaminidase (10 μL of 6 U/mL in 50 mM citrate buffer pH 5.0 containing 1 mg/mL BSA and 0.02% sodium azide, purified in house) was performed on a representative sample (100 μL) of the complete FOS population from 500 μM DGJNAc **239** treated HL60 cells. After 16 h incubation at 37 °C, the enzyme digest was diluted with 90 μL of water. An Amicon Ultra centrifugal filter (Millipore, 10,000 MWCO) was pretreated with 150 μL of water and used to remove proteins following centrifugation at 13,000 g for 15 min at 4 °C. The filter was washed with an additional 100 μL of water and the combined eluates were evaporated to dryness before being reconstituted in 100 μL of a 1:1 mixture of acetonitrile/water for HPLC analysis.

*4.6.2.5.7 Statistical analysis of FOS analysis*

Experiments were performed in triplicate. To test for significance the Prism 4.0a software was used to perform a student t-test using a 99% confidence interval.

**4.6.2.6 Cell metabolism and cytotoxicity assay**

In order to test an inhibitor for the interference with cell metabolism and associated cellular toxicity the following protocol was adapted from the CellTiter 96® $AQ_{ueous}$ Non-Radioactive Cell Proliferation Assay (Promega, Southampton, U.K.). The corresponding compound in a variety of increasing concentrations is incubated with the cell line to be tested for 24 or 72 h. 100 μL of the cell line to be tested contained in their growth medium were transferred into a 96-well

plate, 20 μL of development solution was added to each well and the mixture incubated for 4 h at 37 °C and 5% $CO_2$ before absorbance of the newly formed formazan was measured at 490 nm (Molecular Devices SPECTRAmax M5 Rom v2.1.35). The development solution is made up of a 20:1 mixture of 3-(4,5-dimethylthiazol-2-yl)-5-(3-carboxymethoxyphenyl)-2- (4-sulfophenyl)-2H-tetrazolium (MTS) in PBS (pH 6.5, sterile filtered and stored at -20 °C protected from light) and phenazine methosulfate (PMS) in PBS (0.92 mg/mL, sterile filtered), which are combined immediately before usage. This method was employed to rule out cellular toxicity in the case of the FOS assay involving the pyrrolidine **68** derivatives. Cellular toxicity for all cell lines involved in the cell invasion assay were tested against toxicity from DGJNAc **239** and pyrrolidine **68**.

#### 4.6.2.7 Cell invasion assay – Boyden-chamber setup

##### *4.6.2.7.1 3 day protocol of cell invasion*

The protocol was adapted from the instructions for the QCM™ 24-Well cell invasion assay (Merk Millipore, Watford, U.K., ECM 554) and involves steps spread over 3 days. The following protocol uses cells grown in a 225 $cm^2$ flask and employs 12 wells in total of a 24 well plate. Day 1: Cells having been grown for 2-3 passages following thawing, are placed in starvation medium (FCS free, no trypsination at this stage) for 24 h. Day 2: Following a visual inspection the cells are washed with PBS (30 mL) and incubated for 15 min with 9 mL of trypsin (Sigma Aldrich) at 37 °C and 5% $CO_2$. To the detached cells 15 mL of quenching medium (Bovine serum albumin 50 mg/mL in starvation medium; sterile filtered) is added and the cells are centrifuged into a pellet (300 x g, 5 min). The pellet is redissolved in quenching medium and the cell number adjusted accordingly. To allow for rehydration 300 μL of pre-warmed starvation medium containing drug or distilled water (sterile filtered) at the final concentration is added to the top insert and incubated for 15-30 min at RT. The solution in the insert is then aspirated and discarded. The prepared cell solution is adjusted to the final concentration using drug or distilled

water and 250 μL are added to the corresponding top insert. With exception to the negative control, where FCS free media is used, all bottom inserts are made up to the final concentration with drug and distilled water in regular cell growth medium containing FCS (chemo-attractant) and 500 μl are added to the corresponding bottom well. The thus prepared plate is then incubated at 37 °C at 5% $CO_2$ for 24-64 h. Day 3: The remaining wells on the 24-well plate are filled with 225 mL of pre-warmed cell detachment buffer (contained in kit). The well insert is lifted up and the cell solution contained is carefully aspirated and discarded and the insert with the invaded cells attached to the bottom is placed in the well containing detachment buffer. Following the transfer of all the inserts to the new wells the plate is incubated for 30 min at 37 °C and gently shaken every 10 min. The inserts are then discarded and 75 μL of CyQUANT dye/lysis buffer (1:75 mixture of dye/lysis buffer)[155] was added to each well and the resulting solution incubated at RT for 15 min. Of the resultant solution 200 μL are transferred into a 96 well plate and fluorescence was determined (Molecular Devices SPECTRAmax M5 Rom v2.1.35, excitation 485 nm, emission 538 nm).

##### *4.6.2.7.2 Statistical analysis*

Experiments were performed in triplicate whenever possible and otherwise in duplicate. To test for significance the Prism 4.0a software was used to perform a student t-test using a 95% confidence interval.

#### 4.6.2.8 Protein concentration determination

Protein concentrations were determined as follows: In a 50:1 ratio bicinchoninic acid solution (Sigma-Aldrich, B9643) was combined with copper(II) sulfate solution (Sigma-Aldrich, C2284) and 200 μL of this solution was added to a 10 μL protein sample in a 96-well plate. Following incubation at 37 °C for 30 min absorbance was measured at 600 nm (Molecular Devices UVmax

kinetic microplate reader and SOFTmax 2.35 software). Protein content in triplicate was determined in comparison to a protein standard (bovine serum albumin, Sigma-Aldrich, P0914).

## 4.7 References Chapter 4


1. (a) Hirschfeld, J.; Jonsson, B.; Rasmuson, M., Inheritance of a new group-specific system demonstrated in normal human sera by means of an immuno-electrophoretic technique. *Nature* **1960**, *185*, 931-932; (b) Hirschfeld, J., Immune-electrophoretic demonstration of qualitative differences in human sera and their relation to the haptoglobins. *Acta. Path. Micro. Im.* **1959**, *47*, 160-168.

2. Daiger, S.; Schanfield, M.; Cavallisforza, L., Group-specific component (GC) proteins bind vitamin-D and 25-hydroxyvitamin-D. *P. Natl. Acad. Sci. Usa* **1975**, *72*, 2076-2080.

3. Cleve, H.; Constans, J., The mutants of the vitamin-D-binding protein - more than 120 Variants of the GC/DBP system. *Vox Sang.* **1988**, *54*, 215-225.

4. Constans, J.; Viau, M., Group-specific component - evidence for 2 subtypes of GC1 gene. *Science* **1977**, *198*, 1070-1071.

5. Cleve, H.; Patutschnick, W., Neuraminidase treatment reveals sialic acid differences in certain genetic variants of the Gc system (vitamin-D-binding protein). *Hum. Genet.* **1979**, *47*, 193-198.

6. Abbas, S.; Linseisen, J.; Slanger, T.; Kropp, S.; Mutschelknauss, E. J.; Flesch-Janys, D.; Chang-Claude, J., The Gc2 allele of the vitamin D binding protein is associated with a decreased postmenopausal breast cancer risk, independent of the vitamin D status. *Cancer Epidemiol. Biomarkers Prev.* **2008**, *17*, 1339-1343.

7. Kawakami, M.; Blum, C. B.; Ramakrishnan, R., Turnover of the plasma bindng protein for vitamin D and its metabolites in normal human subjects. *J. Clin. Endocrinol. Metab.* **1981**, *53*, 1110-1116.

8. Schoentgen, F.; Metz-Boutique, M.-H.; Jollès, J.; Constans, J.; Jollès, P., Complete amino acid sequence of human vitamin D-binding protein (group-specific component): evidence of a three-fold internal homology as in serum albumin and α-fetoprotein. *Biochim. Biophys. Acta* **1986**, *871*, 189-198.

9. Braun, A.; Bichlmaier, R.; Cleve, H., Molecular analysis of the gene for the human vitamin-D-binding protein (group-specific component): Allelic differences of the common genetic GC types. *Hum. Genet.* **1992**, *89*, 401-406.

10. Braun, A.; Kofler, A.; Morawietz, S.; Cleve, H., Sequence and organization of the human vitamin D-binding protein gene. *Biochim. Biophys. Acta Gene Struct. Expression* **1993**, *1216*, 385-394.

11. Verboven, C.; Ragijns, A.; De Maeyer, M.; Van Baelen, H.; Bouillon, R.; De Ranter, C., A structural basis for the unique binding features of the human vitamin D-binding protein. *Nat. Struct. Biol.* **2002**, *9*, 131-136.

12. (a) Head, J.; Swamy, N.; Ray, R., Crystal structure of the complex between actin and human vitamin D-binding protein at 2.5 angstrom resolution. *Biochemistry (Wash.)* **2002**, *41*, 9015-9020; (b) Otterbein, L. R.; Cosio, C.; Graceffa, P.; Dominguez, R., Crystal structures of the vitamin D-binding protein and its complex with actin: Structural basis of the actin-scavenger system. *Proc. Natl. Acad. Sci. U. S. A.* **2002**, *99*, 8003-8008; (c) Verboven, C.; Bogaerts, I.; Waelkens, E.; Rabijns, A.; Van Baelen, H.; Bouillon, R.; De Ranter, C., Actin-DBP: The perfect structural fit? *Acta Crystallogr. Sect. D. Biol. Crystallogr.* **2003**, *59*, 263-273.

13. Van Baelen, H.; Bouillon, R.; De Moor, P., Vitamin D-binding protein (Gc-globulin) binds actin. *J. Biol. Chem.* **1980**, *255*, 2270-2272.

14. McLeod, J. F.; Kowalski, M. A.; Haddad Jr., J. G., Interactions among serum vitamin D binding protein, monomeric actin, profilin, and profilactin. *J. Biol. Chem.* **1989**, *264*, 1260-1267.

15. Calvo, M.; Ena, J. M., Relations between vitamin D and fatty acid binding properties of vitamin D-binding protein. *Biochem. Biophys. Res. Commun.* **1989**, *163*, 14-17.

16. McVoy, L. A.; Kew, R. R., CD44 and annexin A2 mediate the C5a chemotactic cofactor function of the vitamin D binding protein. *J. Immunol.* **2005**, *175*, 4754-4760.

17. (a) Cooke, N. E.; Haddad, J. G., Vitamin D binding protein (Gc-globulin). *Endocr. Rev.* **1989**, *10*, 294-307; (b) Haddad, J. G., Plasma vitamin D-binding protein (Gc-globulin): Multiple tasks. *J. Steroid Biochem. Mol. Biol.* **1995**, *53*, 579-582.

18. Speeckaert, M.; Huang, G.; Delanghe, J. R.; Taes, Y. E. C., Biological and clinical aspects of the vitamin D binding protein (Gc-globulin) and its polymorphism. *Clin. Chim. Acta* **2006**, *372*, 33-42.

19. Ngwenya, B. Z.; Yamamoto, N., Activation of peritoneal macrophages by lysophosphatidylcholine. *Biochim. Biophys. Acta* **1985**, *839*, 9-15.

20. Yamamoto, N.; Homma, S.; Millman, I., Identification of the serum factor required for in vitro activation of macrophages: Role of vitamin D3-binding protein (group specific component, Gc) in lysophospholipid activation of mouse peritoneal macrophages. *J. Immunol.* **1991**, *147*, 273-280.

21. Yamamoto, N.; Homma, S., Vitamin-D3 binding-protein (Group-specific component) is a precursor for the macrophage-activating signal factor from lysophosphatidylcholine-treated lymphocytes. *Proc. Natl. Acad. Sci. U. S. A.* **1991**, *88*, 8539-8543.

22. Yamamoto, N.; Kumashiro, R., Conversion of vitamin D3 binding protein (group-specific component) to a macrophage activating factor by the stepwise action of β-galactosidase of B cells and sialidase of T cells. *J. Immunol.* **1993**, *151*, 2794-2802.

23. Yamamoto, N., Structural definition of a potent macrophage activating factor derived from vitamin D-3 binding protein with adjuvant activity for antibody production. *Mol. Immunol.* **1996**, *33*, 1157-1164.

24. Yamamoto, N. Macrophage activating factor from vitamin D binding protein. US5326749, 1994.

25. Yamamoto, N.; Naraparaju, V.; Asbell, S., Deglycosylation of serum vitamin D-3-binding protein leads to immunosuppression in cancer patients. *Cancer Res.* **1996**, *56*, 2827-2831.

26. Nagasawa, H.; Sasaki, H.; Uto, Y.; Kubo, S.; Hori, H., Association of the macrophage activating factor (MAF) precursor activity with polymorphism in vitamin D-binding protein. *Anticancer Res.* **2004**, *24*, 3361-3366.

27. (a) Uto, Y.; Yamamoto, S.; Takeuchi, R.; Nakagawa, Y.; Hirota, K.; Terada, H.; Onizuka, S.; Nakata, E.; Hori, H., Effect of the Gc-derived Macrophage-activating Factor Precursor (preGcMAF) on Phagocytic Activation of Mouse Peritoneal Macrophages. *Anticancer Res.* **2011**, *31*, 2489-2492; (b) Uto, Y.; Yamamoto, S.; Mukai, H.; Ishiyama, N.; Takeuchi, R.; Nakagawa, Y.; Hirota, K.; Terada, H.; Onizuka, S.; Hori, H., β-Galactosidase Treatment Is a Common First-stage Modification of the Three Major Subtypes of Gc Protein to GcMAF. *Anticancer Res.* **2012**, *32*, 2359-2364.

28. Aliprantis, A. O.; Diez-Roux, G.; Mulder, L. C. F.; Zychlinsky, A.; Lang, R. A., Do macrophages kill through apoptosis? *Immunol. Today* **1996**, *17*, 573-576.

29. Mytar, B.; Siedlar, M.; Wołoszyn, M.; Ruggiero, I.; Pryjma, J.; Zembala, M., Induction of reactive oxygen intermediates in human monocytes by tumour cells and their role in spontaneous monocyte cytotoxicity. *Br. J. Cancer* **1999**, *79*, 737-743.

30. Yamamoto, N.; Willett, N. P.; Lindsay, D. D., Participation of serum proteins in the inflammation-primed activation of macrophages. *Inflammation* **1994**, *18*, 311-322.

31. Mohamad, S.; Nagasawa, H.; Uto, Y.; Hori, H., Tumor cell alpha-N-acetylgalactosaminidase activity and its involvement in GcMAF-related macrophage activation. *Comp. Biochem. Physiol.* **2002**, *132*, 1-8.

32. Bin Mohamad, S.; Nagasawa, H.; Sasaki, H.; Uto, Y.; Nakagawa, Y.; Kawashima, K.; Hori, H., Gc protein-derived macrophage activating factor (GcMAF): Isoelectric focusing pattern and tumoricidal activity. *Anticancer Res.* **2003**, *23*, 4451-4457.

33. Yamamoto, N.; Naraparaju, V., Immunotherapy of BALB/c mice bearing Ehrlich ascites tumor with vitamin D-binding protein-derived macrophage activating factor. *Cancer Res.* **1997**, *57*, 2187-2192.

34. Koga, Y.; Naraparaju, V.; Yamamoto, N., Antitumor effect of vitamin D-binding protein-derived macrophage activating factor on Ehrlich ascites tumor-bearing mice. *Proc. Soc. Exp. Biol. Med.* **1999**, *220*, 20-26.

35. Toyohara, Y.; Hashitani, S.; Kishimoto, H.; Noguchi, K.; Yamamoto, N.; Urade, M., Inhibitory effect of vitamin D-binding protein-derived macrophage activating factor on DMBA-induced hamster cheek pouch carcinogenesis and its derived carcinoma cell line. *Oncology Letters* **2011**, *2*, 685-691.

36. Nonaka, K.; Onizuka, S.; Ishibashi, H.; Uto, Y.; Hori, H.; Nakayama, T.; Matsuura, N.; Kanematsu, T.; Fujioka, H., Vitamin D binding protein-macrophage activating factor inhibits HCC in SCID mice. *J. Surg. Res.* **2012**, *172*, 116-122.

37. Yamamoto, N.; Suyama, H.; Yamamoto, N.; Ushijima, N., Immunotherapy of metastatic breast cancer patients with vitamin D-binding protein-derived macrophage activating factor (GcMAF). *Int. J. Cancer* **2008**, *122*, 461-467.

38. Yamamoto, N.; Suyama, H.; Nakazato, H.; Yamamoto, N.; Koga, Y., Immunotherapy of metastatic colorectal cancer with vitamin D-binding protein-derived macrophage-activating factor, GcMAF. *Cancer Immunol., Immunother.* **2008**, *57*, 1007-1016.

39. Yamamoto, N.; Suyama, H.; Yamamoto, N., Immunotherapy for Prostate Cancer with Gc Protein-Derived Macrophage-Activating Factor, GcMAF. *Transl. Oncol.* **2008**, *1*, 65-72.

40. Yamamoto, N.; Ushijima, N.; Koga, Y., Immunotherapy of HIV-Infected Patients With Gc Protein-Derived Macrophage Activating Factor (GcMAF). *J. Med. Virol.* **2009**, *81*, 16-26.

41. Gumireddy, K.; Reddy, C.; Swamy, N., Mitogen-activated protein kinase pathway mediates DBP-maf-induced apoptosis in RAW 264.7 macrophages. *J. Cell. Biochem.* **2003**, *90*, 87-96.

42. Gregory, K. J.; Zhao, B.; Bielenberg, D. R.; Dridi, S.; Wu, J.; Jiang, W.; Huang, B.; Pirie-Shepherd, S.; Fannon, M., Vitamin D Binding Protein-Macrophage Activating Factor Directly Inhibits Proliferation, Migration, and uPAR Expression of Prostate Cancer Cells. *Plos One* **2010**, *5*, e13428.

43. (a) Hanahan, D.; Weinberg, R., The hallmarks of cancer. *Cell* **2000**, *100*, 57-70; (b) Hanahan, D.; Weinberg, R. A., Hallmarks of Cancer: The Next Generation. *Cell* **2011**, *144*, 646-674.

44. Kanda, S.; Mochizuki, Y.; Miyata, Y.; Kanetake, H.; Yamamoto, N., Effects of vitamin D-3-binding protein-derived macrophage activating factor (GcMAF) on angiogenesis. *J. Natl. Cancer Inst.* **2002**, *94*, 1311-1319.

45. Kisker, O.; Onizuka, S.; Becker, C.; Fannon, M.; Flynn, E.; D'Amato, R.; Zetter, B.; Folkman, J.; Ray, R.; Swamy, N.; Pirie-Shepherd, S., Vitamin D binding protein-macrophage activating factor (DBP-maf) inhibits angiogenesis and tumor growth in mice. *Neoplasia* **2003**, *5*, 32-40.

46. Kalkunte, S.; Brard, L.; Granai, C. O.; Swamy, N., Inhibition of angiogenesis by vitamin D-binding protein: Characterization of anti-endothelial activity of DBP-maf. *Angiogenesis* **2005**, *8*, 349-360.

47. Pacini, S.; Morucci, G.; Punzi, T.; Gulisano, M.; Ruggiero, M., Gc protein-derived macrophage-activating factor (GcMAF) stimulates cAMP formation in human mononuclear cells and inhibits angiogenesis in chick embryo chorionallantoic membrane assay. *Cancer Immunol., Immunother.* **2011**, *60*, 479-485.

48. Pacini, S.; Punzi, T.; Morucci, G.; Gulisano, M.; Ruggiero, M., Effects of Vitamin D-binding Protein-derived Macrophage-activating Factor on Human Breast Cancer Cells. *Anticancer Res.* **2012**, *32*, 45-52.

49. Yamamoto, N. Diagnostic and prognostic indices for cancer and aids. US5620846, 1997.

50. Yamamoto, N. Diagnostic and prognostic ELISA assay of Serum plasma α-N-acetylgalactosaminidase for cancer. US5712104, 1998.

51. Korbelik, M.; Naraparaju, V.; Yamamoto, N., The value of serum alpha-N-acetyl galactosaminidase measurement for the assessment of tumour response to radio- and photodynamic therapy. *Br. J. Cancer* **1998**, *77*, 1009-1014.

52. Reddi, A.; Sankaranarayanan, K.; Arulraj, H.; Devaraj, N.; Devaraj, H., Serum alpha-N-acetylgalactosaminidase is associated with diagnosis/prognosis of patients with squamous cell carcinoma of the uterine cervix. *Cancer Lett.* **2000**, *158*, 61-64.

53. CRUK; How many stages of cancer are there? http://www.cancerresearchuk.org/cancer-help/about-cancer/cancer-questions/how-many-stages-of-cancer-are-there

54. Greco, M.; Mitri, M. D.; Chiriacò, F.; Leo, G.; Brienza, E.; Maffia, M., Serum proteomic profile of cutaneous malignant melanoma and relation to cancer progression: Association to tumor derived alpha-N-acetylgalactosaminidase activity. *Cancer Lett.* **2009**, *283*, 222-229.

55. Svasti, J.; Bowman, B., Human group-specific component - changes in electrophoretic mobility resulting from vitamin-D binding and from neuraminidase digestion. *J. Biol. Chem.* **1978**, *253*, 4188-4194.

56. Svasti, J.; Kurosky, A.; Bennett, A.; Bowman, B., Molecular-basis for the 3 major forms of human-serum vitamin-D binding-protein (Group-specific component). *Biochemistry (Wash.)* **1979**, *18*, 1611-1617.

57. Coppenhaver, D.; Sollenne, N.; Bowman, B., Post-translational heterogeneity of the human vitamin-D-binding protein (Group-specific component). *Arch. Biochem. Biophys.* **1983**, *226*, 218-223.

58. Viau, M.; Constans, J.; Debray, H.; Montreuil, J., Isolation and characterization of the O-glycan chain of the human vitamin-D binding-protein. *Biochem. Biophys. Res. Commun.* **1983**, *117*, 324-331.

59. Gejyo, F.; Chang, J.; Burgi, W.; Schmid, K.; Offner, G.; Troxler, R.; Vanhalbeek, H.; Dorland, L.; Gerwig, G.; Vliegenthart, J., Characterization of the B-chain of human-plasma alpha-2-HS-glycoprotein - the complete amino-acid-sequence and primary structure of its heteroglycan. *J. Biol. Chem.* **1983**, *258*, 4966-4971.

60. Nilsson, B.; Nordén, N. E.; Svensson, S., Structural studies on the carbohydrate portion of fetuin. *J. Biol. Chem.* **1979**, *254*, 4545-4553.

61. Ishii-Karakasa, I.; Iwase, H.; Hotta, K., Structural determination of the O-linked sialyl oligosaccharides liberated from fetuin with endo-α-N-acetylgalactosaminidase-S by HPLC analysis and 600-MHz 1H-NMR spectroscopy. *Eur. J. Biochem.* **1997**, *247*, 709-715.

62. Ishii-Karakasa, I.; Iwase, H.; Hotta, K.; Tanaka, Y.; Omura, S., Partial purification and characterization of an endo-α-N-acetylgalactosaminidase from the culture medium of Streptomyces sp. OH-11242. *Biochem. J* **1992**, *288*, 475-482.

63. Oda, S.; Sato, M.; Toyoshima, S.; Osawa, T., Purification and characterization of a lectin-like molecule specific for galactose/N-acetyl-galactosamine from tumoricidal macrophages. *J. Biochem.* **1988**, *104*, 600-605.

64. Suzuki, N.; Yamamoto, K.; Toyoshima, S.; Osawa, T.; Irimura, T., Molecular cloning and expression of cDNA encoding human macrophage C-type lectin: Its unique carbohydrate binding specificity for Tn antigen. *J. Immunol.* **1996**, *156*, 128-135.

65. Prohaska, R.; Koerner Jr., T. A. W.; Armitage, I. M.; Furthmayr, H., Chemical and carbon-13 nuclear magnetic resonance studies of the blood group M and N sialoglycopeptides from human glycophorin A. *J. Biol. Chem.* **1981**, *256*, 5781-5791.

66. Ju, T.; Otto, V. I.; Cummings, R. D., The Tn antigena-structural simplicity and biological complexity. *Angew. Chem. Int. Ed.* **2011**, *50*, 1770-1791.

67. Brockhausen, I., Mucin-type O-glycans in human colon and breast cancer: Glycodynamics and functions. *EMBO Reports* **2006**, *7*, 599-604.

68. Iida, S.; Yamamoto, K.; Irimura, T., Interaction of human macrophage C-type lectin with O-linked N-acetylgalactosamine residues on mucin glycopeptides. *J. Biol. Chem.* **1999**, *274*, 10697-10705.

69. Higashi, N.; Morikawa, A.; Fujioka, K.; Fujita, Y.; Sano, Y.; Miyata-Takeuchi, M.; Suzuki, N.; Irimura, T., Human macrophage lectin specific for galactose/N-acetylgalactosamine is a marker for cells at an intermediate stage in their differentiation from monocytes into macrophages. *Int. Immunol.* **2002**, *14*, 545-554.

70. van Vliet, S. J.; Saeland, E.; van Kooyk, Y., Sweet preferences of MGL: carbohydrate specificity and function. *Trends Immunol.* **2008**, *29*, 83-90.

71. Napoletano, C.; Zizzari, I. G.; Rughetti, A.; Rahimi, H.; Irimura, T.; Clausen, H.; Wandall, H. H.; Belleudi, F.; Bellati, F.; Pierelli, L.; Frati, L.; Nuti, M., Targeting of macrophage galactose-type C-type lectin (MGL) induces DC signaling and activation. *Eur. J. Immunol.* **2012**, *42*, 936-945.

72. Jorgensen, C.; Christiansen, M.; Laursen, I.; Krogsoe, L.; Hojrup, P.; Blou, L.; Houen, G., Large-scale purification and characterization of nonglycosylated Gc globulin (vitamin D-binding protein) from plasma fraction IV. *Biotechnol. Appl. Biochem.* **2006**, *44*, 35-44.

73. Christiansen, M.; Jorgensen, C. S.; Laursen, I.; Hirschberg, D.; Hojrup, P.; Houen, G., Protein chemical characterization of Gc globulin (vitamin D-binding protein) isoforms; Gc-1f, gc-1s and gc-2. *Biochim. Biophys. Acta: Proteins Proteomics* **2007**, *1774*, 481-492.

74. Joergensen, C. S.; Laursen, I.; Houen, G. Purification process for large scale production of GC-globulin, the GC-globulin produced hereby, a use of Gc.globulin and a GC-globulin medicinal product. US6806355, 2004.

75. Kistler, P.; Nitschmann, H., Large Scale Production of Human Plasma Fractions. *Vox Sang.* **1962**, *7*, 414-424.

76. Gobom, J.; Nordhoff, E.; Mirgorodskaya, E.; Ekman, R.; Roepstorff, P., Sample purification and preparation technique based on nano-scale reversed-phase columns for the sensitive analysis of complex peptide mixtures by matrix-assisted laser desorption/ionization mass spectrometry. *J. Mass Spectrom.* **1999**, *34*, 105-116.

77. Borges, C. R.; Jarvis, J. W.; Oran, P. E.; Nelson, R. W., Population studies of Vitamin D binding protein microheterogeneity by mass spectrometry lead to characterization of its genotype-dependent O-glycosylation patterns. *J. Proteome Res.* **2008**, *7*, 4143-4153.

78. Rehder, D. S.; Nelson, R. W.; Borges, C. R., Glycosylation status of vitamin D binding protein in cancer patients. *Protein Sci.* **2009**, *18*, 2036-2042.

79. Ravnsborg, T.; Olsen, D. T.; Thysen, A. H.; Christiansen, M.; Houen, G.; Højrup, P., The glycosylation and characterization of the candidate Gc macrophage activating factor. *Biochim. Biophys. Acta: Proteins Proteomics* **2010**, *1804*, 909-917.

80. Niedbala, M.; Madiyalakan, R.; Matta, K.; Crickard, K.; Sharma, M.; Bernacki, R., Role of glycosidases in human ovarian-carcinoma cell-mediated degradation of subendothelial extracellular-matrix. *Cancer Res.* **1987**, *47*, 4634-4641.

81. Albert, B.; Johnson, A.; Lewis, J.; Raff, M.; Roberts, K.; Walter, P., Cell Junctions, Cell Adhesion, and the Extracellular Matrix. In *Molecular Biology of the Cell*, Fifth ed.; Garland Science: New York, 2008.

82. Jones, P. A.; De Clerck, Y. A., Extracellular matrix destruction by invasive tumor cells. *Cancer Metastasis Rev.* **1982**, *1*, 289-317.

83. Fauve, R. M., Some aspects of the macrophage-cancer relationship. *Res. Immunol.* **1993**, *144*, 265-268.

84. Bosmann, H. B., Glycoprotein degradation. Glycosidases in fibroblasts transformed by oncogenic viruses. *Exp. Cell Res.* **1969**, *54*, 217-221.

85. (a) Simizu, S.; Ishida, K.; Osada, H., Heparanase as a molecular target of cancer chemotherapy. *Cancer Sci.* **2004**, *95*, 553-558; (b) Kramer, R. H.; Vogel, K. G.; Nicolson, G. L., Solubilization and degradation of subendothelial matrix glycoproteins and proteoglycans by metastatic tumor cells. *J. Biol. Chem.* **1982**, *257*, 2678-2686.

86. Bosmann, H. B.; Hall, T. C., Enzyme activity in invasive tumors of human breast and colon. *Proc. Natl. Acad. Sci. U. S. A.* **1974**, *71*, 1833-1837.

87. Bernacki, R.; Niedbala, M.; Korytnyk, W., Glycosidases in cancer and invasion. *Cancer Metastasis Rev.* **1985**, *4*, 81-101.

88. (a) Dennis, J.; Granovsky, M.; Warren, C., Glycoprotein glycosylation and cancer progression. *Bba-Gen Subjects* **1999**, *1473*, 21-34; (b) Ohyama, C., Glycosylation in bladder cancer. *International Journal of Clinical Oncology* **2008**, *13*, 308-313.

89. Meany, D. L.; Chan, D. W., Aberrant glycosylation associated with enzymes as cancer biomarkers. *Clinical Proteomics* **2011**, *8*.

90. Bosmann, H. B.; Bernacki, R. J., Glycosidase activity. Glycosidase activity in L5178Y mouse leukemic cells and the activity of acid phosphatase, β-galactosidase and β-N-acetylgalactosaminidase and β-N-acetylglucosaminidase in a synchronous L5178Y cell population. *Exp. Cell Res.* **1970**, *61*, 379-386.

91. Bosmann, H. B.; Bieber, G. F.; Brown, A. E.; Case, K. R.; Gersten, D. M.; Kimmerer, T. W.; Lione, A., Biochemical parameters correlated with tumour cell implantation. *Nature* **1973**, *246*, 487-489.

92. Dobrossy, L.; Pavelic, Z. P.; Vaughan, M.; Porter, N.; Bernacki, R. J., Elevation of lysosomal enzymes in primary Lewis lung tumor correlated with the initiation of metastasis. *Cancer Res.* **1980**, *40*, 3281-3285.

93. Yagi, F.; Eckhardt, A.; Goldstein, I., Glycosidases of Ehrlich ascites tumor-cells and ascites fluid purification and substrate-specificity of alpha-N-acetylgalactosaminidase and alpha-galactosidase - comparison with coffee bean alpha-galactosidase. *Arch. Biochem. Biophys.* **1990**, *280*, 61-67.

94. Whitehead, J. S.; Fearney, F. J.; Kim, Y. S., Glycosyltransferase and glycosidase activities in cultured human fetal and colonic adenocarcinoma cell lines. *Cancer Res.* **1979**, *39*, 1259-1263.

95. Klohs, W. D.; Mastrangelo, R.; Weiser, M. M., Release of glycosyltransferase and glycosidase activities from normal and transformed cell lines. *Cancer Res.* **1981**, *41*, 2611-2615.

96. Chatterjee, S. K.; Chowdhury, K.; Bhattacharya, M.; Barlow, J. J., Beta-hexosaminidase activities and isoenzymes in normal human ovary and ovarian adenocarcinoma. *Cancer* **1982**, *49*, 128-135.

97. Narita, M.; Taniguchi, N.; Makita, A.; Kodama, T.; Araki, E.; Oikawa, K., Elevated activity of β-hexosaminidase and sulfhydryl modification in the B-variant of human lung cancer. *Cancer Res.* **1983**, *43*, 5037-5042.

98. Wielgat, P.; Walczuk, U.; Szajda, S.; Bien, M.; Zimnoch, L.; Mariak, Z.; Zwierz, K., Activity of lysosomal exoglycosidases in human gliomas. *J. Neurooncol.* **2006**, *80*, 243-249.

99. Szajda, S. D.; Waszkiewicz, N.; Stypulkowska, A.; Dadan, J.; Zwierz, K., Lysosomal exoglycosidases in serum and urine of patients with pancreatic adenocarcinoma. *Folia Histochem. Cytobiol.* **2010**, *48*, 351-357.

100. Thompson, J. N.; Stoolmiller, A. C.; Matalon, R.; Dorfman, A., N-acetyl-β-hexosaminidase: role in the degradation of glycosaminoglycans. *Science* **1973**, *181*, 866-867.

101. Dimitroff, C.; Sharma, A.; Bernacki, R., Cancer metastasis: A search for therapeutic inhibition. *Cancer Invest.* **1998**, *16*, 279-290.

102. Mehlen, P.; Puisieux, A., Metastasis: A question of life or death. *Nat. Rev. Cancer* **2006**, *6*, 449-458.

103. Niedbala, M. J.; Crickard, K.; Bernacki, R. J., In vitro degradation of extracellular matrix by human ovarian carcinoma cells. *Clin. Exp. Metastasis* **1987**, *5*, 181-197.

104. Woynarowska, B.; Wikiel, H.; Bernacki, R., Human ovarian-carcinoma beta-N-acetylglucosaminidase isoenzymes and their role in extracellular-matrix degradation. *Cancer Res.* **1989**, *49*, 5598-5604.

105. Fleet, G. W. J.; Fellows, L. E.; Smith, P. W., Synthesis of deoxymannojirimycin fagomine deoxynojirimycin 2-acetamido-1,5-imino-1,2,5-trideoxy-D-mannitol 2-acetamido-1,5-imino-1,2,5-trideoxy-D-glucitol 2S, 3R, 4R, 5R-trihydroxypipecolic acid and 2S, 3R, 4R, 5S-trihydroxypipecolic acid from methyl 3-O-benzyl-2,6-dideoxy-2,6-imino-α-D-mannofuranoside. *Tetrahedron* **1987**, *43*, 979-990.

106. Fleet, G. W. J.; Smith, P. W.; Nash, R. J.; Fellows, L. E.; Parekh, R. B.; Rademacher, T. W., Synthesis of 2-Acetamide-1,5-imino-1,2,5-trideoxy-D-mannitol and of 2-Acetamido-1,5-imino-1,2,5-trideoxy-D-glucitol, a Potent and Specific Inhibitor of a Number of β-N-Acetylglucosaminidase. *Chem. Lett.* **1986**, 1051-1054.

107. Woynarowska, B.; Wikiel, H.; Sharma, M.; Carpenter, N.; Fleet, G.; Bernacki, R., Inhibition of human ovarian-carcinoma cell-mediated and hexosaminidase-mediated degradation of extracellular-matrix by sugar analogs. *Anticancer Res.* **1992**, *12*, 161-166.

108. Michalik, A.; Hollinshead, J.; Jones, L.; Fleet, G. W. J.; Yu, C.-Y.; Hu, X.-G.; Van Well, R.; Horne, G.; Wilson, F. X.; Kato, A.; Jenkinson, S. F.; Nash, R. J., Steviamine, a new indolizidine alkaloid from Stevia rebaudiana. *Phytochemistry Lett.* **2010**, *3*, 136-138.

109. Ramessur, K. T.; Greenwell, P.; Nash, R.; Dwek, M. V., Breast cancer invasion is mediated by beta-N-acetylglucosaminidase (beta-NAG) and associated with a dysregulation in the secretory pathway of cancer cells. *Br. J. Biomed. Sci.* **2010**, *67*, 189-196.

110. Thompson, A. L.; Michalik, A.; Nash, R. J.; Wilson, F. X.; Well, R. V.; Johnson, P.; Fleet, G. W. J.; Yu, C.-Y.; Hu, X.-G.; Cooper, R. I.; Watkin, D. J., Steviamine, a new class of indolizidine alkaloid [(1R,2S,3R,5R,8aR)-3- hydroxy-meth-yl-5-methyl-octa-hydro-indolizine-1,2-diol hydro-bromide]. *Acta Crystallogr. Sect. Sect. E: Struct. Rep. Online* **2009**, *65*, o2904-o2905.

111. Hu, X.-G.; Bartholomew, B.; Nash, R. J.; Wilson, F. X.; Fleet, G. W. J.; Nakagawa, S.; Kato, A.; Jia, Y.-M.; van Well, R.; Yu, C.-Y., Synthesis and Glycosidase Inhibition of the Enantiomer of (-)-Steviamine, the First Example of a New Class of Indolizidine Alkaloid. *Org. Lett.* **2010**, *12*, 2562-2565.

112. Millar, A. W.; Brown, P. D.; Moore, J.; Galloway, W. A.; Cornish, A. G.; Lenehan, T. J.; Lynch, K. P., Results of single and repeat dose studies of the oral matrix metalloproteinase inhibitor marimastat in healthy male volunteers. *Br. J. Clin. Pharmacol.* **1998**, *45*, 21-26.

113. Evans, J. D.; Stark, A.; Johnson, C. D.; Daniel, F.; Carmichael, J.; Buckels, J.; Imrie, C. W.; Brown, P.; Neoptolemos, J. P., A phase II trial of marimastat in advanced pancreatic cancer. *Br. J. Cancer* **2001**, *85*, 1865-1870.

114. Sparano, J. A.; Bernardo, P.; Stephenson, P.; Gradishar, W. J.; Ingle, J. N.; Zucker, S.; Davidson, N. E., Randomized phase III trial of marimastat versus placebo in patients with metastatic breast cancer who have responding or stable disease after first-line chemotherapy: Eastern Cooperative Oncology Group trial E2196. *J. Clin. Oncol.* **2004**, *22*, 4683-4690.

115. Coussens, L.; Fingleton, B.; Matrisian, L., Matrix metalloproteinase inhibitors and cancer—trials and tribulations. *Science* **2002**.

116. Markman, M., Challenges associated with evaluating the clinical utility of non-cytotoxic pharmaceutical agents in oncology. *J. Cancer Res. Clin. Oncol.* **1997**, *123*, 581-582.

117. Goffin, J. R.; Anderson, I. C.; Supko, J. G.; Eder Jr., J. P.; Shapiro, G. I.; Lynch, T. J.; Shipp, M.; Johnson, B. E.; Skarin, A. T., Phase I trial of the matrix metalloproteinase inhibitor marimastat combined with carboplatin and paclitaxel in patients with advanced non-small cell lung cancer. *Clin. Cancer Res.* **2005**, *11*, 3417-3424.

118. Hempel, S.; Buettner, G.; O'Malley, Y.; Wessels, D.; Flaherty, D., Dihydrofluorescein diacetate is superior for detecting intracellular oxidants: Comparison with 2 ',7 '-dichlorodihydrofluorescein diacetate, 5(and 6)-carboxy-2 ',7 '-dichlorodihydrofluorescein diacetate, and dihydrorhodamine 123. *Free Radic. Biol. Med.* **1999**, *27*, 146-159.

119. Noda, T.; Amano, F., Differences in nitric oxide synthase activity in a macrophage-like cell line, RAW264.7 cells, treated with lipopolysaccharide (LPS) in the presence or absence of interferon-gamma (IFN-gamma): Possible heterogeneity of iNOS activity. *J. Biochem., Tokyo* **1997**, *121*, 38-46.

120. I would like to thank Dr. H. Kramer for machine time and his assitance at Oxion Proteomics Facility, Oxford Centre for Gene Function, Department of Physiology, Anatomy and Genetics, University of Oxford, South Parks Road, Oxford, OX1 3QX.

121. (a) Link, R.; Perlman, K.; Pierce, E.; Schnoes, H.; Deluca, H., Purification of human-serum vitamin D-binding protein by 25-hydroxyvitamin-D3-sepharose chromatography. *Anal. Biochem.* **1986**, *157*, 262-269; (b) Swamy, N.; Roy, A.; Chang, R.; Brisson, M.; Ray, R., Affinity purification of human plasma vitamin-D-binding protein. *Protein Expression Purif.* **1995**, *6*, 185-188.

122. (a) Miura, Y.; Kato, K.; Takegawa, Y.; Kurogochi, M.; Furukawa, J.-I.; Shinohara, Y.; Nagahori, N.; Amano, M.; Hinou, H.; Nishimura, S.-I., Glycoblotting-assisted O-glycomics: Ammonium carbamate allows for highly efficient o-glycan release from glycoproteins. *Anal. Chem.* **2010**, *82*, 10021-10029; (b) Method for releasing reducing glycan by ammonium salt. EP2322532, 2009; (c) Ludger Ltd; Orela Glycan Release Kit. **2008**.

123. The O-glycan release and HPLC analysis technique were developed by Dr. D. Alonzi at Oxford Glycobiology Institute, Department of Biochemistry, University of Oxford, South Parks Road, Oxford, OX1 3QU.

124. Rountree, J. S. S.; Butters, T. D.; Wormald, M. R.; Boomkamp, S. D.; Dwek, R. A.; Asano, N.; Ikeda, K.; Evinson, E. L.; Nash, R. J.; Fleet, G. W. J., Design, Synthesis, and Biological Evaluation of Enantiomeric beta-N-Acetylhexosaminidase Inhibitors LABNAc and DABNAc as Potential Agents against Tay-Sachs and Sandhoff Disease. *Chemmedchem* **2009**, *4*, 378-392.

125. Rountree, J. S. S.; Butters, T. D.; Wormald, M. R.; Dwek, R. A.; Asano, N.; Ikeda, K.; Evinson, E. L.; Nash, R. J.; Fleet, G. W. J., Efficient synthesis from D-lyxonolactone of 2-acetamido-1,4-imino-1,2,4-trideoxy-L-arabinitol LABNAc, a potent pyrrolidine inhibitor of hexosaminidases. *Tetrahedron Lett.* **2007**, *48*, 4287-4291.

126. Boomkamp, S. D.; Rountree, J. S. S.; Neville, D. C. A.; Dwek, R. A.; Fleet, G. W. J.; Butters, T. D., Lysosomal storage of oligosaccharide and glycosphingolipid in imino sugar treated cells. *Glycoconjugate J.* **2010**, *27*, 297-308.

127. Alonzi, D. S.; Neville, D. C. A.; Lachmann, R. H.; Dwek, R. A.; Butters, T. D., Glucosylated free oligosaccharides are biomarkers of endoplasmic-reticulum alpha-glucosidase inhibition. *Biochem. J.* **2008**, *409*, 571-580.

128. Neville, D.; Coquard, V.; Priestman, D.; te Vruchte, D.; Sillence, D.; Dwek, R.; Platt, F.; Butters, T., Analysis of fluorescently labeled glycosphingolipid-derived oligosaccharides following ceramide glycanase digestion and anthranilic acid labeling. *Anal. Biochem.* **2004**, *331*, 275-282.

129. Nishimura, Y.; Satoh, T.; Kudo, T.; Kondo, S.; Takeuchi, T., Synthesis and activity of 1-N-iminosugar inhibitors, siastatin B analogues for alpha-N-acetylgalactosaminidase and beta-N-acetylglucosaminidase. *Bioorg. Med. Chem.* **1996**, *4*, 91-96.

130. Saotome, C.; Wong, C.; Kanie, O., Combinatorial library of five-membered iminocyclitol and the inhibitory activities against glyco-enzymes. *Chem. Biol.* **2001**, *8*, 1061-1070.

131. Best, D.; Chairatana, P.; Glawar, A. F. G.; Crabtree, E.; Butters, T. D.; Wilson, F. X.; Yu, C.-Y.; Wang, W.-B.; Jia, Y.-M.; Adachi, I.; Kato, A.; Fleet, G. W. J., Synthesis of 2-acetamido-1,2-dideoxy-D-galacto-nojirimycin [DGJNAc] from D-glucuronolactone: the first sub-micromolar inhibitor of alpha-N-acetylgalactosaminidases. *Tetrahedron Lett.* **2010**, *51*, 2222-2224.

132. (a) Best, D.; Wang, C.; Weymouth-Wilson, A. C.; Clarkson, R. A.; Wilson, F. X.; Nash, R. J.; Miyauchi, S.; Kato, A.; Fleet, G. W. J., Looking glass inhibitors: scalable syntheses of DNJ, DMDP, and (3R)-3-hydroxy-l-bulgecinine from d-glucuronolactone and of l-DNJ, l-DMDP, and (3S)-3-hydroxy-d-bulgecinine from l-glucuronolactone. DMDP inhibits β-glucosidases and β-galactosidases whereas l-DMDP is a potent and specific inhibitor of α-glucosidases. *Tetrahedron Asymmetry* **2010**, *21*, 311-319; (b) Anzeveno, P. B.; Creemer, L. J., Efficient synthesis of (+)-nojirimycin and (+)-1-deoxynojirimycin. *Tetrahedron Lett.* **1990**, *31*, 2085-2088.

133. Weymouth-Wilson, A. C.; Clarkson, R. A.; Jones, N. A.; Best, D.; Wilson, F. X.; Pino-Gonzalez, M.-S.; Fleet, G. W. J., Large scale synthesis of the acetonides of L-glucuronolactone and of L-glucose: easy access to L-sugar chirons. *Tetrahedron Lett.* **2009**, *50*, 6307-6310.

134. Schueller, A. M.; Heiker, F.-R., Synthesis of 2-acetamido-1,2-dideoxy-d-galacto-nojirimycin (2-acetamido-1,2,5-trideoxy-1,5-imino-d-galactitol) from 1-deoxynojirimycin. *Carbohydr. Res.* **1990**, *203*, 308-313.

135. Kang, S. H.; Ryu, D. H., Intramolecular cyclization of C2 symmetric and meso-iodo amino alcohols: A synthetic approach to azasugars. *Tetrahedron Lett.* **1997**, *38*, 607-610.

136. Clark, N. E.; Metcalf, M. C.; Best, D.; Fleet, G. W. J.; Garman, S. C., Pharmacological chaperones for human α-N-acetylgalactosaminidase. *Proc. Natl. Acad. Sci. U. S. A.* **2012**, *109*, 17400-17405.

137. Van Diggelen, O. P.; Schindler, D.; Kleijer, W. J.; Huijmans, J. M.; Galjaard, H.; Linden, H. U.; Peter-Katalinic, J.; Egge, H.; Dabrowski, U.; Cantz, M., Lysosomal α-N-acetylgalactosaminidase deficiency: A new inherited metabolic disease. *Lancet* **1987**, *2*, 804.

138. Glunde, K.; Guggino, S. E.; Solaiyappan, M.; Pathak, A. P.; Ichikawa, Y.; Bhujwalla, Z. M., Extracellular Acidification Alters Lysosomal Trafficking in Human Breast Cancer Cells. *Neoplasia* **2003**, *5*, 533-545.

139. Shafat, I.; Vlodavsky, I.; Ilan, N., Characterization of mechanisms involved in secretion of active heparanase. *J. Biol. Chem.* **2006**, *281*, 23804-23811.

140. (a) Ho, C.-W.; Popat, S. D.; Liu, T.-W.; Tsai, K.-C.; Ho, M.-J.; Chen, W.-H.; Yang, A.-S.; Lin, C.-H., Development of GlcNAc-Inspired Iminocyclitiols as Potent and Selective N-Acetyl-beta-Hexosaminidase Inhibitors. *ACS Chem. Biol.* **2010**, *5*, 489-497; (b) Steiner, A. J.; Schitter, G.; Stuetz, A. E.; Wrodnigg, T. M.; Tarling, C. A.; Withers, S. G.; Mahuran, D. J.; Tropak, M. B., 2-Acetamino-1,2-dideoxynojirimycin-lysine hybrids as hexosaminidase inhibitors. *Tetrahedron-Asymmetry* **2009**, *20*, 832-835.

141. Prof. A. Kato, Department of Hospital pharmacy, University of Toyama, 2630 Sugitani, Toyama 930-0194, Japan.

142. Mellor, H.; Neville, D.; Harvey, D.; Platt, F.; Dwek, R.; Butters, T., Cellular effects of deoxynojirimycin analogues: uptake, retention and inhibition of glycosphingolipid biosynthesis. *Biochem. J.* **2004**, *381*, 861-866.

143. Rang, H. P.; Dale, M. M.; Ritter, J. M.; Flower, R. J., General Principles. In *Rang and Dale's Pharmacology*, Sixth ed.; Elsevier: Philadelphia, 2007.

144. Actelion Pharmaceuticals US, Inc; Prescribing information for Miglustat. http://www.zavesca.com/pdf/Zavesca-full-prescribing-information.pdf

145. Pfizer; Prescribing information Miglitol. http://labeling.pfizer.com/ShowLabeling.aspx?id=581

146. Glawar, A. F. G.; Best, D.; Ayers, B. J.; Miyauchi, S.; Nakagawa, S.; Aguilar-Moncayo, M.; García Fernández, J. M.; Ortiz Mellet, C.; Crabtree, E. V.; Butters, T. D.; Wilson, F. X.; Kato, A.; Fleet, G. W. J., Scalable syntheses of both enantiomers of DNJNAc and DGJNAc from glucuronolactone: The effect of N-alkylation on hexosaminidase inhibition. *Chem. Eur. J.* **2012**, *18*, 9341-9359.

147. The pyrrolidine iminosugar along with its N-butyl and N-hydroxyethyl side chain derivatives were synthesised by Dr. S. Jenkinson at Chemistry Research Laboratory, 12 Mansfield Road, Oxford, OX1 3TA.

148. The carboxylic acid derivative of the pyrrolidine iminosugar was synthesised by Dr. R. F. Martínez at Chemistry Research Laboratory, 12 Mansfield Road, Oxford, OX1 3TA.

149. CRUK; Most common cancer in women in the UK. http://www.cancerresearchuk.org/cancer-info/cancerstats/incidence/commoncancers/#Top3

150. Hulkower, K. I.; Herber, R. L., Cell migration and invasion assays as tools for drug discovery. *Pharmaceutics* **2011**, *3*, 107-124.

151. Albini, A.; Iwamoto, Y.; Kleinman, H. K., A rapid in vitro assay for quantitating the invasive potential of tumor cells. *Cancer Res.* **1987**, *47*, 3239-3245.

152. Orkin, R. W.; Gehron, P.; McGoodwin, E. B.; Martin, G. R.; Valentine, T.; Swarm, R., A murine tumor producing a matrix of basement membrane. *J. Exp. Med.* **1977**, *145*, 204-220.

153. Kleinman, H. K.; McGarvey, M. L.; Hassell, J. R.; Star, V. L.; Cannon, F. B.; Laurie, G. W.; Martin, G. R., Basement membrane complexes with biological activity. *Biochemistry (Wash.)* **1986**, *25*, 312-318.

154. Merk Millipore; User guide for QCM 24-well cell invasion assay. http://www.millipore.com/userguides.nsf/a73664f9f981af8c852569b9005b4eee/860c5f3ae955a8068525790d0054127f/$FILE/ECM554.pdf

155. Jones, L. J.; Gray, M.; Yue, S. T.; Haugland, R. P.; Singer, V. L., Sensitive determination of cell number using the CyQUANT® cell proliferation assay. *J. Immunol. Methods* **2001**, *254*, 85-98.

156. Neve, R. M.; Chin, K.; Fridlyand, J.; Yeh, J.; Baehner, F. L.; Fevr, T.; Clark, L.; Bayani, N.; Coppe, J.-P.; Tong, F.; Speed, T.; Spellman, P. T.; DeVries, S.; Lapuk, A.; Wang, N. J.; Kuo, W.-L.; Stilwell, J. L.; Pinkel, D.; Albertson, D. G.; Waldman, F. M.; McCormick, F.; Dickson, R. B.; Johnson, M. D.; Lippman, M.; Ethier, S.; Gazdar, A.; Gray, J. W., A collection of breast cancer cell lines for the study of functionally distinct cancer subtypes. *Cancer Cell* **2006**, *10*, 515-527.

157. Rasheed, S.; Nelson-Rees, W. A.; Toth, E. M.; Arnstein, P.; Gardner, M. B., Characterization of a newly derived human sarcoma cell line (HT 1080). *Cancer* **1974**, *33*, 1027-1033.

158. Dickens, J. P.; Crimmin, M. J.; Beckett, R. P. Dioxolane intermediates. GB2287023, 1995.

159. Tonn, J.-C.; Kerkau, S.; Hanke, A.; Bouterfa, H.; Mueller, J. G.; Wagner, S.; Vince, G. H.; Roosen, K., Effect of synthetic matrix-metalloproteinase inhibitors on invasive capacity and proliferation of human malignant gliomas in vitro. *Int. J. Cancer* **1999**, *80*, 764-772.

160. (a) Maegawa, G. H. B.; van Giersbergen, P. L. M.; Yang, S.; Banwell, B.; Morgan, C. P.; Dingemanse, J.; Tifft, C. J.; Clarke, J. T. R., Pharmacokinetics, safety and tolerability of miglustat in the treatment of pediatric patients with GM2 gangliosidosis. *Mol. Genet. Metab.* **2009**, *97*, 284-291; (b) Nirogi, R. V. S.; Kandikere, V. N.; Shukla, M.; Mudigonda, K.; Maurya, S.; Boosi, R.; Yerramilli, A., Liquid chromatographic tandem mass spectrometry method for the quantification of miglitol in human plasma. *Arzneim.-Forsch.* **2006**, *56*, 328-336.

161. Zengel, P.; Ramp, D.; Mack, B.; Zahler, S.; Berghaus, A.; Muehlenweg, B.; Gires, O.; Schmitz, S., Multimodal therapy for synergic inhibition of tumour cell invasion and tumour-induced angiogenesis. *BMC Cancer* **2010**, 92.

162. (a) Wilkins, M. R.; Lindskog, I.; Gasteiger, E.; Bairoch, A.; Sanchez, J.-C.; Hochstrasser, D. F.; Appel, R. D., Detailed peptide characterization using PEPTIDEMASS - A World-Wide-Web-accessible tool. *Electrophoresis* **1997**, *18*, 403-408; (b) Gasteiger, E.; Hoogland, C.; Gattiker, A.; Duvaud, S.; Wilkins, M. R.; Appel, R. D.; Bairoch, A., Protein Identification and Analysis Tools on the ExPASy Server. *John M. Walker (ed): The Proteomics Protocols Handbook, Humana Press* **2005**, 571-607.

# 5 CONCLUSION

The subject of this thesis has been both the synthesis and biological evaluation of iminosugars. This was done on the backdrop of identifying novel glycosidase inhibitors as potential anti-cancer agents. Based on the evidence in the literature the two glycosidases, α-*N*-acetyl-galactosaminidase and β-*N*-acetyl-hexosaminidase, were identified as promising selective biological targets for anti-cancer therapy.

The synthetic journey from piperidines to azetidine iminosugars began by confirming the previously reported highly potent β-*N*-acetylhexosaminidase inhibition ($IC_{50}$ 140 nM, human placenta) of pipecolic amide **10** (Figure 5.1). Structure activity relationship data was collected on this 6-ring amino acid along with further 5-ring systems, including the potent pyrrolidine inhibitor **68** ($K_i$ 27 nM, HL60). This allowed for their potent inhibition potential to be rationalized by comparing DFT calculation based molecular models and the biological activity of the L-ribo azetidine **78L** was successfully predicted using this model. Inspired by the ideas of this theoretical exercise, synthetic routes to azetidine iminosugars in novel chemical space were devised. The existing methodology for the formation of *cis*-azetidines was significantly extended by inclusion of an oxidative protocol, which allowed for the formation of the enantiomeric pair of *ribo* azetidine α-amino-acids and methyl amides. This represents the first synthesis of a 3-hydroxy-2-carboxy-azetidine with no protection on the endocyclic nitrogen or OH3. Substantial progress has also been made towards the development of *trans*-azetidine methodology, which should give access to all possible stereoisomers of the azetidine scaffold, subject to further optimization of the orthogonal protecting group setup employed. Furthermore, the most powerful α-*N*-acetyl-galactosaminidase inhibitor, DGJNAc **239**, was successfully derivatised on the endocyclic nitrogen using reductive amination. It can therefore be concluded that this thesis saw the successful synthesis of highly potent inhibitors for both novel glycosidase anti-cancer targets.

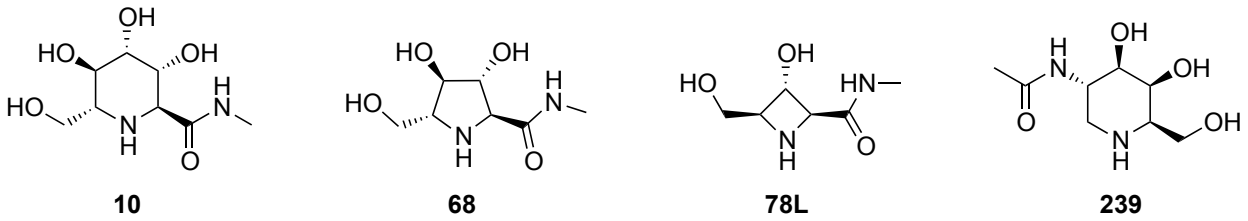


**Figure 5.1** 6-, 5- and 4-ring iminosugars.

The newly synthesised iminosugars were subjected to extensive biological evaluation including: *in vitro* enzymatic inhibition assays, assessment of lysosomal glycosidase inhibition on a cellular level and a Boyden chamber cell invasion assay. Although the *in vitro* assay on the immunosuppressive effects of α-*N*-acetyl-galactosaminidase could not be completed, current ongoing investigations show promising preliminary results when DBP is isolated directly from blood plasma. The importance of a quality control mechanism for evaluating the degree and identity of the glycan on DBP was identified and MALDI-Ms showed an absence of glycosylation on the commercial DBP. A comparison of the *in vitro* enzymatic inhibition strength with cellular inhibition of lysosomal glycosidases was drawn for *N*-alkyl derivatives of both DGJNAc **239** and pyrrolidine **68**. A general principle emerged that *N*-butyl side chains promote cell and organell penetration, while hydrophilic side-chain characteristics like *N*-hydroxyethyl and carboxylic acid derivatives restrict the iminosugar to extra cellular space, which is consistent with the biodistribution observed for iminosugars currently in the clinic. With regard to cancer cell invasion it was found that β-*N*-acetyl-hexoaminidase inhibitors can retard the migration of even the highly aggressive breast cancer cell line MDA-MB-231 through the ECM. Non-toxic iminosugars would make a promising addition to a cocktail of protease inhibitors as an answer to the diversity of hydrolytic enzymes secreted by invasive cancer cells.

I would hope that the promising results in terms of *cis*- and *trans*-azetidine synthesis methodology along with glimpses gleaned of the potential held by iminosugars as anti-cancer agents will stimulate future research by my two groups and other investigators interested in the exciting field of iminosugars.

# Appendix A – Publications arising from work within this thesis

Digital object identifiers (DOI) provided as hyperlinks below citation.

## Related to Chapter 2:

Araújo, N.; Jenkinson, S. F.; Martínez, R. F.; Glawar, A. F. G.; Wormald, M. R.; Butters, T. D.; Nakagawa, S.; Adachi, I.; Kato, A.; Yoshihara, A.; Akimitsu, K.; Izumori, K.; Fleet, G. W. J., Synthesis from D-altrose of (5R, 6R, 7R, 8S)-5,7-dihydroxy-8-hydroxymethylconidine and 2,4-dideoxy-2,4-imino-D-glucitol, azetidine analogues of swainsonine and 1,4-dideoxy-1,4-imino-D-mannitol. *Org. Lett.* **2012**, *14*, 4174- 4177.

DOI: http://dx.doi.org/10.1021/ol301844n

## Related to Chapter 3:

Glawar, A. F. G.; Jenkinson, S. F.; Thompson, A. L.; Nakagawa, S.; Kato, A.; Butters, T. D.; Fleet, G. W. J., 3-Hydroxyazetidine Carboxylic Acids: Non-Proteinogenic Amino Acids for Medicinal Chemists. *ChemMedChem* **2013**, *8*, 658-666.

DOI: http://dx.doi.org/10.1002/cmdc.201200541

## Related to Chapter 4:

Best, D.; Chairatana, P.; Glawar, A. F. G.; Crabtree, E.; Butters, T. D.; Wilson, F. X.; Yu, C.-Y.; Wang, W.-B.; Jia, Y.-M.; Adachi, I.; Kato, A.; Fleet, G. W. J., Synthesis of 2-acetamido-1,2-dideoxy-D-galacto-nojirimycin [DGJNAc] from D-glucuronolactone: the first sub-micromolar inhibitor of alpha-*N*-acetylgalactosaminidases. *Tetrahedron Lett.* **2010**, *51*, 2222-2224.

DOI: http://dx.doi.org/10.1016/j.tetlet.2010.02.063

Glawar, A. F. G.; Best, D.; Ayers, B. J.; Miyauchi, S.; Nakagawa, S.; Aguilar-Moncayo, M.; García Fernández, J. M.; Ortiz Mellet, C.; Crabtree, E. V.; Butters, T. D.; Wilson, F. X.; Kato, A.; Fleet, G. W. J., Scalable syntheses of both enantiomers of DNJNAc and DGJNAc from glucuronolactone: The effect of *N*-alkylation on hexosaminidase inhibition. *Chem. Eur. J.* **2012**, *18*, 9341-9359.

DOI: http://dx.doi.org/10.1002/chem.201200110